Analysing micro-residues on prehistoric stone tools by Raman microscopy and determining their origins

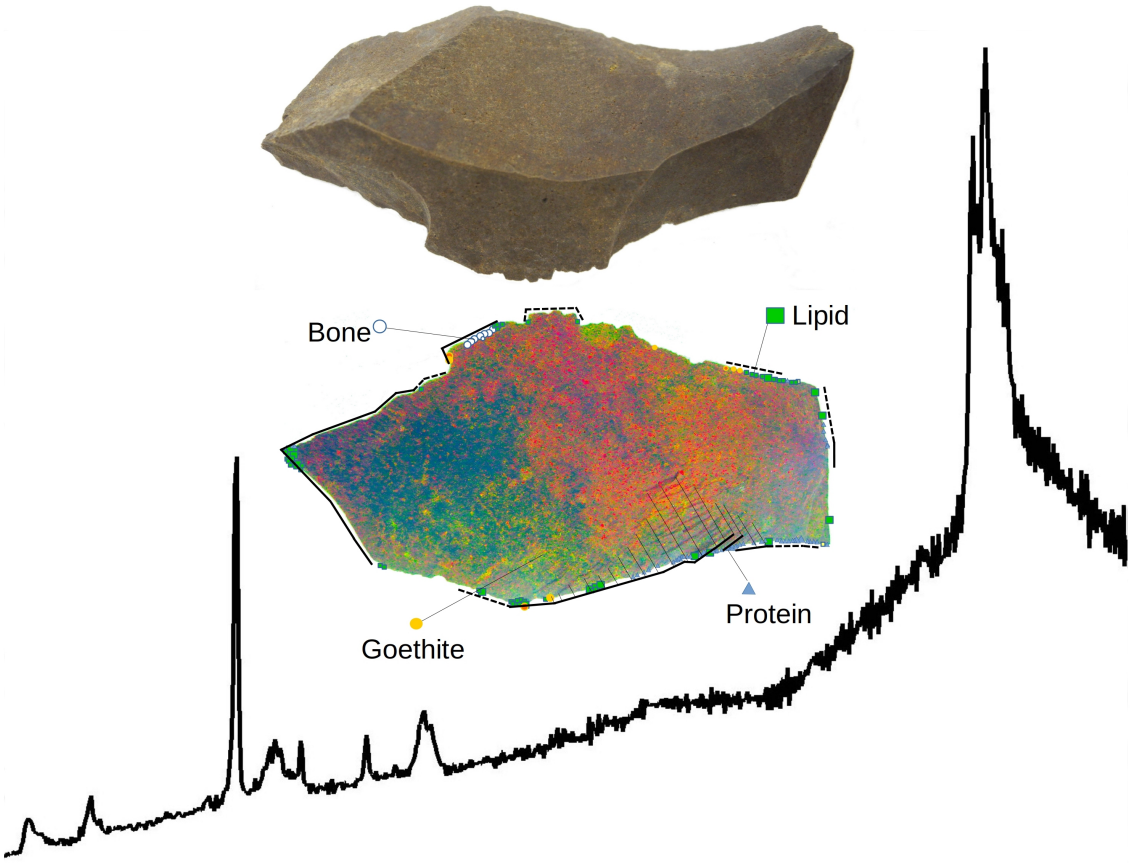

A THESIS SUBMITTED IN FULFILMENT OF THE REQUIREMENTS FOR THE AWARD OF THE DEGREE

DOCTOR OF PHILOSOPHY

FROM THE

UNIVERSITY OF WOLLONGONG

By

LUC BORDES

CENTRE FOR ARCHAEOLOGICAL SCIENCE,
School of Earth, Atmospheric and Life Sciences

2019

Declaration

I, Luc Bordes, declare that this thesis, submitted in fulfilment of the requirements for the award of Doctor of Philosophy, in the School of Earth, Atmospheric and Life Sciences, University of Wollongong, is wholly my own work unless otherwise referenced or acknowledged. The document has not been submitted for qualifications at any other academic institution.

Luc Bordes

26 March 2019

List of figures

List of tables

Abstract

This thesis aims to contribute to the determination of prehistoric stone tool function from traces of use for reconstructing and understanding hominin prehistoric behaviour. While macro-morphological approach provides important information about the context of tool use, it does not provide secure evidence of how the tool was actually used or what materials were processed. Retouched tools that do not match formal types, and unretouched flake tools are potentially even more problematic for morphological based interpretations of function.

Microscopic use-wear analysis is an essential technique to determine use of stone tools, but it needs to be complemented by residue analysis for more robust functional interpretations. Conventional use-wear analysis identifies residues in the first stages of optical microscopy, followed by targeted analysis of residues, which often need to be removed. However, optical recognition of in situ, amorphous micro-residues is difficult. Additionally, stone artefacts not preselected for macro-residues may have low levels of preservation, and in that case cannot always benefit from pre use-wear analysis.

Raman microscopy offers an alternative initial approach to residue analysis because it is a fast, non-destructive analytical technique, with high spatial resolution and it can rapidly identify a wide range of organic and mineral residues (bone, lipids, proteins, cellulose, lignin, starch and iron oxides).

This thesis develops a new methodology, to enhance the use of spectroscopic technique in discriminating use-related residues from contaminants, and to provide interpretations both independent of, and complementary to, conventional use-wear analysis. Indeed, micro-residues on prehistoric stone tools can arise from diverse origins that may be incidental to tool-use, naturally occurring in sediment, and arising from post-depositional processes and from other sources including ancient and modern contamination. To learn about hominin behaviour from stone tools, it is critical to filter the possibilities and retain only use-related materials. Consequently, Raman microscopy is positioned as a potential first step, but needs to develop its own micro-residue discrimination strategy. A whole set of criteria and complementary observations are needed, including correlation between use-wear and micro-residues distributions, which require systematic spatial localisation and secure identification. Initial Raman microscopy is bringing a new approach and has the advantages of being complementary to and independent of conventional use-wear residue analysis. Additionally, to interpret stone artefacts micro-residues Raman analysis, this work developed a reference material database that is critical to compare with analysed residues on prehistoric stone tools.

Raman references for different chemical compounds, modern and natural materials have been developed here, as well as targeted stone tools experiment to investigate type of micro-residues deposited.

This thesis has been also planned from the beginning to be part of the “Out of Asia” ARC Laureate Project, which was designed to improve understanding of the timing and dispersal of prehistoric hominin populations into South Asia and Australia. In this project, archaeochemistry, including different types of spectroscopic methods (Infrared, Raman, GC-MS), was planned to contribute to understanding hominin behaviour by analysing stone artefacts recovered from selected archaeological sites and to determine their function. Consequently, two available prehistoric stone artefacts collections were selected, from Liang Bua and Denisova cave, to apply the developed methodology in Raman spectroscopy for reconstructing and understanding hominin prehistoric behaviour.

Analysis results of different sets of artefacts collected from these two prehistoric sites allow to observe continuity or variation of stone tools use and behaviour through time, which requires comparisons of worked materials and particular ways of using stone tools recovered from different archaeological layers.

This thesis shows that Raman spectroscopy applied to prehistoric stone tools is a successful analysing method and can be considered as a technique with a potential pivotal role in relating use-wear and other complementary techniques like GS-MS. Indeed, as Raman spectroscopy is a non destructive technique and leaves intact micro-residues on stone surfaces, any tagged concentrated spot of micro-residues (e.g., lipids) could be targeted in a second step of analysis with application of any complementary techniques on material having being securely linked to prehistoric use on stone artefacts. In that perspective, this thesis can open a way forward to optimise information from lithic functional analysis by combining, and ensuring that, the different analysing methods (use-wear analysis, spectroscopic analysis, GC-MS separative methods) will better complement each other in the future.

Keywords: Raman microscopy, Liang Bua, Denisova Cave, Micro-residues, Stone tools

Acknowledgements

Connection to the PhD project

I would like to thanks especially Dr Elspeth Hayes in connecting me to this PhD project with the local help in France from Dr Liz Kish.

Supervisors

I would like to thanks my main supervisor Prof Richard Roberts, and my co-supervisors Dr Linda Prinsloo and Prof Richard Fullagar. Especially Linda for her supervision on the Raman spectroscopy part and Richard for advising me on use-wear analysis, and his precious help about English language corrections in the manuscript.

Other member of CAS:

I would like to thanks Dr Mike Morley, Dr Anna Kotarba-Morley, Dr Susan Luong, for their welcome and collaboration.

Access to resin collection:

Thanks to Philip Green giving me access to his Australian resin collection and for expertise during the 2016 workshop.

Goat skin collection:

Thanks to Dr Nicolas Gill who provided me some goat bone and skin reference materials.

Sharing PhD UOW experience:

Thanks to other CAS PhD students: Conor Mcadams, Maria Schaarschmidt, Anna Romanyukha, Dafne Koutamanis for sharing PhD experience at UOW.

Welcoming at UOW:

Thanks to Prof Anthony Dosseto and Dr Gabriel Enge for their welcome when I arrived at UOW in August 2015.

Chapter 1 Introduction

1.1 Background

Determining prehistoric stone tool function from traces of use is a key for reconstructing and understanding hominin prehistoric behaviour, in part because the most common archaeological finds found in prehistoric sites are stone artefacts. Organic materials (from food remains or shaped tools made of plant and animal tissue are less well-preserved, although, because of their partially mineralised apatite structure, bone, ivory and antler remains are also commonly encountered in some old prehistoric sites, either as consumed animal products or as shaped tools.

Stone materials have been used by hominin, including our own genus *Homo*, for over two million years (Kimbel et al., 1996; Prat et al., 2005; Harmand et al., 2015), in the making of a range of different tools intended to be used, with abundant stone flake debris resulting from flaking processes—some of which has traces of use. Other rocks were used with pounding and grinding actions and were sometimes first shaped to make polished or ground stone tools. Lithic technologists generally classify stone tools according to the manufacturing processes used to make particular implements like choppers, bifaces, blades, points, Levallois flakes, burins. (Debenath and Dibble, 1994; Odell, 1996). Byproducts (e.g., core, flaking debris) of this manufacturing processes are also informative for understanding tool making technology (Ahler, 1989). The use of different types of hammer stones (e.g., hard or soft stone; antler or wood) and pounding implements can be also determined by functional studies, and contributes to understanding the makers' gestures in that process (e.g., Driscoll and Garcia-Rojas, 2014).

Stone tool classification systems are generally based on their production technology, shape and by measurement of parameters like length, width, cross section, edge angles and dimensions of the used edges. (Inizan et al., 1999). Stone tools have been labeled as scrapers, points, projectile elements, blades, hand axes and other terms that imply function, mainly on the basis of their shape, recognition of their active parts and tool ergonomy (Lovita, 2011). While this macro-morphological approach provides important information about the context of tool use, it does not provide secure evidence of how the tool was actually used or what materials were processed. Retouched tools that do not match formal types (e.g., with more complex design or multiple used edges) and unretouched flake tools are potentially more problematic for morphological based interpretations of function (Dibble, 1987; Hardy et al., 2001). Indeed, use-wear and residue studies show that tool typology may not be strongly linked with the processing of specific materials (Hardy et al., 2008). Morphological studies can

rarely determine the specific, or range of, worked materials. For example, hafted stone points of similar design could be mounted as armatures on hunting projectiles or as bits on stick handles to drill holes in shell—i.e. for completely unrelated tasks.

Another way of classifying stone tools is to identify their function by knowing more accurately (1) the actions involved or mode of use (e.g., cutting, sawing, scraping or grinding); (2) the nature of materials on which they were used (e.g., bone, plant, skin or pigment); and (3) the broader task and context of their use (e.g., cutting meat for cooking, scraping skin in a tanning process, cutting plant material for medicine preparation). Experiment-based use-wear studies have successfully provided a more reliable methodology for determining such details about prehistoric stone tool function since the 1960s. For example, several researchers used optical and electron microscopy to recognise different patterns of experimental use-wear and relate these to the working of a particular soft or hard material, and even more precisely to plant, wood, bone, or skin material (e.g., Semenov, 1964; Odell, 1975; Hayden, 1979; Anderson, 1980; Keeley, 1980; Olausson, 1980; Kamminga, 1982; Beyries, 1984; Fullagar, 1986; van Gijn, 1990). The experimental wear patterns recognised on stone tools assigned significance to combinations of various forms of wear (polish, striations, scarring and edge rounding) and to particular contexts (e.g., hafting, use and manufacture traces), all of which help in the reconstruction of the prehistoric gestures.

1.2 Context of this study in relation with “Out of Asia” project and aims of this thesis

This PhD work is part of the development of archeochemistry in the Centre for Archaeological Science under the auspices of the “Out of Asia” ARC Laureate Project (awarded to Prof Richard “Bert” Roberts, University of Wollongong), which was designed to improve understanding of the timing and dispersal of prehistoric hominin populations into Southeast Asia and Australia. In this project, archaeochemistry, including different types of spectroscopy methods (Infrared, Raman, Gas Chromatography coupled with Mass Spectrometry (GC-MS)), was planned to contribute to understanding hominin behaviour by analysing stone artefacts recovered from selected archaeological sites and to determine their function. In the Out of Asia Project, prehistoric sites were selected between Denisova Cave in Siberia and Madjedbebe, the oldest known human occupation site in Australia, to track dispersal and behavior of modern and archaic humans (Fig. 1.1). Stone artefacts from two key sites, Denisova Cave (Fig. 1.1, site 1) and Liang Bua (Fig. 1.1, site 7) were selected for analysis in this thesis.

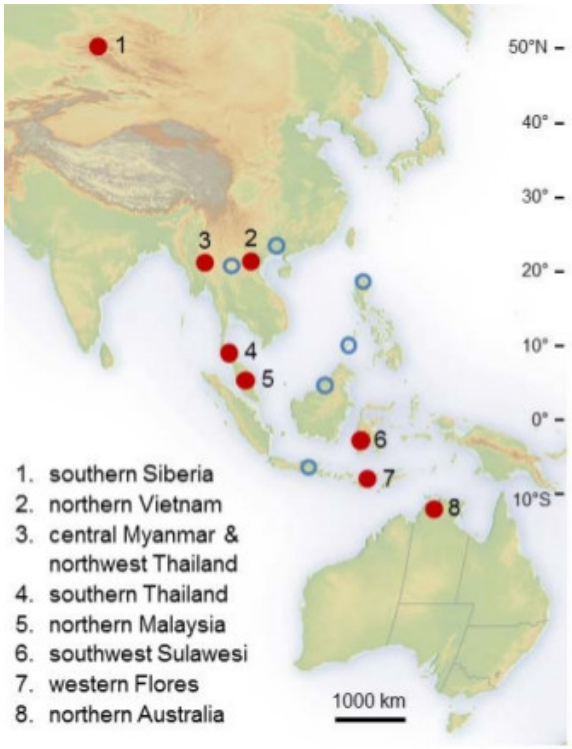

Figure 1.1: Prehistoric sites included in the Out of Asia Project.

Genetic evidence estimates that Denisovans, a new hominin group identified from DNA from human remains in Denisova Cave diverged around 800,000 years ago from the branch leading to modern humans and Neanderthals, remains of which have also been found the Altai Mountains (Krause et al., 2010; Reich et al., 2010; Meyer et al., 2012). Remarkably, Denisovan DNA has been obtained from modern-day inhabitants of Melanesia, Polynesia and Australia, indicating that Denisovans evidently interbred with the pioneering wave of modern humans to enter Southeast Asia, perhaps as early as 75,000 years ago, leaving Aboriginal Australians with a genetic legacy of this encounter (Rasmussen et al., 2011; Reich et al., 2011; Meyer et al., 2012). *Homo floresiensis* (commonly called 'Hobbits') remains, of an ancient lineage possibly related to *Homo erectus*, occupied the Indonesian island of Flores from ~1 million years ago until 60,000 years ago, when they were probably replaced by modern humans (Brown et al., 2004; Morwood et al., 2004; Morwood et al., 2005; Sutikna et al., 2016).

An innovative approach of this PhD thesis is to investigate residues by combining spectroscopic methods with conventional use-wear study of stone artefacts from these two sites. The main aim of this research is to shed light on continuity of tool function and resource-use by sampling artefacts from well-dated archaeological layers, during phases of occupation of these caves. Along with this overarching objective, I have three specific aims:

1 - To develop a methodology for application of Raman microscopy to determine residue origins and stone tool function;

2 - To assess the potential of this methodology by applying it to two archaeological assemblages, from Denisova Cave and Liang Bua;

3 - To assess environmental and cultural factors in the differential preservation of residue materials.

Apart from their high significance in human evolution, these two sites were chosen because of the availability of these stone artefact collections in the Centre for Archaeological Science (CAS), and because they had been collected and stored to optimise conditions for use-wear and residue analysis. This PhD is the first to report results of extended analyses by Raman spectroscopy on both of these collections, and follows publication of preliminary methodological work on artefacts from Liang Bua (Bordes et al., 2017) and Denisova Cave (Bordes et al., 2018).

1.3 Spectroscopic analysis to complement use-wear studies

Study of residues has been complementing use-wear functional studies since the 1970s (e.g., Briuer, 1976; Shafer and Holloway, 1979; Anderson, 1980; Loy, 1983; Fullagar, 1986). However, in recent decades, lithic analysts have been complementing functional studies with analytical methods from archaeological chemistry to identify molecular traces (Pollard and Heron, 1996). Systematic application of archaeochemistry techniques to functional studies has been limited by several factors such as site context, artefact recovery methods, residue preservation, and instrument availability.

Use-wear remains the backbone of lithic functional analysis (Fullagar and Matheson, 2014; Hayes, 2015), but can give only access to indirect micro-traces of the material worked by a

given stone tool. Moreover, that technique is sometimes reaching its limits to distinguish similar wear patterns from different worked materials and different wear patterns obtained by working the same material with different stone (Fullagar, 1986). In the case of expedient stone tools (e.g., on unretouched flake tools), polish from use can be faint and discontinuous along an edge; and overlapping wear from handling can render more complex the identification of used edges and the material that came into contact with the tool (Rots, 2010). Moreover, some rocks, like quartzite, can make interpretations of use-polish challenging.

When preserved on stone artefacts, residues can complement use-wear study and strengthen functional interpretations. Indeed, residues still present on stone artefacts can provide direct proof of specific material which have been in contact with them. Different techniques have been used to investigate archaeological residues in situ on stone tools. Visible light microscopy (VLM) has been used to investigate plant and animal residues (Hardy et al., 2001; Robertson et al., 2009), but some authors underline the difficulties of identifying residues with only optical microscopes (Monnier et al., 2012). For example, it was shown that, based on their microscopic morphological appearance, animal residues could be mistaken for plant residues (Wadley et al., 2007). Other residues like skin flakes can also be confused with bone residues, observed under VLM (Langejans, 2012). Some common archaeological residues like bone are reported as being difficult to identify, especially when no internal structure can be observed, in part because the material is squashed or degraded on the rock surface of artefacts (Jarhen et al., 1997; Lombard, 2004; Guarino et al., 2006). Other difficulties can arise from the mixing of organic residues with sediment and naturally occurring minerals on stone artefact surfaces; and the stone artefact colour can create confusion (e.g., white bone residues on white milky quartz background). With only VLM, the level of confidence to identify many residues on stone tools will never be 100% certain, even for an experienced observer. This level of confidence will further decrease considerably with decreasing size of residues and poorer preservation of amorphous residues.

The problem of residue identification using optical or VLM is not only qualitative, but also quantitative. Indeed, when a high number of stone artefacts is required, the number of residues increases accordingly. Consequently, with a fixed time budget for analysis, there will be less time for VLM observation per artefact (reducing likelihood of secure identifications), or fewer artefacts that can be analysed. Another complementary technique to identify residues is to apply chemical stains or dyes, which attach specifically to a particular residue molecule and enhance VLM observation (Lamb et al., 2005; Hayes, 2015; Stephenson, 2015). However,

each dye can target only one or a few types of residues at once, and residues usually need to be removed from the targeted stone tool surface for various tests. A further limitation of that technique is that the specificity of dyes to organic residue molecules which could have been altered over long time, or being present as complex organic mix, or again closely associated with minerals, may be questionable. Concerning these issues, Infrared and Raman spectroscopic analysis have advantages over VLM. Spectroscopy can identify multiple residues with a higher confidence level than the VLM methods, leading to accurate spectral fingerprints of a great range of materials. Furthermore, these methods are non destructive and other analytical methods can be applied subsequently. Scanning electron microscopy (SEM) has been used both on experimental stone tools (Jarhen et al., 1997; Anderson, 1980) and prehistoric artefacts (Anderson, 1980) to observe residues. SEM with energy dispersive X ray spectroscopy (EDS) capacity can probe the elemental composition of these residues. Recent advance in SEM technology open the possibility to observe in situ residues on uncoated stone artefact surfaces, bringing excellent capability for identification of smaller residues (Rots et al., 2017), but focusing on such samples need at least several minutes, and image quality is sometimes degraded due to charging effects.

In FT-IR (Fourier-Transform Infrared Spectroscopy), different prehistoric organic residues can be detected (Prinsloo et al., 2014). Residues with animal (including human) tissue (including blood, ancient DNA, hair, and feathers) have been identified. Other analysed residues include adipocere, proteins, lipids (Cesaro et al., 2012); bone and fat residues (Solodenko et al., 2015); tar and bitumen residues on Palaeolithic tools (Monnier et al., 2013); and glue and mud plaster (Shaham et al., 2010). Plant residues have also been detected, like phytoliths, starches, pollen grains, cell walls and fibres. Additionally, this technique allows detection of mineral residues such as calcite (Cesaro et al., 2012). It should be noted that large experimental Infrared databases on both animal and plant residues have also recently been built (Monnier et al., 2017).

Raman spectroscopy was first used to analyse mineral pigments (Hernanz et al., 2006; Ospitali et al., 2006). Recent advances in spatial resolution, and the use of multiple laser red-shifted lines have enabled the detection of a growing number of similar archaeological residues (as found with FT-IR) such as human remains and hair (Edwards et al., 2007), resin, plant residues (e.g., plant fibre or starch grain), bone and fat. One big advantage of Raman spectroscopy is its analytical speed: analysis can be achieved for each residue by recent instruments in a matter of seconds rather than in minutes for FT-IR and SEM. Consequently,

the new generation of Raman instruments allows new strategies for investigating stone artefact function in larger samples and more systematically rather than being constrained by the limitations of older instruments, which were primarily restricted to confirming material identifications targeted by VLM observations.

Spectroscopic residue analysis followed two different approaches of residue analysis: (1) sample extraction analysis and (2) in situ analysis. Extracting the residues is the older technique, preferred for macro-residues (Chapter 1, Section 1.5), preferred because it allows an isolated analysis of the targeted residue, and prevents the potential problem of an additional mineral background signal. In more recent work, direct multi-sampling of macro-residues has been achieved (Vahur et al., 2011). Extraction analysis is limited by the amount of residue attached to the stone tool and, in some cases, where the residues are so small and in such low abundance, extraction cannot be achieved and not enough material can be analysed to give reliable results (Galanidou, 2006). Extraction can be done directly by dry sampling or by dissolving an area of the stone artefact with a solvent. The direct, dry sampling method is suitable when sufficient residue is attached to the stone tools (Shaham et al., 2010), but it might not be possible to recover residues embedded in irregularities of the surface. The extraction technique is destructive because it can remove a substantial amount of attached residue and can dissolve a residue film from the targeted surface. For this reason, in the case of very precious samples or where only small amounts of material remain on the artefact surface, “in situ” analysis which is less “destructive”, would be preferred. In these situations, spectroscopic methods like Infrared and Raman spectroscopy have advantages over other extraction methods.

1.4 Analysing strategy including micro-traces study and residues spectroscopic analysis

Having outlined how spectroscopic analysis is complementary to use-wear analysis, how can we combine them together to most effectively study stone artefacts and their function ?
One strategy is to undertake a first step of micro-trace study with VLM residue observation followed by a second step of spectroscopic analysis, following the conventional approach currently used by most analysts (Cesaro et al., 2012; Monnier et al., 2013). In this strategy, the role of Raman or Infrared spectroscopy is to confirm the identification of targeted residues identified by VLM. This strategy accords with historical development of these techniques; VLM observation of micro-traces is first applied, followed by spectroscopy methods. The older

generation of spectroscopic instruments, which could only achieve slow rates of analysis, was appropriate for systematic detection of large residues, justifying this secondary checking role. One big advantage of this approach for researchers is that the analysis can be applied straightforwardly to residues, already considered on stone artefacts as related to tool use, and it is equally appropriate for extracted residues.

However, it appears that achieving the spectroscopic analysis after the use-wear study (polish, scarring, edge rounding, striations) is a limited strategy when applied to artefacts that have not been selected for their exceptional residue preservation, especially as these spectroscopic techniques are fitted now to analysis micro-residues on less preserved samples, which can pass undetected, below the threshold of VLM observation.
Indeed, a strategy with use-wear and residue VLM observation as the first step could result in false negative assessments; for example, when no identifiable shaped residues are detected, because they are too small, amorphous, smeared on the surface or mixed with attached sediment. In the latter cases, the VLM analysed artefacts might be rejected for further spectroscopic study because of poor preservation, when the residues exist but were below threshold limits of detection. Consequently, the classical approach might result in bias because only residues on intensively used stone tools will be analysed, and expedient stone tools will be missed.

Furthermore, with the classical approach, spectroscopy analysis is strongly driven by the initial micro-traces study and thus focuses only on micro-residues recognised previously by VLM and tends to be a confirmation of only what has been initially identified. Very small, shapeless, smeared micro-residues embedded in surface irregularities missed during the VLM observation step will be probably also ignored by subsequent spectroscopy. Documenting the distribution of micro-residues may also be less reliable, because the focus tends to be on the most heavily used surfaces and edges, neglecting micro-residues from less intensively used areas or arising from other origins (incidental). From a practical point of view, two arguments are against this conventional approach. First, use-wear analysts sometimes apply solvents to clean the artefacts in order to fully examine all surface features, and consequently chemically alter the micro-residues and/or obliterate completely the microscopic remains on tool surfaces (Hogberg et al., 2009). These methods of micro-traces analysis cannot be considered non destructive and may not always be justified as a first step in the study of stone artefacts. Second, targeting exactly the same micro-residues under VLM so they are visible with spectroscopy instruments is very time consuming, even with the new generation of Infrared

and Raman instruments that are equipped with VLM capacity. To conclude about the strategy concerning initial stage of VLM analysis, one needs to take into account that relating micro-residues to tool use is more difficult for less well-preserved artefacts when only micro-residues are present (Chapter 1, sections 1.6 to 1.7) with additional risk of modern contamination (Chapter 3, section 3.2).

An alternative strategy is to undertake spectroscopy analysis as the first step, before VLM observation. Indeed, it is logical to first apply non destructive analyses more sensitive to contamination, before other methods that demand additional steps of surface cleaning and increase risk of exposure to modern contaminants. This strategy has been followed by Hogberg (Hogberg et al., 2009), mainly because of the surface cleaning issue outlined above. This spectroscopy-first strategy, renders the spectroscopy results independent from the use-wear study and encourages study of less well preserved artefacts and micro-residues not observed under VLM.

As this 'spectroscopy-first' strategy, Raman spectroscopy is not any more a simple confirmation of previously identified residues, and need to be used more as a stand-alone technique which need to assert micro-residues found on stone artefacts as use-related (Chapter 1, section 1.7). However, to achieve this, Raman analysis needs to be systematic in coverage of entire edges and tool surfaces to achieve micro-residues distributions and is consequently much more time consuming. Nevertheless, its important to note that if Raman analysis replaces VLM observation as the first step, the spectroscopy results still need to be related to micro-traces observations in a second step to be validated as use-related residues, especially because their distribution need to be meaningful with polished part of stone tools (Chapter 3, section 3.10). This new approach is available to researchers only now because of a new generation of spectroscopic instruments, which have the capacity to analyse a spot in a few seconds at high spatial resolution. This sub-micron spatial resolution (Chapter 2, sections 2.1.2 and 2.1.3) allows to analyse micro-residues in attached sediment, and select sub-micron smeared residues on stone tool surfaces and sort different mixtures (e.g., mixed residues composed of organic and mineral materials). This alternative strategy is more suited to the study of systematically selected stone artefacts from archaeological layers where the preservation conditions are still unknown and have the advantage to lower exposure to contamination before this analysis.

The choice between these two strategies, outlined above, depends, in part, on the process of selecting artefacts for study, residue preservation conditions, and likely residue distributions on the artefacts. For example, when stone tools can be clearly oriented with known functional contexts and residues observed easily under VLM (e.g., a hafted arrow point), the first strategy will be less time consuming and generally appropriate for the research questions; and the subsequent spectroscopy analysis will be faster and target directly the area of interest (e.g., arrow tip or hafted zone). However, when no strong functional hypothesis links the stone artefact morphology and poor preservation conditions leave no shaped residue features on its surface, the second strategy would be preferred for the reasons outlined above.

Artefacts from both prehistoric sites studied (Liang Bua and Denisova Cave) were not sorted and have been sampled directly from archaeological layers. Most of them were delivered to the laboratory covered by sediment or attached to a pedestal of sediment, which render them suitable for high standards of analysis, but prevent the direct evaluation of residue preservation. Consequently, in this thesis, I focus on Raman spectroscopy and its fast capability for investigating micro-residues (Chapter 2, sections 2.1.2 and 2.1.3), and explore fully the potential of this alternative strategy, using Raman spectroscopy as a stand-alone technique and linking its results with use-wear study afterward, in order to obtain more objective conclusions. However, this strategy demanded that I develop a new methodology for selecting use-related micro-residues, rejecting others (Chapter 3).

1.5 Preservation of residues on prehistoric stone tools

As discussed above, the analysing strategy and information obtained from residues is highly dependent on their preservation on prehistoric artefacts. Preservation of microscopic residues, like macroscopic remains, is dependent on their molecular nature, post-depositional weathering of artefacts and burial conditions (Wadley et al., 2007; Peta, 2009; Langejans et al., 2010). Size and abundance of use-related residues are mainly a result of preservation conditions but could also result from the duration of stone tool contact with a given material or how the tool was used and stored in the past. In conditions of good preservation, a large residue distribution or bigger residues might be visible with the naked eye. As discussed above, most previous spectroscopic analyses of stone tools have been done on macro-residues, visible by naked eye or low magnification observation (Shaham et al., 2010; Vahur et al., 2011; Carcimaru et al., 2012). Whatever the analysis technique used, preservation of macro-residues is also a key criteria for artefact selection. On other hand, some authors

(Langejans et al., 2012) have attempted to find and identify micro-residues on a whole range of archaeological stone artefact samples with success, showing that preservation of residues is not “black or white” and that micro-residues could be preserved when macro-residues are lacking. Such studies question the conventional way of selecting prehistoric artefacts according to the best preserved residues. Indeed, micro-residues could remain embedded in cracks and small rock surface depressions, and be resilient to alteration or removal by post-depositional processes or other factors. Moreover, preservation at a local scale can vary across an archaeological site, and particular artefacts might be protected by overlying rock, being away from ground water flow, by a protective sediment layer or by other circumstances. As these factors depend on so many parameters, they are difficult to evaluate (Langejans et al., 2010), and we cannot exclude that the smallest residues could survive even when conditions are not favourable, perhaps after thousands of years. Another complexity affecting residue preservation is chemical alteration of the initial material to another product over time. Some residues after thousands of years of alteration, are recognisable as traces of worked material, only after identification of their end products.

1.6 Different origins of residues attached to stone tools

Identifying residues attached to a stone tool by VLM observation or analysing it by spectroscopic analysis (whatever the instruments used, SEM, Infrared, Raman, GC-MS.) does not mean that the residues are related to what the tool was used for processing or that the residues necessarily provide any information about its function. Indeed, if an ultimate aim is to shed light on prehistoric hominin activities (Chapter 1, Section 1.1), we need to determine which residues will give information about tool function. Residues can have many origins apart from use (Rots et al., 2016), and could have been deposited on stone artefacts from before the time when the tool-stone was first extracted as raw rock material in prehistory until after arrival in the laboratory for analysis (Fig. 1.2**)**. Residues can also be indirectly related to stone tool use, being only incidental to the main task. For example, plant fibres can contact with stone tools while cutting meat on a palm woven mat; and pigment or fat can be transferred to tools by hominin hands involved in a previous task. Residues can also come from a common hominin activity on site. If an artefact used on wood has been laid on ground where bone processing had been undertaken, preserved bone residues on the tool are not linked to its function.

Residues can arise also from post-depositional processes, include anthropogenic modifications during surface exposure of the artefacts before burial. During this phase, water flowing over an artefact could have also deposited oxides, other minerals or plant material. Natural processes could have continued after burial depending on the geological nature of sediment layers, humidity, temperature and other conditions. micro-organisms like fungi and bacteria also contribute to the presence of organic residues. Another possible origin of residues can be the sediment layer, in which artefacts had been found, resulting from geological environment or from anthropogenic processes. From that surrounding sediment, preserved organic artefacts, like bones, present in archaeological layers could have been in contact with stone artefacts leading to bone residues on surface and edges. Others residues, such as rootlets, are commonly transferred from sediments in which artefacts were buried. Finally, modern contamination can be the source of residues found on stone tools, and derive from excavation, artefact extraction, storage and handling. These different residue origins, each perhaps deposited at a different time, can also be superposed on the same stone tool, rendering their interpretation even more complex.

It is tempting to think that highly specific residues found on stone artefacts will have a higher chance of being prehistoric in origin and a higher chance of being use-related. However, even a starch grain identified as an Indonesian plant species or a specific chemical substance (e.g., a cholesterol or camphor) does not have a higher chance of being linked with tool function, than any bone fragment with no taxonomic identification. Indeed, in the modern world, natural chemical substances are widely used in common everyday domestic products (e.g., camphor in clothes cleaning, insect repellent) and plant and animal materials are spread widely. Indeed, it is not excluded that the aforementioned rare Indonesian species of plant be from a local origin (e.g., a local botanical garden). In other words, modern spectroscopic methods (Raman, IR, GC-MS, SEM etc.) are a useful means of identifying the chemical nature of residues, but are only the first step in the complete investigation that needs to be done at the “crime scene” (the artefact surface)—including critical assessment of all the clues relevant to residue origins and artefact function. Fortunately, some contaminants can only be derived from modern chemicals (e.g., polypropylene, polyester, fibreglass, viscose) and can be removed from the list of suspects linked with tool function.

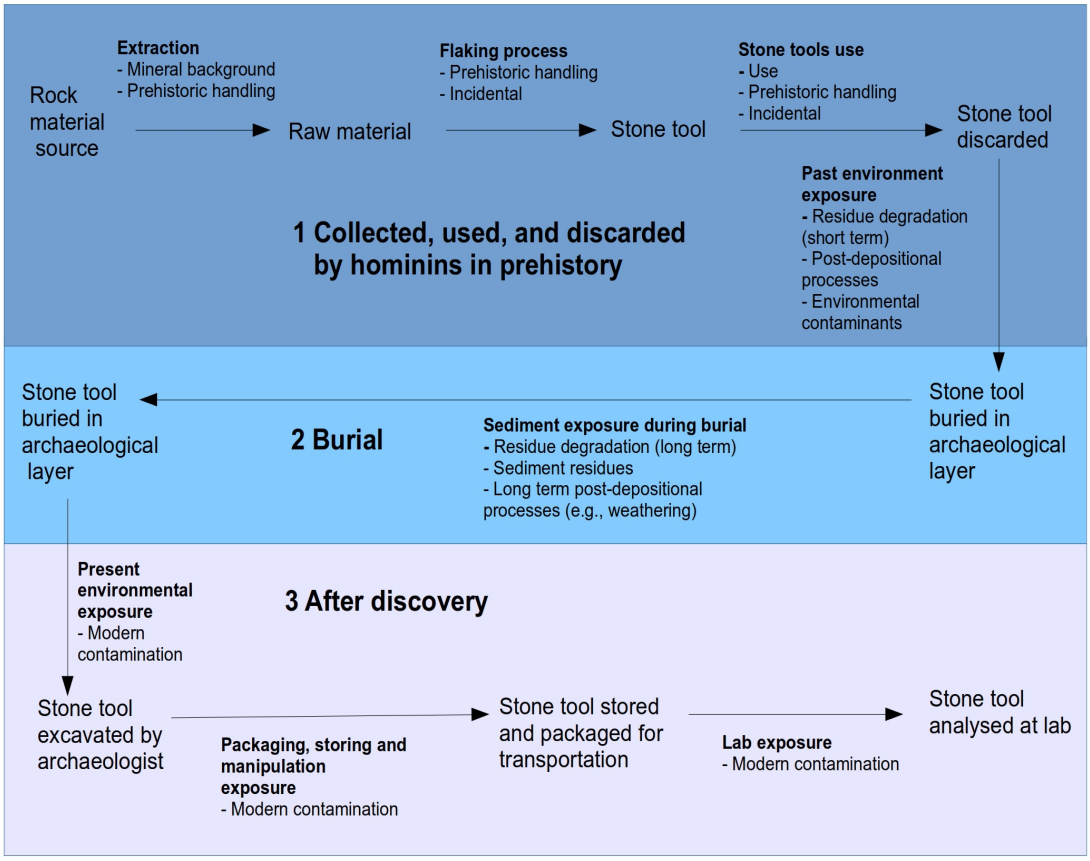

Figure 1.2: Micro-residues possible origins.

1.7 Micro-residue analysis on prehistoric artefact

In the discussion above, I mentioned macro and micro-residues on stone artefacts, yet they need to be carefully distinguished in stone tool analysis and often need to be studied with a different strategy. I define macro-residues as being larger than hundred microns, often more clearly shaped, and identifiable by VLM. For example fragments of bone, hair, feather, fish, scale and bundles of plant fibres will be considered as such. These macro-residues are those that are frequently found on fresh experimental stone tools (Pedergnana et al., 2017) and on selected prehistoric artefacts with excellent preservation. As emphasised above (Chapter 1, section 1.4), spectroscopy methods can characterise the chemical nature of these macro-residues but may be not essential to identify them as it could be done often more quickly and straightforwardly under optical microscope (VLM).

On the other hand, as emphasised in section 1.3, spectroscopic methods are increasingly useful for study of prehistoric stone artefacts that are not pre-selected for their residue preservation or morphology and which can have any preservation state and commonly have only smaller and scarcer residues. Because of their small size (less than 100 microns) and no visible distribution, these micro-residues can be only be observed with microscopes at higher magnification. Micro-residues are more difficult to interpret as use-related residues than macro-residues, being more difficult to distinguish from modern contaminants, or from residues resulting from post-depositional processes. These issues become even more critical when micro-residues share similar features to pseudomorph mineral grains (e.g., calcite) and organic particles, are amorphous, or are showing different confusing colours. Even if observer experience and the use of residue databases expand the confidence in identification, VLM is always likely to have a non negligible percentage of false identifications. This misidentification increases with smaller residues, and it is then necessary to complement VLM observations with other identification techniques. Additionally, as the number of micro-residues requiring identification increases, in order to relate them confidently to use (Chapter 3), the need for a quick and more secure identification method like Raman spectroscopy is even more critical.

1.8 Relating micro-residues to prehistoric stone tool use

After identifying micro-residues on a stone artefact, the main difficulty is to relate them to prehistoric use, and eliminate other possible origins (Chapter 1, section 1.6). To argue that micro-residues are archaeologically related to use, it is important to have, at the same time, multiple strands of evidence (Lombard et al., 2009; Langejans, 2011; Langejans et Lombard, 2014), by detecting repeatedly the same residue, and getting a clear distribution of these attached residues on the stone artefacts. Indeed, a single residue or residue type is seldom sufficient for determining the use of a stone tool, and some researchers (Wadley et al., 2007) have found by experience that archaeological residues often preserve collectively in relatively high abundance. Spatial distribution seems to be another key criteria to recognise use-related micro-residues, contamination and post-depositional micro-residues. Indeed, establishing a spatial relationship between used edges and tool surfaces resulting from use with the distribution of micro-residues seems to be the logical link between micro-traces and spectroscopic analysis. This doesn't mean that prehistoric use-related residues cannot occur outside the zone on a tool directly in contact with materials used, as emphasised by a recent experimental study working stone tools with fresh material (Xauflair et al., 2016), but I argue

that the preservation of such micro-residue distributions beyond the polished or other worn zones on a tool after thousands years is still not completely understood.

Moreover, fresh experimentations almost always generate on stone artefacts well preserved macro-residue distributions, and they cannot be confidently compared with surviving micro-residue distributions that are documented on prehistoric stone tools. Finally, only micro-residues with a clear spatial relationship with use polish and/or other forms of use-wear, linked with human action, can be demonstrated to be use-related. Other micro-residues, found in insufficient numbers and with no significant distribution linked with use polish (or micro-traces) cannot be demonstrated to be use-related, and are considered here to be incidental residues (Chapter 1, section 1.9). Confronted with the multiple aspects of elucidating micro-residues origins, one of the main directions of this present work is to develop a new methodology and select important criteria for determining use-related archaeological micro-residues, described and illustrated by examples in Chapter 3.

1.9 Micro-residues unrelated to stone tool function but linked to a prehistoric human activity or working context

If micro-residues cannot be linked with prehistoric artefact function, but cannot either be rejected as resulting from modern contamination or from natural post-depositional processes, hypotheses about incidental use or contact with a material resulting from human activities need to be considered. In this thesis, which focuses on use-related residues, incidental micro-residues resulting from past human activities, will also be included in the discussed results as they can contribute to understanding the prehistoric context of stone tools use.

1.10 Thesis outline

From what has been discussed above, we will try to define here the main directions:

1. In **Chapter 1**, I have assessed the viability of Raman spectroscopy as a robust, fast spectroscopic analysis technique described in **Chapter 2**, well adapted to common stone artefact various morphologies and their uneven surfaces. I have also discussed Raman spectroscopy as a complement to VLM use-wear and residues to be applicable to different states of artefact preservation and to macro or micro-residues (Bordes et al., 2017).

2. In **Chapter 3**, I develop a standalone strategy to efficiently filter out non use-related micro-residues and to systematically locate concentrated areas of use-related residues on tools. Raman spectroscopy is applied as an independent first step of in situ, non destructive analysis complementary to conventional analysis and compatible with other potential analytical techniques (e.g., GC-MS). My focus is on use-related micro-residues, but I also consider incidental residues arising from prehistoric activities, natural post-depositional processes and potential sources of contamination.

3. In **Chapter 4**, I document some modern materials library and experimental spectral databases, relevant for analysing artefacts from the archaeological sites. I examine materials collected around Denisova Cave in the Altai Mountains, Siberia, and around Liang Bua and similar areas in Southeast Asia.

4. In **Chapters 5 and 6**, I document results with my interpretations of hominin behaviour from stone artefact use at Denisova Cave and Liang Bua, respectively. I consider the nature of evidence for change and continuity in tool function through time. Contamination, natural post-depositional processes and residue preservation on artefacts from each site, Denisova Cave and Liang Bua, are reported and compared.

5. In **Chapter 7**, I summarise the main conclusions of this study, discuss the performance of Raman spectroscopy as a method for micro-residue analysis, and consider some potential directions for future research.

Chapter 2 Analysis techniques and methods

2.1 Raman microscopy

2.1.1 Theory

2.1.1.1 Raman effect

Monochromatic incident light interacts with any material in three different ways; namely it may be reflected, absorbed or scattered. In Raman spectroscopy (Colthup et al., 1990; Ferraro, 2002; Keresztury, 2002; Smith and Dent, 2005), we observe electromagnetic radiation scattered by vibrational units (which can be molecules, ions or parts of molecules where this interaction occurs) when they are irradiated with a monochromatic laser source. This interaction of the incident oscillating electric field (laser excitation light with amplitude E_0 and frequency υ_0) with phonons of frequency υ_m induces a dipole moment $\vec{P}$, which depends of the polarisability tensor of the vibrational unit α:

$$\vec{P} = \alpha \times \overrightarrow{E_0}(cos2\pi\upsilon_0 t)$$

α polarisability tensor terms can be individually described as functions of the normal vibration coordinates Q using a Taylor approximation:

$$\alpha_{ij} = \alpha_{ij}^0 + (\frac{\delta\alpha_{ij}}{\delta Q})_{Q=Q_0} \quad \text{i, j=x, y(or z)}$$

with the scattered electric field proportional to $\vec{P}$:

$$P_i = \sum_j \alpha_{ij} \times E_j = \overbrace{\sum_j \alpha_{ij}^0 E_{0_j} \cos(2\pi\upsilon_0 t)}^{\text{Rayleigh}} + \overbrace{\underbrace{\frac{E_{0_j} Q_0}{2}(\frac{\delta\alpha_{ij}}{\delta Q})_{Q=Q_0} \times [\cos(2\pi(\upsilon_0 - \upsilon_m)t) + \cos(2\pi(\upsilon_0 + \upsilon_m)t)]}_{\text{Stokes/Anti-Stokes}}}$$

The equation above shows that two different scattering effects can occur: one without change of frequency is Rayleigh quasi-elastic scattering ($\upsilon \sim \upsilon_0$), and the other with change in frequency is Raman inelastic scattering ($\upsilon = \upsilon_0 \pm \upsilon_m$) which occurs only if vibrations change polarisability ($\partial\alpha_{ij}/\partial Q \neq 0$). Almost all incident photons are quasi-elastic scattered at the same

energy as the incident excitation light, but only a very small part of the light (1 photon on 10 millions) is inelastically scattered and at a different energy (or wavelength) (Fig. 2.1).

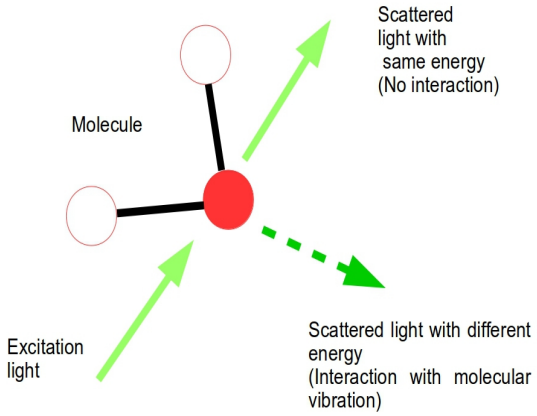

Figure 2.1: Light scattered from molecule (or vibrational unit).

In Raman scattering, a molecule (or vibrational unit) with initial energy (E_0) is excited to a virtual state (E_v) and then relaxed to a different vibrational state with higher or lower energy than the original state (E_{vib}) due to interaction with molecular vibrations (Fig. 2.2). This interaction results as a transition between two vibrational levels of a given molecule (or vibrational unit). If the initial level is an excited vibrational level, the measured vibrational energy is greater than the excitation energy, leading to anti-Stokes radiation. If the initial level is the fundamental vibrational level, the measured vibrational energy is less than the excitation energy leading to Stokes radiation. Stokes transitions are far more likely than anti-Stokes transitions because of the higher population of the fundamental vibrational level in a given molecule (or vibrational unit) at ambient temperature (Maxwell-Bolzmann law), and Stokes transitions are commonly used in Raman spectroscopy to observe molecular vibrations (Fig. 2.2).

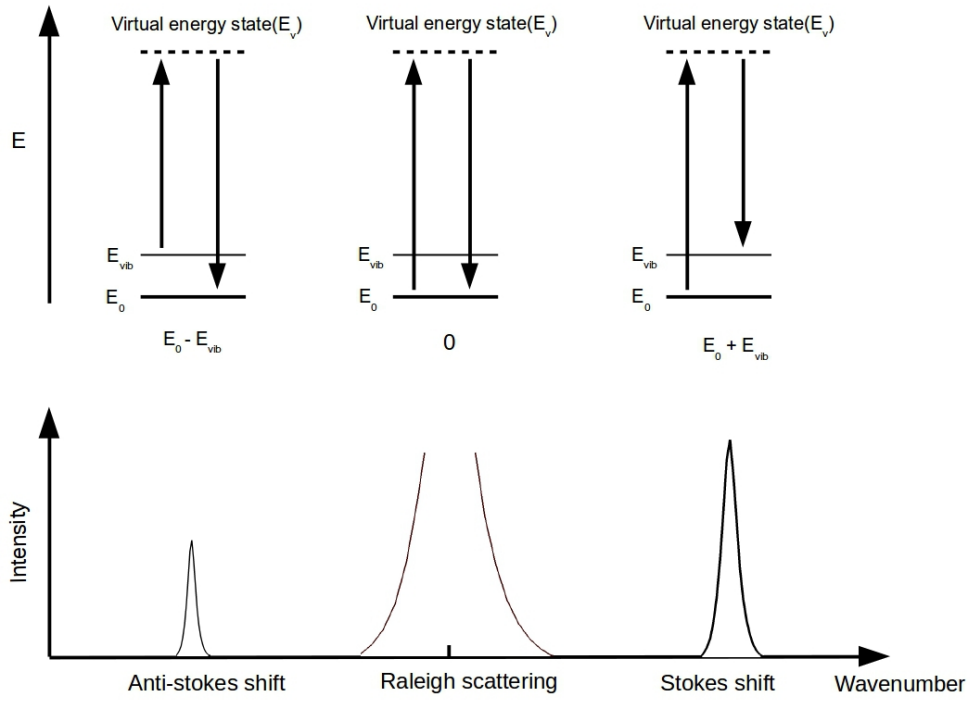

Figure 2.2: Two types of radiation arising from the light scattering process: Stokes radiation and anti-Stokes radiation.

Because Raman spectroscopy measures the difference between the incident and scattered light, the positions of the vibrational bands are not dependent on the wavelength of laser excitation. This relative difference between monochromatic incoming photon energy (laser) and scattered photon energy is called “Raman shift”, and expressed in wavenumber units (cm^{-1}) (Fig. 2.3, B). Two processes other than normal Raman scattering can take place as a result of excitation by the laser; namely the resonance Raman effect and fluorescence (Fig. 2.3, A) as described in the following sections.

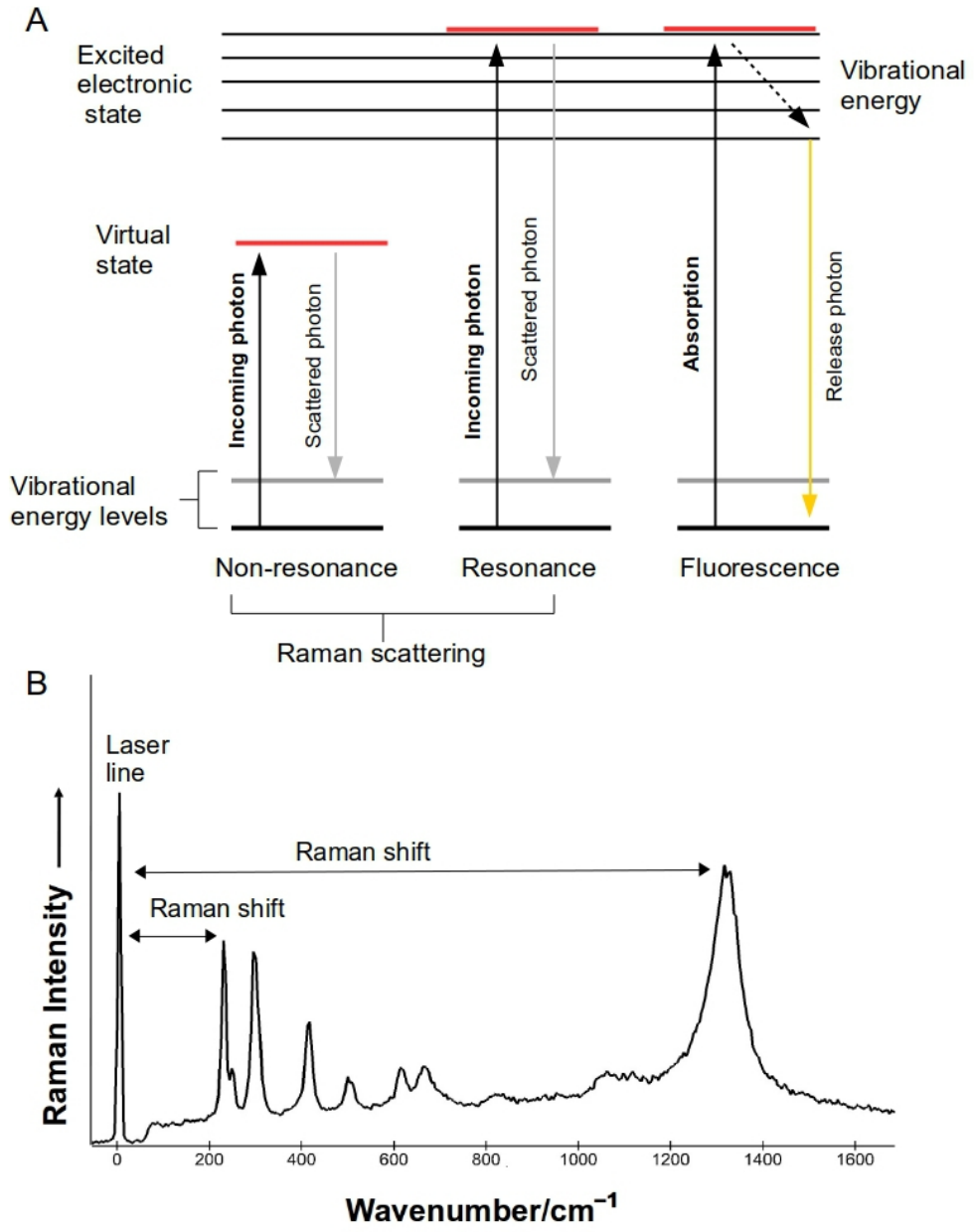

Raman shift = Incoming photon energy - Scattered photon energy

Figure 2.3: Normal, resonance Raman conditions in competition with fluorescence effect (A), example of molecular vibrational spectral fingerprint composed of a set of vibrational bands, each shifted from laser line by a specific "Raman shift" expressed in wavenumber units (cm^{-1}) on the X axis and Raman Intensity on the Y axis (B).

2.1.1.2 Resonance Raman spectroscopy

An important phenomenon in Raman spectroscopy is the resonance effect, which is of particular importance for coloured molecules (organic pigments) (Spiro, 1987; Keresztury, 2002; Adar, 2013). Raman scattering can be obtained by using any monochromatic light excitation leading to a transition from the fundamental vibrational level to a virtual energy level before de-excitation back to a vibrational mode of lower energy (Fig. 2.3, A) . In normal Raman conditions or out of resonance conditions, the molecule (or vibrational unit) absorbing electronic energy from the ground electronic state to an excited electronic state is very different from this virtual energy level. However, in resonance conditions, when the molecule absorbs light with an energy level close to that of the incoming photon energy (Fig. 2.3, A), the transition probability toward this virtual energy level will be greatly increased by coupling with the electronic transition corresponding to the molecule light absorption. This increases greatly the transition probability, in creating a resonance effect which will lead to intensity enhancement of Raman scattering by 10^3 to 10^4 times, hence leading to a considerable intensity increase of Raman bands.

Furthermore, in resonance conditions, mainly vibrational transitions in the molecule corresponding to molecular vibration modes affecting the specific part of the molecule absorbing the incident light will be enhanced. This light absorbing part of the molecule (pigment), usually includes at least one double bond conjugated system. As a result, using different incident laser light wavelengths (green laser emitting at 532 nm or red laser emitting at 785 nm) to excite the same organic pigment will lead to different resonance conditions, concerning different molecular vibrational modes, which will be enhanced differently, depending on the excitation wavelength.

2.1.1.3 Fluorescence

Fluorescence (Lakowicz, 1999; Sauer et al., 2011; Valeur and Berberan-Santos, 2012) arises from the de-excitation of absorbed light from a broad range of vibrational levels belonging to excited electronic states. This effect results in the appearance of very broad spectral bands which compete in intensity with Raman scattered bands. When fluorescence is strong, the Raman signal could be completely hidden in fluorescence background noise, which is a limiting factor for coloured materials absorbing light in visible wavelength range. Origins of this fluorescence can arise from the scattering molecules themselves, or from small amounts of

mineral impurities or organic matter.

However, in some cases, it could be interesting to take advantage of some specific narrow fluorescence bands arising from a particular material, as any Raman instrument can be used as a fluorescent spectrometer in using laser induced fluorescence (LIF) (Solarz and Paisner, 1986; Kaye et al., 2015). As fluorescence is a light re-emitting effect, which has far higher quantum yield than Raman scattering effect, low concentrated material can be easily detected in LIF mode. One example of the application of LIF in this work is the neodymium rare earth element substituted in bone apatite present on Liang Bua stone artefacts. The neodymium substitution leads to laser induced fluorescence, which was used in this study to decrease bone mapping times and improve spatial resolution (Chapter 6, section 6.3.2.4).

2.1.1.4 Molecular vibrational modes in Raman scattering: Example of hydroxyl apatite

The incident photons will thus interact with a molecule (or vibrational unit), and the amount of energy change (either lost or gained) by a photon is characteristic of the nature of each bond (vibrational mode) present. Not all vibrational modes will be observable with Raman spectroscopy (depending upon the symmetry of the molecule (or vibrational unit) but sufficient information is usually present to enable a very precise characterisation of the molecular structure.

For example, bone is a matrix of organic matter supported on a mineral scaffold. Bone mineral (biological apatite) is mainly composed of carbonated hydroxylapatite expressed by the general formula $Ca_5(PO_4,CO_3)_3OH$. The Raman spectrum of bone is dominated by vibrations originating from the phosphate anion formed from one phosphorus atom bound to four oxygen atoms in a tetrahedral arrangement (Fig. 2.4).

Bone apatite is mainly composed of hydroxylapatite expressed by the general formula $Ca_5(PO_4)_3(F,OH,Cl)$ as structure can be occupied not only by OH^-, but also by the substituting ions F^- and /or Cl^- (Wopenka et al., 2005). In addition, apatite can incorporate numerous ions and; anionic complexes (such as AsO_4^{3-} , SO_4^{2-} , CO_3^{2-}, SiO_4^{4-}) can replace PO_4^{3-}; and a large number of metal cations (such as K^+, Na^+, Mn^{2+}, Ni^{2+}, Cu^{2+}, Co^{2+}, Zn^{2+}, Sr^{2+}, Ba^{2+}, Pb^{2+}, Cd^{2+}, Y^{3+}) and trivalent ions of rare-earth elements can substitute for Ca^{2+} (Wopenka et al., 2005).

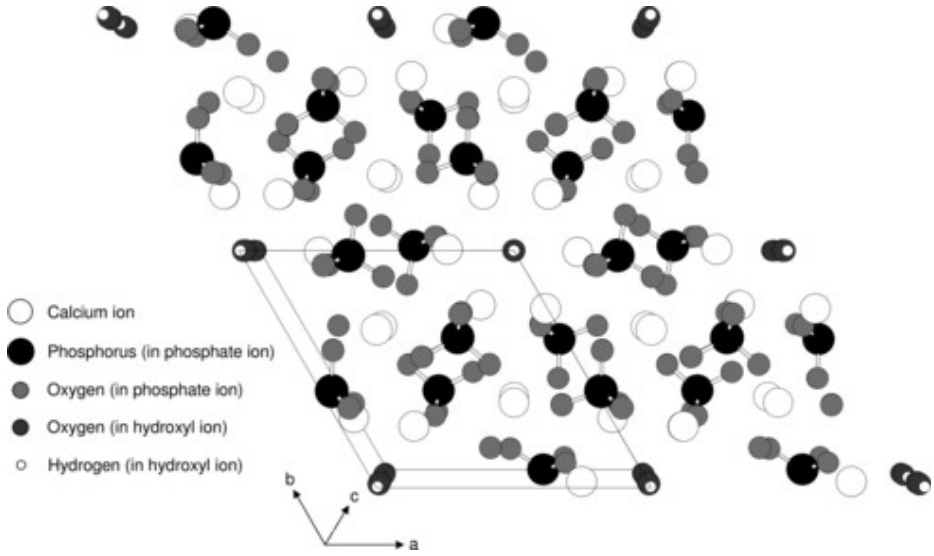

Figure 2.4: Crystal lattice structure of calcium hydroxy-apatite (HAP) and the HAP unit cell (Beckett et al., 2011).

The spectrum of the isolated tetrahedral PO_4^{3-} anion with T_d symmetry consist of four Raman active vibrational modes (Fig. 2.5). $\nu 1$ (A_1) corresponding to the symmetric stretching vibrational mode of PO_4^{3-} anion located at 963 cm^{-1} (Fig. 2.5, A, E). The doubly degenerate bending mode $\nu 2$ (E) is centred at 434 cm^{-1} (Fig. 2.5, C, E), the triply degenerate bending mode $\nu 4$ (F_2) at 593 cm^{-1} and the triply degenerate anti-symmetric $\nu 3$ stretching mode at 1017 cm^{-1} (F_2) (Fig. 2.5, B, D, E) (Elliot, 1994; Pye et al., 2003; Antonakos et al., 2007). This last mode is weak in intensity and not seen on the Raman spectrum given in the example here (Fig. 2.5).

Carbonate ions are also present in the bone apatite structure. The isolated CO_3^{2-} geometry ion is planar with three equal symmetrically arranged C–O bonds and have D_{3h} point-group symmetry. Among the six possible vibrational modes, only one is Raman active namely the symmetric $\nu 1(A'_1)$ stretching mode, theoretically centred around 1063 cm^{-1} (Elliot, 1994; Antonakos et al., 2007), which is upshifted to 1076 cm^{-1} for our bone apatite example (Fig. 2.5) when distorted carbonate anions are in the crystal lattice and its symmetry lowered to C_{2v}. Carbonate ions can substitute in the apatite structure either in the OH-site (“A-type” substitution) or in the PO_4 site (“B-type” substitution) (Wopenka et al., 2005).

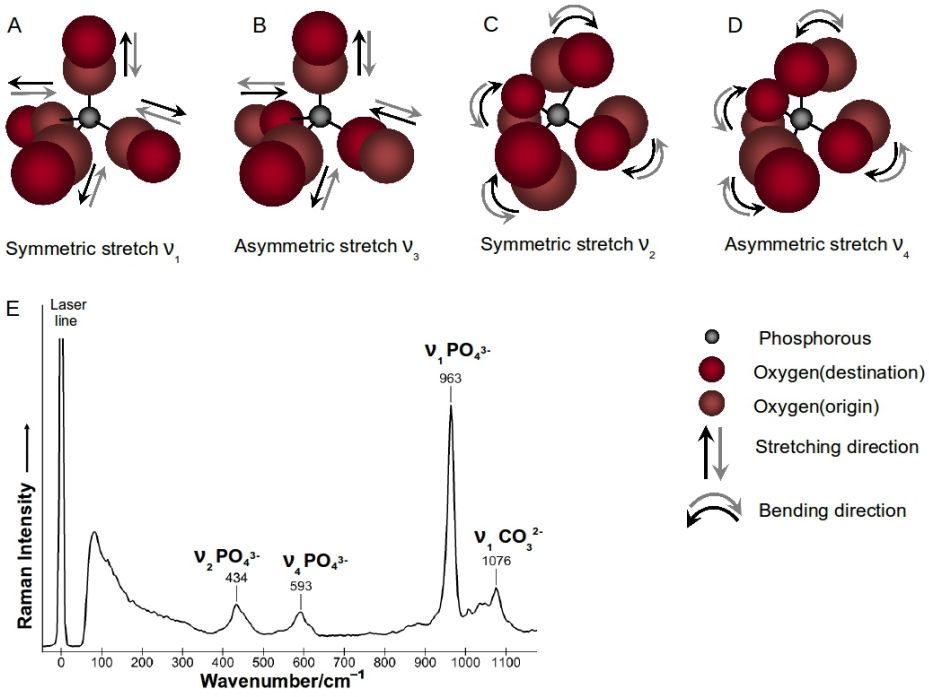

Figure 2.5: Different vibrational modes for PO_4^{3-} anion in bone apatite (Smith and Dent, 2005) and attribution on Raman spectrum.

Reduction of the PO_4^{3-} anion symmetry from T_d to C_s symmetry in an apatite crystal lattice results in a splitting of the F_2 to the 2 A_1 and A_2 modes that appear at lower shifted energies in the Raman spectrum of phosphates (Elliot, 1994; Antonakos et al., 2007). However, in well crystallised bone apatite, crystallites are not randomly oriented and the effect of preferred orientation on PO_4^{3-} anion modes frequency can be observed on appearance of fine structure PO_4^{3-} anion modes (Elliot, 1994; Antonakos et al., 2007). For v_1 CO_3^{2-} mode, three bands centred at 1034, 1050, and 1076 cm^{-1} are visible, two bands centred at 434, and 448 cm^{-1} for $v2$ PO_4^{3-} anion mode, and 2 bands at 593 and 613 cm^{-1} for PO_4^{3-} anion $v4$ mode (Fig. 2.6).

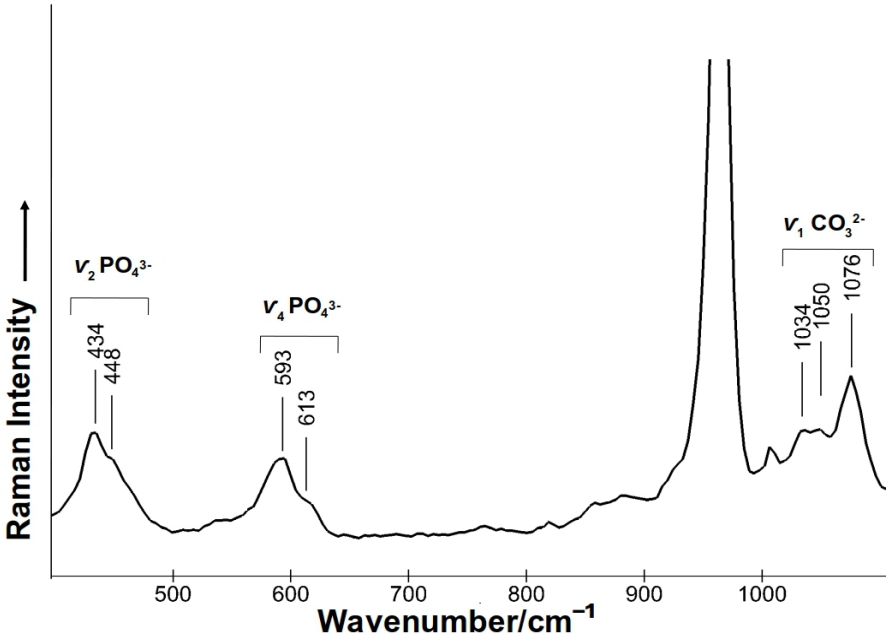

Figure 2.6: Details of additional vibrational modes of CO_3^{2-} and PO_4^{3-} anion modes in bone apatite due to crystallite orientation.

Moreover, the main PO_4^{3-} *v*1 stretching vibrational band is useful to probe the short range atomic disorder of apatite structure. This disorder can arise from either ionic substitutions or from crystallite size and provoke broadening of FWHM (Full Width at Half Maximum) and shifting of *v*1 band (Wopenka et al., 2005). With respect to *v*1 broadening, the same authors found that synthetic apatite has a narrower *v*1 band than geological apatite, which has a narrower band than bone and dentine apatite. Furthermore *v*1 mode FWHM can be used to probe bone crystallinity and detect diagenetically altered bone (Dal Sasso et al., 2018).

The main *v*1 vibrational band position is typically centred at 962 cm^{-1} for synthetic hydroxyapatite but can vary from 960 to 967 cm^{-1} for different bone/dentine hydroxyapatite and geological apatite (Thomas et al., 2007; Thomas et al., 2011). Ionic substitution influence the frequency of this phosphate band (Freeman et al., 2001; Thomas et al., 2007; Thomas et al., 2011) as fluoride in synthetic apatite structure (fluorapatite) can upshift the *v*1 mode to 964 cm^{-1}, but other ions like Sr^{2+}, Ba^{2+} and Mn^{2+} can downshift it to 947 cm^{-1}, with increasing concentration (Thomas et al., 2007; Thomas et al., 2011). Carbonated apatite is reported with upshifted values between 964 and 967 cm^{-1} (Antonakos et al., 2007). In animal fresh bone, *v*1 band has been reported with values downshifted to 958-959 cm^{-1} (Sauer et al., 1994; Konstantinos et al., 2012). Finally heated apatite having carbon present in its structure has been reported with *v*1 continuously downshifted to 943 cm^{-1} (Puceat et al., 2004).

2.1.2 Raman instrument

All Raman spectra were recorded with a WITec® alpha 300R confocal Raman microscope (WITec® Instrument Corp., Germany) equipped with two UHTS300 spectrometers and two CCD detectors: a visible DV401 detector for use with 532 nm excitation and second DV401 detector for 785 nm excitation (Fig. 2.7, A-B). The excitation sources were two diode lasers operated at 532 nm and 785 nm wavelengths with 38 mW and 120 mW maximum power output respectively (Fig. 2.7, 01). Used samples excitation laser power under microscope objectives were ranging from these values down to few milliwatts depending of the position of the attenuation scew at the exit of both laser diodes. Zeiss® microscope objectives (20X and 50X magnifications) were used (Fig. 2.7, 03), achieving for the X50 objective (0.8 of numeric aperture) a sub-micron spatial resolution in XY plane and under three microns resolution in Z axis (Fig. 2.8) The samples were placed on a piezo-driven, feedback-controlled scanning stage (Fig. 2.7, 04).

The Raman microscope can operate as an optical microscope with white illumination (Fig. 2.7, 09) or in Raman analysing mode by switching mirror/beam splitters directing light from the sample either toward the video camera or toward a monochromator. Each laser source is coupled to a single mode fibre (Fig. 2.7, 02), which guides the laser light toward the microscope. Each laser source can be selected by a moving mirror before its holographic beamsplitter (Fig. 2.7, 05), which reflects laser light toward the sample. A piezo-driven objective (Fig. 2.7, 03) focuses either lamp light or the laser beam on the sample, and its Z position can be moved to adjust the focus on the sample surface. In Raman mode, back scattered light is collected by the same objective through a holographic beam splitter, and the laser frequency is filtered by a notch filter (Fig. 2.7, 05). Then, scattered light is directed by a multi-mode optic fibre (Fig. 2.7, 06) toward the selected monochromator: (1) for red excitation (785 nm) equipped with 600 gr/mm and 1200 gr/mm grating, or (2) a second identical monochromator for green excitation (532 nm) equipped with 600 gr/mm and 1800 gr/mm grating (Fig. 2.7, 07). Finally scattered photons are counted by a Peltier effect cooled CCD detector (Fig. 2.7, 08), mounted on each monochromator. The Raman system is controlled by the WItec® software.

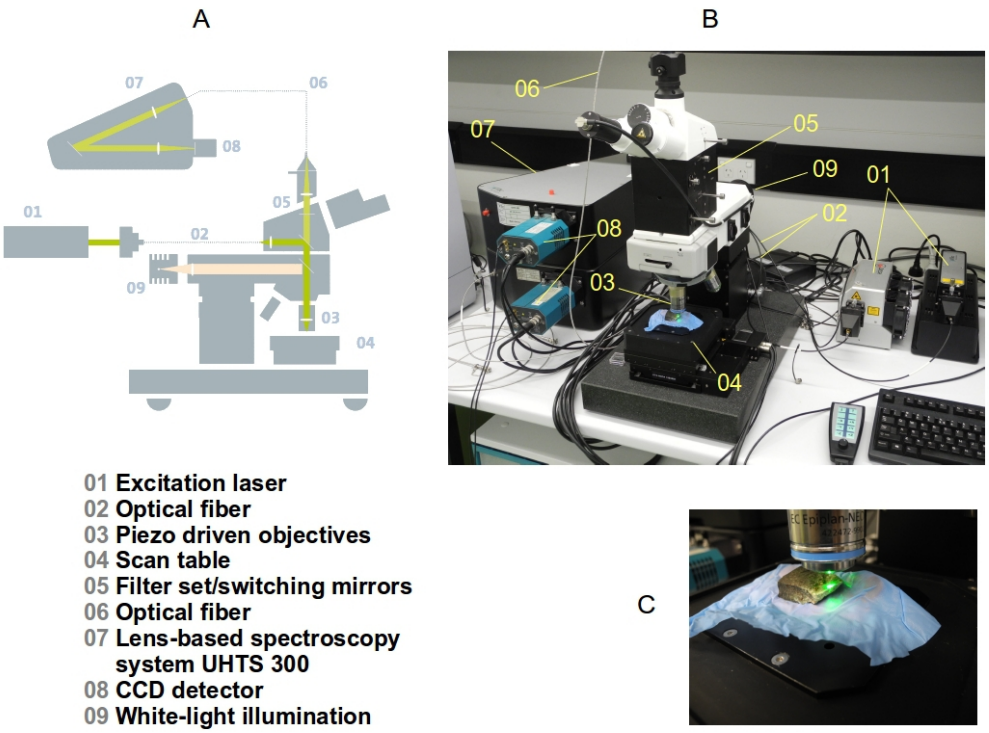

Figure 2.7: Scheme of Raman microscope (Villa Montero, 2014) (A), photo of WItec® Raman microscope (Luc Bordes) (B), photo of detail of a stone artefact set on Blu-Tack® support covered by a nitrile glove cut patch under microscope objective during measurement (Luc Bordes) (C).

2.1.3 Applying Raman confocal microscopy to micro-residue analysis

Each stone artefact selected from the 2004 Liang Bua excavation (Chapter 6, section 6.2) was initially analysed in three steps:

1. An initial analysis before cleaning, followed by
2. A systematic micro-residue observation and analysis after a 5 s ultrasonication, followed by
3. A final analysis after a further 15 min ultrasonication.

To reduce analysing time, artefacts from the Denisova excavation (Chapter 5) and 2015 Liang Bua excavation (Chapter 6) were analysed in two steps:

1. An initial analysis before cleaning, followed by

2. Systematic micro-residue observations and analysis after a 10 s ultrasonication.

Because of the difficulty in systematically analysing unwashed stone artefacts partially or totally obscured by adhering sediment, the procedure for Raman analysis of artefacts from the 2016 Liang Bua excavation (Chapter 6) was made more efficient, with only one step of systematic micro-residue observation and analysis after a 10 s ultrasonication.

Washed sediment samples were also analysed after drying. For study of washed sediments, Petri drying dishes (Chapter 2, section 2.4) were directly placed under the microscope for analysis. Other sediment samples were placed on glass microscope slides for analyses. For in situ study of stone artefacts, all edges were investigated systematically along a strip, approximately 200 µ from the edge. Polished edges were regularly examined for smeared micro-residues (Chapter 3, section 3.5), even when no other traces were visible on the surface. Probing rate was adapted to micro-residue concentration. When a concentration of micro-residues was found, the inland surface beyond the 200 µ standard analysing strip, was often checked to investigate the residue's spatial distribution. Because of time limitations, the surface away from the edge was not studied in detail, with the focus on particular points of interests and additional spots selected in a random manner.

When extended areas were encountered with strong coloured mineral pigments (e.g., haematite, goethite, manganese oxide), Dstretch® software was very useful to illustrate spatial distribution on the entire side of an artefact; and Raman spectroscopy was only needed to control their identification at several spots. DStretch® is a program that employs a decorrelation stretch algorithm to enhance images by increasing hue and contrast and by rendering these in artificial colours (Harman, 2008; Rifkin et al., 2015). This program is applying a Karhunen-Loeve transform to the colors of the image which diagonalises the covariance matrix of the colours. The contrast for each colour is then stretched to equalise the colour variances. Next the colours are uncorrelated and fill the colorspace. Finally, the inverse transform is used to map the colours back to an approximation of the original. Dstretch® colour spaces used for this work are 'LAB' (Chapter 6, artefact LAB5580a, LB5524, LB5225) and 'YWE' (Chapter 6, artefacts LB5213 and LB5126). Coloured area showed by Dstretch® were randomly probed with Raman microscopy on the surface of the artefacts relatively to other area to confirm that the concentrations of pigment (mainly haematite and goethite) were real.

Spectral Raman mapping was limited to small targeted areas on the artefact because of

uneven surfaces and frequent fluorescence, which had to be quenched, before spectra could be obtained. Generally, the green 532 nm laser line was used as the excitation source for both mineral and organic micro-residues, as a better signal-to-noise ratio was obtained than for 785 nm excitation. Furthermore, the risk of burning micro-residues was less for green excitation than for red excitation, and a larger spectral range (0 - 3500 cm^{-1}) could be covered in one spectral window. Consequently, the red laser was only used when the fluorescence was too high, as, for example, with some particular plant fibres. Care was taken to increase the laser power progressively for each spot probed, in order to collect the spectra below the threshold of damage due to laser heating. In some instances, unavoidable over-heating helped to distinguish between organic and inorganic micro-residues.

In analysing micro-residues, the high spatial resolution of Raman confocal microscopy was very useful to analyse small targeted volumes at the surface of stone artefacts. With a X50 objective, the Raman instrument used is capable of achieving one micron surface and three microns depth spatial resolution. Indeed, micro-residues can be located in holes, cracks or half masked by residual sediment; and fluorescence can arise from the rock surface or from organic material around the targeted spot. Consequently, positioning the analysing volume with accuracy is critical to get reliable spectral data and optimise their signal-to-noise ratio (Fig. 2.8**)**. The confocal attributes of the Raman system are extremely useful in rejecting scattered light from material located outside the analysed volume, targeting particular parts of a residue (e.g., intact tissue or the tip of a fibre). This micro-residue targeting needs also to follow very uneven surfaces, while changing constantly the microscope focus, light illumination, and tuning of the laser power for each micro-residue heat sensitivity and damage threshold. Moreover, some fluorescent micro-residues (e.g., some plant materials including resin) require switching to red laser excitation. This adaptation of the Raman analysis to optimise each spot of analysis and constantly change of focus over an uneven surface explains why no automation of the system can be applied to a whole stone artefact and why the analysing process needs to be done spot by spot, with manual control.

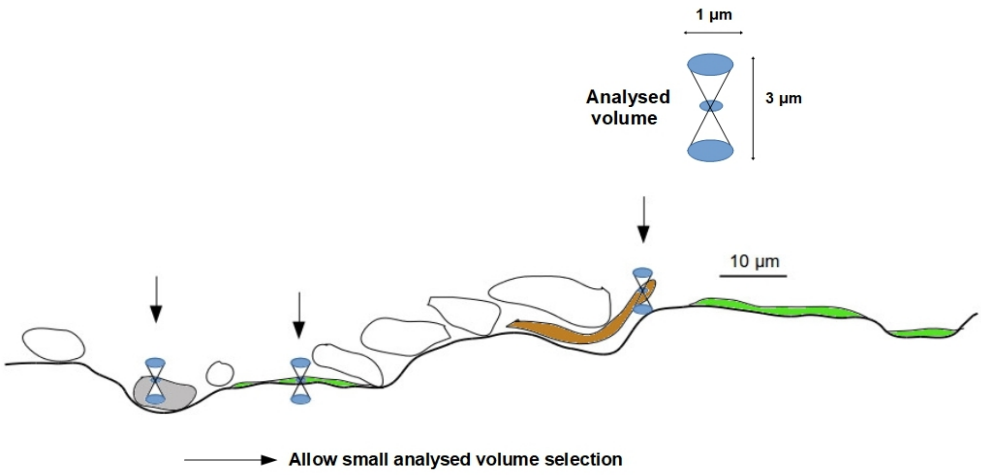

Figure 2.8: Usefulness of high spatial selection in Raman confocal microscopy to target a variety of micro-residues attached or loose on the surface.

2.2 Optical microscopy

Optical microscopes included an Olympus stereozoom SZ61 with external fibre optic light source, and an Olympus BX51 metallographic microscope with vertical incident illumination and 5x, 10x, 20x and 50x objectives. The main aims of my use-wear study were to establish the distribution and intensity of use-polish (including abrasive smoothing, alignments and striations), and to locate, in some cases, other forms of use-wear (e.g., scarring, edge rounding, and striations). It was not my intention to achieve a detailed use-wear analysis to identify function and worked material based on use-wear. Some researchers have attempted quantification of surface reflectivity to evaluate polish intensity (Keeley, 1980; Dumont, 1982). Anderson experimented optical interferometry to characterise use-wear on plant working tools (Anderson et al., 2006). Surface roughness had been recorded with laser profilometry (Stemp and Stemp, 2001; Stemp and Stemp, 2003) and laser scanning confocal microscopy quantitative surface mapping have been applied on stone tools use-wear (Evans et al., 2008).

However, for my study, due to time limitation, the use-wear analysis was simplified, and I retained only four types of polish intensity, visible at low and high magnification: not polished, discontinuously polished, continuously polished, and highly polished (Fig. 2.9). Discontinuous polish refers to an edge or surface area that does not show continuous polish but rather has discontinuous patches of adjacent polished edges and areas that are not clearly linked (Fig. 2.9, A). Continuous polish refers to use-wear that shows clearly continuous polish over edges

and surfaces that are easy to follow (Fig. 2.9, B). High polish refers to edges and areas with very high reflective gloss, often visible macroscopically (Fig. 2.9, C). These observations of polish are subjective and are not intended to provide a quantitative or absolute scale measurement of use-polish, but rather to give an idea of relative intensity. The symmetry and extent of polish along edges to the adjacent inland surfaces were also documented because they are indicators of contact zones and the angle at which the tool was held during any task. Symmetry and extent of polish potentially provide important criteria for distinguishing scraping and cutting actions. Gradient of the polish from the edge to the inland surface is also potentially important for assessing the difference between use polish and a natural alteration that mimics use-polish. When a completely homogeneous reflective surface is widespread on the entire side of an artefact, in the absence of any other surface use-wear (e.g., striations, directionality and alignments), it is interpreted as a surface alteration or 'natural polish'. Additionally, some use-wear forms, such as striations, were only observed systematically in later stages of this study, particularly on stone artefacts from the 2016 collection from Sector XXVI.

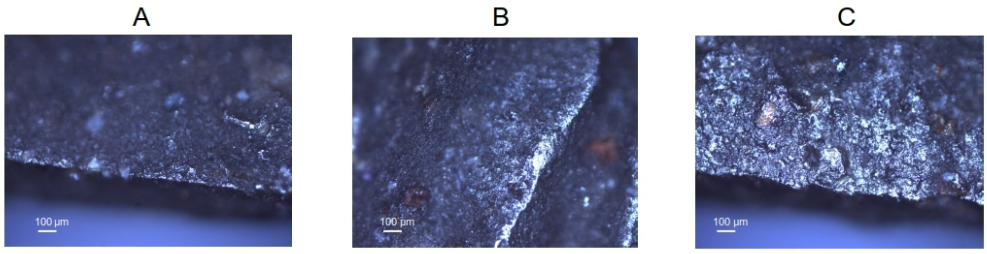

Figure 2.9: Images showing examples of three types of polish intensity distinguished on same artefact LB5563c: Discontinuous polish (A), continuous polish (B), high polish with inland extension (C).

Artefacts have been oriented in figures to best show the surfaces with micro-traces, and have shown the approximate location of the flaking platform (proximal end) and labels (right and left) for the margins or edges. For central dorsal ridges (which sometimes have traces of use), they are referred to right or left dorsal sides, meaning the side towards the right or left flake margins, respectively.

2.3 Handling samples

In order to avoid contamination (including from human contact), the artefacts were handled

with nitrile gloves (latex, powder and protein free). For each change of artefact, nitrile gloves were changed to avoid transferring contamination between different samples. Gloves were changed systematically when any other objects were manipulated. The artefacts were placed on a stable support fashioned by Blu-Tack® (a synthetic rubber compound) to accommodate the shape of each artefact. This enabled the positioning of each sample under the Raman microscope with the incident light (laser) normal to the point of analysis. The support was covered with a piece of nitrile glove to prevent contamination from the Blu-Tack® (Fig. 2.7, C**)**. Basic precautions such as storing the samples in clean bags and boxes were taken before and after each analysis. Sediment samples were placed on slides, and were directly analysed under the Raman microscope. During analysis standby, artefacts where covered by a clean nitrile glove to prevent additional airborne contamination.

2.4 Extraction from pedestal, sampling sediment and washing artefact

When samples were available with their attached sediment block (i.e., for both the 2016 and 2015 collections), the following procedure was applied (Fig. 2.10):

1. The pedestal (artefact on sediment block) was photographed prior to and after artefact extraction, to document the orientation of upper and lower artefact surfaces and the overlying/underlying sediment (Fig. 2.10, B). During transportation, some pedestals were fragmented with artefacts loose in the sediment, and it was not possible to observe artefact orientation.

2. The artefact was gently removed from the pedestal (Fig. 2.10, C), and the inner sediment (directly attached to the stone artefact) was extracted by gravity or small strokes and stored in a clean centrifuge tube.

3. The artefact was then placed into a beaker and submerged in Millipore® water. The beaker was placed in an ultrasonic bath for ten seconds (Fig. 2.10, D).

4. The ultrasonicated (washed) artefact was placed stored in a clean plastic bag or box with a lateral opening to allow the sample to dry, but protecting it from airborne contamination from above.

5. Part of the washed sediment with water was poured into a Petri dish or box and

evaporated in the oven at 60 ºC overnight (Fig. 2.10, E). Another part was secured in a plastic tube and stored in a refrigerator for future analysis.

6. Finally, a sample of the outer sediment was then extracted from the sediment block and stored in a clean centrifuge tube (Fig. 2.10, F).

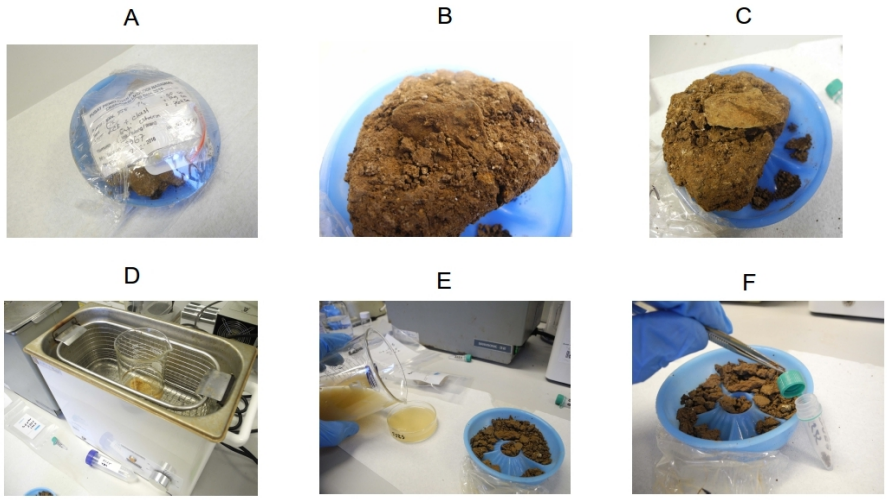

Figure 2.10: Stone artefact in pedestal, packaged (A); Stone artefact in pedestal (B); Stone artefact extracted from pedestal (C); Stone artefact in beaker in ultrasonic bath (D); Pouring washed sediment solution in Petri dish/box (E); Sampling outer sediment in pedestal (F).

2.5 Scanning electron microscopy (SEM) and energy dispersive spectroscopy (EDS) probe

A scanning electronic microscope (SEM) and energy dispersive spectroscopy (EDS) probe study complemented the Raman spectroscopy by determining elemental analysis of selected micro-residues. Uncoated samples were analysed using a bench-top Phenom XL SEM with a CeB_6 source and a built-in EDS, housed at the School of Earth, Atmospheric and Life Sciences , University of Wollongong. Back-scattered electron (BSE) images/secondary electron (SE) images were collected at 5/10 kV at low vacuum (60 Pa) and medium vacuum (10 Pa). Semi-quantitative EDS spot analyses/line analyses/maps were collected at 10 kV at medium vacuum using a larger spot size. These data were processed using Phenom ProSuite elemental identification software. Recent advances in this new generation of SEM instruments allow fast focusing. However, focusing time on uncoated environment samples still takes a few minutes and prevented me from systematically analysing a high number of micro-residues—unlike Raman spectroscopy where focusing time is counted in seconds. Furthermore, the

depth and spatial resolution (typically 2-5 microns depth) of SEM-EDS analysis depends on the excitation electron beam energy and the element to be detected in a given material. Therefore, controlling the analysis volume for very finely smeared micro-residues, closely attached to the artefact surface proved to be more problematic than with a confocal system (for which in depth spatial resolution is constant).

2.6 Summary

A key aim of this study was to investigate the potential of Raman microscopy to contribute to functional analysis of stone tools. Consequently, the main instrument used in this study was a Raman microscope. Optical microscopes provided complementary data on artefact manufacture, use-wear and visible residues. The SEM provided specific information about the elemental composition of particular residues.

Chapter 3 Developing a method to discriminate micro-residues attached to prehistoric stone artefacts

3.1 A methodology to discriminate use-related micro-residues

To reliably analyse micro-residues on prehistoric artefacts with optimal results, Raman spectroscopy needs to be applied as an independent technique, and should not focus on residues previously recognised either with naked eye observation or with visible light microscopy. In this approach, with conventional use-wear study occurring after Raman micro-residue analysis, no residues that were previously classified as use-related, are targeted preferentially. As seen in Chapter 1, the advantage of first screening micro-residues using Raman spectroscopy, is to prevent the Raman results from being influenced by the results of other methods, such as conventional use-wear and VLM residue analyses. Thus, the correlation between results from both methods can be independent and thus more objective. However, in this approach, relating micro-residues found on stone artefacts to prehistoric stone tool use poses a difficulty for the Raman analyst, who requires a new methodology for evaluating residues origins.

In this study, I developed a such methodology to discriminate use-related micro-residues from other residues that could arise from modern contamination, post-depositional processes or incidental use. To achieve this discrimination, I applied the experience gained in rejecting micro-residues that were not securely related to stone tool use, and progressively built a list of important criteria to consider for an optimal micro-residue filtering strategy. Any residue needs to meet the requirements for all these criteria to be considered potentially as use-related (i.e., linked with prehistoric use). Applying each of these criteria (Fig. 3.1) to a given micro-residue can be time consuming, so filtering steps were arranged in a way to reduce analysis time. For example, it is not necessary to check for the origin of a given micro-residue in sediment, if its Raman spectral fingerprint matches a known lab contaminant. Similarly, it would be inefficient to spend time mapping a complete distribution of a micro-residue that is present on all samples and has a high probability of arising from post-depositional processes.

The criteria (Fig. 3.1**)** are hierarchical and the scheme recognises the identification of known modern contaminants as an unavoidable first step, simply to avoid spending days repeating analyses of obvious pen ink, modern dyed fibres or epoxy resin (Appendix I, table 3**)**. Taking into account spatial distribution (as an isolated or collective occurrence), is the logical second step, as modern contaminants have a high probability of isolated occurrence on artefact surfaces. In contrast, when one type of micro-residue is widespread over all surfaces of a stone artefact, and cannot be related to use, it is possibly related to a natural process that

took place over time. The third step is to check if a given micro-residue systematically occurs on the same side of an artefact (e.g., always on the surface that is first exposed during excavation). Checking whether the origin of any micro-residue found on one archaeological artefact is also found in the layer sediment and attached sediment is another important step. Considering recurrence of the same micro-residues on a whole set of studied artefacts is also a key criteria in this filtering strategy. Indeed, the probability of having *exactly* the same traces of use, (exactly the same set of residues, occurrence and spatial distribution) on several artefacts in a random sample of artefacts even from the same layer is very low. Correlation with polish distribution is the final step, which checks how one given micro-residue is related to areas where pressure was applied (and where polish is most developed) during the use of a stone tool. This final step is time consuming, as residue distributions need to be established and correlated, but is not necessary for micro-residues that are rejected in earlier steps.

It's important to keep in mind that even if a type of micro-residue cannot be related directly to use of the stone tool, it could still originate from a prehistoric activity, incidental to the use of the tool or be the result of a post-depositional process in the past; and does not need to be automatically considered as modern contamination.

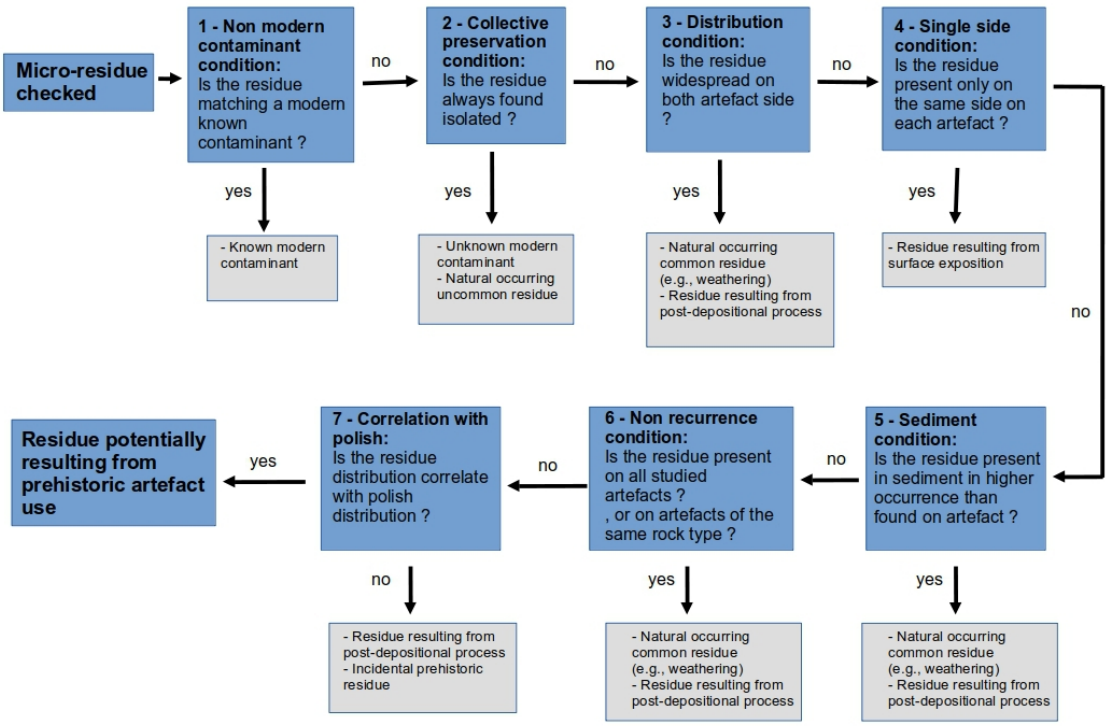

Figure 3.1: Sequence of steps to determine whether residues result from prehistoric use.

3.2 Discrimination of modern contaminants

Each time an unknown Raman spectral fingerprint was encountered on a stone artefact, it was compared to spectra in a database of modern contaminants (Appendix I, table 3). If the spectral fingerprint is easily recognised as originating only from a modern source (e.g., epoxy resin, fibre, glass), it is rejected as related to tool use. If it is identified as a natural compound (e.g., plant fibre, starch grain), it could be a modern contaminant, related to tool use or unrelated to tool use. In this case, the spatial distribution of the residue has to be taken into account before it can be considered as potentially use-related. Sometimes an unknown modern contaminant can be recognised without exact identification because it is associated with a well-known modern contaminant (e.g., see plant fibre and aromatic resin on artefact LB5526b, Chapter 6, section 6.3.2.1). Determining associated contaminants can save investigation time compared with matching their spectral signature to a specific material, which can be a very time consuming process, given the high number of modern material candidates.

The range of modern contaminants encountered during this study suggests six main sources responsible for their transfer to artefact surfaces:

- Contamination during excavation of the stone artefact

- Contamination from sample packaging

- Contamination from contact with instruments and other objects or materials during analysis stages

- Contamination from handling

- Airborne contamination

- Contamination by water used for cleaning

3.2.1 Contamination during the excavation of stone artefacts on site

At archaeological sites, specific contamination can arise during excavation of the stone artefact itself, from contact with tools or from contact with the excavators' bodies or clothes. Once the stone artefact is unearthed, it is also in contact with possible airborne contaminants. Modern dyed fibres were identified in the attached sediment or surfaces of unwashed artefacts. As Raman spectroscopy is well suited to analyse coloured material, such as organic pigments and modern dyed fibres arising from modern clothes worn by people working on the archaeological site can easily be identified. For example, on a studied artefact from Denisova Cave, it has been found a modern dyed fibre which could have been identified with archaeologist gloves used to hold them during sampling on site (Indeed the fibre from these gloves had been carefully sampled to check the eventuality of such contamination, and analysed as a reference (Fig. 3.2).

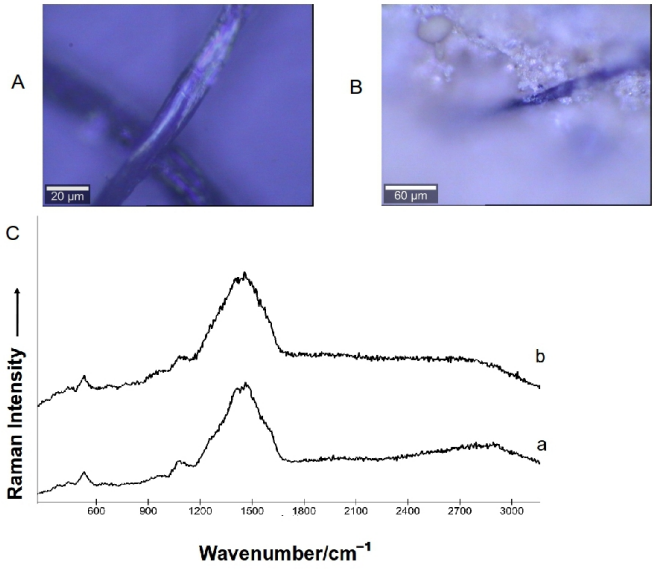

Figure 3.2: Example of matching Raman spectrum from a contamination fibre on Denisova Cave artefact DC12 unwashed artefact (B, C, b) with an Russian archaeologist glove fibre reference (A, C, a).

A particular contamination source arising from the archaeological work on site was identified as iron oxide marks left on some stone artefacts, probably mainly by metal trowels used during the excavation. The iron oxides contain haematite, maghemite and organic matter which cannot be rejected straightforwardly based on Raman spectral data, because iron oxides are materials known to have been used in prehistory. However taking further criteria into account (Chapter 3, section 3.9), the source can be identified and contaminants filtered

out. To minimise on site contamination during stone artefact recovery for Raman micro-residue analysis, artefacts need to be collected and packaged as soon as possible after discovery, with minimal contact, and by wearing gloves. A layer of sediment should be left around the artefacts. Metal tools used to excavate prehistoric sites are probably unavoidable, but metal tool contact with the sampled artefact should be avoided/minimised (Chapter 3, section 3.9). It is important to know what tools (e.g., metal, wood and brushes) were on site, and which tools and what parts were in contact with artefacts. Such details can help to explain other residue contaminants, which can originate from contact with people working on the site. Interpretations of all micro-residues and use-wear can be affected by on site contamination, and need to be considered more cautiously when the risk of contact with people, archaeological tools, clothing and other modern materials is high.

3.2.2 Contamination from samples packaging

Stone artefacts are commonly stored in Ziplock® bags, and Parafilm® is sometimes used for packaging from site to lab. Plastic boxes were used in this study for temporary storage, especially to protect drying samples after washing airborne contamination. Plastic box micro-residues, sometimes found on studied artefacts are easy to identify because of the very specific Raman spectrum of the plastic. However material like Parafilm® and Ziplock® bags (Fig. 3.3, C**,** b and c) can be more problematic as the main bands of their Raman spectra can be confused with lipid micro-residues found on artefacts. Even though weaker Raman bands make it possible to discriminate directly between these modern micro-residues, in poor signal-to-noise conditions, the identification can be more difficult. Plastic box residues were identified on artefacts, always as loose and isolated micro-residues particles, but Ziplock® bags don’t seem to be transferred, as this material was never identified during artefacts analysis. The use of Parafilm®, to wrap artefacts or as a contact material, was avoided in this study.

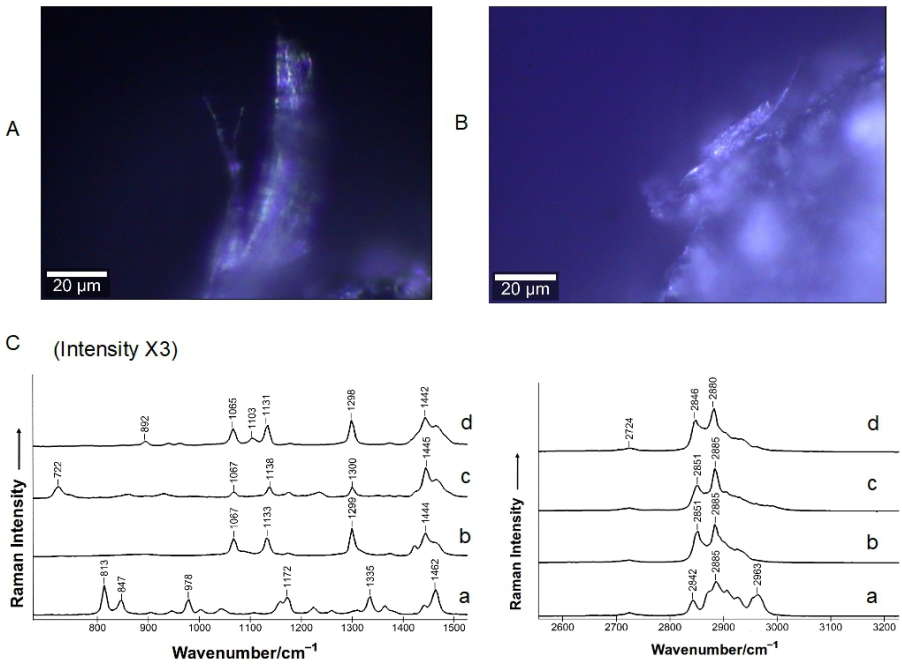

Figure 3.3: Plastic box fibres analysed on Denisova Cave artefact DC2 (A-B), Raman spectrum of plastic box (C, a), Ziplock® bags (C, b), Parafilm® (C, c), and a lipid micro-residue found on prehistoric artefact (C, d).

3.2.3 Contamination from handling

Ideally, for any spectroscopic analysis of prehistoric artefacts, direct contact with the samples should be avoided unless some gloves are worn. However, sometimes artefacts with a long curation history are received for study, and they might have been exposed to contact with bare human hands (Bordes et al., 2017). Therefore, it was useful to determine which types of micro-residues are deposited on stone artefact surfaces by direct handling. In this study, many individual particles were identified as protein and lipid micro-residues on all edges of some artefacts, most notably on artefacts excavated more than ten years ago, with little information about how they had been manipulated during previous microscopic observation or other analyses. Their frequency and widespread distribution cast doubt on their classification as archaeological micro-residues linked with tool-use, and their presence could be due to contamination from handling. In order to test this hypothesis, four basic experiments were undertaken and the results show that even after heating stone flakes to temperatures above 600°C some isolated protein and lipid micro-residues remain on the flakes (Bordes et al., 2017). In addition to the presence of protein and lipid micro-residues on untouched stone flakes, results show that handling causes the same kind of micro-residues (Table 3.1**)**.

Table 3.1: Summary of micro-residues found on handling experiments (proteins, unidentified lipids, saturated fatty acids)						
Blank stone flake 1	**Unwashed and untouched blank stone flake**	**Untouched after 10 s cleaning**	**Untouched after 15 min cleaning**	**Washed sample after 5 min handling**	**Handled after 10 s cleaning**	**Handled after 15 min cleaning**
Micro-residues analysed	Lipids	Lipids	Lipids	Proteins Proteins + Lipids	Proteins Saturated fatty acids	Proteins Saturated fatty acids
Blank stone flake 2	**Unwashed and untouched blank stone flake**	**After 5 min handling**	**Handled after 15 min cleaning**			
Micro-residues analysed	None	Proteins Saturated fatty acids Lipids	Proteins Saturated fatty acids			
Blank stone flake 3	**Unwashed and heated at 600°C**					
Micro-residues analysed	None					
Blank stone flake 4	**Unwashed and heated at 600°C**	**After 5 min handling**				
Micro-residues analysed	Proteins	Proteins Saturated fatty acids Lipids				

Lipid micro-residues detected using Raman spectroscopy had a distinctive appearance (as observed under the 50X microscope attached to the WiTec® Raman instrument), namely a shiny aspect when originating from fresh handling (Fig. 3.4**).**

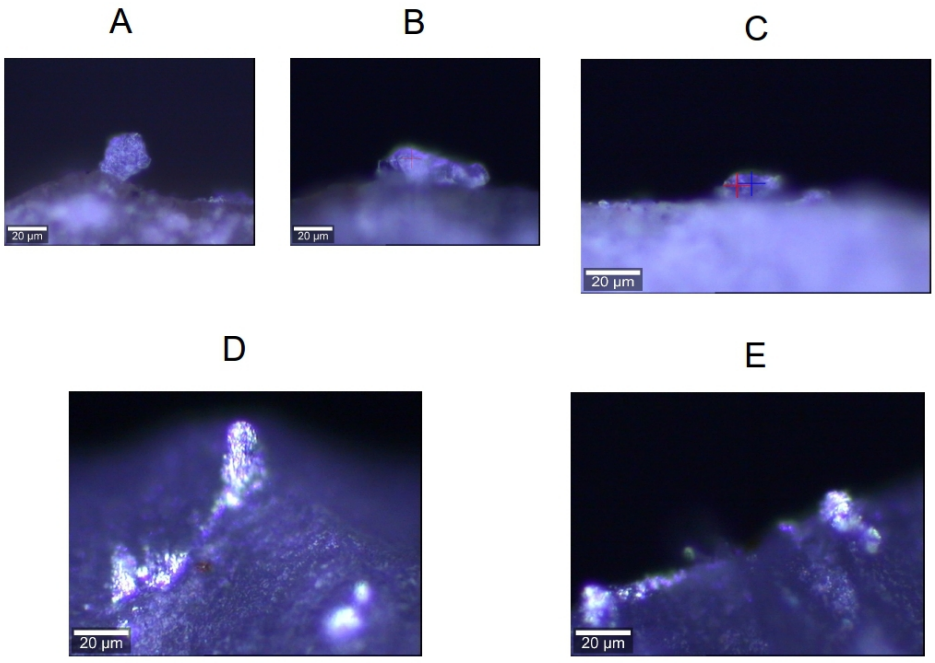

Figure 3.4: Protein (A) and saturated fatty acid micro-residues on archaeological artefacts (B-C), saturated fatty acid micro-residues from fresh handling on experimental stone flakes (D-E).

The Raman spectra of protein and fatty acid micro-residues were compared (Figs. 3.5 to 6) to investigate the possibility of distinguishing between archaeological and fresh micro-residues.

The Raman spectrum of a protein is characterised by Amide I (1600–1690 cm^{-1}) and Amide III (1230–1300 cm^{-1}) vibrations of the peptide backbone. A strong broad peak at ~1454 cm^{-1} corresponds to CH_2 and CH_3 bending modes (Rygula et al., 2013). Side chains phenylalanine and tyrosine bands are observed between 1007–1008 cm^{-1} and 856–859 cm^{-1} respectively. The Raman spectrum of a typical micro-residue found on the prehistoric stone artefacts (Fig. 3.5, a) has been compared with protein spectrum recorded for our handling experiments (Fig. 3.5, b). It clearly shows that both spectra are very similar but with small differences such as variation in relative intensities of the Amide I (1656 cm^{-1}), phenylalanine (~1007 cm^{-1}) and tyrosine (859 cm^{-1}) peaks. The S-S vibrational band at 513 cm^{-1} is sometimes observed, but because of its weak intensity, can often be masked by the background noise. Unfortunately, these differences are not consistent and vary according to analysis position, making it difficult to distinguish systematically between different types of proteins. Furthermore, archaeological micro-residues are most likely mixtures, and the spectral range between 500 and 1000 cm^{-1} is often noisy due to fluorescence, making protein discrimination according only on spectral data even more difficult.

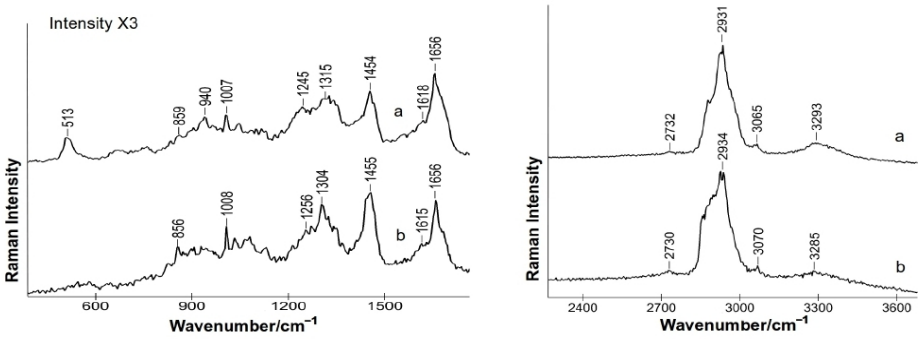

Figure 3.5: Raman spectrum of a typical protein micro-residue obtained on Liang Bua artefacts (a) compared to the Raman spectrum obtained from protein micro-residues originating from handling the artefacts (b) (Bordes et al., 2017).

Raman spectra of lipid micro-residues detected on artefacts are characterised by very strong CH_2 and CH_3 stretching vibrations (2800-2950 cm^{-1}), bending CH_2/CH_3 vibrational bands at 1463, 1443 cm^{-1}, a CH_2 twisting mode at 1300 cm^{-1}, and C-C stretching at 1133, 1105 and 1067 cm^{-1} (Czamara et al., 2015), typical of saturated fatty acids (SFA). Spectra recorded on

the Liang Bua artefacts (Fig. 3.6, a) and on the stone blank from the handling experiments (Fig. 3.6, b) were compared to palmitic and stearic acids (Fig. 3.6, c and d). The spectra are very similar, and differ only slightly, such as the presence of a shoulder at 1424 cm^{-1} and a more intense 1177 cm^{-1} band for spectra from handling experiments. Unfortunately, these small differences are difficult to observe in all conditions especially with a low signal-to-noise ratio, making systematic distinctions (between contamination due to modern handling and saturated fatty acid micro-residues due to prehistoric use or handling) rather difficult based on their Raman signal (Bordes et al., 2017).

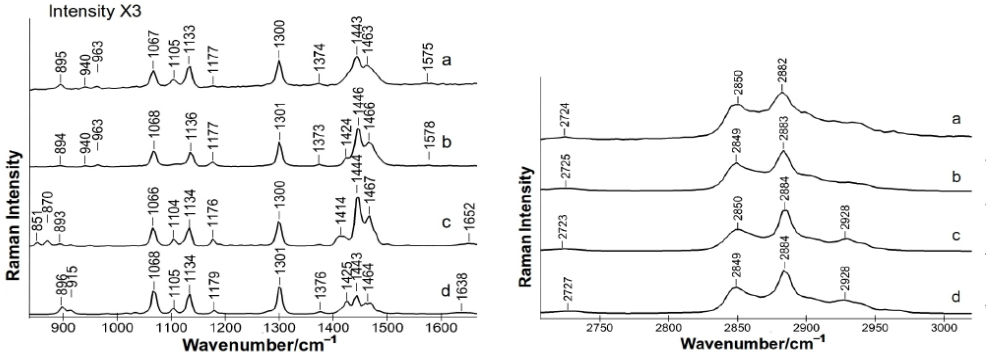

Figure 3.6: Raman spectrum of a typical fatty acid micro-residue found on Liang Bua artefacts (a) in comparison to contamination from handling (b), stearic acid (c) and palmiric acid (d) (Bordes et al., 2017).

Nevertheless, neither protein nor fatty acid smeared micro-residues resulting from handling were found (Chapter 3, section 3.5), and correlation of their spatial distribution in relation to polished edges is another criterion that can discriminate between them. However, avoiding bare hand contact with stone artefacts and using gloves is critical for avoiding unwanted additional protein and lipid residues that can interfere with the correct interpretation of use-related residues.

3.2.4 Contamination from contact during the analysing stage

To avoid micro-residues originating from my hands, the artefacts were only handled with nitrile gloves (latex, powder and protein free). The artefacts were placed on a support fashioned by Blu-Tack® (a synthetic rubber compound) to accommodate the shape of each artefact. This enabled the positioning of each sample under the Raman microscope with the incident light (laser) normal (i.e., perpendicular) to the point of analysis. The support was covered with a

piece of nitrile glove to prevent contamination from the Blu-Tack®. In this manner, the only material in contact with the stone artefacts was nitrile (Chapter 2, fig. 2.7, C). As a result nitrile micro-residues were sometimes identified on edges of studied artefacts. The spectral fingerprint of nitrile, with two unique bands at 1533-1535 and 2240-2241 cm^{-1} (Fig. 3.7), is easily distinguishable, so it's a convenient material to use for this purpose.

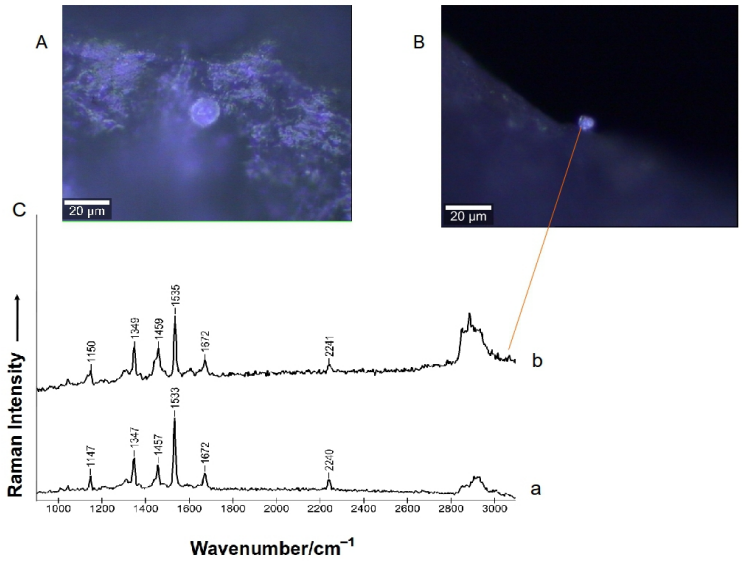

Figure 3.7: Image of blue nitrile glove micro-residues on artefact LB5068 (A) and on artefact LB4340 (B), reference Raman spectrum of blue nitrile glove (C, a), Raman spectrum of the blue nitrile micro-residue analysed on Liang Bua stone artefact LB4340 (C, b).

Another important source of contamination could arise from the use of powdered nitrile gloves, which release a great number of starch grains, which attach to sample surfaces upon contact. Indeed, the use of this type of glove should be avoided at all costs in organic micro-residues analysis. Even if starch grain morphology could be used to identify these starch grains as contamination by specialists (e.g., Torrence and Barton, 2006; Haslam et al., 2011; Messner, 2011), they could be present in great numbers and different sizes, and be more or less distributed on stone artefact edges, and could be misleading when superimposed on others important significant archaeological starch grains or others micro-residues. Such a contamination happened during analysis of artefact LB4130 when powered gloves were used by accident (Fig. 3.8).

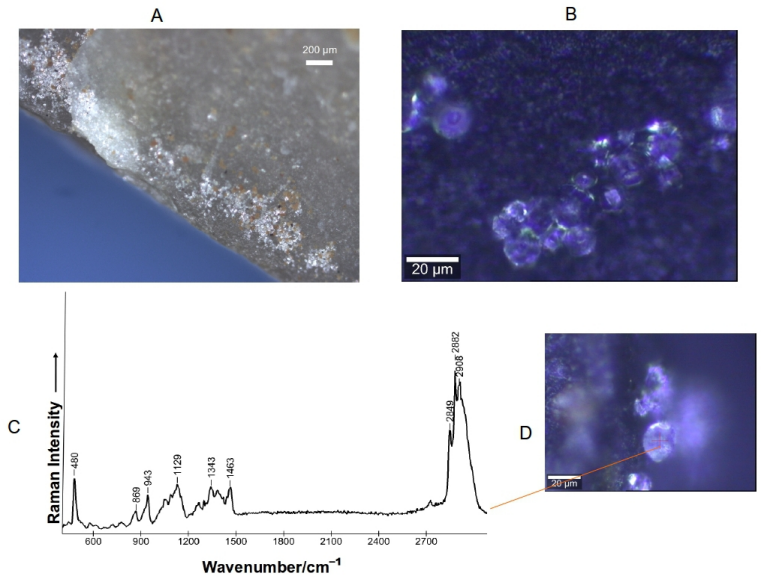

Figure 3.8: Image of starch grains contamination with distribution along an artefact edge (A), and in a group with different sizes (B), Raman spectrum of starch grain contamination.

Pen ink was another, initially misleading, contamination micro-residue analysed on a few of the stone artefacts. A black micro-residue found in the middle of the right distal edge of artefact LB228 (Bordes et al., 2017), which had been through an ultrasonication cleaning process two times (total 2 hours) to check its attachment to the surface. Similar micro-residues were not found in the sediment or in washed sediment removed from the sample. The micro-residues appears as a patch of black droplets on the polished edge (Fig. 3.9, A), which potentially links it to some prehistoric tool-use. The Raman signal is dominated by two bands at 1591 and 1383 cm^{-1} and less intense bands at 1620, 1545, 1247, 1178, 917, 809 and 611 cm^{-1} (Fig. 3.9, B, a). The appearance of the micro-residues and their strong attachment to the artefact suggested that it could be a resin-like material, but its Raman spectra do not match any spectrum in our current database of Australian resins or, as far as we could establish, any resin described in the literature (Edwards et al., 1996; Daher et al., 2010). In fact, the spectrum is quite similar to that of crystal violet (Pozzi et al., 2013) (Fig. 3.9, B, b), a modern synthetic dye mainly used in pen ink.

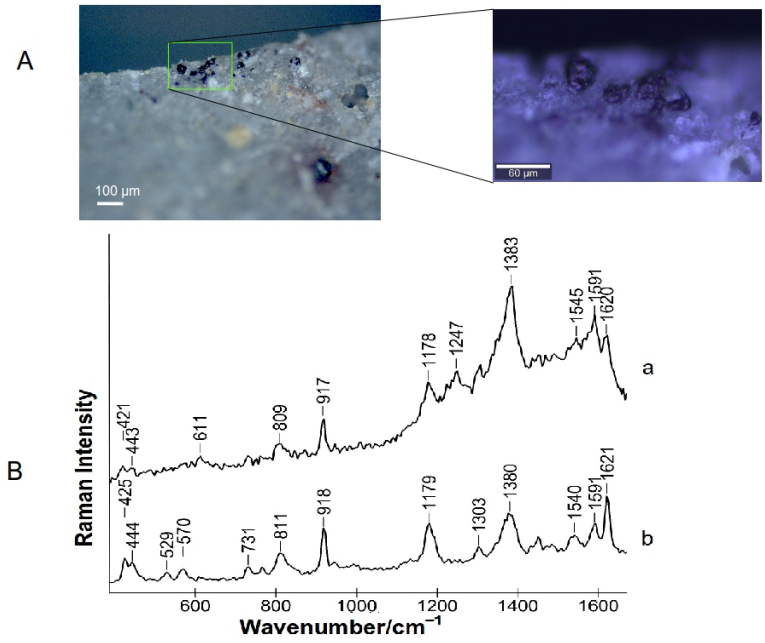

Figure 3.9: Patch of black pen ink droplets on stone artefact LB182 edge (A), Raman spectrum of analysed black micro-residues (B, a) compared with crystal violet pen ink (B, b).

3.2.5 Airborne contamination

To evaluate airborne contaminants in the MicroTrace laboratory at the Centre of Archaeological Science, clean glass microscope slides were placed in different areas of the room, namely above the Raman microscope, under the ventilation shaft in the roof and at the lab entrance. After one week, the slides were removed and the accumulated dust analysed using Raman spectroscopy (Table 3.2).

Table 3.2: List of airborne micro-residues found on microscope slides set in different areas of the Raman laboratory

Contaminant check	Analysed material	Number found	Position of the microscope slide
Contaminant check 1			**Over Raman microscope**
	Fluorescent fibre	1	
	Glass fibre	1	
	Indigo dyed fibre	1	
	Plant fibre	1	
	Protein	2	
Contaminant check 2			**Over Raman microscope**
	Black dyed fibre type 2	1	
	Black dyed fibre type 3	1	
	Cellulose fibre	1	
	Glass fibre	1	
	Indigo dyed fibre	1	
	Plant fibre	1	
	Polyester fibre	1	
	Protein	4	
	Quartz	1	
	Starch grain	2	
Contaminant check 3			**Over Raman microscope**
	Black dyed fibre type 1	1	
	Glass	1	
	Plant fibre	2	
	Protein	1	
Contaminant check 4			**Under roof ventilation**
	Black dyed fibre type 1	1	
	Calcium carbonate	1	
	Carbonised material	1	
	Cellulose fibre	1	
	Charcoal	1	
	Glass	1	
	Glass fibre	1	
	Plant fibre	1	
	Polyester fibre	1	
	Protein	2	
	Starch grain	1	
Contaminant check 5			**Under roof ventilation**
	Black dyed fibre type 1	1	
	Carbonate	1	
	Cellulose fibre	2	
	Indigo dyed fibre	2	
	Plant fibre	2	
	Protein	1	
	Starch grain	1	
Contaminant check 6			**Lab entrance**
	Black dyed fibre type 1	3	
	Plant fibre	1	
	Protein	2	

Among contamination found on these slides, only those that could be misleading within our prehistoric micro-residues study (protein, dyed fibre, pure cellulose fibre, natural plant fibre and starch grains) are discussed in more detail. Protein micro-residues seem to be common in airborne contamination as identified on several slides. Raman spectra obtained on these micro-residues cannot distinguish them from handling protein residues or identify any particular type of protein. However, these residues usually appear isolated, loose from the surface, hence not as smeared micro-residues, and randomly distributed.

Many modern fibres were also detected on the monitoring slides. Four types of black dyed modern fibre with specific Raman spectral signatures were identified, with one type (Type 1) the most common (Fig. 3.10, A, a). All spectra to some extend have fluorescence backgrounds, but the Raman Resonance effect allows enough signal-to-noise ratio to establish distinct spectral signatures and to identify some of these dyes. Indigo was identified as one of the dyes (Fig. 3.10, D, d) and is commonly used to colour modern clothes (e.g., denim), showing a clear contamination from the clothes from people working in the laboratory. These airborne fibres can also enter the laboratory through the ventilation system, or by people moving through the laboratory access door. Potential contamination by modern dyed fibres is not surprising, considering the great varieties used nowadays in modern materials used as building material, or coming from clothing, as shown also by polyester fibres often found on our monitoring slides.

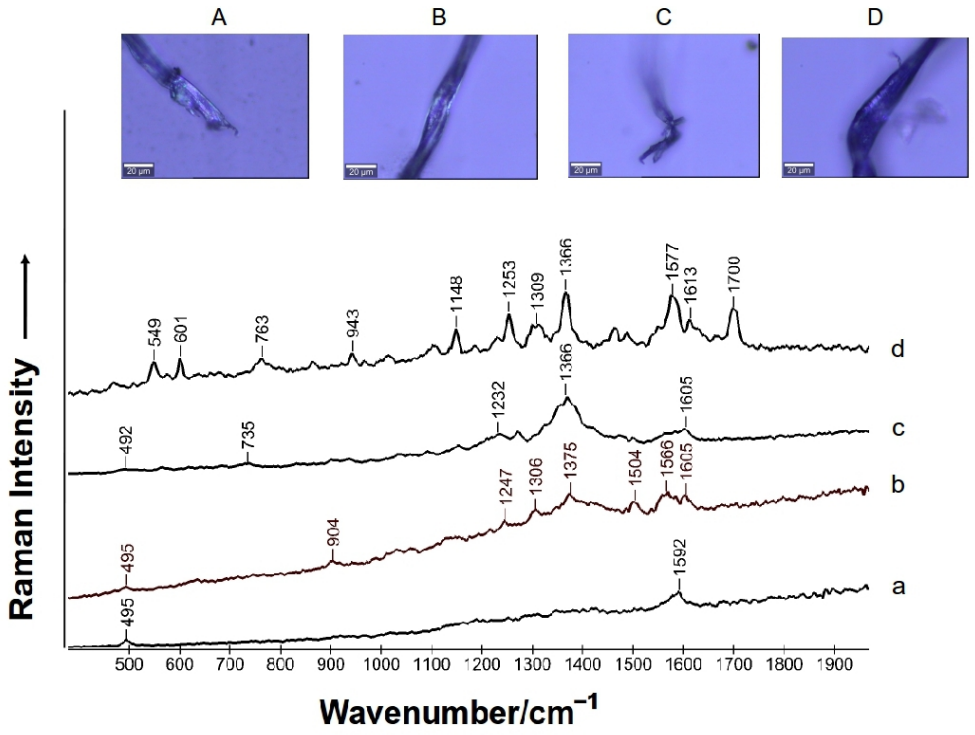

Figure 3.10: Four different types of dyed fibres found among airborne contamination. Type 1, dyed fibre (A, a); Type 2, dyed fibre (B, b); Type 3, dyed fibre (C, c); Indigo fibre (D, d). 532nm laser excitation.

Colourless fibres were also detected among airborne contaminants, some of them probably of manufactured origin, such as pure cellulose, and others probably of natural origin, such as plant fibre. Raman spectra on pure cellulose (Fig. 3.11, A, a) show high intensity, sharp Raman bands of cellulose at 1099, 1121 cm^{-1} (C-O and O-C-O stretching modes) and C-H deformation mode at 902 cm^{-1} (Argawal et al., 1997); and low frequency bands of cellulose are visible at 382, 462 and 513 cm^{-1}, but with no visible lignin band. These bands are also high in intensity compared to cellulose C-H stretching bands centred at 2898 cm^{-1}. Plant fibre spectra are characterised by a lower signal-to-noise ratio and broader cellulose bands with a lignin band at 1604 cm^{-1} (Fig. 3.11, B, b). Raman spectra obtained on plant fibres had weak signal-to-noise ratios and fluorescent backgrounds, which may be an indication of their natural origin compared to the high signal-to-noise ratio typical of spectra of modern fibres made of pure cellulose material (Kavkler et al., 2011). Moreover these airborne fibres occur isolated and very often loosely attached or free of the artefact surfaces.

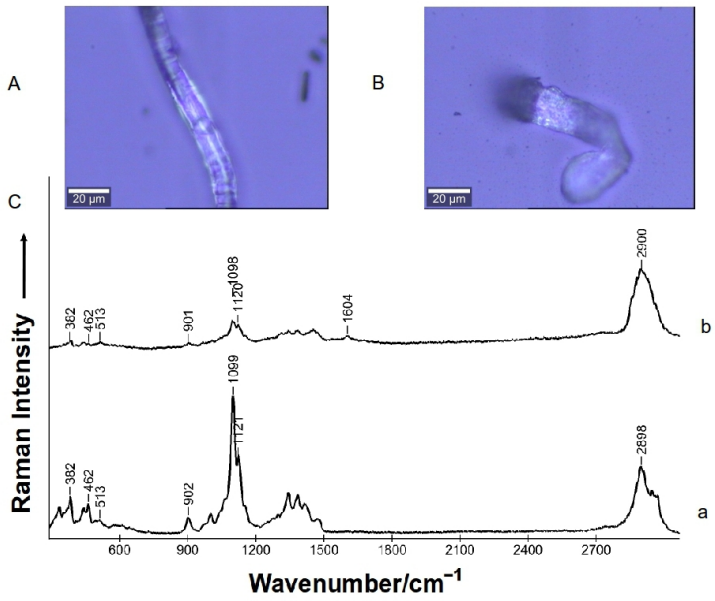

Figure 3.11: Manufactured pure cotton fibre (A), natural plant fibre containing cellulose and lignin (B), Raman spectrum of manufactured pure cotton fibre (C, a), Raman spectrum of natural plant fibre containing cellulose and lignin (C, b).

Polyester contaminant micro-residues were sometimes encountered on studied artefacts, either as fibres or as amorphous residues. While loose fibres could easily be classified as contaminants, especially when mixed with pure cellulose, amorphous polyester contaminant micro-residues could be more misleading, and can sometimes be interpreted wrongly as attached resin or plant like residues with only visual VLM observation.

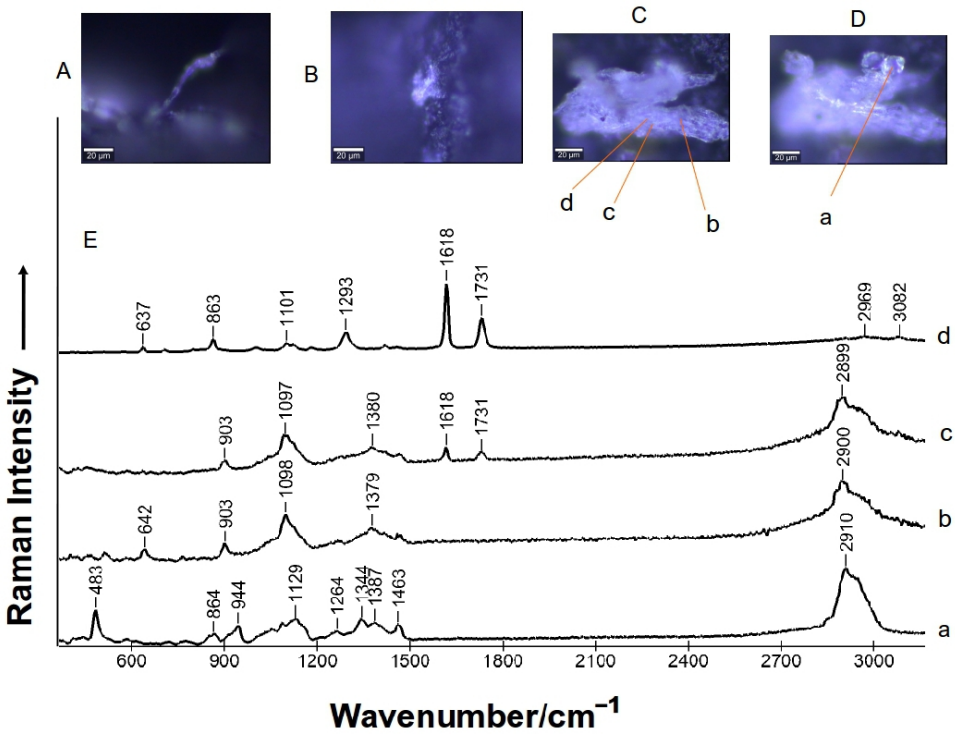

Figure 3.12: Small polyester fibre on artefact LB4829 (A), polyester shapeless residues on artefact LB4582 (B), composite polyester-cellulose residue on artefact LB3958 (C), same residue with a different focus showing attached two starch grains (D), starch grain spectrum (E, a), cellulose (E, b), mixed cellulose-polyester (E, c), pure polyester (E, d).

Presence of polyester in airborne contamination probably originates from modern clothes, in which it is used in large quantities in association with synthetic cellulose (viscose). Such mixed contaminant residues were encountered on some of the artefacts studied (Fig. 3.12, C, E, c) and can be associated with other contaminants such as starch grains (Fig. 3.12, D, E, a) trapped in modern clothes. With its high spatial sub-micron resolution, Raman spectroscopy is capable of separately analysing each component of such mixed micro-residues, which is critical to recognise them as contamination.

3.2.6 Contamination from water used to clean artefacts

Various freshly flaked stones were washed with different sources of water available in our lab to evaluate possible contamination. Isolated starch grains were sometimes observed on stone flakes washed with simple distilled water, but none was spotted when using Milipore® water. Such potential contamination stresses the importance of using a highly purified source of

water when analysing micro-residues, especially if starch grains need to be studied as potential use-related residues on stone artefacts. Quality of the water source used needs to be monitored, and glassware carefully cleaned and rinsed with water of the same quality.

3.3 Isolated and collective micro-residues

Another important criteria to filter out residues not related to use is to observe its occurrence as an isolated residue or as a group of micro-residues. To be considered as a group, every spatially associated micro-residues needs to have a similar Raman spectral fingerprint, hence indicating that they are the same material. Indeed, an isolated residue is more likely to arise from contamination than is a group of residues; so an increasing number of closely related micro-residues improves the chance of them being the result of stone tool use. For example, similar spectral fingerprints were found for a bundle of fibres on artefact LB4204 indicating that all the fibres originate from the same plant (Fig. 3.13**)**

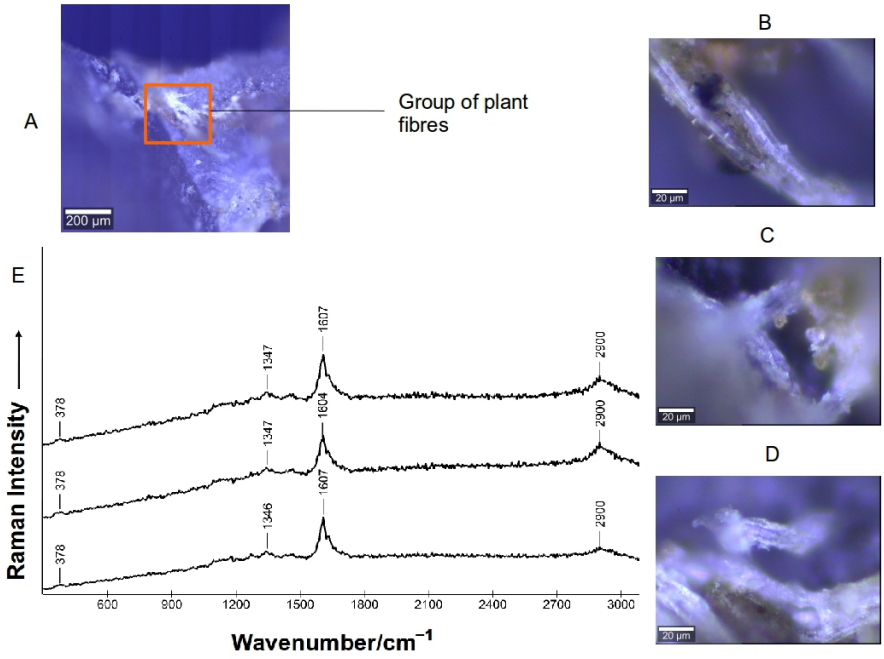

Figure 3.13: Group of fibres on LB4204 main edge (A), individually analysed fibre inside this group led to the same signal (B, C, D), Raman spectra of three different fibres among this group (E).

In contrast, some micro-residues with a similar visual aspect and found spatially close to each other can be made of distinct material. For example, two micro-residues found on LB5126 were identified as a protein and a lipid (Fig. 3.14**)**.

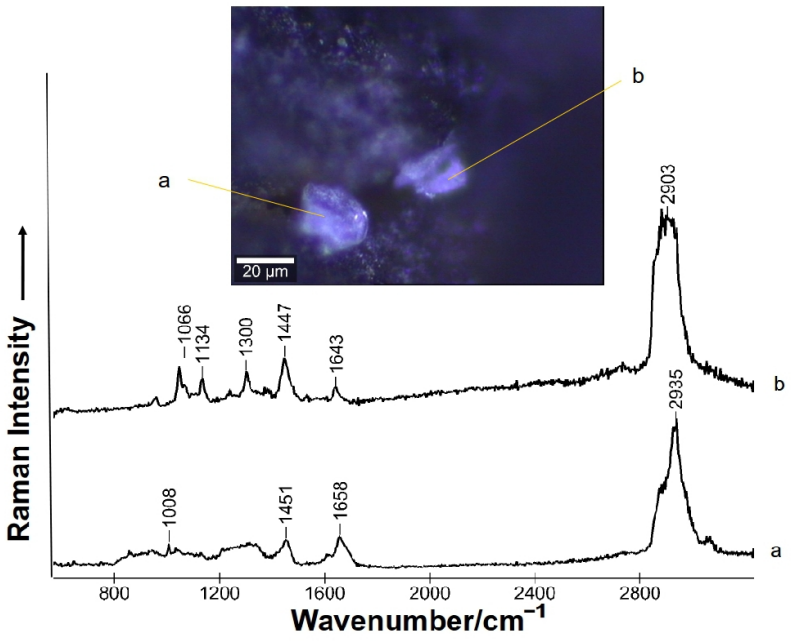

Figure 3.14: Micro-residues with similar visual aspect and found close to each other on LB5126, with distinct spectral fingerprints, protein (a), lipid (b).

3.4 Micro-residues position on the artefact surface

It is important to consider that micro-residues could occupy different positions in relation to an artefact surface. The position of a micro-residue can easily be evaluated by moving focus in microscope mode, prior to analysis. They are seldom found buried in surface holes or cracks in porous rocks. Commonly they are attached directly in contact with the rock surface or are 'loose'—only partly in contact with it. Objects embedded in the surface have a high chance of being a mineral forming part of the mineral background or part of a rock inclusion. Objects completely loose from the surface have a higher chance of originating from the inner sediment or being another contaminant. However, these criteria are insufficient for classifying a residue as use-related, and have only consideration. When considered together with appearance, number and distribution of micro-residues, loose micro-residues might be use-related; and a strong adhering micro-residue can be a contaminant. Individual micro-residues (Chapter 3, section 3.5) could have different degrees of contact with the rock surface but 'smeared' micro-residues (Chapter 3, section 3.5) are always be in complete contact with the surface, by definition. Some examples of micro-residues with different possible positions and identifications are shown in Fig 3.15. Multiple positions of the same micro-residue in a concentrated area, is a good indicator of their relation to tool use, as a worked material has a

higher probability of having different aspects and different degrees of attachment to the rock surface (e.g., Fig. 3.15, D) than an isolated micro-residue that is always found loose on the surface.

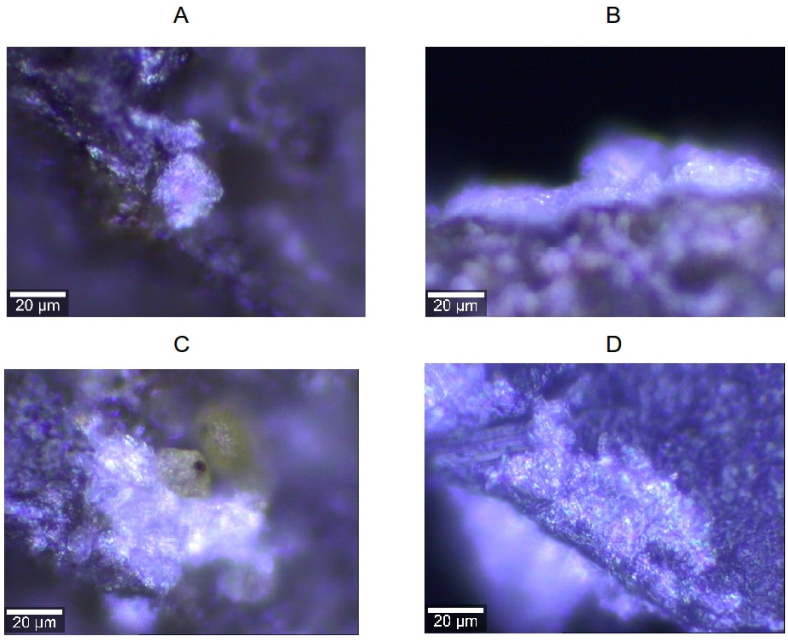

Figure 3.15: Individual lipid micro-residue loose from the surface (A), individual lipid micro-residue partially in contact with surface on edge (B), Individual lipid micro-residue in contact with surface (C), smeared shiny lipid micro-residue showing strong contact with surface with presence of additional individual micro-residues in background (bottom left of the image, on edge) (D).

3.5 Individual and smeared residues

Micro-residues made of the same material could also have very different visual appearances. Micro-residues, which can be recognised as discrete particles with limited shape are designated here by the term “individual residue” (Fig. 3.16). Individual fatty acid micro-residues were previously detected through their Raman spectra on prehistoric artefacts and potentially originate from tool use (Bordes et al., 2017). However, as other sources can produce lipids on stone artefacts such as human handling (Bordes et al, 2017) individual micro-residues alone could be difficult to relate to stone tool use, especially when they are not found in a group or display a clear spatial distribution in relation to use-polished areas. Some individual micro-residues show variation in their aspect under the microscope (Fig. 3.16); some of them look more opaque or transparent, more solid or soft, smooth or grainy. Hence, there is a need to achieve individual spectroscopic analyses on each of them.

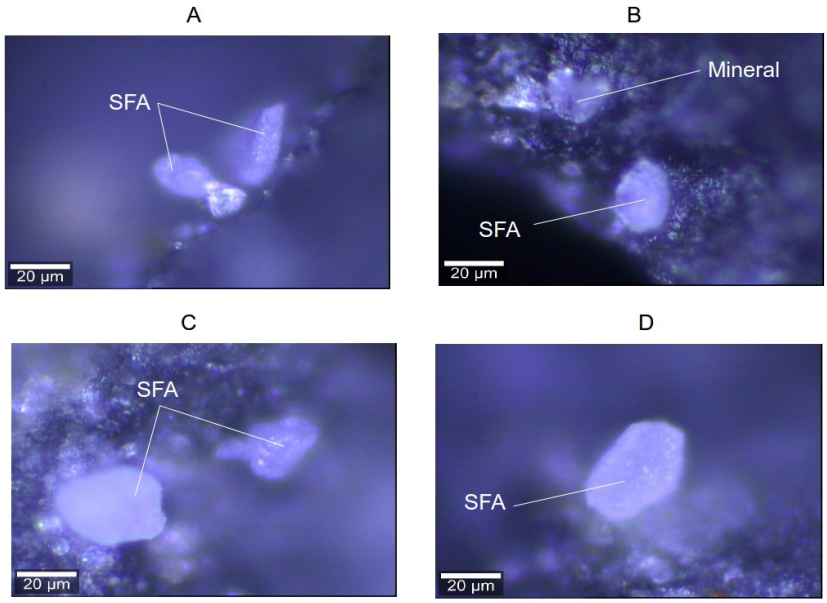

Figure 3.16: Individual solid saturated atty acid (SFA) micro-residues found on Denisova Cave artefacts DC2 and DC12 (A-D).

Polymorph mineral grains can have very similar aspects as organic micro-residues, and have odd shapes. It is very often quite difficult to identify individual micro-residues with only VLM observation, because the same material can have different shape, texture, variation in colour and opacity (Fig. 3.17). Moreover, individual residues can be made of several different materials as a mix of mineral and organic material (Fig. 3.18). In the case of these mixed micro-residues, confocal Raman spectroscopy is very useful to selectively analyse their different parts and identify their different compounds.

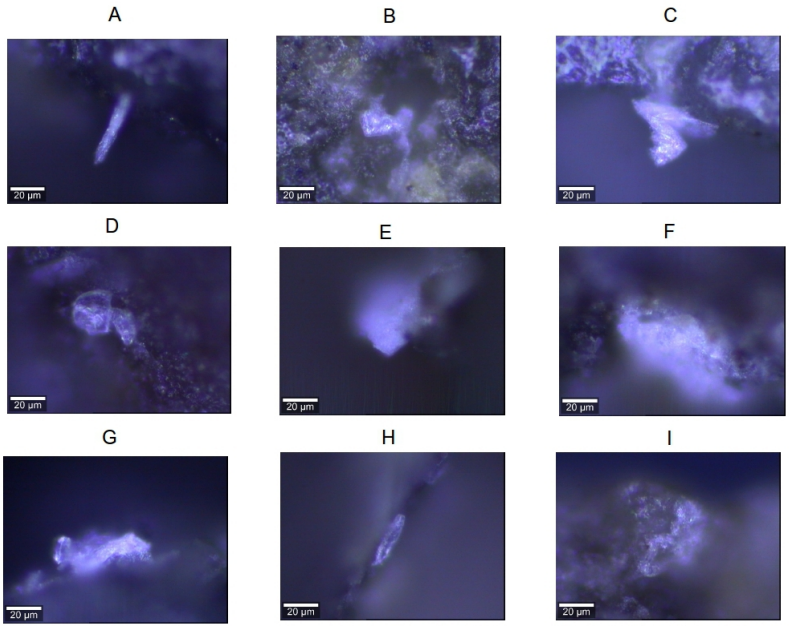

Figure 3.17: Protein (A, C), plant material (B), starch grain (D), calcite (E), fossil bone (F), unsaturated fatty acid) UFA (G), saturated fatty acid (SFA) (H), plant material (I).

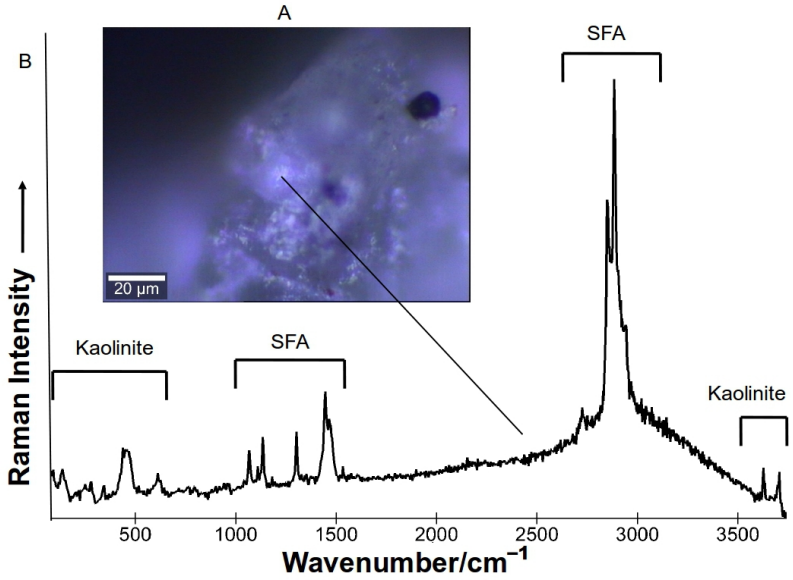

Figure 3.18: A mixed SFA/kaolinite individual micro-residue on LB5126 artefact (A), Raman spectrum of a mixed SFA/kaolinite individual micro-residue on LB5126 artefact (B).

Micro-residues which appear as a layer or film smeared on the rock surface with different surface extension will be designated by the term “smeared residue”. In contrast to individual residues, smeared fatty acid residues, by definition, indicate a close attachment to the surface of stone tools and do not originate from casual handling (Bordes et al, 2017). As no smeared residues have been recognised among modern contaminant residues, either from an airborne source or handling, they have a higher chance of being linked to prehistoric use. Smeared residues are by definition closely bound to the surface, filling its cracks and irregular depressions, as opposed to an individual residue, which can be either attached directly or in a loose position on/above the surface. For some of these smeared residues, which are distributed closely with use-wear on worked artefact edges and surfaces, it is particularly critical to infer their relation to stone tool use; and especially so for some micro-residues like fatty acids. Directional smeared striations were sometimes observed following the orientation of striations in use-polish (Fig. 3.19). These directional smeared micro-residues show that their formation is probably linked to the same process, which produced the stone tool polish by applying a certain amount of pressure, along a preferential direction on the artefact, on a limited area. Considering this, smeared micro-residues can be more securely linked with stone tool use, but caution is needed when clues exist about other causes of pressure that could have caused micro-residues to be smeared on the surface. For example, for stone artefacts with metal marks (Chapter 3, section 3.9), a metal tool could have caused sufficient pressure to alter individual residues and alter the artefact surface, thus mimicking use-wear. Therefore, understanding that both individual and smeared micro-residues are complementary is important for determining whether micro-residue concentration as use-related.

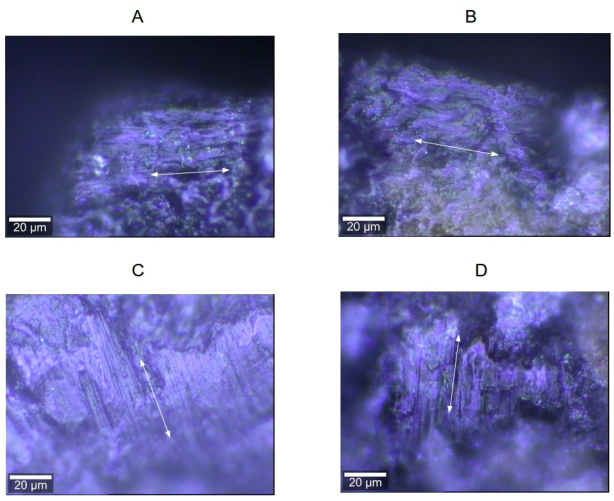

Figure 3.19: Images of fatty acid smeared residues: Artefact DC2, dorsal side (A), artefact DC12, dorsal side (B), artefact DC27, dorsal side (C), artefact DC4, dorsal side (D).

Indeed, when smeared lipids are spatially associated with individual micro-residues, with the same Raman spectral signature, it greatly strengthens an interpretation of prehistoric tool use. Individual and smeared micro-residues co-exist for the processing of different kinds of material including bone, lipids, protein, plant material, resin and mineral pigment. Smeared residues are even more difficult to relate to a particular material under VLM observation, and can be easily confused with polished areas (Fig. 3.20).

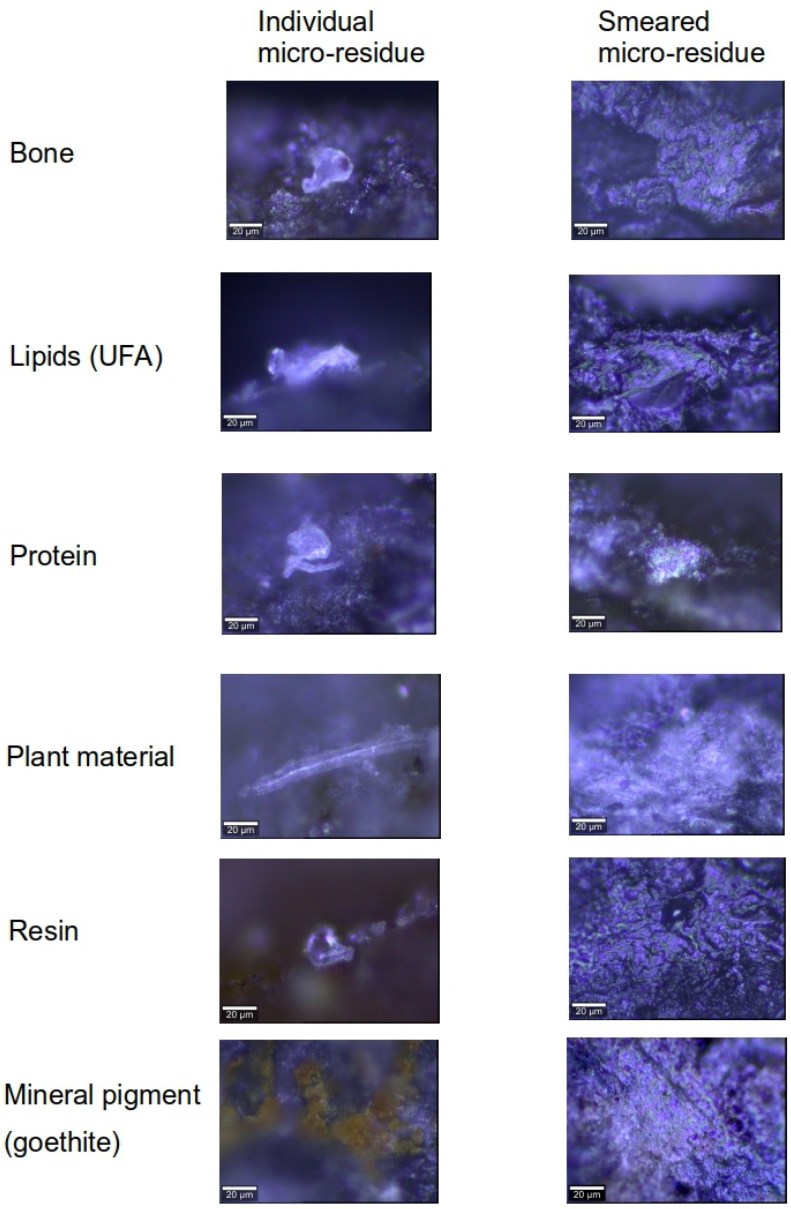

Figure 3.20: Images of individual and smeared analysed micro-residues for different materials.

3.6 Widespread distributions

Widespread distribution of a micro-residue on the whole surface of a stone artefact is likely to result from post-depositional processes, which could include mineral deposition of manganese oxide or iron oxide or a biological process (e.g., a biofilm, resulting from micro-fungal and bacterial activity). Widespread residue distribution could also indicate an origin from the surrounding sediment layer. The origin of micro-residues in sediment could be natural (e.g., mineral grains) or anthropogenic (e.g., organic residues from prehistoric or modern human activity on site). To be classified as a ‘widespread’, a residue is easily detected in any area chosen randomly on both surfaces or along edges.

3.7 Presence of micro-residues in sediment

The presence of micro-residues in the layer sediment is an efficient way of discriminating any micro-residue that may have originated from the sediment and transferred to the artefact. Analysis of the sediment samples does not aim to identify every mineral or organic object but rather to check for the presence or absence of micro-residues on the artefacts that can potentially be use-related (e.g., bone, protein, lipids, plant fibre). The relative abundance of mineral grains and different micro-residues found in sediment samples and on artefacts needs also to be noted.

When micro-residues found on artefact surfaces are completely absent from inner and outer sediment samples, we can clearly reject the possibility that they originate from the sediment. But if micro-residues on samples surfaces are also detected in one of the sediment samples, their relative abundance needs to be evaluated on the artefacts and all sediment samples. Indeed, in the case of abundant archaeological residues (e.g., bone) on an artefact, their presence in the outer sediment does not mean that all bone residues attached to the analysed stone artefact originate from the sediment. The concentrations of residue in the outer and inner sediments need to be high enough to explain that bone could have been transferred to the stone tool (Fig. 3.21). In contrast, a higher concentration of a micro-residue on artefacts compared with a low abundance in sediment samples suggests that its origin is from the artefact surface. In a third last case, in which a similar abundance of residues can be found on the artefact surface and both inner and outer sediment samples, no decisive origin either from artefact or from sediment can be determined and this criterion won't be sufficient argument to infer the relation between micro-residues and stone artefact use. Additional criteria, such as

position (Chapter 3, section 3.4) or aspect of micro-residues (Chapter 3, section 3.5), will need to be considered.

This criterion of residue abundance is particularly useful for evaluating mineral or micro-residues, which could be common in sediment (e.g., iron oxide and manganese oxide) but difficult to affirm as use-related. However, as for bone residues, a few very rare haematite grains in sediment cannot explain the presence of hundreds of grains on stone tool edges. In this study, I had separated inner and outer sediment, expecting to observe increasing amounts of micro-residues toward outer sediment, implying diffusion of some micro-residues from artefact surface toward sediment. No such abundance gradient was evident from visual inspection (which has been checked with Raman analysis), although no quantification of abundance was undertaken. Consequently, analyses of both outer and inner sediment samples were mainly used to double check for micro-residue presence.

Analysis of washed sediment (i.e., washed from the artefact) is a useful check for the presence of micro-residues similar to those found on the artefact surface. Some residues such as individual bone micro-residues and fragments, plant fibres or starch grains, are far more likely to detach themselves from stone tools and be found in the washed sediment. In contrast, lipids and proteins are more strongly attached to artefact surfaces, and were not found in washed sediment. Analysis of washed sediment is an excellent check to assess the presence of micro-residues in very low abundance that could be missed from analysis of residues on a stone artefact. So, if micro-residues are found in washed sediment but not in previously analysed artefact observations, extended time of artefact analysis is needed to try to spot and analyse them, because they are probably present and were missed.

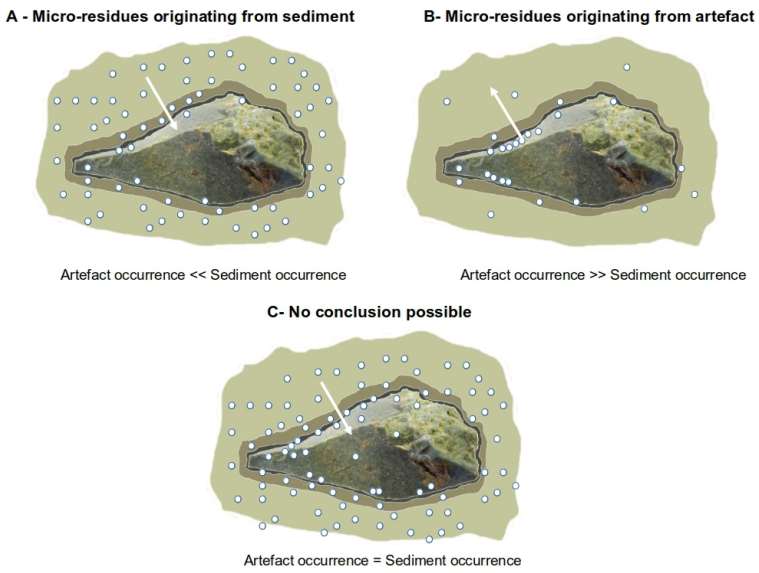

Figure 3.21: Higher abundance of residues in sediment than on the artefact (A) and lower abundance in sediment than on the artefact (B). Same abundance as in sediment (C).

3.8 Presence of micro-residues as artefact mineral background

Mineral background needs to be analysed and minerals found in the tool stone (artefact raw material) need to be determined. Indeed, if potentially use-related mineral micro-residues are found on a stone artefact, one needs to check for its presence as part of the mineral background of the tool stone. Organic materials are not likely to be confused with mineral background but some natural hydrocarbons (e.g., kerogen and bitumen) can be part of a naturally outcropping rock. Hydrocarbons cannot be confused with plant and animal lipids because their Raman spectral fingerprint is very distinct (Orange et al., 1996). A way to analyse artefact mineral background is to randomly select a few zones completely devoid of any residues and analyse several spots to determine the main mineral composition of the surface. Mineral background can easily be distinguished as its signal will be always increase when lowering the spectroscope focus down towards the stone surface (i.e., lowering the microscope objective) and can often be analysed beneath smeared organic residues. Mineral background is also indicated by the high recurrence of spectra on analysed spots devoid of any residues signal. Uncommon mineral inclusions can sometimes be encountered but can usually be properly interpreted by analysing their spectrum, their embedded position in a rock surface (Chapter 3, section 3.4) and by observing their crystalline aspect.

3.9 Single side distributed micro-residues

Another criterion for rejecting a modern contaminant, is illustrated by residues found on the Liang Bua archaeological site, during excavation. Some shiny and black iron oxide micro-residues containing haematite and maghemite (Fig. 3.22), coated by a layer of organic material were found on a few stone artefacts from this site. These residues were considered of possibly use-related because they were distributed on a use-polished edge, appeared in groups with a specific pattern and were not present in the layer sediment.

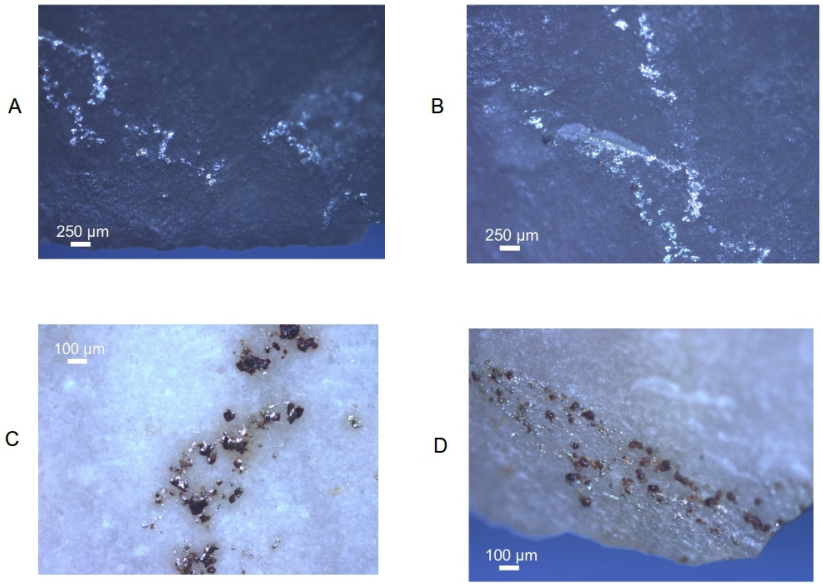

Figure 3.22: Liang Bua artefact LB4582 with shiny iron oxide trowel marks (A, B), Liang Bua artefact LB4340 with shiny iron oxide trowel marks (C, D)

These micro-residues were very difficult to understand because they were sometimes located outside polished zones, existing either on small, well-bounded areas of less than few hundred microns or on very extended areas all over one side of the artefact. It was difficult to reject them directly as a contaminant because haematite could be a prehistoric pigment worked by humans in the past and also occurs naturally in sediments and rocks. The fact that it was documented during excavation which side of the artefact was facing up (towards the surface) and which was facing down was the key to understanding these micro-residues. Indeed, they occur systematically on the side of artefacts facing up, indicating that the residues probably originated from exposure of that upper surface at the archaeological site and this information gave direction to investigate the source of modern contamination.

Conventional use-wear studies often identify marks made by trowels and sieves, and it was suspected that the marks originated from steel trowels used to excavate the tools on-site. Therefore an experimental tool was deliberately touched with a steel tool and comparison of the VLM image and Raman spectra of these micro-residues with those on the artefacts show that they are the same (Fig. 3.23, A-C). SEM-EDS analysis confirmed the identification of iron oxides in combination with carbon. (Fig. 3.23, D). Silicon is present as an underlying mineral background included in analysed depth volume. Another visual characteristic of these micro-residues was the presence of oriented striations seen frequently at higher magnification (X50 objective), and which were also observed on experimentally stones scratched with metal tools (Fig. 3.23, A-B). This iron oxide contamination most likely arises from common metal tools used during archaeological excavation such as a trowel. Artefacts LB4340 and LB4582 are good examples of such metal mark contamination (Fig. 3.24).

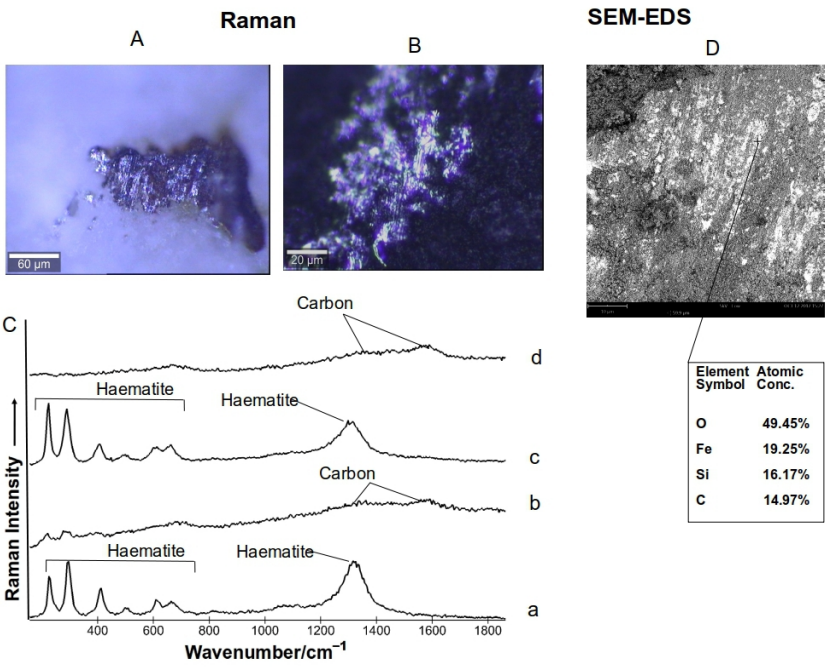

Figure 3.23: Image of shiny iron oxide metal marks on LB4340 Liang Bua artefact (A), Raman spectra showing organic material spectrum at low laser power (C, b) and haematite spectrum at higher laser power after organic matter burning (C, a), image of shiny iron oxide metal marks obtained with metal point on experimental stone artefact (B), Raman spectra showing organic material spectrum at low laser power (C, d) and haematite spectrum at higher laser power after organic matter burning (C, c), analysed shiny iron oxide metal marks done with metal point on experimental stone artefact by SEM-EDS confirming presence of iron oxide and carbon (D).

Identifying this source of contamination illustrates the value of recording the position of collected artefacts on site and advantages of having them extracted with a layer of surrounding sediment. Removing artefacts in blocks of sediment can also help to limit contact with these metal tools.

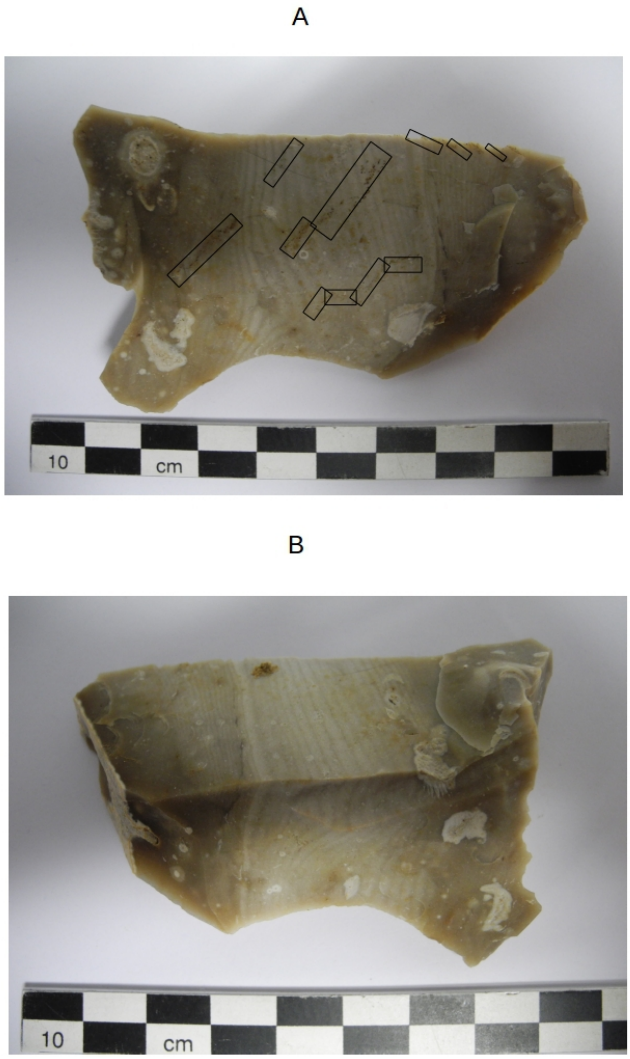

Figure 3.24: LB4340 artefact top surface with metal marks (A), LB4340 artefact under surface without metal marks (B).

3.10 Correlation of micro-residues distribution with polish distribution

This criterion is based on the relation between use-polished surfaces and micro-residue distributions. For example, we can expect that micro-residues resulting from sawing bone with a tool edge will have more concentrated bone residues on that edge than on the opposite edge. This implies that to evaluate this criterion, at least several (at least two) analysed micro-

residues have to be considered. An isolated micro-residue found on a polished edge is not very meaningful, but two micro-residues on this polished area indicate a higher probability of being use-related than if one of these micro-residues occurs on a polished edge and the other on an opposite or adjacent non used edge. Obviously, the higher number of micro-residues detected, the more robust will this distribution correlation criterion be. Practically, evaluating the overlap of polished areas with the analysed micro-residues distribution is a good way to test this criterion (Fig. 3.25). For example, DC12 showed a good correlation between its polished edges and smeared saturated fatty acid micro-residues (Fig. 3.25), but poor distribution with protein individual micro-residues (Fig. 3.26).

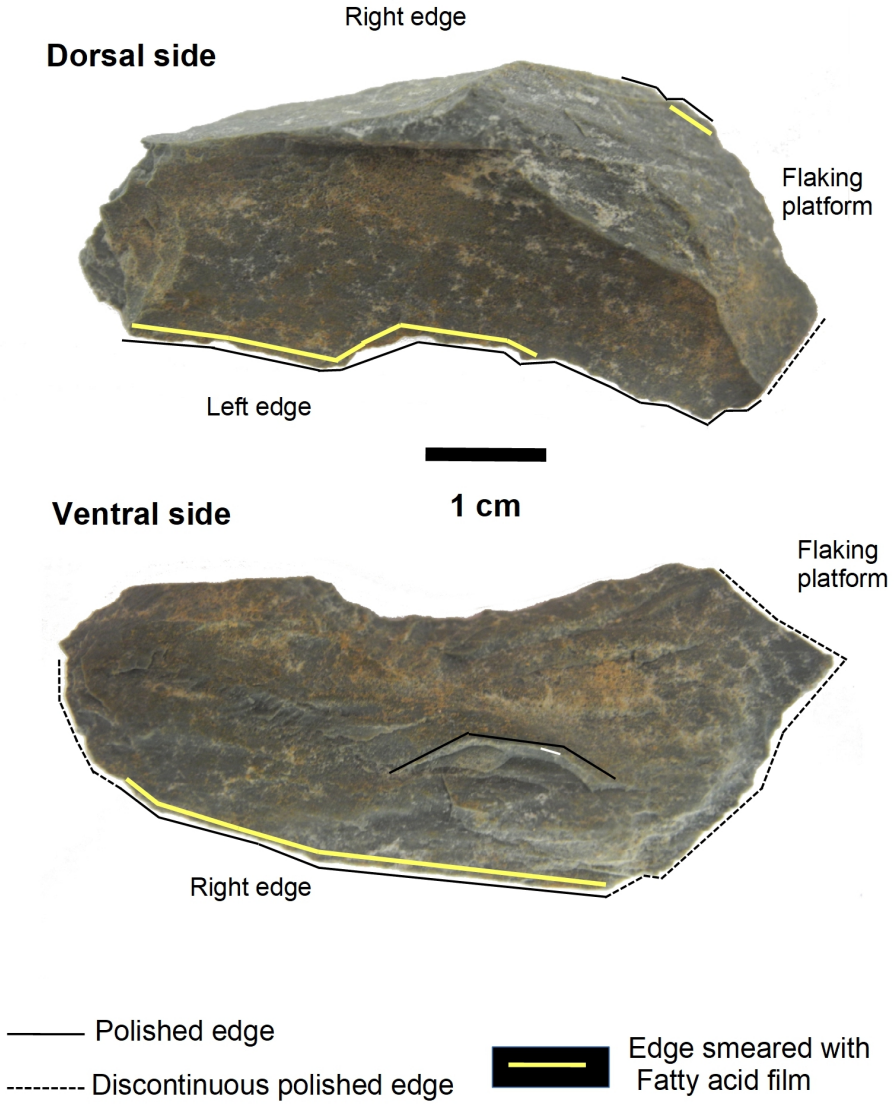

Figure 3.25: DC12 Denisova Cave artefact illustrating good correlation between polished edges and smeared saturated fatty acid micro-residues.

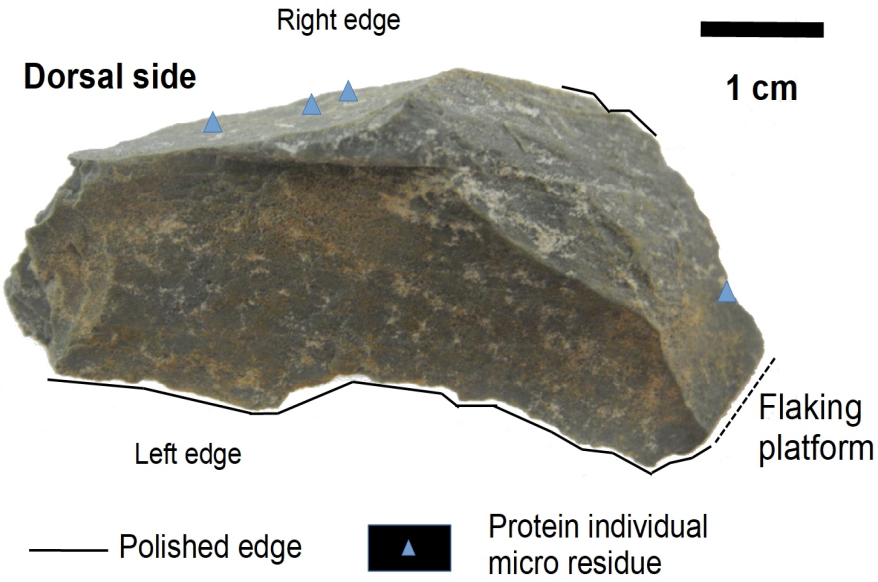

Figure 3.26: DC12 Denisova Cave artefact showing no correlation between polished edges and protein individual micro-residues.

It isn't useful to consider this correlation criterion for micro-residues with a widespread distribution (Chapter 3, section 3.6). Correlation between micro-residues and use-polish distributions is an important criterion but needs to be considered together with all the other criteria (presence in sediment, individual and smeared residues, isolated or group of residues). One can object that residues are not always distributed on polished areas. Indeed, some researchers have recently shown that stone tool experiments using fresh materials indicate, that some micro-residues can be initially located away from the used and polished edges (Xhauflair et al., 2016). Such micro-residues may be use-related, but their relative preservation on these different areas of the artefact after thousands of years is still unknown. Moreover, it is very likely that pressure during use increases the chance of attaching material on the rock surface, embedding it in cracks and small depressions of the surface, hence increasing its chance of survival against degradation processes. For example, it's obvious that cutting fresh material like a tomato is going to spread red juice all over the surface of the stone tool, but it will be probably be close to the edge; some tomato skin squeezed by the pressure and embedded in edge irregularities will have a better chance of surviving thousands of years, when all juice on the surface will likely have disappeared. The chemistry of each material plays a crucial role in residue sensitivity to degradation processes. In experimental and

archaeological case studies, I have observed that a high concentration of some micro-residues, such as bone, are often in close alignment with highly polished areas, either directly on edges or at small distance (few hundred of microns) inland, which tends to confirm this statement. It is also important to observe and probe with spectroscopy, any increasing number of micro-residues associated with more highly polished zones (Fig. 3.27) along artefacts edges, and their decrease with less polished zones; the implication is that the downward pressure applied to the tool surface probably generated both residue abundance and polish intensity.

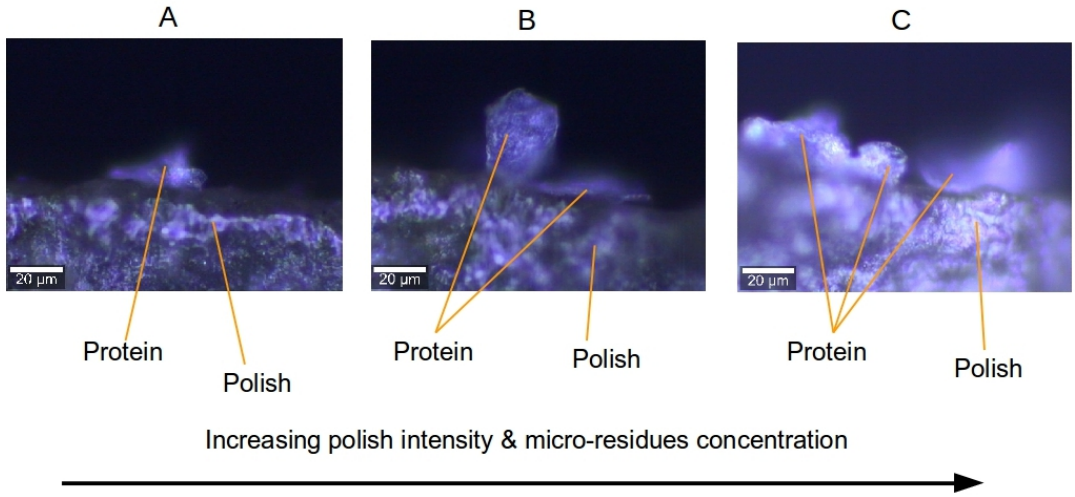

Figure 3.27: Narrow strip of polish and few protein micro-residues (A), wider strip of polish and increasing number of protein micro-residues (B), high polished edge and concentration of protein micro-residues (C).

Establishing micro-residue distributions has the advantage of mapping residue concentrations or combinations of residues, indicating which edges were used for working (different) materials. Indeed, we should not assume that prehistoric tools were specialised or not; multiple edges may have been used for the same material or different materials.

Systematic mapping of micro-residues also contributes to understanding incidental and use-related micro-residues, which is of tremendous importance in identifying prehistoric actions in relation to the use of stone tools. As defined in the introduction (Chapter 1, section 1.6), I do not want to confuse use-related micro-residues with any incidental prehistoric material that came in contact with stone tools (e.g., grass on which the stone tool had been used or bone from some post-depositional contact). Indeed, use-related micro-residues should be recurrent and concentrated in association with traces of use, particular polish. In contrast, incidental residues should most often be present away from polish and other traces of use or be very

restricted in their distribution on edges that have no indications of use. One examples of such incidental micro-residues is discussed in chapter 6 (Chapter 6, section 6.3.2.4) about grass material found on artefact LB5164.
Even if this criterion is key to distinguishing use-related micro-residues from micro-residues arising from other origins, a last example is useful to highlight the importance of considering all the criteria together:

Micro-residues on Liang Bua artefact LB5527 edges were systematically analysed by Raman spectroscopy before and after washing: individual, loose bone micro-residues were found on the edge of the unwashed artefact. Some residues appear on polished edges, sometimes in apparent concentrations, but always isolated. In this case, distribution is not a decisive criterion for rejecting these micro-residues; some are located on use-polished edges although others are located outside of them (Fig. 3.28**).** Bone micro-residues were found in outer sediment and washed sediment but with no clear gradient towards or away from the artefact. However, total absence of smeared bone residues on unwashed Artefact 5527 indicates that these isolated and loose individual micro-residues likely derive from the sediment.

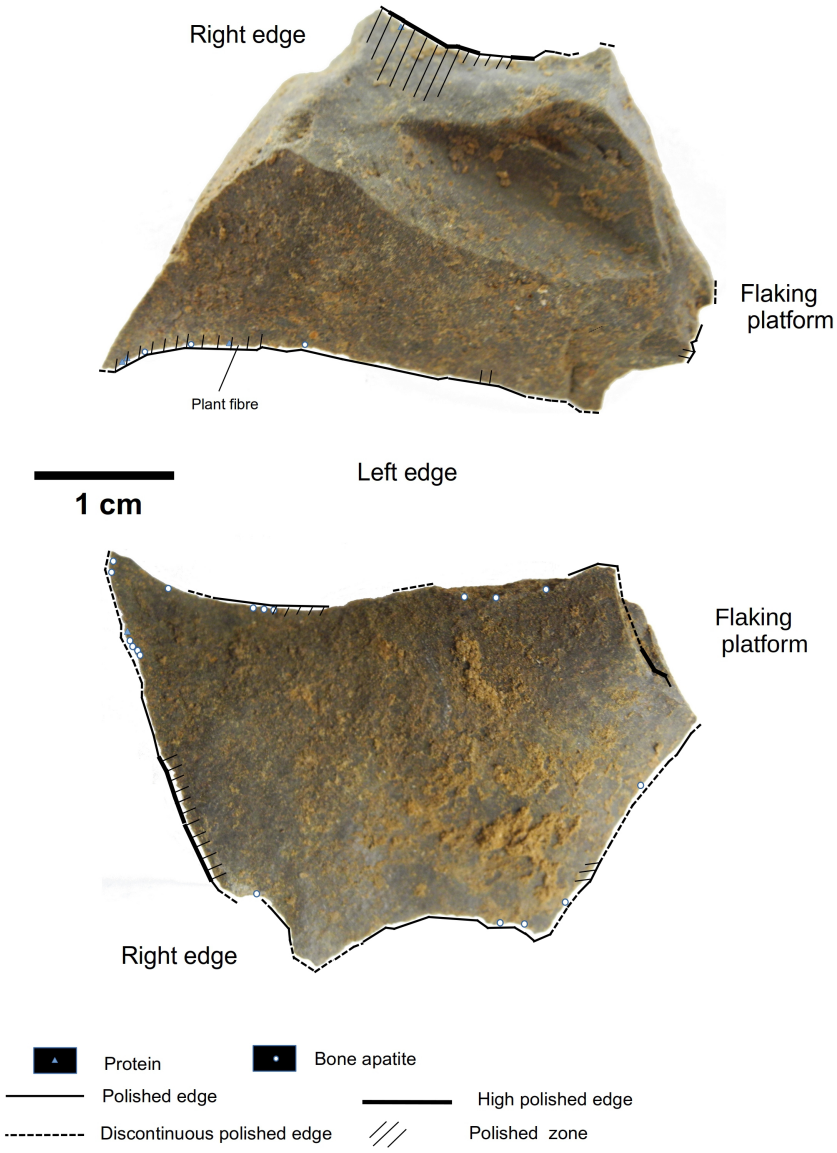

Figure 3.28: Correlation between micro-residues and polish distribution on unwashed Liang Bua artefact LB5527.

Confirmation of this hypothesis can be found after washing (Fig. 3.29). No bone micro-residues were found after washing, with no smeared bone residues. Instead, a concentration of fatty material more firmly attached to the polished surface was detected with a higher probability of being related to artefact use. A few plant residues were detected but not in high abundance and only outside the main areas of use-polished zones, suggesting that they are not related to the use and likely incidental. Consequently, only fatty materials and proteins, unfortunately not supported by enough key plant or any animal residues to get more specific information, can assigned to use of artefact LB5527, but bone, in significant amounts, cannot be demonstrated in this case to be use-related.

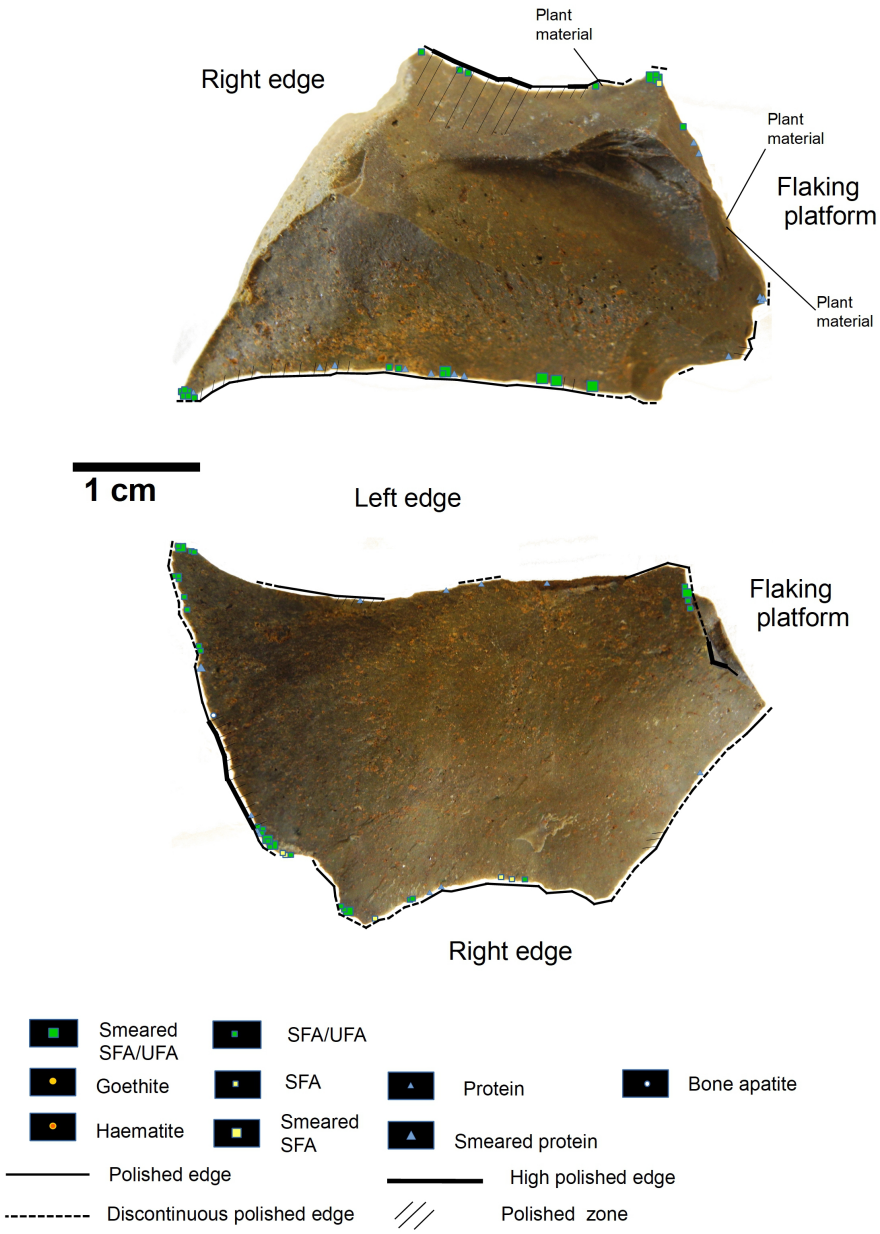

Figure 3.29: Correlation between micro-residues and polish distribution on washed Liang Bua artefact LB5527.

This example illustrates that if Raman spectroscopy cannot provide specific data on the nature of the material worked, however the hierarchy of criteria are sufficient to identify micro-residues origin. This example also emphasises that the probability of being use-related does not depend only on the amount of material on a given artefact, but also on distributions along the edges and a potential origin from sediment.

3.11 Recurrence in a set of artefacts

Considering the recurrence of the same type of micro-residue in a set of studied artefacts, it is useful to discriminate some micro-residues, which cannot be use-related. Micro-residues found on every artefact in a sample set are very unlikely to result from prehistoric use. Indeed, the probability that every artefact within a random selected set is used to work the same material is low. For example, the fact that bone micro-residues were found on every Denisova Cave artefact and in sediment samples (Chapter 5, section 5.3.2), shows that they cannot be related to artefact use. It's interesting that key archaeological material like bone can be discriminated by other criteria and that the spectral identification alone is in fact telling us little of the origin of material present on prehistoric artefacts. This criteria is especially useful to discriminate micro-residues arising from natural process on stone tools made of the same stone or rock type. As another example, all Liang Bua artefacts made of volcanic tuff show recurrence of kaolinite clay (Chapter 6, section 6.3.2.3) with no traces of this material on artefacts made of other stones or (e.g., quartz and chert). The kaolinite is probably linked to a weathering process and cannot be use-related. This criteria emphasises the importance of understanding artefact samples, in the context of the archaeological site, and in the context of each archaeological layer.

Chapter 4 Reference materials and experimentation with modern stone artefacts

4.1 Developing Raman spectral references and database

Developing a reference material database is critical to compare with analysed residues on prehistoric stone tools. Indeed, although for many chemical compounds, modern and natural materials, some Raman spectra references are available in the literature, accurate spectral comparisons can only be done with the help of a locally developed database. Many references in the literature often lack a particular wavenumber annotation for a band of interest or are only given for a restricted wavenumber range, sometimes excluding vibrational bands of interest. Furthermore, slight variations in the positions of Raman bands, fluctuation of the spectral background due to instrumentation, local variations in analysed materials or measuring conditions create differences between literature references, which in some cases are confusing. Moreover, Raman spectral references of natural materials found in archaeological contexts are few and researchers need to rely on those found in other fields of research (e.g., the food industry) to identify particular residues. Such spectral references, out of archaeological context, are often not fully comparable to results obtained in archaeological research. Subsequently, references recorded with the same instrument and experimental conditions make it possible to compare Raman spectra accurately and confirm securely the identification and composition of some micro-residues.

Database was developed in a progressive opportunistic way, mostly guided by the micro-residues found on archaeological stone tools, rather than attempting to be comprehensive.

4.2 Pure chemical references

Raman spectra of pure chemical references were recorded directly on microscope slides in solid or liquid state. The references were chosen based on the main components that are expected to remain as residues after long periods of time and a list of these chemicals can be found in appendix (Appendix I, table 2).

For lipids, it was useful to record references for sterols, saturated fatty acids (SFA), unsaturated fatty acids (UFA) and Triacylglycerols (TAG) (Fig. 4.1**).** SFA can be easily identified by their high intensity C-H stretching mode at 2285 cm^{-1}, absence of C=C stretching mode and sharp bands between 1443 and 1069 cm^{-1}, notably a narrow band at 1301 cm^{-1} (Fig. 4.1, a**)**. Triglycerides (or Triacylglycerols (TAG)) have similar fingerprints as corresponding fatty acids, but show an additional ester vibrational bands in the 1720-1750 cm^{-1} range (Czamara et

al., 2015). In the case of tripalmitin, the main ester band is centred at 1746 cm^{-1} (Fig. 4.1, b**)**. UFA can be identified by C=C stretching band at 1658 cm^{-1}, =C-H stretch at 3009 cm^{-1} and a broad shoulder centred at 1260-1270 cm^{-1} on the =C-H deformation band at 1305 cm^{-1}(Fig. 4.1, c) (Czamara et al., 2015). Cholesterol has a distinct shape for the C-H stretching region and unique bands at 1676 cm^{-1} and 705 cm^{-1} (Fig. 4.1, d**)**. These bands are useful to identify cholesterol, especially when spectra are acquired with recording times of only a few seconds and when background noise often mask weaker vibrational bands.

This chemical database aids the identification of the main chemical compounds of a given micro-residue on stone artefacts. Compound categories present can be confirmed as lipid, carbohydrate, protein, etc. However, it will seldom be possible to make a more specific identification as archaeological residues seldom are pure compounds but rather a mixture of compounds. A combination of compounds can sometimes be used to identify some particular material (e.g., cellulose and lignin for plant material), but often, residue identification is more efficient if comparisons are directly made with a natural materials database (Chapter 4, section 4.3.2) (Appendix I, table 4). For this reason, references of pure chemical compounds are useful but not sufficient and a comprehensive list of more complex materials (synthetic and natural) needed to be developed.

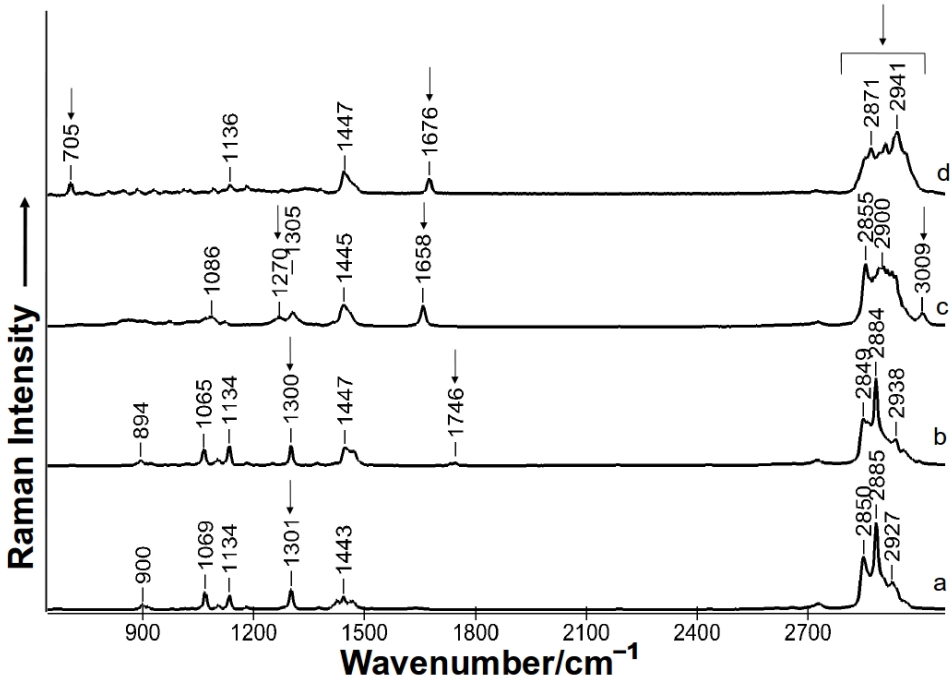

Figure 4.1: Spectra of different lipids: Palmitic acid (SFA) (a), tripalmitin (triglyceride) (b), oleic acid (UFA) (c), cholesterol (d).

4.3 Modern material references

A variety of synthetic and natural materials was analysed, directly deposited on microscope slides.

4.3.1 Synthetic material references

The aim of analysing modern synthetic materials is to identify contamination originating from material close or in direct contact with the stone artefacts when exposed to a laboratory environment during analysis (Chapter 3, section 3.2.4). Some of these materials like nitrile blue gloves, plastic boxes (polypropylene) and Blue tack® were identified as micro-residues transferred on stone artefacts. Easily discarded when their Raman signal is known, but more time consuming to identify when not already in a database and considered as unknown material (Chapter 3, section 3.2). Obviously, in view of the large spectrum of modern materials used nowadays, a researcher needs to develop a list of modern material references specific to collection protocols and storage materials according to a specific laboratory environment. A list of these materials for our laboratory can be found in appendix (Appendix I, table 3).

4.3.2 Natural materials references

Raw material references analysis was not undertaken systematically for the whole range of archaeological material that can be encountered as micro-residues attached to stone tools. Indeed, an exhaustive strategy for developing such a complete database will be almost impossible, too time consuming and mostly useless for the short time of this study. Instead, new material references were analysed according to the kind of micro-residues found on the prehistoric artefacts under study. A list of the material analysed is presented in appendix (Appendix I, table 4). For example, when natural fibre micro-residues were identified on Liang Bua artefacts, several different kinds of plant and wooden fibres were analysed for comparison purposes. As for all unknown prehistoric material residues, Raman spectroscopy is not very likely to identify plant or animal exact species, then some close natural materials were acceptable for our study even if not directly found in the past environment of archaeological sites (e.g., database of Australian resin, kino and gum), and helpful for first spectral identification either on experimental or prehistoric artefacts.

On the other hand, others raw material references analysis was undertaken because of the opportunity to access a particular collection of potential preserved archaeological materials, namely private resin collection of Philip Green of Australian resin, kino (*Eucalyptus*) and gum. Indeed, resins are an important type of potential prehistoric residue which can be informative on different past technologies, especially hafting techniques.

Resin and kino are quite challenging to analyse with Raman spectroscopy because they tend to melt under laser beam excitation and in many cases have a strong fluorescence background. The 785nm excitation was used when the level of fluorescence was too high using 532 nm excitation, that it prevented any spectrum to be recorded. To avoid fluorescence, smaller particles with a more translucent aspect were targeted. Laser power level was increased slowly to reduce the chance of melting the analysed resin. In another strategy, using the same laser power, but switching between the X50 to X20 objectives was sometimes useful to decrease the focus area and prevent melting. Consequently some resin and kino samples were successfully analysed only with 785 nm excitation (Fig. 4.2), and others with both excitations (Fig. 4.3). In the latter case, 532nm excitation was preferred because it was faster, the full wavenumber range being obtained at once within an unique spectral window, including a higher signal-to-noise ratio on CH stretching bands around 3000 cm^{-1}.

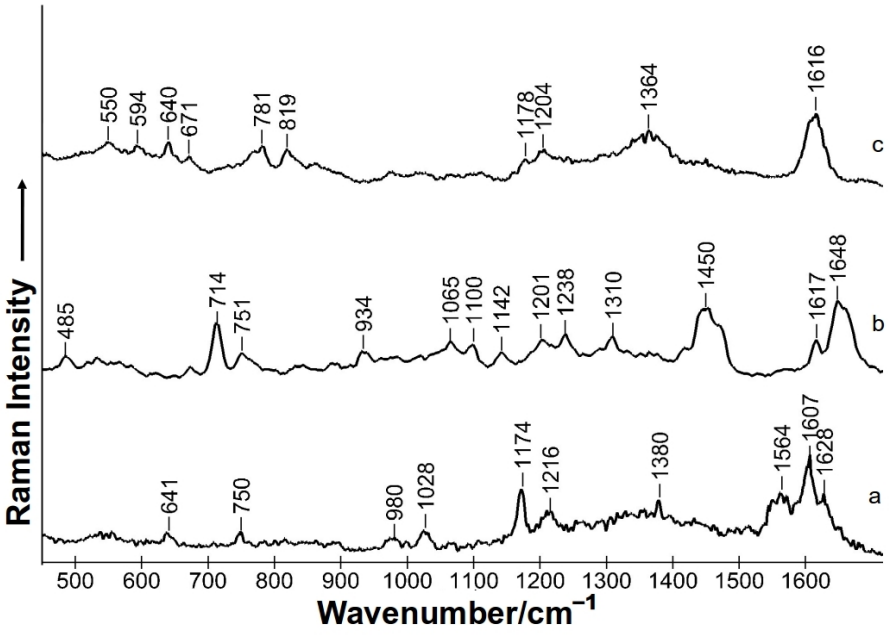

Figure 4.2: Spectra of different resins with 785 nm excitation: Grass tree (*Xanthorrhoea quadrangulata*) (a), white cypress (*Callitris glaucophylla*) (b), Eucalyptus (*Angophora costata*) kino (c).

According to (Daher et al., 2010), a weak vibrational band at 3086 cm^{-1} can be informative for presence of diterpenic resin. This band was present for Callitris and Bunya pine resins (Fig. 4.3, b-c), indicating these materials probably have diterpenic resin content. Vibrational bands between 1600-1670 cm^{-1}, including stretching C=O vibrational modes at 1670 cm^{-1} and stretching ($C=CH_2$) olefinic group stretching 1650 cm^{-1} modes are also useful to distinguish resin (Fig. 4.3, a-c) from gum (Fig. 4.3, d) with very weak features in 1800-1500 cm^{-1} range as the vibrational modes for gum originates from polysaccharides and are devoid of such molecular bonds (like aromatic group) in this region (Edwards et al., 1996; Vandenabeele et al., 2000). Kino exudate is historically referred as a "gum" but with a lower content in carbohydrate (Patten et al., 2010). Interestingly, every Eucalyptus kino sample spectrum analysed as reference in that work had a very distinct fingerprint compared to the gum sample (Fig. 4.3, d), but close to a resin spectral fingerprint (e.g., Eucalyptus*) (Angophora Costata),* including a strong aromatic mode centred at 1617 cm^{-1} *for kino (Fig.* 4.2, c) which are not present in our gum sample, indicating that eucalyptus kino probably include additional aromatic compounds.

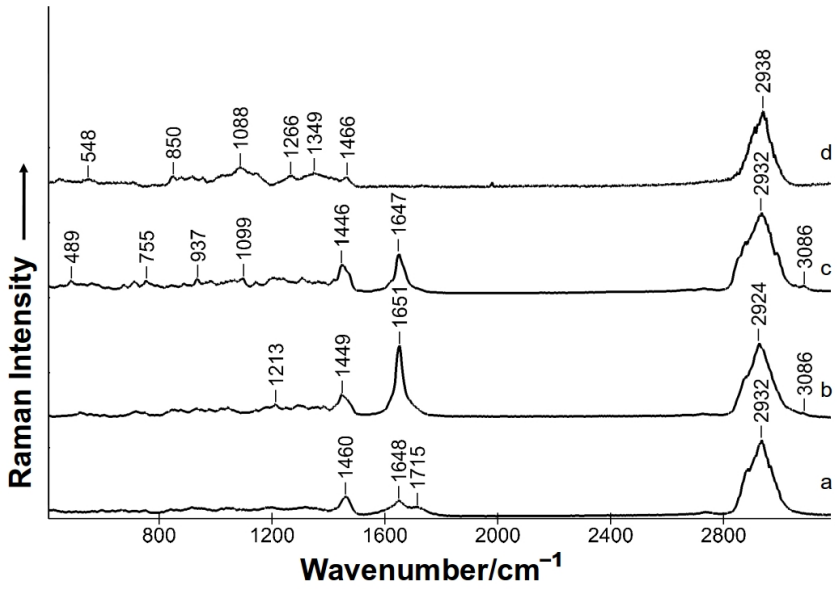

Figure 4.3: Spectra of different resins and a gum with 532 nm excitation: Spinifex (*Trioda pungens*) (a), Bunya pine (*Araucaria bidwillii*) (b), Cypress pine (*Callitris rombodia*) (c), South African acacia gum (d).

4.4 Raman analysis of an experimental tools collection from 1980

Stone flakes were selected from a collection of experimental tools that were used as the basis for documenting residues and wear patterns in the early 1980s (Fullagar, 1986). These experimental tools were used to investigate micro-residues short term preservation (30 years), and to observe their distribution on true stone artefact surfaces. These tools were used to process a variety of materials including animal flesh, bone and skin and a variety of plants and trees. Micro-residues identified on their working edges and surfaces are summarised in (Table 4.1), with residues abundance frequency. We classified abundance as such:

Very common: Micro-residues are widespread and found very easily.

Common: Micro-residues which are found easily, but only in limited areas or with specific distributions.

Uncommon: Micro-residues are not easy to find and occur in fewer numbers in spatially-constrained areas.

Rare: Micro-residues are found single or very infrequently on the artefact and in the sediment.

Table 4.1 : Summary of results of Raman analysis on an experimental 1980 collection

Artefact	Stone	Material	Use	Duration /Nb of strokes	Types of micro-residue analysed	Relative abundance
X38	Flint	Typha	Scraping & cutting	30-40 min	Protein Protein + Calcium nitrate	Very common Uncommon
X150	Flint	Typha	Scraping	45 min	Protein Protein + Calcium nitrate Starch grain	Common Common Rare
X64	Flint	Casuarina wood	Sawing	45 min	Plant fibre Plant material	Very common Very common
X84	Flint	Palm tree	Scraping	10 min / 1000	Protein Protein + Calcium nitrate Calcium nitrate SFA Protein + SFA Starch grain	Very common Common Uncommon Uncommon Uncommon Uncommon
X85	Flint	Palm tree	Scraping	20 min / 1500	Protein Protein + SFA + Calcium nitrate Plant fibre Protein + Calcium nitrate Protein + Calcite	Common Common Uncommon Uncommon Uncommon
X86	Flint	Black palm	Sawing	20 min / 1500	Protein Protein + Calcium nitrate Plant fibre Starch grain	Common Common Uncommon Uncommon
X88	Flint	Rattan	Sawing	45 min	Protein	Common
X96	Flint	Tooth	Engraving	1 min / 50	Protein Starch grain	Common Rare
X106	Flint	Bamboo	Scraping	20 min	Protein Plant fibre Smeared plant material	Common Uncommon Uncommon
X107	Flint	Bamboo	Scraping	5 min	Protein SFA Protein + SFA	Common Common Uncommon
X127	Flint	Blood	Cutting	0 min / l	Specific protein (haemoglobin)	Very common
X230	Flint	Fresh possum skin	Scraping	5 min	Smeared SFA	Uncommon
X290	Hornfel	Fresh possum skin	Scraping	5 min	Smeared SFA SFA Protein fibre Protein Starch grain	Common Common Common Common Rare
X27	Flint	Bone	Sawing	15 min	Bone + Collagen	Very common
X284	Flint	Cow bone	Sawing	20 min	Bone + Collagen Smeared bone Smeared SFA + Bone Smeared SFA	Very common Common Common Common
X287	Flint	Cow bone	Sawing	20 min	Bone + Collagen	Very common
X309	Flint	Fresh cow bone	Scraping	45 min	Bone + Collagen Collagen fibre (protein) Plant fibre	Very common Common Rare
X288	Flint	Meat	Cutting	20 min	Collagen fibre Smeared protein SFA fibre SFA	Very common Very common Uncommon Uncommon
X143	Flint	Kangaroo	Butchering	10 min	Lipids Plant fibre SFA	Common Uncommon Uncommon

4.4.1 Plant materials

The experimental tools used to work plant material like wood, bamboo, rattan, palm tree, typha from the 1980 collection was analysed and micro-residues like plant fibres, starch grains, individual SFA, proteins were identified (Table 4.1). As an example, individual starch grains can be identified by their characteristic spectral fingerprint. The Raman bands at 483-484 cm^{-1} (C-C-C bending, C-O torsion), 1462-1467 cm^{-1} (CH, CH 2, C-O-H bending) and very strong band at 2912-2915 cm^{-1} (C-H stretching) are diagnostic of starch (Fig. 4.4, a-b) together with bands at 865-867, 941-942, 1130-1136, and 1343-1348 cm^{-1} (Fig. 4.4) (Holder, 2010; Bordes et al., 2017).

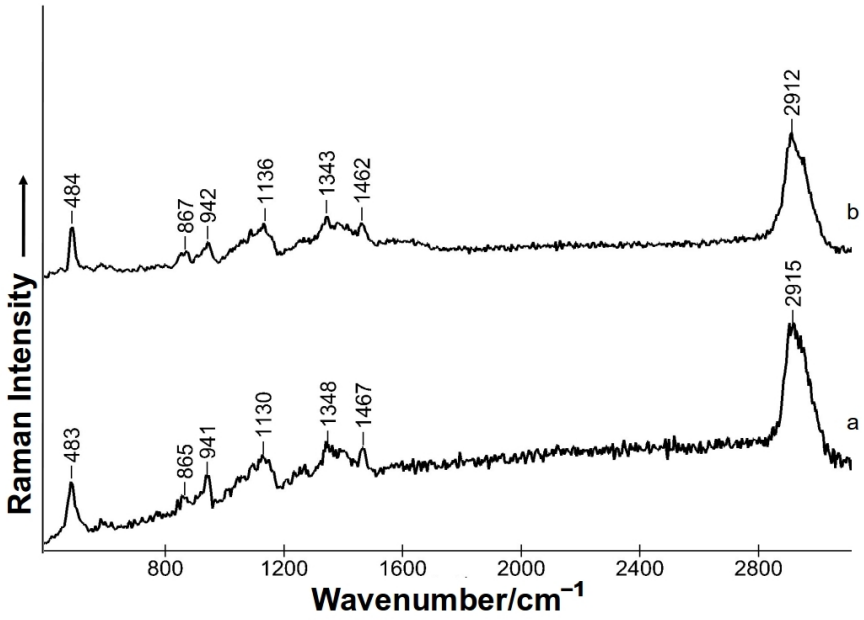

Figure 4.4: Spectra of two different starch grains with 532 nm excitation: Typha (X150) (a) and palm tree (X84) (b).

Identification of amorphous starch and starch grains by Raman spectroscopy is quite useful because their optical identification can sometimes be difficult, and because they are small objects (often a few microns in diameter), with variation in shape or can be amorphous, closely associated or even be mixed with sediment of other organic micro-residues. However, the identification of starch on a stone tool need to be attributed to tool-use very cautiously, because starch grains can easily arise from modern contamination (Chapter 3, section 3.2.5). Raman spectral information of starch grains cannot determine any specific plant species.

Numerous plant proteins were analysed on different experimental stone tools from the 1980 collection. The Raman spectrum of a protein is characterised by amide I (1600-1690 cm^{-1}) and a broad amide III (1230-1300 cm^{-1}) vibrational band of the peptide backbone (Rygula et al., 2013). A strong broad peak at ~1454 cm^{-1} corresponds to CH_2 and CH_3 bending modes. A small sharp side-chain phenylalanine band is observed at 1006-1008 cm^{-1} which is also systematically observed for proteins.

A particular association of calcium nitrate (sharp band at ~1050 cm^{-1}) with protein micro-residues was frequently identified on stone tools which were used on plants from an old artefact collection (Bordes et al., 2017). Calcium nitrate did not occur on the rock surface immediately around the micro-residues, but it is only associated with them. (Fig. 4.5). In spectra where the intensity of this band was high, it was possible to observe two weaker bands located at 710-715 cm^{-1} and 740-748 cm^{-1}, identifying this compound as calcium nitrate **(**Pérez-Alonso et al., 2004**)**. Calcium nitrate was found associated with pure protein, as well as mixed protein and fatty acid micro-residues analysed on stone tools which were used to work plant material (Table 4.1), but never in pure fatty acid micro-residues. It was also not detected on fresh experimental stone tools (Table 4.3). The presence of calcium nitrate has been reported as a degradation products from burials (Pérez-Alonso et al., 2004 ; Bradtmoller et al., 2016), which suggests that they could be a product from plant protein degradation.

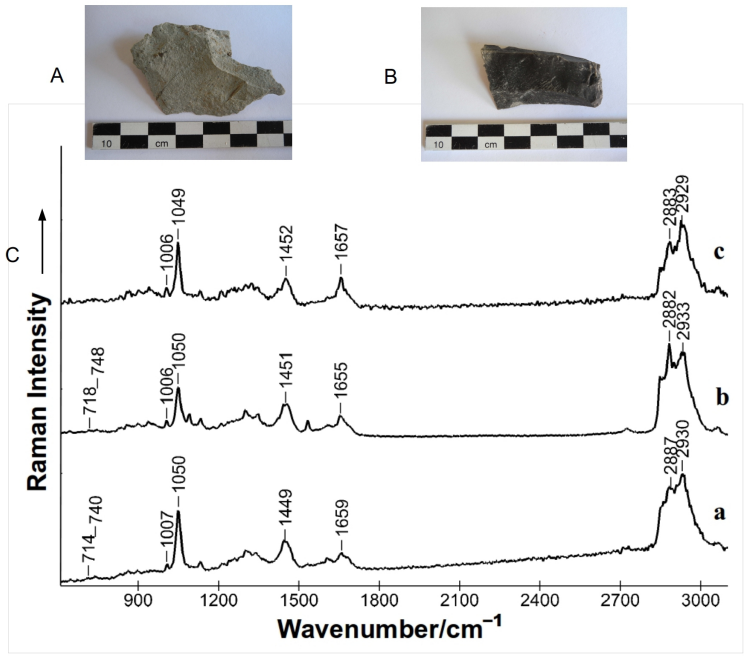

Figure 4.5: Images of experimental tools with protein micro-residues with calcium nitrate content: Experimental artefacts X150 (A), used on typha and X86 (B), used on palm tree. Raman spectra of protein micro-residues with calcium nitrate content on Liang Bua artefact (LB45) (C, a) and experimental artefacts X150 (C, b) and X86 (C, c).

4.4.2 Animal materials

The distribution and type of residues on the experimental tools used for processing animal products varied according to tool function. On artefacts used to saw or cut bone (X284, X309), bone and collagen are very common, however, collagen fibre is absent on X284, but present on X309 (Fig. 4.6), with occurring frequency only second to bone containing collagen residues. On the other hand, on experimental artefact X288 used to cut meat, the more common micro-residues are collagen fibres and smeared proteins. However, X290 use to scrape skin shows some individual and smeared SFA micro-residues in far more abundance than collagen (Table 4.1**)**. The Raman spectrum of collagen fibre is typical of protein with amide I band at 1670 cm^{-1} and CH deformation band at 1464 cm^{-1} and phenylalanine band at 1006 cm^{-1}. At higher wavenumbers, intense C-H stretching modes occur with a maximum at 2933 cm^{-1}. Due to the weak signal-to-noise ratio usually on collagen fibre, the position of weaker vibrational bands cannot be accurately determined. However, main band positions are in agreement with published spectra for collagen (Rygula et al., 2013), but are not only characteristic for collagen proteins. Compared with other protein micro-residues found on other experimental stone tools, the upshifted position of collagen amide I band and its lower relative intensity might potentially be useful to identify this specific protein (Fig. 4.6, D**)**. But on a practical level, variation in these spectral features for different collagen micro-residues found on experimental artefacts as well as weak signal-to-noise ratio with green laser excitation (532nm), render collagen not easy to specifically be recognised among others proteins using Raman spectroscopy. Indeed, the dependence of collagen fibrils orientation on Raman spectra have been observed (Bonifacio et Sergo, 2010). However, collagen fibrils are quite distinctive in appearance by their long thin fibre aspect under optical microscope (Fig. 4.6, A, B, C**),** and often found in high numbers or even in bundles. So this particular aspect, together with a Raman protein spectral fingerprint (Fig. 4.6, D), will be enough to recognise these micro-residues as collagen. Because of this difficulty, when collagen is not found as fibrils but as amorphous individual residues, or smeared collagen, it would be quite difficult to recognise as such, and to distinguish from other protein micro-residues in Raman spectroscopy. However, collagen can be identified securely when analysed in bone (Chapter 4, section 4.5.2) as it's composing its main proteinaceous material.

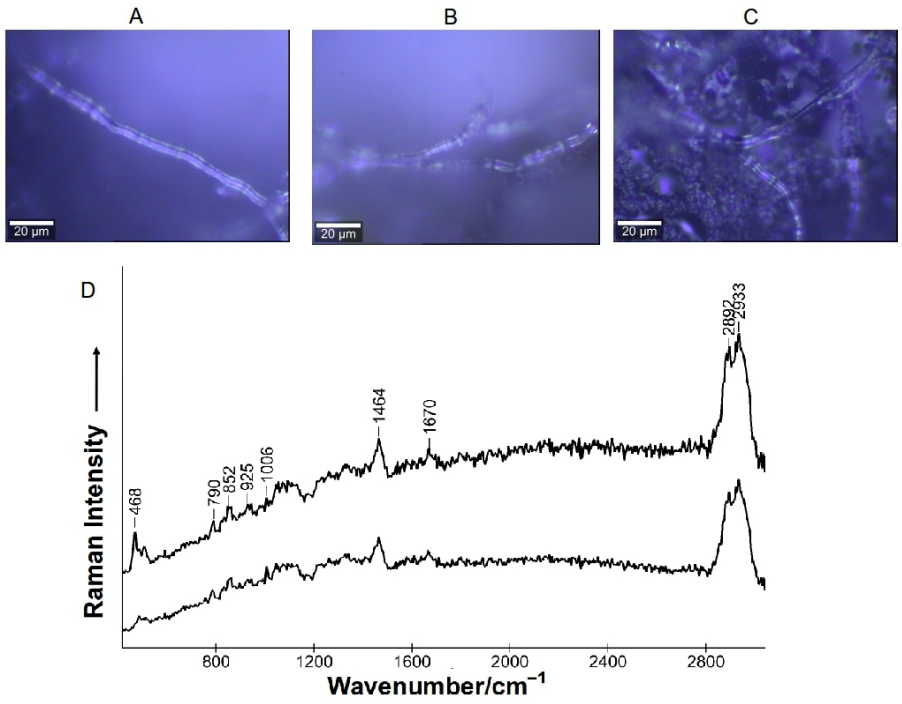

Figure 4.6: Collagen fibrils analysed on experimental artefact X309: Images (A-C) and two Raman spectra (D).

Animal material processing using experimental stone tools produced also protein micro-residues (Table 4.1**).** Compared to plant protein (Fig. 4.7), these micro-residues weren't associated with a clear distinct spectral signature. This situation is probably arising from a lack of signal-to-noise ratio obtained generally with protein micro-residues, which prevents the observation of weak vibrational bands, which could allow to distinguish between different types of proteins. As a consequence, the detection of protein micro-residues on stone artefacts will be rather non-specific of a particular plant or animal and have to be determined by other techniques oriented to protein analysis (e.g., Cross-over Immunoelectrophoresis (CIEP) (Hogberg et al., 2009).

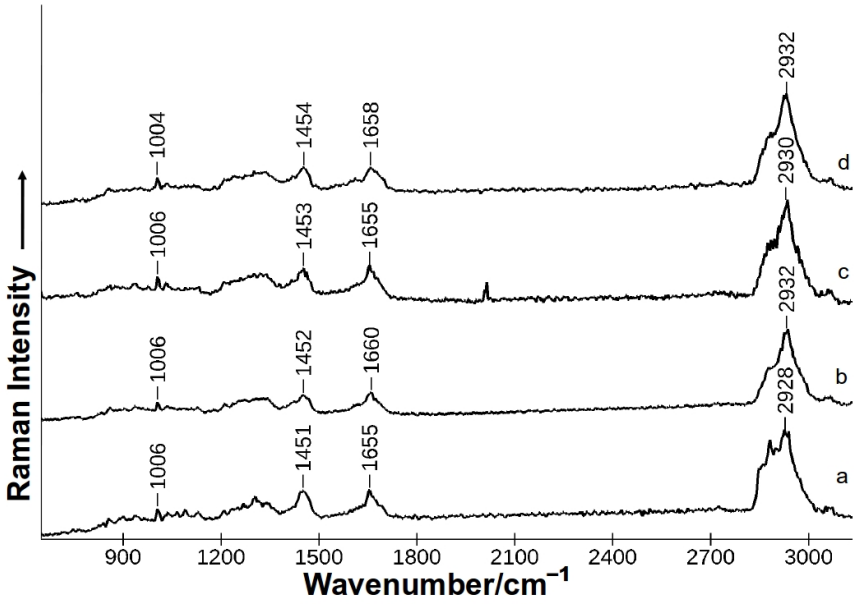

Figure 4.7: Protein residues analysed from different materials on experimental artefacts: Scraping typha (X150) (a), sawing black palm (X86) (b), scraping deer skin (D3) (c), scraping kangaroo skin (X230) (d).

Artefacts X284 (cow bone) and X290 (possum skin) produced also numerous individual and smeared saturated fatty acids (SFA) (Chapter 3, section 3.5). The spectrum is typical for SFA (Chapter 4, section 4.2). These SFA micro-residues sometimes show variations in relative band intensities and small spectral differences between different materials, (e.g., plant or animal), but often too slight to allow systematic recognition in all background noise conditions (Fig. 4.8**)**, as found for protein micro-residues (Fig. 4.7), SFA micro-residues will remain unspecific of any particular species of animal or plant in Raman spectroscopy. The reason for this differs from the problem of low signal-to-noise for proteins as SFA spectra have good signal-to-noise ratios which makes it possible to observe weak vibrational bands. However, SFA micro-residues on the archaeological tools showed very little variation (except those from originated from fresh handling, (Chapter 3, section 3.2.3). This lack of variation between SFAs deposited by processing different materials can be explained as follows: Firstly, the Raman spectra are dominated by bands originating from palmitic, stearic and myristic acids, the main components of plant and animal material, obscuring bands from less concentrated components, which can be more characteristic of a particular plant or animal. Secondly, SFA micro-residues may be end products of degradation of fatty acids originally present on the

tools 30 years ago. Finally, Raman signal is known to be strongly dependent on molecular orientation, hence SFA solid state structure and molecular packing is likely to have a greater influence on Raman spectra than slight variations in lipid composition (Motoyama, 2012). However, abundance and association with other specific key micro-residues (bone, plant fibre) can help to relate them to the processing of a particular material.

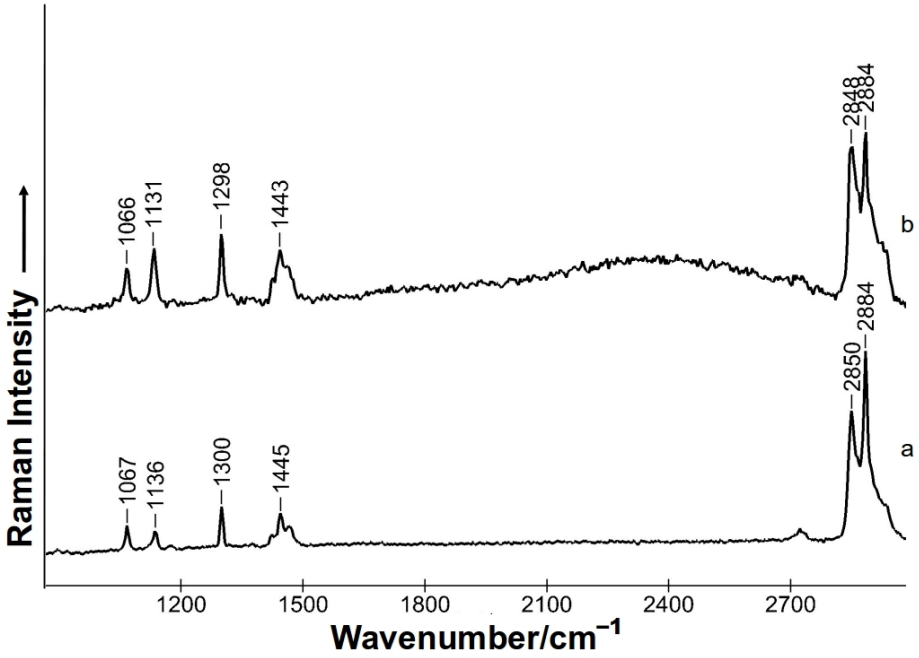

Figure 4.8: Saturated fatty acids analysed on X107 (bamboo cutting) (a), X290 (possum skin scraping) (b).

Animal materials tend to generate far higher amounts of SFA individual micro-residues and especially extended surfaces of smeared SFA micro-residues (Fig. 4.9**)** compared to plant materials. Smeared areas located on polish showing oriented striations can often be observed (Chapter 3, section 3.5), indicating their relation to stone tool use (Fig. 4.9, B**)**. Smeared aspect of these micro-residues indicate that pressure was applied on the worked material that transferred it on to the stone surface and parallel striations indicate the directionality of the working movement. It should be noted that these striations are found always strictly parallel and located on the polished area covered by smeared residues, contrary to the divergent striations (like a field line) arising from natural fractures found on the smooth glossy mineral background.

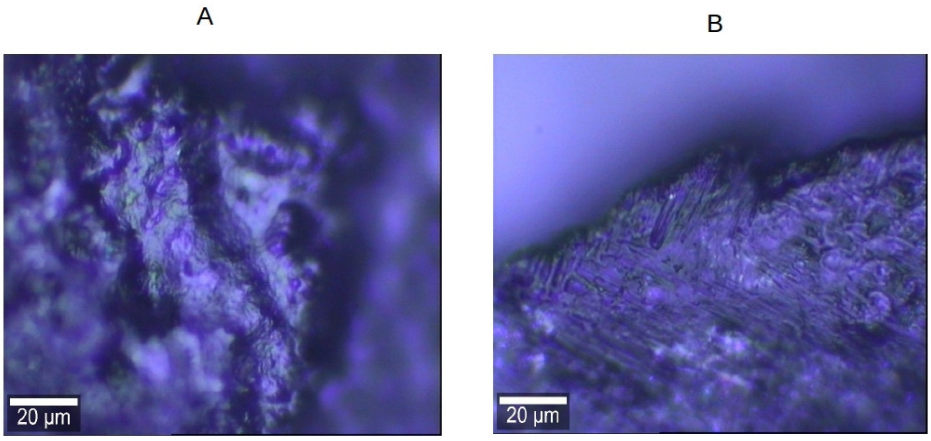

Figure 4.9: SFA smeared areas on X290 (A), SFA smeared area on X284 with presence of striations (B).

Another micro-residue of potential interest for archaeology, analysed in this collection, was 30 year old dried blood (Fig. 4.10, A-B). Blood is a potential key residue to be found on prehistoric artefacts. Indeed, blood had been successfully identified using Raman spectroscopy in the 5300 year old Iceman's tissue samples (Janko et al., 2012), that illustrates that this particular protein can be preserved for thousands of years. Raman spectra show distinct bands at 1588, 1359, 1316, 1228, 1132, 1001 and 752 cm^{-1}, which could be all assigned to vibrational modes of porphyrin which is a major unit in haemoglobin (Asghari-Khiavi et al., 2009) (Fig. 4.10, C, b**)** and are consistent with Raman bands observed for fresh blood (Fig. 4.10, C, a, D**)**. However, it is interesting to note that in analysis of blood on X157 experimental artefact, the spectrum obtained is arising from resonance Raman effect (Chapter 2, section 2.1.1.2). On Raman spectrum of porphyrin with 532 nm excitation, no main protein vibrational bands are observed and in particular not the most intense amide usually observed around 1660 cm^{-1} (Rygula et al., 2013), because of the fluorescence background, and low protein signal in comparison with strong intensity enhancement on porphyrin pigment. Because of this resonance effect on porphyrin, being an organic pigment absorbing in 500-560 nm visible light range, Raman spectroscopy using green visible laser excitation can be a powerful probing tool for ancient blood in selectively enhancing its specific porphyrin unit (Spiro and Strekas, 1974; Wood and McNaughton, 2002).

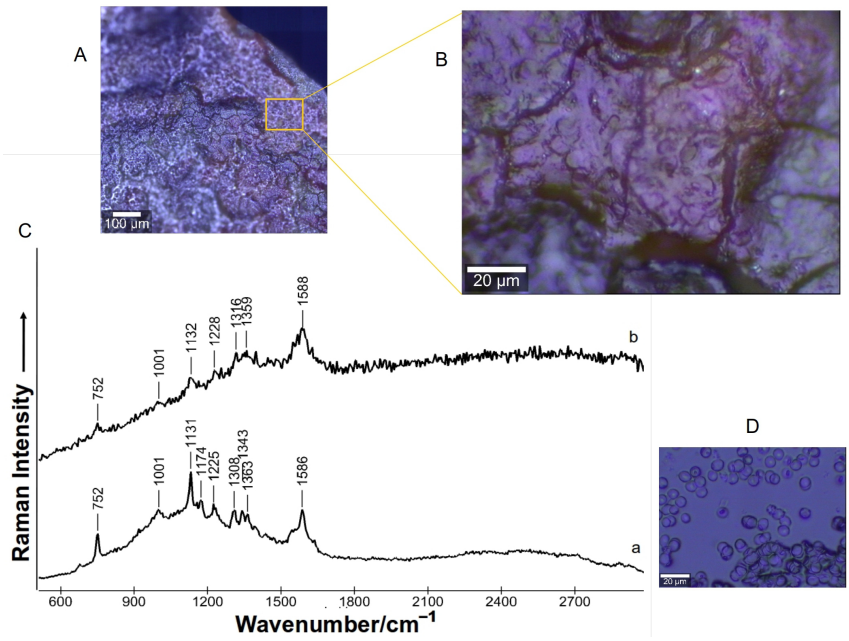

Figure 4.10: 30 year old dry human blood analysed on experimental artefact X127, X20 microscope objective (A), image of cracked blood smeared surface detail showing apparent blood cell, X50 microscope objective (B), Raman spectrum obtained on fresh blood (C, a), Raman spectrum obtained on blood on experimental artefact X127 (C, b) (532nm excitation), image of fresh blood cell deposited on microscope glass slide, X50 microscope objective (D).

Examining the results from the set of micro-residues analysed on artefacts from dated collection (Table 4.1**)**, identifying stone tool use is fairly easy, if the majority of significant micro-residues are specific, like plant fibre, starch or bone. But other micro-residues with a non-specific Raman signature like saturated fatty acids or proteins, can arise either from animal or plant sources. In that case, their relative abundance, and association with other micro-residues can be useful to sort out which kind of material was processed by the tool.

For example, I found often high abundance of protein on stone tools used on plant and this abundance of protein can be an indicator of plant working, even in the absence of plant fibres on some aged experimental artefacts (Table 4.1**).** Moreover, these proteins are found among a diversified set of others micro-residues as proteins with calcium nitrate, mixes of protein and SFA, and starch grains (Table 4.2).

In contrast, micro-residues found on stone tools from new experiments are always easier to interpret (Chapter 4, section 4.5) as key micro-residues like plant fibres are always found in great numbers on experimental artefacts used on plant. On the other hand, on artefacts which worked on animal, animal proteins can be recognised mainly by the distinct shape of collagen

fibril. Bone, SFA or collagen are always found in higher abundance for bone, skin or meat working respectively. Stone tools which worked animal have a more limited range of unspecified micro-residues as mixed residues of protein with SFA or protein with calcium nitrate was not detected on animal processed artefacts. This contrast in micro-residue sets can be critical to evaluate plant working tools in the case of low preservation of plant fibre.

Table 4.2: Summary of micro-residues found on stone tools from an old experimental collection

Material worked	Relative abundance of micro-residue types
Bone	Bone + Collagen > SFA >> Protein
Skin	SFA/UFA >> Collagen fibre >> Protein
Meat	Collagen fibre, protein >> SFA
Plant	Plant fibre, protein, protein + SFA, protein + calcium nitrate, SFA, starch grain

4.5 Raman analysis of experimental artefacts used in targeted experiments

Targeted new experiments were undertaken to compare results with those found on prehistoric artefacts from Liang Bua and Denisova Cave (Chapters 5 and 6). In these experiments, stone types similar to those found at these sites were used to work plant and animal materials to allow future use-wear and polish comparisons. However, in this study, we have concentrated on micro-residue analysis. The plant materials processed with flakes made of Denisova Cave and Liang Bua site rocks, were investigated (Table 4.3). For animal materials, a set of experiments on fallow deer bone and skin (Table 4.3) were undertaken to get a better understanding of lipid micro-residues found on Denisova Cave artefacts (Chapter 5, section 5.3.3). Local material from Flores, Indonesia or South Siberia, Russia was used when available, but other materials was also collected in Australia. As my aim was to access broad category of material, species collections was not critical at this stage. Moreover, as underscored previously, Raman spectroscopy is not a spectroscopic technique fitted to identify particular animal or plant species, especially when they are at different stages of degradation.

Table 4.3: Targeted new experiments

Artefact	Material worked	Aging time	Use	Duration	Types of micro-residue analysed	Frequency
D1	Fresh Fallow deer (*Dama dama*) bone	3 months	Cleaning, extracting bone marrow and scraping	5 min	Smeared bone + Collagen Bone + Collagen Smeared mixed SFA/UFA	Very common Very common Uncommon
D2	Fresh Fallow deer (*Dama dama)* jaw bone	3 months	Sawing	5 min	Bone + Collagen Smeared bone + Collagen Smeared mixed SFA/UFA + Bone Smeared mixed SFA/UFA Protein	Very common Very common Uncommon Uncommon Rare
D3	Fresh Fallow deer (*Dama dama)* skin	3 months	Scraping	10 min	Smeared mixed SFA/UFA Individual mixed SFA/UFA Collagen fibre (protein) Protein	Common Common Uncommon Uncommon
D4	Fern (*Athyrium filix-femina)*	2 weeks	Cutting	3 min	Plant fibre Carotenoid Smeared carotenoid	Common Common Common
D5	Rowan (*Sorbus aucuparia)*	2 weeks	Cutting and Scraping	3 min	Wooden fibre Smeared wooden fibre Oxalate Individual SFA	Common Common Rare Rare
D8	Siberian pine (*Pinus sibirica*)	1 month	Cutting and Scraping	20 min	Smeared wood Wooden fibre Plant fibre Smeared resin	Common Common Uncommon Uncommon
D9	Nettle (*Urtica dioica)*	9 months	Cutting	5 min	Plant fibre Smeared mixed SFA/UFA Individual mixed SFA/UFA	Common Common Common
D10	Birch bark (*Betula pendula)*		Cutting	5 min	Smeared wood Wooden fibre Fluorescent plant fibre	Common Common Uncommon
D11	Fresh Goat (*Capra hircus)* skin	2 months (5 ºC)	Scraping	10 min	Smeared protein Protein Smeared mixed SFA/UFA Individual mixed SFA/UFA Collagen fibre Wooden material Plant material	Common Common Uncommon Uncommon Uncommon Rare Rare
B1	Indonesian bamboo (*Bambuseae sp.)*	1 year	Cutting	5 min	Gramineae fibre (low cellulose + lignin) Smeared gramineae Starch grain Cellulose fibre Individual mixed SFA/UFA Smeared mixed SFA/UFA Smeared Starch Oxalate Protein	 Very common Common Common Common Uncommon Uncommon Rare Rare Rare
B2	Indonesian bamboo (*Bambuseae sp.*)	1 year	Cutting and scraping	10 min	Gramineae fibre (low cellulose + lignin) Smeared gramineae Starch grain Cellulose fibre Individual mixed SFA/UFA Smeared mixed SFA/UFA	Very common Common Common Common Uncommon Uncommon
B3	Fountain grass (*Pennisetum setaceum*)	1 day	Cutting	3 min	Gramineae fibre (low cellulose + lignin) Smeared gramineae Starch grain Oxalate Calcite	Very common Common Uncommon Uncommon uncommon
B4	Lomandra (*Lomandra longifolia*)	1 day	Cutting	3 min	Plant fibre (cellulose + lignin) Smeared plant fibre (cellulose + lignin) Plant material (lignin) Starch grain Oxalate	Very common Common Uncommon Uncommon Uncommon
B5	Tussock grass (*Poa labillardiere*)	1 day	Cutting	3 min	Plant fibre (cellulose + lignin)	Very common

					Smeared plant fibre (cellulose + lignin) Individual mixed SFA/UFA Smeared mixed SFA/UFA Plant material (lignin) Starch grain Oxalate	Common Uncommon Uncommon Uncommon Uncommon Uncommon
B6	Fresh local bamboo (*Bambuseae sp.)* (Australia)	1 day	Cutting	5 min	Gramineae fibre (low cellulose + lignin) Smeared gramineae Carotenoid Smeared carotenoid Starch grain Smeared SFA + Plant material Individual mixed SFA/UFA Smeared mixed SFA/UFA Oxalate	Very common Common Common Common Uncommon Uncommon Uncommon Uncommon Uncommon
B7	Dry local bamboo *(Bambuseae sp.)* (Australia)	1 day	Cutting	5 min	Gramineae fibre (low cellulose + lignin) Smeared gramineae Individual mixed SFA/UFA Smeared mixed SFA/UFA	Very common Common Uncommon Uncommon

4.5.1 Plant materials

Plant materials were processed using experimental flakes made of typical rocks (e.g., silicified tuff, flint) which were used by prehistoric hominids at Liang Bua (Table 4.3, B1-B7). This set of experiments was undertaken to identify a particular plant fibre and micro-residues composed of cellulose and lignin found on Liang Bua artefacts (Chapter 6, section 6.2.2.3 and section 6.2.2.4). Comparing different types of plants, lignin bands present in range 1600-1660 cm^{-1} can be informative for identifying some categories of plants (Fig. 4.11**).** Indeed, the very strong aryl ring stretching band from lignin at 1608 cm^{-1} is a clear doublet with a second peak at 1631 cm^{-1} and another band could be observed at 1173 cm^{-1} (Fig. 4.11, b**)** which according to (Wang et al., 2014) is characteristic of grass plant species, including bamboo, containing higher amounts of hydroxycinnamic acids (ferulic and p-coumaric acids) in cell walls (Takei et al., 1995; Ram et al., 2003). In contrast, wooden material like mulga wood (*Acacia aneura*) (Fig. 4.11, a), has a lower intensity lignin aryl stretching vibration at 1599 cm^{-1} accompanied by a upshifted shoulder peak at 1658 cm^{-1}, assigned to coniferyl alcohol and conifer-aldehyde (Agarwal et al., 1999). Wood and grass material seems to have generally higher intensity lignin bands compared to cellulose vibrational bands (369-377 cm^{-1}, 1092-1125 cm^{-1}), but this relative difference is to be considered cautiously as species of plants can have variable contents of lignin, also depending on the part of the plant (leave, stem, root). Other plants, like lomandra (*Lomandra longifolia*) (Fig. 4.11, c) show an intermediate situation between grass and wood with a more balanced ratio between cellulose and lignin intensity and 1638 cm^{-1} band lignin position.

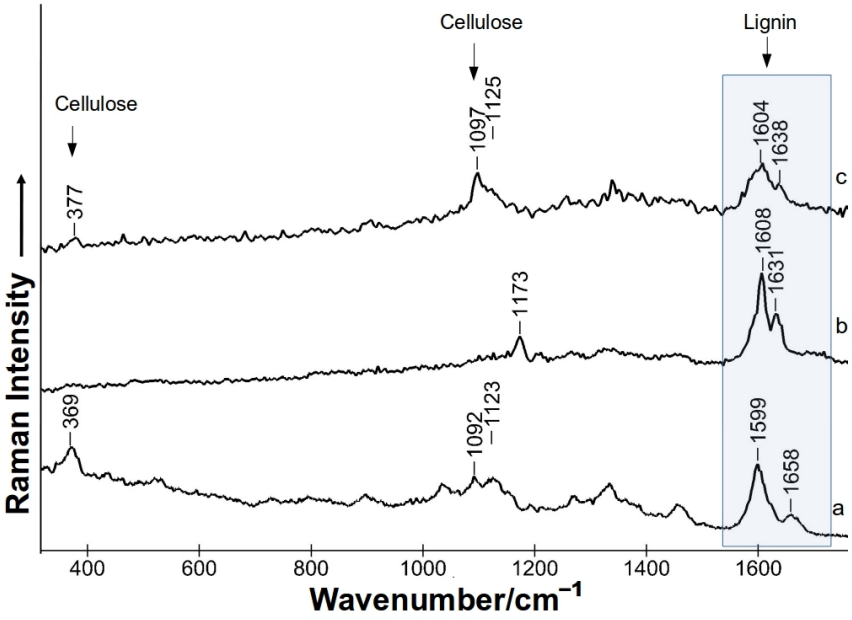

Figure 4.11: Mulga wood (*Acacia aneura*) (a) compared to experiments on Indonesian bamboo *(Bambuseae sp.)*, artefact B1 and B2 (b) and experiment on Lomandra (*Lomandra longifolia*) artefact B4 (c).

Plant materials were also analysed on experimental flakes made of typical rocks used by prehistoric hominin at Denisova Cave (Table 4.3, D4-D10). These stone tools were used to process plant material to reconstruct realistic prehistoric activities like shaping and shaving a spear shaft in Siberian pine (*Pinus sibirica*) (Fig. 4.12, A), cutting rowan (*Sorbus aucuparia)* branches (Fig. 4.12, B), or incising birch tree (*Betula pendula)* to collect a strip of bark (Fig. 4.12, C-D).

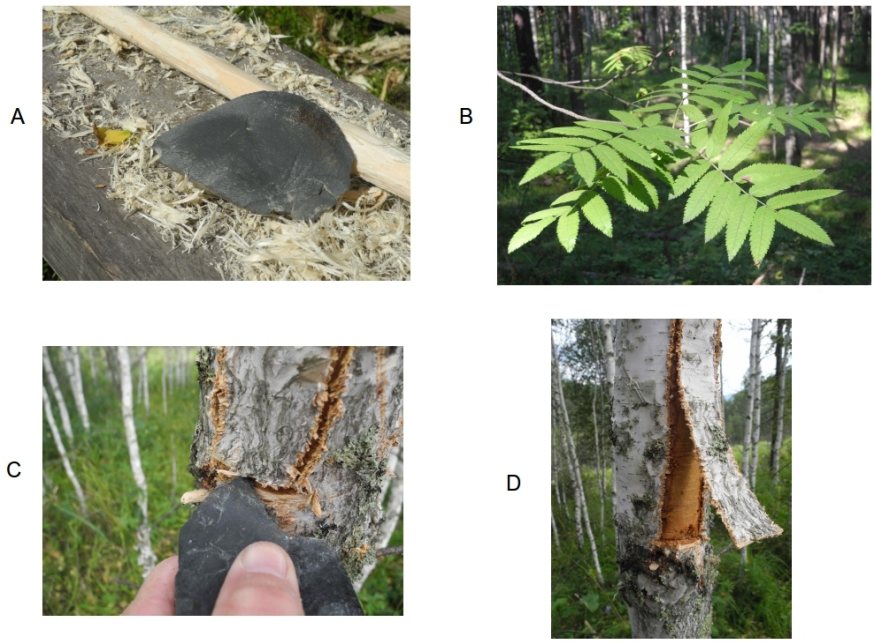

Figure 4.12: D8 experimental artefact used to craft a spear in Siberian pine (*Pinus sibirica*) (A), Rowan (*Sorbus aucuparia)* branch used for experimental artefact D5 (B), incising birch (*Betula pendula)* bark to collect bark strip with artefact D10 (C), almost detached strip of bark (D).

These experiments provided an opportunity to start developing a spectral database, not of plant fibres, but also of other types of micro-residues like carotenoid, resin, starch grains, SFA (saturated fatty acids), UFA (unsaturated fatty acids), and oxalate crystals.

A carotenoid pigment was identified on experimental tools D4 (fern) (*Athyrium filix-femina)* and fresh local bamboo *(Bambuseae sp.)* (Table 4.3, B6). These residues occurred as either individual or smeared micro-residues. Main carotenoid bands are rather easy to recognise and centred at 1525 (ν1, C=C stretching), 1162 (ν2, C-C, stretching), 1101 cm^{-1} (ν2 C=CH, deformation mode) despite a strong fluorescent background (Fig. 4.13, C). (Merlin, 1985). This material was only observed and analysed on recent experiments and not on the older 30 year old experiments.

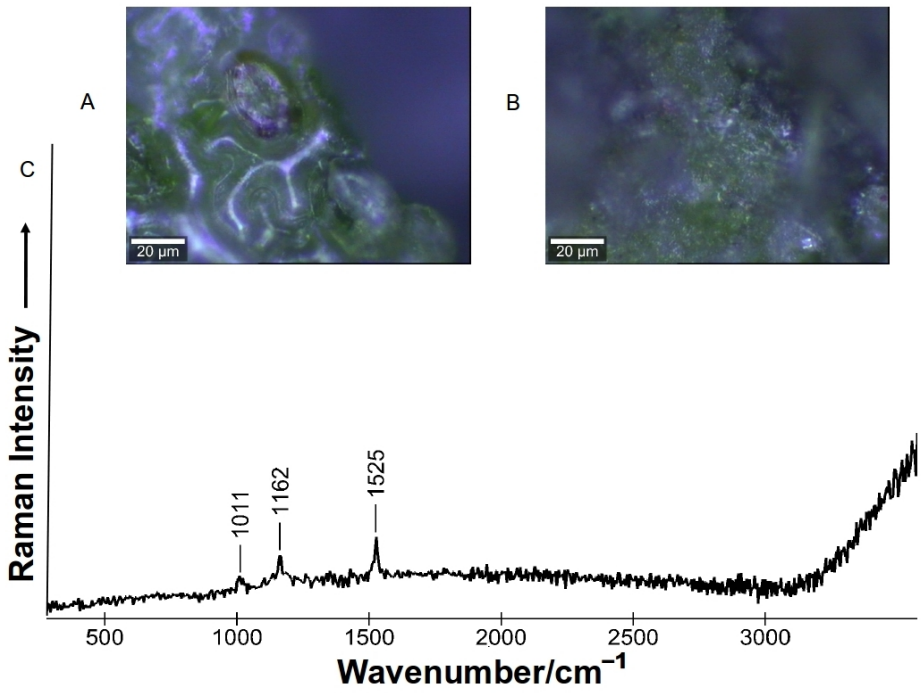

Figure 4.13: D4 fern (*Athyrium filix-femina)* experiment micro-residues, Individual (A), smeared (B), and carotenoid Raman spectrum (C).

On D8 (*Pinus sibirica*) experimental tool, smeared wooden material and resin was successfully analysed (Fig. 4.14**)**. These two fragile materials are difficult to analyse using Raman spectroscopy because of their high sensitivity to laser beam heating and requires low laser power measurements (Chapter 4, section 4.3.2). Moreover, the noise from fluorescence and the mineral background render the task even more challenging, even on fresh experimental stone tools. Wooden material has typical cellulose and lignin fingerprints (Figs. 4.14, A, a and 4.11)**.** Resin display similar bands centred around 1600 cm^{-1} but with a upshifted maximum at 1611 cm^{-1} , and specific vibrational bands could be observed at 1447 cm^{-1} and 711 cm^{-1} (Fig. 4.14, B, b**)** (Daher et al., 2010) (Chapter 4, section 4.3.2). Additionally, the absence of cellulose bands is helpful to distinguish at first glance resin material from wooden or plant material. On smeared residues, the intensity of main vibrational bands of these two materials can be also mapped to observe their spatial distribution on stone tool edges and surfaces (Fig. 4.15**).**

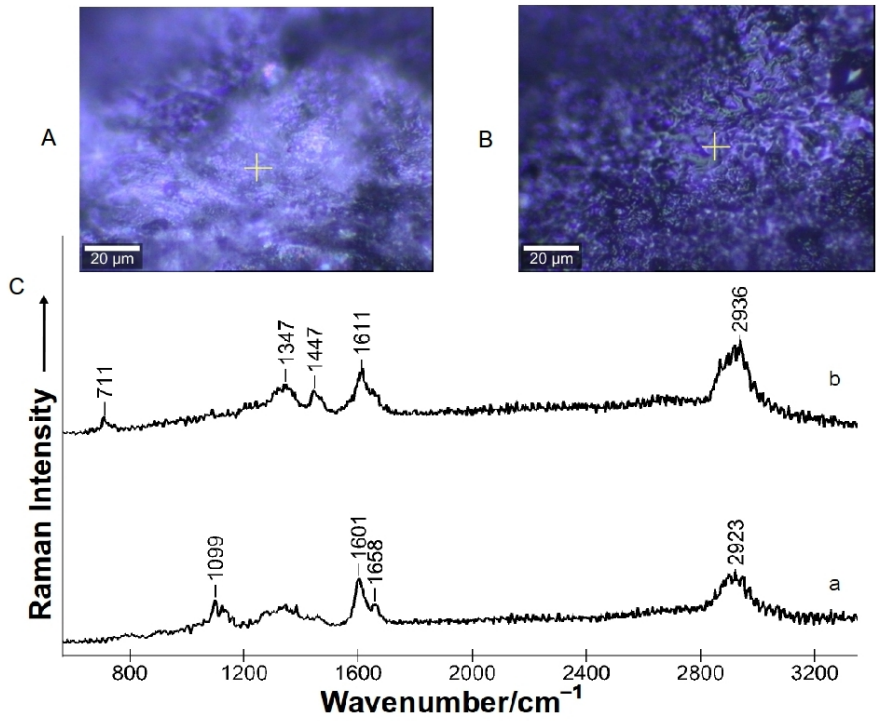

Figure 4.14: D8 experimental tool used to scrape Siberian pine (*Pinus sibirica*): Smeared wooden material (A), smeared resin material (B), smeared wooden material Raman spectrum (C, a), smeared resin material Raman spectrum (C, b).

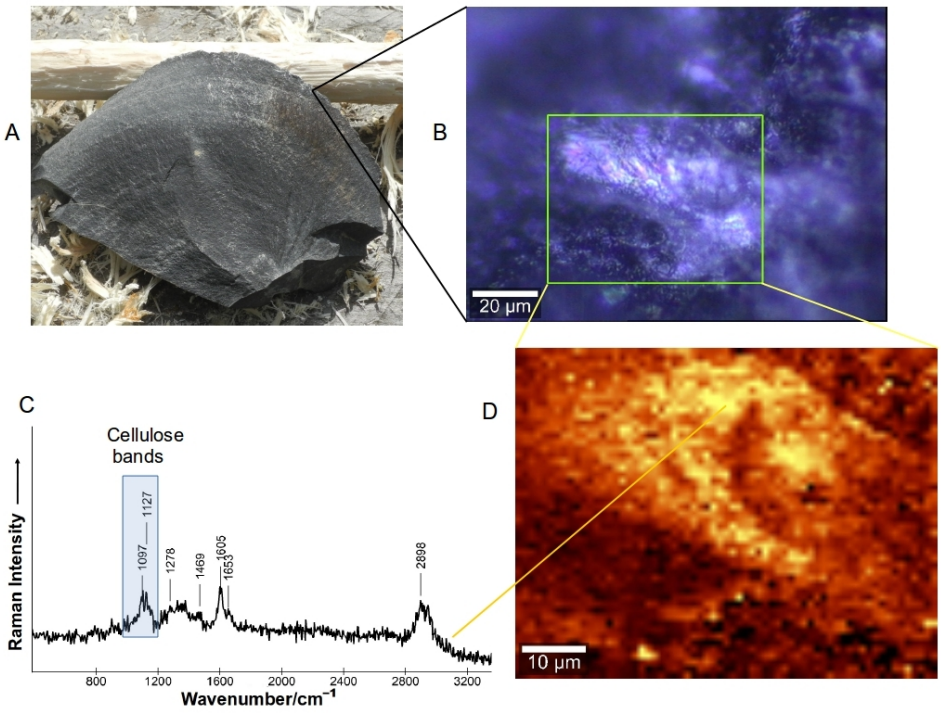

Figure 4.15: D8 stone artefact used to scrape Siberian pine (*Pinus sibirica*) (A), smeared wooden material micro-residue (B), smeared wooden material Raman spectrum (C), spectral mapping image obtained with cellulose bands integrated intensity (D).

4.5.2 Animal materials

Skin and bone from a Fallow deer (*Dama dama*) were obtained from a three months old carcass and worked with three stone tools. One tool (Table 4.3, D1) was used to clean bone and extract marrow from it, another tool D2 was used to saw the jaw bone, and a third one (D3) was used to scrape fresh deer skin (Fig. 4.16**)**.

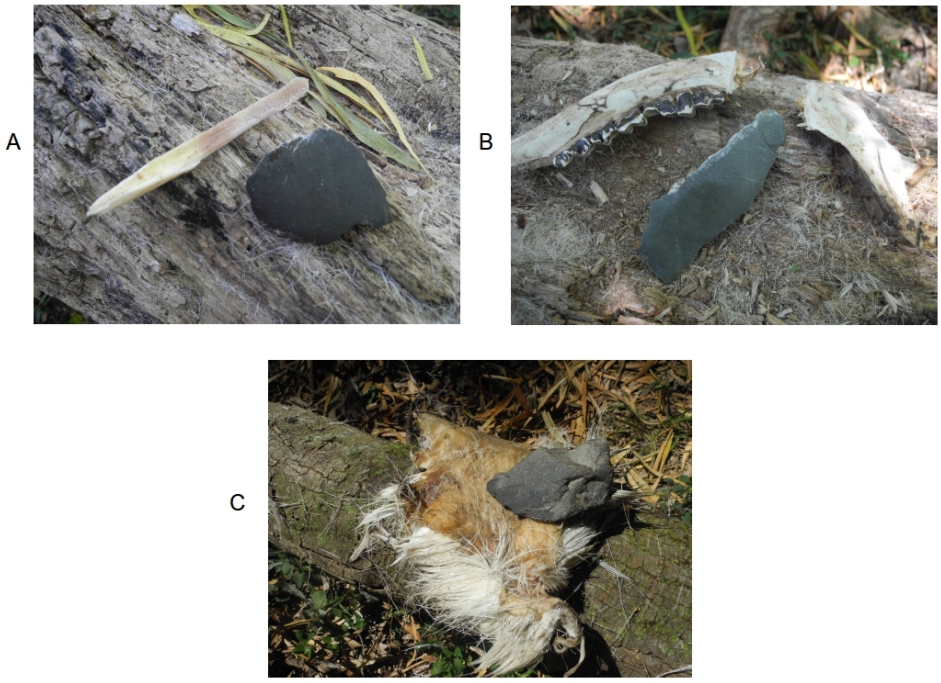

Figure 4.16: Deer bone scraping with experimental artefacts D1 (A), deer jaw cutting with experimental artefact D2 (B), deer skin scraping with experimental artefacts D3 (C).

The micro-residues detected on experimental stone tools are summarised in Table (4.3). Bone and smeared bone micro-residues occur commonly on experimental artefacts used on deer bone (Table 4.3, D1, D2) (Fig. 4.17). Raman spectrum is typical of carbonated hydroxyl apatite which is the main component of animal bone (Chapter 4, sections 4.6.2 and 4.7) and shows the presence of collagen by the appearance of protein typical fingerprint (Fig. 4.17, D, b-c). It should be noted that collagen protein signal in bone is distinct from collagen fibrils described in section 4.3.2 (Fig. 4.6**)** and that amide I band is not upshifted at 1670 cm^{-1} position as for collagen fibrils but shows some position variation down to 1660 cm^{-1}, similar to other unspecific proteins encountered. As already observed on collagen from experimental old collection (Chapter 4, section 4.4.2), these variations can be probably explained by collagen alteration

and orientation (Bonifacio et al., 2010). Additionally, collagen is not the only type of protein present in bone and other molecules like (e.g., osteonectin) (Termine et al., 1981) which link collagen to the apatite mineral structure can contribute to the spectrum to a lesser extent.

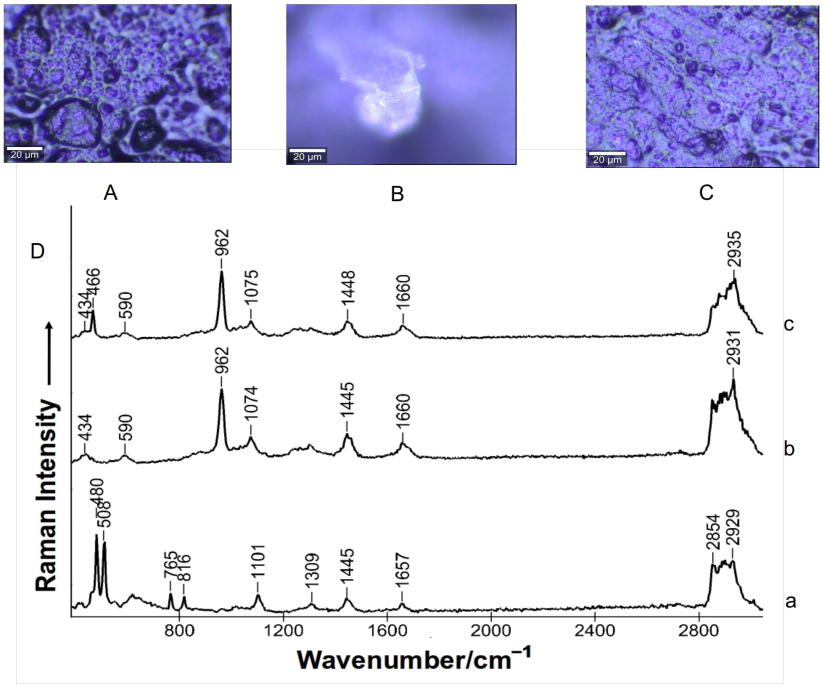

Figure 4.17: Smeared bone micro-residue on D1 (A), bone individual micro-residue on D1 edge (B), smeared FA micro-residue on D1 (C), Raman spectrum of smeared mixed SFA/FA on D1 with feldspar rock background (D, a), Raman spectrum of individual bone micro-residue on D1 (D, b), Raman spectrum of smeared bone on D1 with quartz rock background (D, c).

In addition to bone apatite, individual and smeared micro-residues with unsaturated fatty acid (UFA) content was found second in abundance on stone tools used on bone. In contrast, on experimental stone tool used on deer skin (Table 4.3, D3) the situation is different, with common individual and smeared mixed SFA/UFA micro-residues, as bone and collagen fibres are only uncommon in that case**.** The difference with SFA (saturated fatty acid) identified on older experimental tools (Chapter 4, section 4.3, Fig 4.8**)** is that mixed SFA/UFA micro-residues have unsaturated fatty acid content which is indicated by the presence of sharp bands at 1657 and 3011 cm^{-1} (C=C stretch and =C-H stretching) respectively and a shoulder centred at 1260-1270 cm^{-1} (=C-H deformation) (De Gelder et al., 2007; Czamara et al., 2015) (Fig. 4.18). The presence of another C=C stretch band centred at 1679 cm^{-1} suggests the presence of a trans isomer (Czamara et al., 2015) and a band at 1610 cm^{-1} might be attributed to a conjugated cis isomer mode with multiple C=C-C=C modes (Melchiorre et al., 2015) (see Chapter 5, section 5.3.3 for more UFA spectral details, Figs. 5.14 and 5.15) (Bordes et al.,

2018).

Smeared SFA/UFA residues can be spatially localised by Raman mapping of the integrated intensity of the main C-H streching bands (Fig. 4.19). The Raman spectra of these SFA/UFA micro-residues show very little variation between different materials worked and can therefore not be used to distinguish between plant or animal. Indeed, the main components of SFA (palmiric, stearic, myristic acids) and UFA (linoleic, oleic acids) dominate the Raman spectral features, making the detection of other common fatty acids (SFA or UFA) that might be diagnostic for specific materials very difficult. The consequence of this lack of spectral variation in our study is that SFA/UFA micro-residues cannot be related to a particular plant or animal material, and is then be considered as an unspecific type of micro-residue, if only considering their Raman spectrum. However, in a similar way to SFA micro-residues, considering these micro-residues in association within a set, including other specific micro-residues like bone, or plant material could be more informative. These mixed fatty acid micro-residues with unsaturated fatty acid content were identified both on artefacts from Denisova Cave and Liang Bua and are further discussed in chapter 5 (section 5.3.3) and chapter 6 (section 6.3.2.4).

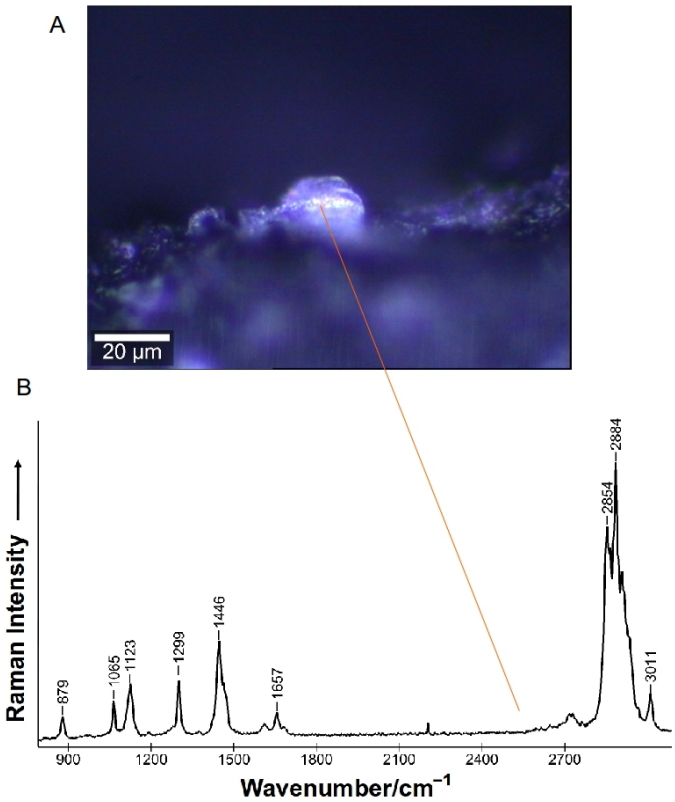

Figure 4.18: Image of individual mixed SFA/FA micro-residue found on D3 (A) and Raman spectrum (B).

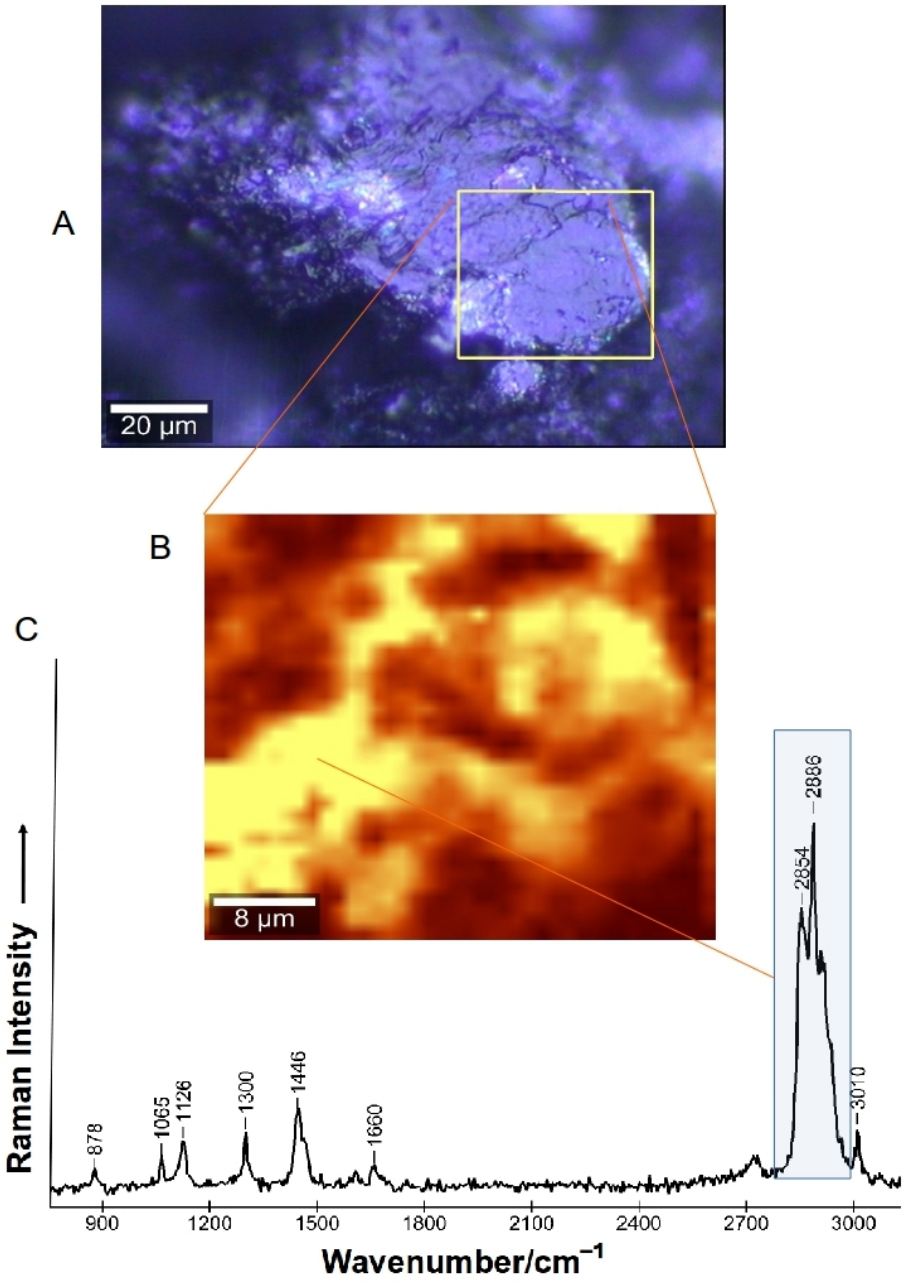

Figure 4.19: Raman spectral imaging of smeared mixed SFA/UFA on D3 proximal left edge. Image of smeared mixed SFA/UFA on D3 proximal left edge (A), integrated intensity of the most intense Raman bands (C-H stretching) was used for mapping (B), typical SFA/UFA Raman spectrum obtained on this smeared micro-residue (C).

In contrast with aged stone tool experiments (Table 4.1), the use of new experimental tools is easier to determine, and differences between plant or animal use is obvious because generally

the whole set of micro-residues can be found on their surfaces and edges (Table 4.3). Furthermore, macro-residues are present with distinctive identification features (bundle of fibre for plant or bone fragment and collagen fibrils bundles for animals) which can be observed directly by optical microscope. Nevertheless, I followed the same approach to consider relative abundance and variation in specific and unspecific micro-residues as for aged stone tools. For artefacts used to process animals the same relative abundance of residues was found for bone and skin working (Table 4.4). The only difference is the nature of lipids analysed which are partially unsaturated. For plants, a predominance of plant fibres makes the identification of plant use quite straightforward. Additionally, in some cases, carotenoid pigments, starch grains and oxalate crystals define unambiguously this set of stone tools as used to process plant materials. Comparing these results with the results of the aged tools collection, leads to the following conclusions. Animal specific micro-residues like bone and lipids are still present, while plant specific micro-residues like plant fibre seems to have mostly disappeared and lipids are not as well preserved as for animal residues. Therefore it's seems useful to not only rely on plant fibre presence, but consider also other micro-residues like abundance of protein, protein mixed with lipids and protein containing nitrate as additional indications for plant working.

Table 4.4: Summary of micro-residues found on stone tools from targeted new experiments

Material worked	**Relative abundance of micro-residue types**
Bone	Bone + Collagen > SFA >> Protein
Skin	SFA/UFA >> Collagen fibre >> Protein
Plant	Plant fibre >= SFA/UFA > Protein, starch grain, oxalate

4.6 Preservation and alteration experiments

4.6.1 Fatty acid preservation experiment

I undertook a few experiments to understand the aging process of fatty acid residues on stone flakes, in particular the relation between micro-residues with only SFA content and micro-residues with saturated and unsaturated fatty acid mixtures (SFA/UFA). For the first experiment, some pork fat was smeared on a stone flake similar to some stone tools found at Denisova Cave. The artefact was buried 5-10 cm underground for 3 months during the hot and rainy climate of an Australian summer. After one month the Raman signal from the pork fat was compared to a reference spectrum recorded before burial. To the naked eye, the initial aspect

of the fresh pork fat on the stone tool was a translucent layer covering, the whole surface coated by the fat (Fig. 4.20, A).

Initial Raman spectrum obtained on fresh pork fat shows a mix between unsaturated and saturated fatty acids as indicated by the presence of the unsaturated fatty acids band centred at 1658 cm^{-1} (Fig 4.21, A, c), a high frequency band at 3010 cm^{-1} (Fig 4.21, B, c), along with a shoulder band visible at 1267 cm^{-1}. Presence of a band centred at 1752 cm-1 (Fig 4.21, A, c) indicate that unsaturated and saturated fatty acids are present in the pork fat as components of triglycerides (Chapter 4, section 4.2). After one month, the same artefact was dug out and analysed again after cleaning with 10 s sonication to get rid of the attached sediment. Visible appearance of the pork fat had drastically changed. Most of it had probably been washed off or degraded by micro-organisms except a small area. One month aged fat had a white solid appearance distinct from its initial aspect. Raman analysis on this one month aged pork fat shows also a different spectral signature (Fig. 4.21, A, b). Raman spectrum shows the characteristic features of saturated fatty acids (see section 4.1), with three adjacent bands at 1462, 1444, 1423 $cm^{-1,}$ one sharp band at 1300 cm^{-1} and a three bands features with two prominent bands at 1132 and 1065 cm^{-1}. Furthermore the high frequency range shows also the characteristic features of saturated fatty acids with a strong sharp band at 2884 cm^{-1} and a shoulder band at 2850 cm^{-1} (Fig. 4.21, B, b). Nevertheless presence of a band at 1659 cm^{-1} and 3015 cm^{-1} still indicated the presence of unsaturated fatty acids (Chapter 4, section 4.2) in this aged fat residue, but the lower intensity of these bands indicate a smaller relative proportion of unsaturated fatty acids in the residue. Presence of triglycerids is also still indicated by a downshifted band at 1736 cm^{-1} perhaps indicating a change in fatty acid content. One aged pork fat content had been probably altered to triglycerids bearing fatty acids which lost theirs unsaturated bonds hence increasing the proportion of saturated fatty acid. The three months aged fat shows the same similar visual aspect as the one month aged fat but the covered area is even smaller (Fig. 4.20, B). Raman spectrum of this fat shows no fundamental spectral differences but the two bands marking unsaturated fatty acid are weaker, indicating that the degradation to saturated fatty acid is an ongoing process (Fig 4.21, A-B, a).

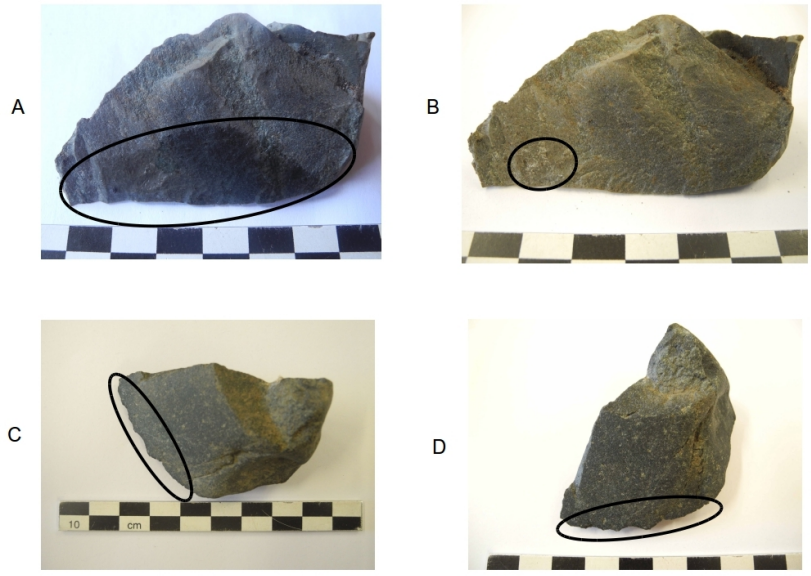

Figure 4.20: Image of experimental stone flake after working fresh fat on edge (A), reduced area of white pork fat observed after three months of burial (B). Image of deer skin scraping fresh experimental stone flake (C) and observed after three months of burial (D).

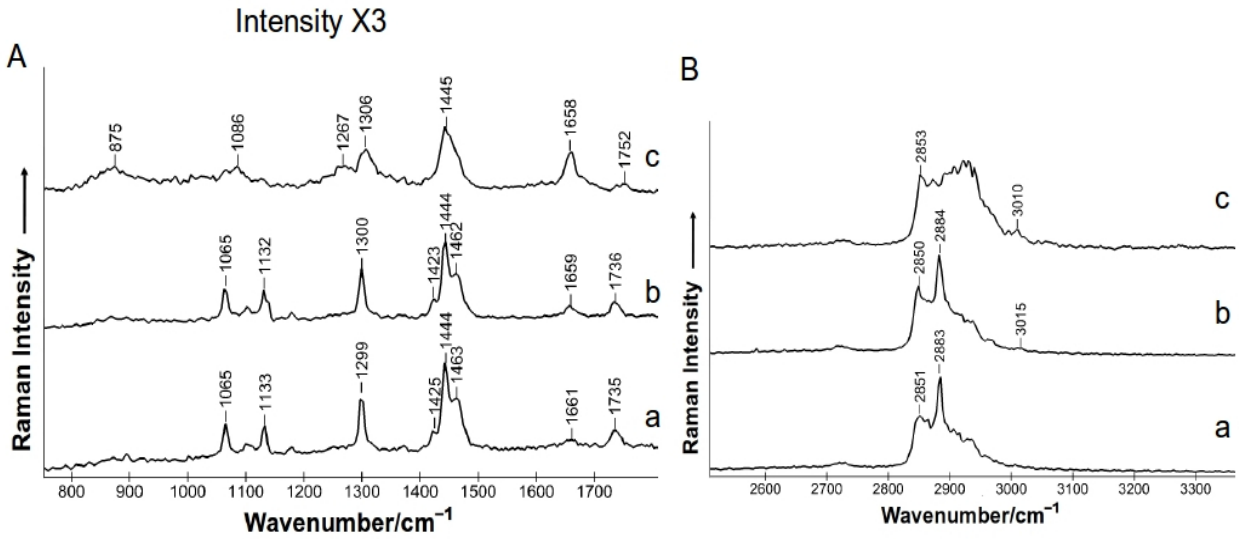

Figure 4.21: Raman spectrum of pork fat on an experimental stone flake (c), after 1 month (b), after 3 months (a). Low wavenumbers range (A) and high wavenumbers range (B).

In the the second experiment, artefact D3 (Chapter 4 part 4.5.2), which had been used on deer skin, was also buried to evaluate the aging effect on a different animal fat. This material was

deposited on stone flake by scraping the deerskin on a tree trunk outdoors, to recreate the context of a prehistoric activity (Fig. 4.16, C). This artefact was buried 10 cm away from the pork fat experiment and was also dug up and analysed by Raman spectroscopy after one and three months. On the initial stone flake, deer fat was observed as a darker area close to the working edge (Fig. 4.20, C). Under VLM, this micro-residue appears not only attached to the surface of the experimental flake but even smeared on it (Chapter 3, section 3.5). Initial Raman spectrum obtained on fresh deer fat shows a mix between unsaturated and saturated fatty acids (Fig. 4.22, A-B,c). Raman spectrum on one month aged deer fat shows no difference with initial fat, indicating excellent preservation of these smeared residues (Fig. 4.22, A-B, b). After 3 months, Raman analysis shows drastic change in deer fat residue spectrum (Fig. 4.22 A-B, a). Only characteristic features of free saturated fatty acids are visible with two main adjacent bands at 1463 and 1443 cm^{-1}, one sharp band at 1298 cm^{-1} and a three bands features with two prominent bands at 1133 and 1065 cm^{-1}. Furthermore the high frequency range shows also the characteristic features of free saturated fatty acid with a strong sharp band at 2882 cm^{-1} and a shoulder band at 2846 cm^{-1}. These two short experiments show that important variations in the degradation timing that can exist between different fatty materials during a short three months period. However, on long term, these results show that buried fatty residues tend to be altered toward fatty mixtures which contain always less proportion of unsaturated fatty acid. This result is coherent with the process of unsaturated fatty acid oxidation reported in literature (Regert et al., 1998).

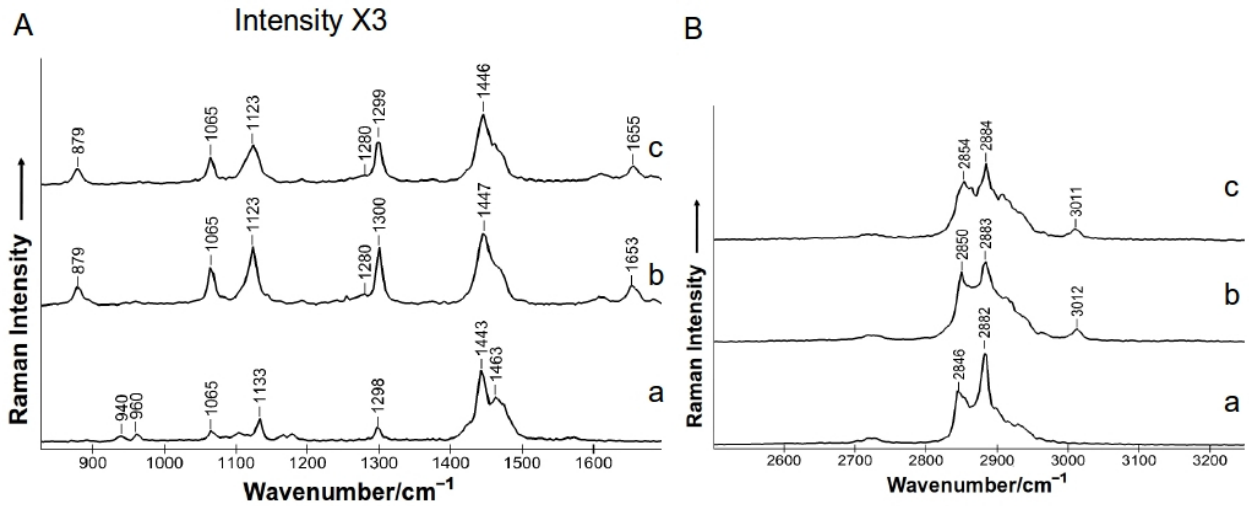

Figure 4.22: Raman spectrum of deer fat on experimental stone flake D3 (c), after 1 month (b), after 3 months (a). Low wavenumbers range (A) and high wavenumbers range (B).

4.6.2 Bone heating experiment

To understand better the origin and unusual Raman spectra of apatite micro-residues obtained on Denisova Cave and Liang Bua stone artefacts and in the sediment (Chapter 5 and 6), a simple bone heating experiment was undertaken. More over, burned bone is a potential key residue, which can be informative about hominid food consumption behaviour. Previous studies were undertaken on bone calcination using X-ray diffraction (Galeano et al., 2014) and FTIR spectroscopy (Lebon et al., 2008) and in a recent study Raman spectroscopy was used to investigate changes in heated bone (Gourrier et al., 2017), but only in the low temperature range (<250 ºC).

Bone fragments were heated at 300, 500 and 700 °C for 1 hour. Resulting samples were crushed with a mortar and pestle and analysed by Raman microscopy. Raman spectrum of dry bone before heating (Fig. 4.23, A) shows the typical spectrum of bone apatite with main apatite *v*1 band centred on 963 cm^{-1}, with FWHM (21 cm^{-1}) along with collagen Raman bands (Fig. 4.23, D, c) (Wopenka et al., 2005). Bone heated at 300 and 500 °C appears black and greenish under microscope due to the presence of amorphous carbon (Fig. 4.23, B). The Raman spectrum (Fig. 4.23, D, b) shows the disappearance of collagen and a downshift of the main apatite Raman band to 952 cm^{-1}. The bands at 1007, 1041, 1075 cm^{-1} are replaced by a single band centred at 1029 cm^{-1}. The apatite structure is still confirmed for heated bone by the positions of *v*2 and *v*4 vibrational modes respectively observed at 432 and 584 cm^{-1} (Wopenka et al., 2005), but these bands are observed slightly downshifted compared to unheated bone (Appendix I, table 1).
Moreover, apatite can be still distinguished from amorphous calcium phosphate (ACP) as the FWHM of the *v*1 mode is increased to between 20 and 27 cm^{-1} which is intermediate between the FWHM observed commonly for bone apatite (15-20 cm^{-1}) (Wopenka et al., 2005; Thomas et al., 2011) than for ACP, generally found over 33 cm^{-1} (Sauer et al., 1993; Grauw et al., 1996).

According to this observation, it seems that this particular Raman apatite signature probably reflects an abnormal disordered apatite structure due to the presence of degraded organic material originating from collagen and other proteins in the bone matrix. The presence of amorphous carbon is indicated by the broad bands centred at 1570 and ~1340 cm^{-1} known as the G (sp2 C-C bonds) and D (sp3 C-C bonds) bands respectively (Tzolov et al., 1993).

One author proposed that this downshift for the apatite *v*1 vibration mode results from laser heating of biogenic diagenetic apatite under green laser excitation (532nm) (Puceat et al., 2004). Finally, It could be noted that this spectrum is not depending of the colour of the apatite analysed (which can appear white, green or black) resulting from bone heating in 300 to 500 °C range. This observation is important as it confirms that the presence of altered organic material is not contributing to apatite Raman spectrum and that its depends only on apatite disordered structure which is the consequence of collagen content combustion.

Raman spectrum obtained for bone heated to 700°C is of a recrystallised pure white apatite (Fig. 4.23, C) with narrower vibrational bands. The main apatite band occurs at 965 cm^{-1} with two well defined bands at 1050 cm^{-1} and 1078 cm^{-1}. An additional band is visible at 3575 cm^{-1} and is attributed to an OH vibration indicating the formation of well crystallised hydroxy apatite (Fig. 4.23, D, a).

However, except for this experiment, this hydroxyl band had been very seldom observed on spectra obtained on bone apatite samples or micro-residues measured in this study, indicating that OH incorporation could be reduced in bone material (Pasteris et al., 2004; Wopenka et al., 2005).

This experiment is evidence for a disordered structure of bone apatite, with a broader main apatite band, for samples heated at 300 and 500 °C and results from heat degradation of the collagen initially present in the bone structure. This collagen is replaced by disordered organic material not showing any protein structure and colouring the heated bone to a greenish to black hue. The presence of this amorphous carbon causes disorder in the apatite crystalline structure, explaining this particular modified apatite spectral signature. At 700 °C when all organic material had been combusted the bone is recrystallised as hydroxy apatite.

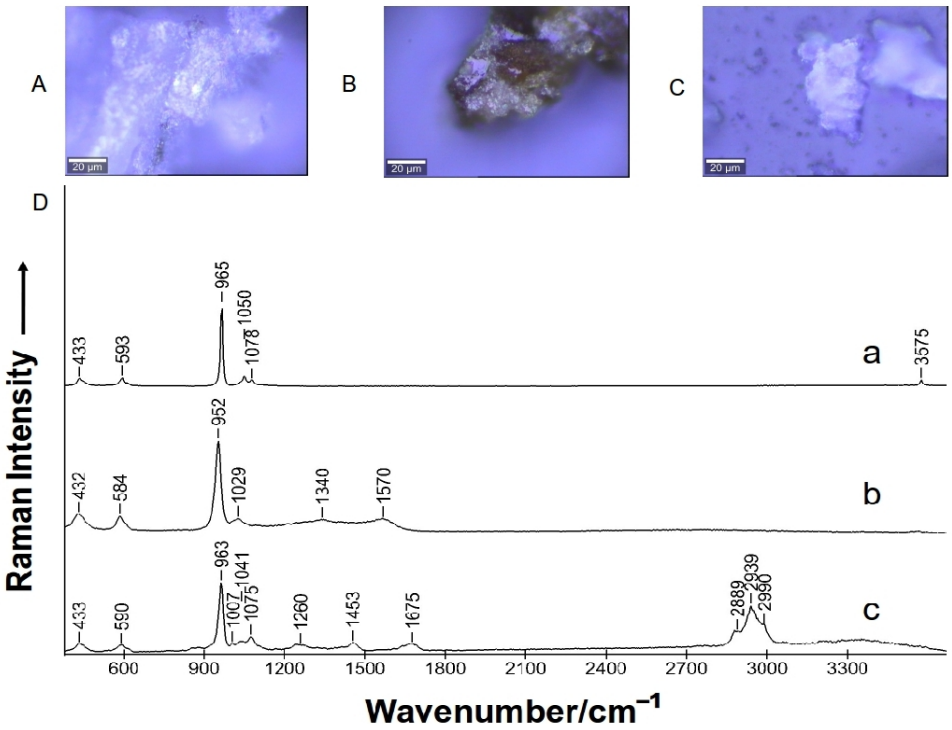

Figure 4.23: Microscope image of dry bone (A), dry bone heated up between 300 and 500 ºC (B), dry bone heated up to 700 ºC (C). Raman spectrum of dry bone (D, c), dry bone heated up between 300 and 500 celsius degrees (D, b), dry bone heated up to 700 celsius degrees (D, a).

4.7 Archaeological macro-bone references

Different prehistoric macro-bones (bone fragments) references were used for this study. For Liang Bua site, several macro-bone samples were analysed from different animal species: ramidae (frogs), muridae (rats) and megachiroptera (flying foxes). For Denisova Cave, a bone artefact DC66, excavated in a layer in the east chamber was used as reference. Additionally, a prehistoric deer bone (10 000 BP) and a mastodon (*Mammut americanum)* bone (130 000 BP) were also analysed for comparison purposes of other archaeological sites. All reference analysis results are summarised in appendix (Appendix I, table 1). On some of these references (DC66, prehistoric deer bone, mastodon bone samples), two different types of apatite Raman spectrum were obtained and allow to distinguish two forms of bone apatite: a mineralised bone apatite containing carbonate ions and better crystallised, and a type of disordered apatite, sensitive to laser heating, that I labelled as altered bone.

Some spectra from these three samples are shown in Fig. 4.24. All three samples have similar spectra in the 400-1200 cm^{-1} region with a carbonate band at 1076-1078 cm- with a shoulder at 1050 cm^{-1} (Fig. 4.24, a-c). This fingerprint is similar to the typical Raman spectrum for bone apatite which is the main compound of bone (Wopenka et al., 2005). However, collagen was not detected in these bone samples.

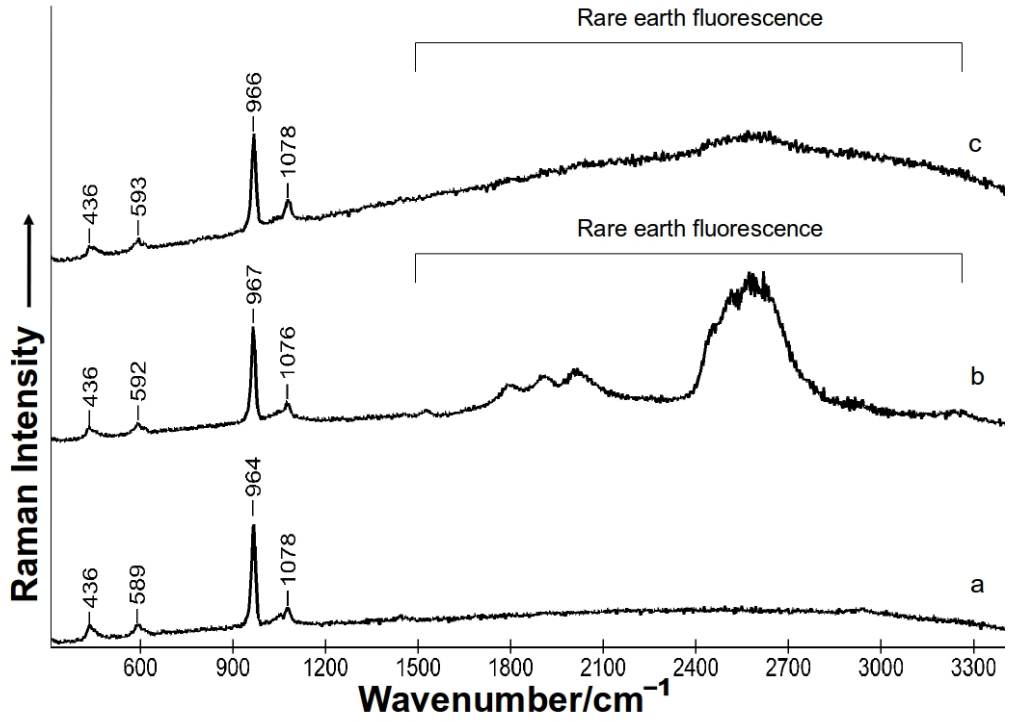

Figure 4.24: Raman spectrum of prehistoric deer bone from Europe (a), prehistoric bone from Liang Bua (ramidae) (b), prehistoric bone from mastondon (*Mammut americanum)* (c).

Fluorescence bands induced by rare earth substitution appear for Liang Bua bone sample (Fig. 4.24, b) and for prehistoric bone sample from mastodon (*Mammut americanum) (*Fig. 4.24 , c). Liang Bua bone sample shows fluorescence bands at 579 nm (Dysprosium, Dy^{3+}), 588, 592, 596, 643, 651 nm (Samarium, Sm^{3+}) (Czaja et al., 2008) and 614, 617, 687, 698 nm (Europium, Eu^{3+}) with 532nm green excitation (Fig. 4.25). Another rare earth element, neodynium (Nd^{3+}) was identified by a series of fluorescence bands at 867, 873, 883, 893, 904, 1055, 1066 nm induced by red 785 nm excitation (Fig. 4.26) (Gaft et al., 2005; Gorobets et al., 2001). This different set of bands obtained with red laser excitation confirms that these bands are arising from fluorescence and not from Raman scattering effect, as the apatite *v*1 vibrational band remains unchanged with both excitation wavelengths. It should be noted that

not all Liang Bua macro-bones analysed as reference lead to rare earth fluorescence bands (Appendix I, table 1).

Mastodon bone spectrum also has bands from rare earth fluorescence but weaker, and with different relative intensities (Appendix I, table 1). It is not known if the presence of this rare earth fluorescence is dependent on the section of bone fragment (inner and outer bone) as it is in contrast with mineralised bone micro-residues found on Liang Bua artefacts which show systematically this type of fluorescence (Chapter 6, section 6.3.2.4). Rare earth element content indicate that this form of bone apatite underwent a rather long process of substitution of its calcium ions by rare earth element showing its antiquity. These rare earth elements are generally transported by underground water in contact with apatite, including fossil bone apatite and their presence are dependent on the geological environment (Herwartz et al., 2013; Metzger et al., 2004). It is relevant to note that this type of mineralised bone apatite containing carbonate and often rare earth substitution has very low sensitivity to laser heating. Nevertheless, a few micron sized micro-residues had been observed to be altered by laser heating on a few rare occasions, when maximum laser power is used, the material is suddenly burn and the other form of analysed apatite is obtained (see below). This observation indicates that a low content in impurities and organic matter can be present in small amounts in that form of apatite. In following chapter, I will then designated this type of mineralised bone apatite for convenience sake as “fossil bone”.

This fossil bone shouldn't be confused with geological apatite found on rare abundance on stone artefact as they have been found in that study having clear distinct spectral features, including different rare earth fluorescence bands, no carbonate apatite Raman band and narrower v1 bands, Fwhm (Full with at half maximum) value being found to be about 10-11 cm^{-1} for geological apatite (Appendix I, table 1).

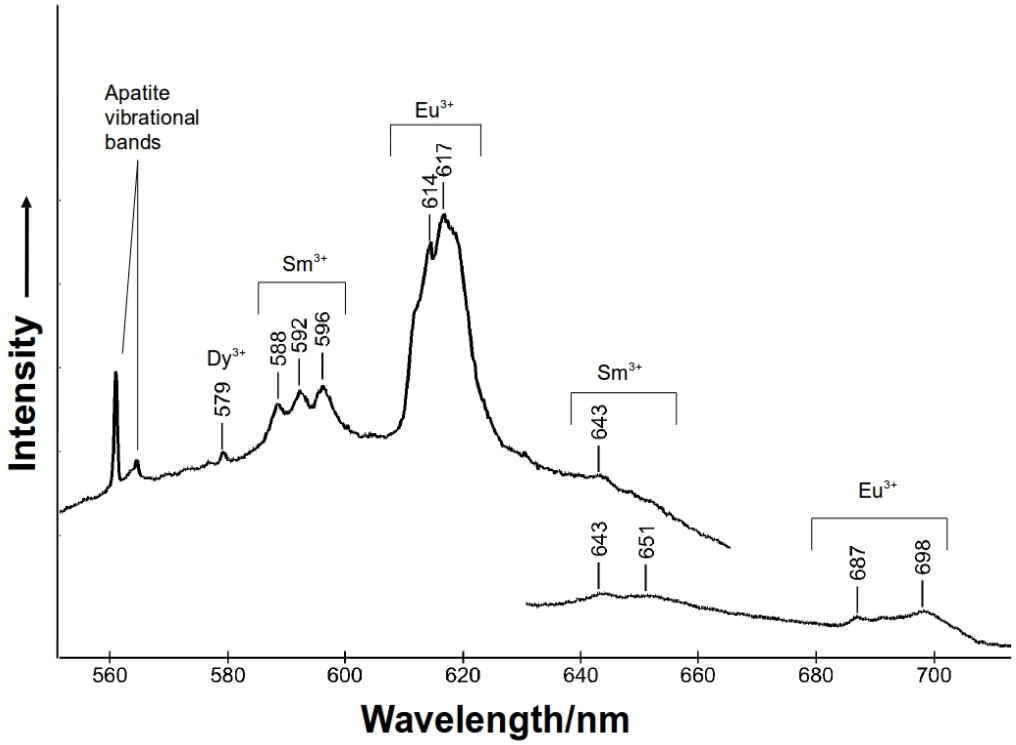

Figure 4.25: Spectrum of Liang Bua ramidae bone showing detail of rare earth fluorescence bands with 532nm excitation.

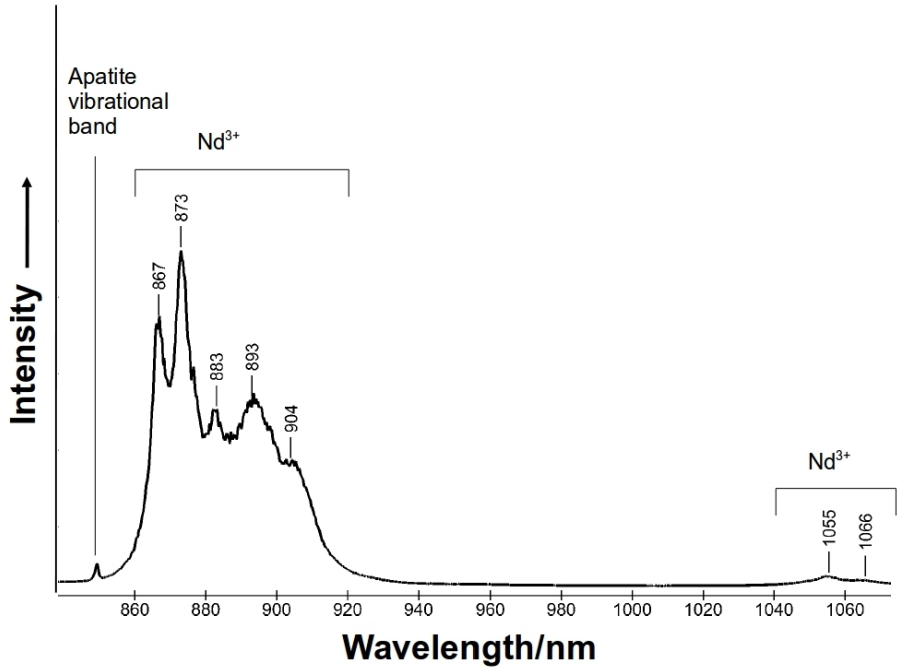

Figure 4.26: Spectrum of ramidae bone showing rare earth fluorescence with 785nm excitation.

Only fossil bone was identified on the Liang Bua macro-bone samples mentioned here, but Denisova Cave bone artefact DC66, old European bone, and mastodon (*Mammut americanum)* bone samples were found instead with high free carbonate content and large amounts of altered bone. Under microscope, altered bone was sometimes observed as amorphous individual particles and sometimes part of bulk old bone, associated with fossil bone apatite.

Altered bone *v*1 phosphate stretching Raman mode was down shifted with typical position varying in a range between 946-959 cm^{-1} (Appendix I, table 1). This *v*1 band is also broadened, with FWHM between 20-35 cm^{-1} which is broader than typical FWHM observed for bone apatite but narrower than amorphous calcium phosphate (ACP) (Sauer et al., 1993; Grauw et al., 1996). Carbonate band at 1075-1078 cm^{-1} and 1050 cm^{-1} band are absent and replaced by a broad shoulder band centred between 1017-1026 cm^{-1} (Fig. 4.27, a-c). Raman spectrum of this type of apatite is different from the spectrum classically observed of bone apatite (Chapter 2 section 2.1.1.4). However, it can be still identified as a phosphate with apatite structure. Indeed, other calcium phosphates have very different sets of vibrational bands (Wopenka et al., 2005) and apatite is the only phosphate that has two bands consistently centred on 431 and 591 cm^{-1}, so the phosphate group can be inferred as still part of apatite like crystalline structure. Considering that such abnormal apatite spectrum have been reported for heated biogenic diagenetic apatite in the same laser excitation conditions (532nm) (Puceat et al., 2004) and that same unusual apatite bands are obtained from heated bone apatite (Chapter 4, section 4.6.2**),** it can be suspected that a heating effect is contributing to that particular apatite spectrum. Additionally, as it has been obtained commonly as bulk part of different old bone reference samples, its identification as bone material is secure (Appendix I, table 1). This form of bone apatite don't display any luminescence from rare earth elements under laser excitation. At this stage, it is not known if rare earth elements are absent in this form of apatite in archaeological samples or if fluorescence can be masked by fluorescence from impurities suspected to be present in this type of apatite which can include organic material and iron oxides with high visible light absorption, according to (Puceat et al., 2004). Indeed, this altered bone is more fluorescent than typical bone apatite probably due to the presence of unspecified organic matter content in different amount which frequently give altered bone apatite its greenish or black colour, as observed for heated bone (Chapter 4, section 4.6.2**)** . It is not known if this organic material is directly related to compounds from collagen degradation or other organic material linked to micro-organism activity. If fossil bone (see previous section) spectrum can be rather straightforwardly recorded even at low power laser excitation, recording a spectrum of this type of bone apatite often requires increasing

laser power to burn progressively organic material which causes this fluorescence. By consequence, Raman spectrum need to be considered as abnormal as resulting directly from laser heating, but I found it more informative than low signal-to-noise spectra obtained with red laser excitation (785 nm).

Indeed, the heating of this form of bone apatite with 532 nm laser excitation lead often to the appearance of an additional broad vibrational band with varying intensities centred at 660 cm^{-1} which can bring information about impurities in this material. This band does not belong to an apatite mode, and has been identified as manganese oxide in +2 and +3 oxidation states, known as hausmanite (Mn_3O_4) (Cordeiro Silva et al., 2012). Production of hausmanite on heated apatite could be explained by manganese dioxide content present in bone apatite either as filling apatite crystal inter space or in crystal lattice as substitution to calcium ions. This production of Mn_3O_4 is probably arising from the oxidation under laser heating of commonly encountered manganese dioxide (MnO_2). Indeed, pure white bone residues without black manganese oxide visible on its surface can show also this vibrational band on their spectrum with laser heating, so manganese oxide is unlikely to arise only from superficial deposits on bone apatite. Manganese oxide have been previously analysed by Raman microscopy in dinosaur bone as a result of bacterial activity consuming fungus which degraded the inner bone (Owocki et al., 2016). Manganese oxide have been also analysed by the same technique in macro prehistoric human bones (Dal Sasso et al., 2018). However presence of manganese, if often encountered in this form of bone apatite is not systematic on all analysed spots, and is an indication of heterogeneity of impurity content.

It's interesting to note that the form of apatite found associated with fossil bone in the archaeological bone references analysed display a very close spectrum compared to altered bone in heating experiment (see section 4.6.2 above), except that no manganese oxide band centred at 660-675 cm^{-1} was found in heated modern bone (Fig. 4.23, b).

Indeed, heated modern bone did not undergo the long process of collagen degradation that occurs in archaeological bone, but collagen and other proteins were rapidly degraded through heating. Observing similar apatite abnormal fingerprints on heated bone is probably due to a disorganised structure because of the loss of its collagen which can be caused either by heating (Chapter 4 section 4.5.2, Fig. 4.23**),** or by micro-organism bone degradation (Fig. 4.27, a-c**).** This latter apatite disorganised structure, originating from bone degradation, is also very sensitive to further laser heating. However, presence of manganese oxide allows distinguishing the micro-organism degradation process from the modern heating process.

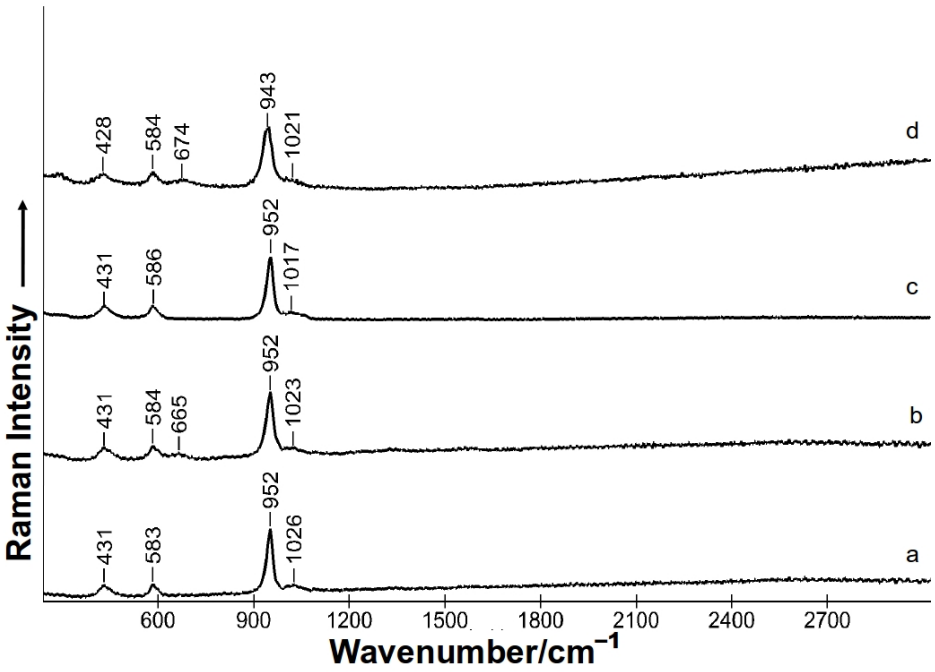

Figure 4.27: Raman spectrum from Denisova Cave DC66 bone artefact (a), Denisova Cave DC66 bone artefact showing manganese oxide content (b), macro-bone fragment from mastodon (*Mammut americanum)* (c), bone fragment from mastodon (*Mammut americanum)* showing manganese oxide content (d).

Chapter 5 Denisova Cave (Russia) stone artefacts analysis

5.1 Archaeological context

Denisova Cave is located in the Bashelaksky Range of the Altai Mountains, Siberia, Russia. This geographic environment is suitable for evaluating my methodology and provides excellent potential for residue preservation, because of the cold climate, relatively stable conditions in the buried cave deposits and because of the chronology, which, although still being refined, certainly spans hundreds of millennia (Fig. 5.1). Moreover, stone, bone and other artefact materials are well-preserved and in deep stratigraphic layers, from which climatic and local environmental data have also been compiled.

The earliest stone artefacts appear at Denisova Cave at the end of the Middle Pleistocene, and are bracketed by RTL ages of 282 ± 56 and 171 ± 43 ka (Derevienko et al., 2003). The Denisovan finger (Sublayer 11.2) and toe (Sublayer 11.4) phalanxes are at least 50,000 years old, and analyses of DNA sequences suggest a split between Neanderthals and Denisovans between 77,000 and 114,000 years ago (Prüfer et al., 2014). It is likely that all hominin groups (at times overlapping but initially only Neanderthals, then Denisovans and later modern humans only) used the cave as an occasional occupation site (Derevienko et al., 2005). In winter, people probably hunted both small and large ungulates (Baryshnikov, 1999); and in summer, people probably collected plants, small mammals, and perhaps fish. Preliminary studies of Pleistocene mammal remains in the East Chamber (Vasiliev et al., 2008, 2010, 2013) indicate the dominance of forest taxa (especially roe deer and Siberian red deer) in Layers 15 and 14, followed by a progressive increase in the proportion of steppe taxa in the overlying Late Pleistocene deposits. These environmental changes may have influenced hominin subsistence strategies and, hence, tool function. The faunal remains from Denisova Cave do not show significant differences between Middle and Upper Palaeolithic food collection strategies. Some cut marks have been identified on the Upper Palaeolithic bones, suggesting an increased role of hunting in modern human subsistence strategies. My ultimate objective is to assess these hypotheses by study of the stone tools used by its prehistoric inhabitants and the materials they used for their subsistence.

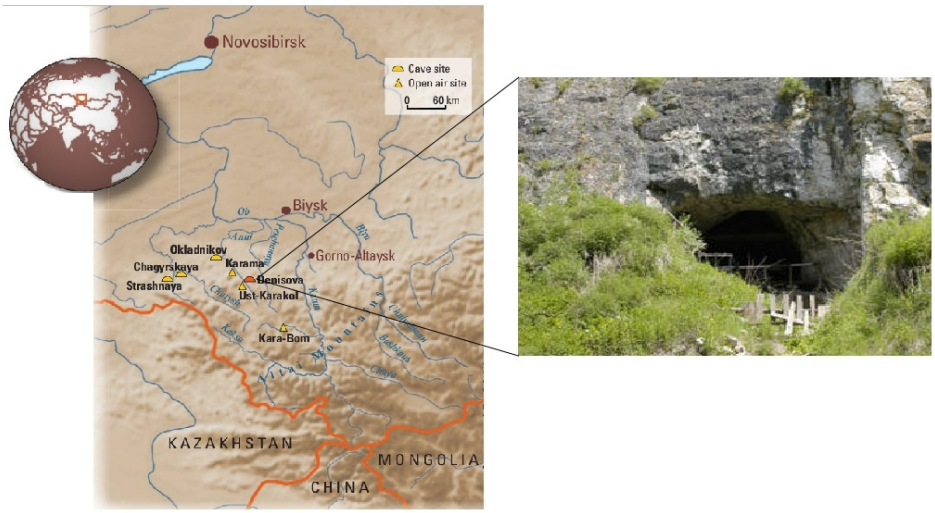

Figure 5.1: Localisation and photo of Denisova Cave.

5.2 Samples

The archaeological specimens analysed comprised 21 stone artefacts from Denisova Cave, collected from the East Chamber section wall between Middle Palaeolithic layers 15 to 11.2. The dating of these layers has been updated recently from ~259–38 ka (Jacobs et al., 2019). The specimens were removed by hand from the walls as they were uncovered, with minimal handling, and placed directly in plastic bags, which were left open at one end to air dry before being sealed for storage and transport to University of Wollongong for analysis. Before Raman analysis, a first step of use-wear study and macro-residues localisation was undertaken, but only on the first set of unwashed artefact DC2, DC12, DC22, DC42, DC52 (Bordes et al., 2018).

5.3 Results

5.3.1 Micro-residues identified as modern contaminants

A few contaminant modern fibres were found on the Denisova Cave stone artefacts, and arise from direct manipulation of the samples on site. For example, dark synthetic glove fibres were found on unwashed artefact DC12, and another dyed modern fibre was found on artefact DC2 (Chapter 3, section 3.2.1). It should be noted that metal mark contamination (Chapter 3,

section 3.9) was only detected on artefact DC52. Several modern contamination fibres from the micro-trace laboratory were also found, including dark dyed modern fibre, indigo fibres and few isolated plant fibres. Other common modern contaminations (e.g., micro-residues from plastic boxes and blue nitrile gloves micro-residues), were found on some samples and result from their manipulation during analysis in the laboratory. As such, they are easy to recognise, having very specific Raman signatures (Chapter 3, section 3.2).

5.3.2 Micro-residues originating from the sediment or from post-depositional processes

Similar to artefacts from Liang Bua, biofilms were also found to have developed on some Denisova Cave specimens (Bordes et al., 2017). Additionally, extended zones on unwashed artefacts DC22, DC37, DC43, DC52 were covered by micro-filaments, probably resulting from fungal activity. These filaments are difficult to analyse because their small diameter (approximately one micron) renders them very sensitive to laser heating, hence showing their freshness as recent biological growing material. However, weak fluorescent protein signals were sometimes obtained, confirming their biological origin (Fig. 5.2).

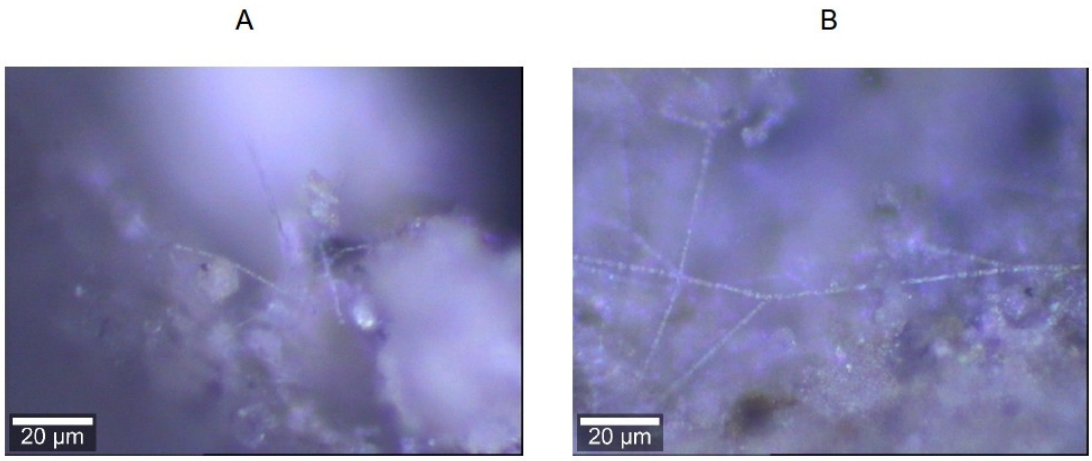

Figure 5.2: Fungi filaments observed on DC22 (A) and DC37 (B).

One significant residue arising also from post-depositional process on the Denisova Cave artefacts and originating from the sediment is apatite. Indeed, white, green and black apatite residues were found in high abundance on all artefacts, in the form of individual micro-

residues or smeared micro-residues. These apatite residues are widespread on all Denisova Cave stone tools, and don't show any specific spatial distribution. Moreover, same apatite residues are also strongly present in the surrounding sediment of all the artefacts. Additionally, same apatite residues have been also found in the attached sediment of one non artefact (DC32) collected from the surface of the cave and on some Denisova artefacts that completely lack polish or any other traces of use (i.e., were not used). The green or black colour of these residues could be explained by the presence of an unspecified organic coating on the apatite itself. The same feature was observed with the same Raman spectrum on artefacts from Liang Bua (Fig. 5.3, a-b) (Chapter 6, section 6.3.2.4). The spectral signature of this form of apatite is also identical to those recorded from altered bone apatite analysed on reference archaeological bone samples (Chapter 4, section 4.7), confirming such identification. Indeed, the main apatite band is downshifted, with absence of a carbonate band at 1075 cm^{-1} and replaced by a weak shoulder band centred at 1027-1030 cm^{-1}. In both cases, a Mn_3O_4 band is present, showing the presence of manganese in apatite. Evidence of manganese oxide in apatite indicates that a chemical process allows manganese oxide (present in the immediate depositional environment) to fill altered bone voids, probably by the combined action of micro- fungi and bacteria (Owocki et al., 2016) (Chapter 4, section 4.7).

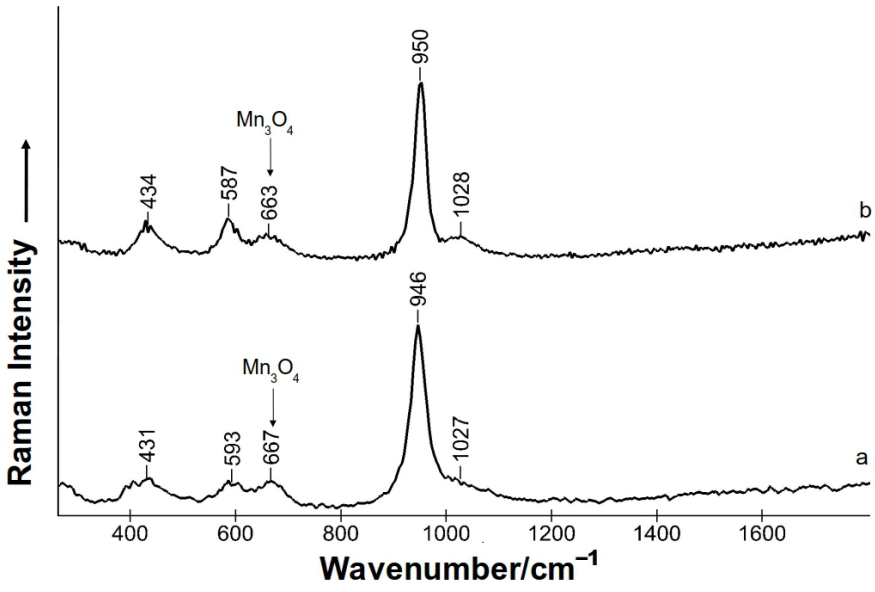

Figure 5.3: Raman spectrum of altered bone apatite found on artefact DC1 from Denisova Cave East Chamber (a), Raman spectrum of altered bone apatite on artefact LB5164 from Liang Bua (b).

Only this specific form of bone apatite was found on Denisova artefacts and in layer sediment. Solid bone micro fragments were never observed, and bone apatite rather systematically appears always as amorphous residues. As no fossil bone apatite was found in coexistence with this altered form of apatite in situ on Denisova Cave artefacts, one hypothesis is that the bone alteration process probably didn't take place on the stone artefacts; and that this material was likely transferred from the sediment, where it is always found in great abundance (Appendix IIa, table 2). Indeed, only a unique fossil bone apatite micro-residue (as defined in Chapter 4, section 4.7) was identified in only one artefact sediment sample (DC27). Consequently, this altered bone apatite, present on all examined artefacts, cannot be identified as a micro-residue linked to use of stone artefact, but probably originates from some prehistoric activity (human or other animal) at the site; underwent a complex alteration process and was transferred to the stone artefacts from the sediment. Indeed, bone macro-residues are recognised in great abundance in other layers. Not less than five human occupation layers were observed during the excavation of Layer 11 in Main Chamber (Derevianko et al., 2014). Furthermore, concentrations of archaeological bone artefacts were found in that layer, suggesting intensive working on bone (Derevianko et al., 2014), and widespread occurrence of altered apatite in the sediment and apatite on stone artefacts in the East Chamber may have a similar origin. In that sector, archaeologists observed that bone was very often already altered by acidic chemical processes (Vasiliev et al., 2013), which are consistent with in situ observations of altered apatite on the studied artefacts.
Further work will be needed to determine the exact origin of these altered bone apatite residues and to explore the possibility of using this spectral signature in other Denisova cave archaeological contexts to establish a useful marker of prehistoric human activities.

5.3.3 Potential use related micro-residues

Eight out of twenty one artefacts studied from Denisova Cave East Chamber returned positive results for lipid micro-residues using Raman microscopy (Table 5.1**)**. Three different fatty acid micro-residues were found on these artefacts. DC2 and DC12 from layer 11.4 having micro-residues composed of a mix of different saturated fatty acids (SFA). Artefacts DC26 and DC27 from Layer 13 have also a mix of different saturated fatty acid residues, but in different proportion (SFA'). Additionally, four other artefacts (DC4, DC13 and DC39) from Layer 13 and Artefact DC11 from Layer 15 have micro-residues composed of a mix of saturated fatty acids and unsaturated fatty acids (SFA/UFA).

Table 5.1: Summary of results obtained by Raman spectroscopy and use-wear analysis on Denisova Cave East Chamber artefacts.					
Artefact number	**Layer**	**Age (ka)**	**Use**	**Use-related residues**	**Use interpretation**
DC36	11.1	120 - 38	Unknown	None	Unknown
DC37	11.2	120 - 38	Unknown	None	Unknown
DC1	11.4	120 - 38	Unknown	None	Unknown
DC2	11.4	120 - 38	Denticulate knife	SFA	Cutting animal material
DC4	11.4	120 - 38	Scraper/cutting flake	SFA/UFA	Scraping/cutting animal material
DC12	11.4	120 - 38	Scraper	SFA	Scraping animal material
DC13	11.4	120 - 38	Scraper	SFA/UFA	Scraping animal material
DC39	11.4	120 - 38	Cutting tool	SFA/UFA	Cutting animal material
DC42	12.2	259 -129	Not used	None	Not used
DC52	12.2	259 -129	Not used	None	Not used
DC43	12.3	259 -129	Unknown	None	Unknown
DC45	12.3	259 -129	Scraper	None	Unknown
DC5	13	259 -129	Unknown	None	Unknown
DC14	13	259 -129	Not used	None	Not used
DC26	13	259 -129	Scraper/cutting flake	SFA'	Scraping/cutting animal material
DC27	13	259 -129	Scraper/cutting flake	SFA'	Scraping/cutting animal material
DC30	13	259 -129	Not used	None	Not used
DC11	15	259 -129	Hacking (cutting with percussion movement) tool	SFA/UFA	Hacking (cutting with percussion movement) animal material
DC22	15	259 - 129	Not used	None	Not used, natural goethite visible on surface
DC23	15	259 - 129	Not used	None	Not used
DC25	15	259 - 129	Not used	None	Not used
DC32	Non artefact	NA	Not used	None	Not used

Saturated fatty acid micro-residues found on DC2 and DC12

Individual lipid micro-residues were observed on both artefacts as white solid objects with a grainy texture. Twenty three individual micro-residues found were analysed successfully on artefact DC2 and six individual micro-residues were analysed on Artefact DC12, giving the same Raman spectral signature. A typical Raman spectrum (532nm excitation), similar to those found for experimental stone tools (Chapter 4, section 4.4) for SFA, is shown in (Fig. 5.4**)**. The individual SFA micro-residues are localised mainly on the two opposite long edges of Artefact DC2, with a high concentration on the right edge on the ventral side (Fig. 5.5). The majority of individual SFA micro-residues on artefact DC2 is located on polished parts of the edges, but some was detected on unpolished edges. On artefact DC12 only a few of these micro-residues were detected, with no specific distribution (Fig. 5.6).

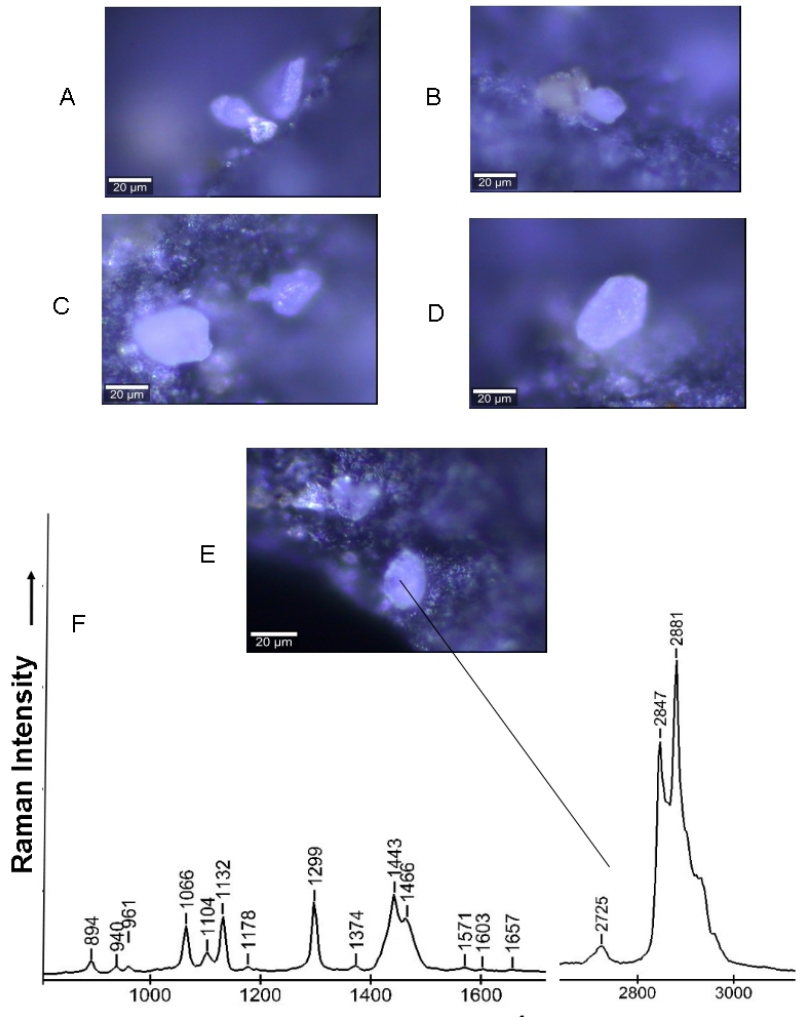

Figure 5.4: Individual saturated fatty acid micro-residues detected on artefacts DC2 and DC12 (A-E) and typical Raman spectrum (F).

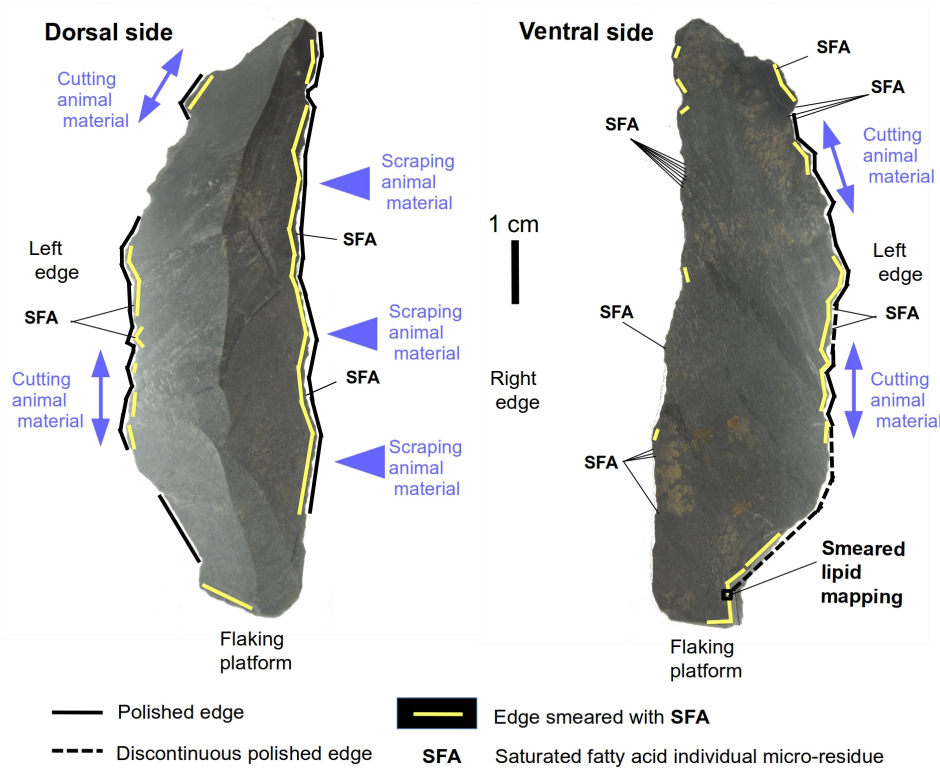

Figure 5.5: Correlation between DC2 SFA micro-residues and polished area distribution.

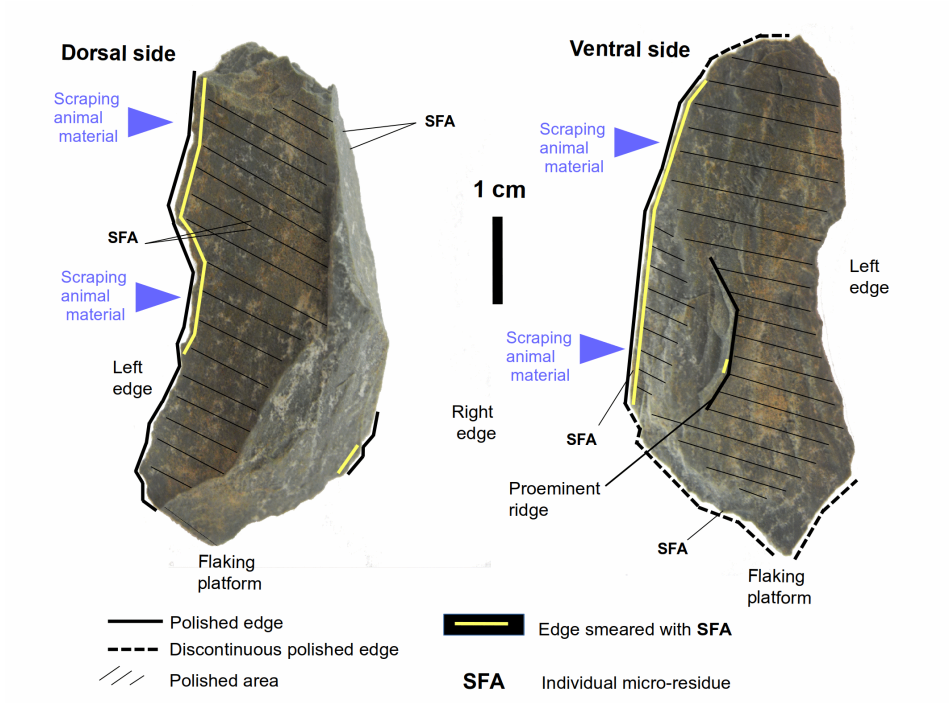

Figure 5.6: Correlation between DC12 SFA micro-residues and polished area distribution.

Probing the rock surfaces of artefacts DC2 and DC12, another residue type was observed that appeared as thin smeared films on the rock surface. These thin films were only visible with microscopic observation, even for more intensively smeared zones (Fig. 5.7). Raman spectra obtained on these smeared micro-residues are identical to individual SFA micro-residues, namely saturated fatty acids. Raman spectral imaging confirmed their spatial distribution on the rock surface as thin discontinuous films (Fig. 5.8). They will be designated by smeared SFA micro-residues to distinguish them from individual SFA micro-residues (Chapter 3, section 3.5). The intensity of the Raman signal decreases rapidly when moving the microscope objective slightly out of focus in both directions, with the mineral background signal increasing with downward focusing, indicating that the films are only a few microns deep. Most surfaces covered by smeared SFAs correspond to polished areas and are not homogeneous in thickness, indicating the filling of irregularities and cracks in the surface. These smeared SFA micro-residues on artefact DC2 were detected on both left and right margins on dorsal side and on the right margin of the ventral side, along parts of platform edge and the left proximal edge (ventral surface) (Fig. 5.5). Artefact DC12 shows distributions of these smeared SFA micro-residues mainly on the left edge on dorsal side and on the right edge on ventral side. Additionally, two other areas with less abundant SFA micro-residues were detected on a section of the right edge on the dorsal side and on a central ridge on the ventral side (Fig. 5.6)

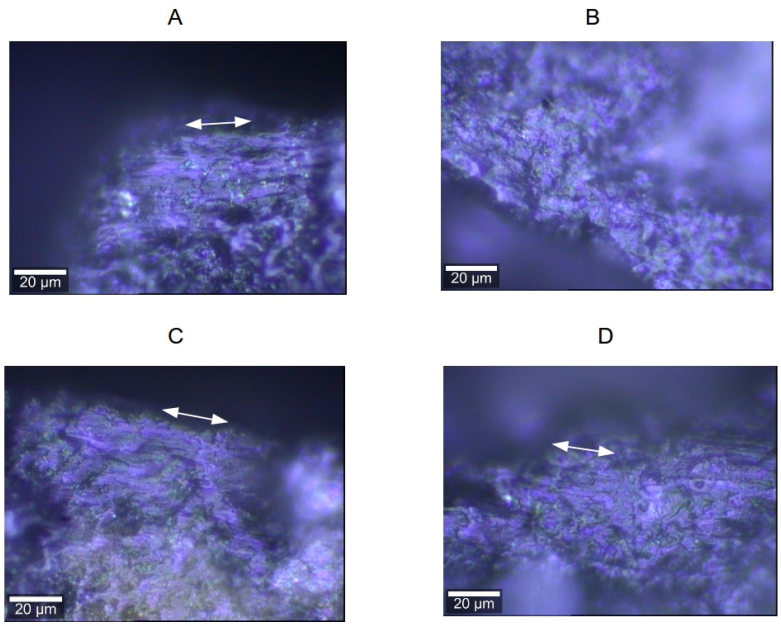

Figure 5.7: Examples of images of SFA smeared areas: DC2, dorsal side (A), DC2, ventral side (B), DC12, dorsal side (C), DC12, ventral side (D). White double arrows show visible striation direction.

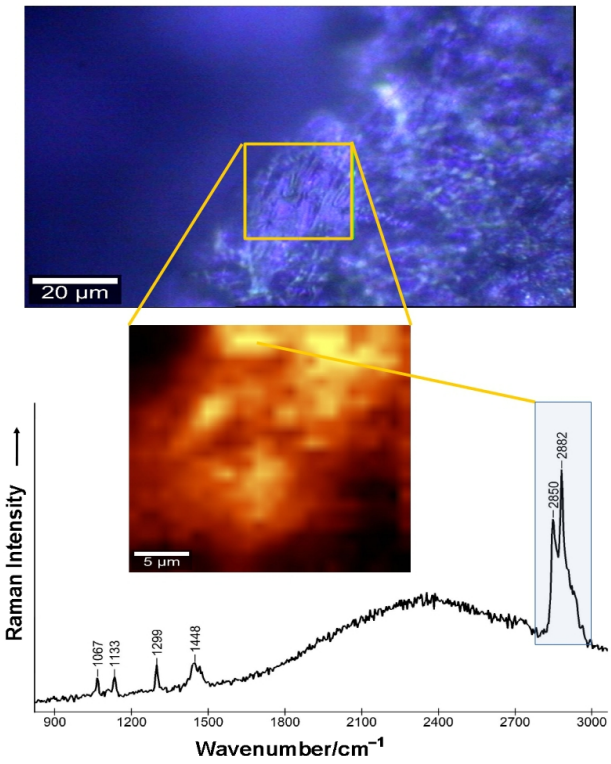

Figure 5.8: Raman spectral image of smeared SFA on DC2 ventral proximal left edge. The integrated intensity of the most intense Raman bands (C-H stretching) was used for mapping.

Smeared SFA micro-residues were found close to the use polish distribution on artefacts DC2 and DC12. Observation of polish distribution on artefact DC2 after washing (Fig. 5.5) shows that the left edge had been polished on both sides, with no polish extending inland. The right edge of artefact DC2 shows a continuous polish on the dorsal side but no polished edge section on the ventral side. Low visibility of polish on right edge on the ventral side may be due to heavy scarring or retouching on that edge (Fig. 5.5). The polish distribution on artefact DC2 seems to indicate that pressure was applied evenly along the left edge of both sides during tool use, suggesting that it was used as a knife with a sawing action that symmetrically applies pressure to both sides of the edge. The polish distribution on tool DC12 shows a different distribution with the left edge polished on the dorsal side (Fig. 5.6), extending from the left edge to the central dorsal ridge. On the ventral side of the tool, it is the opposite right edge which is polished over the whole flat ventral surface. A central prominent ridge (Fig. 5.6**)** in the middle of the ventral surface of artefact DC12 is also heavily polished. Another adjacent zone is devoid of polish against its concave side in the right edge direction because of the presence of this prominent polished ridge on the ventral surface which concentrated the pressure applied on ventral surface. Distribution of polish on this prominent ridge confirms the

scraping direction from the right ventral edge.
These observations suggest that this tool was used as a double sided scraper, working with one edge dorsal side and the opposite edge with ventral side down on the worked material.

The spatial distribution of the smeared SFA residues superimposed onto the polish distribution (Figs. 5.5 and 5.6), shows a good agreement for both artefacts. Nevertheless, a percentage of the areas covered with saturated fatty acid micro-residues on artefact DC2, does not correspond to polished surfaces, such as the flaking platform on the dorsal side and several small areas on the right edge on dorsal side. The smeared SFAs also do not consistently occur on every polished surface, probably because of poor preservation in these areas.

Looking toward an interpretation of these smeared fatty acid micro-residues in terms of stone tool use, results obtained on experimental tools show that they can occur preferentially on stone tools used to work animal material. Experimental stone artefacts used on fresh animal skin more commonly have individual and smeared SFA micro-residues (Chapter 4, sections 4.4.2 and 4.5.2). Fresh bone working also tends to have these fatty residues, but they are less abundant than occurrences of collagen fibres (Chapter 4, section 4.4.2) which haven't been detected on artefacts DC2 and DC12 artefact. Indeed, it can be expected that tissues under skin and inside fresh bone (e.g., marrow) could be rich in fat, hence leading to a higher quantity of smeared and individuals lipid residues on stone tools. Experimental stone artefacts used on fresh animal skin have individual and smeared SFA micro-residues, as the more common residue mix.

Polished areas on artefacts DC2 and DC12 were observed under the optical microscope and a similar polish pattern was observed for DC2 and DC12 (Fig. 5.9) which seems to indicate that these two stone artefacts having same SFA micro-residues have been used to work similar material. Comparison of the polish pattern observed on DC2 and DC12 with the polish pattern on experimental skin scraping tools (Chapter 4, section 4.5.2) support this hypothesis.

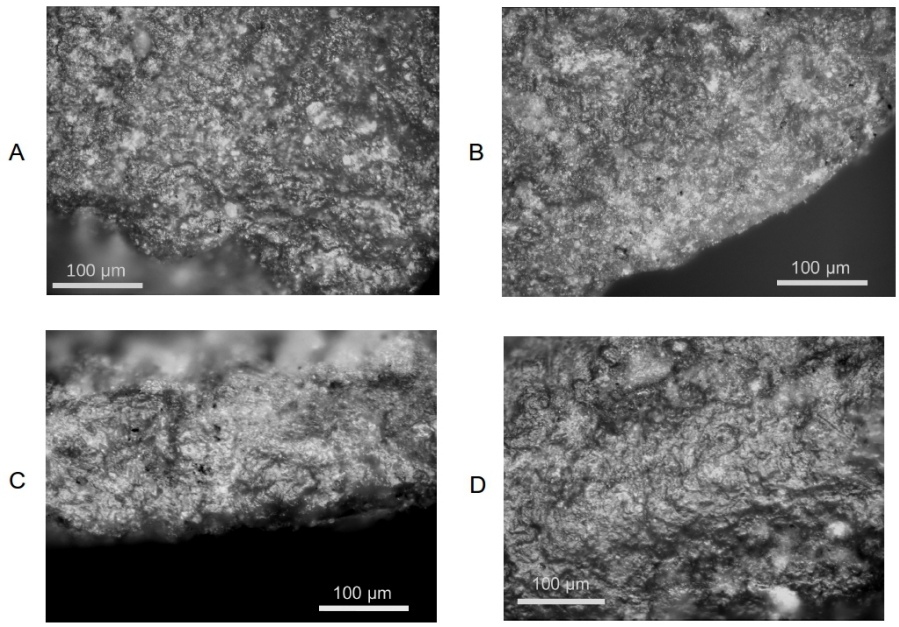

Figure 5.9: Image of artefacts DC2 and DC12 polish: DC2 X20 polish details on ventral side (A-B), DC12 X20 polish details on ventral side edge (C), DC12 X20 polish details on ventral side prominent ridge (D).

Saturated fatty acid micro-residues found on DC26 and DC27

The spectra for lipids on artefacts DC26 and DC27 are typical of SFAs (Chapter 4, section 4.4), but compared with SFA spectra from artefacts DC2 and DC12, the CH_2 twisting mode at 1300 cm^{-1} and C-C stretching modes at 1134, 1104 and 1067 cm^{-1} are lower in relative intensity to the main bending CH_2/CH_3 vibrational bands at 1464 and 1446 cm^{-1} (Fig. 5.10). Additionally, the 894 cm^{-1} band is weaker and low intensity bands at 1177, 1372 and 1574 cm^{-1} (visible on spectra from artefacts DC2 and DC12) are not observed on lipid spectra from artefacts DC26 and DC27. However, the lower signal-to-noise ratio could explain the apparent absence of these low intensity bands. It can be noted that the two weak bands at 940 and 960 cm^{-1} in micro-residue spectra from artefacts DC2 and DC12 are also observed in micro-residue spectra from artefacts DC26 and DC27. These differences, which have been observed consistently for each analysed SFA micro-residue, might be then explained by differences in the proportion of SFA present in the mix which comprise these micro-residues. The highest concentration fatty acids that occur in lipids (from plant and animals) are palmitic and stearic acids and is also the main component of adipocere, the end product of animal fat tissue (Forbes et al., 2004). Therefore, it is probable that palmitic acid is contributing mainly to the micro-residues on artefacts DC2 and DC12, whereas stearic acid could be in a greater

abundance in micro-residues on artefacts DC26 and DC27. Indeed, compared with palmitic acid, stearic fatty acid has CH_2 twisting and C-C stretching modes of lower relative intensity to the main bending CH_2/CH_3 vibrational bands (Chapter 3, section 3.2.3, fig. 3.6).

Smeared SFA micro-residues on DC26 was identified mainly on the dorsal side of the flaking platform (external platform edge), which seems to have been used for scraping, indicated by the polish distribution on the edge and dorsal surface (Fig. 5.11). Additionally, a few small areas with smeared SFA are on the ventral, left distal edge, and the discontinuous polish distribution indicates scraping. Distribution patterns on artefacts DC27 are similar to those on artefact DC26, with smeared SFA micro-residues on the external platform edge and ventral left distal edge, but the polished surface on the dorsal and ventral sides is far more extensive and covers almost all the surface between these two scraping edges (Fig. 5.12). The correlation between smeared SFA micro-residues and polished edge is rather good for this artefact, SFA smeared area being found on the most polished section of these two edges.

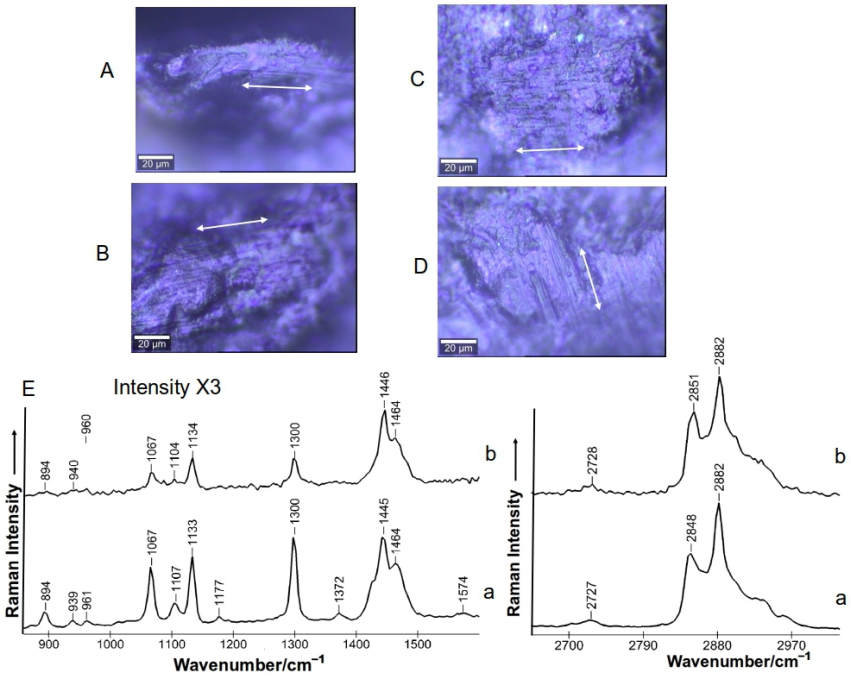

Figure 5.10: Image of smeared SFA micro-residue on DC26 (A-B), DC27 (C-D). White double arrows show visible striation direction. Comparison between DC12 SFA micro-residue Raman spectrum (E, a) and DC27 SFA micro-residue Raman spectrum (E, b).

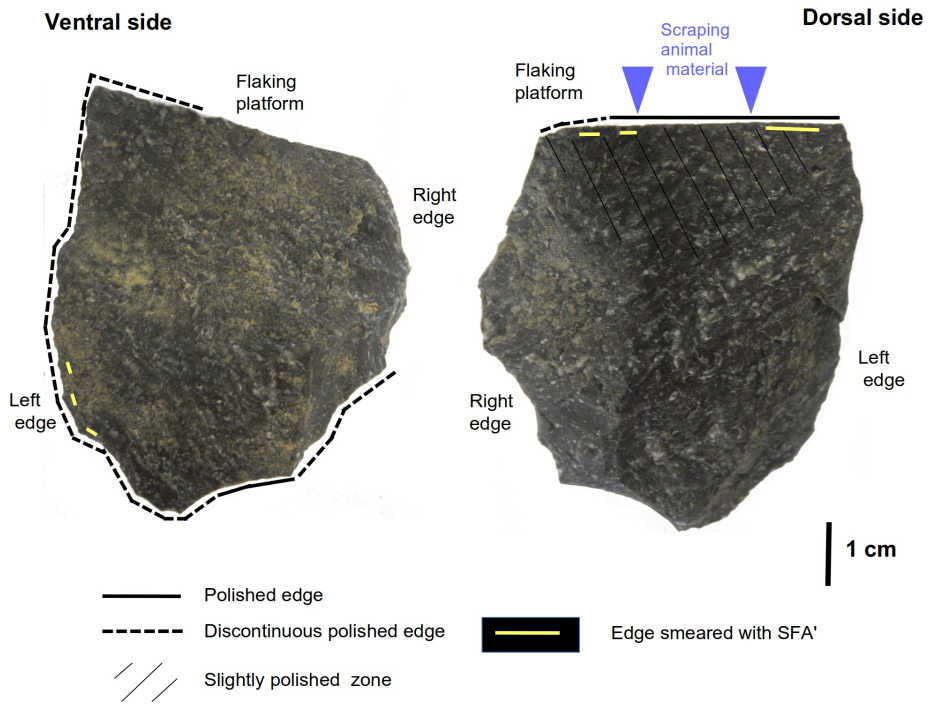

Figure 5.11: Correlation between DC26 SFA micro-residues and polished area distribution.

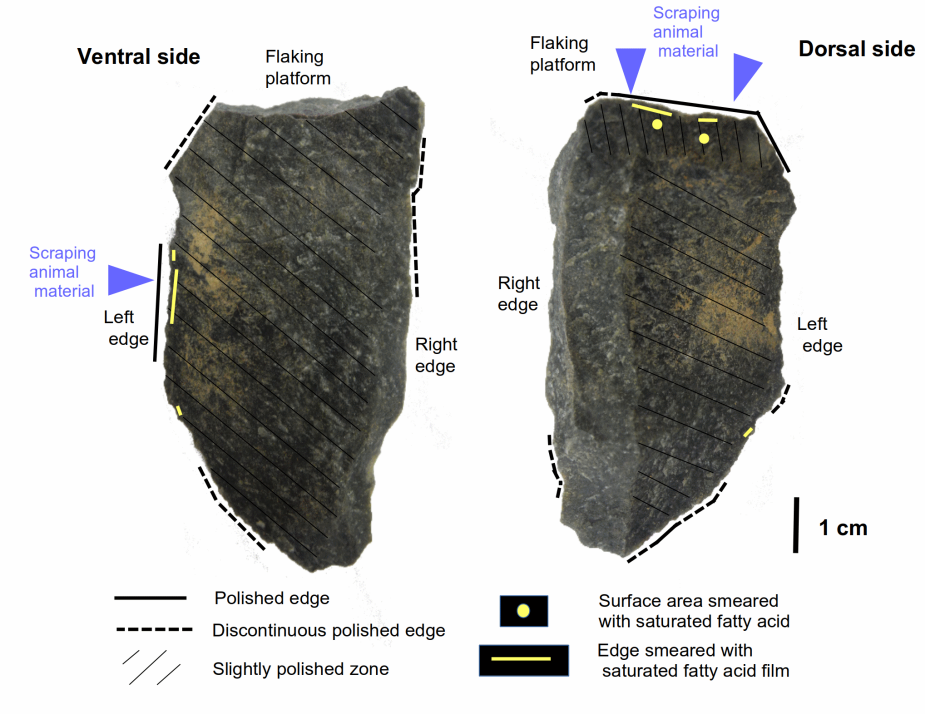

Figure 5.12: Correlation between DC27 SFA micro-residues and polished area distribution.

Unsaturated fatty acids micro-residues found on DC4 and DC13

Raman analysis of artefacts DC4 and DC13 generated 115 and 60 saved Raman spectra respectively, selected from at least three times as many spots probed by the Raman instrument. Similar to results for artefacts DC2 and DC12, individual lipid micro-residues (52 for DC4 and 15 for DC13) as well as smeared lipid micro-residues (43 for DC4 and 18 for DC13) were found in abundance on artefacts DC4 and DC13. However, some major differences were observed. First, individual lipid micro-residues were found in far greater numbers on artefacts DC4 and DC13 and have a different appearance, with a softer structure than the solid white micro-residues found on DC2 and DC12 (Fig. 5.4). Moreover, they are spatially clustered together and very often concentrated around smeared residues as shown in (Fig. 5.13). Second, Raman spectra of individual and smeared lipid micro-residues found on DC4 and DC13 indicate that they are a mixture of saturated and unsaturated fatty acids (Figs. 5.14 and 5.15) with the same Raman spectrum as those found on experimental stone tools (Chapter 4 section 4.5.2)

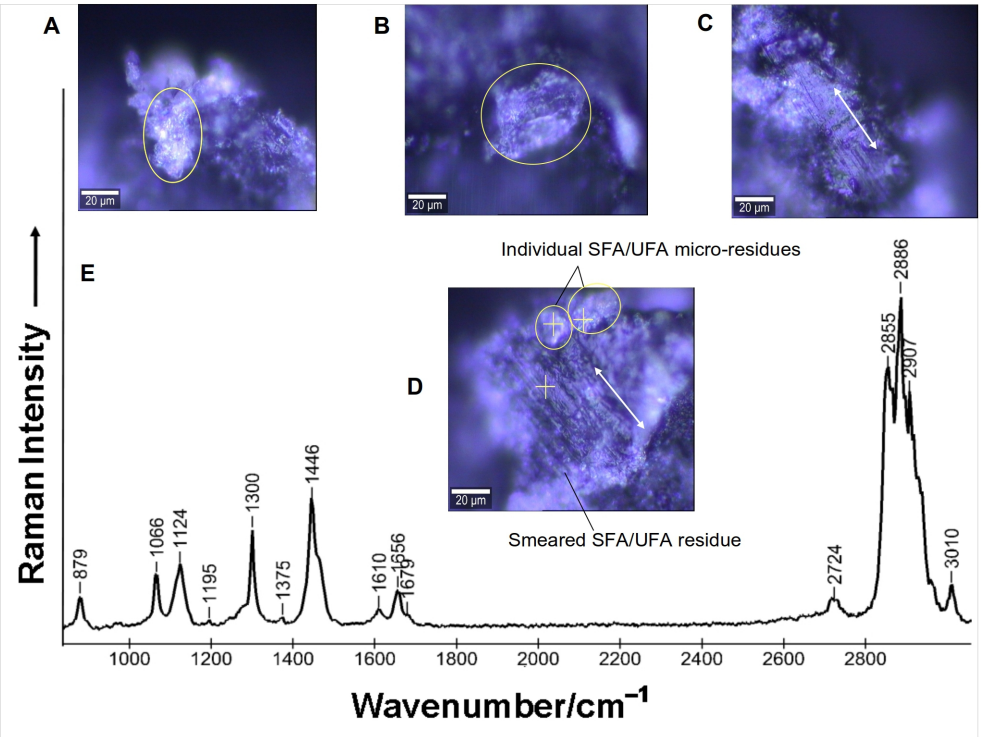

Figure 5.13: Individual mixed SFA/UFA residues on artefact DC4 (A-B), smeared mixed SFA/UFA micro-residue on DC4 (C), association of individual mixed SFA/UFA micro-residues around a central smeared mixed SFA/UFA micro-residue (D). White double arrows show visible striation direction. Typical mixed SFA/UFA micro-residue Raman spectrum (E).

The unsaturated fatty acid content is indicated by the presence of sharp bands at 1656 and 3010 cm^{-1} (C=C stretch and =C-H stretching) respectively and a shoulder centred at 1260-1270 cm^{-1} (=C-H deformation) (De Gelder et al., 2007; Czamara et al., 2015). Trying to go further in the identification of these unsaturated fatty acids, observation of additional low intensity Raman bands at 1610 and 1679 cm^{-1} is useful. Although the 1656 cm^{-1} band could be attributed to cis isomer mode of unsaturated fatty acid, the additional presence of another C=C stretch Raman band centred at 1679 cm^{-1} suggests the presence of a trans isomer of unsaturated fatty acids (Czamara et al., 2015). Then, from this signal, it can be concluded that these micro-residues are containing polyunsaturated conjugated fatty acids having cis and trans isomer configurations.

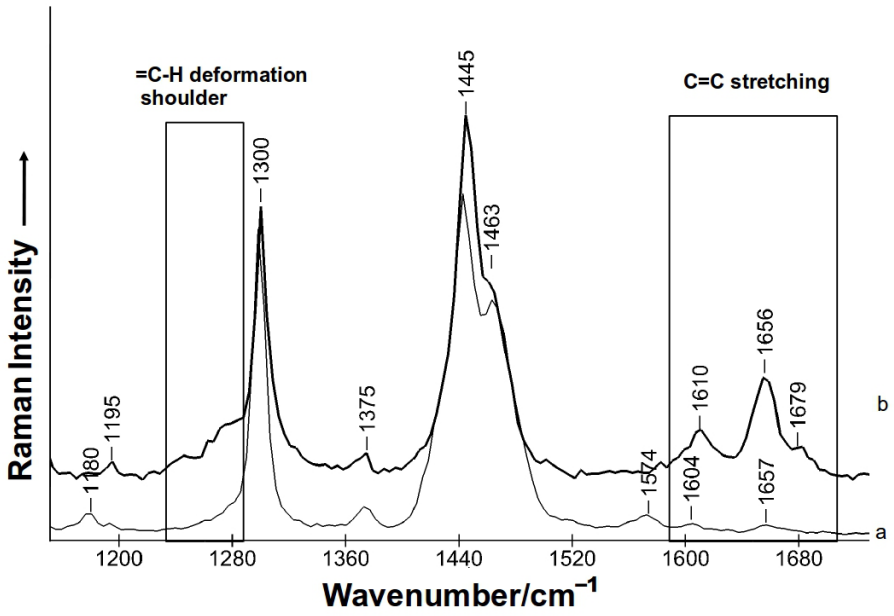

Figure 5.14: Detail of spectral 1100-1700 cm^{-1} range of saturated fatty acids (SFA) found on DC2 and DC12 (a) compared with mixed SFA/UFA found on DC4 and DC13 (b) showing unsaturation spectral markers.

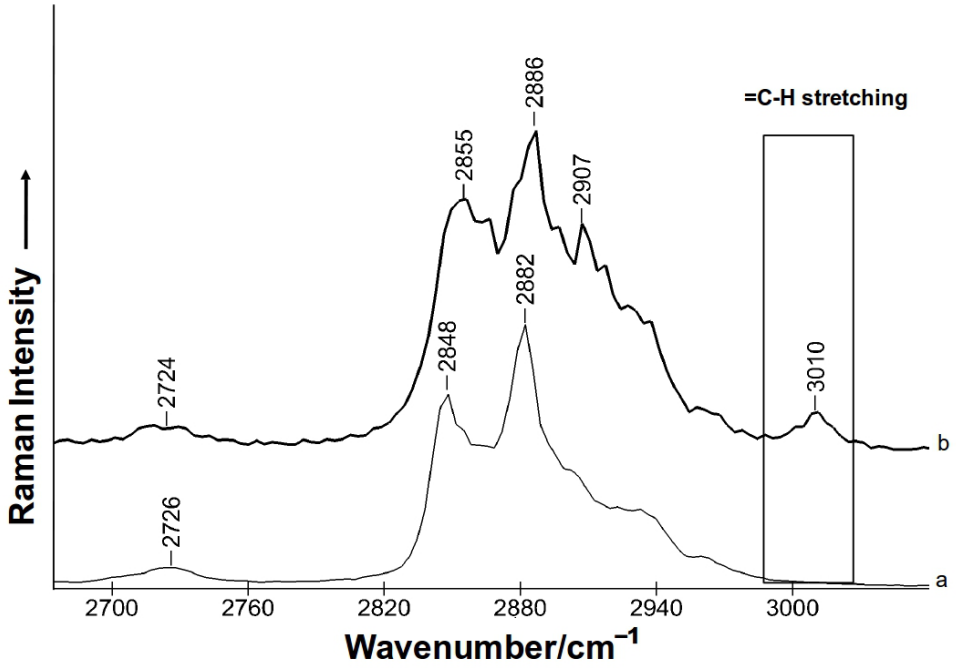

Figure 5.15: Detail of spectral 2700-3100 cm^{-1} range of saturated fatty acids (SFA) found on DC2 and DC12 (a) compared with mixed SFA/UFA found on DC4 and DC13 (b) showing unsaturation spectral markers.

All four edges on the dorsal side of artefact DC4 are highly polished with the right, distal edge and flaking platform exhibiting polish extending onto the surface (Fig. 5.16), indicating it was used for a scraping action. The left margin, which is the only sharp edge of the tool, does not show polish surface extension on its proximal surface, suggesting that it was only used in a cutting/sawing action, combining a scraping action on its distal part. The ventral side shows a highly polished distal edge with surface polish extension indicating also a scraping action. This polish distribution seems to indicate a multi-purpose flake used as a scraper with three edges and as a knife on the only sharp fourth edge (Fig. 5.16). SFA/UFA and smeared SFA/UFA micro-residues are far more concentrated on the left cutting edge of the dorsal side for DC4 (Fig. 5.16), but they are also present on smaller limited area on other edges too, on both sides. This complex distribution indicates that the cutting action could have left apparently more micro-residue on the left edge than the scraping action on the other edges. The polish pattern on DC13 was very similar to that found on DC4, hence indicating a similar worked material (Fig. 5.18).

On artefact DC13, the distal edge shows a higher polish development on each side with extended polished distribution, whereas the left and right edges have extended polished only on ventral side (Fig. 5.17). As no edge on this tool is sharp, it's is logical to conclude that flake have been used mostly as a scraper, mostly on the ventral side which is flat and naturally fitted for this purpose. However, the distal edge had been also used as a scraping edge on both sides. Distribution of isolated fatty acid micro-residues and smeared fatty acid micro-residues show a clear higher concentration on the ventral left edge, which seems also to be the more useful to scrape when the flake is handled, and shows intense resharpening (Fig. 5.17).

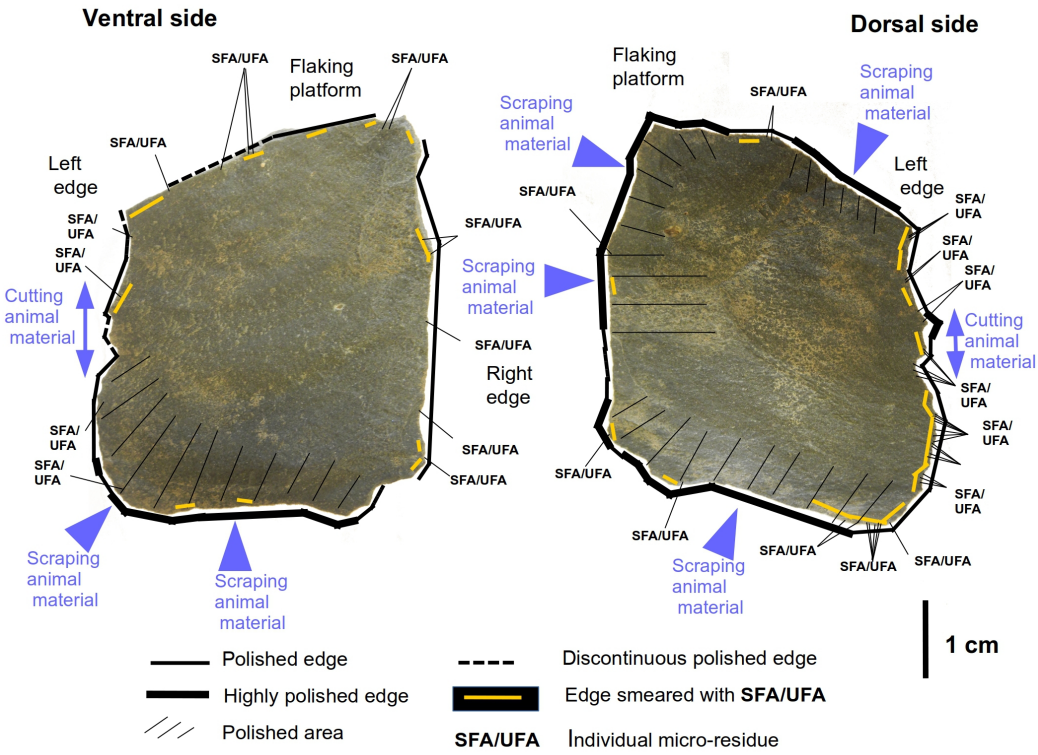

Figure 5.16: Correlation between DC4 SFA/UFA micro-residues and polish distribution.

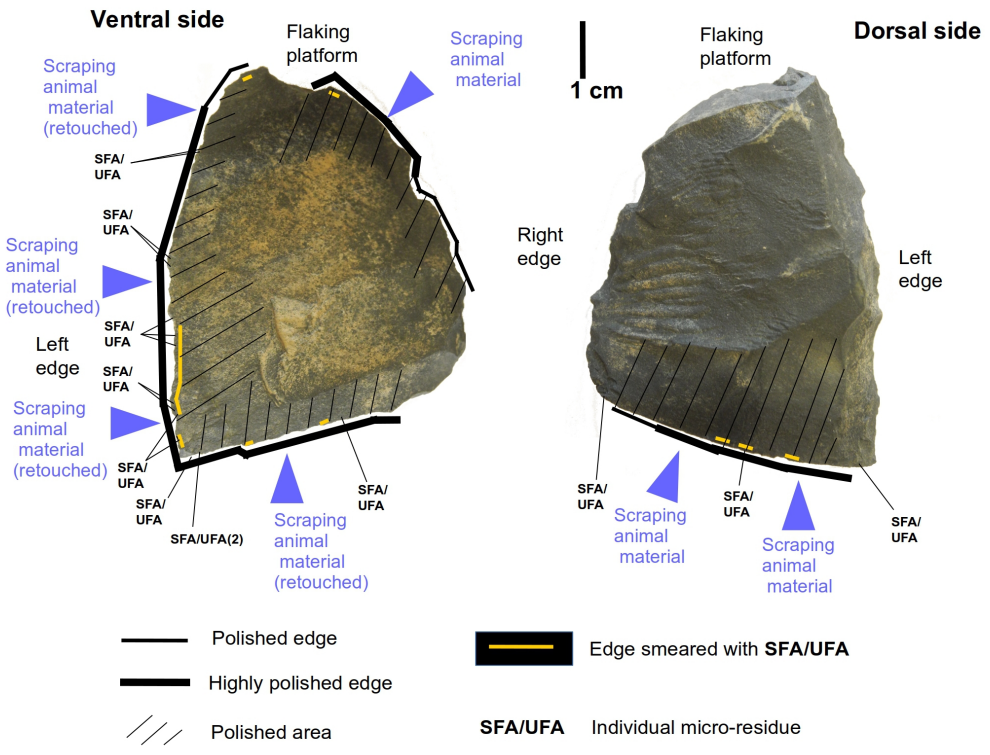

Figure 5.17: Correlation between DC13 SFA/UFA micro-residues and polish distribution.

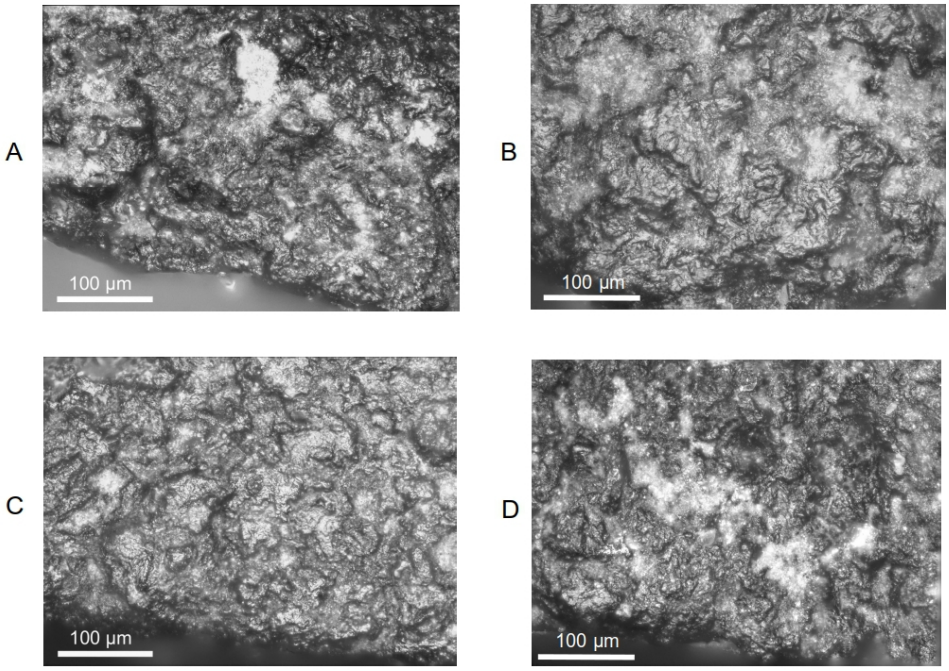

Figure 5.18: Image of edge polish of artefacts DC4 and DC13: DC4 X20 on dorsal side (A), DC4 X20 on ventral side (B), DC13 X20 dorsal side (C), DC13 X20 ventral side (D).

Unsaturated fatty acid micro-residues found on DC39 and DC11

Identical Raman SFA/UFA spectra were obtained on individual residues and smeared micro-residues present on DC39 and DC11, confirming that they have been used on a similar animal material. However, fatty acids were found in far lower abundance on these two artefacts. DC39 has only a smeared SFA/UFA area on the right distal ventral edge (Fig. 5.19) and DC11 has only SFA/UFA individual residues (Fig. 5.20). Nevertheless, these micro-residues were associated with slightly polished ventral distal edge of DC39, are thus use-related, even if the details of use are difficult to determine for this artefact. DC11, on the other hand provides clearer details about its use. Polish was only developed on the distal part of the ventral and dorsal left edge, which seems to be the more useful part of that tool when the flake is handled. On such a short edge length, and considering the greater weight of this artefact compared to other Denisova artefacts studied in this chapter, a hacking action, aiming to cut animal material with percussion, fits well with artefact ergonomy, can be proposed.

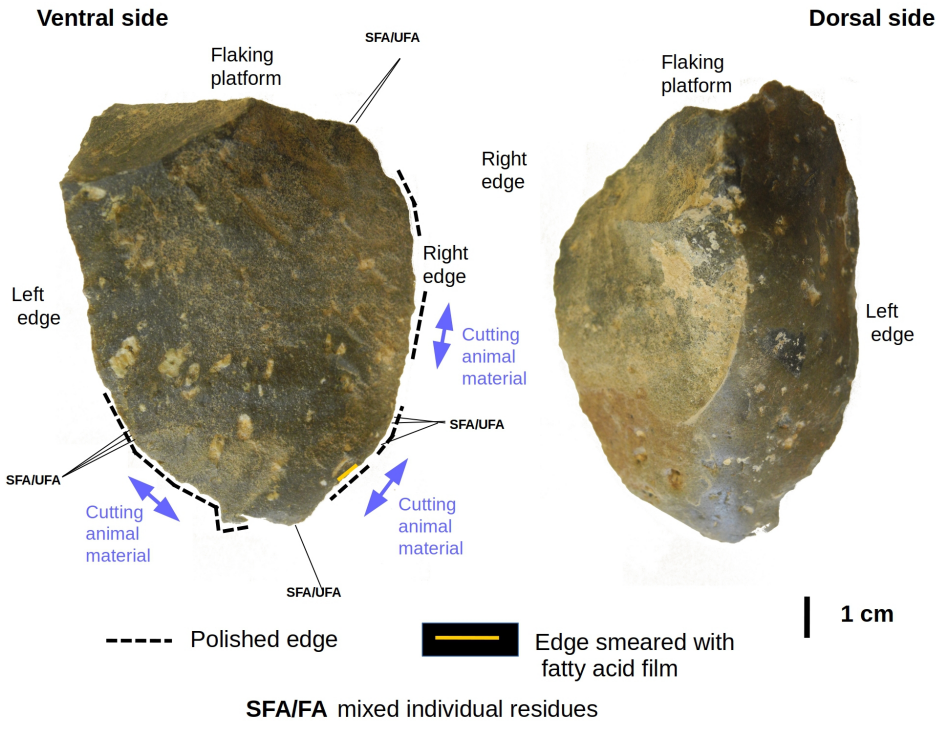

Figure 5.19: Correlation between DC39 SFA/UFA micro-residues and polish distribution.

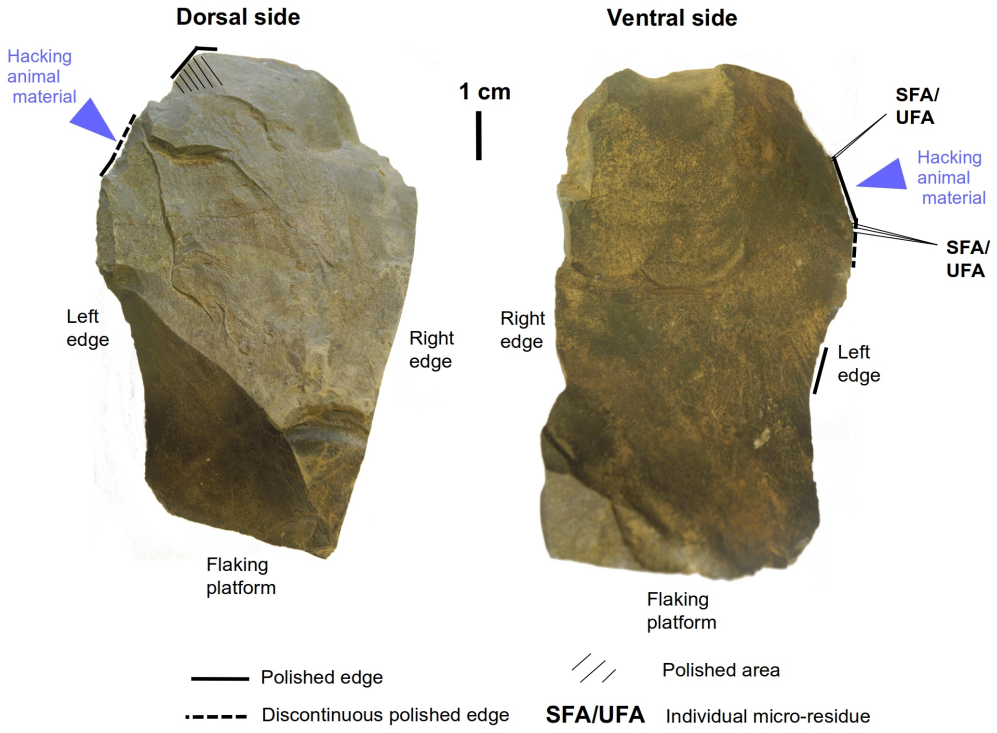

Figure 5.20: Correlation between DC11 SFA/UFA micro-residues and polish distribution.

5.4 Interpretation

Three different fatty acid Raman spectral signatures have been found on these eight stone artefacts: On one side, DC2 and DC12 have SFA micro-residues, DC26 and DC27 have also SFA micro-residues, but composed of different fatty acids mix leading to a slightly different Raman signal. On another hand, DC4, DC11, DC13 and RF39 were found with unsaturated fatty acids, DC4 and DC13 having an excellent state of preservation of fatty acid micro-residues, having associated individual and smeared micro-residues.

In the experiments (Chapter 4, sections 4.4 to 4.5.2), SFA occur more commonly, especially on dry bone and skin working experiments and on all aged experimental tools. In contrast, on recent experimental tools used on fresh material, unsaturated fatty acid micro-residues are common. The common occurrence of SFA micro-residues over micro-residues containing unsaturated fatty acids, can be explained by two characteristics of fatty acids. First, SFAs have a lower melting temperature point than UFAs, hence being solid fat at ambient temperature, in which condition UFAs are liquid as oil. This fatty solid state probably allows

these compounds to attach and stay preferentially on stone tools during use—hence explaining their general occurrence as a result of tool use on animal or plant material. Second, UFA micro-residues degrade into saturated fatty acids with time, making their content converge toward an end of product containing the less degraded molecules (Regert et al., 1998). That hypothesis is supported by pork fat aging experiment which shows a clear decrease of UFA Raman band markers with time (Chapter 4, section 4.6.1).

The presence of UFAs in micro-residues on artefacts DC4, DC11, DC13, RF39 indicate they have been better preserved than on the other stone tools. The fact that these micro-residues occur in greater numbers and more diverse forms also suggests that UFAs are probably better preserved. Explaining the preservation of unsaturated fatty acid on some Denisova Cave stone artefacts (DC4, DC11, DC13, RF39) is possible, considering that these micro-residues are probably a minor component, with a major component of SFA. This association could have preserved UFAs in a more resistant solid state. Furthermore, it's possible that the cold Siberian climate and stable burial conditions could have enhanced preservation (Derevianko et al., 2015). Obtaining such micro-residues with UFA content with similar spectral Raman signature from new experiments working fresh animal or plant material, is another supporting argument that these SFA/UFA micro-residues are not end products, but rather well-preserved lipids.

Looking toward an archaeological interpretation of these lipids, considering only their spectral fingerprint isn't enough, as SFA micro-residues are end products of degradation processes, with different compositions compared with initial worked material. On the other hand, experimental artefacts show that micro-residues containing UFAs are not plant or animal specific (Chapter 4, section 4.5.2). However, observing how these lipids occur on each artefact surface as individual or smeared micro-residues and their relative frequency provides new information. Results obtained on experimental tools show that lipid micro-residues occur preferentially on stone tools used to work animal materials with a relatively high occurrence (Chapter 4, sections 4.4.2 and 4.5.2). Indeed, it can be expected that subcutaneous skin layers and fresh bone marrow could be rich in fat, hence leading to a higher quantity of smeared and individual lipid residues on stone tools. In contrast, plant materials are in greatest relative occurrence before fatty acid micro-residues on most experimental stone tools used on plant (Chapter 4, sections 4.4.1 and 4.5.1). Smeared micro-residues found on stone tools used on plant tissues are also less extensively distributed than those observed on animal materials. Consequently, the high abundance of smeared fatty micro-residues on DC2,

DC12, DC4, DC13, DC26 and DC27 and the absence of use-related plant micro-residues indicate that the tools were more likely used on animal materials. Indeed, only a few isolated plant fibres and starch grains were found on the artefacts (Appendix IIa, table 2), with a high probability of being linked with incidental contact rather than use. Presence of rare plant micro-residues indicates that plant material can survive on the Denisova Cave stone artefacts, but cannot be related to prehistoric stone tools use among stone artefacts analysed here.

Other associated micro-residues can be helpful for determining the kind of animal material that could have been worked with these stone tools. For example, the presence of apatite on the surface of artefacts cannot (on its own) be related to tool use. As already seen (Chapter 3, section 3.6), this material is present widespread on all studied samples and none of it can be identified optically as a solid bone fragment but always as amorphous apatite. Furthermore, although apatite residues are widespread on all 21 analysed Denisova Cave samples, they do not show any specific spatial distribution on the tools and were found often as a continuous layer covering the whole surface of artefacts from the same layers (e.g., Layer 11.4). Moreover, apatite residues are more commonly found than mineral grains in all the sediment samples studied, indicating that this huge amount of apatite present in the sediment had been transferred onto artefacts.

Absence of collagen fibres on the studied artefacts is another characteristic to take in account. As for plant fibre presence, the presence/absence of collagen is not a result of a poor preservation, since some use-related protein residues were identified on some artefacts (Appendix IIa, table 2); and indicates that protein material can survive intact. Looking at the experimental tools, it can be observed that collagen fibres associated with bone are commonly found on experimental stone tools used to work bone and meat (X284, X288, X309, D1 and D2), but weren't identified adjacent to lipid micro-residues on Denisova Cave stone artefacts. So taking into account experimental results (Chapter 4, sections 4.4 and 4.5), and considering the prominent presence of SFA/UFA individual micro-residues and SFA/UFA smeared micro-residues and the absence of bone and collagen use-related micro-residues on the Denisova stone artefacts, I propose that the most common tissue, on which these prehistoric tools worked, was animal skin.

Support for that interpretation can be found in polish details observed on these artefacts resulting from further use-wear optical analysis (Appendix IIa, table 1). Similar use-polish patterns were identified on artefacts DC2 and DC12 (Fig. 5.9), or for DC4 and DC13 (Fig.

5.18), and are similar to the pattern of polish distributions on experimental skin scraping tools (Fig. 5.21, C-D).

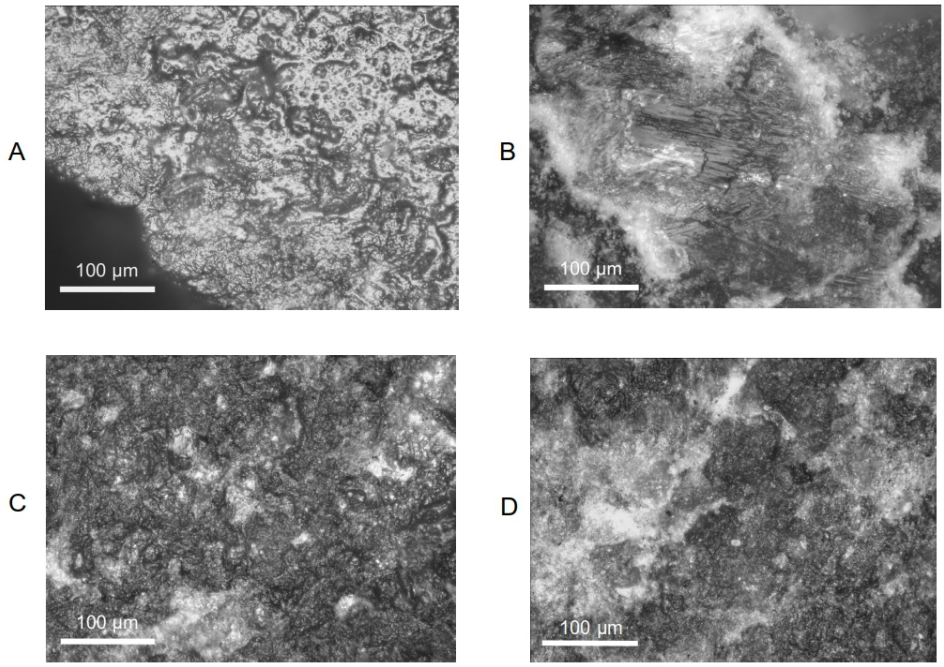

Figure 5.21: Polished area observed (X20) on experimental stone artefact D1 (bone) (A), D2 (meat) (B), D3 (skin) (C & D).

5.5 Conclusion on Denisova artefacts analysis

Results from Denisova Cave East Chamber artefact analysis are in good agreement to previous works about hunting behaviour in Middle Palaeolithic showing that hominins use large ungulates for various purposes (Baryshnikov, 1999). Butchering deer or other animals, and scraping their skins, can have been one of the main activities in the cave. Even if fewer micro-residues are preserved in older levels, a similar material spectral fingerprint, and the location and extent of polish suggest that this activity could have been perpetuated continually through the middle Palaeolithic. The set of stone artefacts studied here were sampled only for this period, so it was not possible to analyse proposed continuities with the Upper Palaeolithic period, but that objective can be targeted for future Denisova Cave micro-residues analysis.

Chapter 6 Liang Bua (Indonesia) stone artefacts analysis

6.1 Archaeological context

Liang Bua is a limestone cave located on the island of Flores, Indonesia (Fig. 6.1), with a cultural sequence spanning ~190 ka. During this time, it has been proposed that the cave was occupied successively by at least two human species, initially by *Homo floresiensis*, and later by *Homo sapiens* (modern humans), currently with no evidence of temporal overlap (Sutikna et al., 2016). The revised dating of *Homo floresiensis* bone remains (LB1) in the cave (Morley et al., 2017) of ~50 ka years ago is close to the time of arrival of modern humans, who are believed by some to be the cause of extinction of *Homo floresiensis* (Callaway, 2016). Indeed the youngest *H. floresiensis* osteological remains date to ~60 ka year ago and youngest associated stone tools with this new hominin species to ~50 ka year ago, which constrains possible overlapping occupation of both species.

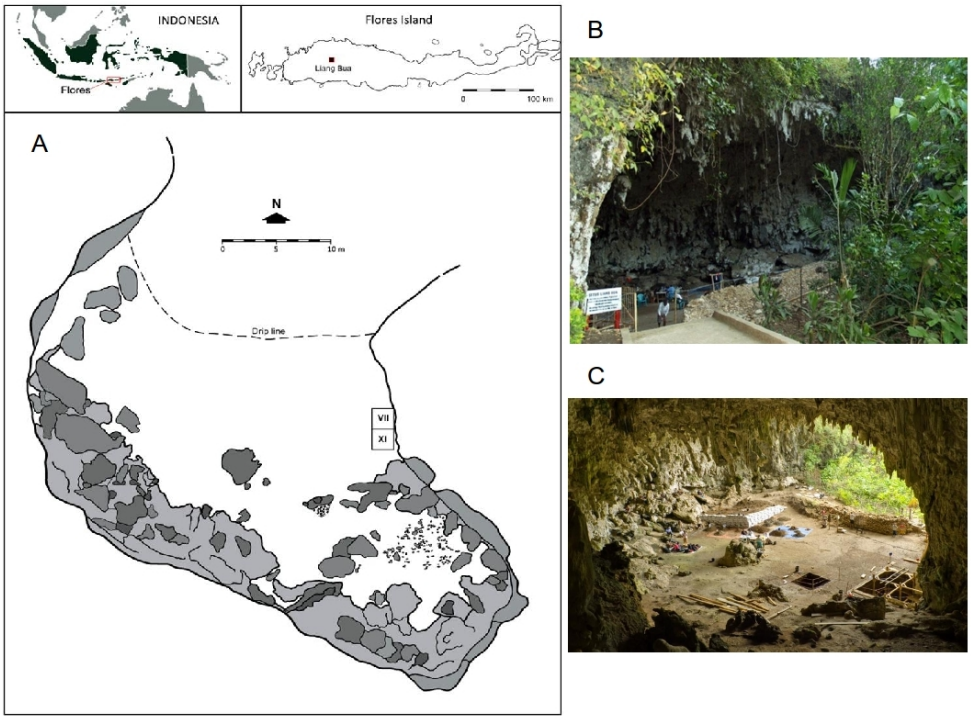

Figure 6.1: Drawing of Liang Bua cave and localisation (A), Liang Bua cave entrance (B), inside view of the cave (C) (Sutikna et al., 2016).

Previous work on the stone artefacts excavated at Liang Bua (Moore et al., 2009) found little variation in stone artefact manufacture techniques between artefacts assigned to modern humans and *Homo floresiensis*, based on the lithic reduction sequence. Nevertheless, a noticeable shift to chert as preferred knapping material, artefacts more frequently exposed to fire, and the abrupt appearance of flakes with prominent edge gloss were documented within the artefact assemblages of modern human (Moore et al., 2009).

6.2 2004 and 2015 collected stone artefacts

6.2.1 Samples

Five artefacts, LB45, LB182, LB228, LB250 and LB337 were obtained among an older collection extracted from sector 11 during 2004 excavation. These five artefacts had been used to evaluate the viability of the analysing method (Bordes et al., 2017). Then, ten stone tools had been randomly selected from artefacts collected in sector 25 and 26 from Liang Bua cave in 2015, and were analysed by Raman spectroscopy. For tools from the 2015 collection, before Raman analysis, a first step of use-wear study and macro-residues localisation was undertaken with optical microscopy on some of unwashed artefacts (LB57, LB3958, LB4131, LB4204) by another researcher (Dr Elspeth Hayes).

6.2.2 Results

A complete list of all analysed micro-residues found on these artefacts can be found in Appendix IIa (Tables 3 and 4) and a summary of analysis results is given in table (Table 6.1**).**

6.2.2.1 Micro-residues identified as modern contaminants

Modern contaminants were found on almost every Liang Bua artefact belonging to these two collections. One of the most common was iron oxide marks left by contact with metal tools (Chapter 3, section 3.9), which have been recognised on artefacts LB45, LB250, LB4340, LB4582, LB3952, LB3958, LB4131, LB4204 and LB57 and identified as contamination from metal tools that likely had contact with these artefacts during the excavation (Chapter 3,

section 3.9). Other contaminants like polyester, translucent cellulose fibres and dark dyed fibres are likely to have their origin from excavation site or from lab airborne contaminants, as they are most of the time found loose on the artefact surfaces and in isolation (Chapter 3, section 3.3). Among these airborne contaminants, dyed modern fibres have been found on artefacts LB3952, LB4131, LB4204, LB57 and LB5227 (Chapter 3, section 3.2.5). Among these dyed fibres, both a dye named “reactive blue”, and indigo dye on an isolated fibre were identified on artefact LB5227 (Fig. 6.2); and an indigo dyed fibre on artefacts LB4131 and LB57. If “reactive blue” dye is clearly related to a modern synthetic dye, indigo dye could be more problematic in the prehistoric archaeological Indonesian context. Indeed, archaeological discoveries date the use of indigo dye back to 6000 years ago in the Indonesian archipelago (Richardson and Richardson, 2016) and Flores island is still a producing area of this traditional dyed fibre. Preservation of the indigo dye is rather good, as thousand-year-old indigo fibres were found recently in Peru (Splitstoser et al., 2016). However, in the case of Liang Bua artefacts, filtering criteria (Described in Chapter 3) were critical for rejecting these fibres as resulting from prehistoric use. Indeed, like many other dyed fibres, indigo dyed fibres were always isolated, on every artefact. Multi spot Raman analysis on one fibre found on LB5227 (Fig. 6.2) reveals that they are made of natural fibre containing cellulose and lignin, dyed with indigo. Indigo Raman spectra were similar to the typical signal obtained on ‘jeans’ indigo dyed fibre, confirming that these indigo dyed fibres originate from modern clothes. Presence of one isolated indigo dyed fibre on artefact LB57 both before and after the washing step confirms that this contamination is arising probably from airborne clothes fibre from people working in laboratory. If most of the dyed modern fibres had been found loose over the artefacts surfaces, some of them have been found closer to the attached sediment. Two of these fibres on artefact LB57 and LB4131 were observed being partially covered by sediment (Fig. 6.3) after washing, suggesting that modern airborne contaminants can also be deposited on stone surfaces when exposed in the laboratory and be subsequently covered by sediment during manipulation or artefact movement in stored bags.

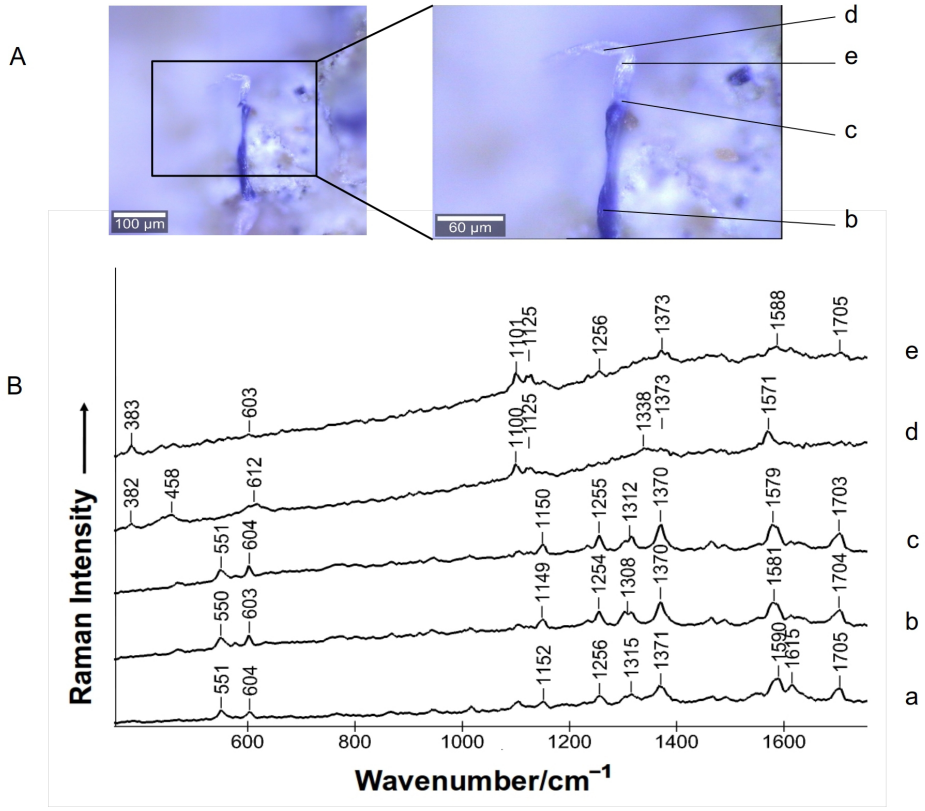

Figure 6.2: Image of indigo dyed fibre on LB5227 (A), Raman spectrum of modern Jean indigo fibre (B, a), Raman spectrum of indigo dyed fibre on LB5227, dyed part showing only indigo pigment (B, b-c), natural fibre extremity without indigo indicating cellulose + lignin content (B, d) and less concentrated dyed part showing cellulose and lignin signal with weak indigo signal (B, e).

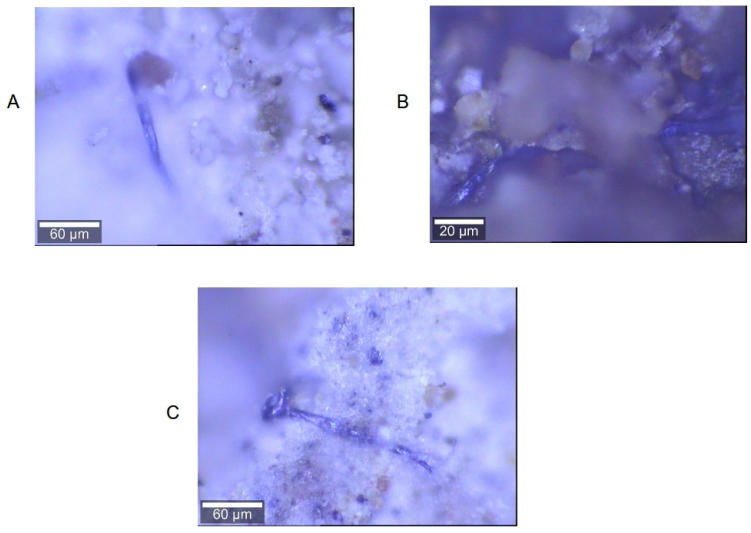

Figure 6.3: Indigo dyed fibre on LB57 emerging from under attached sediment (A), indigo dyed fibre on LB4131 partially covered by sediment (B), dark dyed fibre partially covered by sediment on LB5227 (C).

6.2.2.2 Micro-residues originating from the sediment or from post-depositional processes

Naturally occurring black iron oxide micro-residues were both in the sediment and attached on some Liang Bua artefacts collected in 2004 and 2015. This is the case for artefacts LB182, LB228, LB250, LB45, LB4340, LB4829, LB5227, LB3958. These black iron oxide/hydroxide micro-residues were found coated with organic matter. Under low laser power excitation, the Raman signal obtained from these micro-residues corresponds to unspecified organic material with two broad bands centred at 1592 and ~1380 cm^{-1} (Fig. 6.4, a), respectively known as the G (sp^2 C-C bonds) and D (sp^3 C-C bonds) bands that are typical of amorphous carbon (Tzolov et al., 1993). Increasing the laser power (and thereby burning the organic phase) resulted in spectra of different iron oxides: maghemite (Fig. 6.4, b) with two bands at 681 and 719 cm^{-1} and haematite (Fig. 6.4, c) with its characteristic vibrational bands at 231, 298 and 415 cm^{-1} (Froment and al., 2008). In some cases, the spectra represented a mixture of these minerals with the maghemite contribution to the haematite spectrum at 667 cm^{-1} (Fig. 6.4, d) and recognised as a broadening of this band (Hanesch, 2009). Mixtures of haematite, maghemite and organic matter were also observed (Fig. 6.4, e).

These results indicate that the organic matter is a superficial coating on the iron oxide grains. Their widespread distribution on the surface of the artefacts and high frequency in the sediment suggest that it is a naturally occurring micro-residue at Liang Bua. A possible origin might be the result of micro-organism activity of fungi or bacteria. Previous studies suggested that Mn and Fe rich crusts may form through the action of bacteria in caves (Sebela et al., 2015).

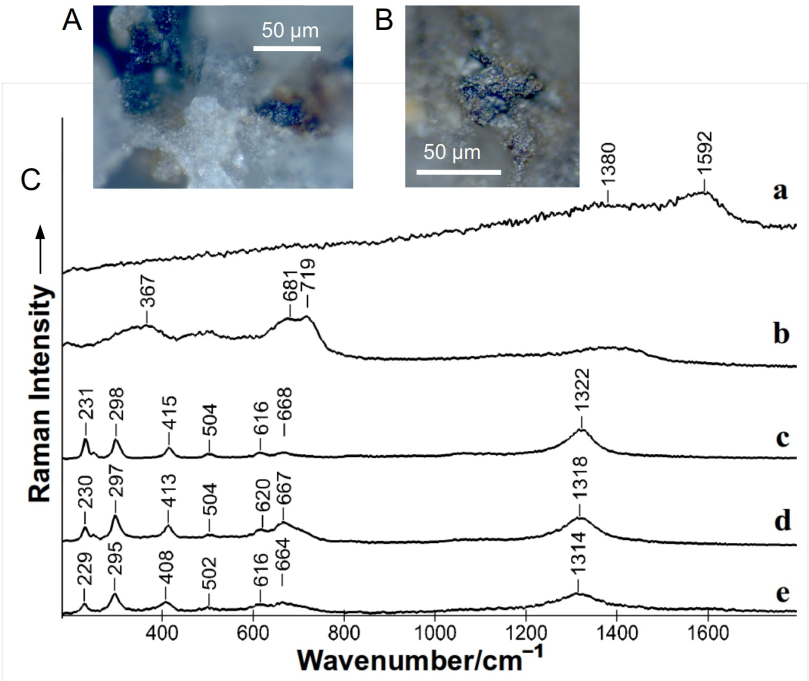

Figure 6.4: Images of black micro-residues found on artefacts LB228 (A) and LB250 (B). Raman spectra recorded on the residues: Recorded with low laser power (C, a) and iron oxide compositions obtained after laser heating: Maghemite (C, b), haematite (C, c), haematite + maghemite (C, d), haematite + maghemite + organic matter (C, e) (Bordes et al., 2017).

Manganese oxide extended crust on stone artefacts or as micro-residues originating from the sediment was found in great abundance on artefacts LB250 and LB337 from the 2004 collection. In contrast, manganese oxide was found in lower abundance and fewer locations on artefacts LB57 and LB4131, belonging to the 2015 collection. Artefact LB250 (Fig. 6.5**,** A) was covered by an extended layer of black to steel grey mineral, with a metallic lustre (Fig. 6.5**,** B-C). Raman spectra obtained for this layer show three broad bands centred around 500, 563 and 621 cm^{-1} consistent with manganese dioxide (MnO_2) (Fig. 6.5**,** D) (Buciuman et al., 1999). As this manganese dioxide surface deposit did not show any recognisable distribution pattern and was also found in the adhering sediments and in sediment layers elsewhere in the cave (Morley et al., 2017), it cannot be considered as linked to the use of the artefact. On the other hand, it can be noticed that manganese dioxide was only found in extended covering or as common mineral residues on the 2016 excavated artefacts (Chapter 6, section 6.3). Even if manganese oxide was deposited naturally in caves together with iron oxides from the action of bacteria (Sebela et al., 2015), evidence from Raman spectroscopy indicates an association

with bone degradation, both on reference bone material (Chapter 4, section 4.7) and, in situ, on 2016 artefacts (see also Chapter 6, section 6.3.2.2). This second origin can explain partially its abundance and extended distribution on these stone tools. However, as artefact LB250 is interpreted as a plant working stone tool, the abundance of manganese oxide needs to be considered more widely as a consequence of bacterial and microbial activity linked with degradation of organic material generally, not only bone.

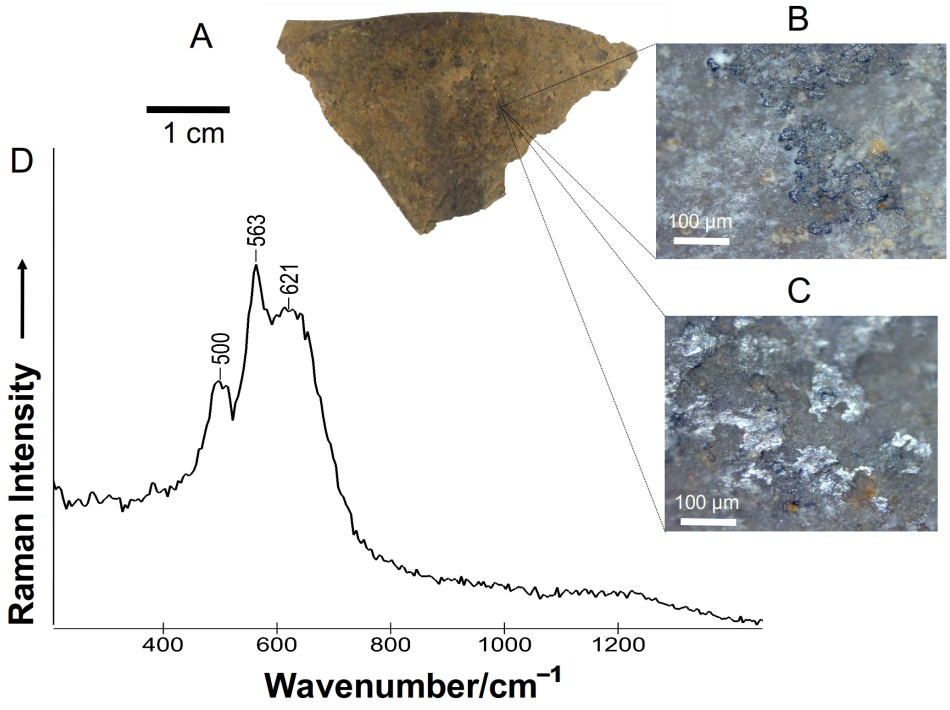

Figure 6.5: Liang Bua artefact LB250 covered by dark stain (A) with a black aspect (B) or a metallic shiny aspect (C), black and shiny metallic widespread residue have the same manganese dioxide (MnO_2) Raman spectrum (D).

More direct traces of micro-organism activity in the cave is indicated by the presence of a biofilm on studied artefacts. Some Liang Bua artefacts have some surface areas covered with biofilm of varying extent (Bordes et al, 2017), with the thickest covering occurring on Pleistocene artefact LB337. Biofilms can consist of bacteria, fungal colonies and other living organisms and regularly occur on stone monuments (Martino et al., 2016). Due to a large fluorescence background under green excitation, the spectra obtained on artefact LB337 were collected using the 785 nm laser line (Fig. 6.6**)**. The main vibrational bands in the spectra at 1236, 1304, 1416, 1530 cm^{-1} (Fig. 6.6, A) are similar to the Raman fingerprint of fungi collected *in situ* on Neolithic paintings (Hernanz et al., 2015). The same typical spectrum was also obtained on individual fungi filaments encountered on the edges of all the other analysed

artefacts (Fig. 6.6, B and C). Variations in the mineral composition of the underlying surface is responsible for the colour differences of the biofilm with bands at 259, 391 and 690 cm^{-1}, originating from iron oxides, present in spectra recorded on yellow areas (Fig. 6.6, A); while bands of cristobalite (419 cm^{-1}) and feldspar (287 and 510 cm^{-1}), which dominate the mineral background of artefact LB337, could be observed in spectra from white areas. Because of time limitation, the presence of biofilm has only been investigated systematically on four artefacts in the 2004 collection, but was noted sporadically on artefacts from Denisova cave (Chapter 5, section 5.3.2) and on other Liang Bua artefacts, notably by the presence of fungi filaments.

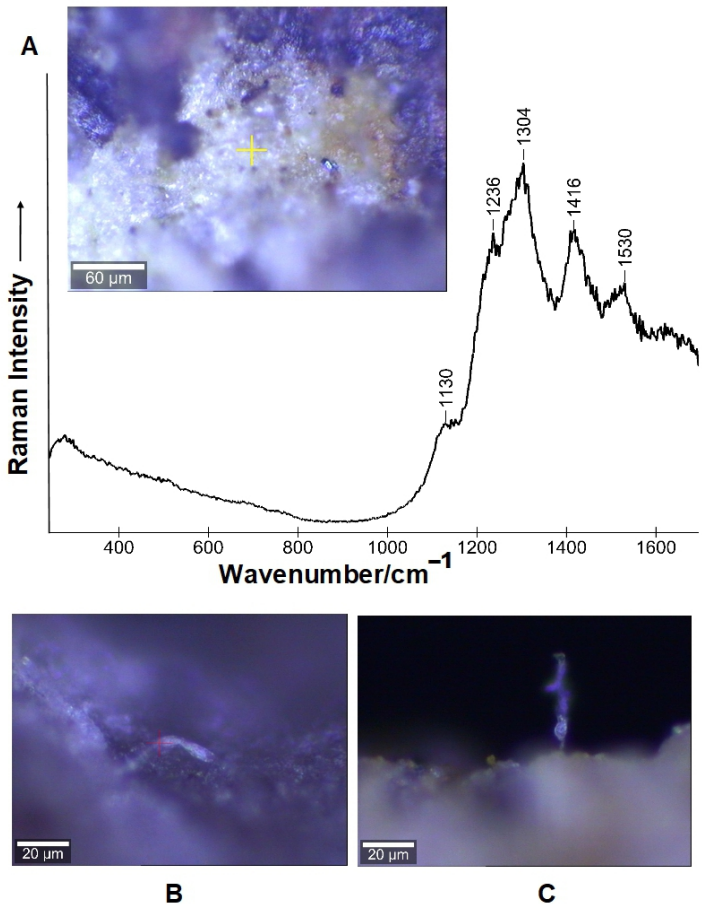

Figure 6.6: Image of biofilm covering artefact LB337 and Raman spectra recorded on it (A), images of typical fungi filaments (B-C) (Bordes et al., 2017).

Geological apatite was also identified as a micro-residue with a sediment origin, especially on artefact LB337. Small white rods (size 10-20 µm) were observed loosely attached to the surface of artefact LB337 (Fig. 6.7, A) and in the sediment that was removed from the artefact

during ultrasonication (Fig. 6.7, B). The Raman spectrum of the rods consists of a strong PO^{4-} vibrational mode at 968 cm^{-1} and two weaker bands at 433 and 592 cm^{-1} (Fig. 6.7, C, a), comparable to published spectra of geological hydroxylapatite (Wopenka et al., 2005) and to spectrum b in (Fig. 6.7, C, b) of a geological apatite sample. In addition to the Raman peaks, strong bands occur in the spectrum of the rods (spectrum a) at 1146, 2083 and 3291 cm^{-1} (564, 600, 645 nm) that can be attributed to luminescence from the rare earth element samarium (Sm^{3+}) with contributions from praseodymium (Pr^{3+}) as their luminescence bands overlap (Czaja et al., 2008; Gaft et al., 2005; Gorobets et al., 2001). Spectrum b recorded on an apatite sample from Australia only has small luminescence bands that can be attributed to Europium. The Raman spectra differ from that of bone apatite (Fig. 6.7, C, c-d) as the totally symmetric P-O stretch vibration occurs at higher wavenumbers (968 cm^{-1} in contrast to 963 cm^{-1} for bone) and the full width at half maximum (FWHM) of this peak is 9 cm^{-1} in comparison to 20 cm^{-1} for spectrum d of fresh bone containing collagen (peaks at 1254, 1451, 1675 and CH stretch vibrations) (Fig. 6.7, C, d). Furthermore the 1072-1074 cm^{-1} peak attributed to carbonate in bone (Fig. 6.7, C, c-d) was absent from the apatite rods analysed. The fact that the Raman spectra of these apatite rods have systematically such a distinct signal from the typical spectral signature obtained on bone, indicate that these objects are probably of geological origin. Furthermore, their uniform shape and size suggest they are not from the random fragmentation of bone material, but result from natural crystal growth.

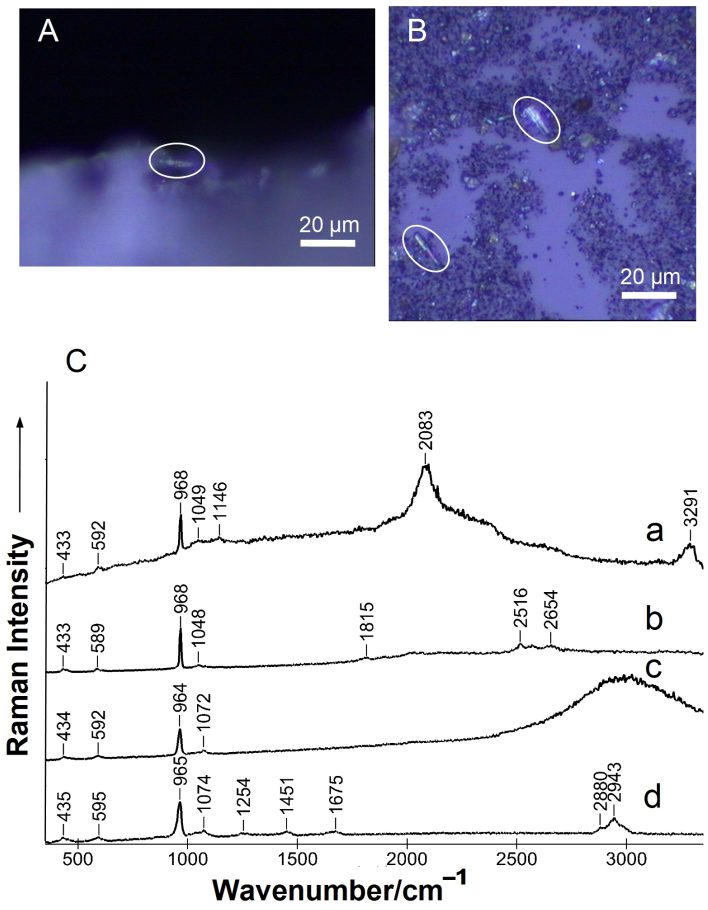

Figure 6.7: Images of apatite rods: On the edge of artefact LB337 (A) and in the sediment washed of the artefact (B). Raman spectra recorded on an apatite rod found in sediment attached to artefact LB337 (C, a), geological apatite reference (C, b), bone fragment found in sediment washed from artefact LB337 (C, c) and bone containing collagen (C, d). (Bordes et al., 2017).

On 2004 and 2015 collected artefacts, apatite micro-residues were identified only in the layer and adjacent sediments belonging to artefact LB4582. For this artefact, the apatite can be identified as fossil bone according to our material references (Chapter 4). However, in the case of this artefact, finding fossil bone in associated layer sediment argues against any link with tool use. Indeed, a concentrated set of several fossil bone micro-residues were found on the main polished edge of the unwashed artefact (Fig. 6.8, A-F), but this very restricted distribution and absence of smeared bone micro-residues (Chapter 3, section 3.5) raises questions about its origin. Moreover, the apparently loose attachment of these fossil bone micro-residues on the edge of artefact LB4582 is supported by the absence of any fossil bone residues staying attached after washing. This result emphasises the fact that even potentially

key archaeological micro-residues like bone, which could display a meaningful distribution in association with polish and other criteria, could originate from the sediment—hence the importance of considering critically others criteria (Chapter 3); and checking the sediment layer for each studied artefact. In the case of artefact LB4582, a bone in contact with the artefact during burial can explain the presence of this concentrated distribution of bone on this restricted edge area. Indeed, any use-related micro-residues would have been found more widely distributed along the polished edge and not only on this restricted spot.

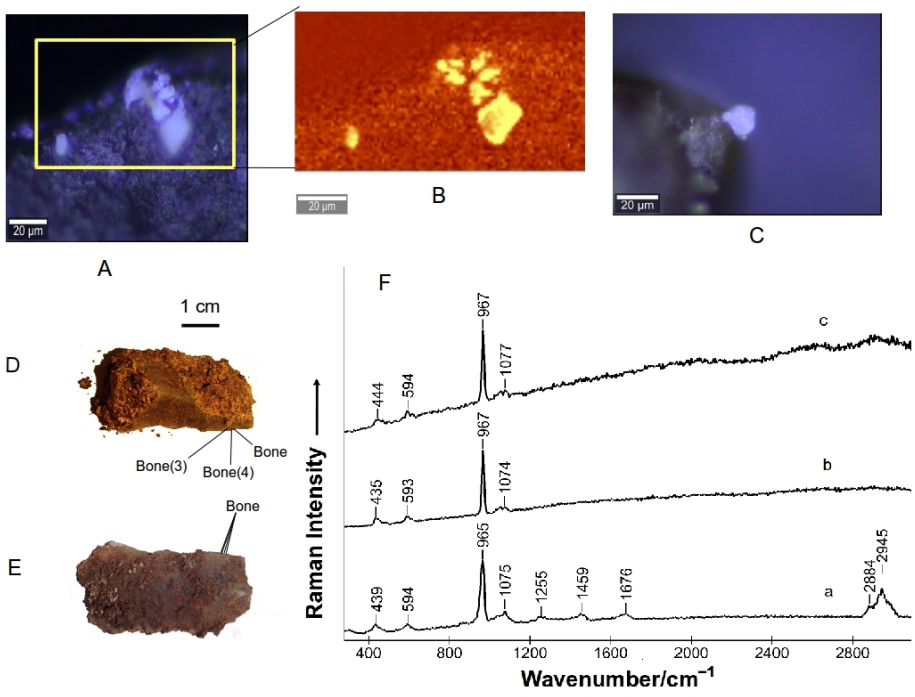

Figure 6.8: Group of fossil bone micro-residues found concentrated on dorsal LB4582 main edge (A), spectral image obtained by scanning bone residues group on intensity of main fossil bone apatite band (967 cm^{-1}) (B), fossil bone micro-residue identified in LB4582 sediment (C), localisation of bone micro-residues, dorsal side LB4582 (D), localisation of bone micro-residues, ventral side LB4582 (E). Comparison of Raman spectra obtained on bone micro-residue found in sediment (F, b), on LB4582 dorsal edge (F, c) with modern dry bone containing collagen (F, a).

Despite Liang Bua cave being located in a tropical forest environment where we could expect plant material arising from the surrounding and underground growing vegetation, plant fibres were almost never encountered in associated layer sediments, except in the sediments of artefacts LB3958 and LB4130. These latter fibres match the typical Raman fingerprint obtained from plant fibres composed of cellulose and lignin (Chapter 4, sections 4.4.1 and 4.5.1).

6.2.2.3 Potential use-related micro-residues

Protein micro-residues were present on a majority of Liang Bua 2004 and 2015 collection artefacts, sometimes appearing as a group of micro-residues and not present in layer sediment. They were generally not widely distributed, but their spatial distribution cannot always be clearly related to polish distribution. These proteins can arise from different origins. One of the sources could be from the handling of artefacts with bare hands (Chapter 3, section 3.2.3). As some non handled artefacts were bearing this kind or residue, another source of protein could be a post-depositional process. Difficulty of sorting different protein origins is due to the lack of a high signal-to-noise ratio on Raman protein spectra that do not systematically distinguish distinct proteins. However, even if non-specific by Raman spectroscopy, clear concentrations of protein micro-residues in association with polished areas were found on some 2016 artefacts (Chapter 6, section 6.3.2.4), so they need to be considered as potentially use-related on some artefacts, but need to be considered carefully in relation to other specific micro-residues like bone or plant material.

Protein associated with calcium nitrate was found on all 2004 artefacts and artefacts LB4340, LB4582, LB4829, LB5003 and LB3952 from the 2015 collection (Fig. 6.9**)** (Appendix IIa, tables 3 and 4). This detected nitrate associated with protein was analysed on some of the reference stone tools from 30 years ago that were used to work plant material and shows similar spectral signatures (Chapter 4, section 4.4.1) but never on recent experimental tools (Chapter 4, section 4.5.1). Consequently, I infer that the protein containing calcium nitrate does not originate from recent modern contamination, but could result either from prehistoric tool use or from post-depositional alteration processes. Furthermore, calcium nitrate was found associated less commonly with starch grains or plant fibres on 2004 and 2015 collection artefacts—so it is suspected that its presence may be linked with plant residue degradation processes.

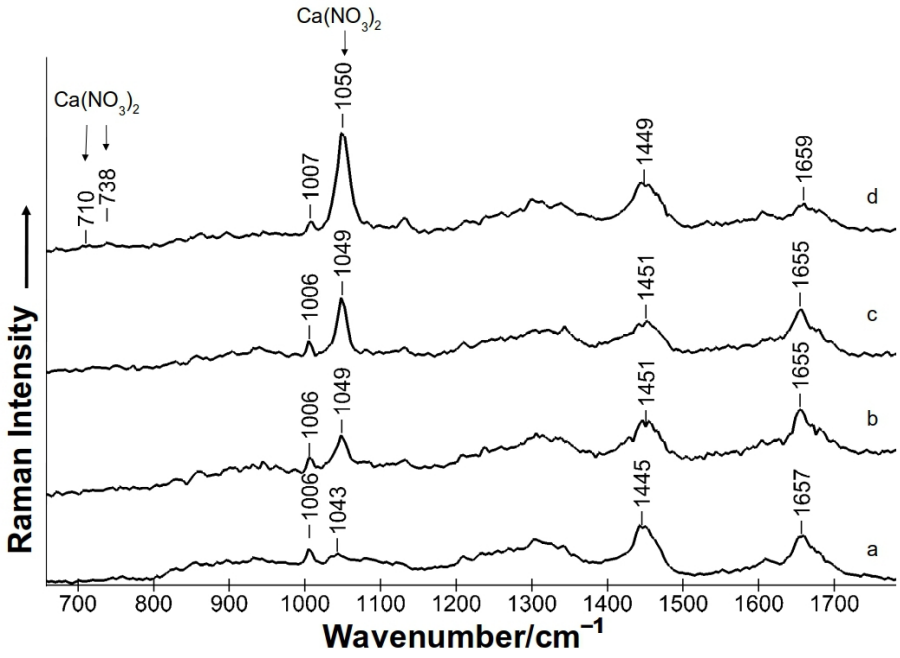

Figure 6.9: Raman spectrum of typical protein micro-residue found on Liang Bua artefacts: Pure protein micro-residue (a), protein residue with low calcium nitrate content (b), protein micro-residue with medium calcium nitrate content (c), protein micro-residue with high calcium nitrate content (d).

Artefacts LB45, LB182, LB250, LB4582 used on plant material with majority of saturated fatty acid individual micro-residues

Potentially use-related SFA (saturated fatty acid) individual micro-residues were found on these four stone artefacts. They were detected either as pure SFA residues, or as mixed with protein residues. When these individual SFA micro-residues were found in association with protein (Fig. 6.10), they could also show calcium nitrate content, but this compound had never been detected associated with pure SFA micro-residue. This observation shows that calcium nitrate presence is linked to protein micro-residues or resulting from their degradation but not in direct association with SFA micro-residues.

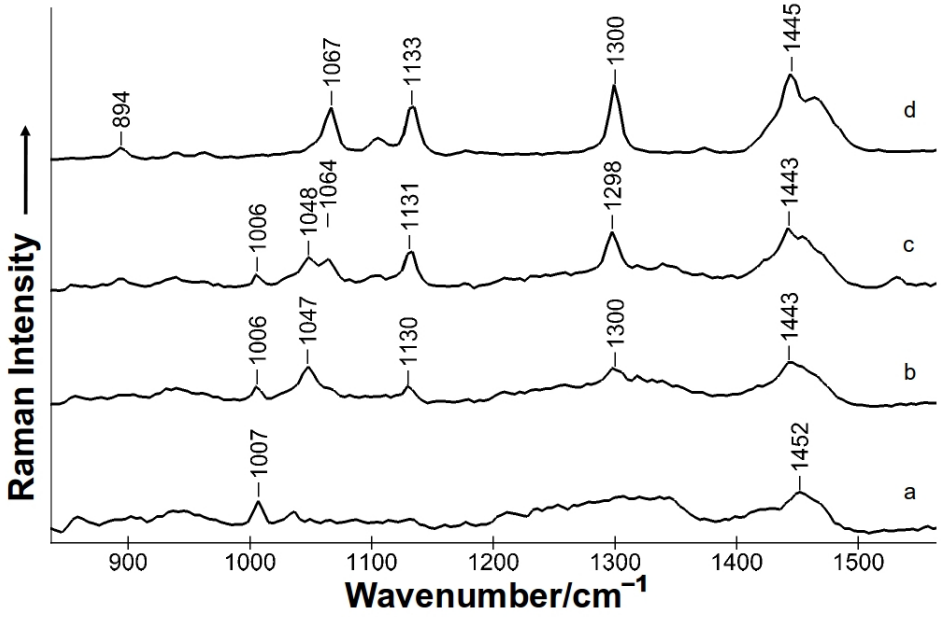

Figure 6.10: Spectra of proteins and protein / fatty acid mixtures associated with calcium nitrate (characteristic peak at 1047-1048 cm^{-1}): Pure protein micro-residue (a), mixed SFA/protein micro-residue with low saturated fatty acid content (b), mixed SFA/protein micro-residue with high saturated fatty acid content (c), and pure SFA micro-residues (d).

Where it was not possible to find particular spatial concentrations of protein residue on Liang Bua artefacts belonging to this artefact collection, SFA micro-residues tended to show such spatial concentration related to polished area on a few artefacts—as for artefacts LB45, LB182, LB337 and LB4582. For example, on artefact LB182, protein residues are located on every edge independently of the intensity of polish but individual SFA residue and mixed individual SFA residue were only present on continuous distal polished edges and highly polished areas including the flaking platform, but not on discontinuous polished or non-polished edges (Fig. 6.11). On artefact LB4582, a concentration of individual SFA micro-residues were found in the middle of the main polished edge, on both sides, although not on other non polished edges (Fig. 6.12). However, both highly polished distal and proximal parts of the main used edge of artefact LB4582 are devoid of SFA micro-residues. It should be noted that this middle part of the main used edge had intense scarring, which could have caused loss of polished edge—particularly likely if the central part of the artefact had been the main working area (Fig. 6.12).

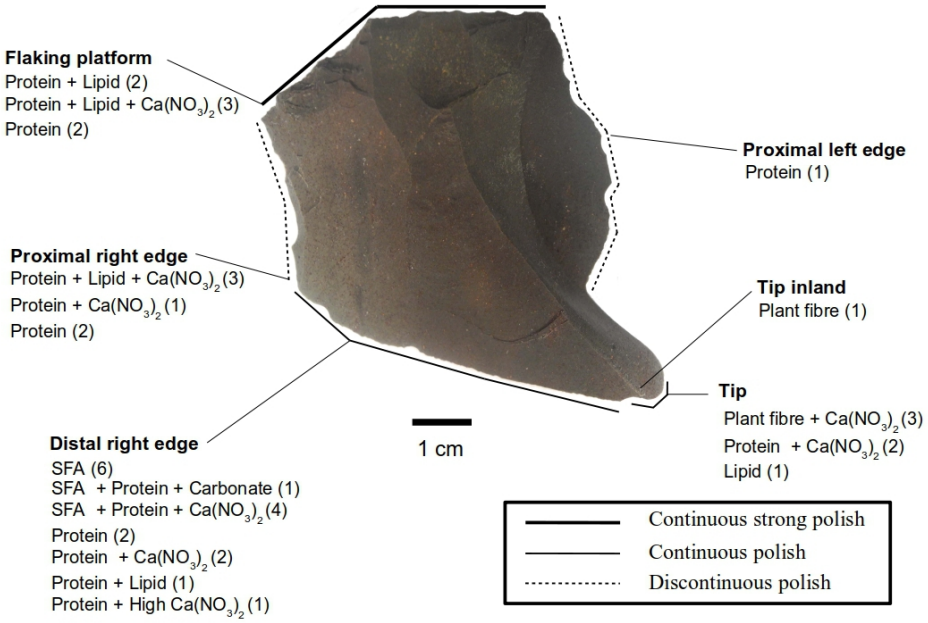

Figure 6.11: Polished edges and residues distribution on dorsal side of artefact LB182. Analysis of proteins, saturated fatty acids (SFA), mixed protein/SFA residues containing or not calcium nitrate, have been summarised for each edge. Numbers of each type of residue for each edge are indicated between brackets (Bordes et al., 2017).

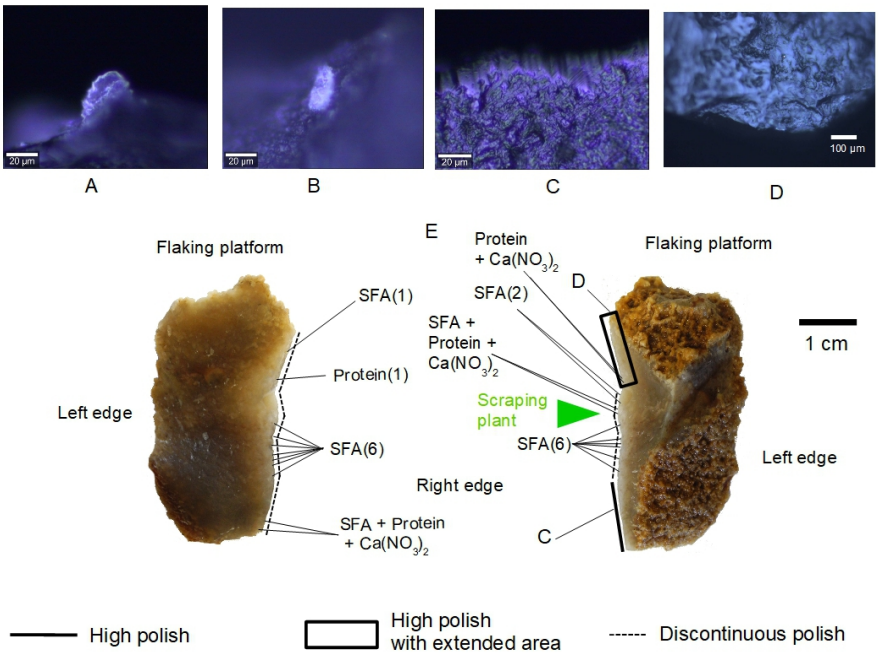

Figure 6.12: Correlation between polish and SFA and protein micro-residues distribution on dorsal and ventral side of artefact LB4582: SFA micro-residue (A), SFA/protein mixed residue containing calcium nitrate (B), highly polished dorsal distal right edge (C), highly polished edge and area on proximal dorsal right edge (D), correlation between polish and SFA and protein micro-residues distribution on dorsal and ventral side of artefact LB4582 (E) .

Taking in account SFA spatial distributions and considering that their Raman spectra could be distinguished from handling SFA (Chapter 3, section 3.2.3) these SFA residues could be interpreted as related to stone tool use. On their own, the nature of these SFA individual micro-residues is difficult to link with a particular animal or plant material because they are probably an end product of fatty acid residues (Chapter 4, section 4.4). Indeed, UFAs commonly degrade into SFAs when exposed to the environment (Regert et al., 1998).

In addition to individual saturated fatty acid micro-residues, an unique smeared area of saturated fatty acid was found on one polished edge of artefact LB250. This kind of smeared SFA residue is not considered the result of handling and, along, with other individually SFA micro-residues found on another edge of LB250 (Fig. 6.13), has a higher likelihood of being use-related (Chapter 3, section 3.5). Furthermore, its two indented edges were likely the main used edges of that stone tool. These indented edges are close to the area where smeared and individual micro-residues were found. They seem to be a good indication of use-related fatty acid micro-residues resulting from prehistoric tool-use. A few plant micro-residues were found on artefacts LB45, LB182 and LB250, indicating that these tools had been used on plant materials, an interpretation that is confirmed by their polish, which is likely linked with high silica content (Bordes et al., 2017). No plant micro-residues were found on artefact LB4582 but similar micro-residues, including individual SFA, protein and protein with calcium nitrate, along with presence of high silica polish, confirm use of this stone tool to process plant tissue. More plant micro-residues with a similar association with individual SFA micro-residues was analysed on Liang Bua artefacts 2015 collection, LB4204 and LB4340 (presented below), and strongly supports use on plant material in both the 2004 and 2015 artefact collections.

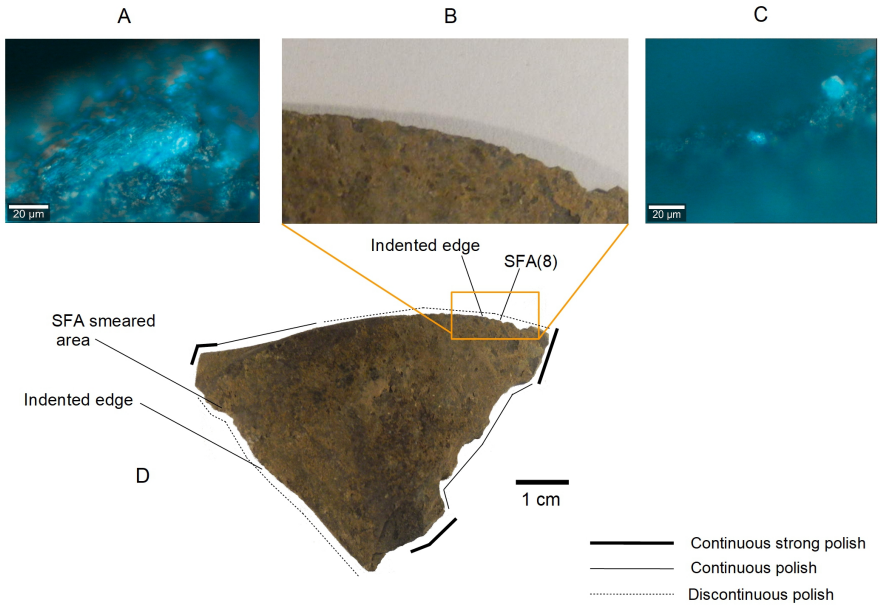

Figure 6.13: Smeared SFA area found on artefact LB250 (A), detail of an indented edge part (B), SFA individual micro-residues found on artefact LB250 (C), distribution of smeared and individual SFA micro-residue in relation with polish and indented edges (D).

Plant fibre on artefact LB4204

Polish distribution on artefact LB4204 indicates that it had been used as a double scraper. Indeed a highly polished area had developed on the proximal edge of the dorsal side during scraping work and the tool edge was retouched until exhaustion (Fig. 6.14, A). Subsequently, the opposite distal edge on the ventral side was used in the same way and lead to a similar extended area of polish on that side (Fig. 6.14, B). The left edge seems to have been used also for scraping on both sides and this edge is well-rounded from use. A group of plant fibre micro-residues was found in the middle of that polished edge, with some concentrated SFA individual micro-residues located more towards the distal part of the same edge. Raman microscopy confirmed that the group of plant fibres was homogeneous and likely originated from the same plant material (Chapter 3, section 3.3, Fig 3.13). Other plant fibres were found scattered on some polished edges and surfaces of that stone tool but were isolated occurrences. The main group of plant fibres (Fig. 6.14, C-D) and SFA micro-residue concentrations can be considered as related to stone tool use, and these plant fibres can be identified as grass material (Chapter 4, section 4.4.1), as shown by typical spectral signatures obtained and compared with different experimentally worked plant fibres (Fig. 6.15).

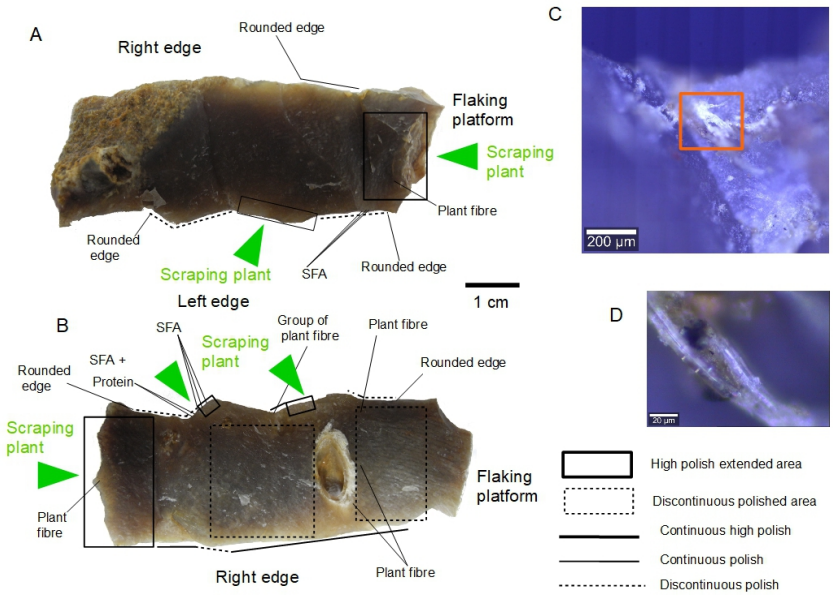

Figure 6.14: Polish and SFA micro-residues and plant fibre micro-residues for artefact LB4204 dorsal side (A), polish and SFA micro-residues and plant fibre micro-residues for artefact LB4204 ventral side (B), group of fibres found on ventral main edge (C), detail of plant fibres (D).

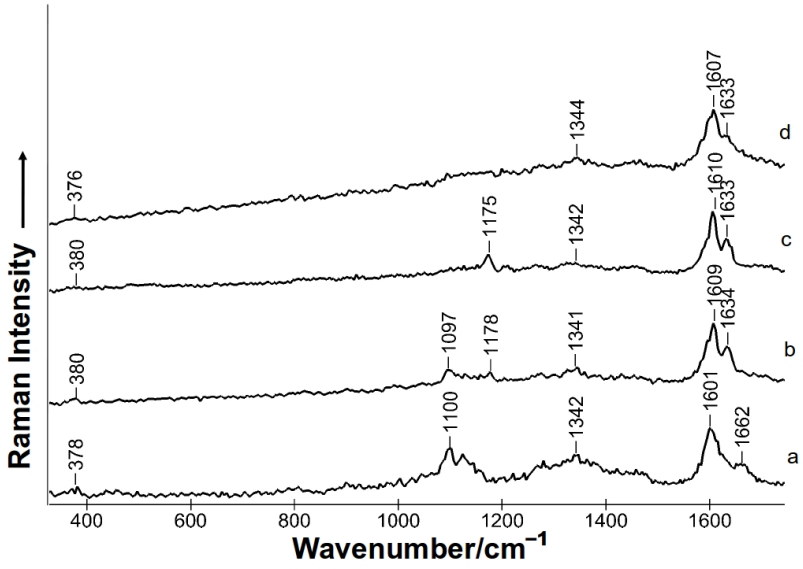

Figure 6.15: Comparison of plant material micro-residues found on LB4204 with different wood, grass and bamboo references (excitation 532 nm): Pine dry wood (*Pinus sp.)* (a), fountain grass (*Pennisetum setaceum*) (b), Indonesian bamboo (*Bambuseae sp.*) (c), plant fibre found on LB4204 (d).

SFA individual micro-residues, plant fibres and charcoal micro-residues on artefact LB4340

According to the polish distribution, this artefact was used as a scraping tool, using mainly both left and right edges on the dorsal side (Fig. 6.16, A**)**. A small part of the left proximal edge was also used for scraping on the ventral side (Fig. 6.16, B**)**. On this artefact, charcoal micro-residues (Fig. 6.16, C-D) were detected in high frequency, especially on the main right edge and are not present in the layer sediment. Charcoal Raman spectra are distinct from common unspecified organic material that can be encountered for black iron oxide residue (Fig. 6.4), and have a narrower 1600 cm^{-1} G (sp^2 C-C bonds) and broader D (sp^3 C-C bonds) bands~1375 cm^{-1} (Francioso et al., 2011) (Fig. 6.16, E). Furthermore, one characteristic of charcoal micro-residues is that they are very resistant to laser burning when laser power is increased. Therefore charcoal particles could be confirmed as use-related micro-residues, resulting probably from a scraping action on burned material, for example, on charred wood or on plant material.

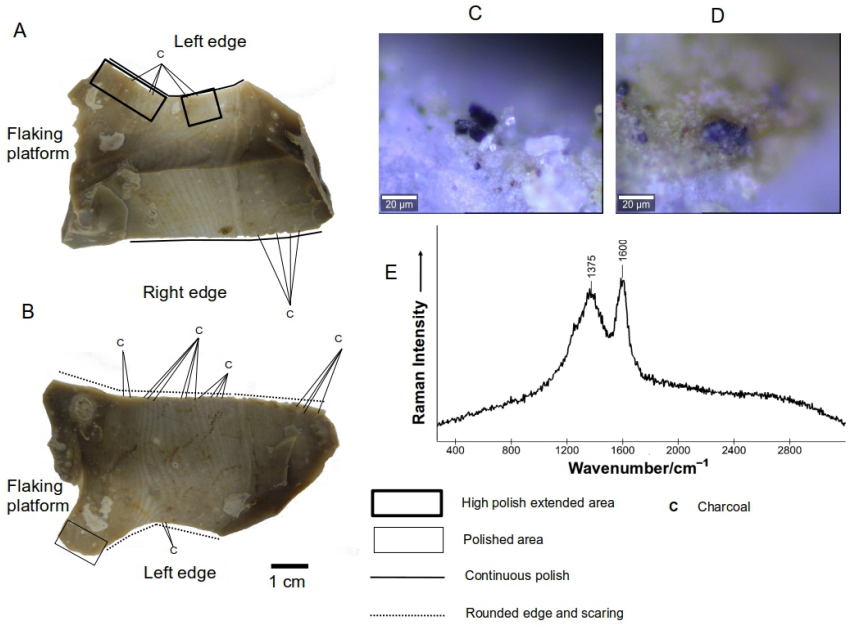

Figure 6.16: Polish and charcoal micro-residues on artefact LB4340 dorsal side (A), polish and charcoal micro-residues on artefact LB4340 ventral side (B), charcoal micro-residues found on ventral left edge (C-D), typical Raman spectrum of charcoal micro-residues (E).

Additionally artefact LB4340 has SFA micro-residues and plant material present on its polished edges (Fig. 6.17). Plant material micro-residues are present on this artefact as either

amorphous plant tissues or distinctively shaped fibres. However, plant material and fibre were isolated on artefact LB4340, and not found as a group of micro-residues as for artefact LB4204, weakening their relation with tool-use. But presence of SFA micro-residues along with these plant fibres tend to indicate that artefact LB4340 could have been used on a similar material to that found on previous artefacts LB4204 and LB4582.

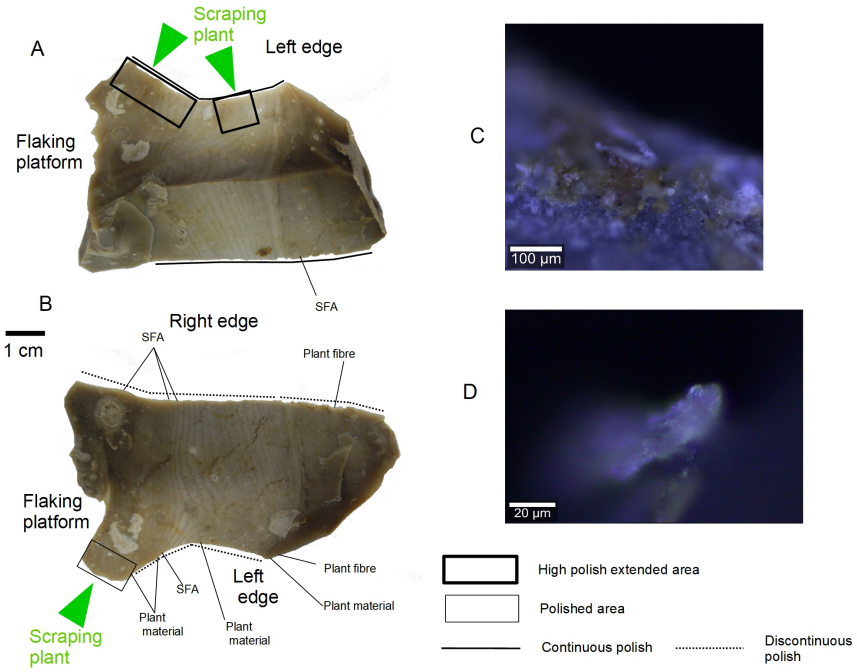

Figure 6.17: Polish, plant fibres and SFA micro-residues on artefact LB4340 dorsal side (A), polish, plant fibres and SFA micro-residues on artefact LB4340 ventral side (B), plant fibre found on ventral left edge (C), plant material micro-residue found on right ventral edge (D).

Artefact LB5227

A concentration of fibres was detected on the dorsal side of this artefact. Not less than nine different fibres were distinguished by Raman spectroscopy. Two different kinds of fibre were analysed: undyed and dyed fibres. The more numerous undyed fibres are natural plant fibres containing cellulose and lignin. They are the only fibres found on artefact LB5227 as a group of micro-residues (Fig. 6.18, C and D, c) (Fig. 6.21, A and B). Two other natural plant fibres found on the same artefact have a similar lignin band doublet to those from LB4204 (Fig. 6.15, d**)** but differ from them by a higher intensity of cellulose bands (Fig. 6.18, B and D, b**).** They have been found always isolated and have an accentuated particular bluish aspect. Other undyed fibres found on artefact LB5223 are pure cellulose fibres without any lignin content

and showing a very high intensity spectrum, indicating a recent modern origin (Fig. 6.18, A and D, a**)**.

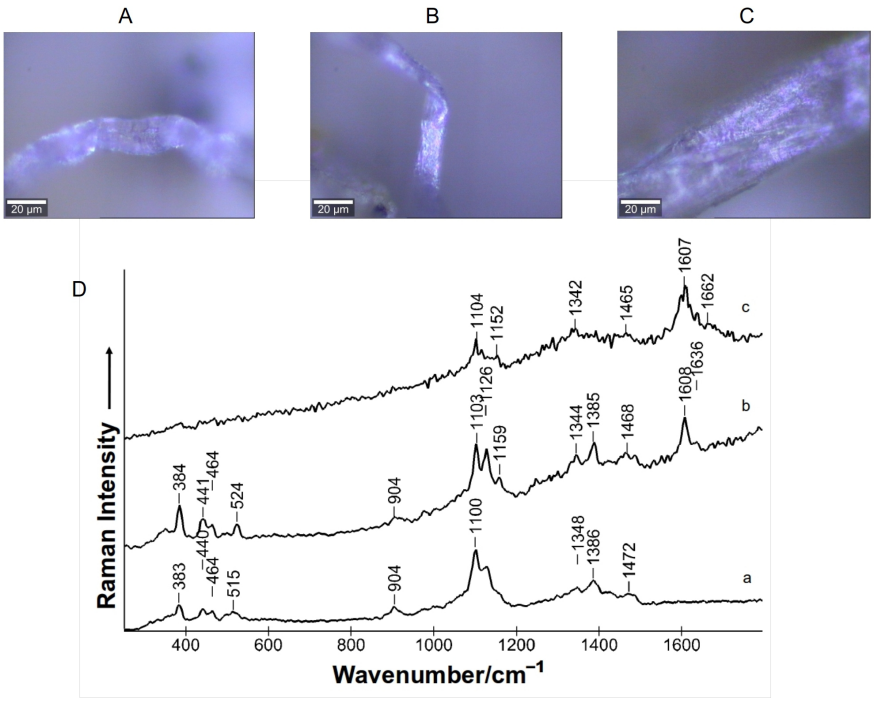

Figure 6.18: Pure cellulose fibre found on LB5227 (A), bluish natural plant fibre found on LB5227 (B), plant fibre found as group on LB5227 (C), Raman spectra of natural plant fibre found on LB5227 (D): Pure cellulose fibre (D, a), bluish natural plant fibre (D, b), plant fibre (D, c).

Six kinds of dyed fibre were analysed on LB5227 (Fig. 6.19). They were always found isolated on artefact LB5227. The more numerous, dark fibres, vary between dark blue and black, with a broad Raman spectral signature, close to those encountered for glove fibre contaminants (Chapter 3, section 3.2.1) (Fig. 6.21, A and D). A second kind of dark dyed fibre caused a distinct Raman fluorescent signature on which only two bands were often visible (Fig. 6.19, D, c). On other kind of dyed fibre, it was possible to obtain a Raman signature similar to those observed for modern dye named “reactive blue” (Fig. 6.19, C and D, b) (Was-Gubala et al., 2014). Some of these dyed fibres were also found to have a “dark and clear” aspect, where the dye covering was in different amounts or altered on some fibre sections. In particular, this was the case for an entangled, long fibre shown in Figures 6.19 (A-B) and 6.21 (C). Some clear sections gave a cellulose and lignin content in their Raman signal (Fig. 6.19 D, a), indicating that these fibres are dyed natural plant fibres. The dye partially covering these fibres was identified as close to the modern reactive blue dyed Raman signature (Fig. 6.19, D, b).

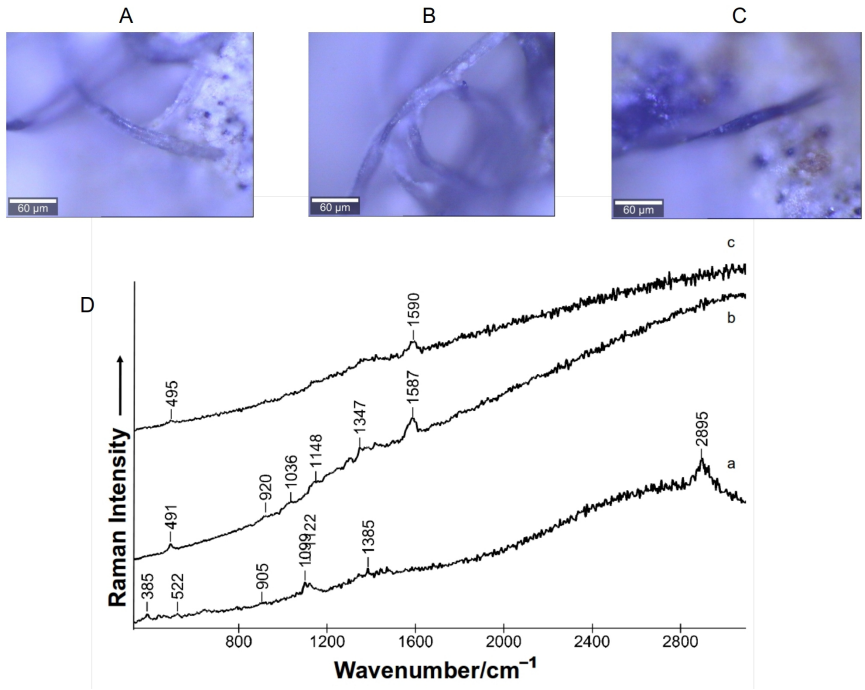

Figure 6.19: Half dark and clear partially dyed fibres found LB5227 (A-B), reactive blue dyed fibre found on LB5227 (C), dyed and partially dyed fibre Raman spectra found on LB5227 (D): Clear plant fibre part of a partially dyed fibre (D, a), reactive blue dyed fibre (D, b), fluorescent dark part of a partially dyed fibre (D, c).

Two modern indigo fibres were also analysed on artefact LB5227 (Fig. 6.21, A), but a third fibre had a slightly darker coloured outer aspect leading to a highly fluorescent signal, and an inner fibre aspect suggesting it was dyed with indigo as well. This latter fibre is probably another indigo dyed modern fibre, maybe mixed with another unidentified dye.

Additionally, one analysis of a coloured isolated dyed fibre had a Raman spectrum indicating an undetermined dye (Fig. 6.20 A-B). The bulk part of this fibre was fluorescent (Fig. 6.20, A, C, b) but the extremity analysis showed a Raman spectrum with a higher signal-to-noise ratio (Fig. 6.20, B, C, a).

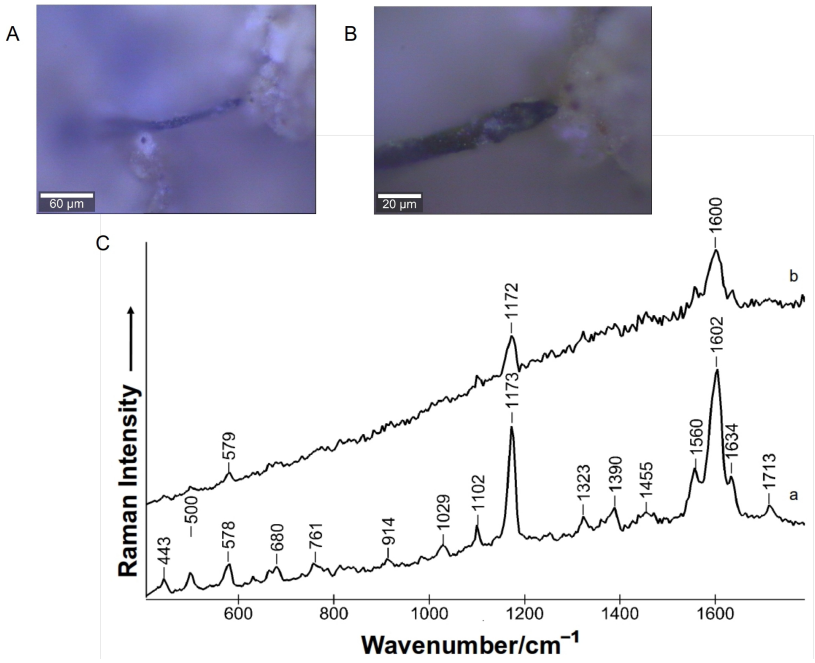

Figure 6.20: Fluorescent dark fibre with unidentified dyed found on LB5227 (A), extremity of dark fibre with unidentified dyed (B), unidentified dyed Raman spectra (C): Less fluorescent fibre extremity with an unidentified dye leading to higher signal-to-noise ratio (a), fluorescent bulk part with an unidentified dye dark leading to low signal-to-noise ratio (b).

With respect to potentially use-related fibres on artefact LB5227, only plant fibres containing lignin and found in higher frequency and sometimes found in groups are likely to be of prehistoric origin (Fig. 6.21, A, B). Nevertheless, it's not straightforward to link these plant fibres to the use of that tool because their spatial distribution is not exclusively included in the darker polished zone observed on this artefact (Fig. 6.21, A). Consequently, it's probable that these plant fibres could have been incidental to the use of that stone artefact.

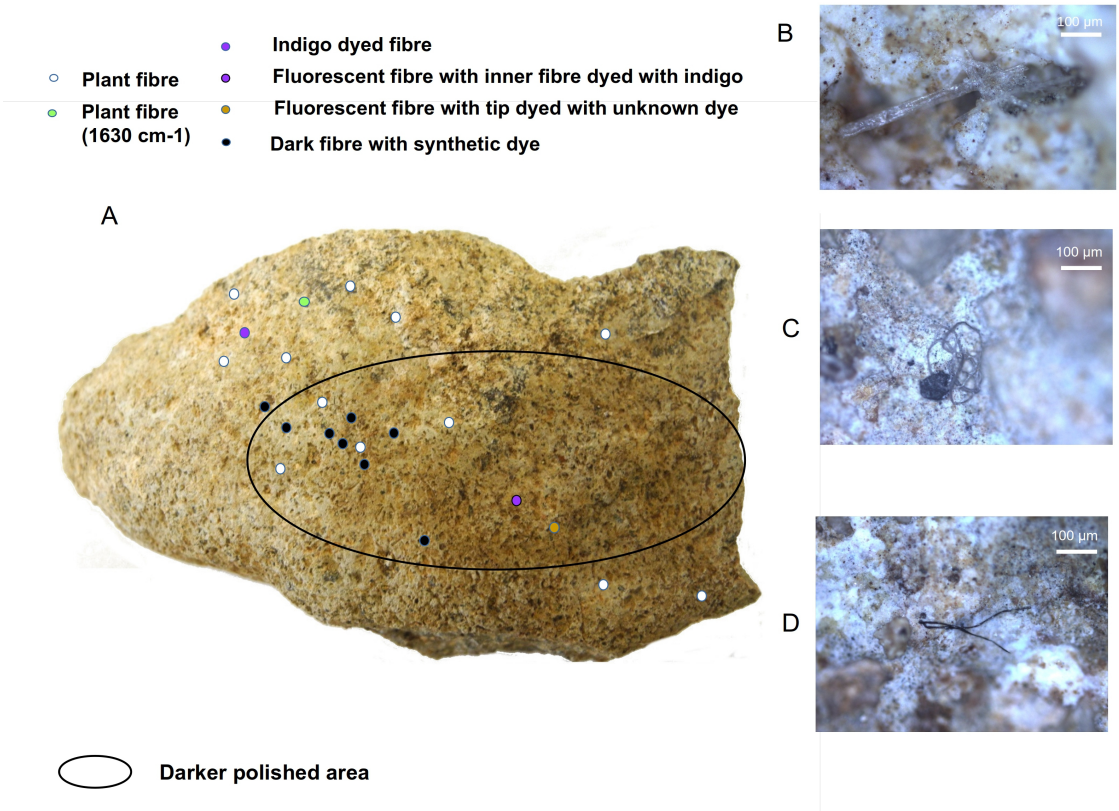

Figure 6.21: Spatial distribution of six types of plant fibre on dorsal side of LB5227 (A), group of plant fibres found on LB5227 (B), entangled dark and clear long dyed fibre found on LB5227 (C), dark dyed fibre found on LB5227 (D).

6.2.2.4 Interpretation

The 2004 and 2015 collections of stone artefacts show the presence of individual SFA (artefacts LB45, LB182, LB250, LB337) and plant fibres (artefacts LB4204, LB4340, LB5227) and charcoal (artefact LB4340) (Table 6.1). On artefact LB4340, it was possible to analyse all these micro-residues and link them to use. Presence of SFA individual micro-residues and plant fibres are commonly found on experimental tools used on plants (Chapter 4, section 4.4.1), supporting an interpretation of stone tool use on plant material along with an indication of use of fire marked by charcoal use related micro-residues on LB4340. If we consider the more common use of tools according to their polish distribution, scraping plant material could have been the more common activity. On these artefacts, layer preservation of micro-residues was not high as shown by individual residues in low concentrations, with a just a few plant

fibres found on the same spot. Although plant species cannot be accurately identified by Raman spectroscopy, plant taxon, like grass material (i.e., Gramineae) was specifically identified on artefact LB4204. Modern contamination “noise” was high on the samples originating from excavation and environment on site, manipulation and laboratory procedures. Consequently, the information brought by Raman spectroscopy analysis is limited on this sample collection, and rarely decisive enough to determine all the materials worked with these tools; and needs to be supported by the polish distribution to be securely related to use.

Table 6.1: Summary of results obtained by Raman spectroscopy and use-wear analysis on 2004 and 2015 collected artefacts.

Artefact	Year	Sector	Layer	Dating (ka)	Rock type	Use as	Significant residues (use-related in bold)	Use interpretation
LB45	2004	XI	9	3	Silicious tuff	Scraper	**Plant fibre, SFA, Protein**	Plant scraping
LB182	2004	XI	22	5–8	Silicious tuff, fine grained	Cutting tool, scraper, piercing tool	**Plant fibre, SFA**	Plant scraping
LB228	2004	XI	31	8–12	Silicious tuff, fine grained	Scraper	None	Unknown
LB250	2004	XI	37	120–60	Silicious tuff, fine grained	Scraper	**Plant material, SFA, Protein, SFA + Protein**	Plant scraping
LB337	2004	XI	43	120–60	Silicious tuff, with presence of cristobalite	Unknown	**SFA, Protein, SFA + Protein**	Unknown
LB57	2015	XXIV	7	1-5	White Chert	Scraper	None	None
LB3952	2015	XXV	52	14.01–11.75	Green Chert	Scraper	None	Plant scraping
LB3958	2015	XXV	52	14.01–11.75	Silicious tuff	Scraper	None	Plant scraping
LB4131	2015	XXV	54	14.01–11.75	Green Chert	Scraper	None	None
LB4204	2015	XXV	53	14.01–11.75	Green Chert	Double side scraper	**Grass fibre, SFA, SFA + Protein**	Plant scraping
LB4340	2015	XXVI	53	14.01–11.75	Green Chert	Cutting tool, scraper	**Charcoal, Plant fibre, SFA, Protein,** Plant fibre	Plant working with use of fire
LB4582	2015	XXVI	56	14.01–11.75	Green Chert	Scraper	**Charcoal, SFA, SFA + Protein, Protein**	Plant scraping with use of fire
LB4829	2015	XXVI	63	18.97–17.45	Dark chert	Scraper	None	None
LB5003	2015	XXVI	63	18.97–17.45	Silicious tuff, fine grained	Scraper	None	None
LB5227	2015	XXVI	67	44.11–18.31	Silicious tuff, with presence of pyroxene	Grinding tool	**Plant fibre**	Plant grinding?

6.3 2016 collected stones artefacts

6.3.1 Samples

From sector XXV and sector XXVI, excavated in 2016, twenty eight collected stone artefacts were analysed.

6.3.2.1 Micro-residues identified as modern contaminants

Several micro-residues from plastic boxes, blue nitrile gloves and Blu-Tack® micro-residues originating during the laboratory manipulation were sometimes found on these artefacts. Frequently polyester micro-residues were found on some artefacts, and are contamination from the laboratory environment, where they are common airborne material arising from people's clothes. Iron oxide marks on artefacts from the 2016 collection (artefacts LB5126, LB5211, LB5213, LB5225 and LB5580a) were interpreted as contamination from metal tools during the excavation (Chapter 3, section 3.9).

Additionally, I also found localised concentrations of shiny, yellowish, metallic micro-residues on artefact LB5211 (Fig. 6.22, B), on both sides of the middle part of the left edge, middle part of the ventral right edge and in a lesser extent on the flaking platform (Fig. 6.22, A). Its Raman analysis shows a unique vibrational band centred at 574 cm^{-1}, which was difficult to interpret (Fig 6.22, C, b), and therefore further analysed with a SEM-EDS probe. Indeed, as these micro-residues were located on polished edges, present as a concentrated group and well attached to the surface it was critical to complete their full identification. A high content in Cu and Zn elements, not arising from the mineral background, was detected (Fig. 6.22, E), indicating that these micro-residues are made of brass. This SEM analysis provides an identification which was confirmed with Raman spectroscopy by analysing an experimental stone flake hit with a brass screw (Fig. 6.22, D and C, a), and comparing the obtained spectrum with the same brass micro-residues signal on artefact LB5211 (Fig. 6.22, C, a and C, b). The presence of brass on this artefact can be explained by contact with a brass part of a tool used during archaeological excavation (e.g., ferrules (often made of brass) holding paintbrush hairs in place could have accidentally rubbed against stone artefact edges.

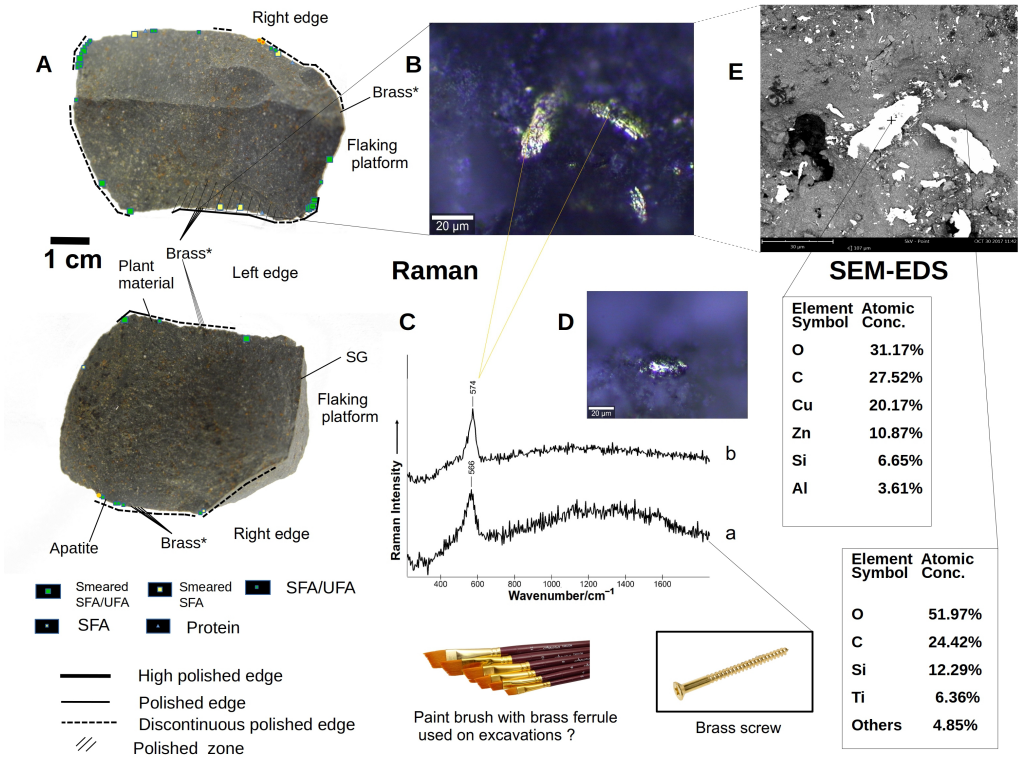

Figure 6.22: Residue distribution on artefact LB5211 showing localisation of brass micro-residues (A), optical image of brass micro-residues on artefact LB5211 (B), Raman spectrum of analysed brass on experimental stone flake hit by brass screw (C, a), Raman spectrum of analysed micro-residues on artefact LB5211 (C, b), optical image of brass micro-residues obtained by hitting experimental stone flake by a brass screw (D), SEM-EDS micro-residues analysis on artefact LB5211 and rock background (E) (exactly same residues as those observed on image B).

A natural fibre was found localised on the left ventral edge of artefact LB5126b associated with a few individual, loosely attached micro-residues identified as an unknown aromatic resin (Fig. 6.23, A-B) (see also Appendix IIa, table 5). Other micro-residues of the same material were found on the same edge on the opposite left dorsal side, in the same edge area; and two more on the ventral flaking platform and right dorsal edge (Fig. 6.53). This restricted distribution clearly indicates an incidental contact of the artefact edge with this particular material. Moreover, this concentration of material is not centred on highly polished edges and no smeared residues of this unknown material was found. But the question remains whether it could be a prehistoric incidental material or a modern incidental contamination contact on archaeological site. A natural fibre attached to two of these micro-residues provides the answer: this fibre was found loose on the edge with a very high signal-to-noise Raman signal, which cannot correspond to very old plant fibres (Chapter 3, section 3.2.5) (Kavkler et al., 2011). Consequently, associated aromatic resin and other isolated scattered individual similar

micro-residues on this artefact need to be also considered as modern contaminants. We have here an unknown material arising probably from accidental contact on the archaeological site during extraction of the sample.

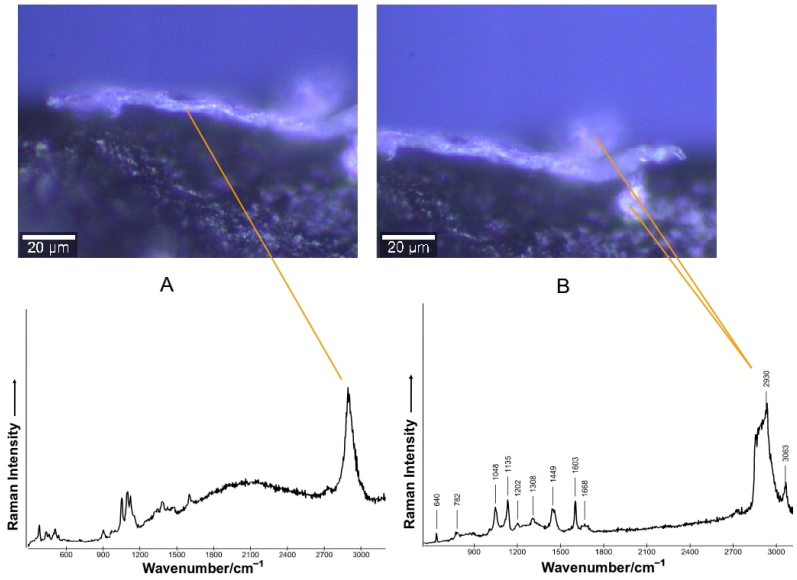

Figure 6.23 : Image of a natural plant fibre with Raman spectrum of the fibre (A), image of natural plant fibre with Raman spectrum of the associated aromatic resin (B).

In contrast with artefacts from 2015 collection, which had numerous dyed fibres, only isolated dyed fibres were found on artefacts LB5212 and LB5580b, during the analysis of stone artefacts from the 2016 collection. The 2016 collection has fewer contaminants than the 2015 collection. This could probably be explained by more careful manipulation and protecting the samples from contamination. Indeed, recovered stone artefacts from the 2016 excavation were removed with a block of surrounding sediment, preserving them partially from contamination from packaging material during storage.

6.3.2.2 Micro-residues originating from the sediment or from post-depositional processes

Manganese oxide micro-residues originating from the attached sediment was found on all artefacts in the 2016 collection, but some artefacts have more extensive covering of manganese, like Artefacts LB5164 and LB5126; and others, like Artefact LB5165, having more manganese micro-residues. Other specimens, like artefacts LB5212, LB5580b and

LB5562b, have more scattered but larger manganese macro-residues, which can be observed with the naked eye. Raman signatures similar to manganese oxide were found on Pleistocene artefacts from the 2004 excavation (Bordes et al, 2017), artefacts LB250 and LB337 (Chapter 6, section 6.2.2.2). A larger amount and greater extent of manganese dioxide was found on artefacts LB5164, LB5165 and LB5126, which were used to work bone; but like artefact LB5068, some tools used on plant material also have (rare) manganese micro-residues. Manganese oxide can be found either as black residue directly on the stone artefact surface, as shiny residues on polished edges or as black spots and smeared residues on bone. The high frequency of manganese oxide on stone artefacts used to work bone is not surprising considering that manganese oxide was identified in altered bone apatite structure of old references bones, probably linked with degradation processes (Chapter 4, section 4.7). However, on artefact LB5164, it is striking that manganese oxide is most abundant on the proximal part of the artefact where SFA micro-residues are all concentrated (Fig. 6.24). Another, artefact LB5580b (Appendix IIb, fig 17), was used intensively on fatty material and also has high number of manganese micro-residues. This observation confirms that manganese oxide can concentrate on different organic-rich materials because microbial and fungal activity similarly affects different materials like bone, fat and plant tissue.

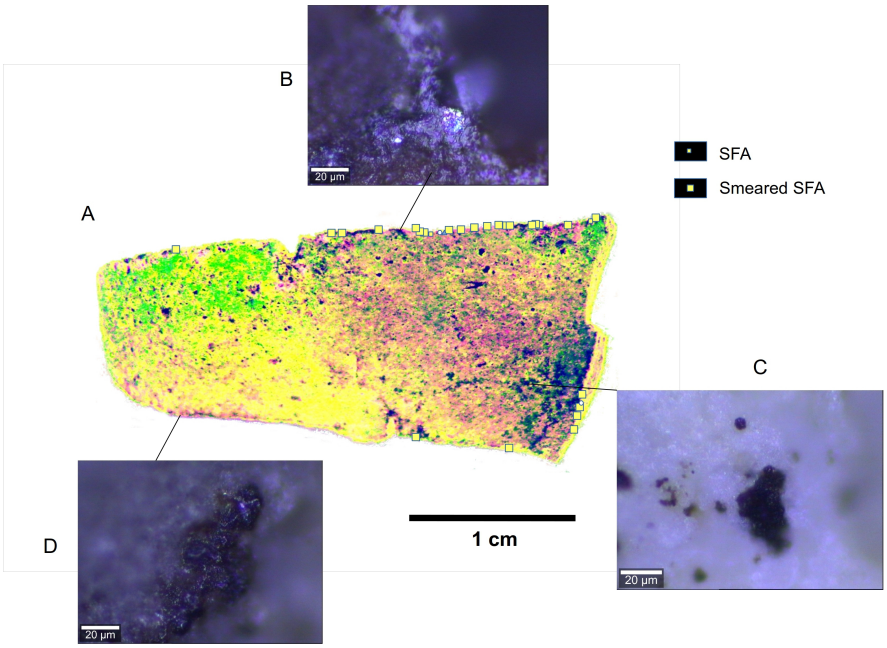

Figure 6.24 : Manganese black colour enhancement on ventral side of artefact LB5164 by Dstretch® (A), image of shiny manganese oxide on polished edge (B), image of spotted manganese oxide on bone residue (C), image of black manganese oxide residue (D).

Identification of manganese oxide residues on Liang Bua artefacts by Raman microscopy has been double checked by SEM-EDS analysis on artefact LB5164 (Fig. 6.25**)** and artefact LB5580b on the same matching spots, their aspect and Raman spectra corresponding to those analysed commonly on all artefacts and sediment samples from that site. Each SEM-EDS analysis revealed systematically content of the element manganese, which was not present in the rock background, on each residue identified by Raman spectroscopy.

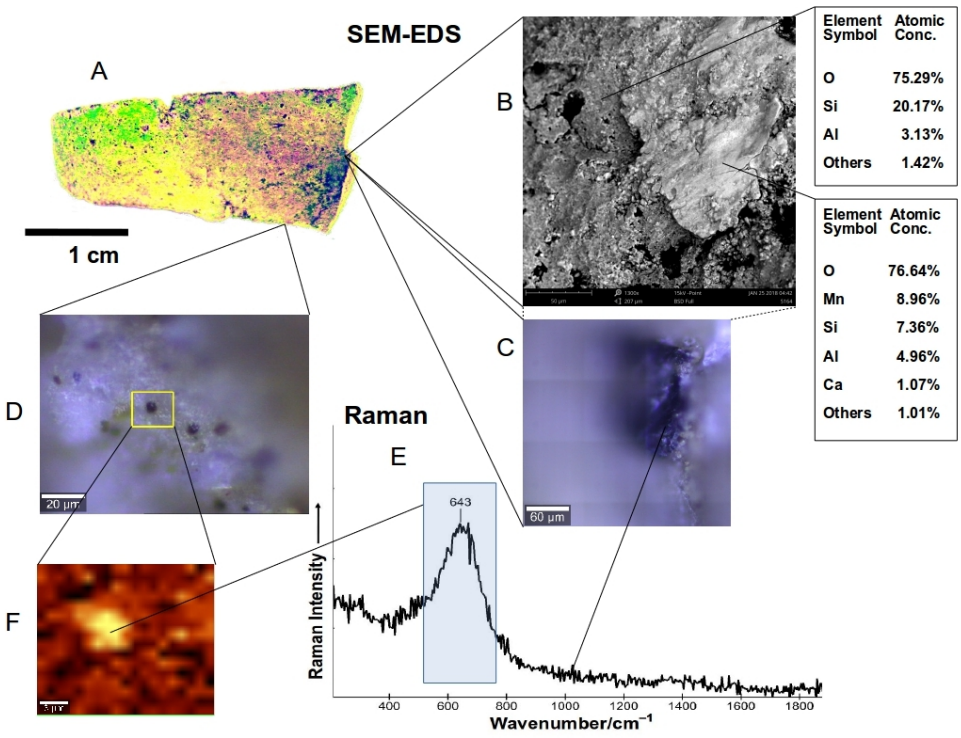

Figure 6.25: Manganese black colour enhancement on ventral side of artefact LB5164 by Dstretch® (A), image of manganese oxide micro-residue by SEM on LB5164 and EDS analysis (B), image of the same manganese oxide micro-residue on LB5164 obtained with Raman optical microscope (C), image of manganese oxide grains on smeared bone residues micro-residues obtained with Raman optical microscope (D), typical Raman spectrum obtained on manganese micro-residues on artefact LB5164 (E), Raman spectral mapping on manganese band integrated intensity on a manganese oxide grain located on a bone smeared residue (F).

6.3.2.3 Micro-residues originating from weathering processes

Pure white kaolinite was found on all artefacts in the 2016 collection, excepted artefacts LB5067, LB5068 LB5580b, LB5525 and LB5526a. Kaolinite always appears as individual micro-residues either attached to the surface or loose, but never embedded in the stone surface. This seems to indicate that this material does not arise from natural inclusions in the

rock. Except on artefact LB5580a, kaolinite is not clearly concentrated near worked edges but is rather found widespread, randomly over the whole stone tool surface. Kaolinite was not found in the sediment, and its purity and the absence of fluorescence seem to indicate it results from a particular, unique chemical process and not from the kaolinite content in the sediment which would have probably mixed with other type of clays. The fact that other artefacts (LB5067, LB5068 LB5580b, LB5525 and LB5526a) belong to different stone types (quartz, chert or chalcedony) and are devoid of kaolinite leads me to conclude that the presence of kaolinite is probably linked to a weathering process of siliceous tuff only. Rock type of artefact LB5067 was not determined but it is clearly distinct from siliceous tuff. Indeed, feldspar form the mineral background in these siliceous tuffs and feldspar minerals are known to convert to kaolinite under acidic environmental conditions, mediated by water (Panchuk, 2017). Kaolinite was found mixed with other residues, mainly with bone micro-residues, but also in some cases with fatty acids micro-residues. These kaolinite mixtures can be found on many artefacts (e.g., LB5126, LB5224a, LB5213, LB5562b, LB5580a, LB5524 and LB5526b) and in some cases completely entrap bone micro-residues (LB5213, LB5580a).

For example, fossil bone and saturated fatty acid were found both mixed in kaolinite micro-residues on artefact LB5213 (Fig. 6.26). Kaolinite shows characteristic mineral bands at 130, 274, 338, 436, 471,756, 794 and 920 cm^{-1} at low wavenumbers and a system of Raman bands dominated by 3625 and 3699 cm^{-1} at high wavenumbers (Fig. 6.26, a) (Frost, 1995; Frost, 1997). Bone apatite can be distinguished by its characteristic phosphate and carbonate bands respectively centred at 966 and 1076 cm^{-1} (Fig. 6.26, b-c), as well as from the rare earth fluorescence bands (Chapter 4, section 4.7). SFA has only a weaker signal on spectrum c (Fig. 6.26, c) with only its main bands at 1451 cm^{-1} and 2886 cm^{-1} being visible.

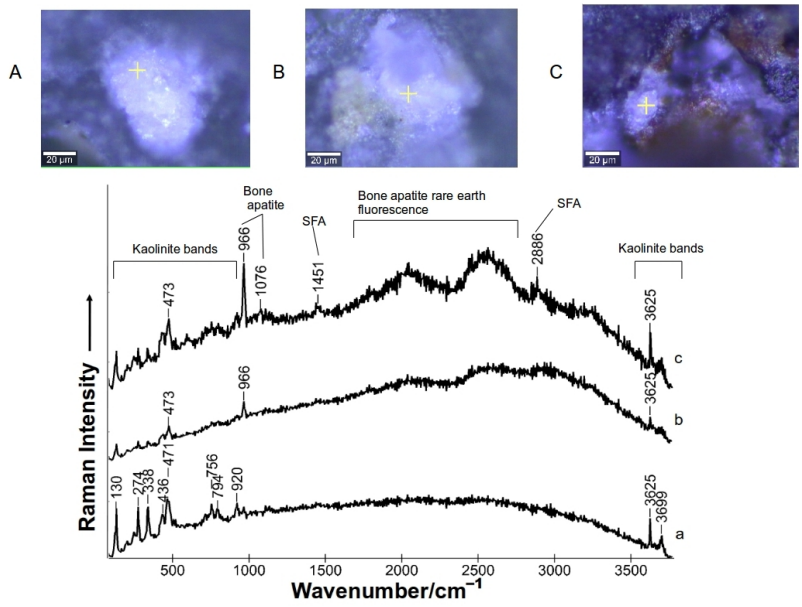

Figure 6.26 : Image of kaolinite micro-residues (A), mixed bone apatite and kaolinite micro-residues (B), mixed bone, SFA and kaolinite (C), Raman spectrum of kaolinite micro-residues (a), mixed bone apatite and kaolinite micro-residues (b), mixed bone, SFA and kaolinite (c).

It is not known if kaolinite weathering products randomly mixed with bone or if a particular affinity of kaolinite with bone could have prevented kaolinite from further leaching away. But kaolinite mineral as a weathering product of acidic attack on rock surface could also have contributed to preserve bone residues on this stone tool from these same aggressive chemical conditions.

6.3.2.4 Potential use-related micro-residues

Artefact with plant micro-residues (LB5068)

On artefact LB5068, protein, individual SFA and starch grains were found specifically on the polished edge, and are potentially use-related. According to the polish distribution, the main working part on that stone tool is the concave distal margin on the ventral side, which was used probably as a notched flake for scraping (Fig. 6.27). This mode of use is clearly indicated by the extended polished area on the ventral side directly behind the working notch. The opposite right and left edges were also slightly used with a cutting action. With respect to micro-residues distribution, a concentration of proteins on the polished edge in the scraping notch could be linked to the use, and confirms protein residues on prehistoric artefacts exist as a result of use, as was also observed on experimental tools (Chapter 4, sections 4.4 and

4.5). If other significant micro-residues like SFA are not specific to animal or plant material, the presence of three starch grains located on the polished area and the absence of bone residues that can also indicate the use of this stone tool on plant material. Finally, a few scattered plant fibres found on the discontinuously polished edge seem to confirm this conclusion.

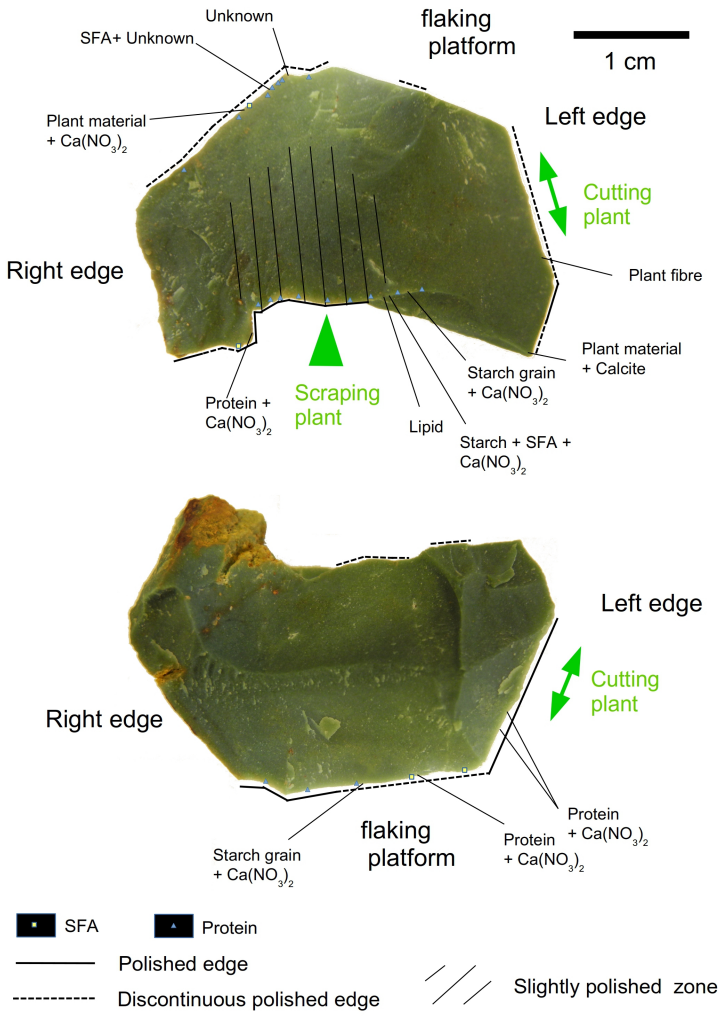

Figure 6.27: Correlation between micro-residues and polish distribution on artefact LB5068.

Even though some artefacts were used on plants (e.g., artefact LB5068), most stone tools collected in 2016 were used on animal material, as indicated by the strong presence of bone residues. For most, I detected two forms of bone apatite: a well-preserved form of bone apatite that I will designate by ‘fossil bone’ and a form of disordered bone apatite designated by ‘altered apatite’. Spectral differences between these two forms of apatite, observed in bone reference samples, has already been described in Chapter 4 (Section 4.7). Presence of these

two forms of apatite was recognised also in distinct micro-residues found in outer and inner sediment samples (Fig. 6.28).

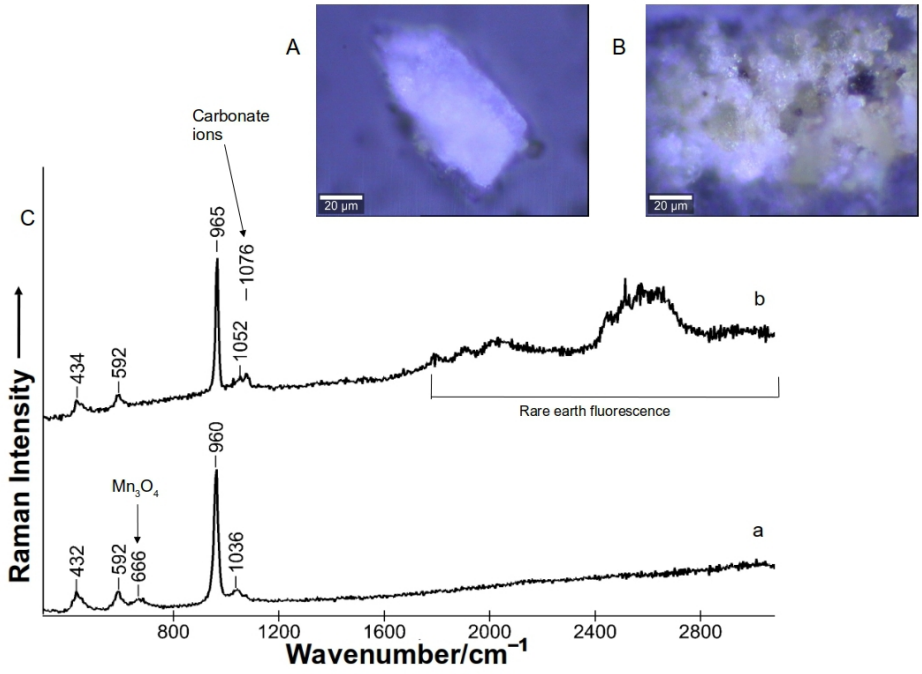

Figure 6.28: Fossil bone apatite fragment (A), altered bone apatite micro-residues (B), Raman spectrum of altered bone apatite (C, a), Raman spectrum of fossil bone apatite fragment (C, b).

Additionally, these two forms of apatite, fossil bone and altered bone apatite were found in situ as part of the same bone micro-residue and smeared bone (see below, artefact LB5164), demonstrating that they are two different phases of the same material having undergone different alteration processes: fossil bone maintaining its structure and accumulating rare earth substitution to calcium ions; and altered bone having a disordered structure due to the presence of degraded organic material and manganese oxide.

Artefacts LB5164, LB5165 with fossil bone and SFA micro-residues

Shaped fragments of bone on artefact LB5164 was analysed. These fragments show the same spectral signature as the fossil bone apatite found in the sediment (Fig. 6.29) confirming identification of this apatite with bone material and showing that it can be present both on the artefacts and in sediment. This bone spectrum display bands from rare earth elements substitution in the bone matrix.

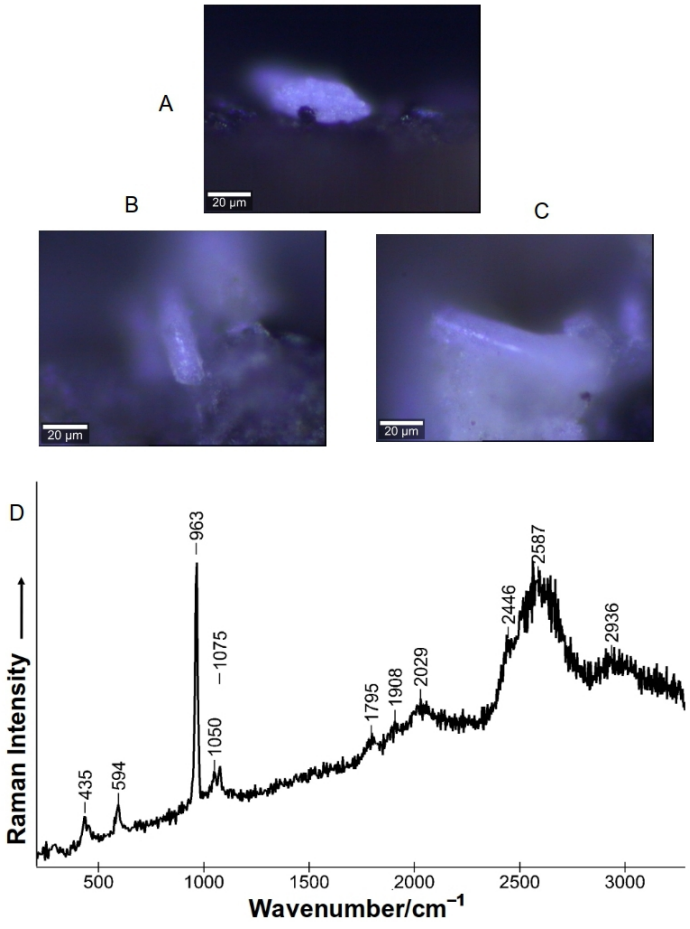

Figure 6.29: Fossil bone apatite fragments on artefact LB5164 (A-C), and Raman spectrum (D).

On the same artefact, bone micro-residues, and large patches of bone were analysed, and found composed simultaneously from both forms of bone apatite, fossil bone and altered bone. Indeed, probing a bone apatite residue on artefact LB5164 in (Fig. 6.30, A-C) and mapping of the position of the main band of apatite in another residue on the same stone tool (Fig. 6.31) shows that fossil bone apatite, with a similar spectral signature to the fragment of bone was mixed with altered bone apatite in same micro-residue. This confirms identification of altered apatite as altered bone in close association with fossil bone, as found also in the LB5165 and LB5164 sediment. It should be noted that altered bone was not found on artefact LB5165, which can be explained by the low amount of bone present on this stone tool compared with artefact LB5164, which has an extended patch of bone on its surface (Fig. 6.32).

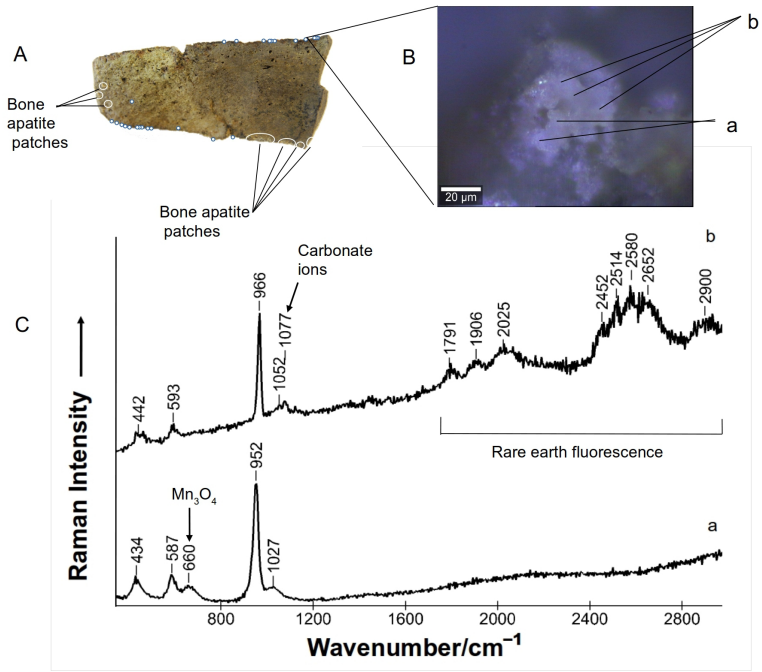

Figure 6.30 : Raman spectra showing two mixed different forms of bone apatite found on LB5164: Fossil bone apatite containing carbonate ion (band at 1077 cm^{-1}) showing complex fluorescing bands arising from rare earth substitution (Eu^{3+}, Sm^{3+}) (b), altered bone apatite containing manganese oxide (a).

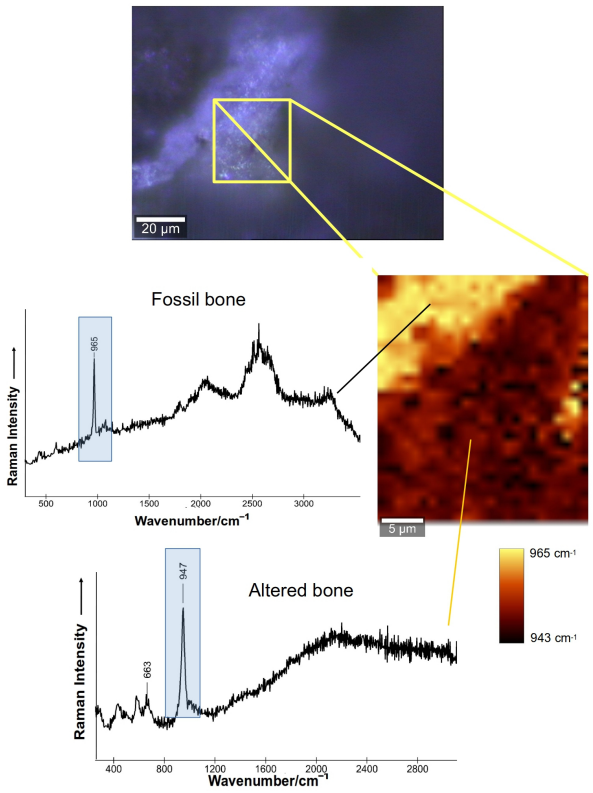

Figure 6.31: Raman mapping of one LB5164 bone apatite micro-residue according to the position of maximum of the apatite main vibrational band. The two forms of bone apatite coexists in this micro-residue.

Even if bone is present in the layer sediment sampled for these artefacts, fossil bone micro-residues on artefacts LB5164 and LB5165, is originating not only from the sediment, but also from the use of these artefacts. Indeed, if some surfaces of artefact LB5164 (like its flaking platform) were covered by a bone apatite patch (Fig. 6.32), without being polished from use, other arguments suggest that fossil bone is partially originating from prehistoric use.

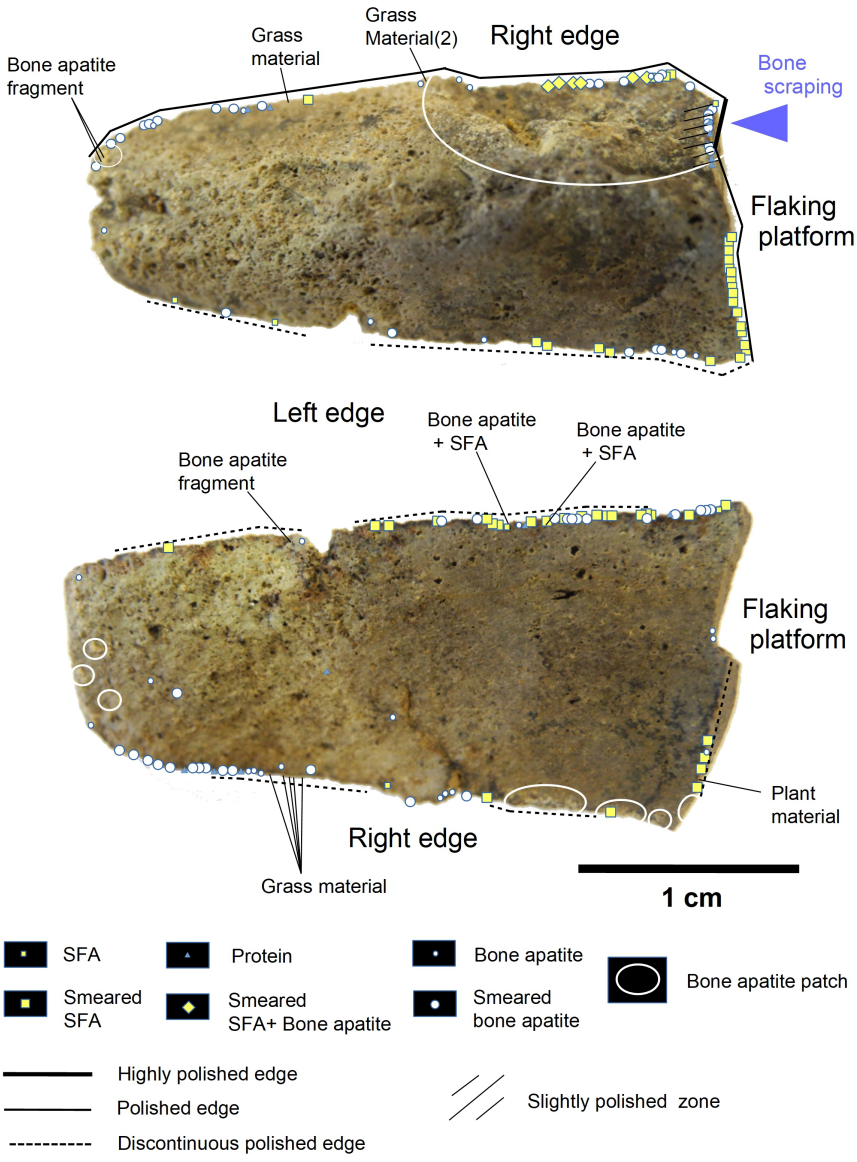

Figure 6.32: Bone apatite and SFA micro-residues distribution on LB5164, correlated with polish distribution.

Firstly, analysis of smeared micro-residues as a mix of fossil bone apatite and SFA (Fig. 6.33) on artefacts LB5165 and LB5164 shows a close association between these two types of micro-residues. Then SFA smeared micro-residues were found in limited distribution on the polished edges of artefacts LB5165 and LB5164 either as individual or smeared micro-residues, and are not found in sediment—all of which supports the hypothesis that they are use-related micro-residues (Figs. 6.32 and 6.34**).** These particular mixed micro-residues could indicate that they were the result of tool use on fresh bone, according to the results of modern experiments (Chapter 4, section 4.5.2). The presence of an extended patch of bone on artefact LB5164 could also confirm that this tool could have worked fresh bone. Secondly, smeared bone apatite residues occur on both of these artefacts in association with polished edges. Consequently, it can be concluded that the fossil bone attached to these stone tools is partially use-related and partially arising from contact with bone in sediment.

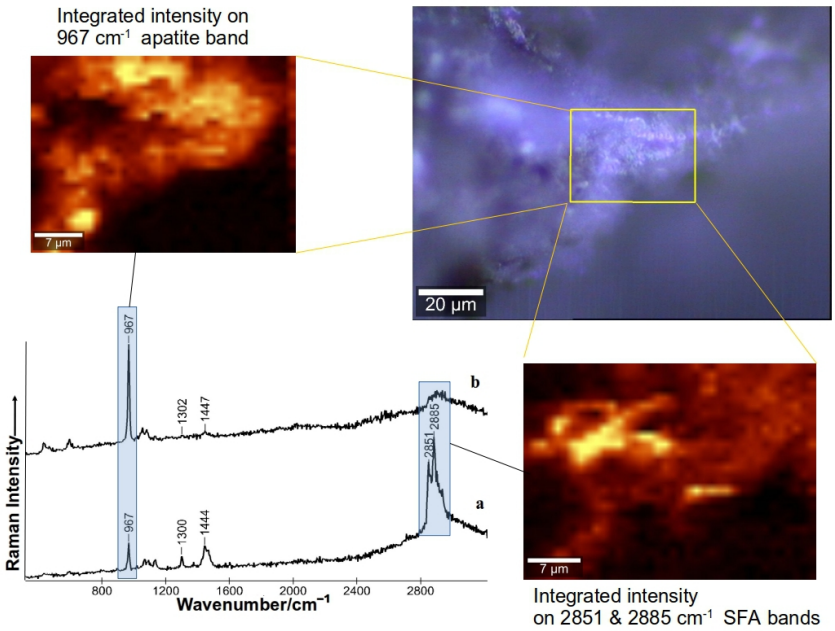

Figure 6.33: Raman mapping of a smeared micro-residue as a mix of fossil bone apatite and SFA.

With respect to the mode of use, artefact LB5164 was probably used as a bone scraper with its dorsal side proximal edge adjacent to the flaking platform showing a highly polished area, smeared bone residues and an adjacent extended patch of bone. Artefact LB5165 was used mainly to scrape bone with the middle section of its left dorsal edge and flat side. Its distal margin could also have been used for a slight cutting action.

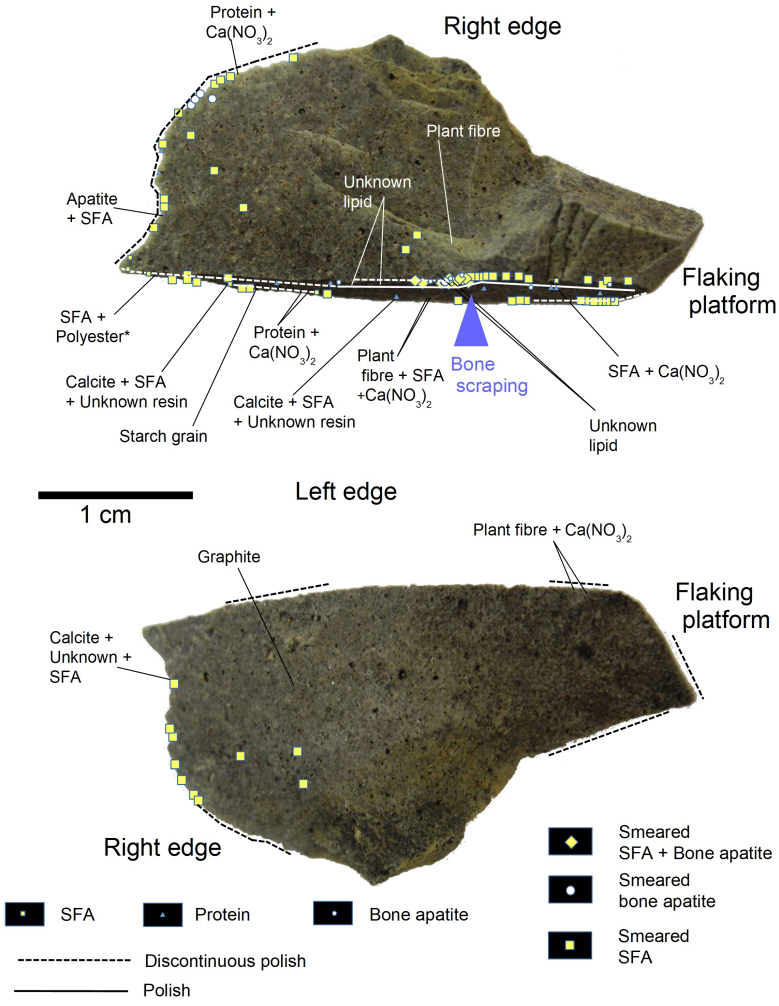

Figure 6.34: Bone apatite and SFA micro-residues distribution on LB5165 and correlation with polish distribution.

Incidental grass micro-residues found on LB5164

In addition to the presence of bone and lipids, a set of plant micro-residues with the same specific spectral Raman signature, was found on the middle of the ventral right edge, on the same edge on the dorsal side and on the flaking platform of artefact LB5164 (Fig. 6.32). As this plant material could not be related clearly to polish distribution, because the flaking platform doesn't bear any use polish, it could have been only incidental to the use of the stone tool, either by being in contact with plant material during its use on bone or by a handling

system. As for artefact LB4204 (Fig. 6.15), typical Raman spectrum of this plant material can be identified on LB5164 as grass material (Gramineae) (Figs. 6.35 and 6.36), (see also Chapter 4, section 4.5.1).

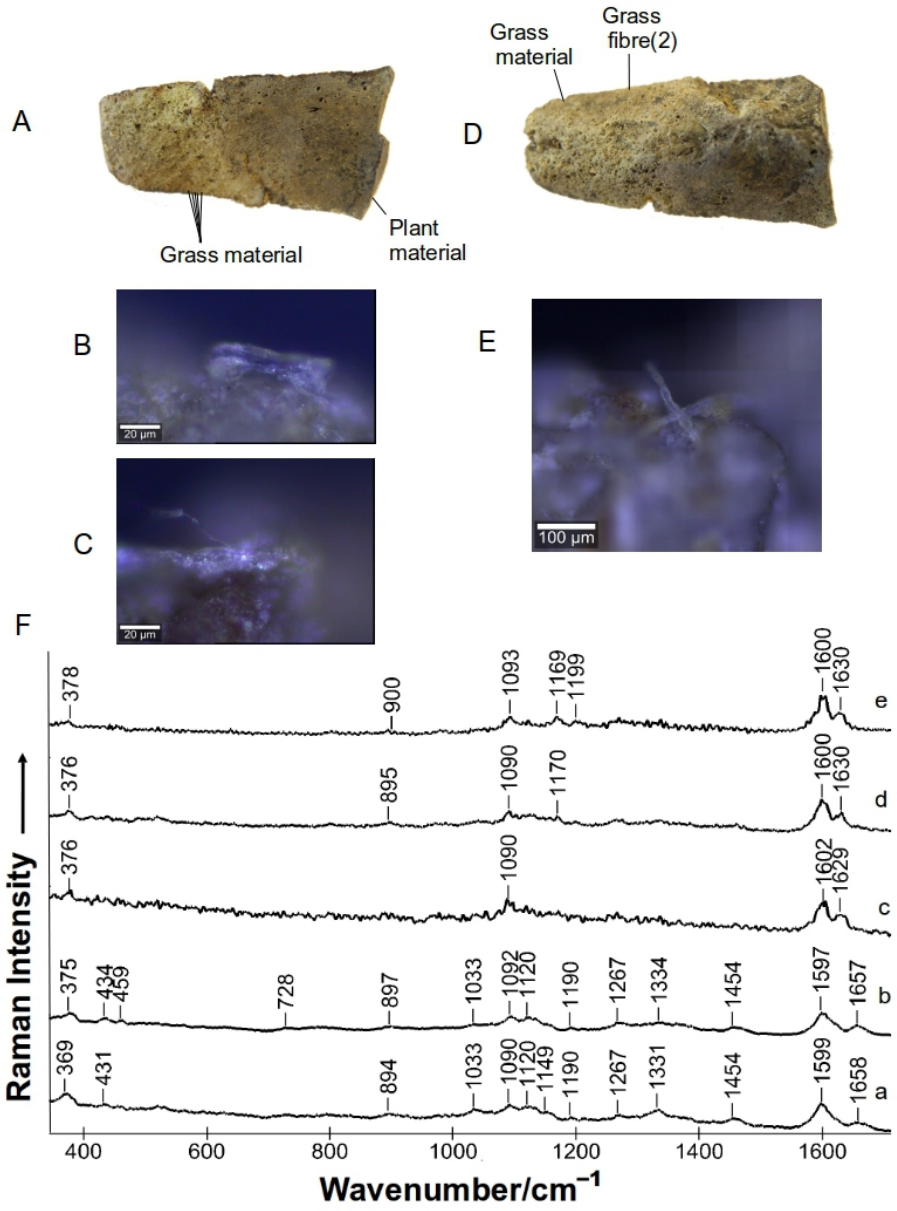

Figure 6.35: Grass material micro-residues localisation on ventral side of artefact LB5164 (A), detail of grass material micro-residues on ventral side of artefact LB5164 (B-C), grass material micro-residues on dorsal side of artefact LB5164 (D), detail of grass material micro-residues on ventral side of artefact LB5164 (E). Comparison of plant material micro-residues found on LB5164 with different wood, grass and bamboo references material (excitation 785 nm): Mulga dry sapwood (*Acacia aneura)* (F, a), pine dry wood (*Pinus sp.*) (F, b) fountain grass (*Pennisetum setaceum*) (F, c), black dry bamboo (*Bambuseae sp.)* (F, d) , plant material found on LB5164 (F, e).

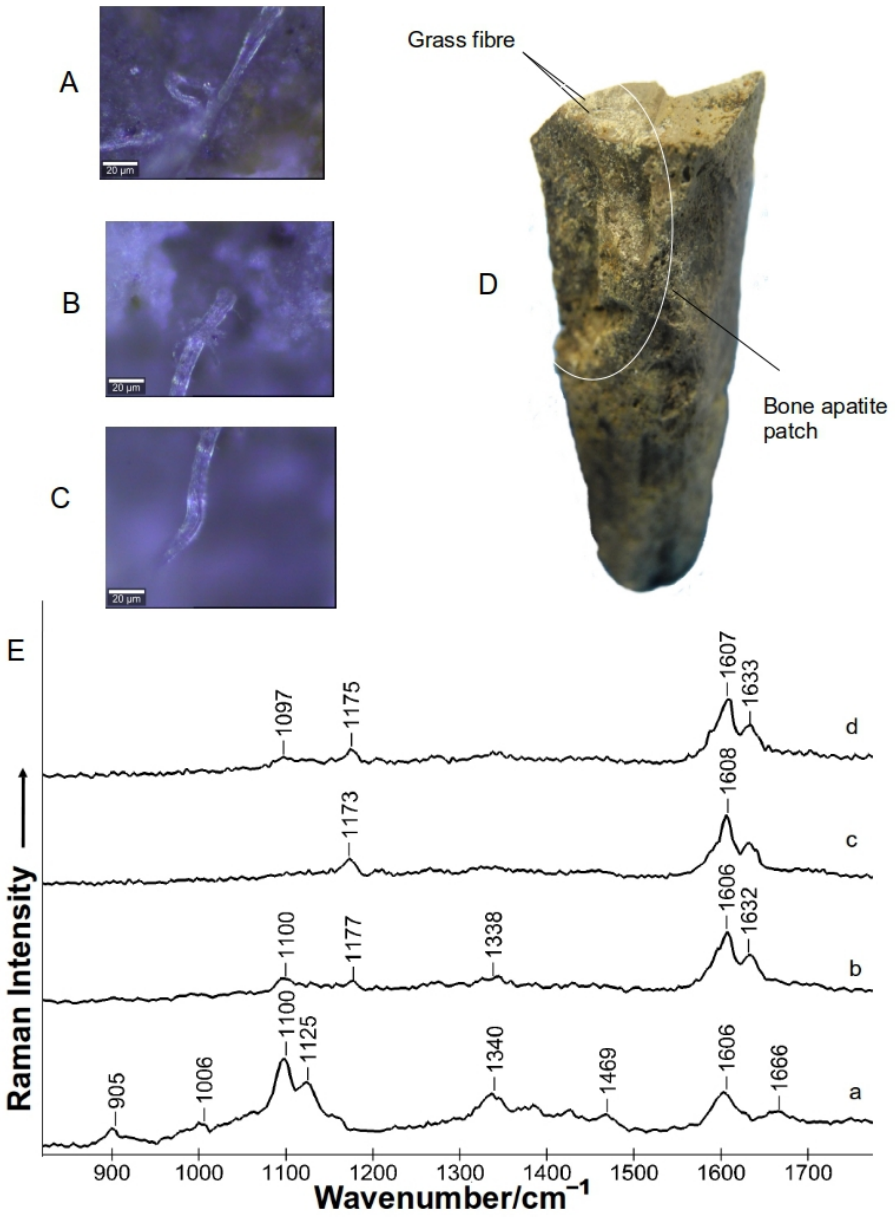

Figure 6.36: Detail of grass micro-residues on flaking platform of artefact LB5164 (A-C), grass micro-residues localisation on flaking platform of artefact LB5164 (D), comparison of plant material micro-residues found on LB5164 with different wood, grass and bamboo references (excitation 532 nm): Rowan wood (*Sorbus aucuparia*) on D5 experimental artefact (E, a), fountain grass (*Pennisetum setaceum*) on B3 (E, b), Indonesian bamboo (*Bambuseae sp.*) on B1 (E, c), plant material found on LB5164 (E, d).

Artefact with multiple material uses: LB5224b

On artefact LB5224b, micro-residues distribution (Fig. 6.37**),** suggests two different uses, corresponding to two opposite edges. On the concave proximal part of the left edge, I found on both sides, bone and SFA micro-residues with a few protein micro-residues. This set of residues could be interpreted as stone tool use on bone, according to experimental patterns of use (Chapter 4, Tables 1 to 4). Symmetry of these micro-residues and polish probably indicate a cutting action on this edge. On the opposite right edge, a high concentration of protein and a few SFA and plant micro-residues were found mainly on the dorsal side. With similar asymmetry, polish intensity was higher on this side and more extensive, suggesting that this edge was probably used in a scraping action. The material worked is very different from that worked by the left edge which has a distinct set of residues, in which bone is absent, but plant material and many protein micro-residues are present and similar to those found on experimental tools used on plants. Distribution of micro-residues can therefore supplement use-wear information to enhance interpretation of tool function and to help identify multiple use.

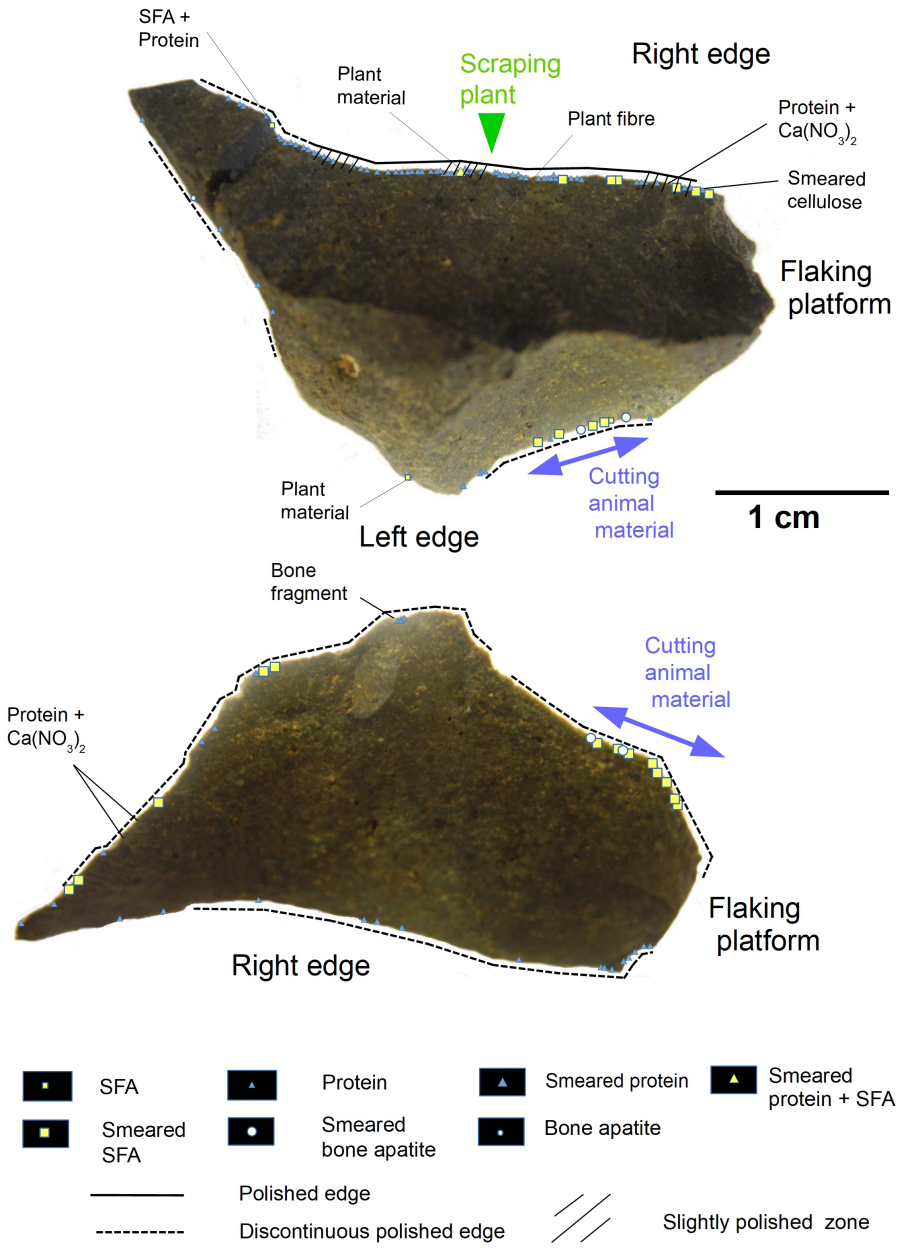

Figure 6.37: Micro-residues distribution on LB5224b correlated with polish distribution.

Stone artefacts used for bone working with use related iron oxides: LB5126, LB5213, LB5125

Three stone artefacts from 2016 collection, artefacts LB5126, LB5213, and LB5125 share the same general morphology, being thick, triangular flakes with a central ridge dividing left and right dorsal sides and a flat ventral surface (Fig. 6.38); and all three share a similar set of micro-residues related to use, and a similar mode of use.

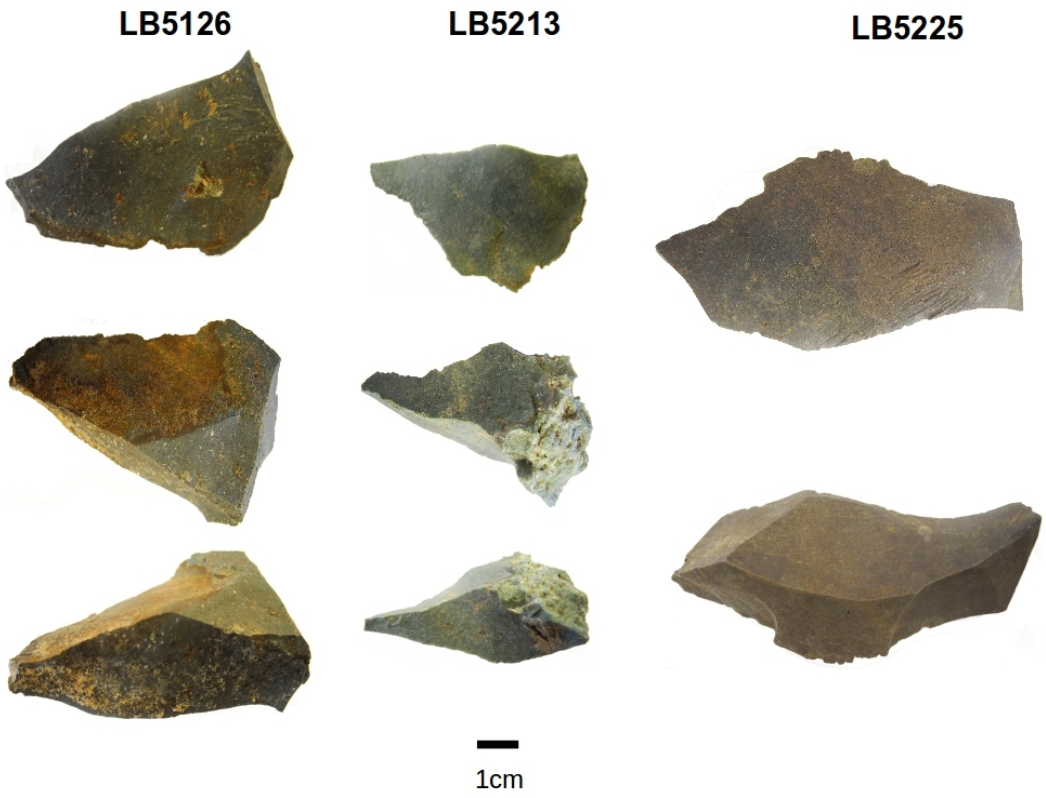

Figure 6.38: Comparison of stone artefacts LB5126, LB5213, LB5225 showing similar morphology.

Stone artefact LB5126:

Artefact LB5126 is one of the stone tools in the 2016 collection with the best preservation of residues. A great amount of smeared and individual fossil and altered bone micro-residues along extended bone apatite patch, was identified on this stone tool, as for artefact LB5164. Coexistence of fossil and altered bone was confirmed on this artefact and I analysed smeared residues located on the polished part of the ventral, left edge (Fig. 6.39). This analysis confirms again the origin of altered apatite as a product of bone degradation, which could either be present as fossil bone or as disordered apatite form, which was distinguished by Raman spectroscopy, even on few micron sized smeared bone residues.

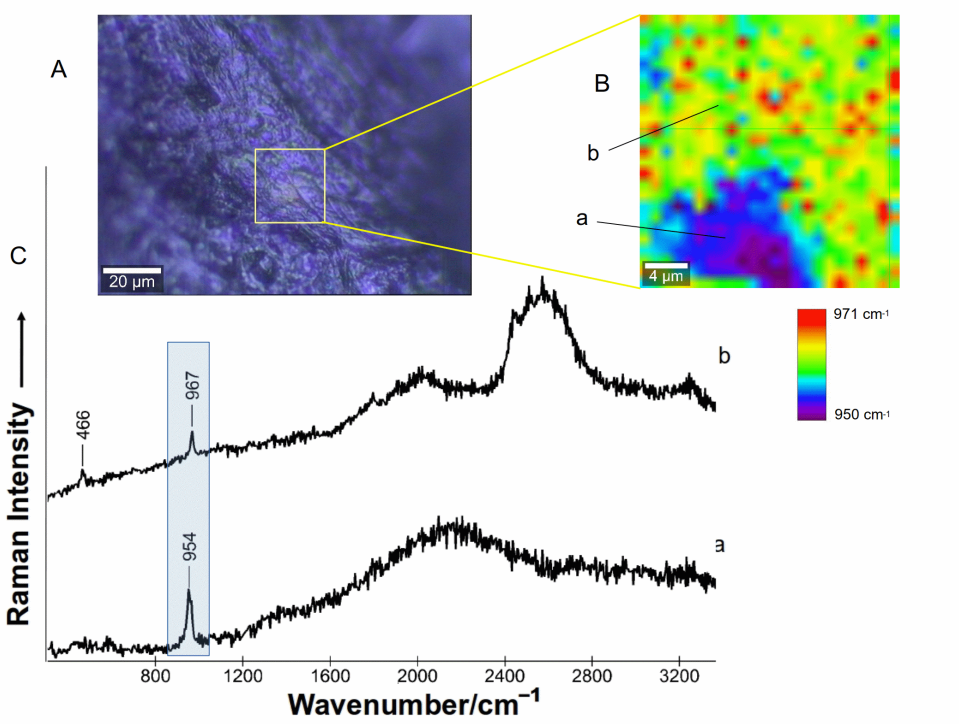

Figure 6.39: Bone apatite smeared residues on a polished area of ventral left edge (A), Raman spectral image with colour depending of the position of the maximum of apatite Raman band which is upshifted for fossil bone (yellow and red, 967 cm^{-1}) and downshifted for altered bone (blue, 954 cm^{-1}) (B), corresponding Raman spectra for altered bone (C, a) and fossil bone (C, b). Note the presence of rare earth fluorescence on fossil bone spectrum (C, b).

Distribution of these bone micro-residues on the ventral side is concentrated on the left edge and the distal margin, as well as along its flaking platform (Fig. 6.40). The distal part of the dorsal right margin were also used on bone, but the more spectacular bone remains are located on the dorsal left side on this tool, where both the left edge and the central ridge had been intensively used on this material. On this side, bone residues can be seen with the naked eye, and are concentrated in association with polish intensity, especially on the left edge of that side (Fig. 6.41). Such an extended distribution of bone suggests fresh bone material working with these edges. In contrast with previous artefacts, artefacts LB5164 and LB5165, apatite bone residues were not found in associated sediment, confirming that the origin of this material is from prehistoric use. This relationship is strengthened by the presence of smeared and individual apatite bone micro-residues along with rare bone micro fragments. SFA smeared and individual micro-residues are also present on this artefact, especially on the right ventral edge and on the distal part of dorsal side, as well as among bone apatite residues. Analysis of both materials links the use of different tool edges to scrape bone, possibly fresh bone.

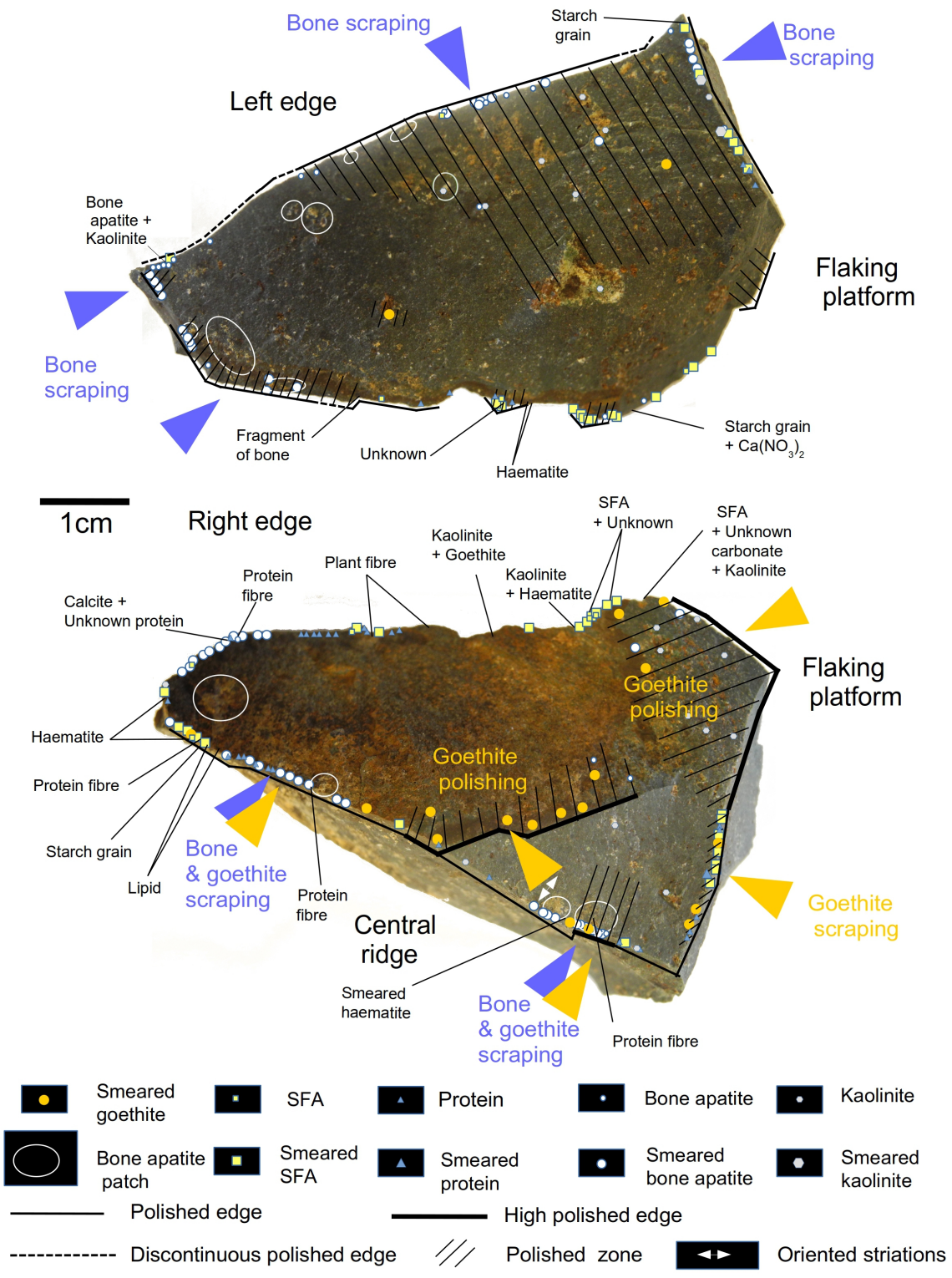

Figure 6.40: Micro-residues distribution on LB5126 ventral and right dorsal side, correlated with polish distribution.

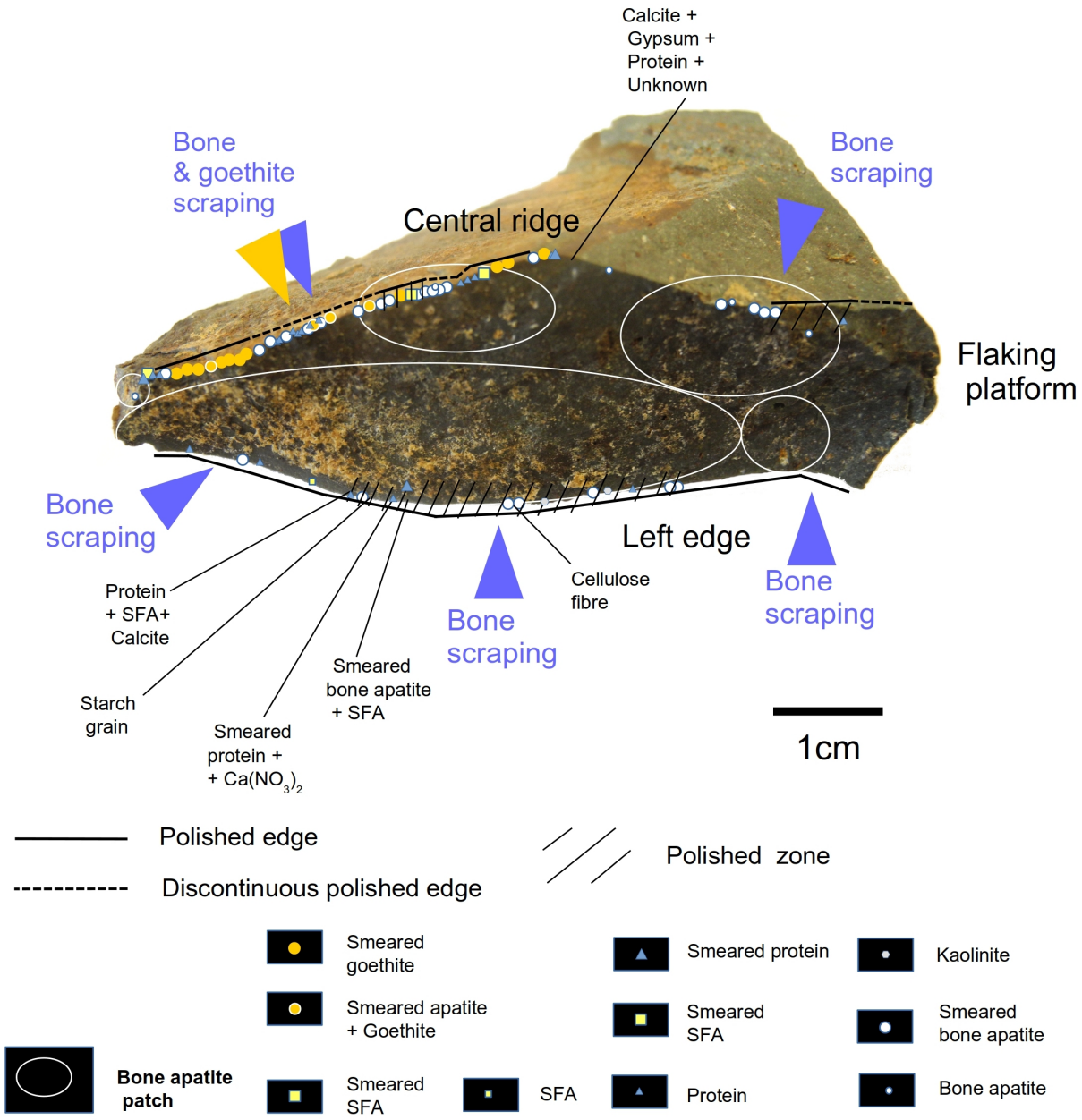

Figure 6.41: Micro-residues distribution on LB5126 dorsal left side correlated with polish distribution.

A natural occurring dark quartz banded formation

A quite obvious feature of LB5126 is a natural dark quartz banded formation running on the right dorsal side, and going through the ventral side along right edge (Fig. 6.42). This layer is exclusively composed of quartz (probed by Raman) in a similar way to the stone mineral background and shouldn't be confused with any use-related residues.

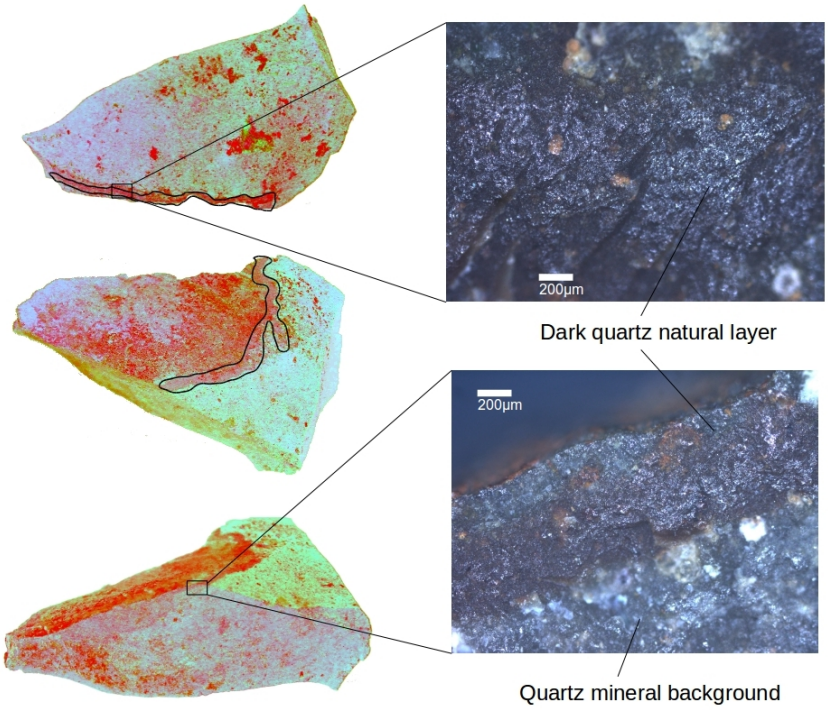

Figure 6.42: Natural dark banded quartz formation embedded in artefact LB5226 emphasised by colour enhancement by Dstretch® software.

Goethite micro-residues found on LB5126

Goethite, showing red to orange hues, was interpreted as a possible use-related residue on this tool, as its presence in sediment is too low to indicate a transfer to the artefact surface in such a large quantity. Among goethite, small amounts of haematite were identified. Goethite mineral does not originate from the stone itself, which is composed exclusively of quartz and has no relation with the natural band of dark quartz observed on this artefact previously (Fig. 6.42).

Distribution of goethite coloured material was observed with Dstretch® visualisation program in association with the most polished area on that tool (Fig. 6.43) and confirmed there by Raman spectroscopy. Goethite occurs in three different forms of micro-residues on this artefact:

(1) as individual mineral grains on the surface with a natural colour range from red to light orange; (2) as smeared goethite; and (3) as mixed smeared bone-goethite micro-residues on polished edges, having a very distinct, non red, shiny and smooth aspect, its colour being often indistinguishable from the polished background.

The presence of this latter form of smeared goethite on the polished edge of artefact LB5126 indicates that this material has undergone pressure during the use of the artefact and bone working, in any case before burial. These smeared goethite micro-residues, located on polished edges, have a very different aspect compared with individual goethite red grains (Fig. 6.44, A-C) spread on larger areas around these worked edges, but still matching typical Raman spectrum already observed on this iron oxide (Hanesh et al., 2009).

Additionally, oriented parallel striations were observed on smeared goethite micro-residues (Fig. 6.44, A-B), which indicate they aren't of natural origin (unlike the adjacent red goethite) and result from a transformation by pressure and movement over the stone tool surface. These smeared goethite micro-residues were found on artefact LB5216 away from any metal tool marks, which otherwise might have produced them during excavation. These smeared goethite residues were recognised especially on the dorsal right and left sides, both on use-polished edges. The right dorsal side was used for working especially goethite, which is smeared on polished areas and notably devoid of bone apatite, which seems to indicate a particular specialised activity on this artefact area.

Other edges on this side, like the central ridge and flaking platform were used for scraping both bone and goethite. Moreover, the ventral side was used on both of these two materials by scraping on left and right ventral edges, along with the central ridge, and again with the left edge of the left dorsal side.

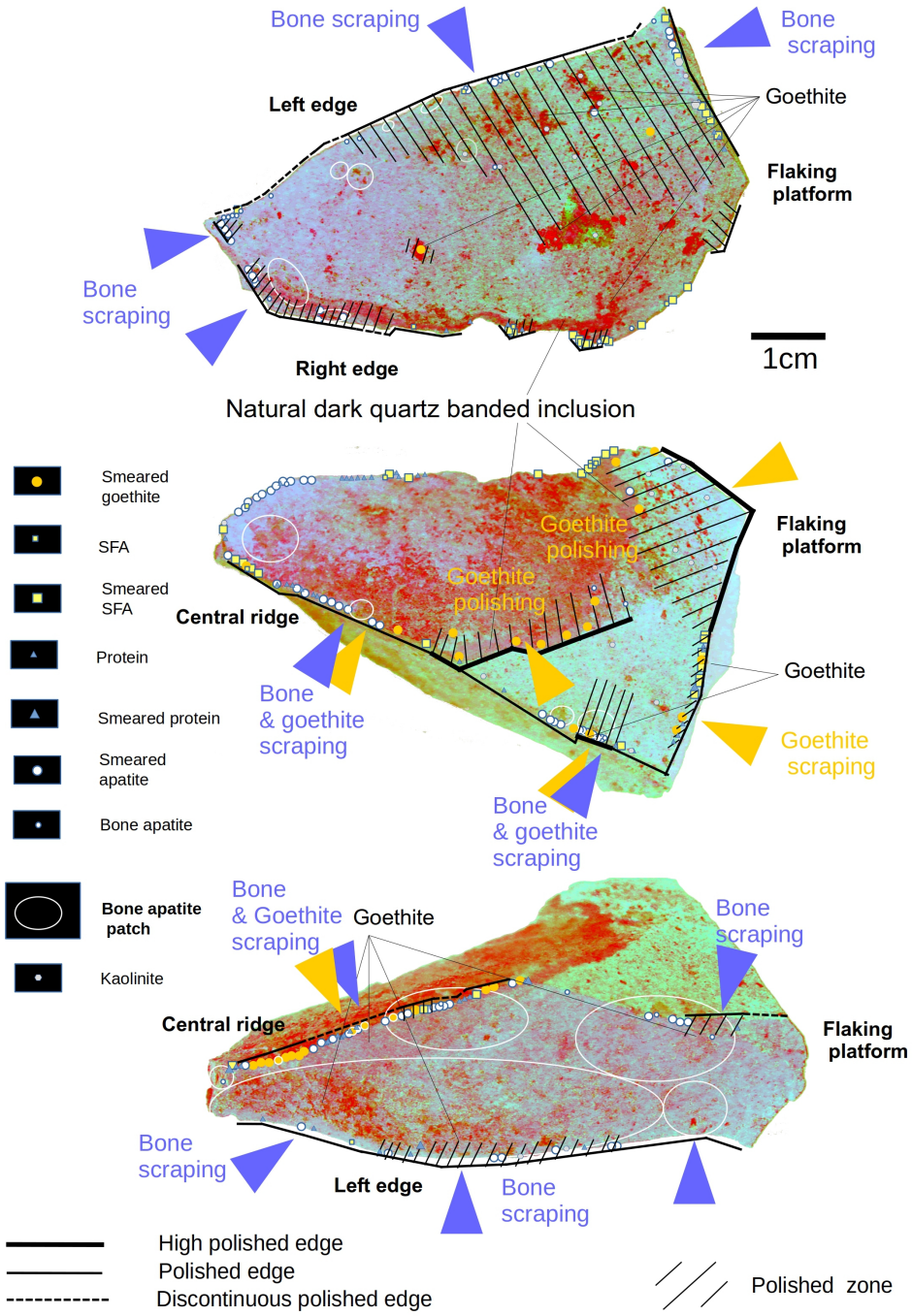

Figure 6.43: Micro-residues distribution on LB5126 with goethite colour enhancement by Dstretch® , correlated with polish distribution.

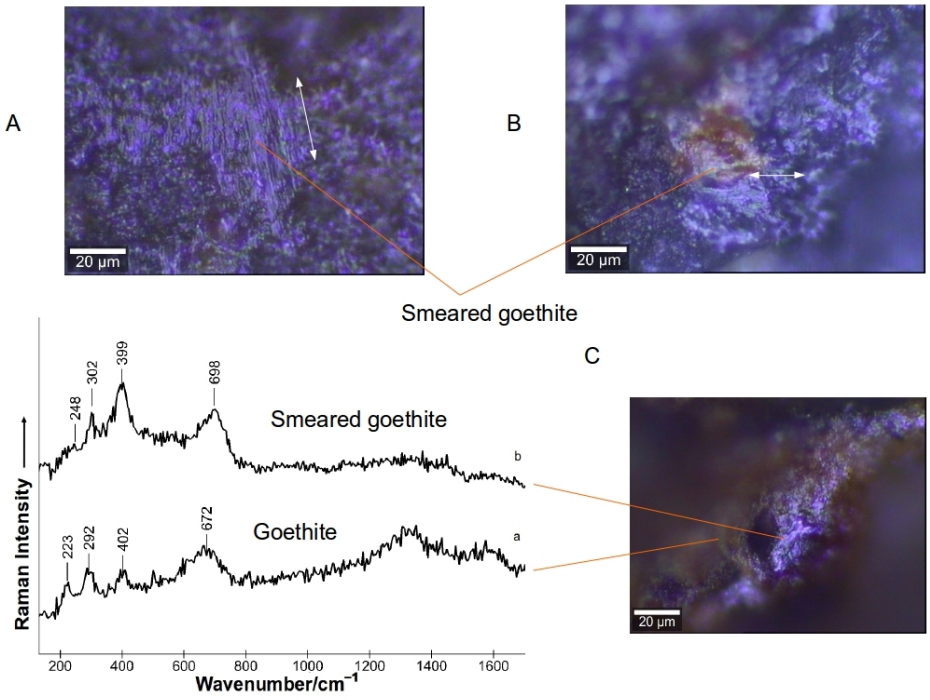

Figure 6.44: Goethite smeared residues on right dorsal polished surface of LB5126 with striation (A-B), Raman analysis of a smeared goethite residue (C, b) and grainy goethite (C, a) residues on central ridge of dorsal left side of artefact LB5126.

Analysis of these mixed smeared residues that are composed of a thin layer of fossil bone apatite and goethite mineral (e.g., Figs. 6.45 and 6.46) confirms that pressure was applied on both goethite and bone during the same action. Some of these mixed smeared residues were also found close to altered bone residues. These specific mixed and smeared micro-residues were concentrated on the central ridge of the left dorsal side (Figs. 6.40 and 6.41), where intensive bone and goethite working are reflected by numerous residues of both materials. This close association and mixing of these two materials are confirmed by SEM-EDS elemental analysis on a few areas selected on the central ridge, on the right dorsal side (Fig. 6.47). Observations of (1) a concentrated spread of rich goethite adjacent to edges for working bone, combined with (2) smeared goethite on polished edges and (3) mixtures of smeared bone and goethite together indicate stone tool use on both materials to achieve an unknown task. On the dorsal right surface, bone residues are in rather low abundance compared with edges used to work both materials (Figs. 6.40 and 6.43), indicating the main material worked on that surface was goethite, probably during a polishing task.

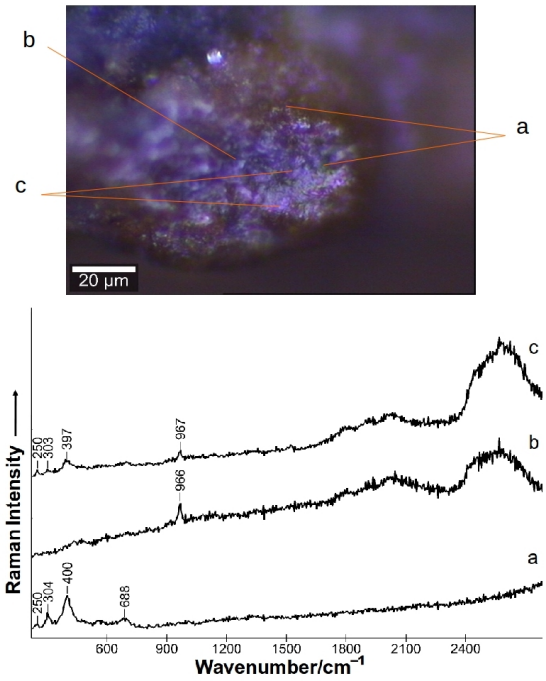

Figure 6.45: Analysis of mixed fossil bone apatite and goethite smeared residues on left edge of dorsal side: Goethite (a), fossil bone (b), fossil bone + goethite (c). Note rare earth fossil bone apatite fluorescence bands on spectrum c.

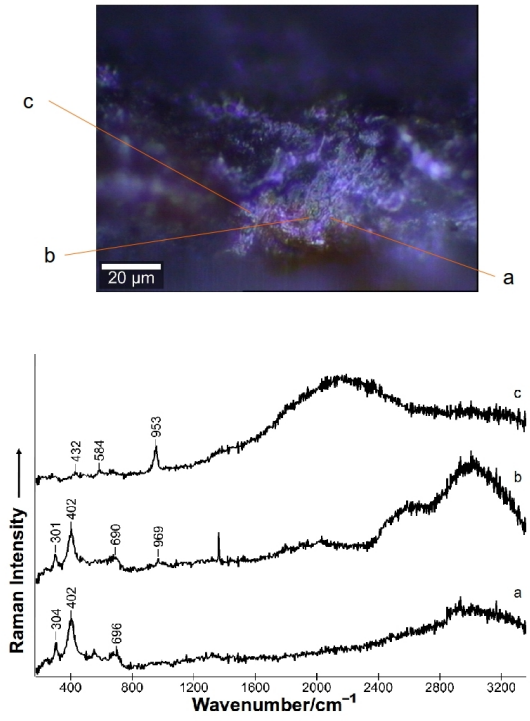

Figure 6.46: Another example of analysis of mixed fossil bone apatite and goethite smeared residues on edge of the dorsal left side in presence of altered bone: Goethite (a), fossil bone + goethite (b), altered bone (c).

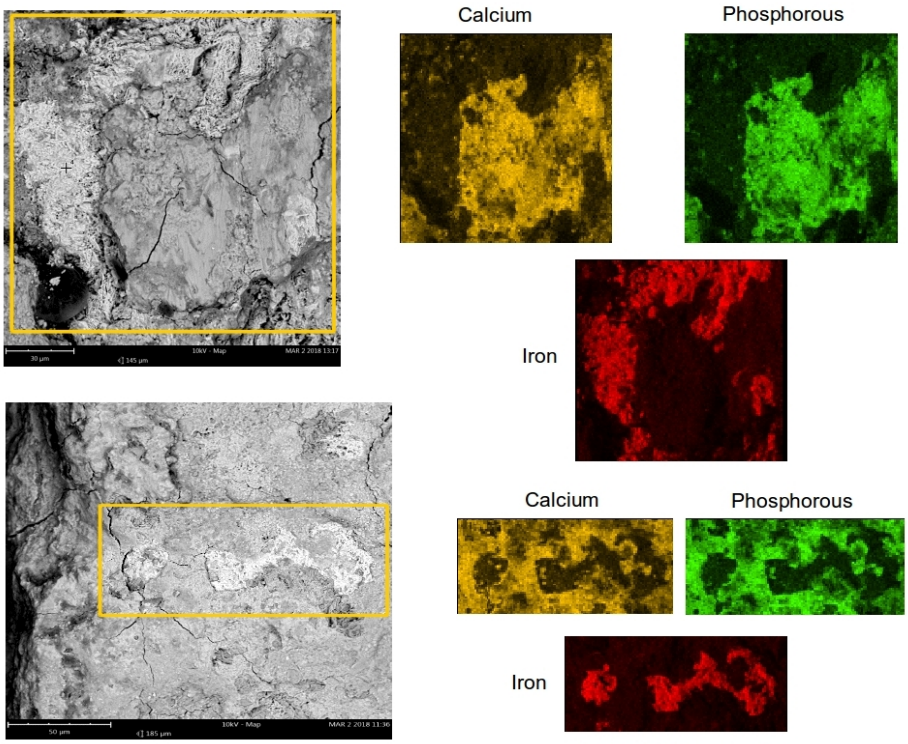

Figure 6.47: Elemental SEM-EDS analysis on two areas selected on central ridge, on dorsal right side, showing iron oxide (identified by Raman spectroscopy as goethite) covered or embedded by bone smeared on the edge.

To summarise my arguments that indicates that goethite is associated with the use of artefact LB5126 :

- Goethite not only occurs as a natural red-orange grain, but also as two other forms with distinct aspect, (1) smeared goethite and (2) smeared goethite mixed with bone.

- Goethite is not distributed uniformly, but shows concentrations in association with polished edges and surfaces or is directly adjacent to them.

- Goethite is not from sediment, nor from rock, nor from the visible dark banded formation, which is only composed of quartz.

Protein micro-residues found on LB5126

Even if they are non-specific residues (plant or animal) (see Chapter 4), individual and a few smeared protein micro-residues were found on artefact LB5126 (Figs. 6.40 and 6.41) and are also linked to the stone tool use. Indeed, concentrations of protein micro-residues occur on the dorsal edges among concentration of other micro-residues (bone, goethite, SFA). Existence of a smeared protein micro-residues confirm this relation to use as those found on artefact LB5126 is similar to traces having been generated in my modern experiments (Chapter 4, section 4.5). It can be noted that a few micro-residues identified as proteins show elongated shapes similar to small sections of fibre but no specific identification can be done with collagen. Indeed, absence of collagen as individual micro-residues is not surprising, as it hasn't been found in bone micro-residues which are either fossil of altered (see above). Being not preserved in bone, its chance of being preserved as isolated residues outside them are probably very low in these conditions.

A similar used artefact with additional presence of unsaturated fatty acids: Artefact LB5213

Artefact LB5213 is similar in shape to artefact LB5126, a thick triangular flake having two angled left and right dorsal surfaces separated by a marked ridge. However, artefact LB5213 has a surface covered by cortex on the proximal dorsal part. The ventral surface have been intensively used (Fig. 6.48**)**. The micro-residues and concentrations on both right ventral and the left distal margin indicate use to scrape bone. During the task, the right distal edge was retouched from the ventral side. This retouch could explain the lack of any high concentration of micro-residues on this part, despite intensive use. Proximal left and right ventral edges also indicate bone scraping activities, but also have overlapping haematite and goethite spread on adjacent polished inland surfaces (Fig. 6.50**).** The central ridge had been also used on bone (Figs. 6.48 and 6.49**)** and with the two coloured materials which have spread on central part of right and left sides (Fig. 6.50**)**. Haematite was detected more frequently than goethite ,but as the conversion of goethite to haematite is rather easy by laser heating, it could be inferred that goethite is present in significant amounts too. Spreading of goethite/haematite is found also on the proximal part of left edge on dorsal left side, in connection with the intensive scraping use of the proximal ventral left edge. On the dorsal side, the central ridge was used to scrape bone and iron oxides along both left and right margins (Figs. 6.48 to 6.50); and are also

associated with goethite/haematite spreading. The goethite and haematite distribution, in a similar way to the previous artefact LB5126, was not randomly widespread but spatially distributed in association with polished areas, leading me to consider the distributions as part of the set of use-related residues found on this stone tool. The same arguments given for artefact LB5126 relating goethite to artefact use and rejecting a natural occurrence of goethite applies to artefact LB5213. As for artefact LB5126, goethite and haematite were found in outer sediment but were not common, so not enough to explain the quantity present on this artefact —thus excluding transfer from the sediment as a source of this material.

Similar smeared haematite and goethite micro-residues (Fig. 6.44**)** were analysed on this tool, mainly on the left edge on dorsal and ventral side, and on proximal part of the central ridge. In contrast with artefact LB5216 on which nor goethite or haematite was not found as part of the rock, artefact LB5213 has a natural haematite vein as a rock inclusion running from the distal part of the left edge to the proximal part of right edge. This vein could be seen on the ventral side and left dorsal side (Fig. 6.50). Presence of this natural vein questions the source of iron oxide as being the stone or another outer source, but does not explain the high amount of goethite and haematite spreaded on the surface of this tool and the specific distribution of this coloured material in relation with used area.

An additional use-related micro-residue was analysed on artefact LB5213. Unsaturated fatty acid, individual and smeared, residues similar to those described already (Chapter 4, section 4.5.2), were found concentrated on the tip and distal left dorsal edge. These residues are distinct from their saturated counterparts found on other worked areas associated with bone, and are not found associated with any other micro-residues. Absence of polish on the artefact tip associated with these micro-residues can be explained by the tip break, which could have happened during the retouching process along the right distal edge. As a result, these UFA micro-residues, being not specific (Chapter 4, section 4.5.2) are difficult to relate to a particular material, other than an unknown fatty material.

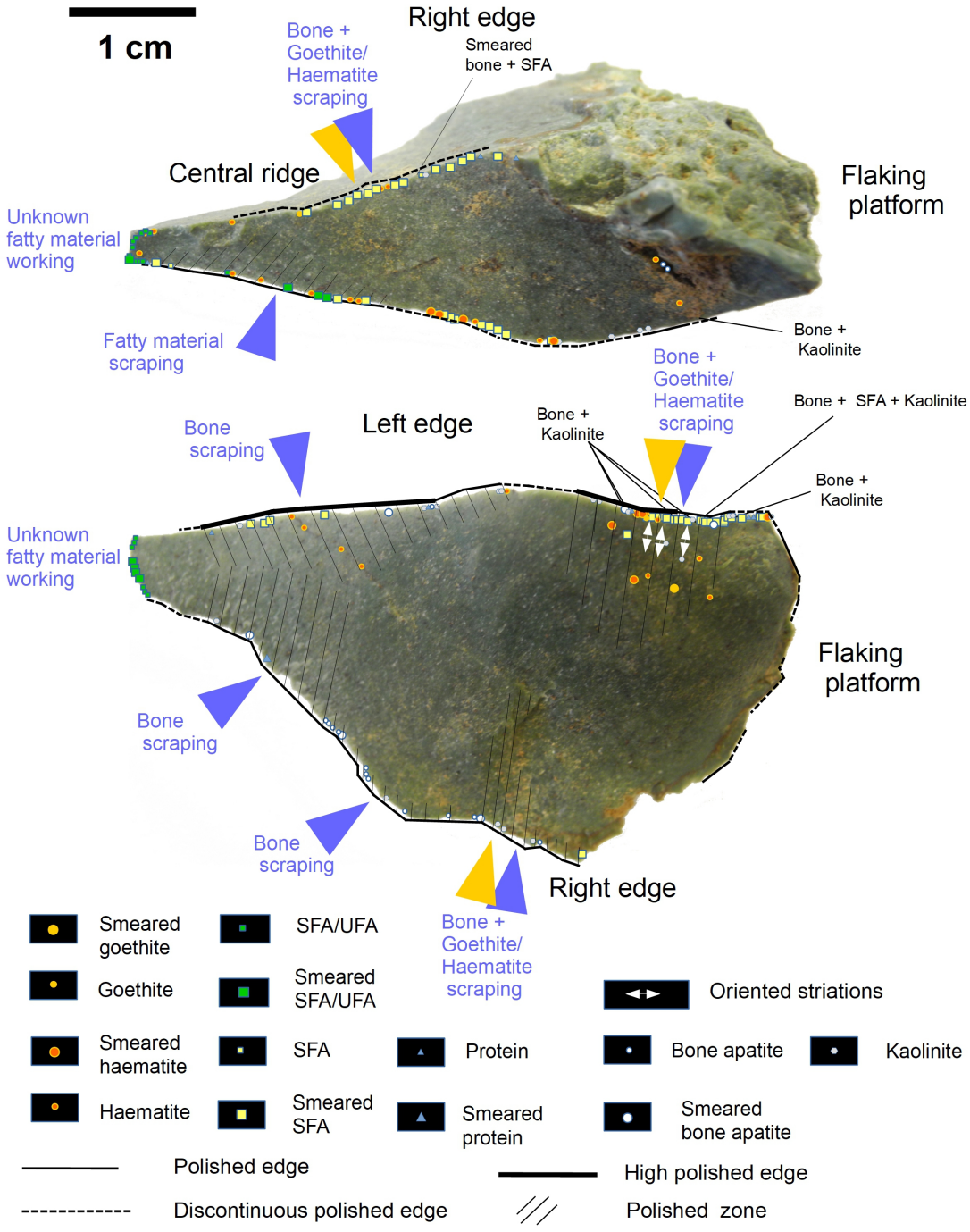

Figure 6.48: Micro-residues distribution on LB5213 ventral and dorsal left side, correlated with polish distribution.

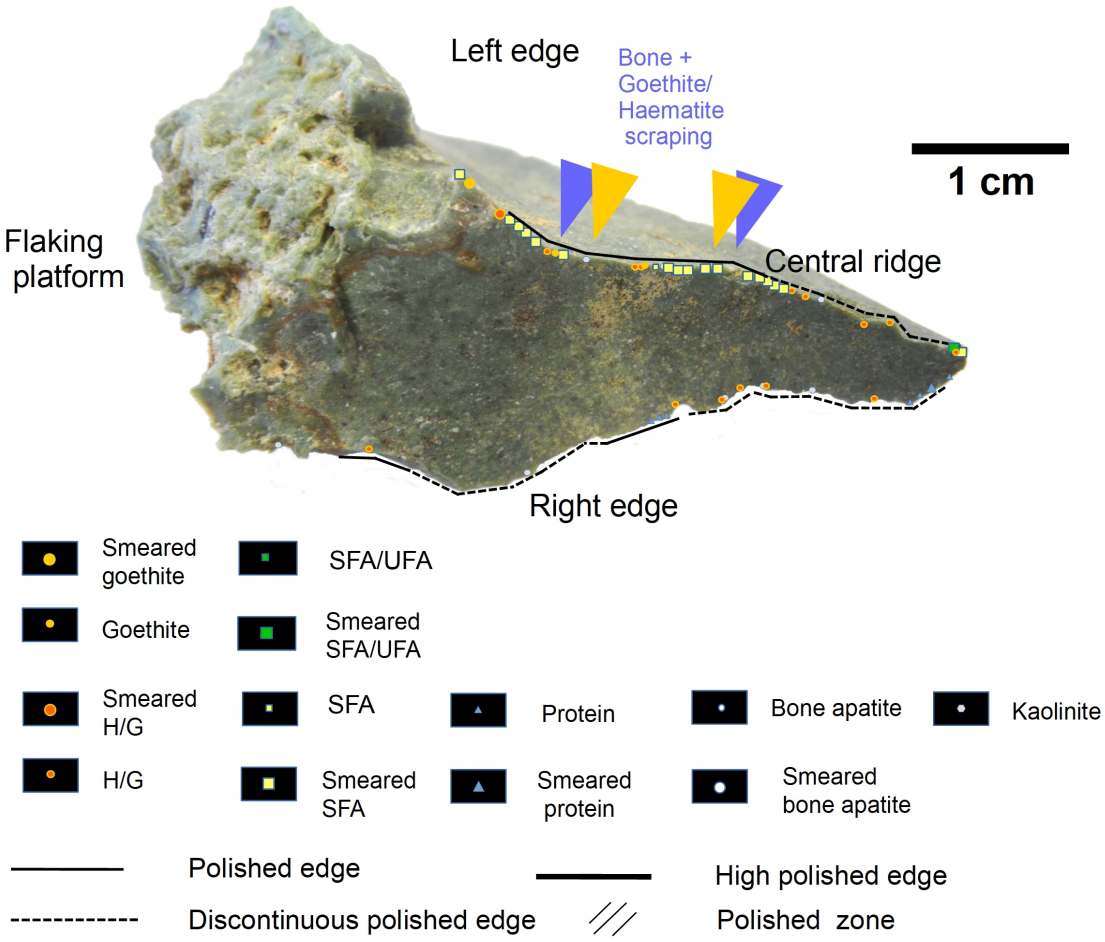

Figure 6.49: Micro-residues distribution on LB5213 dorsal right side, correlated with polish distribution.

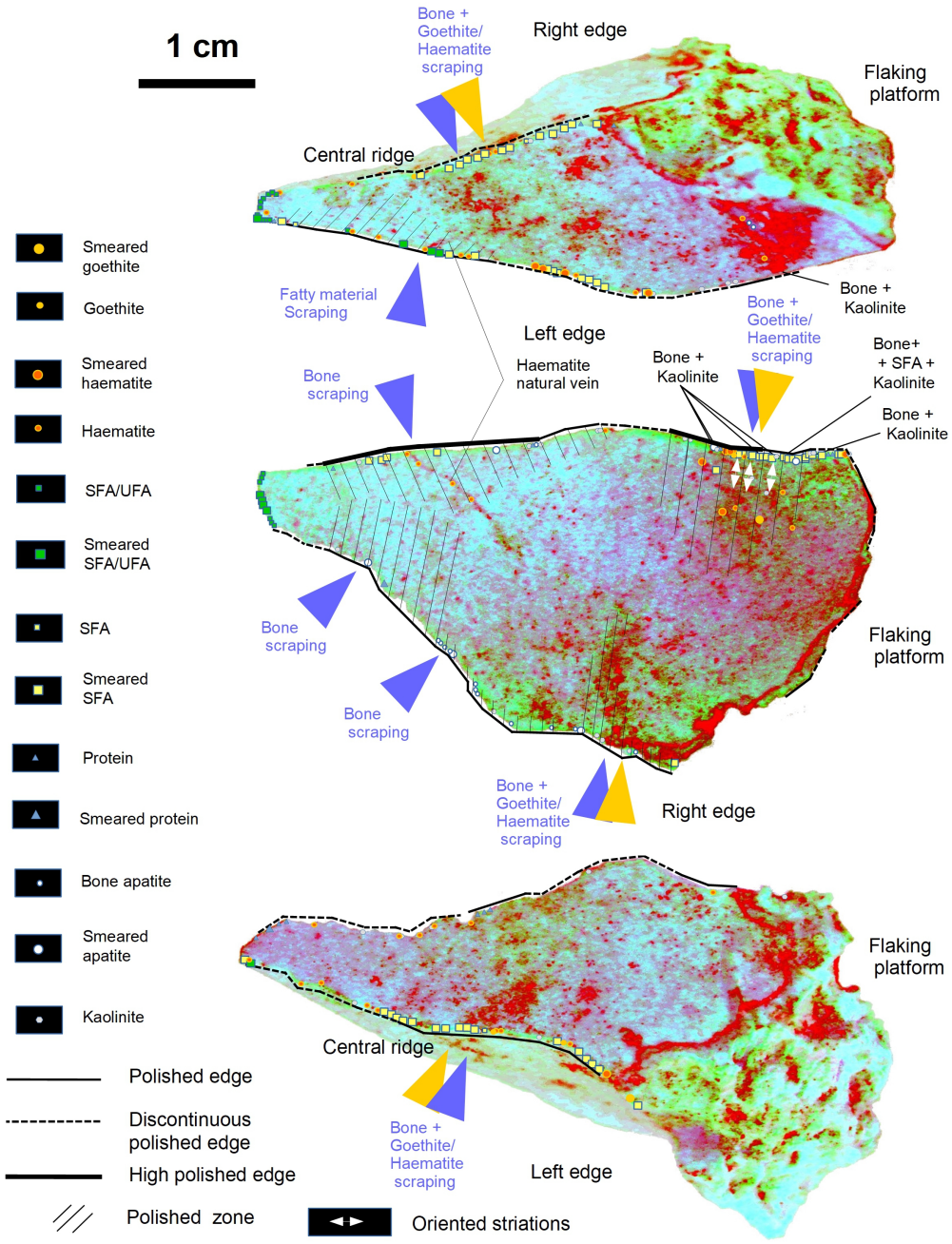

Figure 6.50: Micro-residues distribution on LB5213 with goethite/haematite with colour enhancement by Dstretch®, correlated with polish distribution.

Stone artefact LB5225: A third artefact used on bone with haematite and goethite pigment

On stone artefact LB5225, I detected similar bone and unsaturated fatty acid (UFA) micro-residues as for artefact LB5213. However, bone micro-residues were only found on the medial part of the left edge, both on dorsal and ventral sides (Fig. 6.51). These bone residues can be interpreted as a result of bone scraping with this edge, especially on the ventral side, which shows a high concentration of bone smeared micro-residues. It can be noted that, as LB5126 and LB5213, the dorsal central ridge of LB5225 had being polished and shows concentration of UFA micro-residues on its distal part which indicate a common particular way of use for these all three triangular flakes.

Unsaturated fatty acids are more numerous on artefact LB5225 than found on artefact LB5213, being concentrated on the flake tip, and on ventral left and right edges, with a high concentration of protein. Indeed, the ventral proximal right edge was used to scrape another animal part (probably meat or skin), which could have produced this rather different set of micro-residues. The opposite proximal right edge was probably used in the same way, again with the dorsal side of the flaking platform in downward contact.

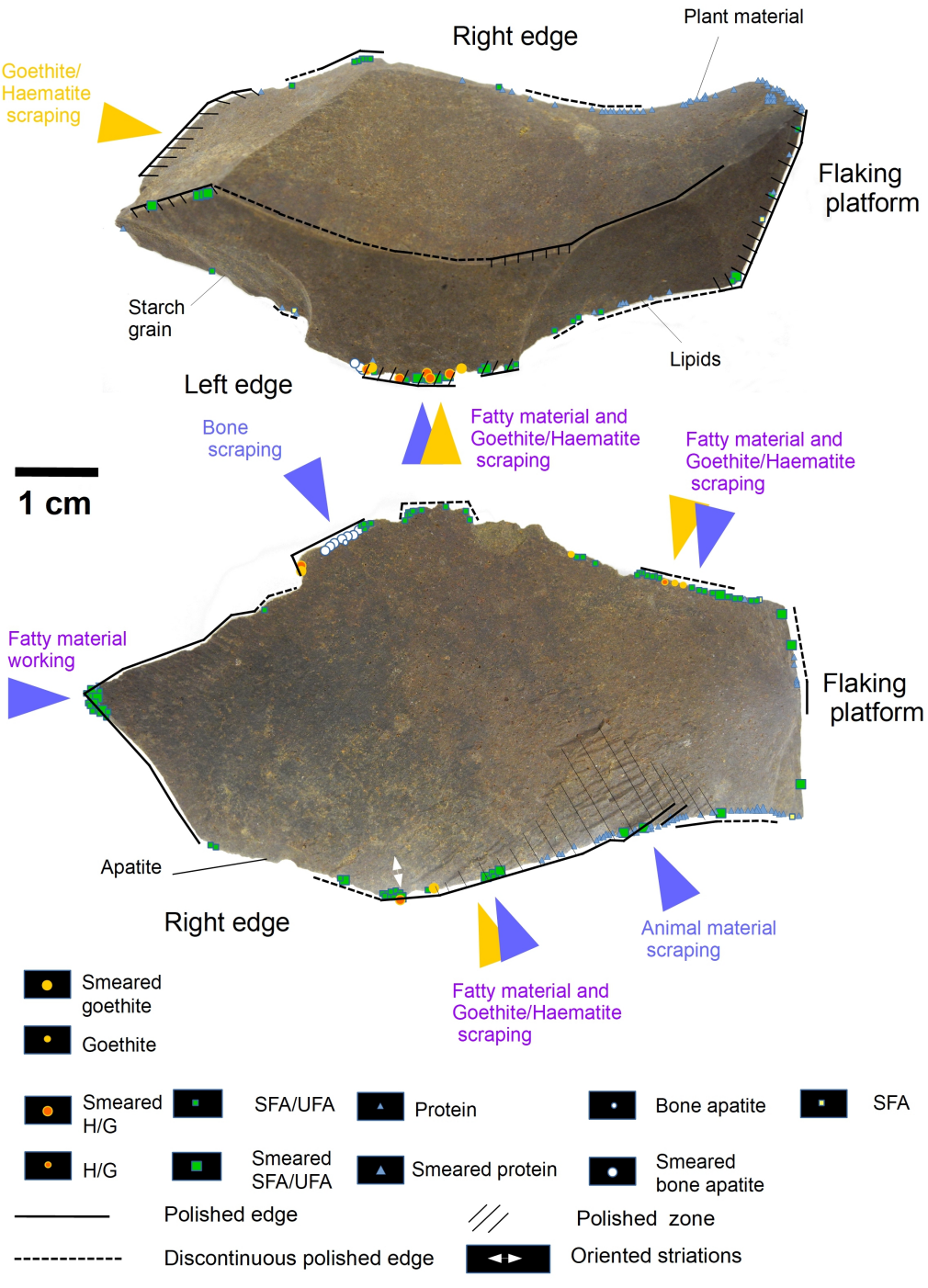

Figure 6.51: Micro-residues distribution on LB5225 dorsal and ventral sides, correlated with polish distribution.

In a similar way as for artefacts LB5126 and LB5213, smeared goethite and haematite micro-residues with the same aspect and Raman spectrum as found on artefacts LB5126 and LB5213 (Fig. 6.44), were found on the dorsal left edge used to worked bone and also on the ventral right edge used scrape other animal material. The dorsal side distal edge, free of bone

and fatty acid micro-residues, seems to have been used mainly on this coloured material. Pigment distribution can be observed quite concentrated in areas located in the vicinity of the main used edges of that stone tool (Fig. 6.52), indicating that this material was used in association with bone and fat, in the same task. The same arguments given for artefact LB5126 relate goethite to tool use and reject a natural occurrence of this material on artefact LB5225.

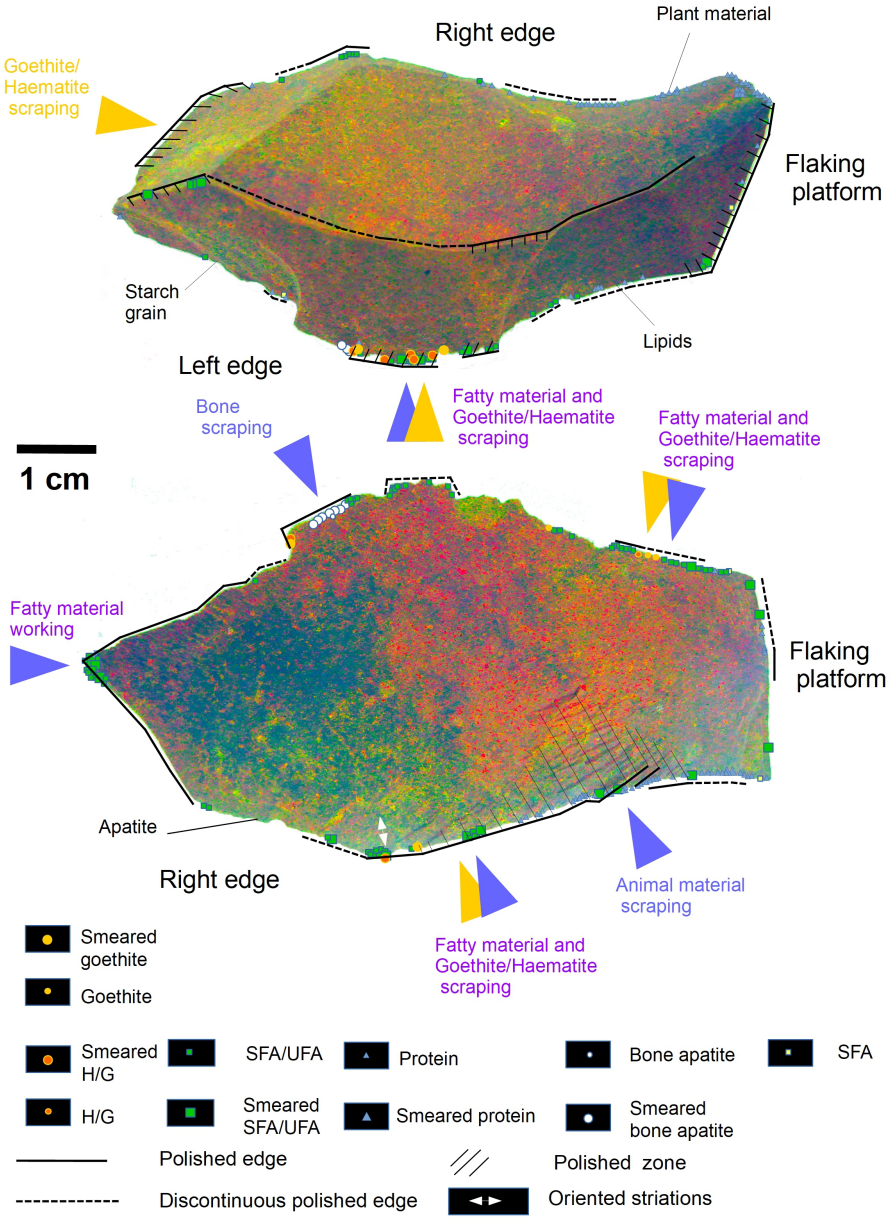

Figure 6.52: Micro-residues distribution on LB5225 with goethite/haematite colour enhancement by Dstretch®, correlated with polish distribution.

Artefact LB5526b: A stone tool dated before ~60 ka with similar morphology and similar use on bone as the previous serie.

Another artefact studied, LB5526b, dated before ~60 ka (Chapter 6, Table 6.2), can be associated very closely with the previous three artefacts (LB5126, LB5213 and LB5225). Indeed, artefact LB5526b shares the same morphology, being a thick triangular flake with a flat ventral side and dorsal side with a central ridge separating right and left dorsal surfaces. As the previous artefacts presented, it shows evidence of intensive bone working on two opposite dorsal lateral edges, but importantly, with also the central ridge used on bone and fatty material, which seems to be a characteristic of all these four flakes (Fig. 6.53). The ventral side was also used on bone with both opposite convergent edges (Fig. 6.54). The distal pointed end of this flake seems to have worked fatty material too, and the flaking platform edge on the left dorsal side was used intensively on bone. Fatty material on this artefact is mainly a mix of saturated and unsaturated fatty acids, as found on artefact LB5525 and on the tip of artefact LB5213. Goethite and haematite were found on the surface of that artefact but in low scattered amounts on all surfaces—that could not be compared to the highly localised concentrations found on the previous artefacts (LB5126, LB5213 and LB5225). Consequently, in this case, these iron oxides which are also present in layer sediment for this sample, have a high probability of arising either from the sediment or from rock weathering, and cannot be, in that case, securely linked with the stone tool use.

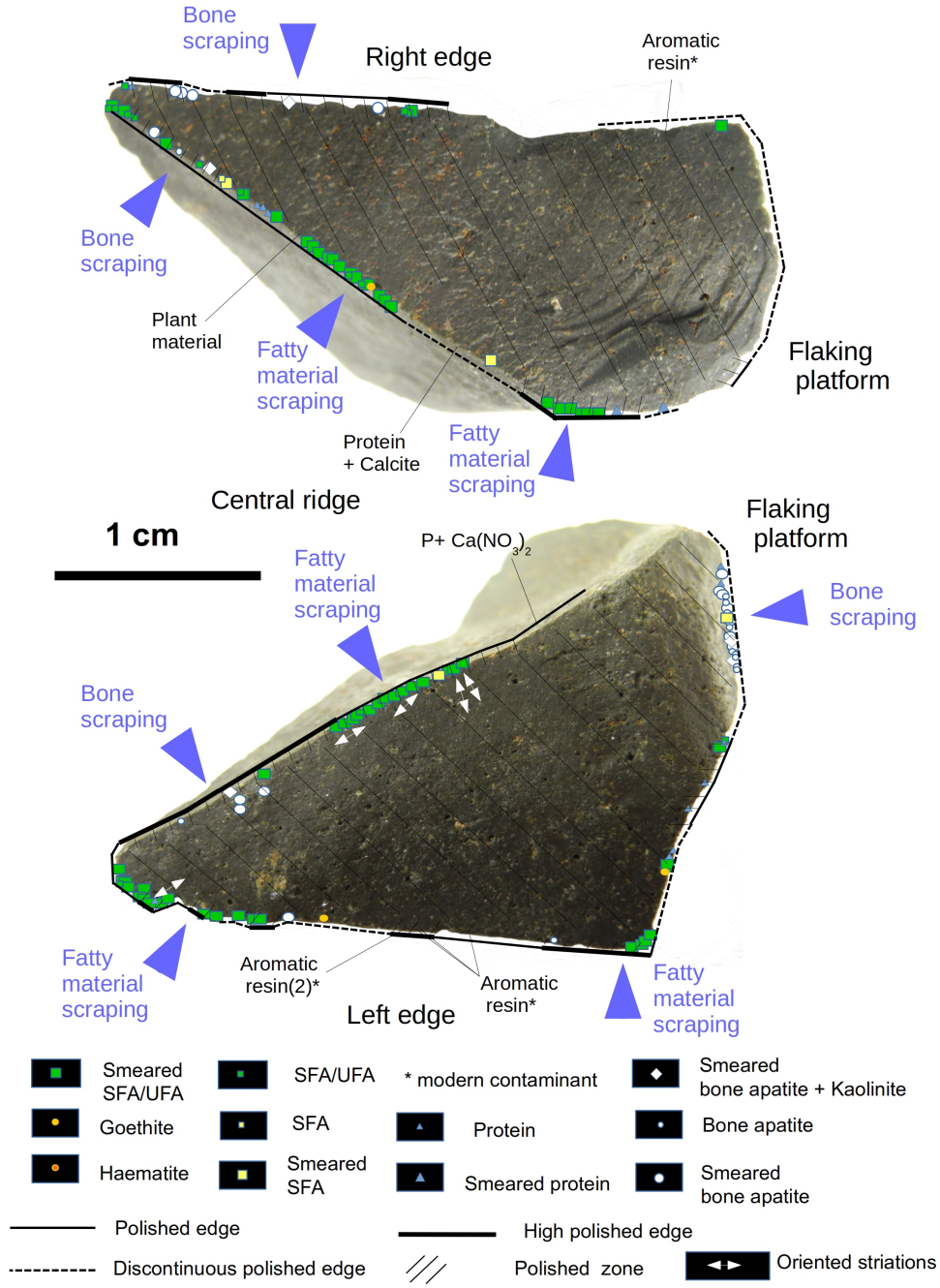

Figure 6.53: Micro-residues distribution on LB5126b dorsal right and left sides, correlated with polish distribution.

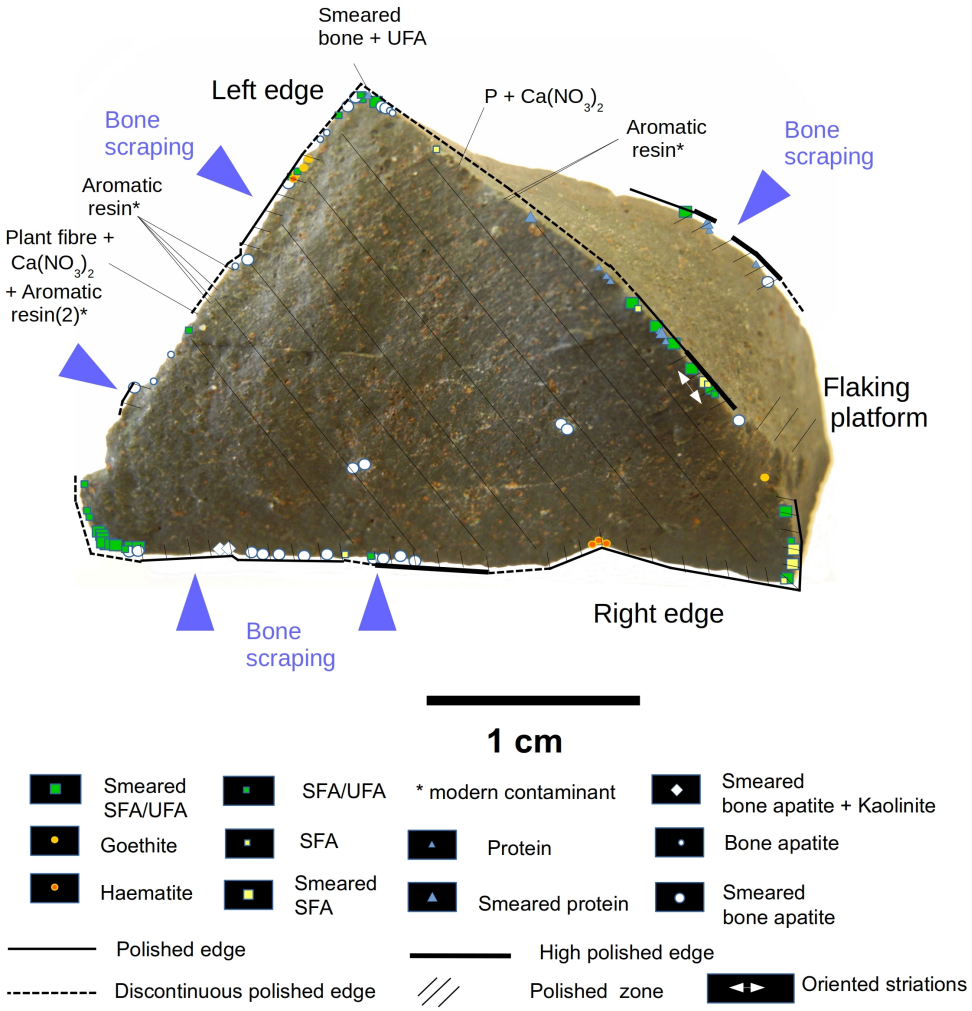

Figure 6.54: Micro-residues distribution on LB5126b ventral side, correlated with polish distribution.

Artefact LB5580a: a stone tool used on bone and iron oxide pigment, dated before ~60 ka

Obvious white and yellow/red coloured residues on side A of this artefact could be seen with the naked eye (Fig. 6.55**)**. White residues were identified as fossil bone, present as smeared and individual residues, often mixed with kaolinite, (Chapter 6, section 6.3.2.3) with presence of additional saturated fatty acid found in one micro-residue. Bone micro-residues and macro fragments of bone were found in the layer (outer) sediment suggesting that some of micro-residues on this stone tools are could have originate from the layer sediment. However, the low bone micro-residues abundance in the sediment is not enough to explain their very high abundance on side A.

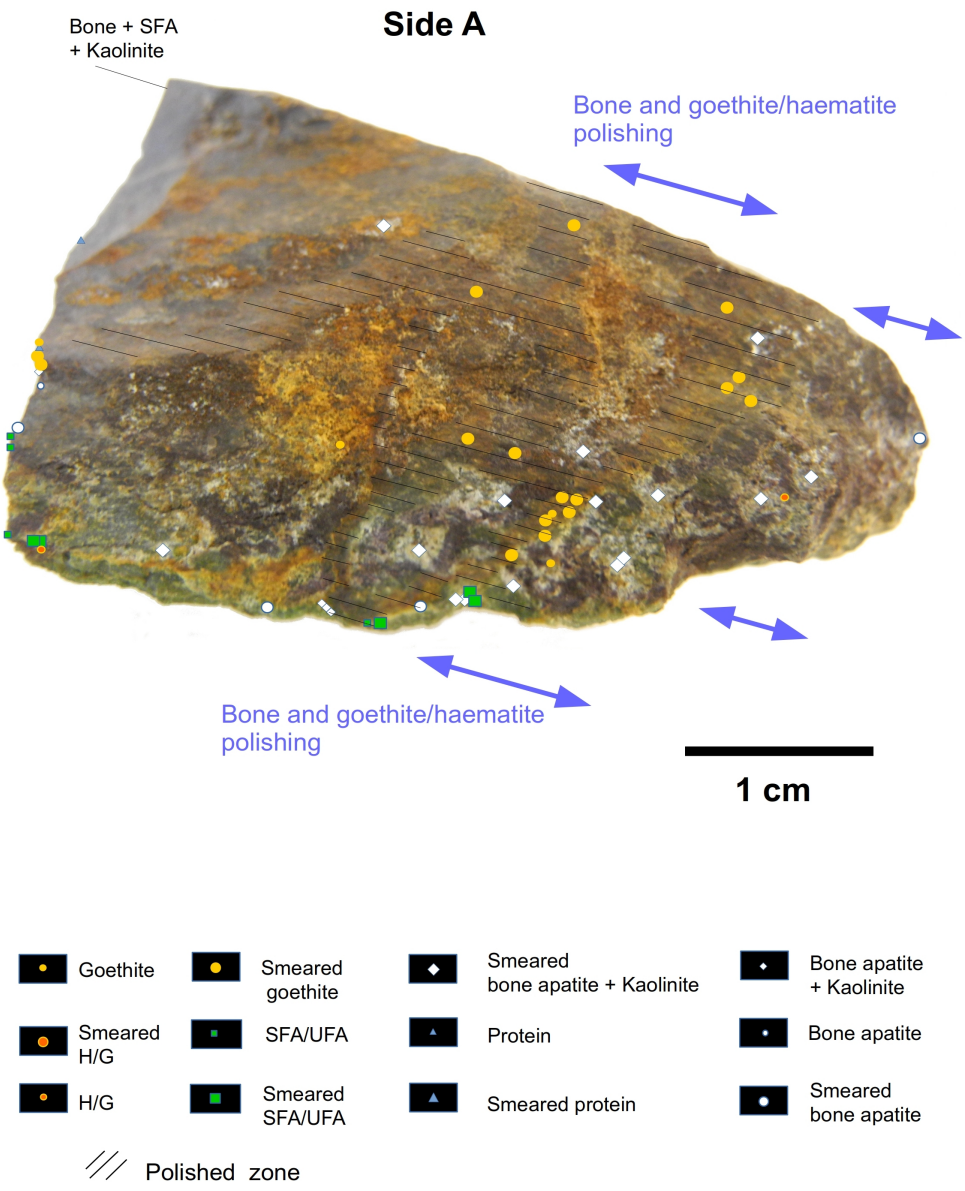

Figure 6.55: Micro-residues distribution on artefact LB5580a side A.

Furthermore, bone is clearly concentrated, mainly on side A, but also on an edge of side C used for scraping (Fig. 6.56)— confirming the association of bone with artefact use. Outside these two concentrated areas only rare occurrences of bone can be found on side D (Fig. 6.56) and no bone micro-residues were found on the cortex (side B) (Fig. 6.57).

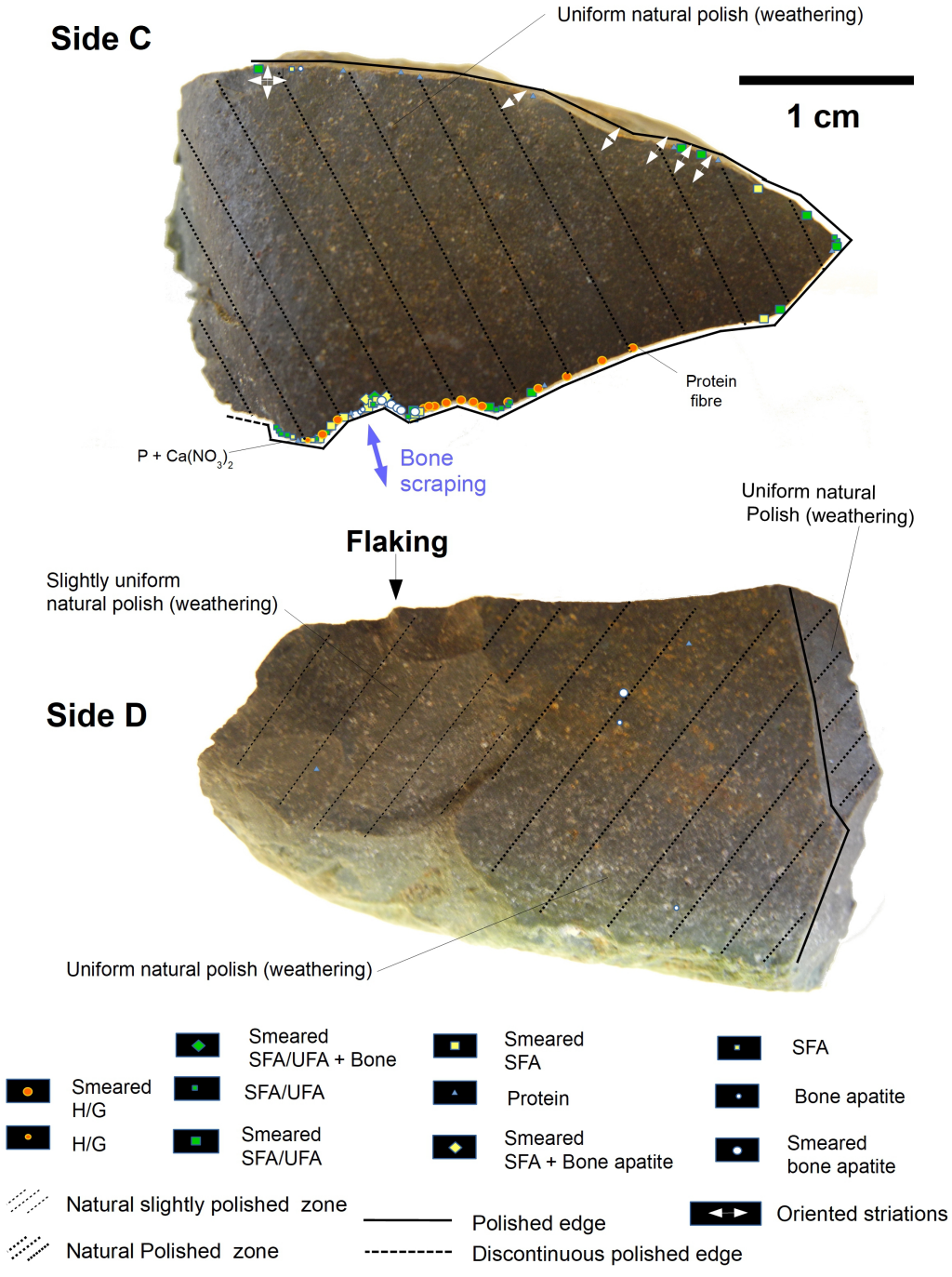

Figure 6.56: Micro-residues distribution on artefact LB5580a, C and D sides.

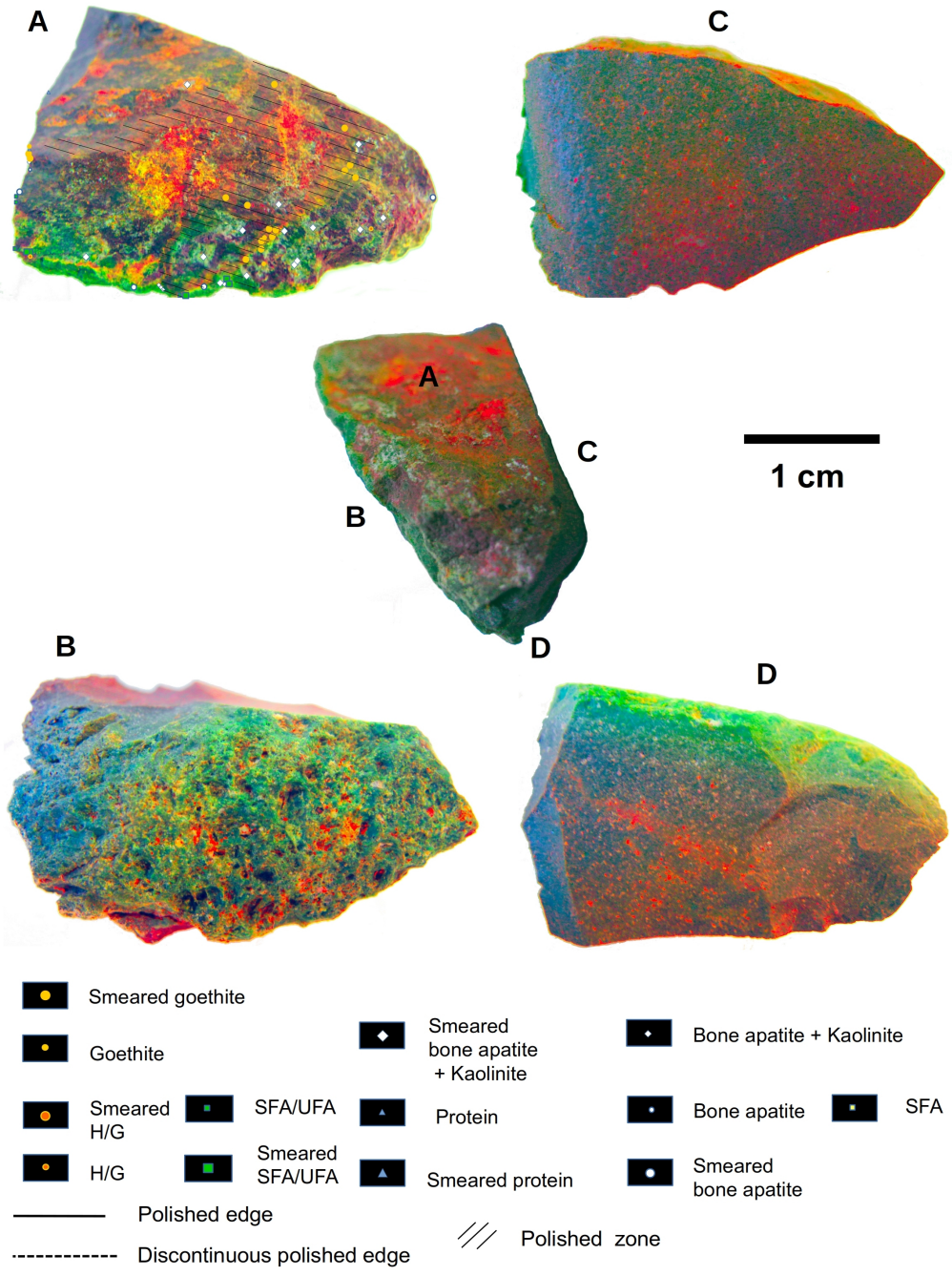

Figure 6.57: Different sides of artefact LB5580a with goethite/haematite colour enhancement by Dstretch®, main coloured side (A), adjacent cortex side (B), smooth side adjacent to the coloured side (C), smooth side opposite to the coloured side (D).

Mixing of bone micro-residues with kaolinite also indicates that this material has degraded and undergone weathering on the rock surface. The high amount of kaolinite on side A of this artefact was observed to completely trap bone micro-residues, both with Raman microscopy and SEM-EDS (Fig. 6.58). As analysed on previous artefact (LB5213), fatty acids were also found associated with kaolinite and bone in some micro-residues.

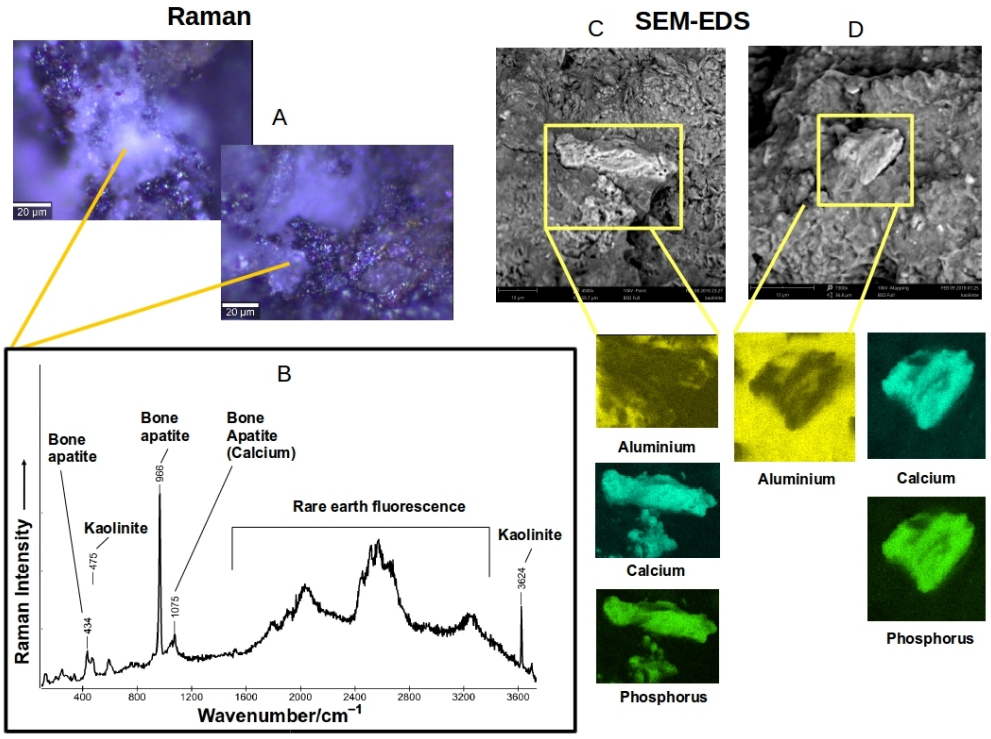

Figure 6.58: Image of kaolinite micro-residues mixed with bone on LB5580a (A), typical Raman spectrum obtained on kaolinite micro-residues showing the presence of fossil bone (B), SEM image of two micro-fragments of bone in white kaolinite covered area on LB5580a and EDS Aluminium (clay) and calcium and phosphorous (bone) elements mapping (C-D).

At this stage, it is difficult to explain such an accumulation of kaolinite weathering on bone, but perhaps the natural porous structure of bone, accentuated in its different state of alteration, could have retained kaolinite from being further leached away from the rock surface, and the presence of kaolinite has contributed to better preservation of bone micro-residues.

Coloured yellow and red mineral residues were found to be mainly goethite (Fig. 6.57), but haematite was found mixed with goethite in lesser amounts. Macroscopically, this coloured material shows clear directional smearing, corresponding to the polished area on the highest part of A side (Fig. 6.55). Microscopically, these two mineral pigments can be found in smeared micro-residues, as found for previous artefacts, on which the residues, I argued, were use-related (LB5126, LB5213, LB5225) (Fig. 6.59).

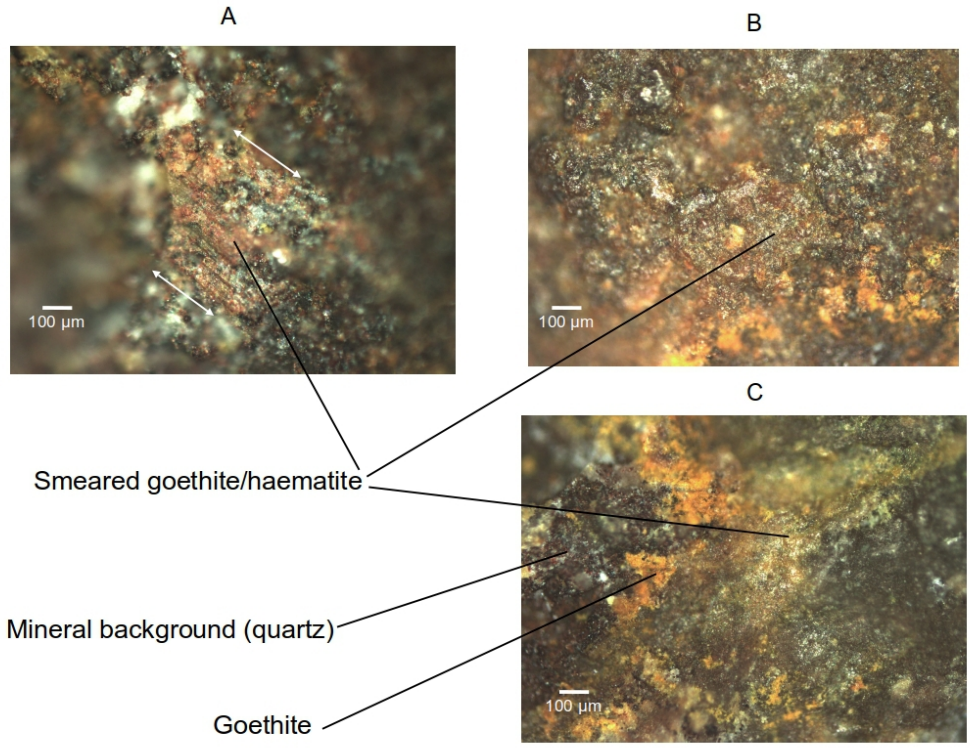

Figure 6.59: Image of smeared goethite areas on LB5580a showing directional smear (white arrow) (A), image of smeared goethite area showing also grainy yellow goethite (B and C).

In some cases, these smeared areas, have a metallic shiny and flattened aspect, contrasting with yellow/red grainy goethite/haematite indicating that they underwent pressure during tool use. They have been documented in a smeared goethite area, with spectral mapping (Fig. 6.60).

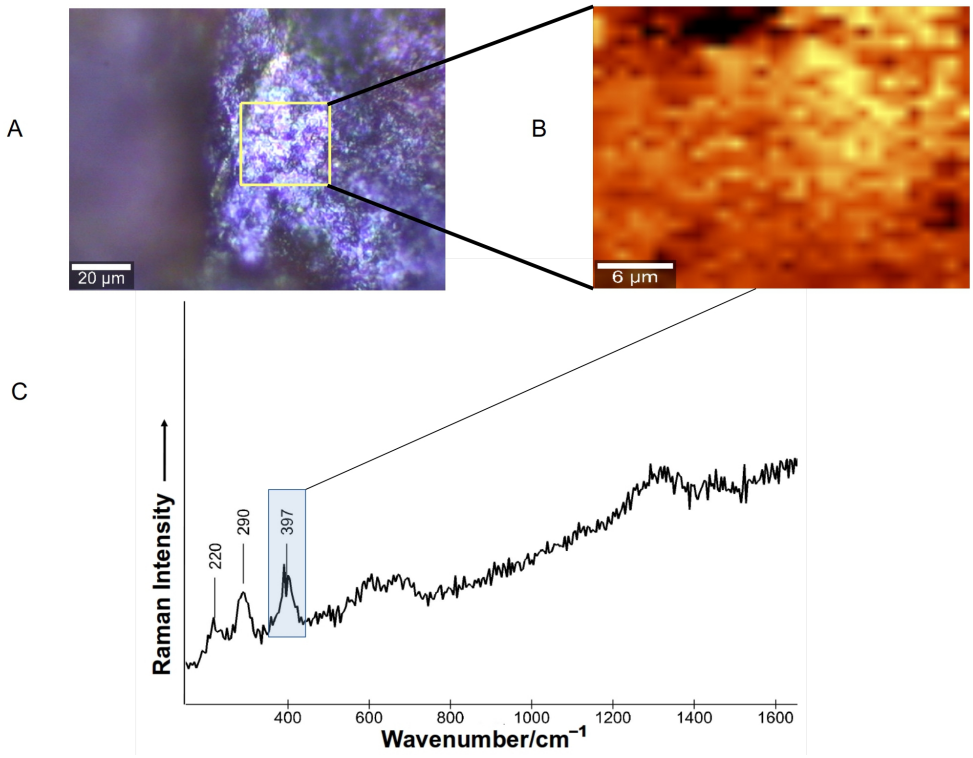

Figure 6.60: Image of smeared goethite micro-residues on LB5580a: (A), Raman mapping of the integrated intensity of goethite main band (B), and typical goethite spectrum obtained on that area (C).

Directionality can be observed on some of these smeared coloured areas with oriented striations visible either at a microscopic scale (Fig. 6.59**),** or a macroscopic scale (Fig. 6.55). Haematite is also present too with numerous, small, individual, micro-residues, frequently found overlying bone (Fig. 6.61).

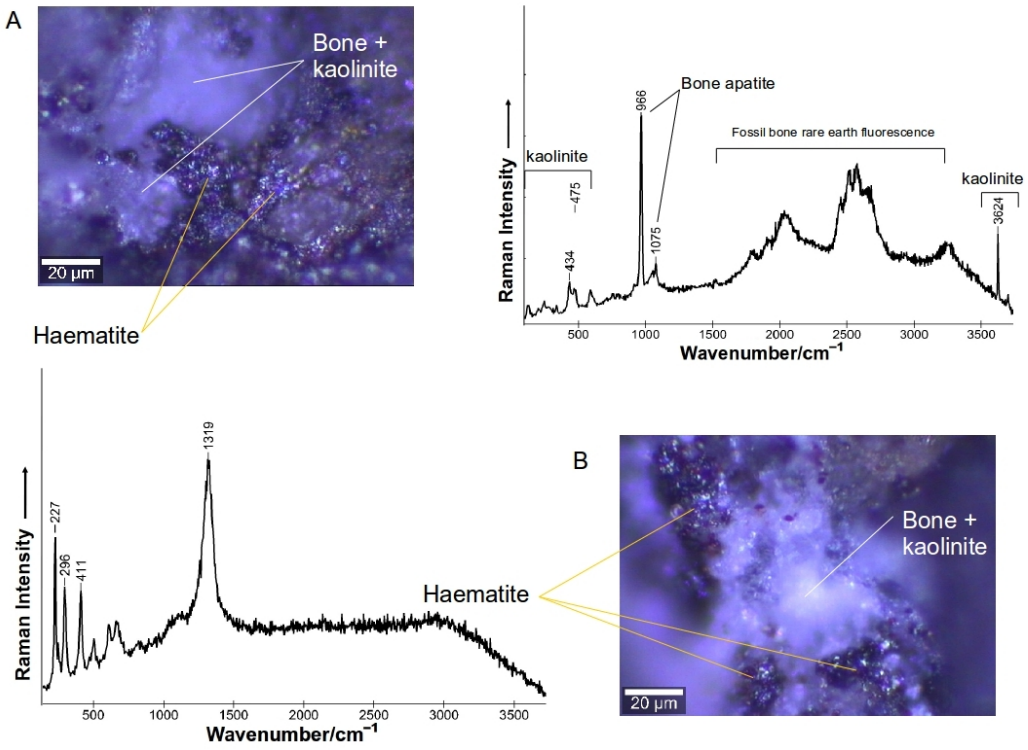

Figure 6.61: Localisation of bone mixed with kaolinite and haematite on two areas of artefact LB5580a with corresponding Raman spectra (A-B).

Goethite and haematite are also present in low amounts, with uniform distribution on two other smooth sides of this artefact (C and D), adjacent to and opposite the main coloured side (A) (Fig. 6.56). These sides result from a naturally weathered rock surface, considering that they are covered by uniform smoothing. Mineral pigment was not detected on the cortex (Side B). Side A, lacking uniform weathering is in very high contrast with Side B, suggesting both bone and iron oxide pigments relate to tool-use, probably by a unidirectional polishing action (Fig. 6.55).

Further to the exceptional preservation of material on Side A, artefact LB5580a was used also on bone on Side C, but probably during a second later episode of use. Indeed, a later flake detachment was observed on Side D (Fig. 6.56**)**, with surface C as the platform. This flake removal is clearly cutting through the weathered surface of Side D as the new flaked surface bears less intense natural smoothing. This notched edge obtained on Side C was then used to scrape bone (Fig. 6.56). Smeared goethite and haematite was found also on this edge but is probably resulting from non intentional pressure on the coloured mineral naturally occurring from weathering on this side. The absence of iron oxides linked to the uses on that edge seems confirm that use is distinct from the joint use of bone and pigment on Side A, and is probably related to a later distinct bone only use task.

In summary artefact LB5580a seems to have been used in two phases:

- First, a polishing task on bone (e.g., final shaping of bone objects) using a large part of side A, in the presence of goethite and haematite pigments

- Second, a very localised scraping task on bone on Side C, after a flake removal on side D.

Using laser induced fluorescence to locate fossil bone micro-residues on LB5580a

Confronted with high coverage of bone on Side A of artefact LB5580a, I took advantage of laser induced fluorescence of neodymium, a rare earth element present in fossil bone micro-residues found on Liang Bua artefacts (Chapter 4, section 4.7), to map fossil bone. Fluorescence has the advantage of being faster than mapping this material by following the Raman apatite band, allows higher spatial resolution, and completes mapping of larger areas in less time. Some examples of comparisons between bone residues fluorescence and Raman spectral mapping on artefact LB5580 side A illustrate this advantage of using this rare earth fluorescence signal (Fig. 6.62). Very coherent spectral images are obtained and they locate fossil bone in both cases, rendering spatial bone distributions by these two distinct interactions of bone apatite with laser light: (1) Raman spectroscopy, with the vibration of PO_4- stretching mode of apatite under green excitation (532 nm) (Fig. 6.62 A-C); and (2) rare earth fluorescence, with fluorescence of neodynium (Nd^{3+}) ions substituted in the apatite crystal lattice under red excitation (785 nm) (Fig. 6.62 A, E-D).

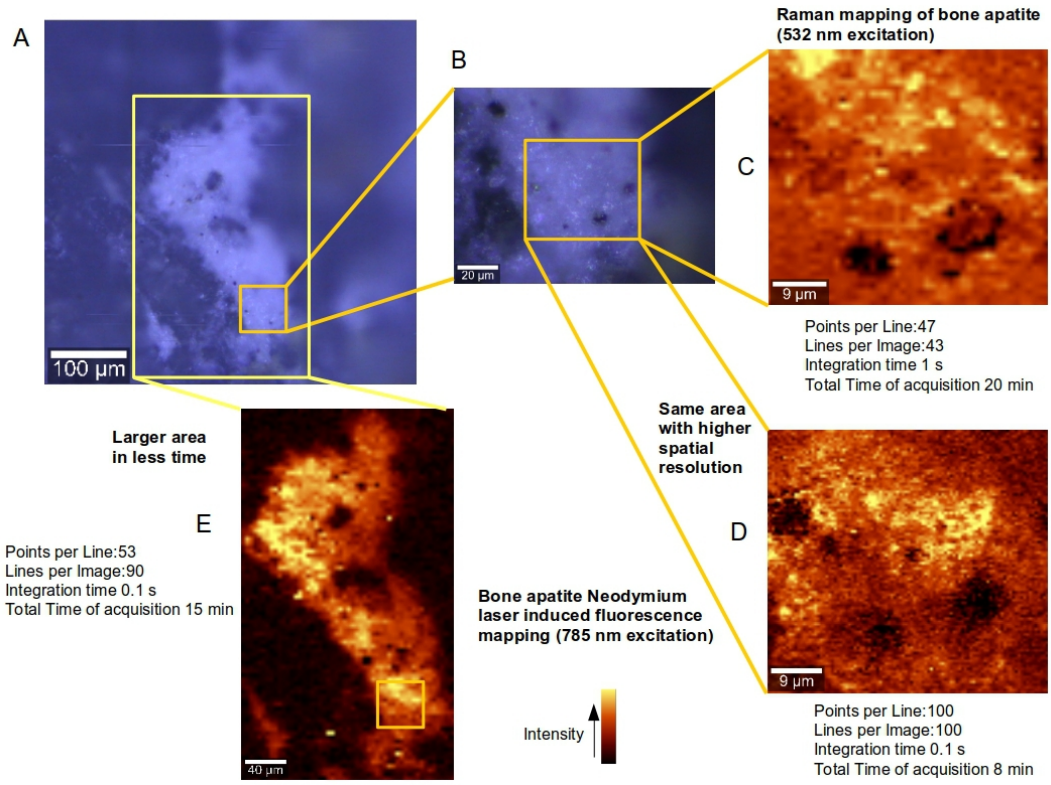

Figure 6.62: Fossil bone residue on artefact LB5580a side A surface (A), selected zone for analysis on fossil bone residue on artefact LB5580a side A surface (B), Raman spectral mapping of PO_4- stretching vibrational mode of apatite on selected zone (C), mapping of neodynium (Nd^{3+}) fluorescence, red excitation (785 nm) on same selected zone (D), mapping of neodynium (Nd^{3+}) fluorescence, red excitation (785 nm) on the entire bone residue (E).

A concentration of bone smeared residues on Side C reveals an example of spectacular striated and smeared bone residue. This edge area was flat enough to achieve a spectral mapping of this smeared bone area using also the specific neodymium fluorescence of fossil bone micro-residues (Fig. 6.63).

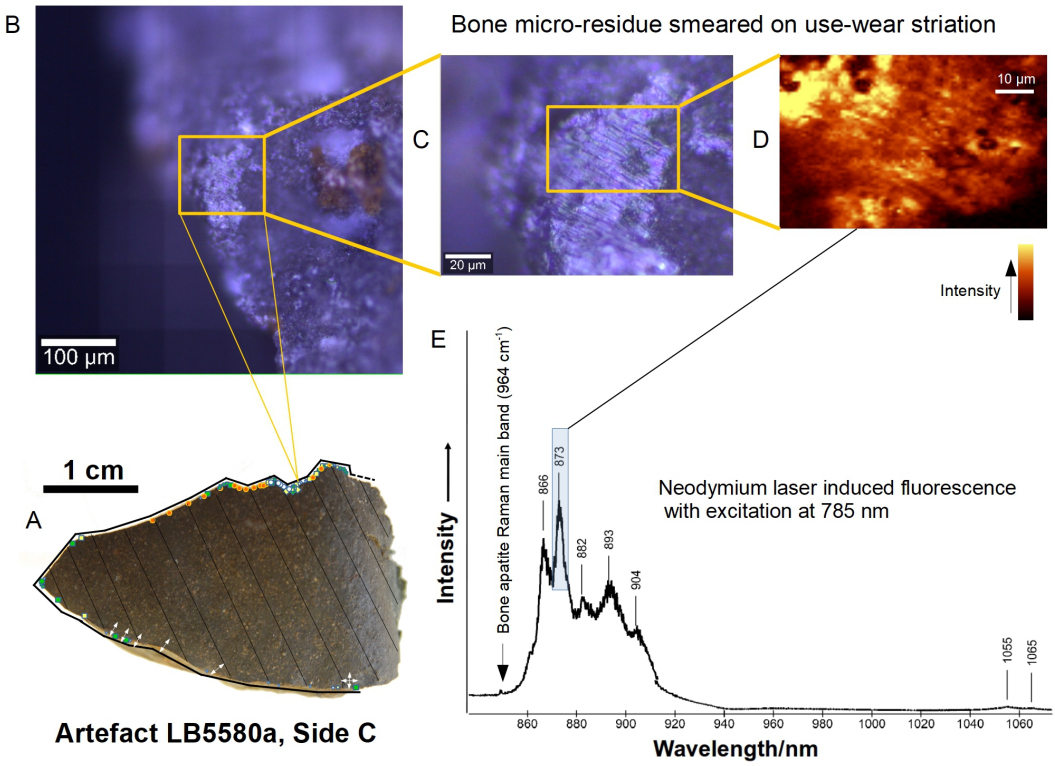

Figure 6.63: Side C of artefact LB5580a showing bone micro-residues concentration (A), image by Raman microscope of a smeared bone residues on used edge, X20 objective (B), image by Raman microscope of a smeared bone residues on used edge showing use-wear striations, X50 objective (C), fluorescence spectral mapping of striated bone micro-residue on neodynium fluorescence bands centred at 873 nm (D), fluorescence spectrum obtained on fossil bone with 785nm laser excitation (E). Note that the Raman vibrational apatite band is still visible on that spectrum but low compared to than fluorescence intensity.

Artefact LB5524: a stone tool use to scrape fatty material and goethite

The dorsal and ventral sides of artefact LB5524 were used to scrape undetermined fatty material. Key residues are difficult to determine (Fig. 6.64). Indeed, plant materials are too few and isolated to be significantly related to use and bone is only showing a small concentration on the dorsal left edge, but these residues were found in such a unique small limited area, that they are probably arising from contact with bone present in sediment. Moreover, presence of fossil bone on artefact LB5524 sediment supports this origin. However, presence of a bone micro-residue mixed with kaolinite on the intensively used dorsal right distal edge may indicate that this unique residue is not arising only from sediment, but as being isolated, this is not sufficient to secure animal origin for fatty material analysed on this part of LB5524.

However, a more certain example of use of LB5524 is indicated on the flaking platform. A high amount of saturated fat was found concentrated and smeared, especially on highly polished edge oriented towards the ventral side (Fig. 6.65). A high amount of goethite is visible and was analysed — in contrast with dorsal and ventral surface where it had been found only in small amounts. Goethite can be found generally grainy in the middle of the surface but smeared goethite can also be found indicating that this material underwent pressure during use. Smeared goethite is found in increasing abundance on the polished edges and furthermore, was found mixed frequently with fatty acid in these same areas (Fig. 6.66**)**. On the opposite edge of the flaking platform, oriented towards the dorsal side (i.e., external platform edge) there is polish from use on the right edge side, but on its central and left edge side, it can be observed scarring damage which probably obliterated large parts of micro-residues and polish. On this badly damaged edge, a unique smeared bone micro-residue suggests an animal origin for the material worked by artefact LB5524 flaking platform. This animal origin is supported by the large amount of fat and strong presence of smeared fat micro-residues found generally in working animal material on experimental tools (Chapter 4, sections 4.4 to 4.5). Artefact LB5524 confirms mostly concurrent use of stone tools on fatty material and iron oxides pigments for period before ~60 ka.

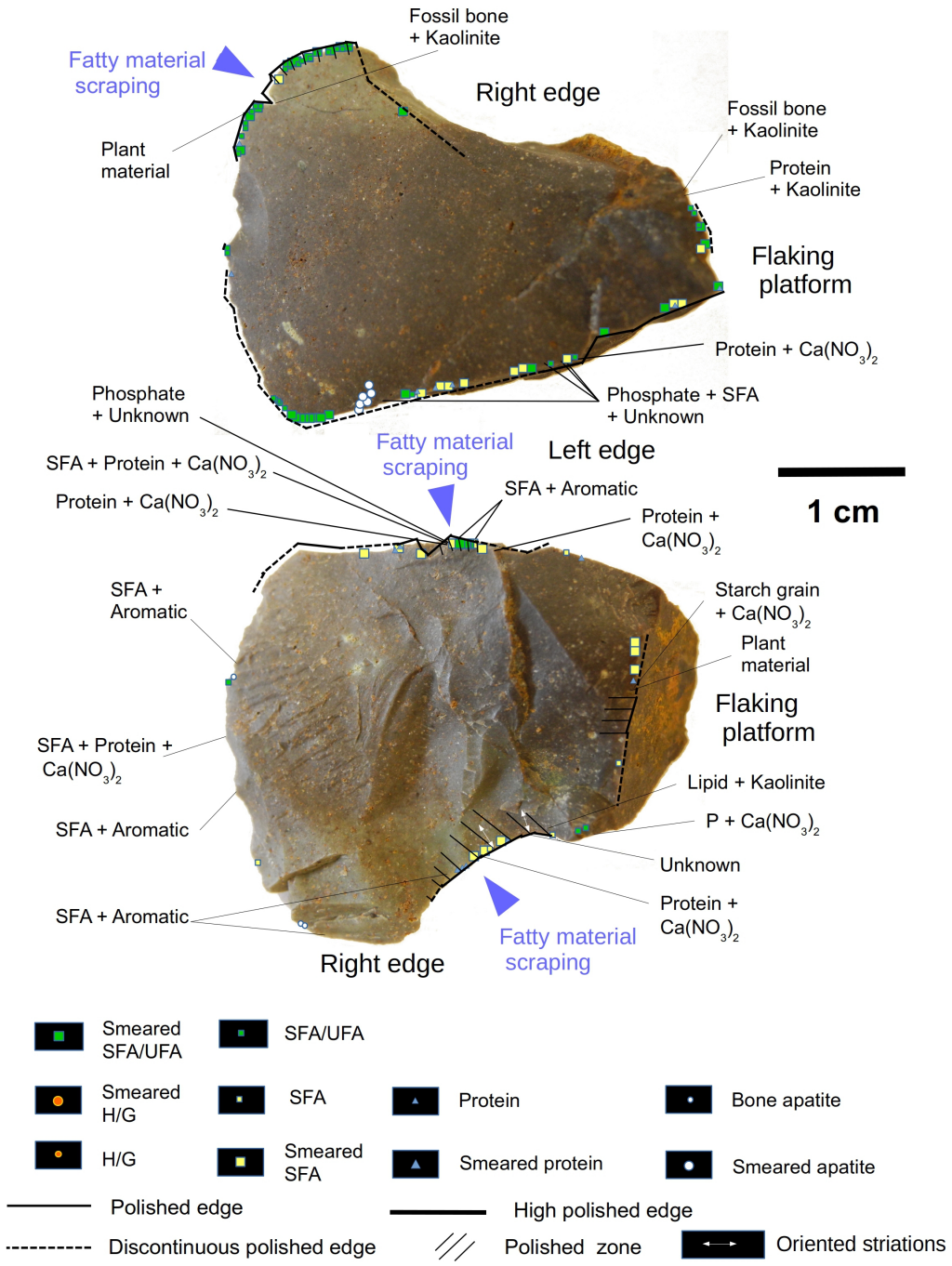

Figure 6.64: Micro-residues distribution on artefact LB5524 and correlation with polish distribution.

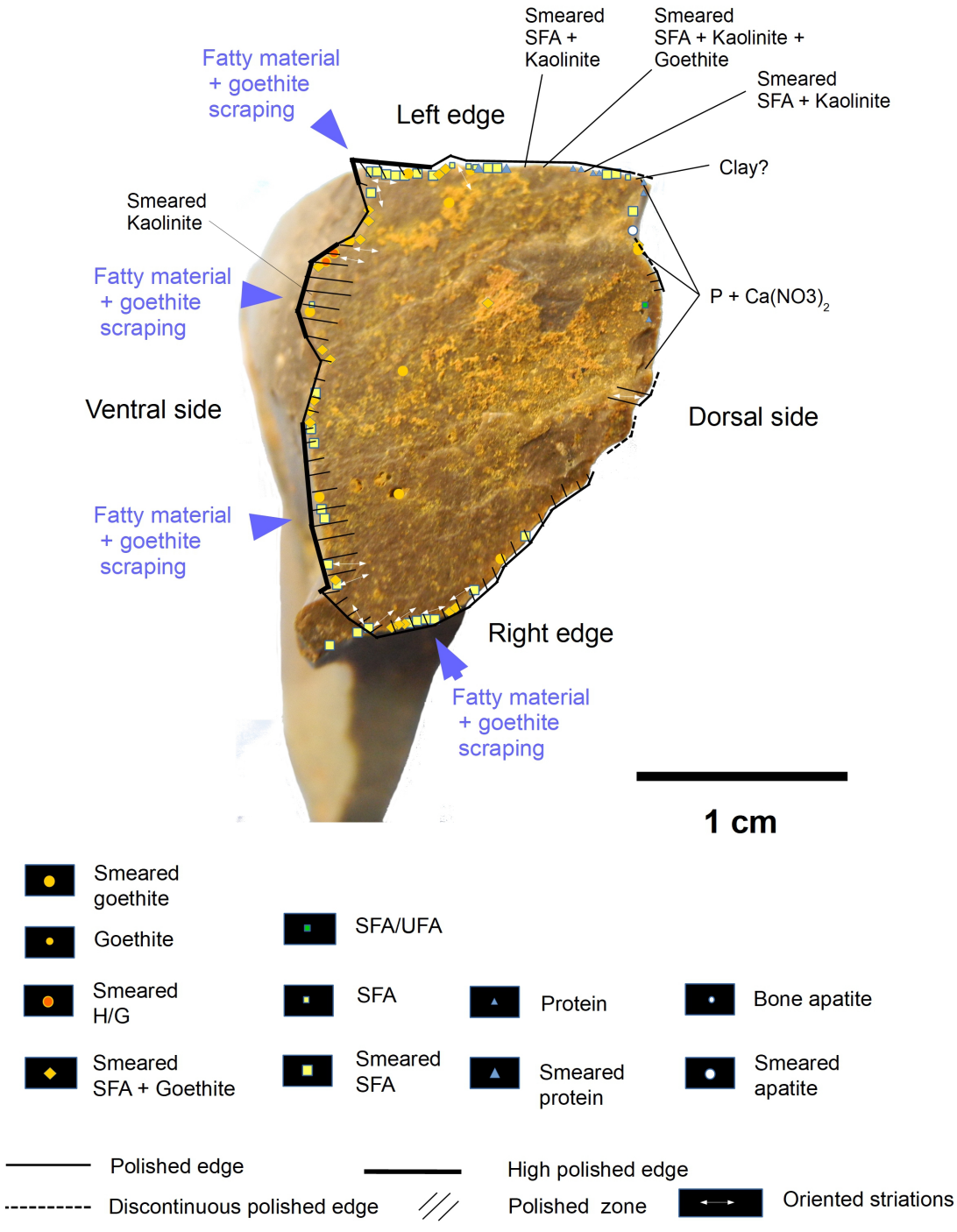

Figure 6.65: Micro-residues distribution on artefact LB5524 flaking platform and correlation with polish distribution.

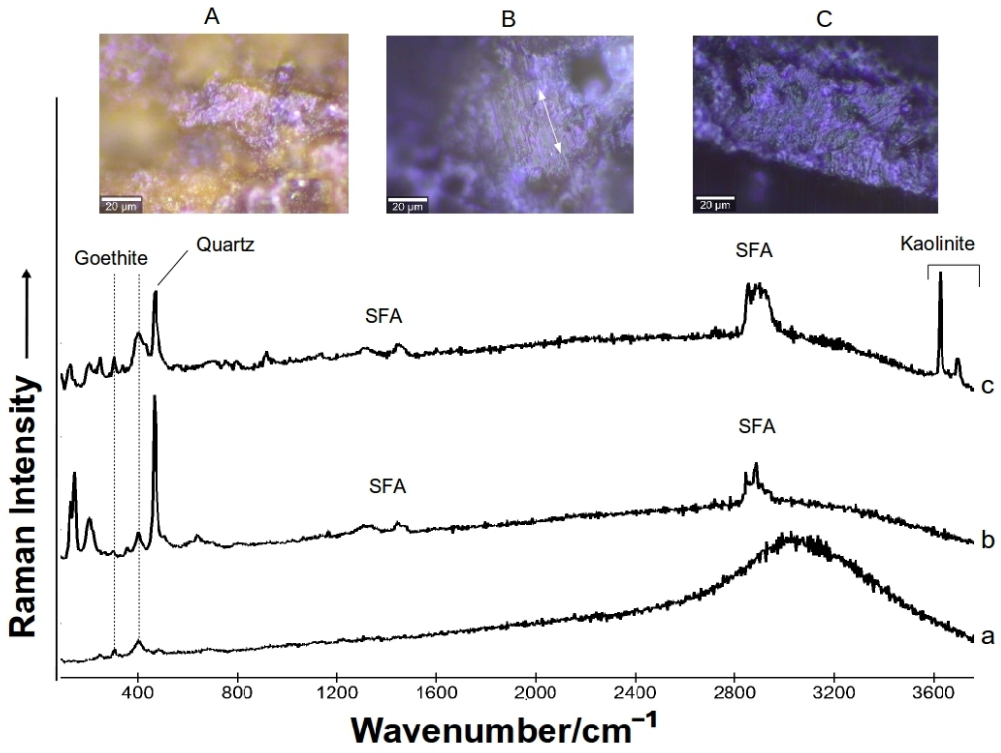

Figure 6.66: Image of smeared goethite micro-residues on flaking platform surface (A), image of smeared goethite mixed with SFA showing oriented striation on polished edge of the ventral side of flaking platform (B), image of smeared goethite mixed with SFA on polished edge of ventral side of flaking platform (C), Raman spectrum of smeared goethite micro-residue (a), Raman spectrum of smeared goethite micro-residue mixed with fat (SFA) (b), Raman spectrum of smeared goethite micro-residue mixed with fat (SFA) and kaolinite (c).

Other artefacts confirming pigment use dated from before ~60 ka

Three others Liang Bua artefacts dated from before ~60 ka confirm the conjoint use of goethite and haematite either with bone or undetermined fatty material:

Artefact LB5533a had been obviously retouched on three distal sides of its ventral surface to create edge fitted with scraping action and bear high covering of goethite (Appendix IIb, fig. 7), mainly concentrated on this ventral surface and concentration on its ridges on dorsal surface which could originated from handling. This artefact, derives from a larger truncated flake, shows on its proximal truncated surface polished edges and coloured yellow material indicating that the goethite deposition is posterior to the truncation. Considering the lower abundance of goethite in sediment compared to its higher abundance on the artefact surface, and goethite distribution not consistent with a natural widespread random covering, this coloured material is likely to be linked with the use of LB5533a on undetermined material.

Indeed, even if two plant materials which have been found on the active edge can suggest that this stone tool could have been used to scrape plant/wood (Appendix IIb, fig. 7), this hypothesis cannot be securely confirmed, taking in account the low number of plant residues, which can arise from incidental contact.

Another artefact LB5533b, extracted from the same sediment block, can be more securely attributed to bone scraping (Appendix IIb, fig. 8) using the opposed edges of its distal dorsal surface and left edge of ventral surface. Goethite and haematite is systematically associated for both of these areas with concentration of bone, and completely absent on the other part of that stone tools, as well as in very low amount in sediment (same layer sediment as LB5533a, because LB5533b has been extracted from same sediment pedestal), showing clearly its relation with bone working on this flake. This association of two materials correlated with the highly polished ridge on the dorsal distal surface can be interpreted as the result of scraping tasks using both bone and pigment. On the left ventral edge, as no marked polished area had been established, one hypothesis is that their presence might originated from prehistoric handling during that particular task.

A last artefact, LB5572, can be interpreted as a nosed scraper used on bone considering concentration of polish on its ventral distal edge (Appendix IIb, fig. 16). Indeed, if some isolated bone residues can also originate from sediment in which bone is common, exclusive distribution of this material on the distal ventral part of this artefact, along with presence of smeared bone residues, tend to indicate its relation to use. Through less marked than for LB5533b, goethite is also localised and associated with bone on this distal part of that tool.

6.3.2.5 Interpretation

Firstly, it can be underlined that compared with the 2004 and 2015 collected artefacts and the two Pleistocene artefacts (LB250, LB337) from 2004 excavation, the 2016 collection included artefacts that were mostly free of dyed fibre as modern contamination. Contact material (nitrile from glove) and a few airborne micro-residues were encountered as minor contamination from laboratory manipulation. This important improvement is due to the samples pedestals, which protect the stone artefacts from environment contamination from the archaeological site to the laboratory. Reducing the micro-wear observation steps before Raman micro-residue analysis contributed also to lower modern background contamination noise on samples. Nevertheless, contact with metal tools on site is still indicated by metal marks on some artefacts, notably on LB5126, LB5211, LB5213, LB5224a, LB5225, LB5580a, LB5524, LB5526b, LB5527.

Additionally, the 2016 artefacts from sector XXV, showed better preservation of residues and this leads to a higher level of confidence in the archaeological information (Table 6.2). One artefact in eleven (artefact LB5068), shows plant-related use, probably a notched scraper. Grass material found on artefact LB5164 shows that a Raman fingerprint can be in some case more specific and restrict the range of material; in that case, to the gramineae family. This plant material, only found in a small limited area, was probably incidental to use or a result of incidental contact with LB5164; but not belonging to main material worked with this stone tool, which is bone. The presence of use-related fossil bone residues on several artefacts (artefacts LB5164, LB5165, LB5126, LB5213, LB5225, LB5580a, LB5526b) contrasts with the 2004 and 2015 collections which are devoid of this material. Such a result indicates clearly the hominin use of stone tools to work bone. The presence of bone residues in some artefact's sediment in varying abundance suggests also bone working as a general hominin activity at the Liang Bua site. Raman analysis of bone residues on this set of stone tools allows us to better understand the high amounts of manganese dioxide on the artefacts. This mineral was often found adhering to the surface of individual or smeared bone apatite and mixed with altered apatite. Indeed, this mineral being a product of bone degradation (Owocki et al., 2016), it is not surprising to find it in association with aged bone attached to prehistoric stone artefacts. On the other hand, this mineral is also common in the cave, probably related to microbial activity (Sebela et al., 2015) and consequently can arise from several origins. Yet, it is found on artefact LB250, without any bone micro-residues. Indeed, microbial activity producing manganese oxide is active not only on bone, but also on other organic worked materials.

Being one of the best preserved, artefact LB5126 is also informative about other stone tools. The extensive patch of bone apatite on that artefact suggests its use on fresh bone, at least on the dorsal left side. Presence of numerous SFA and protein residues located among the bone used edges are additional arguments indicating that a fresh material like meat or fat also could have been worked with the bone. Along this very well-preserved bone material, goethite mineral presence on LB5126 is the more spectacular residue on this tool. Observation of bone and goethite distribution and mixed bone and goethite micro-residue were analysed on different edges used to scrape bone, indicating that these two materials had been worked together during a complex task combining these materials. Moreover, a specialised goethite polishing surface on the right dorsal side was identified, indicating the use of goethite as a red-orange coloured pigment for a polishing task. Determining if the goethite was intentionally deposited on the artefact or already present as a natural deposit from weathering on it surface

is not trivial, but the fact that material was observed on all surfaces of the artefacts, on different perpendicular edges (right and left dorsal side) and that its distribution is in association with used edges and surfaces indicates that this material cannot arise only from a natural weathering deposit. Iron oxides are common in many soil environment and have been recognised as occurring, naturally in Liang Bua cave. Indeed, goethite mixed with clay had been identified in some layers dating between ~41.5–32.8 ka in sector XXIV (Morley et al., 2017). But this micro-stratigraphic sampling cannot be put directly in relation with each stone artefact studied here from sector XI, XXV and XXVI, (with exception about artefact LB57 extracted from sector XXIV (Chapter 6, Table 6.1) which doesn't have any iron oxide covering on its surface), because the cave stratigraphy is complex (Morley et al., 2017). Consequently, I had to rely exclusively on sediment directly attached around stone artefacts to infer origin of any material, mineral or organic found on their surface. Yet in all the case, low abundance of goethite and haematite in sediment indicated that the sediment layer was not the main source of coloured material.

Even considering natural goethite as naturally occurring before burial on the LB5126 and a non-intentional polishing on the right dorsal side, hominins couldn't have missed the coloured traces left from such a red material on clear white bone and may have taken the opportunity of its natural presence on the stone. This activity of bone working with goethite and haematite pigment is confirmed through the period between ~40 ka and ~20 ka by two other artefacts, LB5213 and LB5225, which have the same morphology, being thick triangular flakes with a central dorsal ridge dividing a dorsal left and right surface, all having flat ventral surfaces. All three artefacts having intensively, multiple used edges and surfaces working both goethite and bone, indicating a complex task, and repetitive use. Additionally, it is important to note that all these three artefacts have been used on bone and fatty material with their central ridge, which seems to be a marker of the particular use of these triangular flakes, and indicates a similar way of using them. The age of artefact LB5126, along with two other artefacts used on bone (LB5164, LB5165), indicate that this activity is older than ~40 ka (Table 6.2**)**.

The 2016 artefacts from sector XXVI confirm these results (Table 6.2). The most striking similarity between sector XXV and sector XXVI concerns another triangular flake, artefact LB5526b, with use-related bone residues, and shows the same morphology and the same way of use as the other three artefacts (LB5126, LB5213, LB5225) discussed above. Another important artefact, LB5580a, was used to polish bone and goethite and haematite pigment; and is a key artefact to assert this particular use already observed on LB5126, LB5213, and

LB5225 for sector XXV. This artefact, has a distinct morphology, but nevertheless is showing spectacular macro-residues of bone and pigment related to use. Through its final bone scraping use after flaking retouch, artefact LB5580a shows that combining different materials during a task and adapting the same tool to different uses were within the cognitive capacity of the tool users. Artefact LB5524 also confirms the combining of two materials with its intensively used flaking platform to scrape fatty material and goethite, and confirms use of pigment found already on artefact LB5580a. Bone scraping activity was also confirmed more discretely by scraper LB5562a, with no possible conclusion on LB5562b, because of the presence of bone in the sediment against a unique bone micro-residue found on its edges. Artefacts LB5563a-c, LB5564, LB5565, LB5525 and LB5527 are less well-preserved, didn't retain key specific residues like bone or plant, but show concentrations of fatty acid in association with polished edges including a scraper. On these tools, I found a close association between saturated fatty acids and unsaturated fatty acids. As found on artefact LB5213 these two types of lipids can arise from closely related worked materials in prehistory, but have different preservation potential, being in different states of oxidation. Close association with bone was found for both type of lipids, with the identification of saturated fatty acid (SFA) mixed with bone on artefacts LB5164, LB5126, LB5213 and unsaturated fatty acid/ saturated fatty acid mix (SFA/UFA) on artefact LB5580a. Presence of kaolinite from rock weathering mixed with bone and SFA micro-residues not only securely establishes that these micro-residues are aged prehistoric material, but in the case of artefact LB5580a the kaolinite entraps them completely and could have contributed to their exceptional preservation. Observations of extensive use of multiple edges on scraper tools, in particular smaller artefacts like LB5563a-c (Appendix IIb, figs 11 to 13) is showing a sense of raw material economy, hominins taking advantage in using almost every useful edges on these tools. Such small multiple edges tools, (LB5563c used on three edges and being under three cm long) suggest good dexterity and wit capability.

Table 6.2: Summary of results obtained by Raman spectroscopy and use-wear analysis on 2016 collected artefacts

Artefact	Year	Sector	Layer	Dating (ka)	Rock type	Use as	Significant residues (use-related in bold)
LB5067	2016	XXV	76	44.11–18.31	Silicious tuff	not used	None
LB5068	2016	XXV	76	44.11–18.31	Chert	Scrapper, cutting tool	**Plant fibre, SFA, Protein, starch grain**
LB5211	2016	XXV	82	44.11–18.31	Silicious tuff	Scraper	**UFA, SFA**
LB5212	2016	XXV	82	44.11–18.31	Chert	Scraper	**UFA, SFA**
LB5213	2016	XXV	82	44.11–18.31	Silicious tuff	Scraper	**Bone, Bone + SFA, Bone + Kaolinite**, **SFA, UFA, Protein, Goethite, Haematite**
LB5224a	2016	XXV	83	44.11–18.31	Silicious tuff	Scraper	**SFA, Protein, Bone, Bone + Kaolinite**
LB5224b	2016	XXV	83	44.11–18.31	Silicious tuff	Scraper	**SFA, Bone, protein, plant fibre**
LB5225	2016	XXV	83	44.11–18.31	Silicious tuff	Scrapper, cutting tool	**UFA, Bone, Protein, Goethite, Haematite**
LB5164	2016	XXV	76	120–60?	Silicious tuff	Scrapper, cutting tool	**Bone, SFA, Bone + SFA**, **Protein**, Grass material
LB5165	2016	XXV	76	120–60	Silicious tuff	Scrapper, cutting tool	**Bone, Bone + SFA, Protein, SFA,** Plant fibre
LB5126	2016	XXV	76	120–60	Silicious tuff	Scrapper, polishing tool	**Bone, Bone + Kaolinite, SFA, Protein, Goethite, Haematite, Bone + SFA, Bone + Goethite**
LB5580a	2016	XXVI	75	120-60	Silicious tuff	Scrapper, polishing tool	**Bone, Bone + Kaolinite, Bone + SFA SFA Bone + UFA, UFA, Goethite, Haematite, Kaolinite**
LB5580b	2016	XXVI	75	120-60	Chalcedony	Scraper	**UFA**
LB5562a	2016	XXVI	75	120-60	Silicious tuff	Scraper	**Bone, UFA, Protein,**
LB5562b	2016	XXVI	75	120-60	Silicious tuff	Scraper	**SFA, UFA, Protein,** Pyrite**,** Bone + Kaolinite
LB5563a	2016	XXVI	75	120-60	Silicious tuff	Scraper	**SFA, UFA, Protein**
LB5563b	2016	XXVI	75	120-60	Silicious tuff	Scrapper, cutting tool	**SFA, UFA, Protein**
LB5563c	2016	XXVI	75	120-60	Silicious tuff	Scrapper, cutting tool	**SFA, UFA, Protein**
LB5564	2016	XXVI	75	120-60	Silicious tuff	Scraper	**SFA, UFA, Protein**
LB5565	2016	XXVI	75	120-60	Silicious tuff	Scraper	**SFA, UFA, Protein**
LB5524	2016	XXVI	74	120-60	Silicious tuff	Scraper	**SFA, SFA+ Goethite, UFA, Protein, Goethite**
LB5525	2016	XXVI	74	120-60	Chert	Scraper	**SFA, UFA,** plant material
LB5526a	2016	XXVI	74	120-60	Quartz	Not used	SFA
LB5526b	2016	XXVI	74	120-60	silicious tuff	Scraper	**Bone, Bone + Kaolinite, UFA, SFA, Protein**
LB5527	2016	XXVI	74	120-60	silicious tuff	Scrapper, cutting tool	**SFA, UFA, Protein**
LB5533a	2016	XXVI	74	120-60	Silicious tuff	Scraper	**UFA, Goethite,** Plant material
LB5533c	2016	XXVI	74	120-60	Silicious tuff	Scraper	**Bone, Bone + Kaolinite**, **SFA+ Goethite, SFA + Haematite, Goethite, Haematite**
LB5572	2016	XXVI	75	120-60	Silicious tuff	Nose scraper	**Bone, Bone + Kaolinite**, **Goethite**

6.4 Conclusion on Liang Bua artefacts analysis

Eight artefacts out of fifteen analysed from the 2004 and 2015 collections have use-related micro-residues, six have plant-related residues and two only SFA micro-residues but silicious plant polish (Fig. 6.67**)**. One of these artefacts, LB4340 also has charcoal micro-residues, which suggest the use of fire. From these first results from a dozen artefacts, Raman analysis seems to indicate that scraping plant, including grass, with occasional use of fire were activities conducted by hominins during the period after ~20 ka until few thousand years ago at Liang Bua. Hominins inhabiting the cave from ~40 ka to ~20 ka seem to have used some of their tools on plant material, but majority of artefacts show activities related to animal materials, and high frequency of bone remains on the stone tools (Fig. 6.67**)**. This big contrast does not reflect any relative preservation of this material, as bone and plant were recognised in both collections, but the analysis didn't find any use-related bone on artefacts studied younger than ~20 ka. In that context, strong presence of manganese oxide can be related to bone degradation processes. Some exceptions, like artefact LB250, where polish indicates use on plant material, seem to indicate that the manganese presence is also linked to favourable environmental conditions and its formation before ~60 ka, is probably in relation with a warmer climate and high microbial activity.

By contrast with last glacial period, the period ~120–20 ka shows great continuity in stone tool use centred on bone and animal working, with similar artefacts and with the same way of using (Fig. 6.67**)**. Three artefacts LB5126, LB5213, LB5225 share typology similar morphology and a similar set of micro-residues, showing that bone had been worked with yellow and red pigment (goethite and haematite) in the same way of use. A fourth similar artefact LB5226b, devoid of pigment use, nevertheless shares the same way of use on bone, including specific use of central ridge for scraping, as early as ~120 ka.

As analysed on artefacts LB5580a and LB5524 dated from ~120 ka to ~60 ka, during all this period, hominins were using mineral pigment in conjunction with other material like fresh bone or fat to achieve complex task including polishing and scraping. This demonstrates an ability to combine different materials either to achieve specific treatment (e.g., polishing bone objects, tanning skin) or for symbolic purposes (e.g., shaping animal or human bone and decorating them with pigment). In consequence, if *Homo floresiensis* is well identified as the hominin species inhabiting Liang Bua Cave and the author of the stone artefacts collected in sector XXVI dated from ~120–60 ka, it means that this species may have been used coloured

iron oxide pigments in a similar way to modern humans, at least in association with practical activities such as bone working. If use of pigment for art or practical purposes is well known for modern humans from hundred thousand years ago in South Africa (Henshilwood et al., 2011) and from 40 000 years in Indonesia (Aubert et al., 2014) and for Neanderthal in Europe (Roebroeks et al., 2012), it was in contrast completely unknown for *Homo floresiensis* and could attest possible symbolic behaviour and also confirm higher cognitive capacity of this Hominin species as already indicated by LB1 brain morphology (Falk et al., 2005). Another important insight into *Homo floresiensis* behaviour is the ability to manipulate tools and exploitation of multiple edges on a single artefact, and the sequential use of the same artefact to achieve different tasks. This results is convergent with *Homo floresiensis* wrist morphology which facilitate tool-related manipulative behaviours (Tocheri et al., 2007). Achieving multiple tasks with a stone tool indicates a minimum of planning and wit, higher cognitive ability as already indicated by *Homo floresiensis* stone technology (Morwood et al., 2004; Brumm et al., 2006). Furthermore, the use of only small flakes, some of them smaller than three cm with multiple edges used, underline *Homo floresiensis* high dexterity and a sense of planning for raw material economy, and to minimise energy expenses.

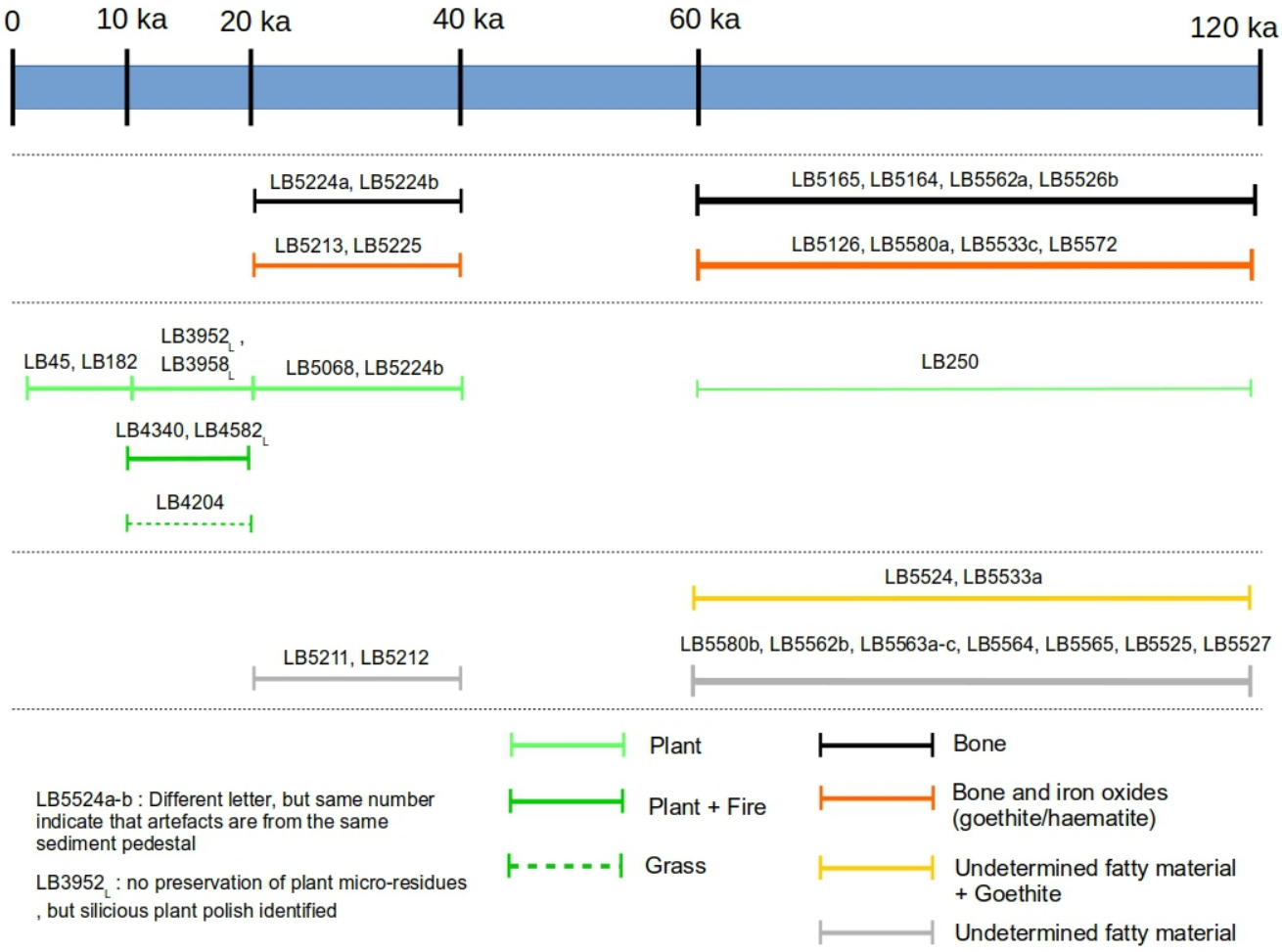

Figure 6.67: Time line with studied stone artefacts dating and use-related micro-residues.

Chapter 7 Discussion and general conclusions

7.1 Developing a new methodology adapted to micro-residues analysis

Investigation of ancient hominin behaviour requires collaboration between multidisciplinary fields of research, and broadly aims to gain insights into past life ways, with diverse approaches including studies of technology, tool function and the history of resource use. In my work, I have been confronted with the need to develop a new approach to tool function that links analyses of residues and use-wear. Integration of these two techniques is, in part, dependent on the preservation of residues, organic and inorganic, on stone artefacts. The conventional approach to study stone tool residues focuses on macro-residues with optically distinct structure. If artefacts are first screened, according to best preservation, macro-residues will likely retain more of their initial shape, be present in higher abundance and be more readily identified by VLM and, under these circumstances, the classical role of spectroscopy, applied afterwards to confirm the chemical nature of these residues, is appropriate (Chapter 1, section 1.4). This linear way of applying use-wear analysis as a first step, followed by detailed residue identification as a second step, results mainly from the earlier historical development of use-wear studies, which are still today more common than residue studies. Until recently, lithic residue analysis was considered to be of secondary importance, as it was confronted with limitations of spectroscopy instruments, low quality conditions of artefact extraction in the field, poor post-excavation conservation, and the particularly high cost of such analysis. For example, washing lithic artefacts in the field to enable technological study, and subsequent handling by use-wear analysts can greatly hinder the efficacy of residue analysis on many organic materials, and reduce the potential information to a minimum; and in consequence, the expenses of time and money on further residue analysis may not be justified.

If this latter approach is without many problems when dealing with well-preserved macro-residues that can be securely identified as resulting from prehistoric use, it reaches its limits when artefacts with a low level of preservation are encountered, and only micro-residues are preserved. Indeed, the problem with smaller, more scattered and less distinctively shaped residues is that the specific residues linked to stone tool use become far more difficult to distinguish from material arising from other origins, such as minerals arising from natural background or from weathering, or from post-depositional processes, modern contamination, incidental contact and from sediment. At this point, analysing only a few targeted micro-residues, many of which can exist on the surface of the analysed artefact, even if high specificity is obtained (e.g., lipid from a herbivore), does not ensure that these traces are

securely linked to prehistoric uses. Even in the best-case scenario, when animal species can be determined, and DNA can reliably distinguish prehistoric species from modern species, a highly specified trace could be modern contamination. Indeed, nowadays, risk of modern contamination of exotic plant or animal species have increased, and naturally occurring micro-traces are widely dispersed by modern transportation as well as by natural dispersal media (e.g., flowing water, rain, wind). If the surface of a stone tool can be viewed as a miniature archaeological excavation field, selectively picking out only a few large residues for analysis would be similar to sampling only the most appealing stone tools, without taking any photography or noting down their exact position; and then trying to understand human behaviour by analysing these artefacts without their context. In contrast, my approach provides a robust method of sampling a wide range of residues and systematically documenting them in situ.

In this project, for Denisova Cave and Liang Bua archaeological sites, samples were not selected according to any particular state of preservation (Chapter 5, section 5.2; Chapter 6, section 6.2.1), but rather by sampling different archaeological layers in a more systematic manner. As these artefacts were recovered with a layer of surrounding sediment (to minimise contamination and keep sediment context with each artefact), such a pre-selection based on tool morphology is eliminated.

These artefact excavation conditions, and the objectives of (1) distinguishing use-related micro-residues from others with different origins and (2) inferring information about prehistoric behaviour, led me to develop an alternative approach. With the latter, spectroscopic micro-residue analysis is not in the trail of the use-wear analysis, merely there to confirm the nature of material worked with stone tools determined by it, but is applied as an independent technique from which results are later correlated with use-wear traces (Chapter 1, section 1.4). A direct consequence of positioning the residue analysis independently from use-wear analysis is that micro-residues need to be analysed more systematically, repeatedly, and in higher frequencies to establish reliable spatial distributions on artefact surfaces. This systematic analysis also ensures the application of full documentation of micro-residues position, form, grouping and distributions, to distinguish use-related micro-residues from other traces arising from different origins (Chapter 3).

Optical identification of amorphous or smeared micro-residues is more complex or impossible in some cases, and systematic chemical identification of such micro-residues is needed to

obtain a degree of certainty as to their nature and origin. An analyst can identify very specific bio-markers with spectroscopy and other techniques, but without a secure demonstration of stone artefact use, the identified residue could be the result of modern contamination, natural post-depositional processes, or some other origin.

7.2 Performance of Raman microscopy as a systematic approach to residue analysis

I selected Raman microscopy as the only available spectroscopic technique able to address the inherent problems of previous approaches because it is capable of analysing targeted single micro-residues, down to micron-size, in situ on stone tools, in a few seconds and on irregular surfaces; it is also capable of probing holes and cracks into this surface. Raman confocal microscopy can achieve, daily, hundreds of micro-residue analyses, identifying a wide range of materials within a reasonable amount of time. Indeed, new generation Raman spectrometers are better suited for this application than older instruments, and prove faster than Infrared absorption instruments in my systematic micro-residue analysis approach. In this role, Raman microscopy reveals itself as a powerful tool, not only in getting chemical fingerprints to elucidate material chemistry, but also for documenting, simultaneously through its objective, how the micro-residues are preserved, which is important for demonstrating prehistoric tool use. Consequently, Raman microscopy can be used to observe the surface context of micro-residues, and with secure chemical identification that does not depend on micro-residue type or aspect, since residues can be analysed as either individual shaped objects or as amorphous smears in situ on the surface (Chapter 3, section 3.5). Moreover, it just so happens that the coexistence of micro-residue types (as discrete particles (individual micro-residues) and as smeared micro-residues) is also a good indication of use because a natural process is unlikely to produce both these types of micro-residues in close relation and in a limited spatial distribution associated with use-polished areas (Chapter 3, section 3.5). Furthermore, observation through the same instrument of use-wear directly linked to the analysed residues (e.g., directional smeared micro-residues aligned with polish micro striations) is a big advantage that can strengthen micro-residue association with use. If both use-polish and residues are present, the relationship between use-wear traces underlying smeared micro-residues (e.g., bone or lipid) can be clearly shown in Raman spectral imaging (Chapter 4, sections 4.5.1 and 4.5.2; Chapters 5,6).

As Raman microscopy not only allows documentation of micro-residues in situ on artefact surfaces but also analysis of sediment samples, the comparison of an artefact residue with outer and inner sediments, and with washed sediment samples provides a first indication of its probable origin (Chapter 3, section 3.7). Establishing the spatial distribution of analysed micro-residues on artefacts and correlating it with polish distribution is a second important criterion to determine if these micro-residues indicate a widespread natural material or a humanly-worked material related to a surface that underwent pressure during performance of a particular task (e.g., cutting, scraping) (Chapter 3, section 3.10). Group occurrence is another critical criterion to consider, as micro-residues always found isolated have high probability of arising from modern contamination sources (e.g., airborne, contact) (Chapter 3, section 3.3). Nevertheless, the possibility of modern contamination needs to be considered at all times, particularly because of the great amount and variety of micron-sized modern materials emitted in our industrial world (Chapter 3, sections 3.2.1 to 3.2.6).

My methodology based on spatial distribution is highly dependent on probing a high number of spots on the sample; so a spectroscopic technique that is capable of chemical identification in a few seconds (to reduce the time of analysis to a minimum) is required. Currently, no automated analysing mode in Raman microscopy is capable of achieving such individual identification of micro-residues over an entire stone tool, or cope with irregular surfaces, complex fluorescence issues and selection of optimal analysing spots on a given micro-residue. So my analysis involves, essentially, a manual individual spot-probing strategy. Consequently, as for other spectroscopic techniques, the analysis time remains one of the main limiting factors constraining investigation of a large number of artefacts. However, I argue that a dozen samples with significant micro-residues, securely linked to their prehistoric use, is better than a hundred samples with micro-residues of doubtful origin. Despite these limitations, the development of such methodology with Raman microscopy to determine residue origins and stone tool function has fulfilled the first specific aim of this study (Chapter 1, section 1.2).

7.3 Analysis performance depending on sample conditions and on different types of material

Not all materials are similar with respect to performance of Raman microscopy, the specificity of material that can be determined, and the difficulty of determining their origin. The latter

imposes constraints on working with different conditions of the stone artefacts after excavation, including handling and storage processes, all of which affect different types of residues differently (Table 7.1)

One of the main archaeologically significant micro-residues found on studied prehistoric artefacts is bone apatite. Bone is one of the archaeological remains that has a higher chance of being preserved on artefacts and is specific of contact with animal material. As this material, degraded, is very resistant to washing, and can adhere strongly to artefacts, it can often be found smeared on the surface, and can be observed even on washed artefacts (Table 7.1). However, sediment also needs to be carefully checked for bone, and the relative occurrence on artefact surfaces and in the surrounding sediment needs to be estimated, particularly as this material has a high chance of being present in archaeological sediments as a consequence of past human activities and other animal behaviour.

For example, my analysis of altered bone apatite on Denisova Cave artefact surfaces shows that post-depositional processes can alter and dissolve this material, and transfer it from the sediment to buried stone tools (Chapter 5, section 5.3.2). A particularly relevant example of transfer of bone from sediment to stone artefacts is found on Liang Bua artefact LB4582, where localised individual fragments of bone originated from contact with a macro-bone lying in sediment (Chapter 6, section 6.2.2.2**)**. Additionally, Raman microscopy is a powerful tool for identifying even micron-sized apatite residues on stone artefact surfaces and distinguishing bone apatite from geological apatite.

Table 7.1 Summary of identification success rate, artefact conditions, specificity and common non-use-related origin for micro-residues encountered in this work

Type of micro-residue	Potential for successful identification with Raman spectroscopy *** high ** moderate * low	Washed artefact	Unwashed artefact	Unwashed artefact/ carefully handled and stored artefact (with gloves)	Artefact with attached pedestal of sediment, carefully handled and stored	Level of specificity attained when use- related
Iron oxides (goethite, haematite)	***	X	X	X	X	Pigment
Manganese	***	X	X	X	X	Pigment
Bone	***	X	X	X	X	Animal
Resin	*	X	X	X	X	Plant material, certain categories of resin can be distinguished (e.g., diterpenic) and gums
Blood	*		X	X	X	Animal
Charcoal	***		X	X	X	Plant
Plant fibre/ plant material	***		X	X	X	Plant, wood and grass can be distinguished, including giant grass (bamboo)
Lipids	***			X	X	non-specific
Protein	**			X	X	non-specific
Starch grain	***				X	Plant
Plant fibre/ plant material, dyed	**				X	Plant with dye (type of dye can be identified)

Additionally, on Liang Bua artefacts, and especially on artefacts from layers older than ~60 ka, using Raman spectroscopy, I was able to distinguish, in situ, two forms of bone apatite (Chapter 6, section 6.3.2.4**)**. One form of bone apatite designated “fossil bone” corresponds to intact bone micro-residues still having carbonate, but with no sign of collagen, which had all been degraded. Fossil bone apatite was often found with traces of rare earth elements, which substitute themselves into the apatite lattice through time and give specific narrow fluorescence bands under green and red excitation (Chapter 4, section 4.7; Chapter 6 section 6.3.2.4). Another form of bone apatite corresponds to a disordered apatite structure that lost all carbonate content but had incorporated in its structure manganese oxide, arising from complex processes of fungal and bacterial biomass degradation in the bone. In situ coexistence of these two forms of bone apatite was indicated by Raman spectroscopy in the same bone micro-residues (also both on smeared and individual bone traces), both on archaeological micro-residues and macro-bone references, confirming the identification of this latter disorganised form of apatite as altered bone.

Lipids are micro-residues that can be easily detected by Raman microscopy, when only a few microns thick and smeared on the surface of stone artefacts. Lipids were often preserved on the studied samples, and their high frequency is a good indicator of the worked areas on used artefacts, as they were systematically found in concentrations on polished edges and surfaces. However, lipids are produced by a wide range of plant and animal tissues, as shown by analyses of experimental tools (Chapter 4, sections 4.4 and 4.5). Additionally, lipids can be transferred easily from any plant and animal material to the artefact surface and could be incidental to tool use, or arise from prehistoric or modern handling (Chapter 3, section 3.2.3). So, great care is needed to interpret their origin critically, with careful consideration of their concentration on polished edges, and their association with other plant and animal micro-residues. These other potential sources impose constraints on interpretations, and it is preferable to analyse unwashed artefacts, or artefacts that have been carefully handled (Table 7.1).

Some lipids found in this study have been identified as saturated fatty acids (SFA), which are probably end products resulting from degradation processes of material originally containing a complex mix of SFA and unsaturated fatty acids (UFA). Because SFA are probably end products of degradation, their Raman fingerprint shows little variation and is not very specific of the worked material (Chapter 4, section 4.4). Nevertheless, in some cases, variation of SFA spectral fingerprints can be observed, as in the case of spectra from artefacts DC26 and DC27 (Chapter 5, section 5.3.3).

Additionally, lipid micro-residues still containing UFA have been found (UFA/SFA). It is relevant to note that Raman microscopy is more sensitive in detecting micro-residues containing UFA because the signal-to-noise ratio is enhanced by the presence of double bonds in these molecules, increasing their polarisation. However, it is not known definitively if these micro-residues with UFA content are the result of better preservation, as was indicated by the systematic presence of UFA on recent experimental stone artefacts and suggested by their differential preservation on artefacts from Denisova Cave (Bordes et al., 2018) (Chapter 5, section 5.3.3) and Liang Bua (Chapter 6, section 6.3.2.4). Indeed, these micro-residues containing UFA were sometimes found concentrated on the same artefact, where SFA were present either on distinct areas (e.g., LB5213) or in close association with them (e.g., LB5226b). These observations suggest that preservation is not the only factor that favours the existence of UFA, and further research is needed to explain their presence.

The same Raman fingerprint as found on these archaeological SFA/UFA micro-residues was obtained on a range of different experimental tool residues, showing that spectral data are insufficient to identify separately plant or animal traces at this stage of research (Chapter 4, sections 4.5.1 and 4.5.2). However, considering their relation with others micro-residues and their occurrence as smeared and individual residues, the lipids can allow us to suggest animal or plant working as an initial hypothesis (Bordes et al., 2018), to be further evaluated by use-wear analysis.

Plant tissue was less common than bone or lipid traces on Liang Bua artefacts, confirming that few stone artefacts were used for plant working. Plant residues were usually short fibres that can be also identified by optical microscopy, but small fragments with no distinctive shape were also found, in which case Raman spectroscopy was critical in their correct identification as plant material. On the other hand, one weakness of Raman microscopy is that, despite the fact that this technique is able to analyse smeared residues, as shown by several successful analyses of experimental tools (Chapter 4, section 4.5.1), old smeared plant micro-residues are more difficult to analyse because of their high level of fluorescence and low laser damage threshold. Hence it is more difficult to associate individual and smeared plant residues than with other micro-residues (e.g., bone), and this constraint of Raman microscopy lowers our ability to securely assert relationships between plant residues and tool use.

Some more specific categories of plant material were distinguished by Raman spectroscopy on artefacts LB4204 and LB5164. Grass tissue displays a particular spectral fingerprint (Chapter 6, section 6.2.2.3) confirmed by experimental comparison (Chapter 4, section 4.5.1). Woody tissue was also distinguished by Raman microscopy, as confirmed by experimental tools and successful blind Test 4 (Appendix III). Bamboo is a subfamily of Poaceae (grasses) that has high silica content, and Raman identification of this category of plant material has particular potential for analysing prehistoric stone tools at other Southeast Asian sites, where siliceous plant processing has been suggested by use-wear studies (Xhauflair at al., 2016).

Raman microscopy had been especially efficient at identifying dyed fibres because of the resonance Raman enhancement effect (e.g., artefact LB5227) (Chapter 6, section 6.2.2.1). This has potential for tracking dye colouring activity, which dates from the late prehistoric period (i.e., by 6000 years ago) in Indonesia. Nevertheless, all dyed fibres analysed on Liang Bua artefacts in this study were found to be from modern contamination, after considering my filtering criteria (i.e., found as an isolated fibre and not found in a group or concentration

associated with a polished area of artefact). Additionally, it was found that dyed fibres were common airborne contaminants (e.g., indigo fibre) and were often found on analysed artefacts in the laboratory or transferred to stone surfaces by handling or other manipulation (Chapter 3, section 3.2.5). In consequence, researchers wanting to successfully analyse dyed fibre residues ideally need to focus on artefacts that are from excavated pedestals and have been carefully handled and stored (Table 7.1).

Starch grains, another type of plant-related micro-residue, were found in low abundance on studied artefacts. Their scarcity does not reflect any difficulty in spotting and analysing these grains, because their characteristic aspect and high signal render their identification quite easy to do in Raman spectroscopy. However, Raman identification of starch is only indicative of a plant origin, and starch spectral signatures cannot be related to a particular plant species (Chapter 4, section 4.5.1). As for plant fibres, poor preservation can be invoked to explain their low archaeological frequency. In these conditions, starch grains are difficult to interpret, especially when found isolated, because they have been one of the more common micro-residues encountered in airborne contamination and from powdered gloves (Chapter 3, sections 3.2.4 to 3.2.5). For these reasons, most starch grains can only be securely linked with use when from artefacts recovered from excavation pedestals and when carefully handled and stored (Table 7.1).

Charcoal is another residue identified with Raman spectroscopy on one artefact from Liang Bua layers younger than ~20 ka (LB4340, Chapter 6, section 6.2.2.3). Associated with plant working evidence, charcoal may indicate the use of fire to work burnt plant material in complex tasks. Charcoal residues need to be compared with charcoal in associated sediments (Table 7.1), as charcoal can be a common material preserved in archaeological layers, and can be a result of human activities and/or natural processes on this site (Morley et al., 2017).

Iron oxide mineral pigment includes micro-residues that are generally difficult to relate to tool use, because they are often ubiquitous in archaeological contexts and in the stone of which the artefact is made. Indeed, iron oxides can occur as result of natural processes, as observed with black iron oxide residues on Liang Bua stone tools LB182, LB228, LB250, LB45 LB4340, LB4829, LB5227, LB3958 (Chapter 6, section 6.2.2.2). They can also be the result of modern contamination left from contact with metal tools during archaeological excavation (Chapter 6, section 6.2.2.1) and in the distinct form of shiny residues composed of

organic matter mixed with iron oxides such as haematite, maghemite or goethite. Nevertheless, in some cases, (e.g., artefacts LB5225, LB5126, LB5213, LB5580a, and LB5524 from layers older than ~60 ka), goethite micro-residues in very high abundance were interpreted as related to tool use, and were associated with a specific task on one surface of each tool (Chapter 6, section 6.3.2.4). Moreover, this residue was shown to be probably associated with the intensive scraping of fresh bone, as reflected by mixed micro-residues containing bone and pigment (Chapter 6, section 6.3.2.4). The identification of coloured iron oxides in close association with other types of use-related residues, such as bone, lipid or plant material, is needed to demonstrate their link to artefact use. Their low background abundance in sediment and rock, relative to their high abundance on the artefact surface and concentration on use-polished areas, provide a strong case for linking mineral pigment and prehistoric artefact use (Table 7.1).

Manganese oxide is another mineral pigment that has been analysed on artefacts investigated in this study. It is invariably interpreted as arising from post-depositional processes, probably from the degradation of organic material by fungal and bacterial activity (Chapter 6, sections 6.2.2.2 and 6.3.2.2). Organic material contained in bone and degraded through time by micro-fauna could be one of the main candidates for the source of manganese, as this mineral was found to be very often strongly associated with bone micro-residues, especially altered bone, both in sediment and on stone artefacts (Table 7.1).

Only resin micro-residues from modern contamination were analysed on artefact LB5526b (Chapter 6, section 6.3.2.1), although this material can be potentially analysed by Raman microscopy and was successfully identified on experimental stone tools (Chapter 4, section 4.5.1). Smeared or individual resin micro-residues can be identified and different types of resin can be distinguished (e.g., diterpenic resin) along with gums (Chapter 4, section 4.3.2). As this material tends to attach itself very strongly to stone surfaces, even washed artefacts can be investigated for resin (Table 7.1) but success of Raman analysis depends on finding micro-residues composed of almost pure resin to be able to measure a Raman spectrum. Indeed, resin mixed with other organic compounds is difficult to identify with this technique because of the high fluorescence of such additives, as shown in my unsuccessful attempts to analyse some resins as reference material (Chapter 4, section 4.3.2). Another issue with analysing resin micro-residues is their tendency to melt under laser heating, which renders their identification difficult to achieve, especially when resin is found as smeared residues only a

few microns thick on artefact surfaces. To overcome these difficulties, IR microscopy can be used to supplement Raman microscopy on resin micro-residues in such cases.

Blood residues were not identified on Liang Bua or Denisova artefacts in my study, but were successfully analysed on one experimental stone tool (Chapter 4, section 4.3.2). Although blood was not identified archaeologically, it is feasible to identify potential blood residues by Raman spectroscopy, because the porphyrin unit in the blood protein haemoglobin produces a specific fingerprint under green laser excitation. The main difficulty of dealing with this material relates to its relatively poor preservation, and, because of this, it is much better to analyse unwashed artefacts (Table 7.1).

7.4 Micro-residues as a data set for interpreting tool function

Identifying different types of associated micro-residues on stone artefacts and determining their spatial distribution are not only necessary to determine their links with prehistoric tool use but they are critical for interpreting the task(s) undertaken with stone artefacts by hominins in the past. The arguments can be complex. For example, based on experimental findings, an archaeological tool with concentrations of individual bone and smeared bone residues on one of its polished edges, along with lipid residues and a few proteins, might be interpreted as having being used on bone material. In contrast, just a few individual bone micro-residues on a polished edge without any other residues in the immediate vicinity is more problematic to interpret, and the sediment should be carefully checked for presence of bone material. In this way, groups of different micro-residues build a context which contributes to the evaluation of micro-residue origins and the likelihood that any of them are linked with use.

Some types of micro-residue and their origins are more easily interpreted than others, as shown by my blind tests results (Appendix III); same methodology was applied. The set of residues including concentrated bone and lipids analysed on both side of one edge in blind test 2 (Appendix III, table 1, fig. 2) might be sufficient to indicate bone sawing. Similarly, a uni-facial distribution of concentrated plant material on one edge in blind tests 4 and 5 provided a correct interpretation of plant scraping (Appendix III, table 1, figs. 4 and 5). In blind test 4, wood was successfully identified and shows that in some cases, different categories of plant material can be identified by Raman spectroscopy. In other cases, interpretation of plant micro-residues is more difficult, as they can be wrongly interpreted when residues from incidental contact are better preserved than the material that the tool was used to process.

For example, in blind test 1 (Appendix III, table 1, fig. 1), plant residues on a tool used to butcher kangaroo were wrongly interpreted as resulting from the main task of cutting plant tissue—probably because too few residues of animal material were detected, as the tool had probably been in contact with plant parts during this process (e.g., from butchering meat on wooden boards or grass; or perhaps grass was present on the animal skin before the task; or because the stone tool had been placed on the ground). Stone artefact use which leaves only lipid micro-residues, without any other specific residues, is also difficult to interpret without further use-wear analysis (Bordes et al., 2018), as demonstrated by the tool in blind test 3 (Appendix III, table 1, fig. 3) used to scrape dry skin but with insufficient micro-residues surviving. Blind tests 6 and 7 (Appendix III, table 1, figs. 6 and 7) further illustrate this problem as concentrated lipids were found on these unused experimental artefacts and wrongly interpreted as originating from use, whereas the residues probably originated from incidental contact with transfer of fatty material from other stone tools handled by the experimenters. Nonetheless, in blind test 6, numerous feldspar-smeared residues were found closely related to lipid micro-residues, and were distinct from the quartz mineralogy of the artefact. Origin of fat was by transference from the hammer. For secure interpretations, lipid micro-residues need to be related to other specific residues and use-wear.

Interpreting a set of micro-residues on an archaeological stone artefact is particularly challenging as we can legitimately argue that micro-residues occur on stone artefacts as palimpsests of successive events. However, even if the sequence of successive events is very difficult to distinguish, restricted localisation of these micro-residue palimpsests provide meaningful information to determine the function and the main type of material worked, and potentially help evaluate use-wear analysis. It is analogous to rock art sites with successive layers of paintings of different ages: if the complexity of all the painting events and their meaning cannot be straightforwardly determined, the fact remains that the concentration of art is showing a painting activity on that site.

Archaeological and experimental observations suggest that Raman microscopy is often not suited to highly specific material identification. Its main contribution is to answer questions about how the stone tools were used and the categories of contact material, rather than to determine precisely what species of animal or plant were worked. The latter requires complementary techniques such as GC-MS to obtain further insights (e.g., Luong et al., 2017, 2018).

7.5 From samples analysis to behavioural interpretations

Another level of interpretation of micro-residues is available by systematic analysis of different sets of micro-residues distributed on parts of the same tool. For example, different uses of two opposite edges can be determined, as in the case of artefact LB5224b (Chapter 6, section 6.3.2.4). Multiple edge use, worked materials, and combinations of different material on the same artefact are important considerations for understanding cognitive and physical capacities of the tool-users, particularly Denisovans and *Homo floresiensis* (Chapters 5 and 6) for which little is known about their behaviour. Concerning *Homo floresiensis*, if we consider that archaeological artefacts older than ~60 ka in Liang Bua are well attributed to them, this study cannot say which animal bone or plant species were utilised, but new information has been gathered about their capacity to use stone tools to scrape, cut and polish different materials like bone, plant and coloured pigment, and combinations of materials (e.g., bone and pigment on LB5126, LB5580a) (Chapter 6, section 6.3.2.4). Some of these tasks took advantage of multiples edges on the same tool (e.g., LB5526b), sequential use of the same tool for different tasks and retouching edges (e.g., LB5580a). Raman analyses suggest hominin dexterity, particularly demonstrated by use of multiple edges of flakes that are sometimes smaller than than three centimeters (LB5563a-c) (Appendix IIb, figs 11 to 13). Consequently the potential of applying this methodology to archaeological assemblages (the second specific aim of this thesis) is not only to confirm the different types of material worked by stone tools at Denisova Cave and Liang Bua, but also to shed light on the use of these artefacts for complex tasks, the full extent of which remains to be elucidated.

7.6 Comparing tool use in different archaeological layers: implications for hominin behaviour and problems of residue preservation

A broader and more difficult level of interpretation based on micro-residue analysis concerns the variation in stone tool use and hominin behaviours through time. This requires comparisons of worked materials and particular ways of using stone tools recovered from a sequence of archaeological layers. Although broader interpretations can be problematic because of the small sample size and because tool use represents such a brief moment of time, we can propose some hypotheses about tool use through time. This addresses the third specific aim of my research (Chapter 1, section 1.2).

At Liang Bua, I propose that more tools were used on plants after the last glacial maximum (~20 ka ago) than is the case for the older artefacts, where bone working is often predominantly associated with pigment (Chapter 6, section 6.4, Fig. 6.67). If preservation is assumed to be similar for all surfaces of any one artefact, then comparison of uses for stone tools in the same layer is likely to be more robust than comparisons of artefacts from different layers, because of the potential differences in their environmental contexts and preservation conditions.

Study of the Denisova Cave and Liang Bua artefacts has revealed a wide range of preservation situations, indicated by micro-residue analyses that extend from identification of few archaeologically use related micro-residues on some artefacts from the 2004 and 2015 Liang Bua artefact collections (Chapter 6, section 6.2.2.3), to the more evenly distributed amounts of fatty residues observed on the Denisova stone tools (Chapter, section 5.3.3) and the abundant well-preserved residues found on artefacts recovered from the 2016 Liang Bua collection (Chapter 6, section 6.3.2.4). These diverse preservation situations indicate that preservation is not uniform between layers and different sites, but also show that, even in unfavourable conditions, micro-residues can potentially be conserved in locally protected areas (e.g., cracks, holes and depressions in the stone surface). A high volume of residues will be easier to link with tool use and will require less time to locate and analyse; conversely lower residue abundance will be harder to link with tool use, and it will be more time consuming to locate and analyse micro-residues. But in both situations, systematic analysis of all residues on artefact perimeters and adjacent surfaces should be the preferred approach because even an apparently high abundance of optically similar residues can be misleading. For example, most white residues on artefact LB5580a were identified as bone apatite (Chapter 6, section 6.3.2.4), but some white material was identified as kaolinite in other areas where it was sometimes found mixed with bone. Residue distributions should always be checked for homogeneity.

Differences of preservation may be a consequence of sample extraction conditions (e.g., recovery of stone artefacts attached to pedestals), rather than the result of regional environmental differences (tropical island vs cold continental) or local site conditions (open rock shelter vs deep cave deposits). Indeed, fewer modern contaminants were found on artefacts from the Liang Bua 2016 collection, which was recovered from attached pedestals and higher amounts of micro-residues were found on them. If robust archaeological

information can be considered as proportional to the amount and number of micro-residues found on one sample, and modern contaminants and other residues arising from sediment or post-depositional processes can be considered as background “noise”, then high abundance of contaminants tends to increase noise and uncertainty about residue origins. However, with a constant low background of contamination, a high number of use-related micro-residues will likely provide archaeologically significant information about tool functions. Indeed, I observed in my study that the artefact recovery method, handling, and storage had more influence on micro-residue preservation than differences linked with climate.

This conclusion is not in agreement with what was expected at the start of this study. I expected that climate would be the main factor explaining differential preservation of micro-residues at Liang Bua and Denisova Cave, located respectively in tropical island and cold continental climatic zones. However, I found that Liang Bua tools from the 2016 collection (recovered from pedestals) have use-related lipid micro-residues containing UFA (Chapter 6, section 6.3.2.4) similar in abundance to those found on some Denisova Cave artefacts (Chapter 5, section 5.3.3). This situation may not be so surprising considering that, despite the Denisova Cave artefacts having spent their burial lives under colder conditions, little is known about the conditions that were present during the time of discard, between stone tool use and their burial. Indeed, these starting conditions for stone artefacts prior to burial can be critical. For example, lipids can be washed away by rain or flowing water soon after residues were deposited on the stone tools. However, if residues are allowed to dry and the tools are then rapidly buried, the residues can solidify and be trapped on the surface under fine sediment, where they may survive for thousands of years. As a modern practical example of this principle, it is easy to clean dishes straight after a meal, but trying to get rid of the greasy caked-on deposits after a few days is much harder work! The influence of starting conditions on lipid preservation and multiple environmental parameters (e.g., humidity, influence of pressure on material worked versus simple deposition, temperature, microbial activity) is apparent from the different rates of degradation observed in my experiments on fat deposition on stone tools that were buried in the same place for the same period of time (Chapter 4, section 4.6.1).

In addition, after artefacts were recovered from Denisova Cave and stored, the change from cold to warm conditions might have triggered rapid degradation of the residues. Warming and cooling of buried artefacts can also happen in the past, during climate fluctuations, but on a different time scale. Although these burial preservation conditions need to be further

investigated on stone tools for different type of material (e.g., lipids, bone), it is likely that initial and final conditions of stone artefact deposition are as important as duration of burial. A shorter duration of burial, but with sudden exposure to a new climatic environment, can be just as critical for preservation as a longer period of burial under more stable conditions, when the artefacts are protected by a closely packed layer of fine sediment.

In this study, differential preservation of particular micro-residues was also observed, depending in part on their material composition. As expected, the mineral parts of bone, apatite and mineral residues generally were found in high abundance on some tools. With respect to organic residues, lipids were found in highest abundance, followed by protein, then by cellulose and lignified plant tissue. Starch grains were very rare and often of uncertain origin (i.e., possible or probable contamination), indicating that starch micro-residues are least well preserved.

Considering this order of preservation, my finding that most artefacts younger than ~20 ka (Chapter 6, section 6.4, Fig 6.67) were used on plant material do not means the absence of this stone tool function in the earlier layers (Chapter 6, section 6.4, Fig. 6.67). Indeed, the lack of plant processing tools in older periods, ~120–60 ka and ~40–20 ka (Chapter 6, section 6.4, Fig 6.67) may reflect poorer plant tissue preservation through time, as artefacts with only concentrations of lipid micro-residues, and not bone, could have been used to process plant tissue, other traces of which did not survive. This hypothesis is supported by analysis of artefact LB250, with a use-polish pattern indicating plant processing but very few plant residues. Consequently, based on the micro-residues, it is possible that stone artefacts were used on plant material from ~120 ka to the past few thousand years but could not be identified by Raman microscopy. Thus Raman microscopy complements and does not replace optical use-wear study (see below). On other hand, bone micro-residues were found to originate from sediment and in contact with artefact LB4582, which has an estimated age of ~20–10 ka (Chapter 6, section 6.4, Fig. 6.67), showing that bone is well preserved from that time. Bone is also preserved in older levels, ~120–20 ka, with several artefacts used for bone working and having a high abundance of bone micro-residues. No bone-working tools were found in deposits younger than ~20 ka (Chapter 6, section 6.4, Fig. 6.67). These data suggest a clear difference in tool function that is not the result of preservation, and likely indicates the importance of stone tools used at the site to process animal tissue from ~120 ka to ~20 ka.
Another significant result is the continuity of tool use on bone and iron oxide pigment from ~120 ka to ~20 ka (Chapter 6, section 6.4, Fig 6.67), in contrast with the actual hypothesis of

a major shift in the cave occupation from *Homo floresiensis*, to modern humans (*Homo sapiens sapiens*) after ~50 ka (Sutikna et al., 2016). This continuity in tool-use is confirmed by the continuous presence of thick triangular flakes with flat ventral surfaces used in a similar way on bone in layers dating to both periods (Chapter 6, section 6.3.2.4).

Raman microscopy analysis of micro-residues on artefacts extracted from layer sequences is thus capable of giving insights into environmental and cultural factors in the differential preservation of residue materials through time, fulfilling the third aim of this thesis (Chapter 1, section 1.2).

7.7 Complementarity of Raman analysis with use-wear analysis

As discussed above, use-wear analysis cannot be separated from micro-residue analysis because analysis of polish and other wear traces are part of the strategy that relates their distributions to the worked area on stone tools. Polish distribution, striations and in some cases scarring traces were used to correlate used edges with micro-residue distributions, as these traces were visible after partial cleaning of studied artefacts. Indeed, it needs to be remembered that (1) micro-residue analysis ideally should avoid the full cleaning of stone artefacts by solvents until the last step of the study, and (2) examination of polish patterns for determining worked material should be done after micro-residue analysis and any complementary residue analyses. Once all residue analyses have been completed, use-wear analysis can be undertaken independently, ideally by another specialist, to determine stone tool function for each artefact. Finally, results from residue and use-wear analyses need to be compared and discussed critically and objectively. This complementary approach of residues and use-wear was applied in my study of Denisova Cave artefacts (Bordes et al., 2018) (Appendix IIa, table 1) and proved useful for interpreting function when either residue or use-wear on its own was inconclusive. Indeed, when it was not possible to identify with Raman microscopy any micro-residues related to use, or there were too few micro-residues to reliably infer the category of material worked, the use-wear study of polish and other forms of wear provided reliable information about tool use. In some other cases, when use-wear analysis was confronted with weakly developed polish and wear that was non-diagnostic of worked material, Raman analysis was critical for identifying key micro-residues on the used edges and determining tool use.

7.8 Limitations of Raman spectroscopy and subsequent chemical analysis of residues

Even with success in analysing a wide range of micro-residues and determining main categories of material (e.g., bone, plant fibre, lipids), and securely linking them to prehistoric use, Raman spectroscopic analysis of ancient residues was not able to identify highly specific markers for plant and animal taxa. Raman spectroscopy is not a primary spectroscopic tool to determine highly specific material, mainly because this technique probes the main composition of a material, and the detailed chemical composition and minor compounds cannot be established. Raman spectroscopy is also highly dependent on the conformation and orientation of packed molecules in a solid state, which does not allow interpretation of small spectral variations that reflect variation in chemical composition of organic micro-residues. However, as shown above, it is possible to divide the micro-residues, which were successfully analysed with Raman spectroscopy, into two groups: (1) animal or plant specific materials like bone and plant, sometimes with more detailed information (e.g., grass or wood); and (2) non-specific micro-residues including lipids and proteins. So, after obtaining an initial array of information from Raman analysis, indicating specific materials, advantage can be also taken from the presence of any concentrated unspecified micro-residues to derive further information. In a first step of analysis, lipids can be related to prehistoric use when they are fairly well preserved and concentrated on a polished area, and lipid distributions can be located easily and quickly with Raman analysis. As Raman spectroscopy is a non destructive technique and leaves intact micro-residues on stone surfaces, any tagged concentrated spot of unspecific micro-residues like lipids could be targeted in a second step of analysis with application of complementary techniques, such as GC-MS, to measure relative proportions of main lipids (e.g., palmitic and stearic acid) or to probe for more specific minor compounds (e.g., sterol) (Luong et al., 2017, 2018).

7.9 The future development of Raman microscopy and ATR FT-IR as complementary techniques for analysing micro-residues

In future developments of Raman analysis, automatic focusing could be of interest to speed up the systematic analysis of micro-residues by mapping larger areas. However, considering the uneven surface of a stone tool, such spectral mapping can only be used to check homogeneity of smeared residues on limited small flat areas (a few thousand microns across) (see also Chapter 2, section 2.1.3). As it involves mechanical displacement in the Z direction

of the microscope objective, it is too slow to be used systematically in the analysing strategy developed in this thesis. However, one can imagine that the future development of a faster focusing system and a 3D displacement stage would allow a whole stone artefact surface to be kept in focus. But the speed of such a system will always be limited by the acquisition time needed to probe each Z position and to adjust focus at each analysed spot. Other additional problems will be the integration of an automatic detection of laser threshold damage to tune the right level of laser power for each analysed spot, and, in some cases, tuning a delay to quench fluorescence or burn impurities, when needed before measurement. Another level of complexity is that Raman measurement signal-to-noise ratio is also dependent on the position of the analysed spot on any given residue, as some part can be more fluorescent than another, or more or less damaged; and can be more or less transparent. Micro-residues (e.g., a fibre) can also move slightly under the laser beam, and the analysing position needs to be constantly readjusted. Consequently, building an automated system that can replace my strategy is not trivial and a dynamic correction of position will need to be applied, meaning that the machine needs to take into account the spatial distribution of a micro-residue fluorescence and to have automatic computer recognition of micro-residue shapes, which can be very complex in some cases.

Surface Enhanced Raman spectroscopy (SERS) (Smith et Dent, 2005; Moskovits, 2006) has been applied in the field of art and archaeology (Bruni et al., 2009; Pozzi et al., 2013; Pozzi et Leona, 2016) and might be an option to consider in analyses of small residues on stone artefacts. This technique has the advantage of enhancing the Raman signal by direct contact of gold or silver nanoparticules or substrates with analysed molecules, to detect very low concentrations of organic molecules, and to quench fluorescence. However, either extraction of the micro-residues from the artefact surface or deposition of a metallic layer on that surface would be needed for this technique, which might be destructive of samples and add complexity to the interpretation of spectral data. Indeed, interaction between metallic surfaces and molecules is highly specific and the SERS effect does not happen for all organic molecules. Moreover, SERS enhancement is dependent on adsorbed molecule orientation, leading also to a difference in intensity enhancement between vibrational modes of the same molecule. In consequence, SERS has to develop from scratch all the spectral references for each type of metal substrate and the conditions of molecule adsorption. Building a SERS reference collection of potential organic traces on stone tools is huge task because of the vast range of different materials, whether use-related or contaminants .

As underlined previously (Chapter 1, section 1.3) IR absorption spectroscopy is classically associated with Raman spectroscopy for the complementary analysis of a great range of ancient materials (Vahur et al., 2011; Cesaro et Lemorini, 2012; Prinsloo et al., 2014; Monnier et al., 2017). At the beginning of my thesis research, ATR-FTIR (Attenuated Total Reflection-Fourier Transform Infrared Spectroscopy), using contact between analysed residues and micro-crystal windows in different IR transmissive materials (e.g., diamond, germanium), was tried unsuccessfully on stone artefacts in the laboratory (with the Bruker®-LUMOS ATR-FTIR instrument). Indeed, although this technique poses no difficulty with flat or prepared samples, the required pressure from the analysing crystal on stone artefact surfaces can often move the whole sample. Indeed, it was difficult to firmly hold irregularly shaped stone artefacts with the instrument sample holder provided. Different media (e.g., sand, polystyrene bead, Blu Tack®) were tried under the stones to lock them in position and limit this movement during analysis, but it was unsuccessful. Other considerations are that ideal contact between the micro-crystal window and micro-residues is difficult to achieve; and the technique cannot be considered as totally non-destructive because the pressure can damage or remove fragile analysed organic materials (e.g., fibres). Another problem is that the micro-crystal window has a high risk of suffering damage on contact with the uneven hard mineral surfaces below analysed residues—and the application of high pressure was usually necessary to get enough signal-to-noise ratio. Additionally, the analysis sequence, including reference measurement and accurate positioning of the crystal, was too slow for a high number of micro-residues to be analysed in a realistic timeframe. Measuring the difference between sample and background in IR spectroscopy can also be problematic either in ATR or in reflection mode because the background signal is constantly changing, generating spectral variations that render data interpretation more complex than in Raman spectroscopy.

7.10 Prospects

Raman spectroscopy applied to prehistoric stone tools can be considered as a valuable method of analysis playing a pivotal role in relation with use-wear analysis and other complementary techniques, such as GC-MS, to better secure micro-residues to stone tool use. The research in this thesis demonstrates that, as non-destructive techniques with high spatial resolution and in situ capabilities, Raman and FT-IR spectroscopy are becoming the standard for initial screening of micro-residues.

To optimise information on lithic functional analysis, the way forward is to ensure that different methods of analysis complement each other. However, it is not a trivial issue to determine the most efficient way of addressing the diverse goals of such collaborations, as each method involves different protocols, which increases the possibility for contamination at every step. Such challenges remain important issues to overcome in future multi-method studies of stone tool function. Specialists in each method need to carefully coordinate their activities to maximise the retrieval of archaeologically-relevant information from ancient residues, while simultaneously minimising the problems inherent in identifying microscopic and molecular traces of past human activities.

References

Adar, F., 2013. Resonance Enhancement of Raman Spectroscopy: Friend or Foe? Spectroscopy. 28(6), 14–21.

Ahler, S.A., 1989. Mass Analysis of Flaking Debris: Studying the Forest Rather Than the Tree. Archeological Papers of the American Anthropological Association. 1, 85–118.

Agarwal, U.P., Ralph, S.A., 1997. FT-Raman Spectroscopy of Wood: Identifying Contributions of Lignin and Carbohydrate Polymers in the Spectrum of Black Spruce (Picea Mariana). Applied Spectroscopy. 51, 1648–1655.

Agarwal, U.P., 1999. An overview of Raman spectroscopy as applied to lignocellulosic materials. in Advances in lignocellulosics characterization. Atlanta, GA, Edition (Argyropoulos DS ed.), 209–225. TAPPI Press.

Anderson, P.C., 1980. A testimony of prehistoric tasks: Diagnostic residues on stone tool working edges. World Archaeology. 12, 181–194.

Anderson, P.C., Georges, J.M., Vargiolu, R., Zahouani, H., 2006. Insight from a tribological analysis of the tribulum. Journal of Archaeological Science. 33(11), 1559–1568.

Antonakos, A., Liarokapis, E., Leventouri, T., 2007. Micro-Raman and FTIR studies of synthetic and natural apatites. Biomaterials. 28, 3043–3054.

Asghari-Khiavi, M., Mechler, A., Bambery, K.R., McNaughton, D., Wood, B.R., 2009. A resonance Raman spectroscopic investigation into the effects of fixation and dehydration on heme environment of hemoglobin. Journal of Raman Spectroscopy. 40, 1668–1674.

Aubert, M., Brumm, A., Ramli, M., Sutikna, T., W Saptomo, E., Hakim, B., J Morwood, M., Van den Bergh, G., Kinsley, L., Dosseto, A., 2014. Pleistocene cave art from Sulawesi, Indonesia. Nature. 514, 223–7.

Baryshnikov, G., 1999. Large mammals and Neanderthal palaeoecology in the Altai Mountains (Central Asia, Russia). Préhistoire Européenne. 14, 49–66.

Beckett, S., Rogers, K.D., Clement, J.G., 2011. Inter-Species Variation in Bone Mineral Behavior upon Heating. Journal of Forensic Sciences. 56, 571–579.

Beyries, S., 1984. Approche functionelle de la variabilite des facies du Mousterien. These de troisieme cycle, Universite de Paris X.

Bonifacio, A., Sergo, V., 2010. Effects of sample orientation in Raman microspectroscopy of collagen fibers and their impact on the interpretation of the amide III band. Vibrational Spectroscopy. 53(2), 314–317.

Bordes, L., Prinsloo, L.C., Fullagar, R., Sutikna, T., Hayes, E., Jatmiko, Wahyu Saptomo, E., Tocheri, M.W., Roberts, R.G., 2017. Viability of Raman microscopy to identify micro-residues related to tool-use and modern contaminants on prehistoric stone artefacts. Journal of Raman Spectroscopy. 48, 1212–1221.

Bordes, L., Fullagar, R., Prinsloo, L.C., Hayes, E., Kozlikin, M.B., Shunkov, M.V., Uliyanov, V.A., Derevianko, A.P., Roberts, R.G., 2018. Raman spectroscopy of lipid micro-residues on Middle Palaeolithic stone tools from Denisova Cave, Siberia. Journal of Archaeological

Science. 95, 52–63.

Bradtmoller, M., Sarmiento, A., Perales, U., Zuluaga, M.C., 2016. Investigation of Upper Palaeolithic adhesive residues from Cueva Morin, Northern Spain. Journal of Archaeological Science: Reports. 7, 1–13.

Briuer, F.L., 1976. New clues to stone tool function: plant and animal residues. American Antiquity. 41(4), 478–484.

Brown, P., Sutikna, T., Morwood, M.J., Soejono, R.P., Jatmiko, Wayhu Saptomo, E., Awe Due, R., 2004. A new small-bodied hominin from the Late Pleistocene of Flores, Indonesia. Nature. 431, 1055–1061.

Brumm, A., Aziz, F., van den Bergh, G.D., Morwood, M.J., Moore, M.W., Kurniawan, I., Hobbs, D.R., Fullagar, R., 2006. Early stone technology on Flores and its implications for Homo floresiensis. Nature. 441, 624–628.

Bruni, S., Guglielmi V., Pozzi, F., 2009. Surface-enhanced Raman spectroscopy (SERS) on silver colloids for the identification of ancient textile dyes: Tyrian purple and madder. Journal of Raman Spectroscopy. 41, 175–180

Buciuman, F., Patcas, F., Craciun, R., R T Zahn, D., 1999. Vibrational spectroscopy of bulk and supported manganese oxides. Physical Chemistry Chemical Physics. 1, 185–190.

Callaway, E., 2016. "Did humans drive 'hobbit' species to extinction?". Nature. *doi:10.1038/nature.2016.19651*.

Carciumaru, M., Ion, R., Nitu, E., Stefanescu, R., 2012. New evidence of adhesive as hafting material on Middle and Upper Palaeolithic artefacts from Gura Cheii-Râs Nov Cave (Romania). Journal of Archaeological Science. 39, 1942–1950.

Cesaro, S.N., Lemorini, C., 2012. The function of prehistoric lithic tools: A combined study of use-wear analysis and \FTIR\ microspectroscopy. Spectrochimica Acta Part A: Molecular and Biomolecular Spectroscopy. 86, 299–304.

Colthup, N., Daly, L., Wiberley, S., 1990. Introduction to Infrared and Raman Spectroscopy, Academic Press.

Cordeiro Silva, G., Soares Almeida, F., Ferreira, A., Ciminelli, V., 2012. Preparation and Application of a Magnetic Composite (Mn_3O_4/Fe_3O_4) for Removal of As(III) from Aqueous Solutions. Materials Research. 15, 403–408.

Czaja, M., Bodyl, S., Gluchowski, P., Mazurak, Z., Strek, W., 2008. Luminescence properties of rare earth ions in fluorite, apatite and scheelite minerals. Journal of Alloys and Compounds. 451, 290–292.

Czamara, K., Majzner, K., Pacia, M.Z., Kochan, K., Kaczor, A., Baranska, M., 2015. Raman spectroscopy of lipids: a review. Journal of Raman Spectroscopy. 46, 4–20.

Daher, C., Paris, C., Le Ho, A., Bellot-Gurlet, L., Echard, J., 2010. A joint use of Raman and infrared spectroscopies for the identification of natural organic media used in ancient varnishes. Journal of Raman Spectroscopy. 41, 1494–1499.

Dal Sasso, G., Angelini, I., Maritan, L., Artioli, G., 2018. Raman hyperspectral imaging as an effective and highly informative tool to study the diagenetic alteration of fossil bones. Talanta. 179, 167–176.

Debenath, A., Dibble, H.L., 1994. Handbook of Paleolithic Typology: Lower and Middle Paleolithic of Europe. University of Pennsylvania Museum of Archaeology and Anthropology, University of Pennsylvania Press. Pages: 256.

De Gelder, J., De Gussem, K., Vandenabeele, P., Moens, L., 2007. Reference database of Raman spectra of biological molecules. Journal of Raman Spectroscopy. 38, 1133–1147.

Derevianko, A.P., Shunkov, M.V., Agadjanian, A.K., Baryshnikov, G.F., Malaeva, E.M., Ulianov, V.A., Kulik, N.A., Postnov, A.V., Anoikin, A.A., 2003. Paleoenvironment and paleolithic human occupation of Gorny Altai: Subsistence and adaptation in the vicinity of Denisova Cave. Novosibirsk Institute of Archaeology and Ethnography SB RAS Press.

Derevianko, A.P., Postnov, A.V., Rybin, E.P., Kuzmin, Y.V., Keates, S.G., 2005. Pleistocene peopling of Siberia: A review of envronmental and behaviour aspects. Indo-Pacific prehistory association bulletin. 3, 57–68.

Derevianko, A.P., Shunkov, M.V., Markin, S.V., 2014. The Dynamics of the paleolithic Industries in Africa and Eurasia in the Late pleistocene and the Issue of the Homo sapiens Origin, Edition. Novosibirsk Institute of Archaeology and Ethnography SB RAS Press.

Dibble, H.L., 1987. The interpretation of Middle Paleolithic scraper morphology. American antiquity. 52(1), 109–117.

Driscoll, K., Garcia-Rojas, M., 2014. Their lips are sealed: identifying hard stone, soft stone, and antler hammer direct percussion in Palaeolithic prismatic blade production. Journal of Archaeological Science. 47, 134–141.

Dumont, J., 1982. The quantification of wear traces: a new use for interferometry. World Archaeology. 14(2), 206–217.

Edwards, H., Farwell, D., Daffner, L., 1996. Fourier-transform Raman spectroscopic study of natural waxes and resins. Spectrochimica Acta Part A: Molecular and Biomolecular Spectroscopy. 52, 1639–1648.

Edwards, H., Wilson, A., Nik Hassan, N., Davidson, A., Burnett, A., 2007. Raman spectroscopic analysis of human remains from a seventh century cist burial on Anglesey, UK. Analytical and Bioanalytical Chemistry. 387(3), 821–8.

Elliot, J.C., 1994. Structure and chemistry of the apatites and other calcium orthophosphates. Amsterdam: Elsevier.

Evans, A.A., Donahue, R.E., 2008. Laser scanning confocal microscopy: a potential technique for the study of lithic microwear. Journal of Archaeological Science. 35, 2223–2230.

Falk, D., Hildebolt, C., Smith, K., Morwood, M., Sutikna, T., Brown, P., 2005. The brain of LB1, Homo floresiensis. Science. 308, 242–245.

Ferraro, J., 2002. Introductory Raman Spectroscopy 2nd Edition.

Forbes, S., Stuart, B., Dadour, I., Dent, B., 2004. A preliminary investigation of the stages of adipocere formation. Journal of Forensic Sciences. 49, 566–574.

Francioso, O., Sanchez-Cortes, S., Bonora, S., Roldan, M.L., Certini, G., 2011. Structural characterization of charcoal size-fractions from a burnt Pinus pinea forest by FT-IR, Raman and surface-enhanced Raman spectroscopies. Journal of Molecular Structure. 994, 155–162.

Freeman, J., Wopenka, B., Silva, M., Pasteris, J., 2001. Raman Spectroscopic Detection of Changes in Bioapatite in Mouse Femora as a Function of Age and In Vitro Fluoride Treatment. Calcified tissue international. 68, 156–62.

Froment, F., Tournié, A., Colomban, P., 2008. Raman identification of natural red to yellow pigments: iron containing ores. Journal of Raman Spectroscopy. 39, 560–568.

Frost, R., 1995. Fourier Transform Raman Spectroscopy of Kaolinite, Dickite and Halloysite. Clays and Clay Minerals. 43, 191–195.

Frost, R., 1997. The Structure of the Kaolinite Minerals; A FT-Raman Study. Clay Minerals. 32, 65–77.

Fullagar, R., 1986. Use-wear and Residues on Stone Tools: Functional Analysis and its Application to Two Southeastern Australian Archaeological Assemblages. PhD thesis, La Trobe University, Australia.

Fullagar, R., 2014 Residues and Usewear. in Archaeology in Practice: A Student Guide to Archaeological Analyses, Edition (J. Balme and A. Paterson ed.), pp 232–263. Blackwell Publishing.

Gaft, M., Reisfeld, R., Panczer, G., 2005. Modern Luminescence Spectroscopy of Minerals and Materials. Springer-Verlag Berlin Heidelberg.

Galanidou, N., 2006. Analytical and Ethical Issues concerning Organic Residues on Paleolithic Chipped Stone Tools from NW Greece. Journal of Field Archaeology. 31, 351–362.

Galeano, S., Garcia-Lorenzo, M.L., Garcia-Lorenzo, M.S., 2008. Bone Mineral Change During Experimental Calcination: An X-ray Diffraction Study. Journal of Forensic Sciences. 59, 1602–1606.

Gorobets, B., Rogojine, A., 2001. Luminescence spectra of minerals Handbook, Moscow.

Gourrier, A., Chadefaux, C., Lemaitre, E., Bellot-Gurlet, L., Reynolds, M., Burghammer, M., Plazanet, M., Boivin, G., Farlay, D., Bunk, O., Reiche, I., 2017. Nanoscale modifications in the early heating stages of bone are heterogeneous at the microstructural scale.(Research Article) (Report). PLoS ONE. 12,e0176179.

Grauw, C.J., De Bruijn, J.D., Otto, C., Greve, J., 1996. Investigation of Bone and Calcium Phosphate Coatings and Crystallinity Determination Using Raman Microspectroscopy. Cells and Materials. 6, 57–62.

Guarino, F.M., Angelini, F., Vollono, C., Orefice, C., 2006. Bone preservation in human

remains from the Terme del Sarno at Pompeii using light microscopy and scanning electron microscopy. Journal of Archaeological Science. 33, 513–520.

Hanesch, M., 2009. Raman spectroscopy of iron oxides and (oxy)hydroxides at low laser power and possible applications in environmental magnetic studies. Geophysical Journal International. 177, 941–948.

Hardy, B., Kay, M., Marks, E., Monigal, K., 2001. Stone tool function at the paleolithic sites of Starosele and Buran Kaya III, Crimea: behavioral implications. Proceedings of the National Academy of Science. 98 (19), 10972–10977.

Hardy, B.L., Bolus, M., Conard, N.J., 2008. Hammer or crescent wrench? Stone-tool form and function in the Aurignacian of southwest Germany. Journal of human evolution. 54, 648–662.

Harman, J., 2015. Using Decorrelation Stretch to enhance rock art images. Paper presented at the American Rock Art Research Association annual meeting on 28 May 2005 (consulted January 2015): http://www.dstretch.com/AlgorithmDescription.html.

Harmand, S., Lewis, J., Feibel, C., Lepre, C., Prat, S., Arnaud, L., Boes, X., Quinn, R., Brenet, M., Arroyo, A., Taylor, N., Clément, S., Daver, G., Brugal, J., Leakey, L., Mortlock, R., Wright, J., Lokorodi, S., Kirwa, C., Roche, H., 2015. 3.3-million-year-old stone tools from Lomekwi 3, West Turkana, Kenya.

Haslam, M., Robertson, G., Crowther, A., Nugent, S., Kirkwood, L., 2011. Archaeological Science Under a Microscope (Terra Australis 30) Studies in Residue and Ancient DNA Analysis in Honour of Thomas H. Loy. ANU E Press.

Hayden, B., 1979. Lithic Use-wear Analysis, New York Academic Press.

Hayes, Elspeth, What was ground?: a functional analysis of grinding stones from Madjedbebe and Lake Mungo, Australia, Doctor of Philosophy thesis, University of Wollongong, 2015. http://ro.uow.edu.au/theses/4491

Henshilwood, C.S., d'Errico, F., van Niekerk, K.L., Coquinot, Y., Jacobs, Z., Lauritzen, S., Menu, M., Garcia-Moreno, R., 2011. A 100,000-Year-Old Ochre-Processing Workshop at Blombos Cave, South Africa. Science. 334, 219–222.

Hernanz, A., Mas, M., Gavilan, B., Hernandez, B., 2006. Raman microscopy and IR spectroscopy of prehistoric paintings from Los Murciélagos cave (Zuheros, Córdoba, Spain). Journal of Raman Spectroscopy. 37, 492–497.

Hernanz, A., Iriarte, M., Bueno-Ramarez, P., de Balban-Behrmann, R., Gavira-Vallejo, J.M., Calderan-Saturio, D., Laporte, L., Barroso-Bermejo, R., Gouezin, P., Maroto-Valiente, A., Salanova, L., Benetau-Douillard, G., Mens, E., 2015. Raman microscopy of prehistoric paintings in French megalithic monuments. Journal of Raman Spectroscopy. 47(5), 571–578.

Herwartz, D., Tutken, T., Jochum, K.P., Sander, P.M., 2013. Rare earth element systematics of fossil bone revealed by LA-ICPMS analysis. Geochimica et Cosmochimica Acta. 103, 161–183.

Hogberg, A., Puseman, K., Yost, C., 2009. Integration of use-wear with protein residue analysis - a study of tool use and function in the south Scandinavian Early Neolithic. Journal of

Archaeological Science. 36, 1725–1737.

Holder, B.H., 2012. Characterization of Starch by Vibrational Spectroscopy, MSc thesis.

Inizan, M.L., Reduron-Ballinger, M., Roche, H., Tixier, J., 1999. Technology and Terminology of Knapped Stone, Edition. Cercle de Recherches et d'Etudes Prehistorique; First edition.

Jacobs, Z., Li, B., V Shunkov, M., B Kozlikin, M., S Bolikhovskaya, N., K Agadjanian, A., A Uliyanov, V., K Vasiliev, S., O'Gorman, K., P Derevianko, A., G Roberts, R., 2019. Timing of archaic hominin occupation of Denisova Cave in southern Siberia.

Jahren, A., Toth, N., Schick, K., Clark, J., Amundson, R., 1997. Determining Stone Tool Use: Chemical and Morphological Analyses of Residues on Experimentally Manufactured Stone Tools. Journal of Archaeological Science. 24, 245–250.

Janko, M., Stark, R.W., Zink, A., 2012. Preservation of 5300 year old red blood cells in the Iceman. Journal of the Royal Society Interface. 9, 2581–2590.

Kamminga, J., 1982. Over The Edge - Functional analysis of Australian stone tools. Occasional Papers in Anthropology. University of Queensland.

Kavkler, K., Demsar, A., 2011. Examination of cellulose textile fibres in historical objects by micro-Raman spectroscopy. Spectrochimica Acta Part A: Molecular and Biomolecular Spectroscopy. 78, 740–746.

Kaye, T.G., Falk, A., Pittman, M., Sereno, P.C., Martin, L.D., Burnham, D.A., Gong, E., Xu, X., Wang, Y., 2015. Laser-Stimulated Fluorescence in Paleontology. PLoS ONE. 10 (5),e0125923.

Keeley, L., 1980. Experimental Determination of Stone Toll Uses: A Microwear Analysis, Edition. University of Chicago Press, Chicago.

Keresztury, G., 2002. Raman Spectroscopy: Theory in Handbook of Vibrational Spetroscopy. Edition. John Wiley & Sons, Chichester.

Kimbel, W., Walter, R., Johanson, D., Reed, K., Aronson, J., Assefa, Z., Marean, C., Eck, G., Bobe, R., Hovers, E., Rak, Y., Vondra, C., Yemane, T., York, D., Chen, Y., Evensen, N., Smith, P., 1996. Late Pliocene Homo and Oldowan Tools from the Hadar Formation (Kada Hadar Member), Ethiopia. Journal of Human Evolution. 31, 549–561.

Konstantinos, K., Malvina, O., Christos, K., 2012. Analysis of bone composition with Raman spectroscopy. Processes, Forth, Patras, Greece.

Krause, J., Fu, Q., Good, J.M., Viola, B., Shunkov, M.V., Derevianko, A.P., Paabo, S., 2010. The complete mitochondrial DNA genome of an unknown hominin from southern Siberia. Nature. 464, 894–897.

Lakowicz, J.R., 1999. Principles of fluorescence spectroscopy, Edition. Second edition. New York : Kluwer Academic/Plenum, 1999.

Lamb, J., Loy, T., 2005. Seeing red: the use of Congo Red dye to identify cooked and damaged starch grains in archaeological residues. Journal of Archaeological Science. 32,

1433–1440.

Langejans, G.H., 2010. Remains of the day-preservation of organic micro-residues on stone tools. Journal of Archaeological Science. 37, 971–985.
Langejans, G.H., 2011. Discerning use-related micro-residues on tools: testing the multi-stranded approach for archaeological studies. Journal of Archaeological Science. 38, 985–1000.

Langejans, G.H., 2012. Micro-residue analysis on early stone age tools from Sterkfontein, South Africa: A methodological enquiry. The South African Archaeological Bulletin. 67, 200–213.

Langejans, G., Lombard, M., 2014. Micro-residues on stone tools: morphological analysis, interpretation and challenges. in International Conference on Use-Wear Analysis. Use-Wear 2012, Edition (Marreiros, J. Bicho, N. Gibaja Bao ed.), pp 55–64. Cambridge Scholars Publishing.

Lebon, M., Reiche, I., Frohlich, F., Bahain, J., Falgueres, C., 2009. Characterization of archaeological burnt bones: Contribution of a new analytical protocol based on derivative FTIR spectroscopy and curve fitting of the v1v3 PO4 domain. Analytical and bioanalytical chemistry. 392, 1479–88.

Lombard, M., 2004. Distribution patterns of organic residues on Middle Stone Age points from Sibudu Cave, Kwazulu-Natal, South Africa. South African Archeological Bulletin. 59, 37–44.

Lombard, M., Wadley, L., 2009. The impact of micro-residue studies on South African Middle Stone Age research. in Archaeological Science Under a Microscope: Studies in Residue and Ancient DNA Analysis in Honour of Thomas H. Loy. ANU Press.

Lovita, R., 2011. Shape Variation in Aterian Tanged Tools and the Origins of Projectile Technology: A Morphometric Perspective on Stone Tool Function. PLOS ONE. 6,e29029.

Loy, T.H., 1983. Prehistoric blood residues: detection on tool surfaces and identification of species of origin.. Science. 220(17), 1269–1271.

Luong, S., Hayes, E., Flannery, E., Sutikna, T., Tocheri, M.W., Saptomo, E.W., Jatmiko, Roberts, R.G., 2017. Development and application of a comprehensive analytical workflow for the quantification of non-volatile low molecular weight lipids on archaeological stone tools. Analytical Methods. 9, 4349–4362.

Luong, S., Tocheri, M.W., Sutikna, T., Wahyu Saptomo, E., Jatmiko, Roberts, R.G., 2018. Incorporating terpenes, monoterpenoids and alkanes into multiresidue organic biomarker analysis of archaeological stone artefacts from Liang Bua (Flores, Indonesia). Journal of Archaeological Science: Reports. 19, 189–199.

Martino, P.D., 2016. What About Biofilms on the Surface of Stone Monuments ? The Open Conference Proceedings Journal. 6, 14–28.

Melchiorre, M., Ferreri, C., Tinti, A., Chatgilialoglu, C., Torreggiami, A., 2015. A Promising Raman Spectroscopy Technique for the Investigation of trans and cis Cholesteryl Ester Isomers in Biological Samples. Applied Spectroscopy. 69, 613–622.

Merlin, J., 1985. Resonance Raman spectroscopy of carotenoids and carotenoid-containing systems. Pure and Applied Chemistry. 57, 785–792.

Messner, T.C., 2011. Acorns and Bitter Roots: Starch Grain Research in the Prehistoric Eastern Woodlands, Edition. University of Alabama Press, Tuscaloosa, AL.

Metzger, C.A., Terry, J.D.O., Grandstaff, D.E., 2004. Effect of paleosol formation on rare earth element signatures in fossil bone. Geology. 32, 497.

Meyer, M., Kircher, M., Gansauge, M., Li, H., Racimo, F., Mallick, S., Schraiber, J.G., Jay, F., Prüfer, K., de Filippo, C., Sudmant, P.H., Alkan, C., Fu, Q., Do, R., Rohland, N., Tandon, A., Siebauer, M., Green, R.E., Bryc, K., Briggs, A.W., Stenzel, U., Dabney, J., Shendure, J., Kitzman, J., Hammer, M.F., Shunkov, M.V., Derevianko, A.P., Patterson, N., Andrés, A.M., Eichler, E.E., Slatkin, M., Reich, D., Kelso, J., Pääbo, S., 2012. A High-Coverage Genome Sequence from an Archaic Denisovan Individual. Science. 338, 222–226.

Monnier, G.F., Ladwig, J.L., Porter, S.T., 2012. Swept under the rug: the problem of unacknowledged ambiguity in lithic residue identification. Journal of Archaeological Science. 39, 3284–3300.

Monnier, G.F., Hauck, T.C., Feinberg, J.M., Luo, B., Tensorer, J.L., Sakhel, H.A., 2013. A multi-analytical methodology of lithic residue analysis applied to Paleolithic tools from Hummal, Syria. Journal of Archaeological Science. 40, 3722–3739.

Monnier, G., Frahm, E., Luo, B., Missal, K., 2017. Developing FTIR microspectroscopy for analysis of plant residues on stone tools. Journal of Archaeological Science. 78, 158–178.

Monnier, G., Frahm, E., Luo, B., Missal, K., 2017. Developing FTIR Microspectroscopy for the Analysis of Animal-Tissue Residues on Stone Tools. Journal of Archaeological Method and Theory. 25, 1–44.

Moore, M., Sutikna, T., Jatmiko, Morwood, M., Brumm, A., 2009. Continuities in stone flaking technology at Liang Bua, Flores, Indonesia. Journal of Human Evolution. 57, 503–526.

Morley, M.W., Goldberg, P., Sutikna, T., Tocheri, M.W., Prinsloo, L.C., Jatmiko, Saptomo, E.W., Wasisto, S., Roberts, R.G., 2017. Initial micromorphological results from Liang Bua, Flores (Indonesia): Site formation processes and hominin activities at the type locality of Homo floresiensis. Journal of Archaeological Science. 77, 125–142.

Morwood, M.J., 2004. Archaeology and age of a new hominin from Flores in eastern Indonesia. Nature. 431, 1087–1091.

Morwood, M.J., Brown, P., Jatmiko, Sutikna, T., Wahyu Saptomo, E., Westaway, K.E., Awe Due, R., Roberts, R.G., Maeda, T., Wasisto, S., Djubiantono, T., 2005. Further evidence for small-bodied hominins from the Late Pleistocene of Flores, Indonesia. Nature. 437, 1012–1017.

Moskovits, M., 2006.Surface-Enhanced Raman Spectroscopy: a Brief Perspective. In Surface-Enhanced Raman Scattering – Physics and Applications. 1–18

Motoyama, M., 2012. Structure and Phase Characterization of Triacylglycerols by Raman Spectroscopy. Bull NARO Inst Livest Grassl Sci. 12, 19–68.

Odell, G.H., 1975. Microwear in perspective: a sympathetic response to Lawrence H. Keeley. World Archaeology. 7, 226–240.

Odell, G.H., 1996. Stone tools Theoretical insights into Human Prehistory. Plenum Press New york and London.

Olausson, D.S., 1980. Lithic technology. 9(2), 58–60.

Orange, D., Knittle, E., Farber, D., Williams, Q., 1996. Raman spectroscopy of crude oils and hydrocarbon fluid inclusions: A feasibility study. Mineral spectroscopy: A tribute to Roger G.Burns The Geochemical society, Special Publication. 5, 65–82.

Ospitali, F., Smith, D.C., Lorblanchet, M., 2006. Preliminary investigations by Raman microscopy of prehistoric pigments in the wall-painted cave at Roucadour, Quercy, France. Journal of Raman Spectroscopy. 37, 1063–1071.

Owocki, K., Kremer, B., Wrzosek, B., Krolikowska, A., Kazmierczak, J., 2016. Fungal Ferromanganese Mineralisation in Cretaceous Dinosaur Bones from the Gobi Desert, Mongolia. PLoS ONE. 10.1371, e0146293.

Panchuk, K., 2017. Physical Geology, Second Adapted Edition.

Pasteris, J.D., Wopenka, B., Freeman, J.J., Rogers, K., Valsami-Jones, E., van der Houwen, J.A., Silva, M.J., 2004. Lack of OH in nanocrystalline apatite as a function of degree of atomic order: implications for bone and biomaterials. Biomaterials. 25, 229–238.

Patten, A.M., Vassao, D.G., Wolcott, M.P., Davin, L.B., Lewis, N.G., 2010. 3.27 - Trees: A Remarkable Biochemical Bounty. in Comprehensive Natural Products II, Edition (ed.), pp 1173–1296. Elsevier, Oxford.

Pedergnana, A., Olle, A., 2017. Building an Experimental Comparative Reference Collection for Lithic Micro-Residue Analysis Based on a Multi-Analytical Approach. Journal of Archaeological Method and Theory. 25, 117–154.

Pérez-Alonso, M., Castro, M.K., Martinez-Arkarazo, I., Angulo, M., Olazabal, M.A., Madariaga, J.M., 2004. Analysis of bulk and inorganic degradation products of stones, mortars and wall paintings by portable Raman microprobe spectroscopy. Analytical and Bioanalytical Chemistry. 379, 42–50.

Peta, J.J., 2009. A Microstratigraphic Investigation into the Longevity of Archaeological Residues, Sterkfontein, South africa. in Archaeological Science Under a Microscope: Studies in Residue and Ancient DNA Analysis in Honour of Thomas H. Loy, Edition (ed.), pp 29–46. ANU Press.

Pollard, A.M., Heron, C., 1996. Archaeological Chemistry, Edition. Cambridge : Royal Society of Chemistry.

Pozzi, F., Lombardi, J.R., Leona, M., 2013. Winsor & Newton original handbooks: a surface-enhanced Raman scattering (SERS) and Raman spectral database of dyes from modern watercolor pigments. Heritage Science. 1, 1–8.

Pozzi, F., Leona, M., 2016. Surface-enhanced Raman spectroscopy in art and archaeology. Journal of Raman Spectroscopy. 47, 67–77

Prat, S., Brugal, J., Tiercelin, J., Barrat, J., Bohn, M., Delagnes, A., Harmand, S., Kimeu, K., Kibunjia, M., Texier, P., Roche, H., 2005. First occurrence of early Homo in the Nachukui Formation (West Turkana, Kenya) at 2.3-2.4 Myr. Journal of Human Evolution. 49, 230–240.

Prinsloo, L.C., Lyn Wadley, L., Lombard, M., 2014. Infrared reflectance spectroscopy as an analytical technique for the study of residues on stone tools: potential and challenges . Journal of Archaeological Science. 41, 732–739.

Prüfer, K., Racimo, F., Patterson, N., Jay, F., Sankararaman, S., Sawyer, S., Heinze, A., Renaud, G., Sudmant, P.H., de Filippo, C., Li, H., Mallick, S., Dannemann, M., Fu, Q., Kircher, M., Kuhlwilm, M., Lachmann, M., Meyer, M., Ongyerth, M., Siebauer, M., Theunert, C., Tandon, A., Moorjani, P., Pickrell, J., Mullikin, J.C., Vohr, S.H., Green, R.E., Hellmann, I., Johnson, P.L.F., Blanche, H., Cann, H., Kitzman, J.O., Shendure, J., Eichler, E.E., Lein, E.S., Bakken, T.E., Golovanova, L.V., Doronichev, V.B., Shunkov, M.V., Derevianko, A.P., Viola, B., Slatkin, M., Reich, D., Kelso, J., Pääbo, S., 2014. The complete genome sequence of a Neanderthal from the Altai Mountains. Nature. 505, 43–49.

Puceat, E., Reynard, B., Lecuyer, C., 2004. Can crystallinity be used to determine the degree of chemical alteration of biogenic apatites? Chemical Geology. 205, 83–97.

Pye, C.C., Rudolph, W.W., 2003. An ab Initio, Infrared, and Raman Investigation of Phosphate Ion Hydration. The Journal of Physical Chemistry A. 107, 8746–8755.

Ram, M., Dowell, F., Seitz, L., 2003. FT-Raman spectra of unsoaked and NaOH-soaked wheat kernels, bran, and ferulic acid. Cereal Chemistry. 80, 188–192.

Rasmussen, M., Guo, X., Wang, Y., Lohmueller, K.E., Rasmussen, S., Albrechtsen, A., Skotte, L., Lindgreen, S., Metspalu, M., Jombart, T., Kivisild, T., Zhai, W., Eriksson, A., Manica, A., Orlando, L., De La Vega, F.M., Tridico, S., Metspalu, E., Nielsen, K., Avila-Arcos, M.C., Moreno-Mayar, J.V., Muller, C., Dortch, J., Gilbert, M.T.P., Lund, O., Wesolowska, A., Karmin, M., Weinert, L.A., Wang, B., Li, J., Tai, S., Xiao, F., Hanihara, T., van Driem, G., Jha, A.R., Ricaut, F., de Knijff, P., Migliano, A.B., Romero, I.G., Kristiansen, K., Lambert, D.M., Brunak, S., Forster, P., Brinkmann, B., Nehlich, O., Bunce, M., Richards, M., Gupta, R., Bustamante, C.D., Krogh, A., Foley, R.A., Lahr, M.M., Balloux, F., Sicheritz-Ponten, T., Villems, R., Nielsen, R., Wang, J., Willerslev, E., 2011. An Aboriginal Australian Genome Reveals Separate Human Dispersals into Asia. Science (New York, N.Y.). 334, 94–98.

Regert, M., Bland, H.A., Dudd, S.N., Bergen, P.F.V., Evershed, R.P., 1998. Free and Bound Fatty Acid Oxidation Products in Archaeological Ceramic Vessels. Proceedings: Biological Sciences. 265, 2027–2032.

Reich, D., Green, R.E., Kircher, M., Krause, J., Patterson, N., Durand, E.Y., Viola, B., Briggs, A.W., Stenzel, U., Johnson, P.L.F., Maricic, T., Good, J.M., Marques-Bonet, T., Alkan, C., Fu, Q., Mallick, S., Li, H., Meyer, M., Eichler, E.E., Stoneking, M., Richards, M., Talamo, S., Shunkov, M.V., Derevianko, A.P., Hublin, J., Kelso, J., Slatkin, M., Pääbo, S., 2010. Genetic history of an archaic hominin group from Denisova Cave in Siberia. Nature. 468, 1053–1060.

Reich, D., Patterson, N., Kircher, M., Delfin, F., Nandineni, M., Pugach, I., Ko, A., Ko, Y., Jinam, T., Phipps, M., Saitou, N., Wollstein, A., Kayser, M., Pääbo, S., Stoneking, M., 2011.

Denisova Admixture and the First Modern Human Dispersals into Southeast Asia and Oceania. American Journal of Human Genetics. 89, 516–528.

Richardson, D., Richardson, S., 2016 http://www.asiantextilestudies.com.

Rifkin, R., 2015. Pleistocene figurative art mobilier from Apollo 11, southern Namibia. International Journal of Art, Archaeology and Conceptual Anthropology. 9, 97–101.

Robertson, G., Attenbrow, V., Hiscock, P., 2009. Multiple uses for Australian backed artefacts. Antiquity . 83, 296–308.

Roebroeks, W., Sier, M.J., Nielsen, T.K., De Loecker, D., Parés, J.M., Arps, C.E.S., Mucher, H.J., 2012. Use of red ochre by early Neandertals. Proc Natl Acad Sci USA. 109, 1889.

Rots, V., 2010. Prehension and Hafting Traces on Flint Tools: A Methodology. Leuven University Press.

Rots, V., Hayes, E., Cnuts, D., Lepers, C., Fullagar, R., 2016. Making sense of residues on flaked stone artefacts: learning from blind tests. PLOS ONE. 11(3).

Rots, V., Lentfer, C., Schmid, V.C., Porraz, G., Conard, N.J., 2017. Pressure flaking to serrate bifacial points for the hunt during the MIS5 at Sibudu Cave (South Africa). PLOS ONE. 12,e0175151.

Rygula, A., Majzner, K., Marzec, K.M., Kaczor, A., Pilarczyk, M., Baranska, M., 2013. Raman spectroscopy of proteins: a review. Journal of Raman Spectroscopy. 44, 1061–1076.

Sauer, G.R., Zunic, W.B., Durig, J.R., 1994. Fourier transform raman spectroscopy of synthetic and biological calcium phosphates. Calcified Tissue International. 54, 414–420.

Sebela, S., Miler, M., Skobe, S., Torkar, S., Zupan, N., 2015. Characterization of black deposits in karst caves, examples from Slovenia. Facies. 61, 1–13.

Semenov, S.A., 1964. Prehistoric Technology: An Experimental Study of the oldest Tools and Artefacts from traces of Manufacture and Wear. Cory Adams & Mackay, London.

Shafer, H.J., Holloway, R.G., 1979. Organic residue analysis in determining stone tool function. In B. Hayden (Ed.). New york Academic Press.

Shaham, D., Grosman, L., Goren-Inbar, N., 2010. The red-stained flint crescent from Gesher: new insights into PPNA hafting technology. Journal of Archaeological Science. 37, 2010–2016.

Smith, E., Dent, G., 2005. Modern Raman Spectroscopy: A Practical Approach. Edition Wiley.

Solarz, R.W., Paisner, J.A., 1986. Laser Spectroscopy and its Applications. CRC Press.

Solodenko, N., Zupancich, A., Cesaro, S.N., Marder, O., Lemorini, C., Barkai, R., 2015. Fat residue and Use-Wear Found on Acheulian Biface and Scraper associated with Butchered Elephant remains at the Site of Revadim, Israel. Plos one.

Spiro, T.G., Strekas, T.C., 1974. Resonance Raman spectra of heme proteins. Effects of

oxidation and spin state. Journal of American Chemistry Society. 96, 338–345.

Spiro, T.G., 1987. Biological Applications Of Raman Spectroscopy. John Wiley & Sons, New York.

Splitstoser, J.C., Dillehay, T.D., Wouters, J., Claro, A., 2016. Early pre-Hispanic use of indigo blue in Peru. Science Advances. 2.

Stemp, W.J., Stemp, M., 2001. Ubm laser profilometry and lithic use-wear analysis: a variable lengh scale investigation of surface topography. Journal of Archaeological Science. 28(1), 81–88.

Stemp, W.J., Stemp, M., 2003. Documenting stages of polish development on experimental stone tools: surface characterization by fractal geometry using UBM laser profilometry. Journal of Archaeological Science. 30(3), 287–296.

Stephenson, B., 2015. A modified Picro-Sirius Red (PSR) staining procedure with polarization microscopy for identifying collagen in archaeological residues. Journal of Archaeological Science. 61, 235–243.

Sutikna, T., Tocheri, M., Morwood, M.J., Roberts, R.G., 2016. Revised stratigraphy and chronology for Homo floresiensis at Liang Bua in Indonesia. Nature. 532, 366–369.

Takei, T., Kato, N., Iijima, T., Higaki, M., 1995. Raman spectroscopic analysis of wood and bamboo lignin. Mokuzai Gakkaishi. 41, 229–236.

Termine, J.D., Kleinman, H.K., Whitson, S., Conn, K.M., McGarvey, M.L., Martin, G.R., 1981. Osteonectin, a bone-specific protein linking mineral to collagen. Cell. 26, 99–105.

Thomas, D.B., Fordyce, R.E., Frew, R.D., Gordon, K.C., 2007. A rapid, non-destructive method of detecting diagenetic alteration in fossil bone using Raman spectroscopy. Journal of Raman Spectroscopy. 38, 1533–1537.

Thomas, D.B., McGoverin, C.M., Fordyce, R.E., Frew, R.D., Gordon, K.C., 2011. Raman spectroscopy of fossil bioapatite - A proxy for diagenetic alteration of the oxygen isotope composition. Palaeogeography, Palaeoclimatology, Palaeoecology. 310, 62–70.

Tocheri, M., M Orr, C., Larson, S., Sutikna, T., J., Wahyu Saptomo, E., Awe Due, R., Djubiantono, T., J Morwood, M., Jungers, W., 2007. The Primitive Wrist of Homo floresiensis and Its Implications for Hominin Evolution. Science (New York, N.Y.). 317, 1743–1745.

Tolkien, J.R.R., 1937. The Hobbit, Edition London George Allen & Unwin.

Torrence, R., Barton, H., 2006. Ancient Starch Research. Left Coast Press, Walnut Creek, CA.

Tzolov, M.B., Tzenov, N.V., Dimova-Malinovska, D.I., Yankov, D.Y., 1993. Surface enhanced Raman scattering of amorphous silicon-carbon films. Applied Physics Letters. 62, 2396.

Vahur, S., Kriiska, A., Leito, I., 2011. Investigation of the adhesive residue on the flint insert and the adhesive investigation of the adhesive residue on the flint insert and the adhesive lum found from Pulli mesolithic settlement site(Estonia) by micro-ATR-FT-IR spectrometry . Estonian Journal of Archaeology. 15, 3–17.

Valeur, B., Berberan-Santos, M.N., 2012. Molecular Fluorescence: Principles and Applications, Edition. Wiley-VCH.

Vandenabeele, P., Wehling, B., Moens, L., Edwards, H., De Reu, M., Van Hooydonk, G., 2000. Analysis with micro-Raman spectroscopy of natural organic binding media and varnishes used in art. Analytica Chimica Acta. 407, 261–274.

Van Gijn, A.L., 1990. The wear and tear of flint: principles of functional analysis applied to Dutch Neolithic assemblages.

Vasiliev, S.K., Shunkov, M.V., Tsybankov, A.A., 2008. Faunal remains of large mammals from Pleistocene deposits in the East Gallery of Denisova Cave. In Issues on the Archaeology, Ethnography and Anthropology of Siberia and Adjacent Regions 14, 26–31 (in Russian). Institute of Archaeology and Ethnography, Siberian Branch, Russian Academy of Sciences Press, Novosibirsk.

Vasiliev, S.K., Shunkov, M.V., Tsybankov, A.A., 2010. Bone remains of large mammals from Pleistocene deposits in the East Gallery of Denisova Cave (based on materials obtained in 2009–2010). In Issues on the Archaeology, Ethnography and Anthropology of Siberia and Adjacent Regions 16, 28–32 (in Russian). Institute of Archaeology and Ethnography, Siberian Branch, Russian Academy of Sciences Press, Novosibirsk.

Vasiliev, S.K., Shunkov, M.V., Kozlikin, M.B., 2013. Preliminary results on the study of megafaunal remains from Pleistocene deposits in the East Gallery of Denisova Cave. In Issues on the Archaeology, Ethnography and Anthropology of Siberia and Adjacent Regions 19, 32–38 (in Russian). Institute of Archaeology and Ethnography, Siberian Branch, Russian Academy of Sciences Press, Novosibirsk.

Villa Montero, M., 2014. Laser Heating and Destruction of Carbon Nanotubes. 10.13140

Wadley, L., Lombard, M., 2007. Small things in perspective: the contribution of our blind tests to micro-residue studies on archaeological stone tools. Journal of Archaeological Science. 34, 1001–1010.

Wang, A., Haskin, L.A., Lane, A.L., Wdowiak, T.J., Squyres, S.W., Wilson, R.J., Hovland, L.E., Manatt, K.S., Raouf, N., Smith, C.D., 2003. Development of the Mars microbeam Raman spectrometer (MMRS). Journal of Geophysical Research: Planets. 108, n/a-n/a.

Was-Gubala, J., Machnowski, W., 2014. Application of Raman Spectroscopy for Differentiation Among Cotton and Viscose Fibers Dyed with Several Dye Classes. Spectroscopy Letters. 47, 527–535.

Wood, B.R., McNaughton, D., 2002. Raman excitation wavelength investigation of single red blood cells in vivo. Journal of Raman Spectroscopy. 33, 517–523.

Wopenka, B., Pasteris, J.D., 2005. A mineralogical perspective on the apatite in bone. Materials Science and Engineering: C. 25, 131–143.

Xhauflair, H., Pawlik, A., Forestier, H., Saos, T., Dizon, E., Gaillard, C., 2016. Use-related or contamination? Residue and use-wear mapping on stone tools used for experimental processing of plants from Southeast Asia. Quaternary International. 10.1016.

“In a hole in the ground there lived a hobbit. Not a nasty, dirty, wet hole, filled with the ends of worms and an oozy smell, nor yet a dry, bare, sandy hole with nothing in it to sit down on or to eat: it was a hobbit-hole, and that means comfort.”

(Tolkien, 1937)

Appendix I material references

Table 1: Typical Raman bands position and other spectral characteristics of different apatite macro-samples, artefacts and micro-residues (on artefact or in sediment) encountered in this study (variation range indicated when observed).

Sample/Micro-residue	*v*2 mode position (cm^{-1})	*v*4 mode position (cm^{-1})	Presence of additionnal manganese band (Mn_3O_4)	*v*1 mode position (cm^{-1})	*v*1 mode FWHM (Full Width at Half Maximum) (cm^{-1})	Carbonate band position, if present (cm^{-1})	Rare earth fluorescence bands maximum, if present (nm)
Geological apatite rock sample	435	588		968	10		566, 596 (Sm^{3+}), 588, 620 (Eu^{3+}), 856, 868, 871, 877, 882, 893, 898, 905, 912, 1055, 1063, 1070 (Nd^{3+})
Geological apatite rod shaped micro-residues found on LB337 (Bordes et al., 2017)	434	593		968	11		566, 600, 645 (Sm^{3+}), 620 (Eu^{3+}) (Nd^{3+} range - not probed)
Geological apatite micro-residues found on DC1	435	594		970	10		566, 599, 645 (Sm^{3+}), 620 (Eu^{3+}) (Nd^{3+} range - not probed)
Dry modern bone exposed sample	437	590		963	21	1077	
Dry modern bone exposed heated 300-500 ºC sample	433-436	584-588		953	22-27		
Dry modern bone exposed heated 700 ºC sample	435	593		965	12	1079	
Denisova (altered) bone apatite micro-residues	431-433	589-595	655-670	947-959	20-35		
DC66 Denisova bone artefact (altered surface)	431-436	582-597	667	947-956	22-30		
Prehistoric deer bone sample (Europe) dated from 10 ka (altered bone)	430-434	585-587	660	954	28-31		
Prehistoric deer bone sample (Europe), dated from 10 ka (mineralised/fossil)	435-436	587-592		965	18-21	1075-1077	
Liang Bua bones macro sample ramidae (frogs), with rare earth fluorescence	436	592		967	18	1076	579 (Dy^{3+}), 588, 592, 596, 643, 651 (Sm^{3+}), 614, 617, 687, 698 (Eu^{3+}), 867, 873, 883, 893, 904, 1057,1066 (Nd^{3+})
Liang Bua bones macro sample ramidae (frogs), muridae (rats), megachiroptera (flying foxes), without rare earth fluorescence	434-439	587-593		966	18-19	1074-1078	
Mastodont bone fossil macro sample, dated from 130 ka (mineralised/fossil)	437	593		967	19	1078	573 (Dy^{3+}), 600 (Sm^{3+}), 607, 622 (Eu^{3+}), 856, 884, 893, 898, 912,1063 (Nd^{3+})
Mastodont bone fossil macro sample, dated from 130 ka (altered bone)	435	586	660	959	25		
Liang bua bone (mineralised/fossil) micro-residues	433-442	589-594		960-968	17-20	1075-1080	578 (Dy^{3+}), 588, 592, 596-597, 634, 643 (Sm^{3+}), 612, 614, 616, 619, 686-687, 697-698 (Eu^{3+}), 866, 872-876, 882-883, 893-894, 904,1055, 1064-1065 (Nd^{3+})
Liang bua altered bone micro-residues	429-439	580-589	660-670	946-953	24-35		

Table 2: List of chemical references.
Lipids
Alaetic acid
5-cholesten-3one
5alpha-cholestan-3beta-ol
7-dehydrocholesterol
Arachidonic acid
Behenic acid
Betulin
Betulinic acid
Calcium palmitate
Cholesterol
Decanoic acid
Elaidic acid
Ergosterol
Linoleic acid
Linoleic acid, 10E, 12Z
Linoleic acid, 9Z, 11E
Myristic acid
Nonadecanoic acid
Octale acid
Oleanolic acid
Oleic acidpalmiric acid
Pentadecanoic acid
Stearic acid
Tannic acid
Trygliceryl tripalmitate
Vaccenic acid
Dye
Crystal violet
Gallic acid
Indigo
Indirubin
Kaempferol

Table 3: Summary of modern materials analysed in Raman spectroscopy.	
Designation	**Material analysed**
Black modern paint XY stage	Dye
Black pen ink	Dye
Blue pen ink	Dye
Blue gloves	Nitrile
Epoxy resin	Resin
Jean white cotton	Cellulose + lignin
Jean blue fibre	Indigo dye
Blue paste	Calcite + lipids
Epoxy resin	Resin
Parafilm	Lipids
Plastic bag	Polymer
Plastic box	Polymer
Polyester fibre	Polyester
Gloves fibre (russian)	Dye
Wrapping plastic film	Polymer

Table 4: Summary of natural materials analysed in Raman spectroscopy.		
Designation	**Genus/Specie**	**Material analysed**
Tooth	Possum	Apatite
Dry bone	Unknown animal	Apatite + collagen
Dry bamboo	Unknown	Cellulose + lignin
Black dry bamboo	Unknown	Cellulose + lignin
Pine	Unknown	Cellulose + lignin
Mulga wood	*Acacia aneura*	Cellulose + lignin
Callitris dark resin	*Callitris glaucophylla*	Diterpenic resin
Callitris light resin	*Callitris glaucophylla*	Diterpenic resin
Callitris resin	*Callitris rhombodia*	Diterpenic resin
Blue flax lily fruit	*Dianella caerulea*	Dye
Viola flower	*Violacea*	Dye
Strelitzia flower	*Strelitzia*	Dye
Pure beewax	NA	Fatty acid
South african gum	Unknown	Gum
Eucalyptus	*Angophora costata*	Kino
Eucalyptus Resin	*Corymbia watsonia*	Kino
Eucalyptus Resin	*Eucalyptus blaxlandii*	Kino
Human blood	NA	Haemoglobin
White egg	Hen	Protein
Pork fat	Pork	Protein + Lipids
Bunya pine resin	*Araucaria bidwilii*	Resin
Pine resin	Unknown	Resin
Xanthorrea	*Xanthorrea quadrangulata*	Resin
Araucaria resin	*Araucaria cunninghamii*	Triterpenic resin
Spinifex	*Trioda pungens*	Triterpenic resin
Spinifex	*Trioda pungens*	Starch grain
Amber	Amber(East coast of England)	Resin

Appendix IIa results tables

Table 1: Results for use-wear optical analysis and Raman analysis for Denisova Cave stone artefacts.							
			Micro-residues analysis by Raman microscopy			VLM use-wear analysis	
Artefact	**Layer**	**Age (ka)**	**Artefact class**	**Significant residues (use-related in bold)**	**Residue origin**	**Task**	**Optical microscopy** **Material worked**
DC36	11.1	120 - 38	Retouched flake	Nd	NA	Uncertain	Flesh and bone
DC37	11.2	120 - 38	Retouched flake	Nd	NA	Uncertain	Animal, cf. antler?
DC1	11.4	120 - 38	Retouched flake	Nd	NA	Uncertain	animal
DC2	11.4	120 - 38	Flake	**SFA**	Animal fat	Cutting	animal
DC4	11.4	120 - 38	Flake	**SFA/UFA**	Animal fat, possibly deer fat	Scraping, Cutting	Uncertain
DC12	11.4	120 - 38	Flake	**SFA**	Animal fat	Scraping	Uncertain
DC13	11.4	120 - 38	Retouched flake	**SFA/UFA**	Animal fat, possibly deer fat	Scraping	Animal, cf. skin
DC39	11.4	120 - 38	Flake	**SFA/UFA**	Animal fat, possibly deer fat	Cutting	Flesh and bone
DC42	12.2	259 - 129	Retouched flake	Nd	NA	Uncertain	None
DC52	12.2	259 - 129	NDA	Nd	NA	Uncertain	None
DC43	12.3	259 - 129	Kombewa flake	Nd	NA	Uncertain	Flesh and bone
DC45	12.3	259 - 129	Retouched flake	Nd	NA	Scraping	Flesh and bone
DC5	13	259 - 129	Retouched flake	Nd	NA	Uncertain	Flesh and bone
DC14	13	259 - 129	NDA	Nd	NA	Not used	None
DC26	13	259 - 129	Split flake	**SFA**	Animal fat	Scraping, Cutting	Uncertain
DC27	13	259 - 129	Retouched flake	**SFA**	Animal fat	Scraping, Cutting	Flesh and bone
DC30	13	259 - 129	Flake	Nd	NA	Not used	Uncertain
DC11	15	259 - 129	Retouched flake	**SFA/UFA**	Animal fat, possibly deer fat	Scraping, Cutting	Flesh and bone
DC22*	15	259 - 129	NDA	Nd	NA	Uncertain	None
DC23	15	259 - 129	NDA	Nd	NA	Uncertain	None
DC25*	15	259 - 129	Flake	Nd			None
			NA: non applicable				**Nd: Not determined**

Table 2: List of analysed micro-residues in Raman spectroscopy for Denisova Cave stone artefact collection.

Artefact	Micro-residues designation	Analysed material	Number analysed	Relative occurrence	Washed sediment after first cleaning	Washed sediment after second cleaning	Layer (outer) sediment	Concentrated/Group /Isolated	Correlation with polish	Micro-residues interpretation
DC1										
Washed sample	Smeared altered bone apatite	Apatite (disordered)	NA	Widespread	Very common	Widespread	Widespread	Concentrated & group	No	Part of sediment
	Altered bone apatite	Apatite (disordered)	NA	Widespread	Very common	Widespread	Widespread	Concentrated & group	No	Part of sediment
	Geological apatite	Apatite (disordered)	1	Rare	No	No	No	Isolated	NA	Unknown
	Protein	Protein	1	Rare	No	No	No	Isolated	NA	Unknown
DC2										
Unwashed sample										
	Smeared altered bone apatite	Apatite (disordered)	NA	Widespread	Very common	Widespread	Widespread	Concentrated & group	No	Part of sediment
	Altered bone apatite	Apatite (disordered)	NA	Widespread	Very common	Widespread	Widespread	Concentrated & group	No	Part of sediment
	Graphite	Graphite	1	Rare	No	No	No	Isolated	NA	Unknown
	Blue Dyed fibre	Dye	1	Rare	No	No	No	Isolated	NA	Modern contamination
	KNO_3	KNO_3	1	Rare	No	No	No	Isolated	NA	Unknown
DC2										
Washed sample	Smeared altered bone apatite	Apatite (disordered)	NA	Widespread	Very common	Widespread	Widespread	Concentrated & group	No	Part of sediment
	Altered bone apatite	Apatite (disordered)	NA	Widespread	Very common	Widespread	Widespread	Concentrated & group	No	Part of sediment
	SFA	SFA	23	Common	No	No	No	Concentrated & group	Yes	**use-related**
	Smeared SFA	SFA	14	Common	No	No	No	Concentrated & group	Yes	**use-related**
	Protein	Protein	6	Uncommon	No	No	No	Isolated	Yes	Unknown
	Starch grain	Starch	3	Uncommon	No	No	No	Isolated	No	Unknown
	Plant fibre, lignin content	Cellulose + lignin	2	Uncommon	No	No	No	Isolated	No	Unknown
	Graphite	Graphite	1	Rare	No	No	No	Isolated	NA	Unknown
	Cellulose fibre*	Cellulose	1	Rare	No	No	No	Isolated	NA	Modern contamination
	Plastic box*	Plastic	1	Rare	No	No	No	Isolated	NA	Modern contamination
	Polyester*	Polyester	1	Rare	No	No	No	Isolated	NA	Modern contamination
DC4										
Washed sample	Smeared altered bone apatite	Apatite (disordered)	NA	Widespread	Very common	Widespread	Widespread	Concentrated & group	No	Part of sediment
	Altered bone apatite	Apatite (disordered)	NA	Widespread	Very common	Widespread	Widespread	Concentrated & group	No	Part of sediment
	UFA	Mix of SFA/UFA	52	Common	No	No	No	Concentrated & group	Yes	**use-related**
	Smeared UFA	Mix of SFA/UFA	43	Common	No	No	No	Concentrated & group	Yes	**use-related**
	Protein	Protein	16	Uncommon	No	No	No	Isolated		

	Geological apatite	Apatite (geologic)	3	Uncommon	No	No	No	Isolated	Yes	Unknown
	Graphite	Graphite	2	Uncommon	No	No	No	Isolated	Yes	Unknown
	Starch grain	Starch	1	Rare	No	No	No	Isolated	NA	Unknown
	Blue glove*	Nitrile	1	Rare	No	No	No	Isolated	NA	Modern contamination
DC5										
Washed sample	Smeared bone apatite	Apatite (disordered)	NA	Widespread	Very common	Widespread	Widespread	Concentrated & group	No	Part of sediment
	Bone Apatite	Apatite (disordered)	NA	Widespread	Very common	Widespread	Widespread	Concentrated & group	No	Part of sediment
Artefact	**Micro-residues designation**	**Analysed material**	**Number analysed**	**Relative occurrence**	**Washed sediment after first cleaning**	**Washed sediment after second cleaning**	**Layer (outer) sediment**	**Concentrated/Group /Isolated**	**Correlation with polish**	**Micro-residues interpretation**
DC11										
Washed sample	Smeared altered bone apatite	Apatite (disordered)	NA	Widespread	Very common	Widespread	Widespread	Concentrated & group	No	Part of sediment
	Altered bone apatite	Apatite (disordered)	NA	Widespread	Very common	Widespread	Widespread	Concentrated & group	No	Part of sediment
	UFA	Mix of SFA/UFA	5	Uncommon	No	No	No	Concentrated	Yes	**use-related**
	Protein	Protein	2	Uncommon	No	No	No	Isolated	Yes	Unknown
DC12										
Unwashed sample	Plant fibre, lignin content	Cellulose + lignin	2	Uncommon	No	No	No	Isolated		
	Plant fibre, lignin content + carotenoid + $Ca(NO_3)_2$	Cellulose + lignin + carotenoid + $Ca(NO_3)_2$	2	Uncommon	No	No	No	Isolated		
	Dark synthetic glove fibre*	Dye	1	Rare	No	No	No	Isolated	NA	Modern contamination
DC12										
Washed sample	Smeared altered bone apatite	Apatite (disordered)	NA	Widespread	Very common	Widespread	Widespread	Concentrated & group	No	Part of sediment
	Altered bone apatite	Apatite (disordered)	NA	Widespread	Very common	Widespread	Widespread	Concentrated & group	No	Part of sediment
	Smeared SFA	SFA	29	Common	No	No	No	Concentrated & group	Yes	**use-related**
	SFA	SFA	6	Uncommon	No	No	No	Isolated	Yes	**use-related**
	Protein	Protein	4	Uncommon	No	No	No	Isolated	No	Unknown
	Graphite	Graphite	2	Uncommon	No	No	No	Isolated	No	Unknown
	Starch grain	Starch	2	Uncommon	No	No	No	Isolated	No	Unknown
	Plant fibre, lignin content	Cellulose + lignin	2	Uncommon	No	No	No	Isolated	No	Unknown
	Dyed plant fibre*	Dye	1	Rare	No	No	No	Isolated	NA	Modern contamination
	Plant fiber with indigo Dye*	Indigo	1	Rare	No	No	No	Isolated	NA	Modern contamination
DC13										
Washed sample	Smeared altered bone apatite	Apatite (disordered)	NA	Widespread	Very common	Widespread	Widespread	Concentrated & group	No	Part of sediment
	Altered bone apatite	Apatite (disordered)	NA	Widespread	Very common	Widespread	Widespread	Concentrated & group	No	Part of sediment
	UFA	Mix of SFA/UFA	15	Uncommon	No	No	No	Concentrated &	Yes	**use-**

								group		**related**
	Smeared UFA	Mix of SFA/UFA	18	Uncommon	No	No	No	Concentrated & group	Yes	**use-related**
	Protein	Protein	2	Uncommon	No	No	No	Isolated	Yes	Unknown
	FA fibre	Mix of SFA/UFA	1	Rare	No	No	No	Isolated	NA	**use-related**
DC14										
Unwashed sample	Smeared altered bone apatite	Apatite (disordered)	NA	Widespread	Very common	Widespread	Widespread	Concentrated & group	No	Part of sediment
	Altered bone apatite	Apatite (disordered)	NA	Widespread	Very common	Widespread	Widespread	Concentrated & group	No	Part of sediment
DC14										
Washed sample	Smeared altered bone apatite	Apatite (disordered)	NA	Widespread	Very common	Widespread	Widespread	Concentrated & group	No	Part of sediment
	Altered bone apatite	Apatite (disordered)	NA	Widespread	Very common	Widespread	Widespread	Concentrated & group	No	Part of sediment
	Protein	Protein	1	Rare	No	No	No	Isolated	NA	Unknown
	Plant fibre, lignin content	Cellulose + lignin	1	Rare	No	No	No	Isolated	NA	Unknown
	Dark Plant fibre, fluorescent Dye*	Dye	1	Rare	No	No	No	Isolated	NA	Modern contamination
Artefact	**Micro-residues designation**	**Analysed material**	**Number analysed**	**Relative occurrence**	**Washed sediment after first cleaning**	**Washed sediment after second cleaning**	**Layer (outer) sediment**	**Concentrated/Group /Isolated**	**Correlation with polish**	**Micro-residues interpretation**
DC22										
Unwashed sample										
	Filaments of protein (Biofilm)	Protein	NA	Widespread	No	No	No	Concentrated & group	No	post-depositional process
	Smeared altered bone apatite	Apatite (disordered)	NA	Widespread	Very common	Widespread	Widespread	Concentrated & group	No	Part of sediment
	Altered bone apatite	Apatite (disordered)	NA	Widespread	Very common	Widespread	Widespread	Concentrated & group	No	Part of sediment
	Protein	Protein	1	Rare	No	No	No	Isolated	NA	Unknown
	Plant fibre, lignin content	Cellulose+lignin	1	Rare	No	No	No	Isolated	NA	Unknown
DC22										
Washed sample	Smeared altered bone apatite	Apatite (disordered)	NA	Widespread	Very common	Widespread	Widespread	Concentrated & group	No	Part of sediment
	Altered bone apatite	Apatite (disordered)	NA	Widespread	Very common	Widespread	Widespread	Concentrated & group	No	Part of sediment
	Goethite	Goethite	NA	Very common	No	No	No	Concentrated & group	No	Natural occurrence on rock surface
	Graphine	Carbon	1	Rare	No	No	No	Isolated	NA	Unknown
DC23										
Washed sample	Smeared altered bone apatite	Apatite (disordered)	NA	Widespread	Very common	Widespread	Widespread	Concentrated & group	No	Part of sediment
	Altered bone apatite	Apatite (disordered)	NA	Widespread	Very common	Widespread	Widespread	Concentrated & group	No	Part of sediment
DC25										
Washed sample	Smeared altered bone apatite	Apatite (disordered)	NA	Widespread	Very common	Widespread	Widespread	Concentrated & group	No	Part of sediment
	Altered	Apatite	NA	Widespread	Very	Widespread	Widespread	Concentrated &	No	Part of

	bone apatite	(disordered)			common		d	group		sediment
DC26										
Washed sample	Smeared altered bone apatite	Apatite (disordered)	NA	Widespread	Very common	Widespread	Widespread	Concentrated & group	No	Part of sediment
	Altered bone apatite	Apatite (disordered)	NA	Widespread	Very common	Widespread	Widespread	Concentrated & group	No	Part of sediment
	Smeared SFA	SFA	12	Uncommon	No	No	No	Concentrated & group	Yes	**use-related**
	Plant fibre, lignin content	Cellulose + lignin	1	Rare	No	No	No	Isolated	NA	Unknown
	Protein	Protein	1	Rare	No	No	No	Isolated	NA	Unknown
DC27										
Washed sample	Smeared altered bone apatite	Apatite (disordered)	NA	Widespread	Very common	Widespread	Widespread	Concentrated & group	No	Part of sediment
	Altered bone apatite	Apatite (disordered)	NA	Widespread	Very common	Widespread	Widespread	Concentrated & group	No	Part of sediment
	Gypsum	Gypsum	NA	Rare	No	No	No	Isolated	No	Unknown
	Smeared SFA	SFA	12	Uncommon	No	No	No	Concentrated & group	Yes	**use-related**
	Haematite	Haematite	2	Uncommon	No	No	No	Isolated	Yes	Unknown
	Plant fibre, lignin content	Cellulose + lignin	1	Rare	No	No	No	Isolated	NA	Unknown
	Protein	Protein	1	Rare	No	No	No	Isolated	NA	Unknown
	Starch grain	Starch	1	Rare	No	No	No	Isolated	NA	Unknown
Artefact	**Micro-residues designation**	**Analysed material**	**Number analysed**	**Relative occurrence**	**Washed sediment after first cleaning**	**Washed sediment after second cleaning**	**Layer (outer) sediment**	**Concentrated/Group /Isolated**	**Correlation with polish**	**Micro-residues interpretation**
DC30										
Washed sample	Smeared altered bone apatite	Apatite (disordered)	NA	Widespread	Very common	Widespread	Widespread	Concentrated & group	No	Part of sediment, post-depositional
	Altered bone apatite	Apatite (disordered)	NA	Widespread	Very common	Widespread	Widespread	Concentrated & group	No	Part of sediment, post-depositional
DC32 Non artefact										
	Smeared altered bone apatite	Apatite (disordered)	NA	Widespread	Very common	Widespread	Widespread	Concentrated & group	No	Part of sediment, post-depositional
	Altered bone apatite	Apatite (disordered)	NA	Widespread	Very common	Widespread	Widespread	Concentrated & group	No	Part of sediment, post-depositional
	Plant fibre, lignin content	Cellulose + lignin	1	Rare	No	No	No	Isolated	NA	Unknown
DC36										
Washed sample	Smeared altered bone apatite	Apatite (disordered)	NA	Widespread	Very common	Widespread	Widespread	Concentrated & group	No	Part of sediment, post-depositional
	Altered bone apatite	Apatite (disordered)	NA	Widespread	Very common	Widespread	Widespread	Concentrated & group	No	Part of sediment, post-depositional

	Dark Plant fibre, fluorescent Dye*	Dye	1	Rare	No	No	No	Isolated	NA	Modern contamination
DC37										
Unwashed sample	Filaments of protein (Biofilm)	UOM	NA	Widespread	No	No	No	Concentrated & group		post-depositional process
DC37										
Washed sample	Smeared altered bone apatite	Apatite (disordered)	NA	Widespread	Very common	Widespread	Widespread	Concentrated & group	No	Part of sediment, post-depositional
	Altered bone apatite	Apatite (disordered)	NA	Widespread	Very common	Widespread	Widespread	Concentrated & group	No	Part of sediment, post-depositional
	Graphite	Graphite	1	Rare	No	No	No	Isolated	NA	Unknown
DC39										
Washed sample	Smeared altered bone apatite	Apatite (disordered)	NA	Widespread	Very common	Widespread	Widespread	Concentrated & group	No	Part of sediment, post-depositional
	Altered bone apatite	Apatite (disordered)	NA	Widespread	Very common	Widespread	Widespread	Concentrated & group	No	Part of sediment, post-depositional
	Protein	Protein	14	Uncommon	No	No	No	Concentrated & group	Yes	Unknown
	UFA	Mix of SFA/UFA	9	Uncommon	No	No	No	Concentrated & group	Yes	**use-related**
	Smeared UFA	Mix of SFA/UFA	2	Uncommon	No	No	No	Isolated	Yes	**use-related**
	Plant fibre, lignin content	Cellulose + lignin	1	Rare	No	No	No	Isolated	NA	Unknown
	Geological apatite	Apatite (geologic)	1	Rare	No	No	No	Isolated	NA	Unknown
DC42										
Washed sample	Smeared altered bone apatite	Apatite (disordered)	NA	Widespread	Very common	Widespread	Widespread	Concentrated & group	No	Part of sediment, post-depositional
	Altered bone apatite	Apatite (disordered)	NA	Widespread	Very common	Widespread	Widespread	Concentrated & group	No	Part of sediment, post-depositional
	Bitumen	bitumen	NA	Widespread	No	No	No	Concentrated & group	No	**Unknown**
DC43										
Unwashed sample	Filaments of protein (Biofilm)	Protein	NA	Widespread	No	No	No	Concentrated & group	No	post-depositional process in situ
DC43										
Washed sample	Smeared altered bone apatite	Apatite (disordered)	NA	Widespread	Very common	Widespread	Widespread	Concentrated & group	No	Part of sediment, post-depositional
	Altered bone apatite	Apatite (disordered)	NA	Widespread	Very common	Widespread	Widespread	Concentrated & group	No	Part of sediment, post-depositional

	Graphite	Graphite	1	Rare	No	No	No	Isolated	NA	Unknown
	Haematite	Haematite	NA	Rare	No	No	No	Isolated	No	Unknown
	Plastic box*	Plastic	1	Rare	No	No	No	Isolated	NA	Modern contamination
	Dark Plant fibre, fluorescent Dye*	Dye	1	Rare	No	No	No	Isolated	NA	Modern contamination
DC45										
Washed sample	Smeared altered bone apatite	Apatite (disordered)	NA	Widespread	Very common	Widespread	Widespread	Concentrated & group	No	Part of sediment, post-depositional
	Altered bone apatite	Apatite (disordered)	NA	Widespread	Very common	Widespread	Widespread	Concentrated & group	No	Part of sediment, post-depositional
	Protein	Protein	3	Uncommon	No	No	No	Isolated	No	Unknown
	Plant fibre, lignin content	Cellulose + lignin	2	Uncommon	No	No	No	Isolated	No	Unknown
	Protein + $Ca(NO_3)_2$	Protein + $Ca(NO_3)_2$	1	Rare	No	No	No	Isolated	NA	Unknown
DC52										
Unwashed sample	Filaments of protein (Biofilm)	Protein	NA	Widespread	NA	NA	NA	Concentrated & group	NA	post-depositional process
	Smeared altered bone apatite	Apatite (disordered)	NA	Widespread	Very common	Widespread	Widespread	Concentrated & group	No	Part of sediment, post-depositional
	Altered bone apatite	Apatite (disordered)	NA	Widespread	Very common	Widespread	Widespread	Concentrated & group	No	Part of sediment, post-depositional
	Protein	Protein	2	Uncommon	No	No	No	Isolated	No	Unknown
	SFA	SFA	2	Uncommon	No	No	No	Isolated	No	Unknown
	Iron oxide “metallic aspect” *	Haematite + UOM	1	Rare	No	No	No	Isolated	NA	Modern contamination
	*** Matching a modern contaminant**	**NA: Non applicable**	**UOM : Undetermined organic material**		**NC : Not counted**					

Table 3: List of analysed micro-residues in Raman spectroscopy for Liang Bua stone artefact 2004 collection.

Artefact	Micro-residues designation	Analysed material	Number analysed	Relative occurrence	Washed sediment after first cleaning	Washed sediment after second cleaning	Layer (outer) sediment	Concentrated/Group /Isolated	Correlation with polish	Micro-residues interpretation
LB182										
Unwashed sample	Black iron oxides	Haematite + Maghemite + UOM	NC	Widespread	Uncommon	Uncommon	Uncommon	Isolated	No	Part of sediment
LB182										
Washed sample	SFA + protein + $Ca(NO_3)_2$	SFA + protein + $Ca(NO_3)_2$	11	Uncommon	No	No	No	Isolated	Yes	**Possibly use-related**
	Protein + $Ca(NO_3)_2$	Protein + $Ca(NO_3)_2$	8	Uncommon	No	No	No	Isolated	No	Unknown
	Protein	Protein	7	Uncommon	No	No	No	Isolated	No	Unknown
	SFA	SFA	7	Uncommon	No	Uncommon	No	Concentrated	Yes	**Possibly use-related**
	SFA + protein	SFA + protein	2	Uncommon	No	Uncommon	No	Isolated	Yes	**Possibly use-related**
	Plant material or fibre, lignin content	Cellulose + lignin	1	Rare	No	Uncommon	No	Isolated	NA	**Possibly use-related**
	Plant material or fibre, lignin content + $Ca(NO_3)_2$	Cellulose + lignin + $Ca(NO_3)_2$	1	Rare	No	No	No	Isolated	NA	**Possibly use-related**
LB228										
Unwashed sample	Carbonate grain	Calcium Carbonate	NC	Uncommon	Uncommon	NA	Uncommon	Isolated	No	Part of sediment
	Charcoal	Carbon	NC	Uncommon	Uncommon	NA	Uncommon	Isolated	No	Part of sediment
	Washed sample									
	Black iron oxides	Haematite + Maghemite + UOM	NC	Uncommon	Uncommon	NA	Uncommon	Isolated	No	Part of sediment
	Protein	Protein	26	Uncommon	Uncommon	NA	No	Isolated	No	Unknown
	Protein + $Ca(NO_3)_2$	Protein + $Ca(NO_3)_2$	6	Uncommon	No	NA	No	Isolated	No	Unknown
	SFA	SFA	3	Uncommon	No	NA	No	Isolated	No	Unknown
	SFA + protein + $Ca(NO_3)_2$	SFA + protein + $Ca(NO_3)_2$	2	Uncommon	No	NA	No	Isolated	No	Unknown
	Bone little fragment	Bone apatite	1	Rare	No	NA	No	Isolated	NA	Unknown
	Patch of dark dropplet*	Crystal violet (pen ink)	1	Rare	No	NA	No	Concentrated & group	NA	Modern contamination
LB250										
Unwashed sample	Charcoal	Carbon	NC	Uncommon	Uncommon	No	Uncommon	Isolated	No	Part of sediment
	Biofilm	UOM	NC	Widespread	common	No	Uncommon	Concentrated & group	No	post-depositional
LB250										
Washed sample	Manganese oxide	MnO_2	NC	Widespread	Uncommon	No	NA	Concentrated & group	No	post-depositional
	Protein	Protein	12	Uncommon	No	Uncommon	No	Concentrated	Yes	**Possibly use-related**

	SFA	SFA	11	Uncommon	No	Uncommon	No	Concentrated	Yes	**Possibly use-related**
	Protein + $Ca(NO_3)_2$	Protein + $Ca(NO_3)_2$	10	Uncommon	No	No	No	Concentrated	Yes	**Possibly use-related**
	SFA + protein + $Ca(NO_3)_2$	SFA + protein + $Ca(NO_3)_2$	6	Uncommon	No	No	No	Concentrated	Yes	**Possibly use-related**
	Organic coated iron hydroxide/oxide “metallic aspect”*	Haematite + UOM	1	Rare	No	No	No	Concentrated & group	NA	Modern contamination
	Plant material or fibre, lignin content	Cellulose + lignin	1	Rare	No	No	No	Isolated	NA	Unknown
	SFA smeared area	SFA	1	Rare	No	No	No	Isolated	NA	**Possibly use-related**
Artefact	**Micro-residues designation**	**Analysed material**	**Number analysed**	**Relative occurrence**	**Washed sediment after first cleaning**	**Washed sediment after second cleaning**	**Layer (outer) sediment**	**Concentrated/Group /Isolated**	**Correlation with polish**	**Micro-residues interpretation**
LB45										
Unwashed sample	Biofilm	Unknown organic material	NC	Widespread	No	No	NA	Concentrated & group	No	post-depositional
	Charcoal	Carbon	NC	Widespread	No	No	NA	Concentrated & group	No	Unknown
LB45							NA			
Washed sample	Manganese oxide	MnO_2	NC	Widespread	Uncommon	No	NA	Concentrated & group	No	post-depositional
	Protein	Protein	8	Uncommon	No	No	NA	Isolated	Yes	**Possibly use-related**
	Protein + $Ca(NO_3)_2$	Protein + $Ca(NO_3)_2$	6	Uncommon	No	No	NA	Isolated	Yes	**Possibly use-related**
	SFA	SFA	4	Uncommon	No	No	NA	Concentrated	Yes	**Possibly use-related**
	Plant material or fibre, lignin content	Cellulose + lignin	2	Uncommon	No	No	NA	Isolated	Yes	**Possibly use-related**
	SFA + protein	SFA + protein	2	Uncommon	No	No	NA	Isolated	Yes	**Possibly use-related**
	SFA + protein + $Ca(NO_3)_2$	SFA + protein + $Ca(NO_3)_2$	2	Uncommon	No	No	NA	Isolated	Yes	**Possibly use-related**
	Organic coated iron hydroxide/oxide “metallic aspect”*	Haematite + UOM	1	Rare	No	No	NA	Concentrated & group	NA	Modern contamination
	Plant material or fibre, lignin content + $Ca(NO_3)_2$	Cellulose + lignin + $Ca(NO_3)_2$	1	Rare	No	No	NA	Isolated	NA	**Possibly use-related**
LB337										
Unwashed sample	Biofilm	UOM	NC	Widespread	common	No	NA	Concentrated & group	No	post-depositional
	Manganese oxide	MNo2	NC	Widespread	Uncommon	Uncommon	NA	Concentrated & group	No	post-depositional
LB337										

Washed sample	Protein	Protein	16	Uncommon	No	No	NA	Concentrated	No	**Possibly use-related**
	SFA	SFA	14	Uncommon	No	No	NA	Concentrated	Yes	**Possibly use-related**
	Protein + $Ca(NO_3)_2$	Protein + $Ca(NO_3)_2$	4	Uncommon	No	No	NA	Isolated	No	Unknown
	Apatite rod	Geologic apatite	2	Uncommon	common	common	NA	X	No	Unknown
	SFA + protein	SFA + protein	1	Rare	No	No	NA	X	NA	**Possibly use-related**
	SFA + protein + $Ca(NO_3)_2$	SFA + protein + $Ca(NO_3)_2$	1	Rare	No	No	NA	X	NA	**Possibly use-related**
	Starch grain	Starch	1	Rare	No	No	NA	X	NA	Unknown
	*** Matching a modern contaminant**	**NA: Non applicable**	**UOM : Undetermined organic material**		**NC : Not counted**					

Table 4: List of analysed micro-residues in Raman spectroscopy for Liang Bua stone artefact 2015 collection.

Artefact	Micro-residues designation	Analysed material	Number analysed	Relative occurrence	Washed sediment after first cleaning	Washed sediment after second cleaning	Layer (outer) sediment	Concentrated/Group /Isolated	Correlation with polish	Micro-residues interpretation
LB4340										
Unwashed sample	Charcoal	Carbon	10	Common	No	No	No	Concentrated & group	Yes	**use-related**
	Plant material or fibre, lignin content	Cellulose + lignin	3	Uncommon	No	Uncommon	No	Isolated	No	Possibly incidental
	Organic coated iron hydroxide/oxide “metallic aspect”*	Haematite + UOM	2	Uncommon	No	No	No	Concentrated & group	No	Modern contamination
	Protein	Protein	2	Uncommon	No	No	No	Isolated	Yes	Unknown
	SFA	SFA	2	Uncommon	No	No	No	Isolated	Yes	**Possibly use-related**
	Starch grain	Starch	1	Rare	No	No	No	Isolated	NA	Unknown
LB4340										
Washed sample	Black iron oxides	Haematite + Maghemite + UOM	NC	Uncommon	No	Uncommon	Uncommon	group	No	From sediment
	Charcoal	Carbon	18	Common	No	No	No	Concentrated & group	Yes	**use-related**
	Organic coated iron hydroxide/oxide “metallic aspect”*	Haematite+UOM	14	Common	No	No	No	Concentrated & group	No	Modern contamination
	Protein	Protein	5	Uncommon	No	Uncommon	No	Isolated	Yes	**Possibly use-related**
	Blue dark grain*	Crystal violet(pen ink)	4	Uncommon	No	No	No	group	Yes	Modern contamination
	Potassium Nitrate	KNO_3	4	Uncommon	No	No	No	Isolated	Yes	Unknown
	Protein + $Ca(NO_3)_2$	Protein + $Ca(NO_3)_2$	4	Uncommon	No	No	No	Isolated	Yes	Unknown
	SFA + aromatic*	SFA + aromatic*	3	Uncommon	No	No	No	Isolated	Yes	Modern contamination

	Plant material or fibre, lignin content	Cellulose+lignin	3	Uncommon	No	Uncommon	No	Isolated	Yes	**Possibly use-related**
	Polyester*	Polyester	2	Uncommon	No	No	No	Isolated	Yes	Modern contamination
	SFA	SFA	2	Uncommon	No	No	No	Isolated	Yes	**Possibly use-related**
	SFA + aromatic + calcium nitrate*	SFA + aromatic + calcium nitrate	1	Rare	No	No	No	Isolated	NA	Unknown
	Blue Nitrile glove*	Nitrile	1	Rare	No	No	No	Isolated	NA	Modern contamination
	SFA + protein + $Ca(NO_3)_2$	SFA + protein + $Ca(NO_3)_2$	1	Rare	No	No	No	Isolated	NA	Unknown
	Starch grain + $Ca(NO_3)_2$	Starch	1	Rare	No	No	No	Isolated	NA	Unknown
Artefact	**Micro-residues designation**	**Analysed material**	**Number analysed**	**Relative occurrence**	**Washed sediment after first cleaning**	**Washed sediment after second cleaning**	**Layer (outer) sediment**	**Concentrated/Group /Isolated**	**Correlation with polish**	**Micro-residues interpretation**
LB4582										
Unwashed sample	Charcoal	Carbon	NC	Rare	No	No	No	Isolated	Yes	Unknown
	Fossil bone	Apatite	11	Uncommon	common	common	common	Concentrated & group	Yes	Part of sediment
	SFA	SFA	5	Uncommon	No	No	No	Group	Yes	**use-related**
	Organic coated iron hydroxide/oxide “metallic aspect”*	Haematite + UOM	4	Uncommon	No	No	No	Group	No	Modern contamination
	Protein	Protein	1	Rare	No	rare	No	Isolated	Yes	Unknown
LB4582										
Washed sample	SFA	SFA	10	Uncommon	No	No	No	Concentrated	Yes	**use-related**
	Iron oxide “metallic aspect” *	Haematite + UOM	5	Uncommon	No	No	No	Concentrated & group	No	Modern contamination
	SFA + protein + $Ca(NO_3)_2$	SFA + protein + $Ca(NO_3)_2$	4	Uncommon	No	No	No	Isolated	Yes	**Possibly use-related**
	Protein + $Ca(NO_3)_2$	Protein + $Ca(NO_3)_2$	2	Uncommon	No	No	No	Isolated	Yes	**Possibly use-related**
	Polyester	Polyester	1	Rare	No	No	No	Isolated	NA	Modern contamination
	Potassium Nitrate	KNo3	1	Rare	No	No	No	Isolated	NA	Unknown
	Calcium Nitrate	$Ca(NO_3)_2$	1	Rare	No	No	No	Isolated	NA	Unknown
	Protein	Protein	1	Rare	No	rare	No	Isolated	NA	Unknown
LB4829										
Unwashed sample	Potassium nitrate	KNO_3	NC	Uncommon	No	No	No	Isolated	Yes	Unknown
	Biofilm	UOM	NC	Uncommon	No	No	No	Isolated	No	post-depositional
	Carbonate	Calcium Carbonate	NC	Rare	No	No	No	Isolated	No	Unknown
	SFA + protein	SFA + protein	2	Uncommon	No	No	No	Isolated	Yes	Unknown

	Fossil bone	Apatite(fossil bone)	1	Rare	No	Uncommon	Uncommon	Isolated	Yes	Part of sediment
	Altered bone	Apatite (disordered)	1	Rare	No	Uncommon	Uncommon	Isolated		Part of sediment
	Protein	Protein	1	Rare	No	No	No	Isolated	No	Unknown
	Protein + $Ca(NO_3)_2$	Protein + $Ca(NO_3)_2$	1	Rare	No	No	No	Isolated	Yes	Unknown
LB4829										
Washed sample	Manganese oxide	MnO_2	NC	Rare	No	No	No	Isolated	No	post-deposional
	Black iron oxides	Haematite + Maghemite + UOM	NC	Rare	No	No	Rare	Isolated	No	Part of sediment
	Protein	Protein	3	Uncommon	No	No	No	Isolated	Yes	Unknown
	Polyester*	Polyester	2	Uncommon	No	No	No	Isolated	Yes	Modern contamination
	SFA + aromatic*	SFA + aromatic	1	Rare	No	No	No	Isolated	NA	Modern contamination
	Plant material or fibre, lignin content	Cellulose + lignin	1	Rare	No	No	No	Isolated	NA	Unknown
Artefact	**Micro-residues designation**	**Analysed material**	**Number analysed**	**Relative occurrence**	**Washed sediment after first cleaning**	**Washed sediment after second cleaning**	**Layer (outer) sediment**	**Concentrated/Group /Isolated**	**Correlation with polish**	**Micro-residues interpretation**
LB5003										
Unwashed sample	Fossil bone	Apatite (fossil bone)	1	Uncommon	No	No	No	Isolated	No	Unknown
	Bone	Apatite (disordered)	1	Uncommon	No	No	No	Isolated	No	Unknown
	Plant material or fibre, lignin content	Cellulose + lignin	1	Rare	No	No	No	Isolated	No	Unknown
	Protein	Protein	1	Rare	No	No	No	Isolated	No	Unknown
	Charcoal	Carbon	NC	Uncommon	No	No	rare	Concentrated	No	Part of sediment
LB5003									No	
Washed sample	Protein	Protein	2	Uncommon	No	No	No	Isolated	Yes	Unknown
	Fossil bone	Apatite (fossil bone)	2	Uncommon	Uncommon	No	No	Concentrated	No	Unknown
	SFA + protein	SFA + protein	2	Rare	No	No	No	Isolated	Yes	Unknown
	Protein + $Ca(NO_3)_2$	Protein + $Ca(NO_3)_2$	1	Rare	No	No	No	Isolated	NA	Unknown
	Aromatic + protein + $Ca(NO_3)_2$	Aromatic + protein + $Ca(NO_3)_2$	1	Rare	No	No	No	Isolated	NA	Unknown
	Polyester*	Polyester	1	Rare	No	No	No	Isolated	NA	Modern contamination
LB5227										
Unwashed sample	Black iron oxides	Haematite + Maghemite + UOM	NC	Uncommon	No	No	No	Isolated	No	post-deposional
	Biofilm	UOM	NC	Uncommon	No	No	No	Isolated	No	post-deposional
	Manganese oxide	MnO_2	NC	Uncommon	Uncommon	Uncommon	Uncommon	Isolated	No	Part of sediment
LB5227										
Washed sample	Plant material or fibre, lignin	Cellulose + lignin	9	Uncommon	No	No	No	Concentrated & group	Yes	**Possibly use-related**

	content									
	Plant fibre, cellulose only with strong signal*	Cellulose	3	Uncommon	No	No	No	Isolated	Yes	Modern contamination
	Dark fibre broad signal*	Dye	3	Uncommon	No	No	No	Isolated	Yes	Modern contamination
	Plant material or fibre, lignin content, bluish, lignin 1630 cm-1	Cellulose+lignin	2	Uncommon	No	No	No	Isolated	Yes	**Possibly use-related**
	Plant fibre, dark and clear fluorescent (reactive blue Dye)*	Dye	2	Uncommon	No	No	No	Isolated	Yes	Modern contamination
	Dark Plant fibre, fluorescent (reactive blue Dye)*	Dye	2	Uncommon	No	No	No	Isolated	Yes	Modern contamination
	Dark Dyed plant fibre (unknown Dye)*	Dye	1	Rare	No	No	No	Isolated	NA	Modern contamination
	Dark fluorescent plant fiber with indigo Dye on inner fibre*	Indigo	1	Rare	No	No	No	Isolated	NA	Modern contamination
	Plant fibre with indigo Dye*	Indigo	1	Rare	No	No	No	Isolated	NA	Modern contamination
LB3952										
Unwashed sample	Organic coated iron hydroxide/oxide “metallic aspect”*	Haematite+UOM	3	Uncommon	No	No	No	Concentrated & group	Yes	Modern contamination
	Protein	Protein	2	Uncommon	No	No	No	Isolated	No	Unknown
	Protein + $Ca(NO_3)_2$	Protein + $Ca(NO_3)_2$	1	Rare	No	No	No	Isolated	NA	Unknown
	Dark Plant fibre, fluorescent Dye*	Dye	1	Rare	No	No	No	Isolated	NA	Modern contamination
LB3952										
Washed sample	Organic coated iron hydroxide/oxide “metallic aspect”*	Haematite + UOM	5	Uncommon	No	No	No	Concentrated & group	Yes	Modern contamination
	Plant material or fibre, lignin content	Cellulose + lignin	2	Uncommon	No	No	No	Isolated	No	Unknown
	Blue Dyed plant fibre*	Dye	1	Rare	No	No	No	Isolated	NA	Modern contamination
	Plant fiber with indigo Dye*	Indigo	1	Rare	No	No	No	Isolated	NA	Modern contamination
	Dark Plant fibre, fluorescent Dye*	Dye	1	Rare	No	No	No	Isolated	NA	Modern contamination
LB3958										

Unwashed sample	Apatite geologic	Apatite geologic	3	Uncommon	No	No	No	Isolated	No	Unknown
	Protein	Protein	2	Uncommon	No	No	No	Isolated	No	Unknown
	SFA + protein	SFA + protein	1	Rare	No	No	No	Isolated	NA	Unknown
LB3958										
Washed sample	Black iron oxides	Haematite + Maghemite + UOM	NC	Uncommon	No	No	No	Isolated	No	post-deposition al
	SFA + protein	SFA + protein	5	Uncommon	No	No	No	Concentrated	No	Unknown
	Protein	Protein	4	Uncommon	No	No	No	Isolated	No	Unknown
	SFA	SFA	1	Rare	No	No	No	Isolated	NA	Unknown
	Organic coated iron hydroxide/oxide “metallic aspect”*	Haematite + UOM	1	Rare	No	No	No	Concentrated & group	NA	Modern contaminat ion
	Polyester + modern cotton fibre*	Polyester + cellulose	1	Rare	No	No	No	Isolated	NA	Modern contaminat ion
	Bone apatite(fossil)	apatite	1	Rare	Bone apatite(alte red)	No	No	Isolated	NA	Unknown
Artefact	**Micro-residues designation**	**Analysed material**	**Number analysed**	**Relative occurrence**	**Washed sediment after first cleaning**	**Washed sediment after second cleaning**	**Layer (outer) sediment**	**Concentrated/Group /Isolated**	**Correlation with polish**	**Micro-residues interpretation**
LB4131										
Unwashed sample	Charcoal	Carbon	NC	Uncommon	No	No	No	Isolated	No	Unknown
	Carbonised material	UOM	NC	Uncommon	No	No	No	Isolated	No	Unknown
	Manganese oxide	MnO_2	NC	Uncommon	No	No	No	Isolated	No	post-deposition al
	Organic coated iron hydroxide/oxide “metallic aspect”*	Haematite + UOM	3	Uncommon	No	No	No	Concentrated & group	No	Modern contaminat ion
	Plant material or fibre, lignin content	Cellulose + lignin	1	Rare	Yes	No	Rare	Isolated	NA	Unknown
	Aromatic Unknown*	Aromatic unknown	1	Rare	No	No	No	Isolated	NA	Modern contaminat ion
	Plant fiber with indigo Dye*	Indigo	1	Rare	No	No	No	Isolated	NA	Modern contaminat ion
LB4131										
Washed sample	Plant material or fibre, lignin content	Cellulose + lignin	2	Uncommon	No	No	Rare	Isolated	No	Unknown
	Dark Plant fibre, fluorescent Dye*	Dye	1	Rare	Yes	No	No	Isolated	NA	Modern contaminat ion
	Polyester*	Polyester	1	Rare	No	No	No	Isolated	NA	Modern contaminat ion
	Iron oxide “metallic aspect” *	Haematite + UOM	1	Rare	No	No	No	Isolated	NA	Modern contaminat ion
LB4204										
Unwashed sample	Plant material or fibre, lignin	Cellulose + lignin	6	Uncommon	No	No	No	Concentrated & group	Yes	**use-related**

	content									
	SFA	SFA	6	Uncommon	No	No	No	Concentrated	Yes	**use-related**
	SFA + protein	SFA + protein	2	Uncommon	No	No	No	Isolated	Yes	**Possibly use-related**
	Dark Plant fibre, fluorescent Dye*	Dye	1	Rare	No	No	No	Isolated	NA	Modern contamination
	Polyester*	Polyester	1	Rare	No	No	No	Isolated	NA	Modern contamination
LB4204										
Washed sample	Plant material or fibre, lignin content	Cellulose + lignin	2	Uncommon	No	No	No	Isolated	Yes	**Possibly use-related**
	Protein	Protein	1	Rare	No	No	No	Isolated	NA	Unknown
	Organic coated iron hydroxide/oxide “metallic aspect”*	Haematite + UOM	1	Rare	No	No	No	Isolated	NA	Modern contamination
LB57										
Unwashed sample	Plant fiber, green highly fluorescent	Dye	4	Uncommon	No	No	No	Concentrated & group	No	Possibly incidental
	Plant material or fibre, lignin content	Cellulose + lignin	3	Uncommon	No	No	No	Isolated	No	Possibly incidental
	Carbonised material	UOM	2	Uncommon	No	No	No	Isolated	No	Unknown
	Plant fiber with indigo Dye*	Indigo	1	Rare	No	No	No	Isolated	NA	Modern contamination
	Iron oxide “metallic aspect” *	Haematite + UOM	1	Rare	No	No	No	Concentrated & group	NA	Modern contamination
LB57										
Washed sample	Plant fiber, green highly fluorescent	Dye	9	Uncommon	No	No	No	Concentrated & group	No	Possibly incidental
	Plant material or fibre, lignin content	Cellulose + lignin	1	Rare	No	No	No	Isolated	NA	Possibly incidental
	Plant fiber with indigo Dye*	Indigo	1	Rare	No	No	No	Isolated	NA	Modern contamination
	Organic coated iron hydroxide/oxide “metallic aspect”*	Haematite + UOM	1	Rare	No	No	No	Concentrated & group	NA	Modern contamination
	Carbonised material	UOM	1	Rare	No	No	No	Isolated	No	Unknown
	*** Matching a modern contaminant**	**NA: Non applicable**	**UOM : Undetermined organic material**		**NC : Not counted**					

Table 5: List of analysed micro-residues in Raman spectroscopy for Liang Bua stone artefact 2016 collection (first part).

Artefact	Micro-residues designation	Analysed material	Number analysed	Relative occurrence	Washed sediment after first cleaning	Washed sediment after second cleaning	Layer (outer) sediment	Concentrated/Group /Isolated	Correlation with polish	Micro-residues interpretation
LB5068										
	Manganese oxide	MnO_2	NC	Uncommon	No	No	No	Isolated	No	post-depositional
	Protein	Protein	19	Uncommon	No	No	No	Concentrated	Yes	**use-related**
	SFA	SFA	4	Uncommon	No	No	No	Isolated	Yes	**Possibly use-related**
	Protein + $Ca(NO_3)_2$	Protein + $Ca(NO_3)_2$	4	Uncommon	No	No	No	Isolated	Yes	**Possibly use-related**
	Starch grain + $Ca(NO_3)_2$	Starch + $Ca(NO_3)_2$	3	Uncommon	No	No	No	Isolated	Yes	**Possibly use-related**
	SFA + carbonate*	SFA + carbonate	1	Rare	No	No	No	Isolated	NA	Modern contamination
	SFA + unknown*	SFA + unknown	1	Rare	No	No	No	Isolated	NA	Modern contamination
	Plant fibre	Cellulose + lignin	1	Rare	No	No	No	Isolated	NA	**Possibly use-related**
	Plant material + calcite	Cellulose + lignin + calcite	1	Rare	No	No	No	Isolated	NA	**Possibly use-related**
	Plant material + $Ca(NO_3)_2$	Cellulose + lignin + $Ca(NO_3)_2$	1	Rare	No	No	No	Isolated	NA	**Possibly use-related**
	Starch + SFA + $Ca(NO_3)_2$	Starch + SFA + $Ca(NO_3)_2$	1	Rare	No	No	No	Isolated	NA	Unknown
	Lipid	Lipid	1	Rare	No	No	No	Isolated	NA	Unknown
	Unknown	Unknown	1	Rare	No	No	No	Isolated	NA	Unknown
	Polyester*	Polyester	1	Rare	No	No	No	Isolated	NA	Modern contamination
	Blue gloves*	Nitrile	1	Rare	No	No	No	Isolated	NA	Modern contamination
LB5165										
Washed sample	Manganese dioxide	MnO_2	NC	Uncommon	No	No	No	Isolated	No	post-depositional
	Haematite	Haematite	NC	Uncommon	No	No	No	Isolated	No	Unknown
	Iron oxide	Iron oxide	NC	Uncommon	No	No	No	Isolated	No	Unknown
	Calcite	Calcite	NC	Uncommon	No	No	No	Isolated	No	Unknown
	Smeared SFA	SFA	56	Common	No	No	No	Concentrated & group	Yes	**use-related**
	Protein	Protein	10	Uncommon	No	No	No	Isolated	Yes	**use-related**
	Smeared bone apatite(fossil & altered) + SFA	Apatite + SFA	8	Uncommon	No	No	No	Concentrated & group	Yes	**use-related**
	Bone apatite(fossil & altered)	Apatite	7	Uncommon	Common	Common	Common	Concentrated & group	Yes	**use-related**
	SFA	SFA	6	Uncommon	No	No	No	Isolated	Yes	**use-**

										related
	Smeared bone apatite	Apatite	5	Uncommon	No	No	No	Concentrated & group	Yes	**use-related**
	Protein + $Ca(NO_3)_2$	Protein + $Ca(NO_3)_2$	3	Uncommon	No	No	No	Isolated	Yes	**use-related**
	Lipid Unknown	Lipid unknown	2	Uncommon	No	No	No	Isolated	Yes	**Possibly use-related**
	Plant fibre + $Ca(NO_3)_2$	Cellulose + lignin + SFA + $Ca(NO_3)_2$	2	Uncommon	No	No	No	Isolated	No	Possibly incidental
	SFA + $Ca(NO_3)_2$	SFA + $Ca(NO_3)_2$	1	Rare	No	No	No	Isolated	NA	Unknown
	SFA + calcite*	SFA + calcite	1	Rare	No	No	No	Isolated	NA	Modern contamination
	SFA + Polyester*	SFA + Polyester*	1	Rare	No	No	No	Isolated	NA	Modern contamination
	Plant fibre	Cellulose + lignin	1	Rare	No	No	No	Isolated	NA	Possibly incidental
	Plant fibre + SFA + $Ca(NO_3)_2$	Cellulose + lignin + $Ca(NO_3)_2$	1	Rare	No	No	No	Isolated	NA	Modern contamination
	Calcite + SFA + Unknown resin*	Calcite + SFA + unknown resin?	1	Rare	No	No	No	Isolated	NA	Modern contamination
	Starch grain	Starch	1	Rare	No	No	No	Isolated	NA	Unknown
	Geological apatite	Apatite	1	Rare	No	No	No	Isolated	NA	Unknown
	Plastic box*	Plastic box*	1	Rare	No	No	No	Isolated	NA	Modern contamination
	Unknown lipid*	Unknown lipid*	1	Rare	No	No	No	Isolated	NA	Modern contamination
	Kaolinite	Kaolinite	1	Rare	No	No	No	Isolated	No	rock weathering
LB5164										
	Manganese dioxide	MnO_2	NC	Very common	No	No	No	Concentrated & group	No	post-depositional
	Haematite	Haematite	NC	Uncommon	No	No	No	Isolated	No	Unknown
	Smeared bone apatite (fossil & altered)	Apatite	53	Common	No	No	No	Concentrated & group	Yes	**use-related**
	Smeared SFA	SFA	49	Common	No	No	No	Concentrated & group	Yes	**use-related**
	Bone apatite (fossil & altered)	Apatite	26	Common	Common	Common	Common	Concentrated & group	Yes	**use-related**
	Protein	Protein	12	Uncommon	No	No	No	Isolated	Yes	**use-related**
	Patch of bone apatite	Apatite	10	Very common	No	No	No	Concentrated & group	Yes	**use-related**
	Plant material (Gramineae)	Cellulose+lignin	10	Uncommon	No	No	No	Concentrated & group	No	Possibly incidental
	SFA	SFA	7	Uncommon	No	No	No	Isolated	Yes	**use-related**
	Smeared bone apatite + SFA	Apatite + SFA	6	Uncommon	No	No	No	Concentrated & group	Yes	**use-related**
	Bone apatite fragment	Apatite	3	Uncommon	No	No	No	Concentrated	Yes	**use-related**
	SFA + Apatite	SFA + Apatite	2	Uncommon	No	No	No	Isolated	Yes	**use-related**

	SFA + Calcite + Protein*	SFA + Calcite + Protein	1	Rare	No	No	No	Isolated	NA	Modern contamination
	Plant fibre	Cellulose+lignin	1	Rare	No	No	No	Isolated	NA	Unknown
	Polyester*	Polyester	1	Rare	No	No	No	Isolated	NA	Modern contamination
LB5126										
	Goethite	Goethite	NC	Very common	Common	Uncommon	Uncommon	Concentrated & group	Yes	**use-related**
	Organic coated iron hydroxide/oxide “metallic aspect”*	Haematite + UOM	NC	Uncommon	No	No	No	Concentrated & group	Yes	Modern contamination
	Manganese oxide	MnO_2	NC	Common	Uncommon	Uncommon	Uncommon	Concentrated & group	Yes	post-depositional
	Smeared bone apatite (fossil & altered)	Apatite	76	Very common	No	No	No	Concentrated & group	Yes	**use-related**
	Protein	Protein	54	Common	No	No	No	Concentrated & group	Yes	**use-related**
	Smeared SFA	SFA	43	Common	No	No	No	Concentrated & group	Yes	**use-related**
	Bone apatite (fossil & altered)	Apatite	21	Common	Common	No	No	Concentrated & group	Yes	**use-related**
	Smeared Goethite	Goethite	19	Common	No	No	No	Concentrated & group	Yes	**use-related**
	Patch of bone apatite (fossil & altered)	apatite	16	Common	No	No	No	Concentrated & group	Yes	**use-related**
	Kaolinite	Kaolinite	14	Common	Common	No	No	Concentrated & group	No	rock weathering
	SFA	SFA	10	Uncommon	No	No	No	Concentrated & group	Yes	**use-related**
	Smeared bone apatite + goethite	Apatite + goethite	4	Uncommon	No	No	No	Concentrated & group	Yes	**use-related**
	Protein fibre	Protein	4	Uncommon	No	No	No	Isolated	Yes	**Possibly use-related**
	Haematite	Haematite	4	Very common	Common	Uncommon	Uncommon	Isolated	Yes	**use-related**
	SFA + calcite (blue tack)*	SFA + calcite	3	Uncommon	No	No	No	Isolated	Yes	Modern contamination
	Plant fibre	Cellulose + lignin	3	Uncommon	No	No	No	Isolated	No	Possibly incidental
	Smeared protein	Protein	3	Uncommon	No	No	No	Isolated	Yes	**use-related**
	Starch grain	Starch	2	Uncommon	No	No	No	Isolated	No	Unknown
	Smeared kaolinite	Kaolinite	2	Uncommon	No	No	No	Isolated	Yes	Possibly incidental
	SFA + unknown carbonate + kaolinite	SFA + unknown carbonate + kaolinite	1	Rare	No	No	No	Isolated	NA	Unknown
	SFA + protein + calcite(blue tack)*	SFA + protein + calcite	1	Rare	No	No	No	Isolated	NA	Modern contamination
	SFA + unknown*	SFA + unknown	1	Rare	No	No	No	Isolated	NA	Modern contamination
	Unknown	Unknown	1	Rare	No	No	No	Isolated	NA	Unknown

	lipid?	lipid?								
	Bone apatite fragment (fossil)	Apatite	1	Rare	No	No	No	Isolated	NA	**use-related**
	Smeared Bone apatite +SFA	Apatite + SFA	1	Rare	No	No	No	Isolated	NA	**use-related**
	Starch grain + $Ca(NO_3)_2$	Starch+ $Ca(NO_3)_2$	1	Rare	No	No	No	Isolated	NA	Unknown
	Cellulose fibre	Cellulose	1	Rare	No	No	No	Isolated	NA	Possibly incidental
	Cellulose fibre*	Cellulose	1	Rare	No	No	No	Isolated	NA	Modern contamination
	Unknown	Unknown	1	Rare	No	No	No	Isolated	NA	**Possibly use-related**
	Smeared protein + calcium nitrate	Protein + $Ca(NO_3)_2$	1	Rare	No	No	No	Isolated	NA	**Possibly use-related**
	Calcite + unknown protein	Protein + calcite	1	Rare	No	No	No	Isolated	NA	Unknown
	Calcite + Gypsum + Protein + Unknown*	Calcite + Gypsum + Protein + Unknown	1	Rare	No	No	No	Isolated	NA	Unknown
	Smeared haematite	Haematite	1	Rare	No	No	No	Isolated	NA	**use-related**
Artefact	**Micro-residues designation**	**Analysed material**	**Number analysed**	**Relative occurrence**	**Washed sediment after first cleaning**	**Washed sediment after second cleaning**	**Layer (outer) sediment**	**Concentrated/Group /Isolated**	**Correlation with polish**	**Micro-residues interpretation**
LB5224a										
	Manganese oxide	MnO_2	NC	Uncommon	No	No	No	Isolated	No	post-depositional
	Haematite	Haematite	NC	Uncommon	No	Uncommon	Uncommon	Isolated	No	Unknown
	Organic coated iron hydroxide/oxide “metallic aspect”*	Haematite + UOM	NC	Uncommon	No	No	No	Concentrated & group	Yes	Modern contamination
	Smeared SFA	SFA	22	Uncommon	No	No	No	Concentrated & group	Yes	**use-related**
	Protein	Protein	12	Uncommon	No	No	No	Concentrated & group	Yes	**use-related**
	SFA	SFA	8	Uncommon	No	No	No	Isolated	Yes	**use-related**
	Kaolinite	Kaolinite	6	Uncommon	No	No	No	Isolated	No	rock weathering
	Starch grain + $Ca(NO_3)_2$	Starch + $Ca(NO_3)_2$	3	Uncommon	No	No	No	Isolated	No	Unknown
	SFA + protein	SFA + protein	2	Uncommon	No	No	No	Isolated	Yes	**Possibly use-related**
	SFA + calcite +protein*	SFA + calcite + protein	1	Rare	No	No	No	Isolated	NA	Modern contamination
	Bone apatite (fossil)	Apatite	1	Rare	Common (only altered)	Common (only altered)	Common (only altered)	Isolated	NA	**Possibly use-related**
	Bone apatite (fossil)+ kaolinite	Apatite	1	Rare	No	No	No	Isolated	NA	**Possibly use-related**
	Plant material	Cellulose + lignin	1	Rare	No	No	No	Isolated	NA	Unknown
	Protein fibre	Protein	1	Rare	No	No	No	Isolated	NA	Unknown

	Cellulose + rutile*	Cellulose + rutile	1	Rare	No	No	No	Isolated	NA	Modern contamination
	Blue gloves + calcite*	Nitrile + calcite	1	Rare	No	No	No	Isolated	NA	Modern contamination
	Gypsum + Modern resin	Gypsum + Modern resin	1	Rare	No	No	No	Isolated	NA	Modern contamination
LB5224b										
	Kaolinite	Kaolinite	NC	Uncommon	No	No	No	Isolated	No	rock weathering
	Manganese oxide	MnO_2	NC	Uncommon	No	No	No	Isolated	No	post-depositional
	Protein	Protein	81	Common	No	No	No	Concentrated & group	Yes	**use-related**
	Smeared SFA	SFA	24	Uncommon	No	No	No	Concentrated & group	Yes	**use-related**
	Smeared bone apatite	Apatite	4	Uncommon	No	No	No	Isolated	Yes	**use-related**
	Protein + $Ca(NO_3)_2$	Protein + $Ca(NO_3)_2$	4	Uncommon	No	No	No	Isolated	Yes	**Possibly use-related**
	Plant material	Cellulose + lignin	2	Uncommon	No	No	No	Isolated	Yes	**Possibly use-related**
	Smeared SFA + protein	SFA	1	Rare	No	No	No	Isolated	NA	**Possibly use-related**
	SFA	SFA	1	Rare	No	No	No	Isolated	NA	**Possibly use-related**
	Bone apatite(fossil & altered)	Apatite	1	Rare	Uncommon(fossil only)	No	No	Isolated	NA	**Possibly use-related**
	Bone apatite fragment(fossil)	Apatite	1	Rare	No	No	No	Isolated	NA	**Possibly use-related**
	SFA + protein	SFA + protein	1	Rare	No	No	No	Isolated	NA	**Possibly use-related**
	Plant fibre	Cellulose + lignin	1	Rare	No	No	No	Isolated	NA	**Possibly use-related**
	Smeared protein	Protein	1	Rare	No	No	No	Isolated	NA	**Possibly use-related**
	Smeared cellulose	Cellulose	1	Rare	No	No	No	Isolated	NA	**Possibly use-related**
	Unknown	Unknown	1	Rare	No	No	No	Isolated	NA	Unknown
	Polyester*	Polyester	1	Rare	No	No	No	Isolated	NA	Modern contamination
LB5213										
	Kaolinite	Kaolinite	NC	Common	No	No	No	Concentrated & group	No	rock weathering
	Manganese oxide	MnO_2	NC	Uncommon	No	Uncommon		Isolated	No	post-depositional
	Organic coated iron hydroxide/oxide “metallic aspect”*	Haematite + UOM	NC	Uncommon	No	No	No	Concentrated & group	No	Modern contamination
	Smeared SFA	SFA	68	Common	No	No	No	Concentrated & group	Yes	**use-related**
	Goethite/Haematite	Goethite/Haematite	36	Very common	Uncommon	Uncommon	Uncommon	Concentrated & group	Yes	**use-related**

	SFA/UFA	SFA/UFA	17	Uncommon	No	No	No	Concentrated & group	Yes	**use-related**
	Bone apatite (fossil & altered)	apatite	14	Uncommon	Uncommon	Uncommon(fossil only)	Uncommon	Concentrated & group	Yes	**use-related**
	Protein	Protein	14	Uncommon	No	No	No	Concentrated & group	Yes	**use-related**
	Smeared SFA/UFA	SFA/UFA	9	Uncommon	No	No	No	Concentrated & group	Yes	**use-related**
	Smeared Goethite/Hematite	Goethite/Haematite	8	Uncommon	No	No	No	Concentrated & group	Yes	**use-related**
	Smeared bone apatite (fossil)	Apatite	6	Uncommon	No	No	No	Isolated	Yes	**use-related**
	Bone apatite (fossil) + kaolinite	Apatite + kaolinite	5	Uncommon	Yes	No	No	Concentrated & group	Yes	**use-related**
	Goethite	Goethite	3	Uncommon	Uncommon	Uncommon	Uncommon	Concentrated & group	Yes	**use-related**
	SFA	SFA	2	Uncommon	No	No	No	Isolated	Yes	**use-related**
	Smeared protein	Protein	2	Uncommon	No	No	No	Isolated	Yes	**use-related**
	Smeared Goethite	Goethite	2	Uncommon	No	No	No	Isolated	Yes	**use-related**
	Bone apatite (fossil) + SFA + kaolinite	Apatite + SFA + kaolinite	1	Rare	No	No	No	Isolated	NA	**use-related**
	Bone apatite (fossil) + SFA	Apatite + SFA	1	Rare	No	No	No	Isolated	NA	**use-related**
	Iron oxide	Iron oxide	1	Rare	No	No	No	Isolated	NA	Unknown
	Indigo Dyed fibre*	Indigo	1	Rare	No	No	No	Isolated	NA	Modern contamination
LB5212										
	Manganese oxide	MnO_2	NC	Uncommon	Uncommon	Uncommon	No	Isolated		post-depositional
	SFA/UFA	SFA/UFA	47	Common	No	No	No	Concentrated & group	Yes	**use-related**
	Smeared SFA/UFA	SFA/UFA	31	Common	No	No	No	Concentrated & group	Yes	**use-related**
	Protein	Protein	9	Uncommon	No	No	No	Isolated	No	Possibly incidental
	Smeared SFA	SFA	5	Uncommon	No	No	No	Isolated	No	Possibly incidental
	Protein + $Ca(NO_3)_2$	Protein + $Ca(NO_3)_2$	1	Rare	No	No	No	Isolated	NA	Unknown
	Bone apatite (altered)	Apatite	1	Rare	Common	No	Common	Isolated	NA	Unknown
	Geological apatite	Apatite	1	Rare	Uncommon	No	No	Isolated	NA	Unknown
	Dark Dyed fibre*	Dye	1	Rare	No	No	No	Isolated	NA	Modern contamination
	Wooden material*	Cellulose + lignin	1	Rare	No	No	No	Isolated	NA	Modern contamination
Artefact	**Micro-residues designation**	**Analysed material**	**Number analysed**	**Relative occurrence**	**Washed sediment after first cleaning**	**Washed sediment after second cleaning**	**Layer (outer) sediment**	**Concentrated/Group /Isolated**	**Correlation with polish**	**Micro-residues interpretation**
LB5211										
	Kaolinite	kaolinite	NC	Uncommon	rare	No	No	Isolated	No	rock weathering

	Organic coated iron hydroxide/oxide “metallic aspect”*	Haematite + UOM	NC	Uncommon	No	No	No	Concentrated & group	No	Modern contamination
	Manganese oxide	MnO_2	NC	Uncommon	No	Uncommon	Uncommon	Isolated	No	post-depositional
	SFA/UFA	SFA/UFA	21	Uncommon	No	No	No	Concentrated & group	Yes	**use-related**
	Smeared SFA/UFA	SFA/UFA	13	Uncommon	No	No	No	Concentrated & group	Yes	**use-related**
	Unknown yellow mineral		9	Uncommon	No	No	No	Concentrated & group	Yes	**Possibly use-related**
	Protein	Protein	3	Uncommon	No	No	No	Isolated	No	Unknown
	Smeared SFA	SFA	3	Uncommon	No	No	No	Isolated	Yes	**Possibly use-related**
	Goethite	Goethite	2	Uncommon	No	No	No	Isolated	No	Unknown
	SFA	SFA	2	Uncommon	No	No	No	Isolated	No	Unknown
	Plant material	Cellulose+lignin	1	Rare	No	No	No	Isolated	NA	Possibly incidental
	Starch grain	Starch	1	Rare	No	No	No	Isolated	NA	Unknown
	Calcite + SFA*	Calcite + SFA	1	Rare	No	No	No	Isolated	NA	Modern contamination
	Haematite	Haematite	1	Rare	No	Uncommon	Uncommon	Isolated	NA	Unknown
	Geological apatite rod	Apatite	1	Rare	No	No	No	Isolated	NA	Unknown
LB5225										
	Goethite	Goethite	NC	Very common	Common	No	No	Concentrated & group	Yes	**use-related**
	Haematite	Haematite	NC	Very common	Common	No	No	Concentrated & group	Yes	**use-related**
	Kaolinite	Kaolinite	NC	Uncommon	No	No	No	Isolated	No	rock weathering
	Manganese oxide	MnO_2	NC	Uncommon	Uncommon	Uncommon	Uncommon	Isolated	No	post-depositional
	Organic coated iron hydroxide/oxide “metallic aspect”*	Haematite + UOM	NC	Uncommon	No	No	No	Concentrated & group	No	Modern contamination
	Protein	Protein	110	Common	No	No	No	Concentrated & group	Yes	**use-related**
	SFA/UFA	SFA/UFA	89	Common	No	No	No	Concentrated & group	Yes	**use-related**
	Smeared SFA/UFA	SFA/UFA	20	Uncommon	No	No	No	Concentrated & group	Yes	**use-related**
	Smeared bone apatite(fossil)	Apatite	10	Uncommon	No	No	No	Concentrated & group	Yes	**use-related**
	Smeared Haematite	Haematite	5	Uncommon	No	No	No	Concentrated & group	Yes	**use-related**
	SFA	SFA	4	Uncommon	No	No	No	Isolated	Yes	**Possibly use-related**
	Smeared protein	Protein	4	Uncommon	No	No	No	Isolated	Yes	**use-related**
	Smeared Goethite	Goethite	4	Uncommon	No	No	No	Isolated	Yes	**use-related**
	Lipid Unknown	Lipid Unknown	1	Rare	No	No	No	Isolated	NA	**Possibly use-related**

	Bone apatite(fossil & altered)	Apatite	1	Rare	No	No	No	Isolated	NA	**use-related**
	Starch grain	Starch	1	Rare	No	No	No	Isolated	NA	Unknown
	Geological apatite	Apatite	1	Rare	No	No	No	Isolated	NA	Unknown
	Plastic bag*	Polyethylene	1	Rare	No	No	No	Isolated	NA	Modern contamination
	*** Matching a modern contaminant**	**NA: Non applicable**	**UOM : Undetermined organic material**		**NC : Not counted**					

Table 6: List of analysed micro-residues in Raman spectroscopy for Liang Bua stone artefact 2016 collection (second part).

Artefact	Micro-residues designation	Analysed material	Number analysed	Relative occurrence	Washed sediment after first cleaning	Washed sediment after second cleaning	Layer (outer) sediment	Concentrated/Group /Isolated	Correlation with polish	Micro-residues interpretation
LB5580a										
	Goethite	Goethite	NC	Very common	Common	No	No	Concentrated & group	Yes	**use-related**
	Haematite	Haematite	NC	Very common	Common	Uncommon	No	Concentrated & group	Yes	**Possibly use-related**
	Kaolinite	Kaolinite	NC	Very common	Common	No	No	Concentrated & group	Yes	**Possibly use-related**
	Manganese oxide	MnO_2	NC	Common	Uncommon	No	No	Isolated	No	post-depositional
	Organic coated iron hydroxide/oxide “metallic aspect”*	Haematite + UOM	NC	Uncommon	No	No	No	Concentrated & group	No	Modern contamination
	Smeared bone apatite (fossil) + kaolinite	Apatite + kaolinite	14	Very common	No	No	No	Concentrated & group	Yes	**use-related**
	Smeared Goethite	Goethite	9	Very common	No	No	No	Concentrated & group	Yes	**use-related**
	Bone apatite (fossil) + kaolinite	Apatite + kaolinite	4	Uncommon	Uncommon	Uncommon	No	Concentrated & group	Yes	**use-related**
	SFA/UFA	SFA/UFA	4	Uncommon	No	No	No	Isolated	No	Unknown
	Smeared bone apatite (fossil)	Apatite	3	Uncommon	No	No	No	Concentrated & group	Yes	**use-related**
	Smeared SFA/UFA	SFA/UFA	3	Uncommon	No	No	No	Isolated	No	Unknown
	Bone apatite (fossil) + SFA + kaolinite	Apatite + SFA + kaolinite	1	Rare	No	No	No	Isolated	NA	**use-related**
LB5580b										
	SFA/UFA	SFA/UFA	49	Common	No	No	No	Concentrated & group	Yes	**use-related**
	Smeared	SFA/UFA	142	Common	No	No	No	Concentrated &	Yes	**use-related**

	SFA/UFA							group		
	Bone apatite (fossil & altered)	Apatite	4	Uncommon	Common	Common	Common(only altered)	Isolated	No	From sediment
	Protein	Protein	3	Uncommon	No	No	No	Isolated	No	Unknown
	Protein + $Ca(NO_3)_2$	Protein + $Ca(NO_3)_2$	3	Uncommon	No	No	No	Isolated	No	Unknown
	Manganese oxide	MNo2	NC	Uncommon	No	No	No	Isolated	No	post-depositional
	Lipid ring*	Lipid	1	Rare	No	No	No	Isolated	NA	Modern contamination
	Dyed fibre*	Dye	1	Rare	No	No	No	Isolated	NA	Modern contamination
	Plant material*	Cellulose + lignin	1	Rare	No	No	No	Isolated	NA	Modern contamination
LB5562a										
	Kaolinite	Kaolinite	NC	Common	Uncommon	No	No	Isolated	No	rock weathering
	Manganese oxide	MnO_2	NC	Uncommon	Uncommon	Uncommon	No	Isolated	No	post-depositional
	Haematite	Haematite	NC	Common	Uncommon	Uncommon				
	SFA/UFA	SFA/UFA	31	Uncommon	No	No	No	Concentrated & group	Yes	**use-related**
	Smeared SFA/UFA	SFA/UFA	23	Uncommon	No	No	No	Concentrated & group	Yes	**use-related**
	Protein	Protein	10	Uncommon	No	No	No	Concentrated & group	Yes	**use-related**
	Protein fibre	Protein	3	Uncommon	No	No	No	Concentrated & group	Yes	**Possibly use-related**
	Smeared bone apatite (fossil)	Apatite	2	Uncommon	No	No	No	Concentrated	Yes	**Possibly use-related**
	SFA	SFA	1	Rare	No	No	No	Isolated	NA	Unknown
	Smeared protein	Protein	1	Rare	No	No	No	Isolated	NA	**Possibly use-related**
	Smeared kaolinite	Kaolinite	1	Rare	No	No	No	Isolated	NA	**Possibly use-related**
	Plant fibre	Cellulose + lignin	1	Rare	No	No	No	Isolated	NA	Possibly incidental
	Plant fibre*	Cellulose + lignin	1	Rare	No	No	No	Isolated	NA	Unknown
	Plant material*	Cellulose + lignin	1	Rare	No	No	No	Isolated	NA	Unknown
	Blue gloves*	Nitrile	1	Rare	No	No	No	Isolated	NA	Unknown
LB5562b										
	Kaolinite	Kaolinite	NC	Uncommon	No	No	No	Isolated	No	rock weathering
	Manganese oxide	MnO_2	NC	Uncommon	Uncommon	Uncommon	No	Isolated	No	post-depositional
	Smeared SFA/UFA	SFA/UFA	27	Uncommon	No	No	No	Concentrated & group	Yes	**use-related**
	SFA/UFA	SFA/UFA	14	Uncommon	No	No	No	Concentrated & group	Yes	**use-related**
	Pyrite	Pyrite	6	Uncommon	No	No	No	Concentrated & group	Yes	**Possibly use-related**
	Haematite	Haematite	4	Uncommon	Uncommon	Uncommon	Uncommon	Isolated	No	Unknown
	Protein	Protein	3	Uncommon	No	No	No	Isolated	Yes	**Possibly use-related**
	Smeared SFA	SFA	2	Uncommon	No	No	No	Isolated	Yes	**Possibly use-related**
	Goethite	Goethite	2	Uncommon	No	No	No	Isolated	Yes	Unknown

	Bone apatite (fossil) + kaolinite	Apatite + kaolinite	1	Rare	No	No	No	Isolated	NA	**Possibly use-related**
	Polyester + SFA*	Polyester + SFA	1	Rare	No	No	No	Isolated	NA	Modern contamination
	Pyrite + goethite	Pyrite + goethite	1	Rare	No	No	No	Isolated	NA	**Possibly use-related**
Artefact	**Micro-residues designation**	**Analysed material**	**Number analysed**	**Relative occurrence**	**Washed sediment after first cleaning**	**Washed sediment after second cleaning**	**Layer (outer) sediment**	**Concentrated/Group /Isolated**	**Correlation with polish**	**Micro-residues interpretation**
LB5563a										
	Kaolinite	Kaolinite	NC	Uncommon	No	No	No	Isolated	No	rock weathering
	Manganese oxide	MnO_2	NC	Uncommon	Uncommon	Uncommon	No	Isolated	No	post-depositional
	Smeared SFA	SFA	28	Uncommon	No	No	No	Concentrated & group	Yes	**use-related**
	SFA/UFA	SFA/UFA	8	Uncommon	No	No	No	Concentrated	Yes	**Possibly use-related**
	Protein	Protein	7	Uncommon	No	No	No	Isolated	Yes	**Possibly use-related**
	Smeared SFA/UFA	SFA/UFA	2	Uncommon	No	No	No	Isolated	Yes	**Possibly use-related**
LB5563b										
	Kaolinite	Kaolinite	NC	Uncommon	No	No	No	Isolated	No	rock weathering
	Manganese oxide	MnO_2	NC	Uncommon	No	No	No	Isolated	No	post-depositional
	Smeared SFA/UFA	SFA/UFA	15	Uncommon	No	No	No	Isolated	Yes	**Possibly use-related**
	SFA/UFA	SFA/UFA	7	Uncommon	No	No	No	Concentrated	Yes	**Possibly use-related**
	Protein	Protein	7	Uncommon	No	No	No	Isolated	Yes	**Possibly use-related**
	Haematite	Haematite	5	Uncommon	No	No	No	Isolated	No	Unknown
	Smeared SFA	SFA	3	Uncommon	No	No	No	Concentrated & group	Yes	**Possibly use-related**
	Lipid	Lipid	1	Rare	No	No	No	Isolated	NA	Unknown
	Plant fibre	Cellulose + lignin	1	Rare	No	No	No	Isolated	NA	Unknown
	Goethite	Goethite	1	Rare	No	No	No	Isolated	NA	Unknown
LB5563b										
	Kaolinite	Kaolinite	NC	Uncommon	No	No	No	Isolated	No	rock weathering
	Manganese oxide	MnO_2	NC	Uncommon	No	No	No	Isolated	No	post-depositional
	Smeared SFA/UFA	SFA/UFA	9	Uncommon	No	No	No	Isolated	Yes	**Possibly use-related**
	SFA/UFA	SFA/UFA	4	Uncommon	No	No	No	Concentrated	Yes	**Possibly use-related**
	Protein	Protein	2	Uncommon	No	No	No	Isolated	Yes	**Possibly use-related**
	Haematite	Haematite	NC	Uncommon	No	No	No	Isolated	No	Unknown
	Smeared SFA	SFA	9	Uncommon	No	No	No	Concentrated & group	Yes	**use-related**
	Unknown	unknown	1	Rare	No	No	No	Isolated	NA	Unknown
	Wooden material*	Cellulose + lignin	1	Rare	No	No	No	Isolated	NA	Modern contamination
	Geological apatite	Apatite	1	Rare	No	No	No	Isolated	NA	Unknown
LB5564										
	Kaolinite	Kaolinite	NC	Uncommon	No	No	No	Isolated	No	rock

										weathering
	Manganese oxide	MnO_2	NC	Uncommon	Uncommon	Uncommon	No	Isolated	No	post-depositional
	Smeared SFA	SFA	15	Uncommon	No	No	No	Concentrated & group	Yes	**use-related**
	SFA	SFA	7	Uncommon	No	No	No	Isolated	Yes	**Possibly use-related**
	Smeared SFA/UFA	SFA/UFA	6	Uncommon	No	No	No	Concentrated & group	Yes	**Possibly use-related**
	Protein	Protein	6	Uncommon	No	No	No	Isolated	Yes	**Possibly use-related**
	Haematite	Haematite	5	Uncommon	No	No	No	Isolated	No	Unknown
	SFA/UFA	SFA/UFA	4	Uncommon	No	No	No	Isolated	Yes	**Possibly use-related**
	Protein + $Ca(NO_3)_2$	Protein + $Ca(NO_3)_2$	4	Uncommon	No	No	No	Isolated	No	Unknown
	Unknown	Unknown	1	Rare	No	No	No	Isolated	NA	Unknown
LB5565										
	Kaolinite	Kaolinite	NC	Uncommon	No	No	No	Isolated	No	rock weathering
	Haematite	Haematite	NC	Uncommon	No	Uncommon	No	Isolated	No	Unknown
	Goethite	Goethite	NC	Uncommon	No	No	No	Isolated	NA	Unknown
	SFA/UFA	SFA/UFA	28	Uncommon	No	No	No	Concentrated	Yes	**use-related**
	Smeared SFA/UFA	SFA/UFA	25	Uncommon	No	No	No	Concentrated & group	Yes	**use-related**
	Smeared SFA	SFA	23	Uncommon	No	No	No	Concentrated & group	Yes	**use-related**
	Protein	Protein	16	Uncommon	No	No	No	Isolated	Yes	**use-related**
	Smeared haematite	Haematite	6	Uncommon	No	No	No	Isolated	No	**Possibly use-related**
	Smeared protein	Protein	5	Uncommon	No	No	No	Isolated	NA	**use-related**
	Protein + $Ca(NO_3)_2$	Protein + $Ca(NO_3)_2$	2	Uncommon	No	No	No	Isolated	Yes	**Possibly use-related**
	Bone apatite (fossil) + kaolinite	Apatite + kaolinite	1	Rare	No	No	No	Isolated	NA	**Possibly use-related**
	Bone apatite(fossil)	Apatite	1	Rare	No	Uncommon	Common(only altered)	Isolated	NA	From sediment
	SFA	SFA	1	Uncommon	No	No	No	Isolated	NA	**Possibly use-related**
	Gypsum	Gypsum	1	Rare	No	No	No	Isolated	NA	Unknown
Artefact	**Micro-residues designation**	**Analysed material**	**Number analysed**	**Relative occurrence**	**Washed sediment after first cleaning**	**Washed sediment after second cleaning**	**Layer (outer) sediment**	**Concentrated/Group /Isolated**	**Correlation with polish**	**Micro-residues interpretation**
LB5524										
	Manganese oxide	MnO_2	NC	Uncommon	No	NA	No	Isolated	No	post-depositional
	Kaolinite	Kaolinite	NC	Common	No	NA	No	Isolated	No	rock weathering
	Haematite	Haematite	NC	Uncommon	No	NA	No	Isolated	No	Unknown
	Organic coated iron hydroxide/oxide “metallic aspect”*	Haematite + UOM	NC	Uncommon	No	NA	No	Concentrated & group	No	Modern contamination
	Smeared SFA	SFA	54	Uncommon	No	NA	No	Concentrated & group	Yes	**use-related**
	SFA/UFA	SFA/UFA	28	Uncommon	No	NA	No	Concentrated & group	Yes	**use-related**
	Smeared SFA/UFA	SFA/UFA	28	Uncommon	No	NA	No	Concentrated & group	Yes	**use-related**

	Protein	Protein	22	Uncommon	No	NA	No	Concentrated & group	Yes	**Possibly use-related**
	Smeared SFA + goethite	SFA + goethite	19	Uncommon	No	NA	No	Concentrated & group	Yes	**use-related**
	Bone apatite(fossil)	Apatite	9	Uncommon	Uncommon	NA	Uncommon	Concentrated & group	No	From sediment
	SFA	SFA	8	Uncommon	No	NA	No	Concentrated & group	Yes	**use-related**
	SFA + aromatic	SFA + aromatic	6	Uncommon	No	NA	No	Isolated	No	Unknown
	Phosphate + SFA	Phosphate + SFA	5	Uncommon	No	NA	No	Isolated	Yes	**Possibly use-related**
	Protein + $Ca(NO_3)_2$	Protein + $Ca(NO_3)_2$	5	Uncommon	No	NA	No	Isolated	No	Unknown
	Fossil bone + kaolinite	Apatite + kaolinite	2	Uncommon	No	NA	No	Isolated	Yes	**Possibly use-related**
	Smeared SFA + kaolinite	SFA + kaolinite	2	Uncommon	No	NA	No	Concentrated	Yes	**use-related**
	Smeared SFA + goethite + kaolinite	SFA + goethite + kaolinite	2	Uncommon	No	NA	No	Isolated	Yes	**use-related**
	SFA + Protein + $Ca(NO_3)_2$	SFA + Protein + $Ca(NO_3)_2$	2	Uncommon	No	NA	No	Isolated	Yes	**Possibly use-related**
	Smeared bone apatite(fossil)	Apatite	1	Rare	No	NA	No	Isolated	NA	Incidental
	Lipid + kaolinite	Lipid + kaolinite	1	Rare	No	NA	No	Isolated	NA	**Possibly use-related**
	Smeared protein	Protein	1	Rare	No	NA	No	Isolated	NA	**Possibly use-related**
	Starch grain + $Ca(NO_3)_2$	Starch + $Ca(NO_3)_2$	1	Rare	No	NA	No	Isolated	NA	Unknown
	Plant material	Cellulose + lignin	1	Rare	No	NA	No	Isolated	NA	Unknown
	Unknown	unknown	1	Rare	No	NA	No	Isolated	NA	Unknown
	Smeared kaolinite	Kaolinite	1	Rare	No	NA	No	Isolated	NA	Unknown
	Kaolinite + gypsum	Kaolinite + gypsum	1	Rare	No	NA	No	Isolated	NA	rock weathering
	Dyed fibre*	Dye	1	Rare	No	NA	No	Isolated	NA	Modern contamination
LB5525										
	Manganese oxide	MnO_2	NC	Uncommon	No	No	No	Isolated	No	post-depositional
	Haematite	Haematite	NC	Uncommon	No	Uncommon	No	Isolated	No	Unknown
	Smeared SFA	SFA	16	Uncommon	No	No	No	Concentrated & group	Yes	**use-related**
	SFA/UFA	SFA/UFA	15	Uncommon	No	No	No	Concentrated & group	Yes	**use-related**
	Smeared SFA/UFA	SFA/UFA	14	Uncommon	No	No	No	Concentrated & group	Yes	**use-related**
	SFA	SFA	13	Uncommon	No	No	No	Concentrated & group	Yes	**use-related**
	Protein + $Ca(NO_3)_2$	Protein + $Ca(NO_3)_2$	5	Uncommon	No	No	No	Isolated	No	Unknown
	Protein	Protein	2	Uncommon	No	No	No	Isolated	Yes	Unknown
	Bone apatite(fossil)	Apatite	2	Uncommon	Uncommon	No	Uncommon	Isolated	No	From sediment
	Smeared	Cellulose +	1	Rare	No	No	No	Isolated	No	Unknown

	plant material	lignin								
	Plant fibre(wood)	Cellulose + lignin	1	Rare	No	No	No	Isolated	No	Unknown
	Plant material + Unknown*	Cellulose + lignin + Unknown	1	Rare	No	No	No	Isolated	No	Unknown
	SFA + Protein	SFA + Protein + $Ca(NO_3)_2$	1	Uncommon	No	No	No	Isolated	NA	Unknown
	Smeared protein	Protein	1	Rare	No	No	No	Isolated	NA	Unknown
	Unknown	Unknown	1	Rare	No	No	No	Isolated	NA	Unknown
	Gypsum	Gypsum	1	Rare	No	No	No	Isolated	NA	rock weathering
	Polyester*	Polyester	1	Rare	No	No	No	Isolated	NA	Modern contamination
LB5526a										
	Manganese oxide	MnO_2	NC	Uncommon	Uncommon	No	Uncommon	Isolated	No	post-depositional
	Haematite	Haematite	NC	Uncommon	Uncommon	No	Uncommon	Isolated	No	Unknown
	Smeared SFA	SFA	19	Uncommon	No	No	No	Concentrated & group	No	Incidental
	Smeared SFA/UFA	SFA/UFA	2	Uncommon	No	No	No	Isolated	No	Unknown
	Protein + $Ca(NO_3)_2$	Protein + $Ca(NO_3)_2$	1	Rare	No	No	No	Isolated	No	Unknown
	Plant material	Cellulose + lignin	1	Rare	No	No	No	Isolated	NA	Unknown
	Bone apatite(fossil)	Apatite	1	Rare	Uncommon	Uncommon	Uncommon	Isolated	No	From sediment
	Unknown	Unknown	1	Rare	No	No	No	Isolated	NA	Unknown
LB5526b										
	Manganese oxide	MnO_2	NC	Uncommon	No	NA	Uncommon	Isolated	No	post-depositional
	Kaolinite	Kaolinite	NC	Common	No	NA	No	Isolated	No	rock weathering
	Haematite	Haematite	NC	Uncommon	Uncommon	No	Uncommon	Isolated	No	Unknown
	Goethite	Goethite	NC	Uncommon	No	No	No	Isolated	NA	Unknown
	Organic coated iron hydroxide/oxide “metallic aspect”*	Haematite + UOM	NC	Uncommon	No	NA	No	Concentrated & group	No	Modern contamination
	Smeared SFA/UFA	SFA/UFA	63	Uncommon	No	NA	No	Concentrated & group	Yes	**use-related**
	Smeared bone apatite(fossil)	Apatite	28	Uncommon	No	NA	No	Concentrated & group	Yes	**use-related**
	Bone apatite(fossil)	Apatite	27	Uncommon	Uncommon	NA	Uncommon	Concentrated & group	Yes	**use-related**
	SFA/UFA	SFA/UFA	26	Uncommon	No	NA	No	Concentrated & group	Yes	**use-related**
	Protein	Protein	21	Uncommon	No	NA	No	Concentrated & group	Yes	**use-related**
	Aromatic resin*	Aromatic resin	14	Uncommon	No	NA	No	Concentrated & group	Yes	Modern contamination
	Smeared SFA	SFA	9	Uncommon	No	NA	No	Concentrated & group	Yes	**use-related**
	Smeared bone	Apatite + kaolinite	6	Uncommon	No	NA	No	Concentrated	Yes	**use-related**

	apatite(fossil)+ kaolinite									
	SFA	SFA	4	Uncommon	No	NA	No	Isolated	Yes	**Possibly use-related**
	Smeared protein	Protein	4	Uncommon	No	NA	No	Concentrated	Yes	**Possibly use-related**
	Smeared bone + UFA	Apatite + UFA	1	Rare	No	NA	No	Isolated	NA	**use-related**
	Plant material	Cellulose + lignin	1	Rare	No	NA	No	Isolated	NA	Incidental
	Plant fibre + $Ca(NO_3)_2$ + Aromatic resin*	Cellulose + lignin + $Ca(NO_3)_2$ + Aromatic resin	1	Rare	No	NA	No	Isolated	NA	Modern contamination
	Protein + $Ca(NO_3)_2$	Protein + $Ca(NO_3)_2$	1	Rare	No	NA	No	Isolated	No	Unknown
	Geological apatite	Apatite	1	Rare	No	No	No	Isolated	NA	Unknown
	Protein + Calcite	Protein + Calcite	1	Rare	No	NA	No	Isolated	No	Unknown
LB5527										
Unwashed sample	Kaolinite	Kaolinite	NC	Common	No	No	No	Isolated	No	rock weathering
	Organic coated iron hydroxide/oxide “metallic aspect”*	Haematite + UOM	NC	Uncommon	No	No	No	Concentrated & group	No	Modern contamination
	Haematite	Haematite	NC	Uncommon	No	Uncommon	No	Isolated	No	Unknown
	Bone apatite(fossil)	Apatite	19	Uncommon	Uncommon	No	Uncommon	Concentrated & group		**Possibly use-related**
	Protein	Protein	5	Uncommon	No	No	No	Isolated	Yes	**Possibly use-related**
	Protein + $Ca(NO_3)_2$	Protein + $Ca(NO_3)_2$	1	Rare	No	No	No	Isolated	No	Unknown
	Plant fibre	Cellulose + lignin	1	Rare	No	No	No	Isolated	No	Unknown
	Gypsum	Gypsum	1	Rare	No	No	No	Isolated	NA	rock weathering
LB5527										
Washed sample	Manganese oxide	MnO_2	NC	Uncommon	No	No	No	Isolated	No	post-depositional
	Kaolinite	Kaolinite	NC	Uncommon	No	No	No	Isolated	No	rock weathering
	Organic coated iron hydroxide/oxide “metallic aspect”*	Haematite + UOM	NC	Uncommon	No	No	No	Concentrated & group	No	Modern contamination
	SFA/UFA	SFA/UFA	36	Uncommon	No	No	No	Concentrated & group	Yes	**use-related**
	Protein	Protein	22	Uncommon	No	No	No	Concentrated & group	Yes	**use-related**
	Smeared SFA/UFA	SFA/UFA	11	Uncommon	No	No	No	Concentrated & group	Yes	**use-related**
	Polyester*	Polyester	5	Uncommon	No	No	No	Isolated	NA	Modern contamination
	SFA	SFA	4	Uncommon	No	No	No	Isolated	Yes	**Possibly use-related**
	Plant fibre*	Cellulose + lignin	4	Uncommon	No	No	No	Isolated	No	Modern contamination
	Plant material	Cellulose + lignin	3	Rare	No	No	No	Isolated	NA	Incidental
	Aromatic	Aromatic	2	Uncommon	No	No	No	Isolated	No	Modern

	resin*	resin								contaminati on
	Protein + $Ca(NO_3)_2$	Protein + $Ca(NO_3)_2$	2	Uncommon	No	No	No	Isolated	No	Unknown
	SFA + Protein	SFA + Protein + $Ca(NO_3)_2$	1	Rare	No	No	No	Isolated	NA	Unknown
	Lipid	Lipid	1	Rare	No	No	No	Isolated	NA	Unknown
	Smeared protein	Protein	1	Rare	No	No	No	Isolated	NA	**Possibly use-related**
	Cellulose fibre	Cellulose	1	Rare	No	No	No	Isolated	No	Modern contaminati on
	Bone apatite(fossil)	Apatite	1	Rare	Uncommo n	No	Uncommon	Isolated	NA	From sediment
	Unknown	Unknown	1	Rare	No	No	No	Isolated	NA	Unknown
	*** Matching a modern contaminan t**	**NA: Non applicable**	**UOM : Undetermined organic material**		**NC : Not counted**					
LB5533a										
	Kaolinite	Kaolinite	NC	Common	NA	NA	No	Isolated	No	rock weathering
	Goethite	Goethite	NC	Common	NA	NA	Uncommon	Isolated	NA	**use-related**
	Haematite	Haematite	NC	Uncommon	NA	NA	No	Isolated	No	Unknown
	Manganese oxide	MnO_2	NC	Common	NA	NA	No	Isolated	No	post-depositional
	SFA/UFA	SFA/UFA	20	Uncommon	NA	NA	No	Concentrated & group	No	**use-related**
	Protein	Protein	10	Uncommon	NA	NA	No	Isolated	Yes	Unknown
	Bone apatite(fossil)	Apatite	4	Uncommon	NA	NA	Uncommon	Isolated	No	From sediment
	Plant material + calcite	Cellulose + lignin + calcite	2	Uncommon	NA	NA	No	Isolated	NA	Incidental
	Smeared SFA/UFA	SFA/UFA	1	Uncommon	NA	NA	No	Isolated	NA	Unknown
	Plant material	Cellulose + lignin	1	Rare	NA	NA	No	Isolated	NA	Incidental
LB5533b					NA					
	Kaolinite	Kaolinite	NC	Common	NA	NA	No	Isolated	No	rock weathering
	Goethite	Goethite	NC	Uncommon	NA	NA	Uncommon	Concentrated & group	Yes	**use-related**
	Haematite	Haematite	NC	Uncommon	NA	NA	No	Concentrated & group	Yes	**use-related**
	Manganese oxide	MnO_2	NC	Common	NA	NA	No	Isolated	No	post-depositional
	Bone apatite(fossil)	Apatite	14	Uncommon	NA	NA	Uncommon	Concentrated & group	Yes	**use-related**
	Smeared Goethite	Goethite	10	Uncommon	NA	NA	No	Concentrated & group	Yes	**use-related**
	Fossil bone + kaolinite	Apatite + kaolinite	9	Uncommon	NA	NA	No	Concentrated & group	Yes	**use-related**
	Smeared Goethite	Goethite	6	Uncommon	NA	NA	No	Concentrated & group	Yes	**use-related**
	Smeared SFA	SFA	3	Uncommon	NA	NA	No	Concentrated & group	Yes	**Possibly use-related**
	Protein	Protein	3	Uncommon	NA	NA	No	Isolated	No	Unknown
	Smeared SFA + goethite	SFA + goethite	3	Uncommon	NA	NA	No	Isolated	Yes	**use-related**
	SFA	SFA	2	Uncommon	NA	NA	No	Isolated	Yes	**Possibly use-related**

	Smeared SFA + haematite	SFA + haematite	2	Uncommon	NA	NA	No	Isolated	Yes	**use-related**
	SFA/UFA	SFA/UFA	1	Rare	NA	NA	No	Isolated	NA	Unknown
	Protein fibre	Protein	1	Rare	NA	NA	No	Isolated	No	Unknown
LB5572										
	Kaolinite	Kaolinite	NC	Common	No	No	No	Isolated	No	rock weathering
	Goethite	Goethite	NC	Uncommon	No	No	No	Concentrated & group	Yes	**Possibly use-related**
	Haematite	Haematite	NC	Uncommon	No	No	No	Concentrated & group	Yes	**Possibly use-related**
	Manganese oxide	MnO_2	NC	Common	No	No	No	Isolated	No	post-depositional
	SFA/UFA	SFA/UFA	21	Uncommon	No	No	No	Concentrated & group	NA	**use-related**
	Protein	Protein	10	Uncommon	No	No	No	Isolated	No	Unknown
	Smeared SFA/UFA	SFA/UFA	6	Uncommon	No	No	No	Isolated	Yes	**use-related**
	Fossil bone + kaolinite	Apatite + kaolinite	3	Uncommon	No	No	No	Isolated	Yes	**Possibly use-related**
	Bone apatite(fossil)	Apatite	2	Uncommon	No	Uncommon	Common	Isolated	Yes	From sediment
	Smeared bone apatite(fossil)	Apatite	1	Rare	No	No	No	Isolated	NA	**Possibly use-related**
	Smeared SFA	SFA	1	Rare	No	No	No	Isolated	NA	Unknown
	SFA	SFA	1	Rare	No	No	No	Isolated	NA	Unknown
	SFA + Protein	SFA + protein	1	Rare	No	No	No	Isolated	NA	Unknown
	Smeared Goethite	Goethite	1	Rare	No	No	No	Isolated	NA	**Possibly use-related**
	Plant fibre*	Cellulose + lignin	1	Rare	No	No	No	Isolated	NA	Modern contamination
	*** Matching a modern contaminant**	**NA: Non applicable**	**UOM : Undetermined organic material**		**NC : Not counted**					

Appendix IIb results figures

Artefact Micro-residues distribution: Liang Bua collection 2016 Sector 25

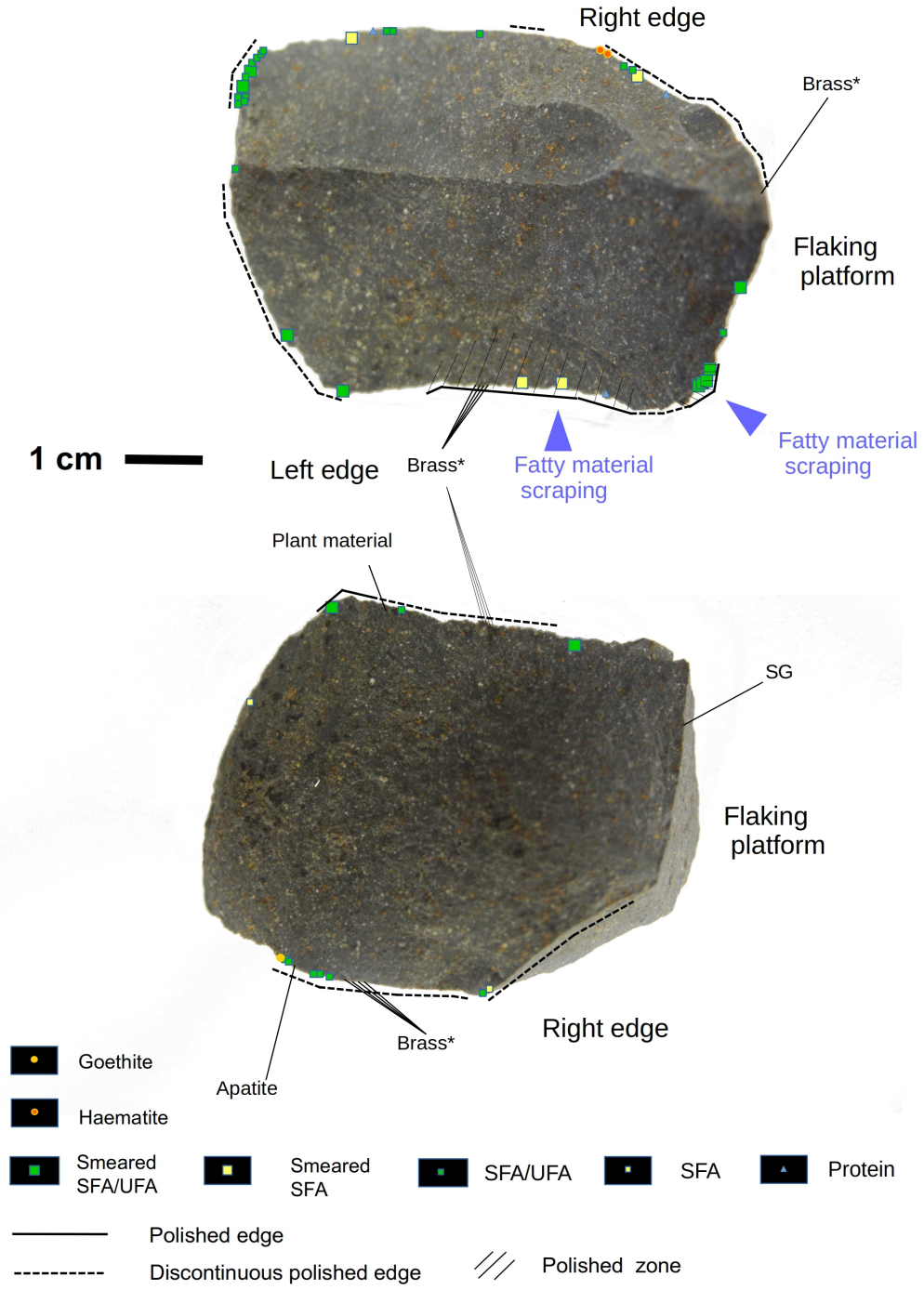

Figure 1: Micro-residues distribution on artefact LB5211.

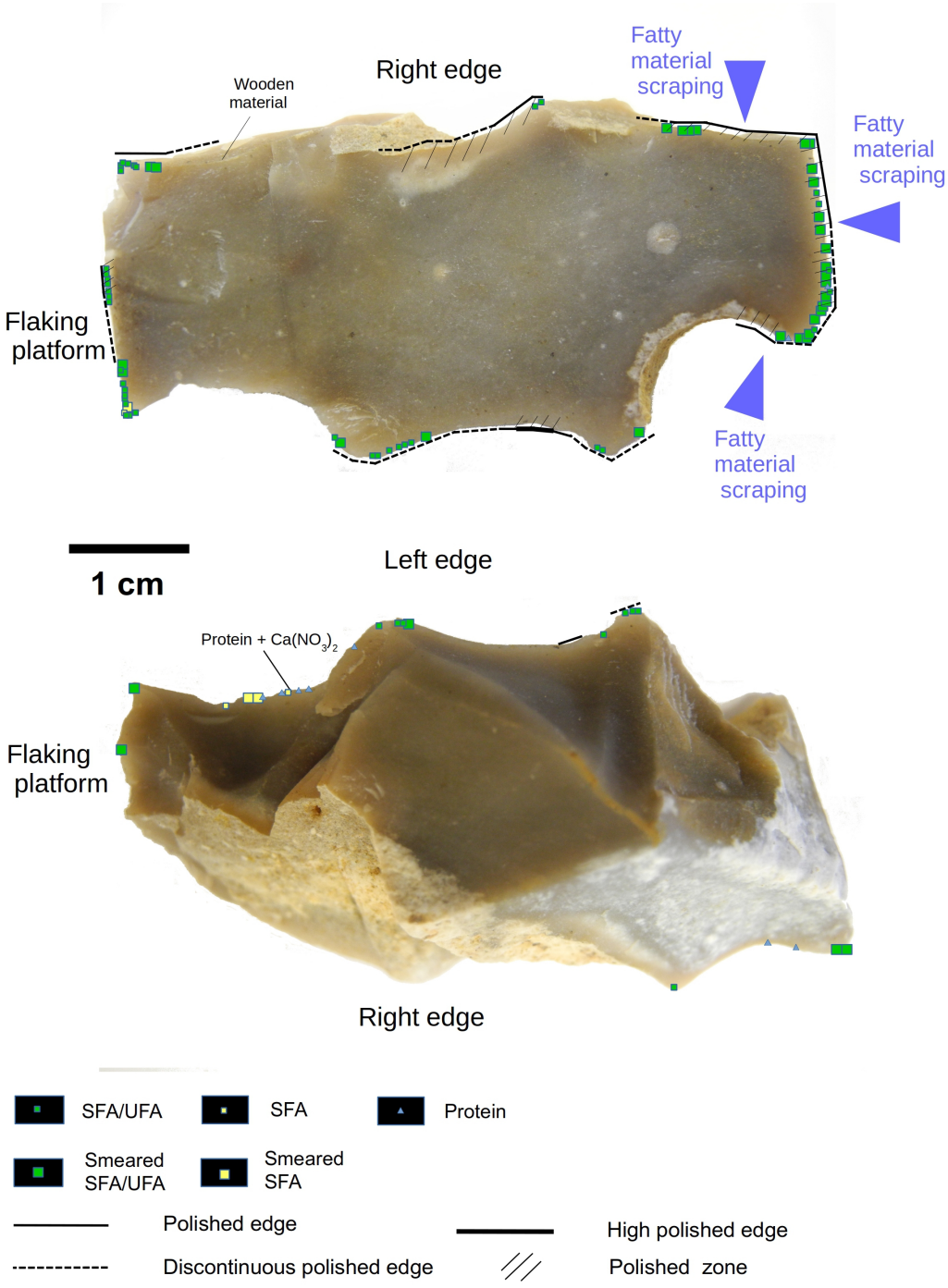

Figure 2: Micro-residues distribution on artefact LB5212.

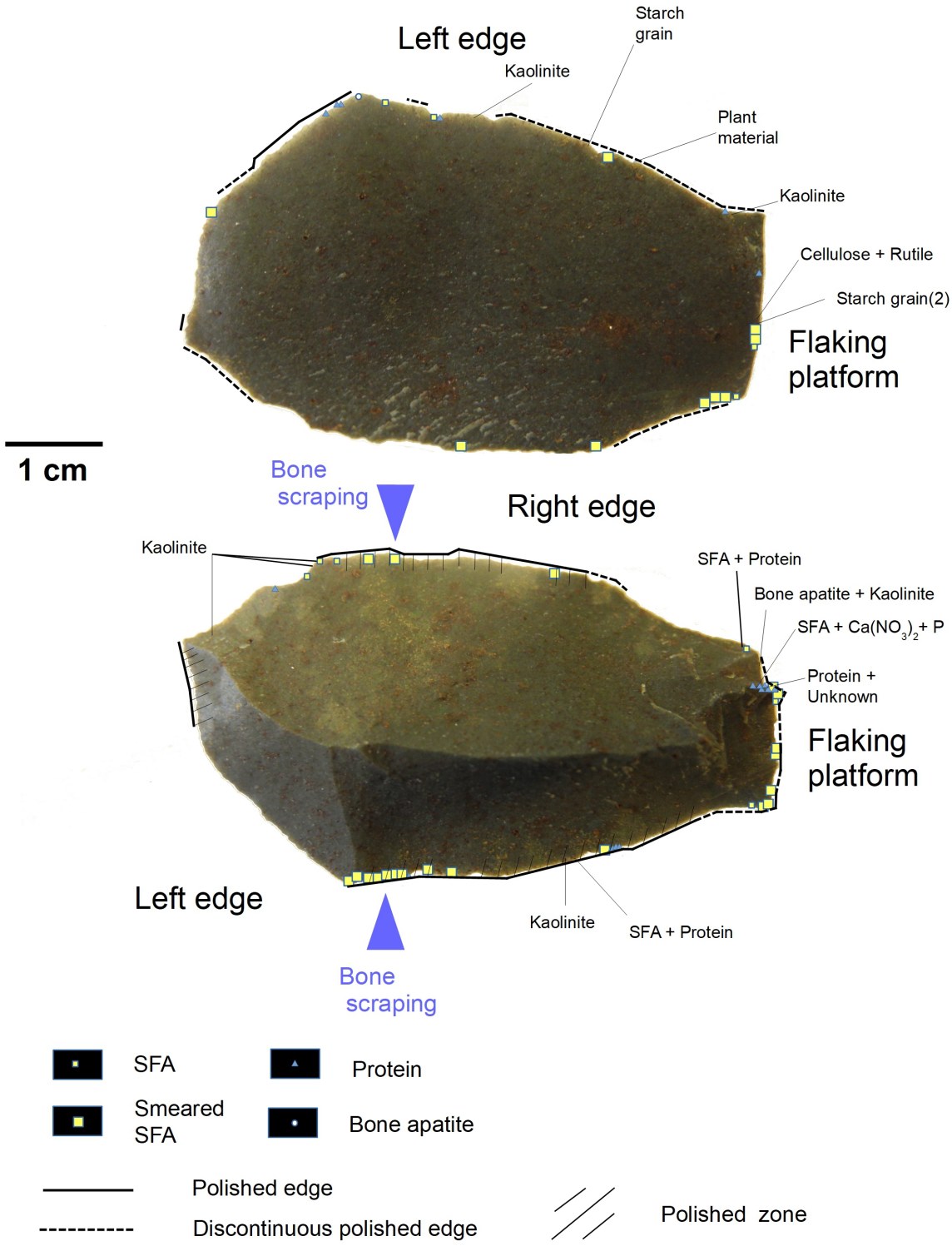

Figure 3: Micro-residues distribution on artefact LB5224a.

Artefact Micro-residues distribution: Liang Bua collection 2016 Sector 26

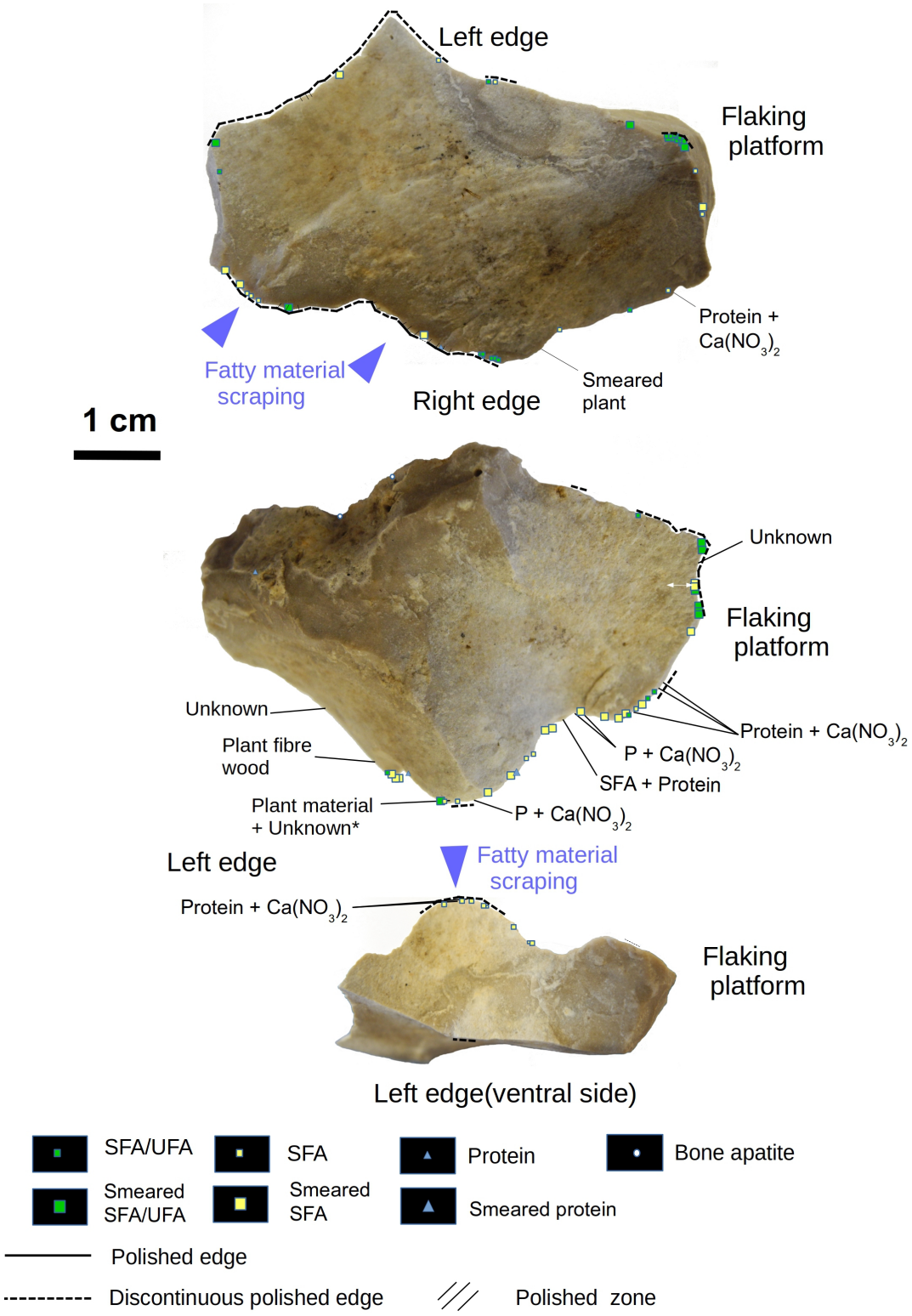

Figure 4: Micro-residues distribution on artefact LB5525.

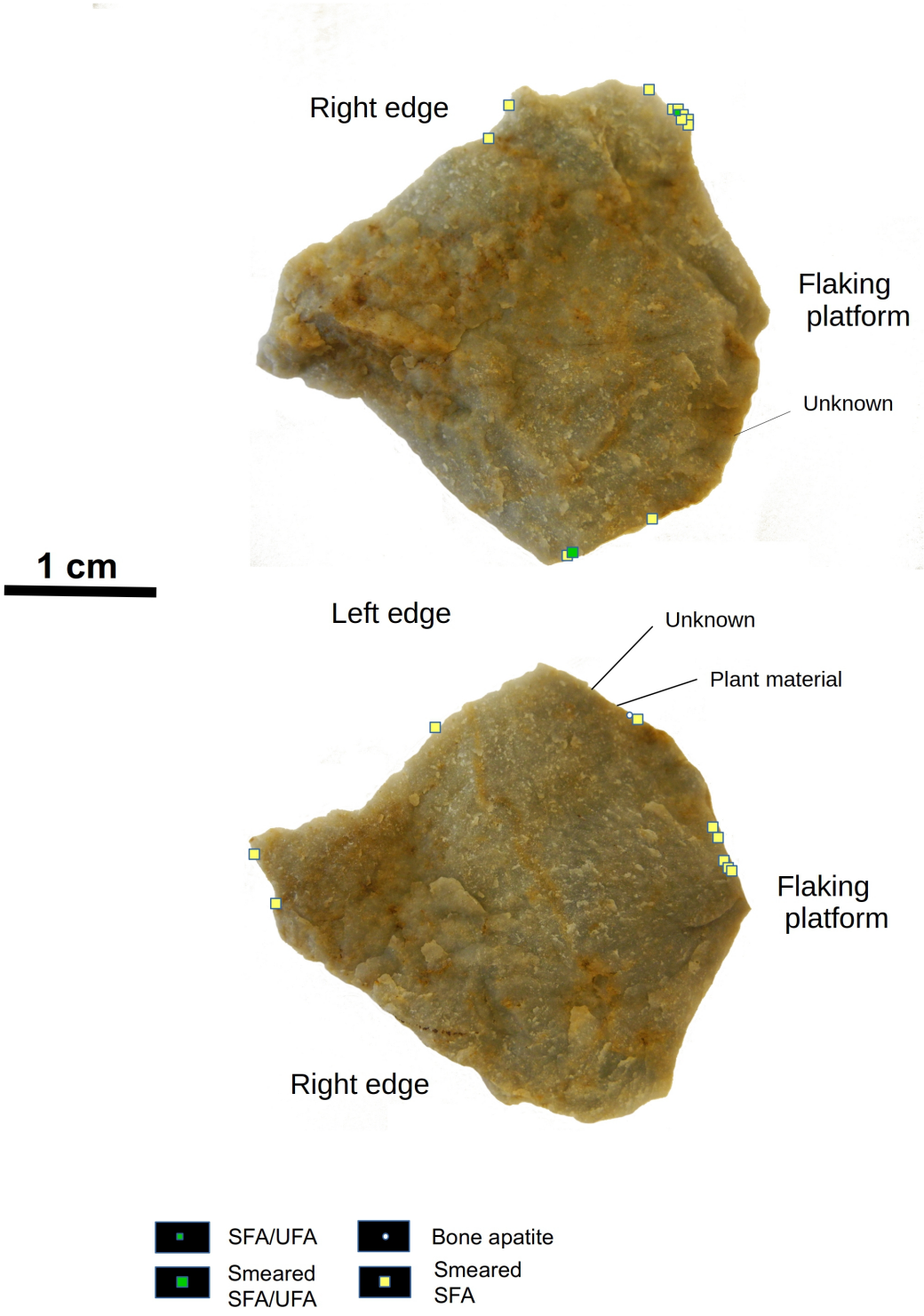

Figure 5: Micro-residues distribution on artefact LB5526a.

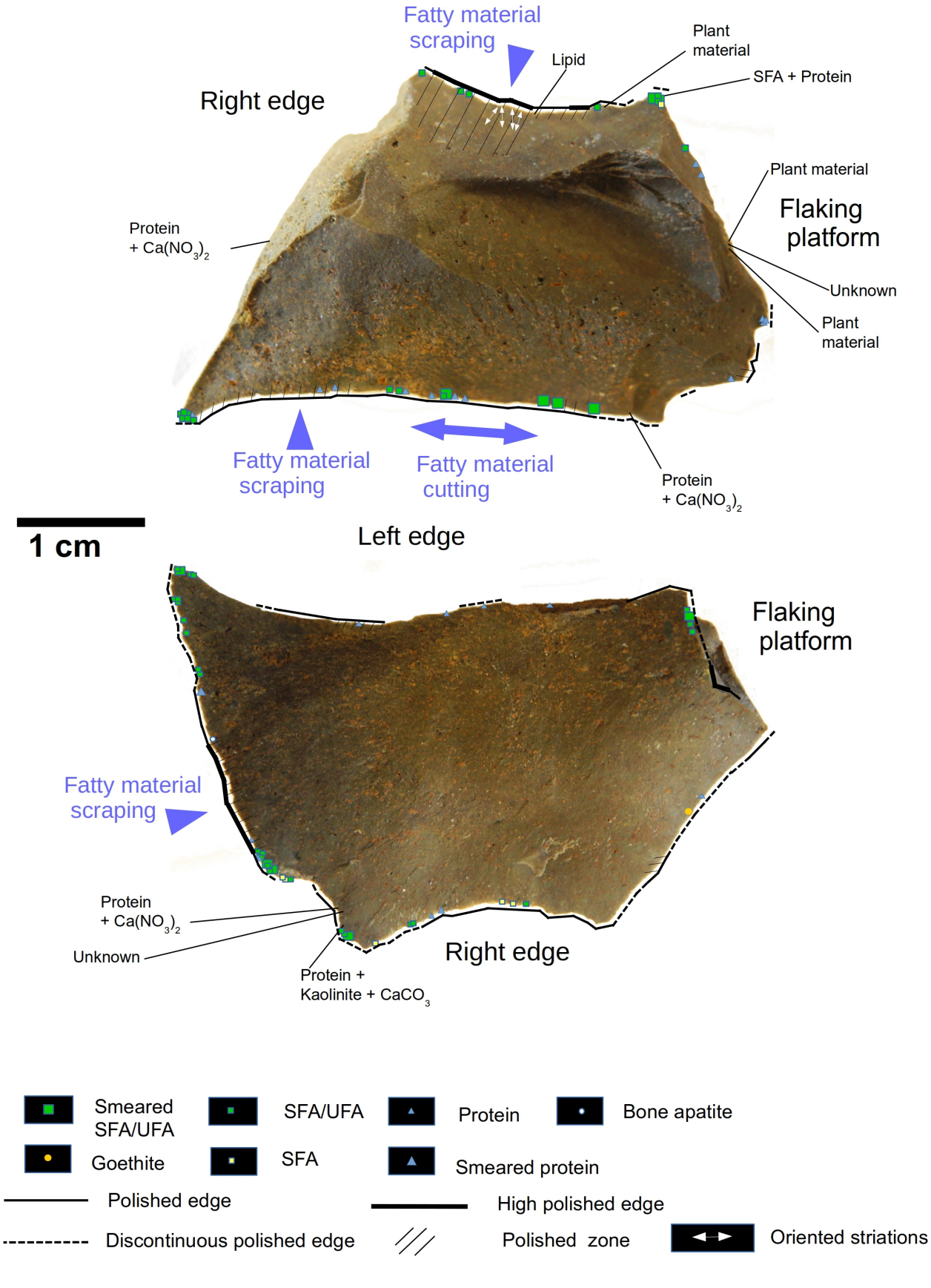

Figure 6: Micro-residues distribution on artefact LB5527.

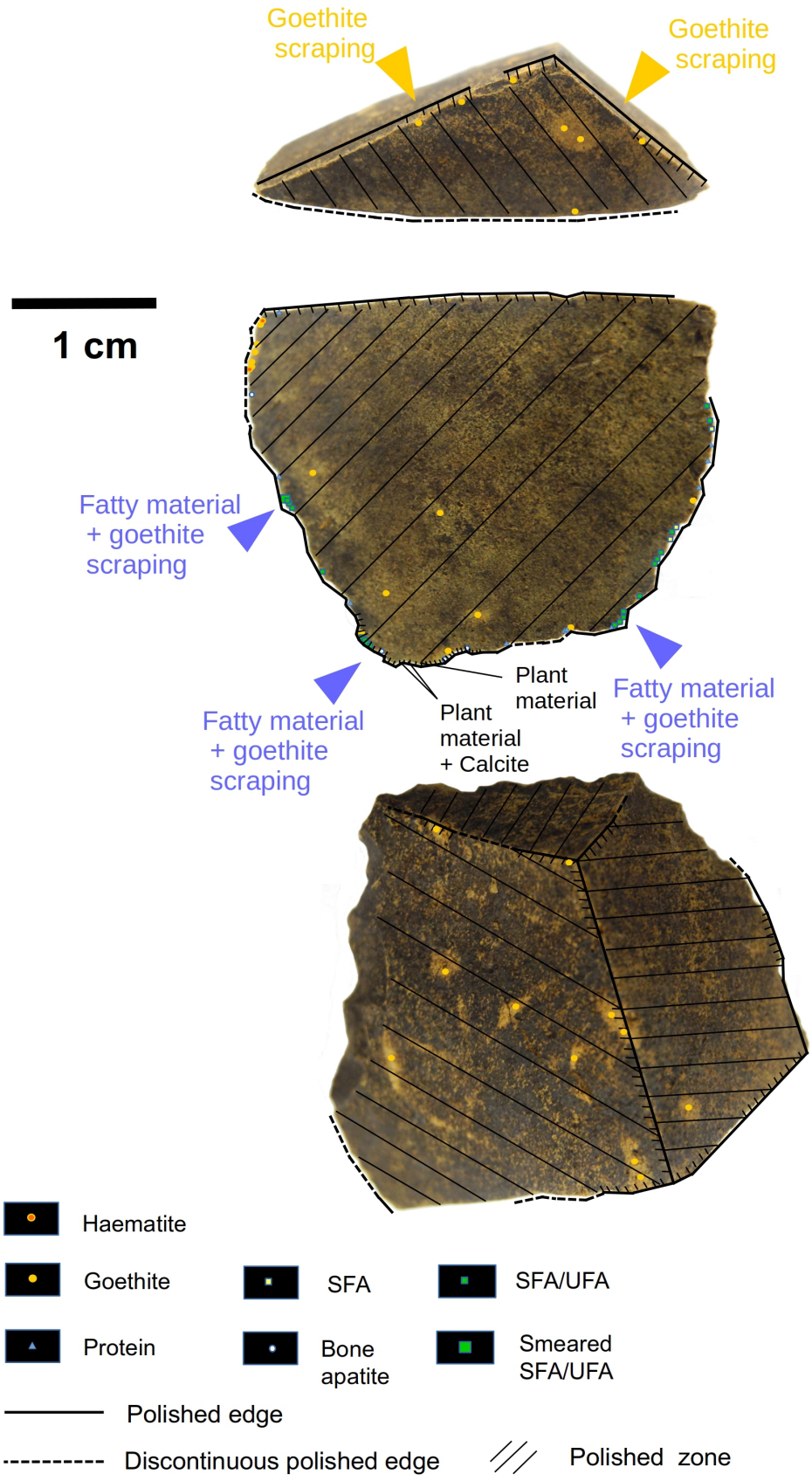

Figure 7 : Micro-residues distribution on artefact LB5533a.

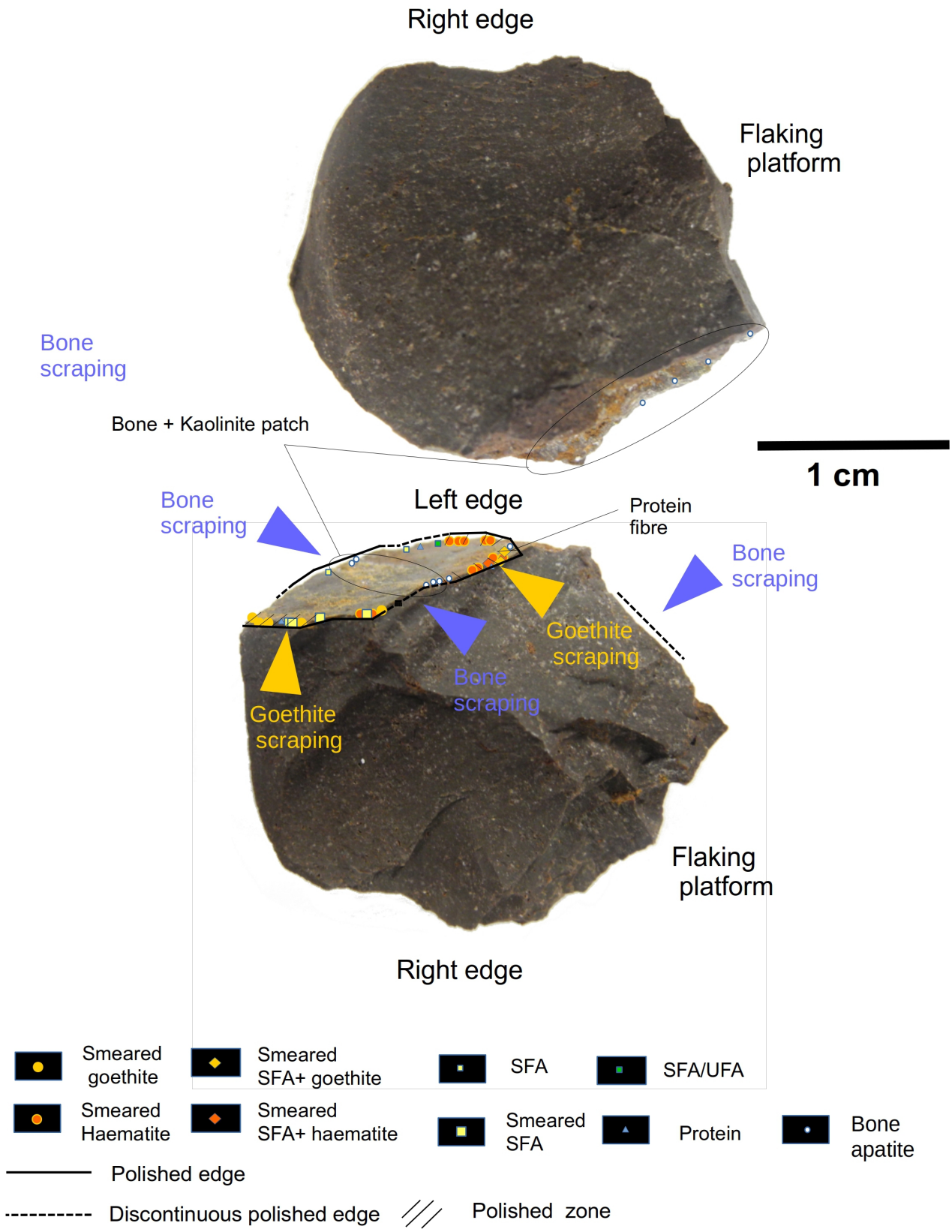

Figure 8: Micro-residues distribution on artefact LB5533b.

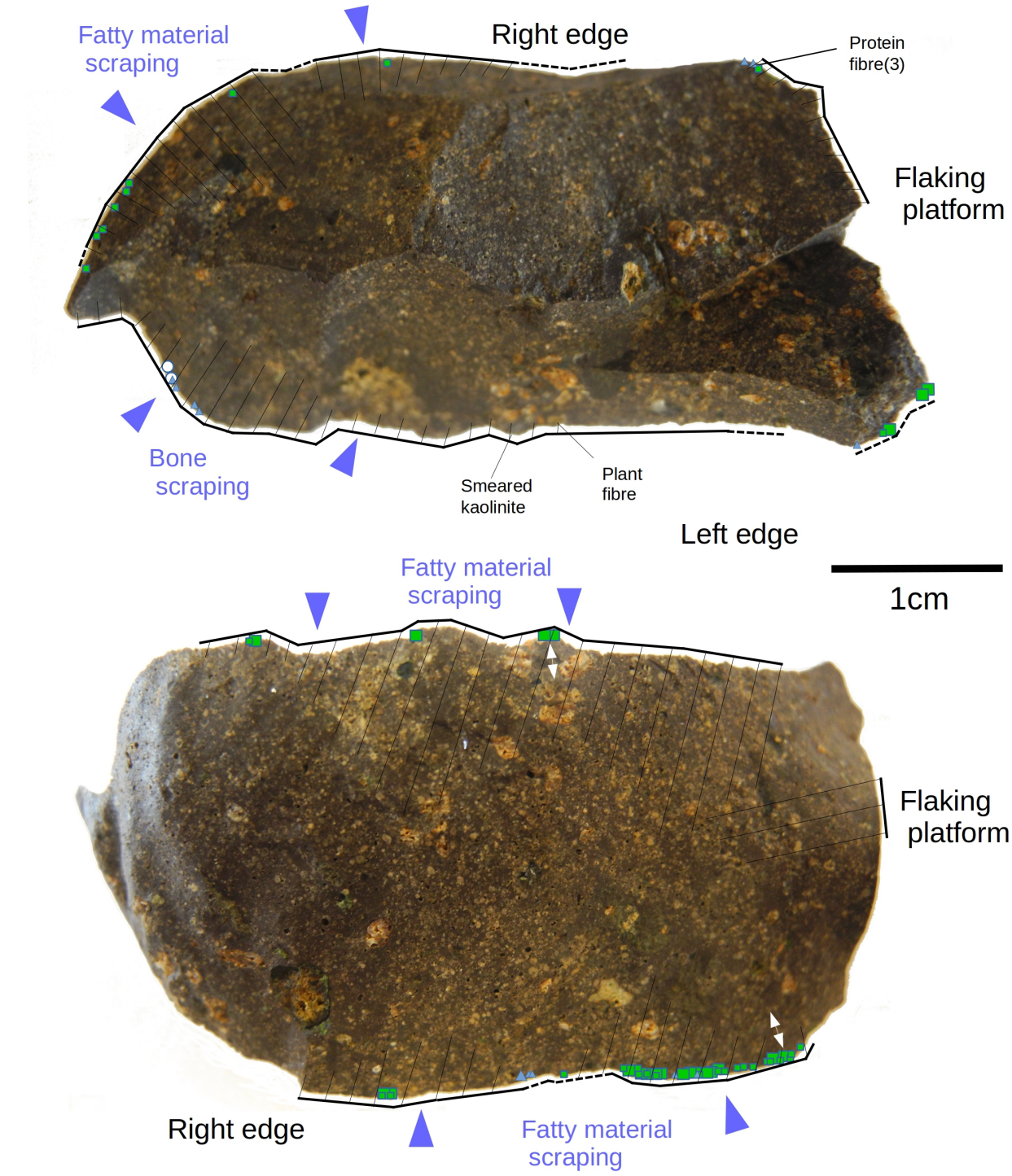

Figure 9: Micro-residues distribution on artefact LB5562a.

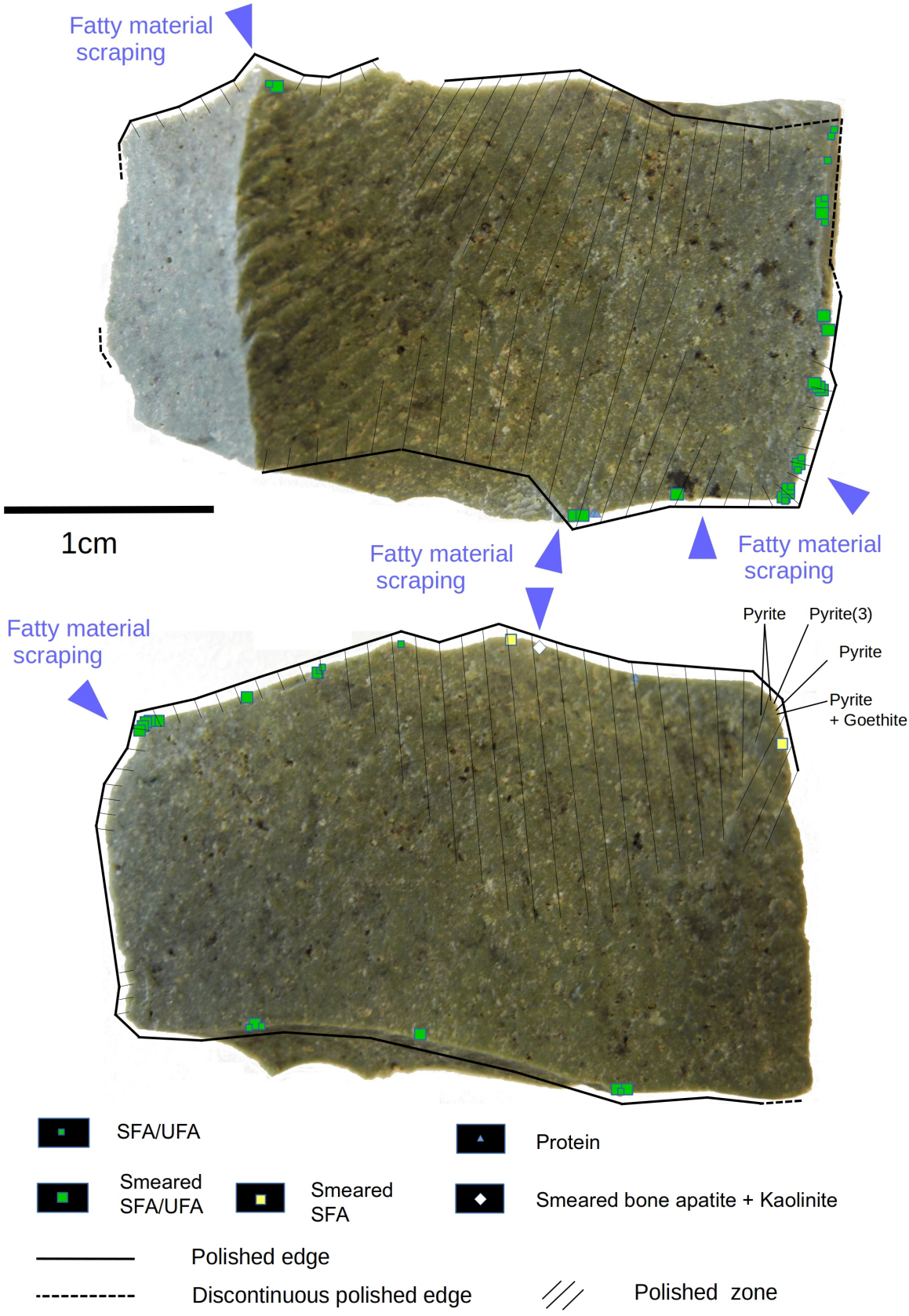

Figure 10: Micro-residues distribution on artefact LB5562b.

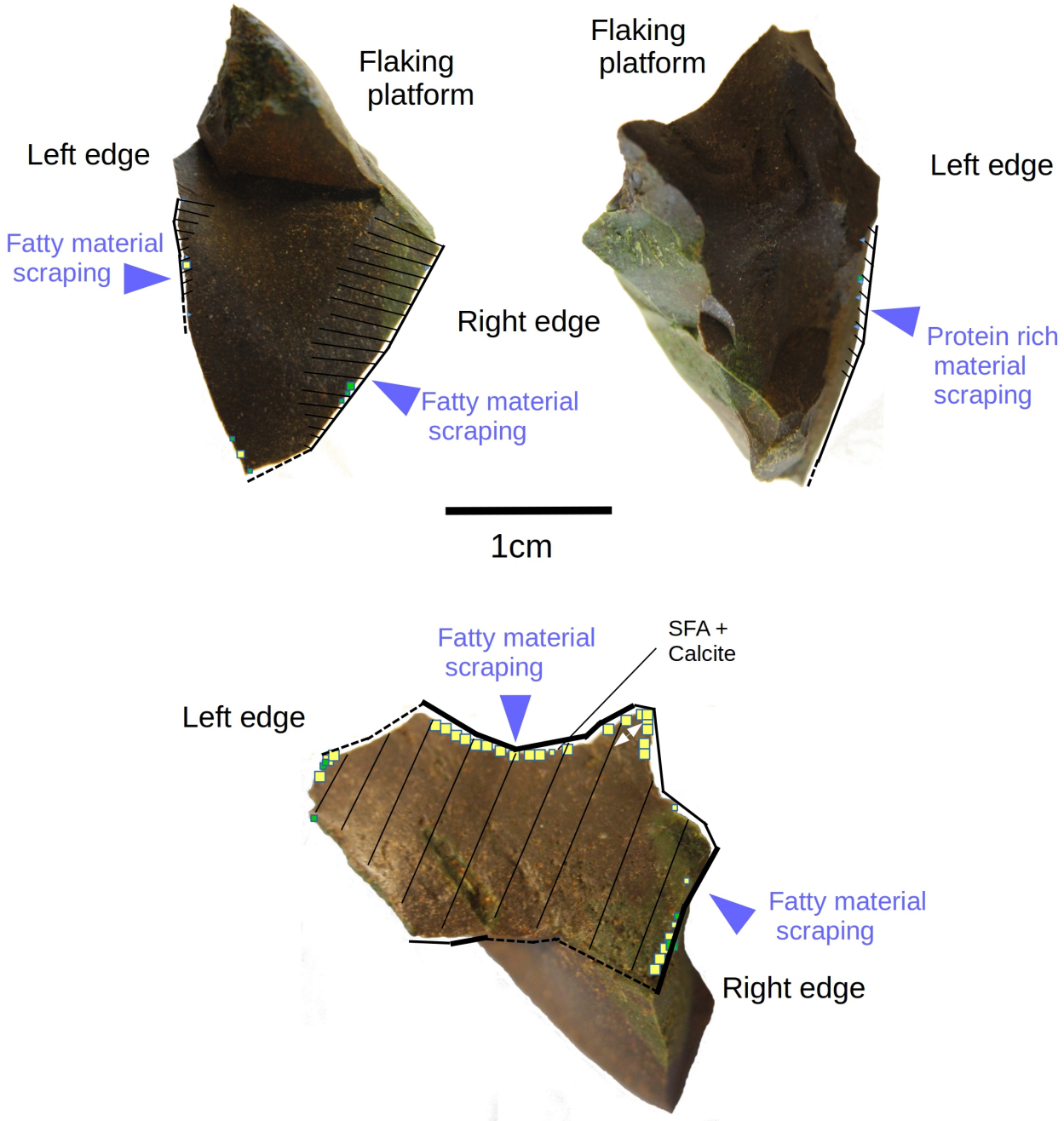

Figure 11 : Micro-residues distribution on artefact LB5563a.

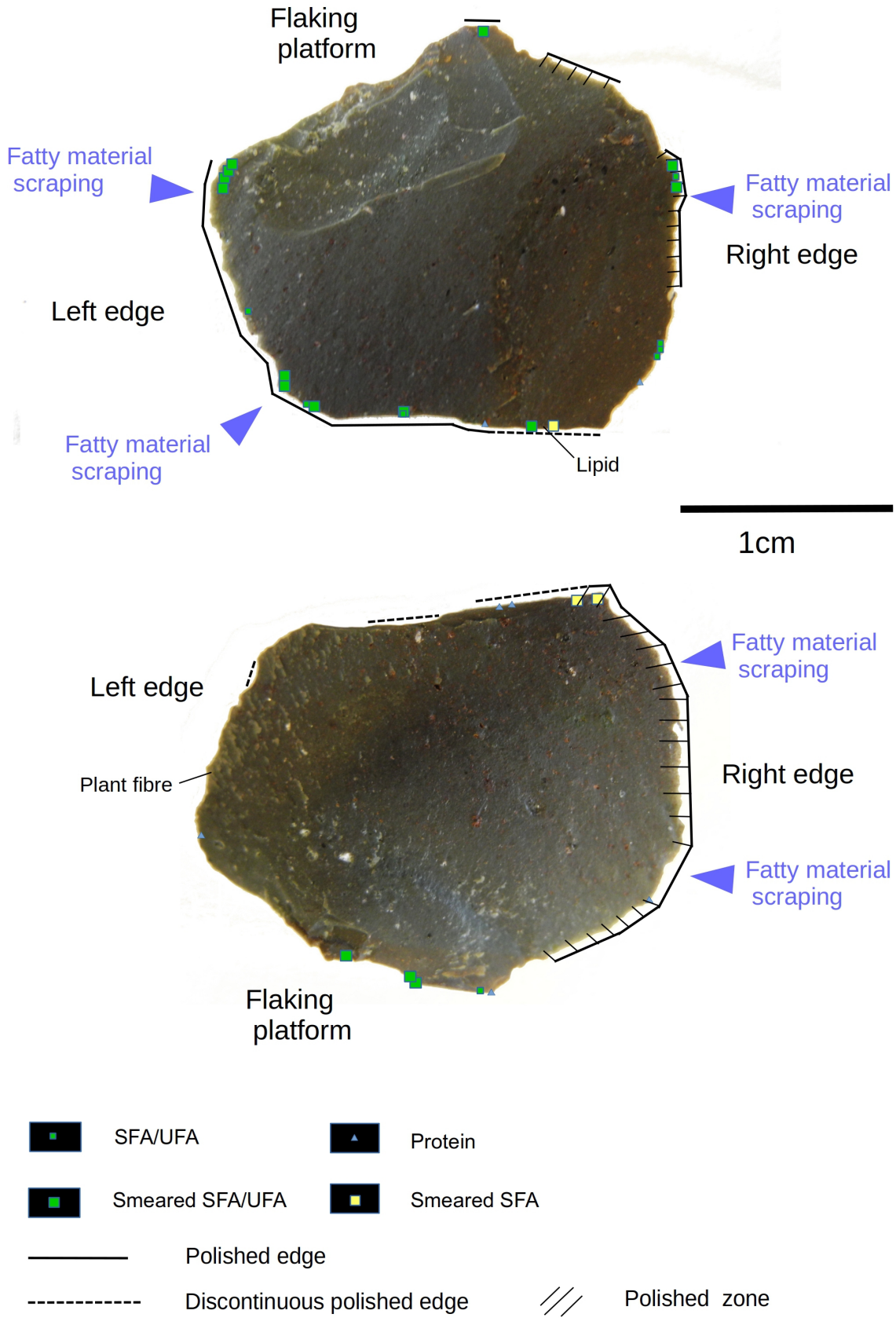

Figure 12: Micro-residues distribution on artefact LB5563b.

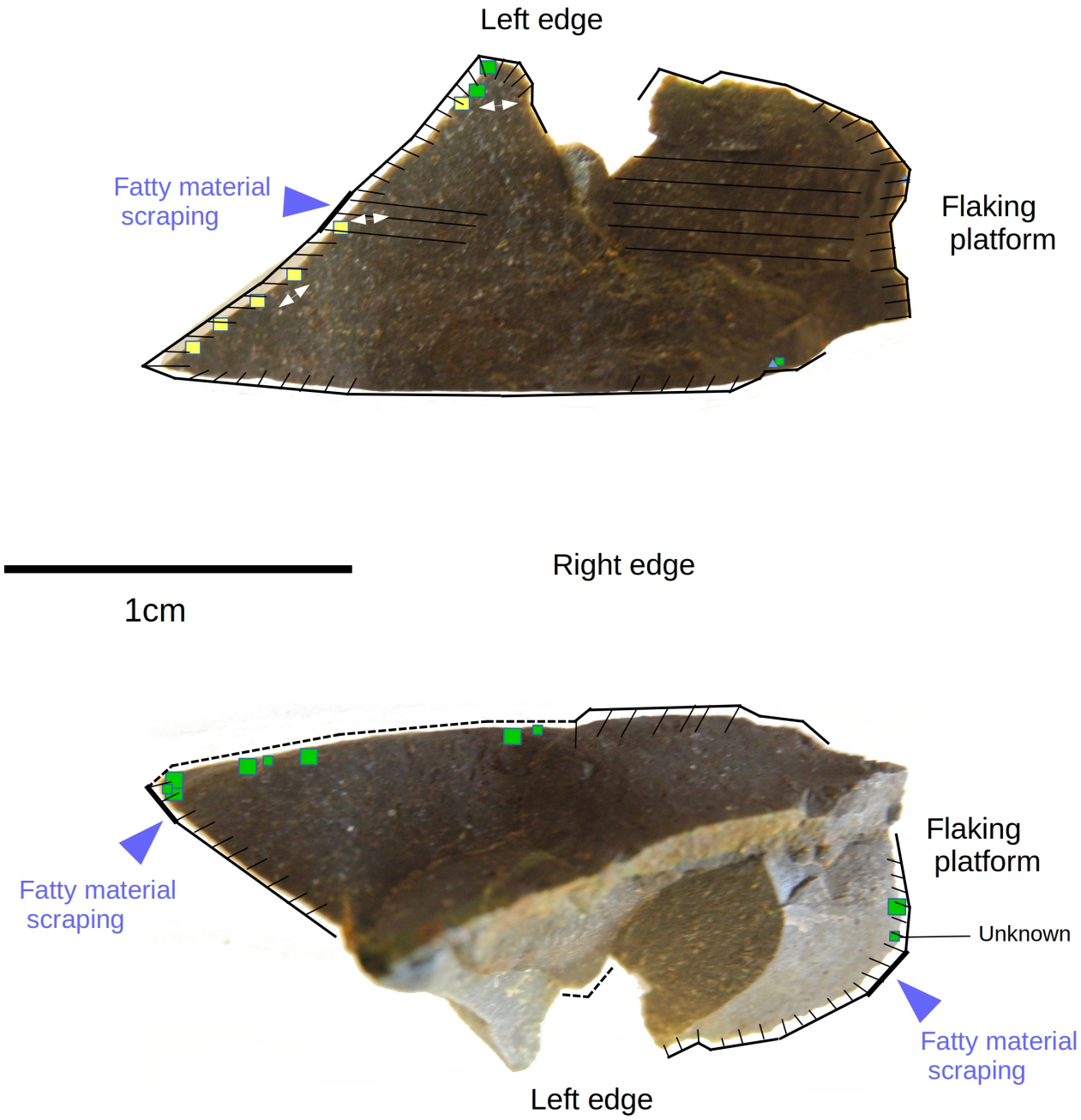

Figure 13: Micro-residues distribution on artefact LB5563c.

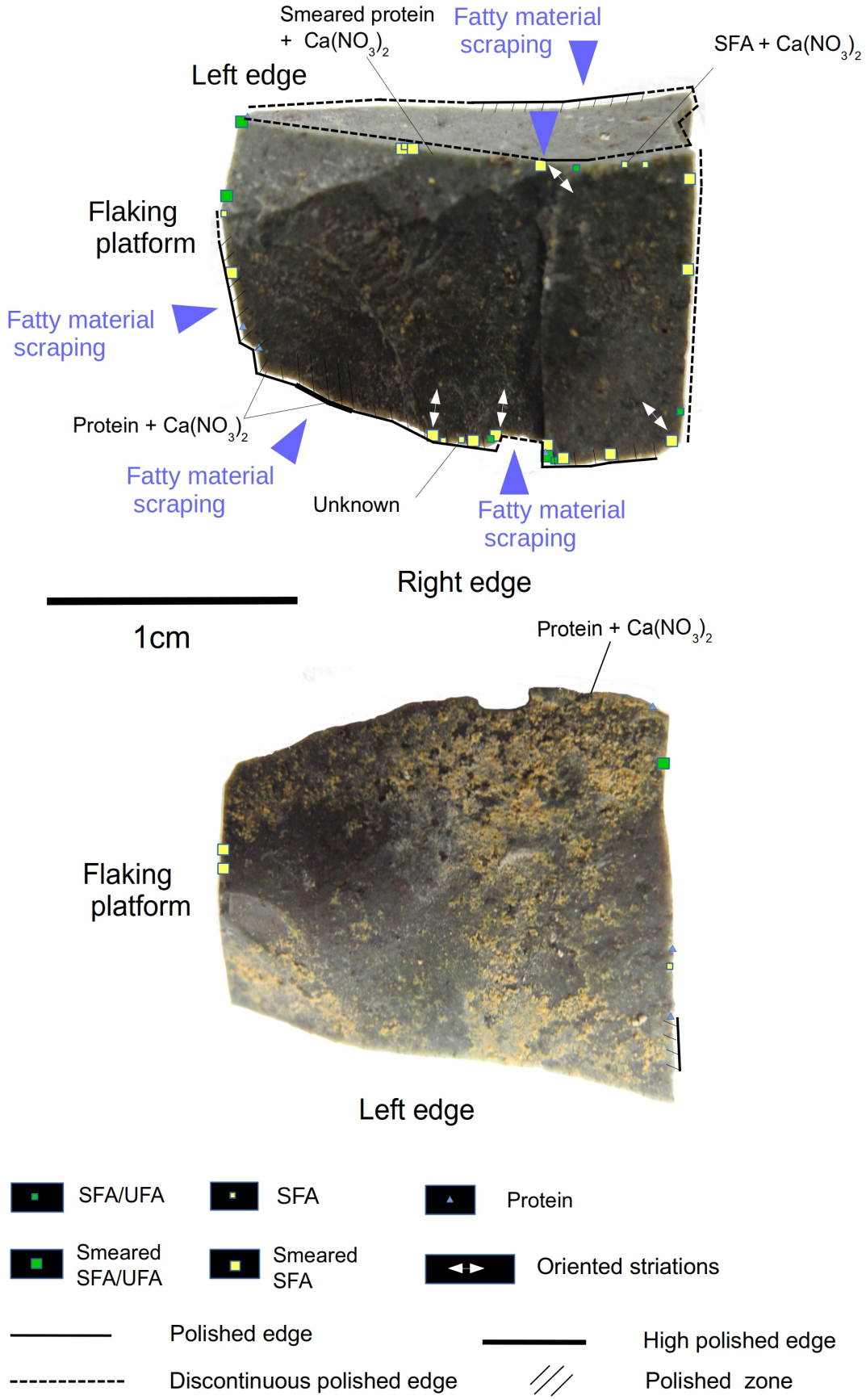

Figure 14 : Micro-residues distribution on artefact LB5564.

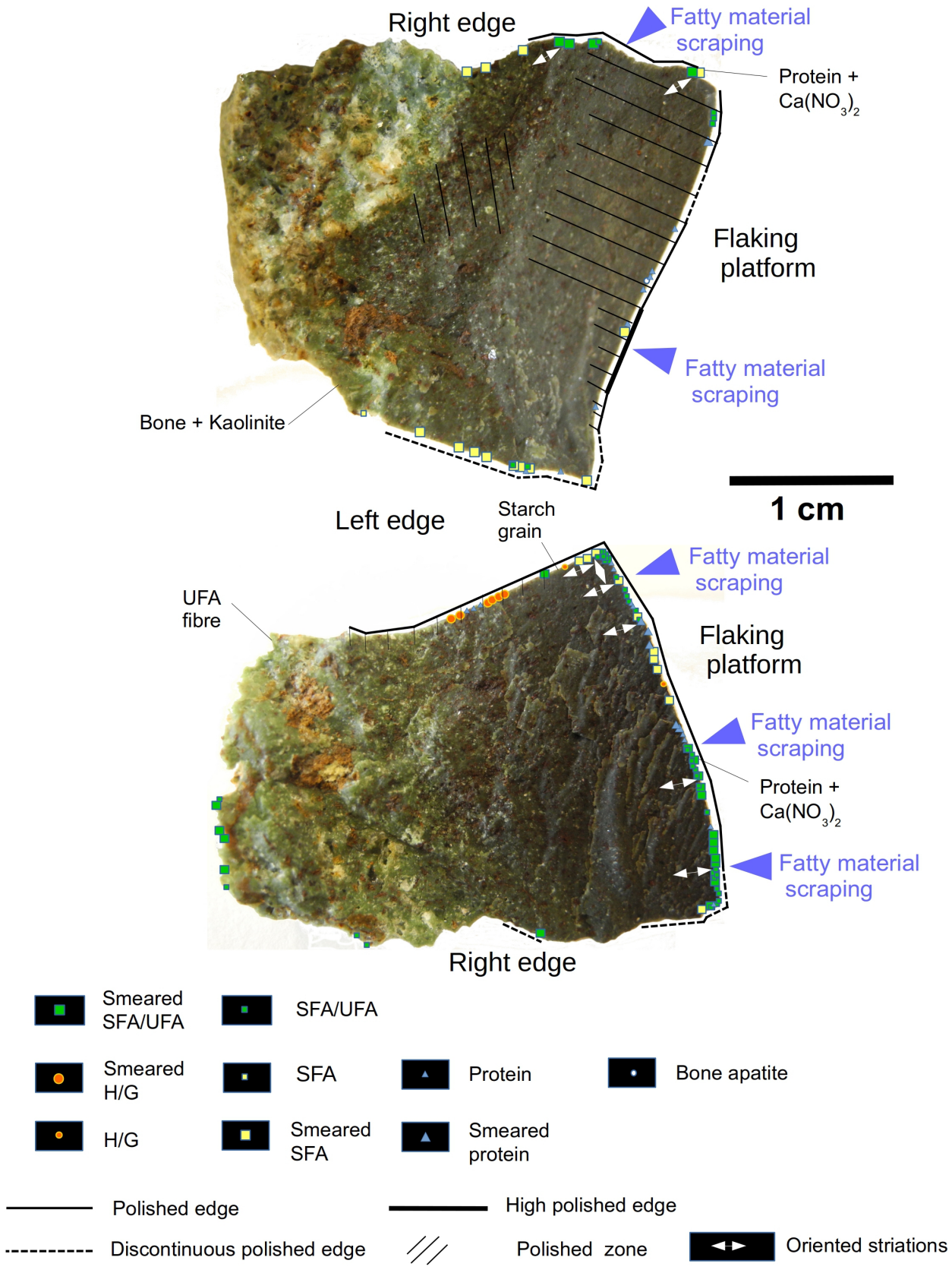

Figure 15: Micro-residues distribution on artefact LB5565.

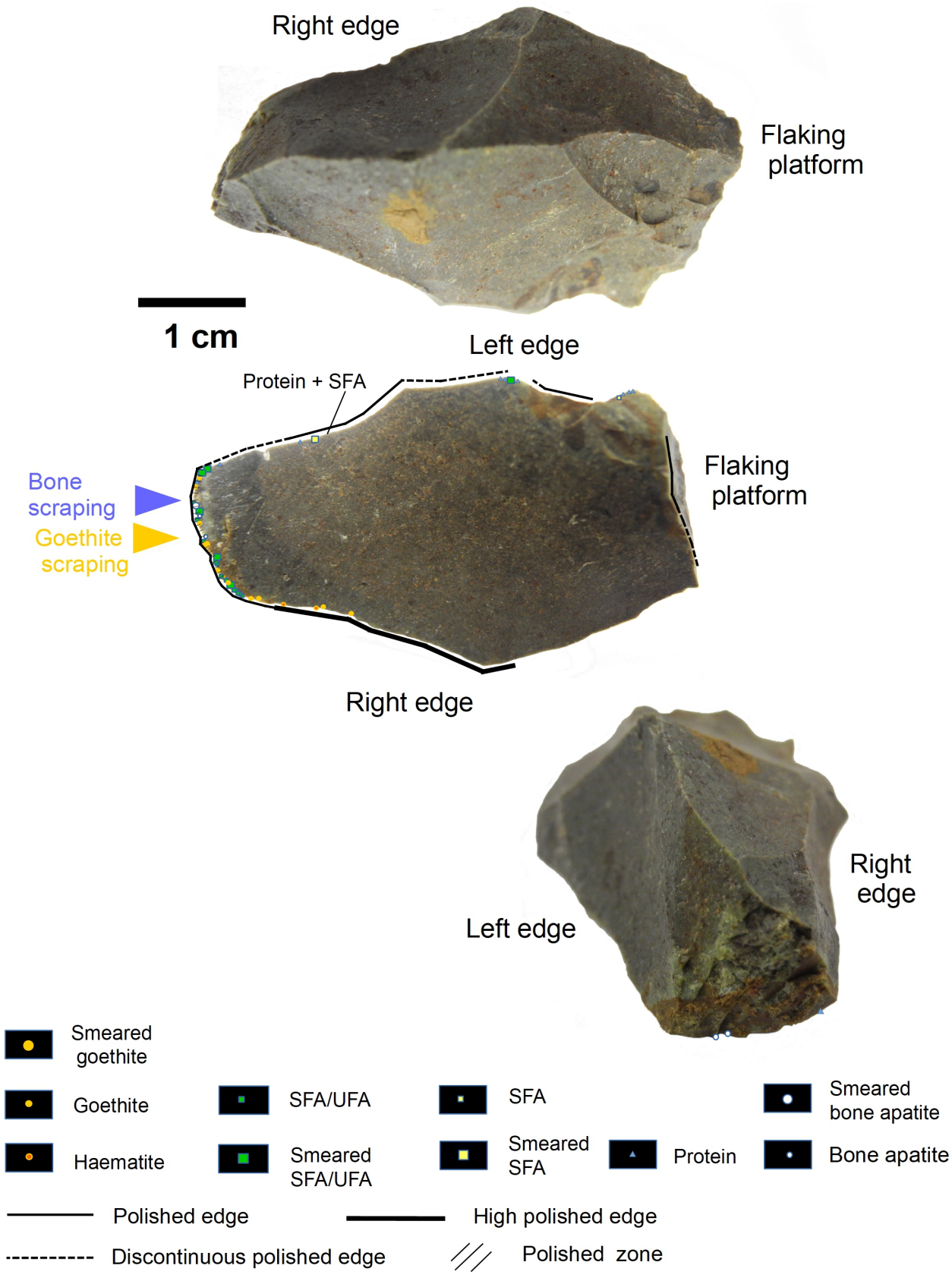

Figure 16: Micro-residues distribution on artefact LB5572.

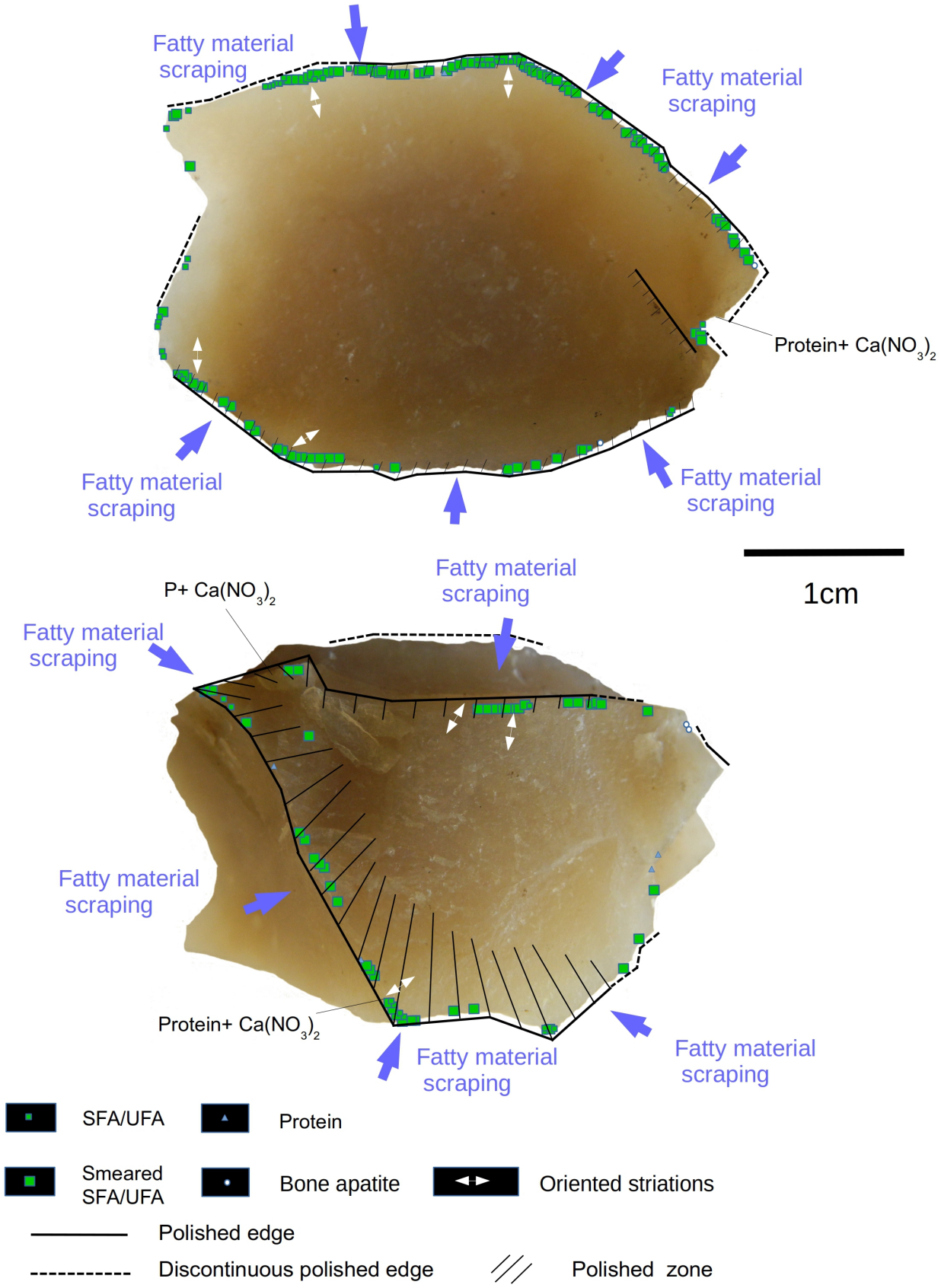

Figure 17: Micro-residues distribution on artefact LB5580b.

Appendix III blind tests

Seven blind stone tools have been selected from an old experimental collection to evaluate the efficiency of the methodology used in this work. Analysis method and interpretation of the micro-residues had been the same as used on archaeological artefacts and as described in chapter two and three except that no cleaning and no sediment sample analysis was needed here. It can be noted that some micro-residues, like collagen, not found on archaeological stone tools, have been found preserved in a similar way as experimental tools used as reference in chapter four. The final rate of success of these blind test is 57% and they are discussed in detail in chapter seven along with the advantage and limits of Raman spectroscopy analysis on each potential archaeological micro-residues.

Table 1 Summary of blind tests

Experiment information				**Use determined after Raman analysis**				
Blind test	**Experiment dating**	**Duration (Minute)**	**Task**	**Use as**	**use-related residues**	**Incidental residues**	**Identified Contamination**	**Use interpretation**
1	1984	50	Butchering fresh *Macropus sp.* wallaby	Cutting tool	**Plant fibre, plant material**, **UFA**	UFA, bone	Dyed fibre, indigo fibre, plastic box, metal mark	Cutting plant
2	1984	35	Sawing *Macropus sp.* kangaroo bone	Sawing tool	**Bone**, **collagen, UFA**,	UFA	Plastic bag, cellulose, unknown aromatic resin	Sawing bone
3	1984	35	Scraping dry *Macropus sp.* kangaroo skin	Not used	**None**	UFA	Dyed fibre, polyester, unknown aromatic resin + gypsum	Not used ?
4	1984	90	Whittling fresh *Melaleuca sp.* wood to a point	Scraper	**Plant fibre, plant material**, **UFA, protein,**	UFA	none	Scraping wood
5	1984	45	Sawing dry *Calamus sp.* rattan from Papua New Guinea	Scraper	**Plant fibre, plant material, UFA, protein**	none	none	Scraping plant material
6	2018		Hammer retouch, not used	Scraper	**UFA, protein, feldspar**	none	none	Scraping unknown fatty material, mineral
7	2018		No retouch, not used	Scraper	**UFA, protein**	none	none	Scraping unknown fatty material

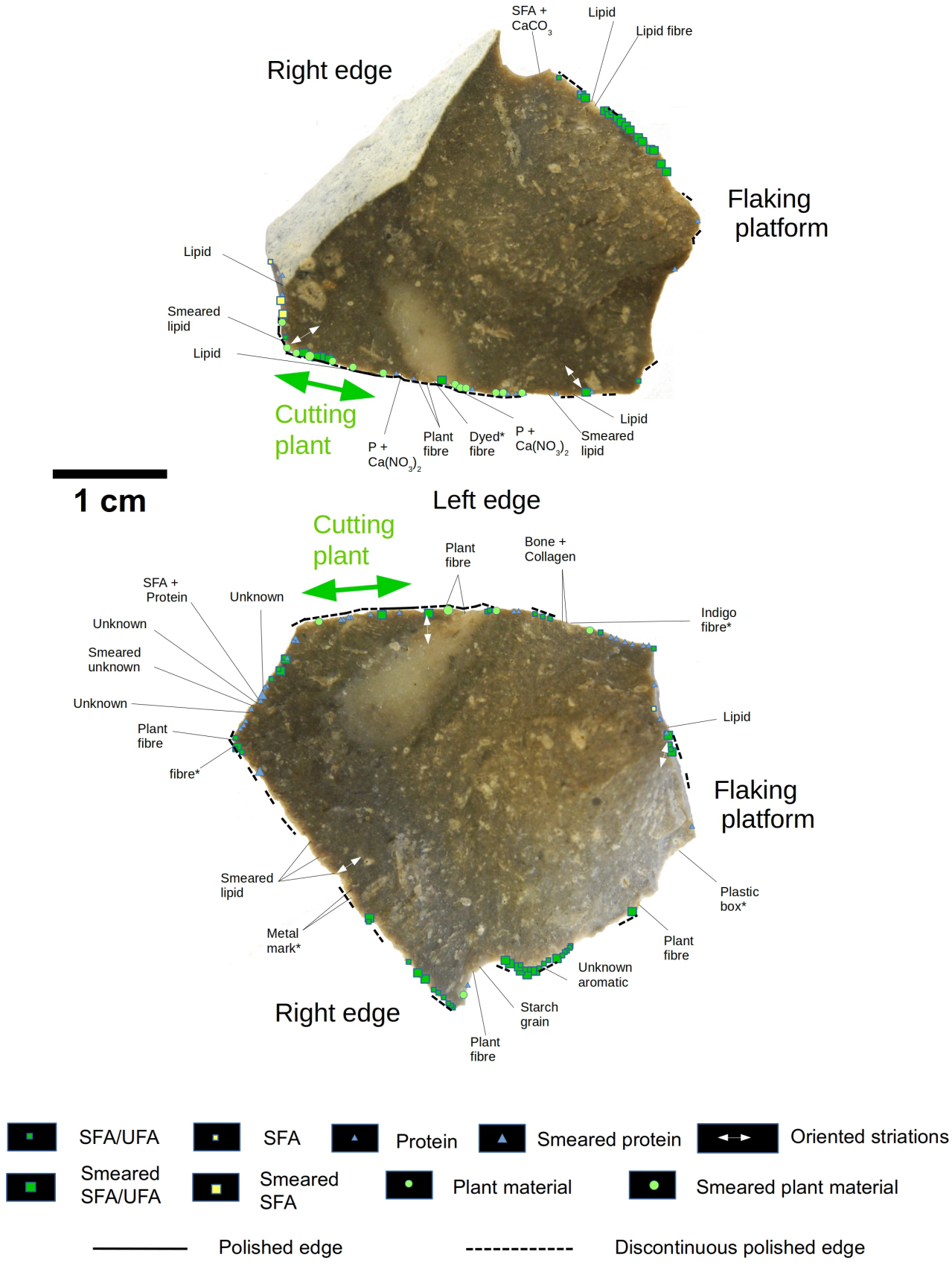

Figure 1 : Micro-residues distribution on artefact Blindtest1.

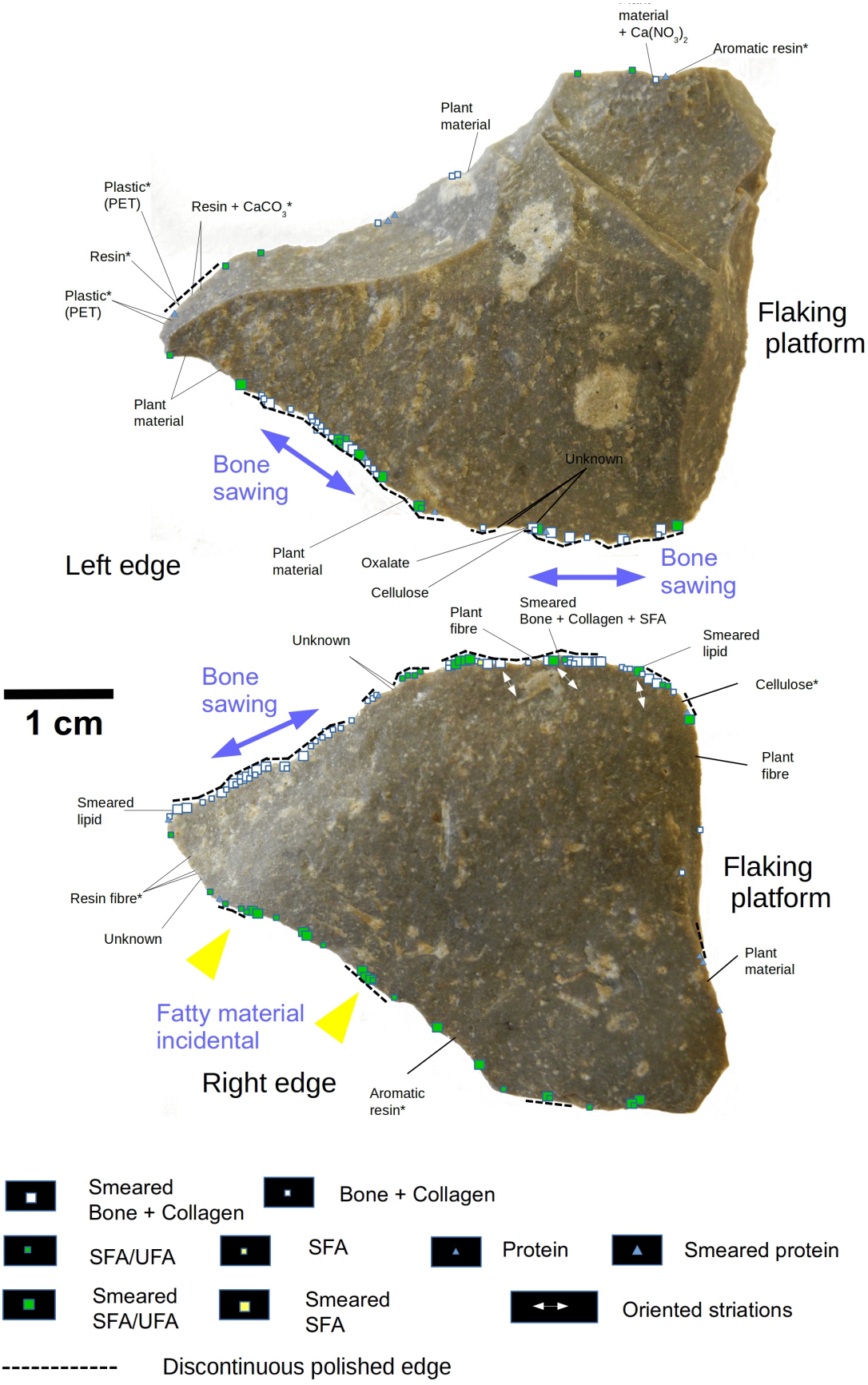

Figure 2 : Micro-residues distribution on artefact Blindtest2.

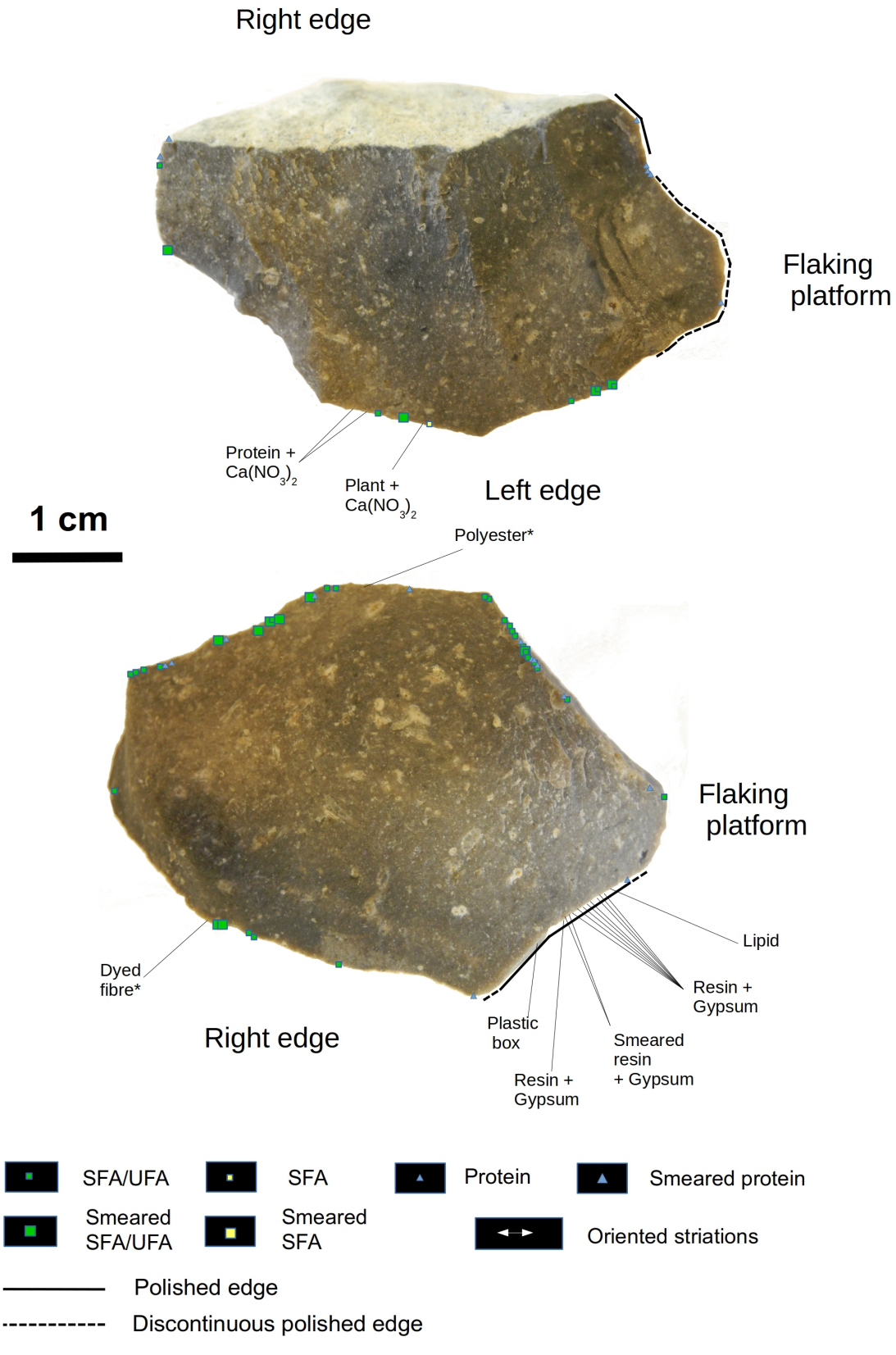

Figure 3 : Micro-residues distribution on artefact Blindtest3.

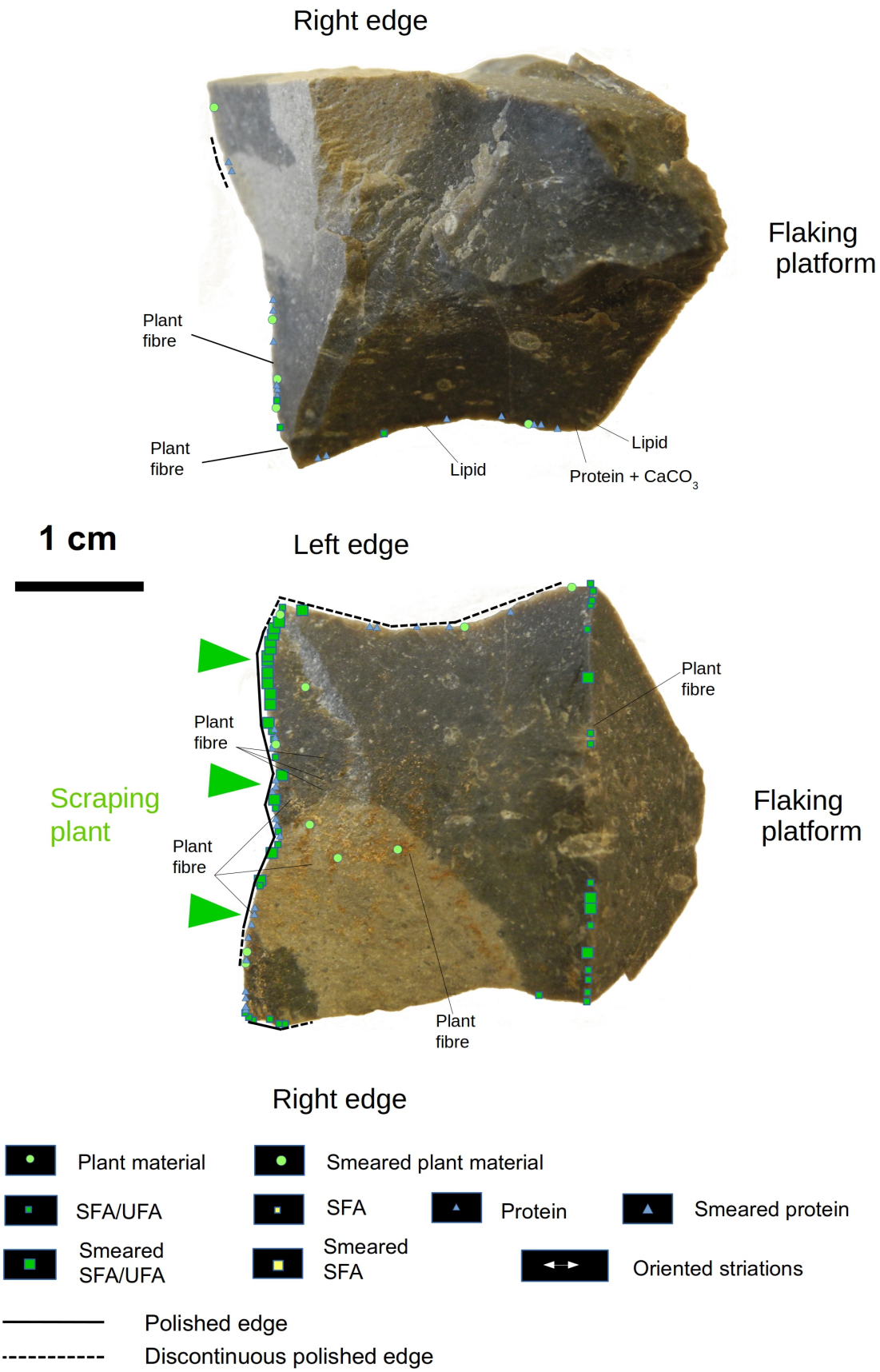

Figure 4 : Micro-residues distribution on artefact Blindtest4.

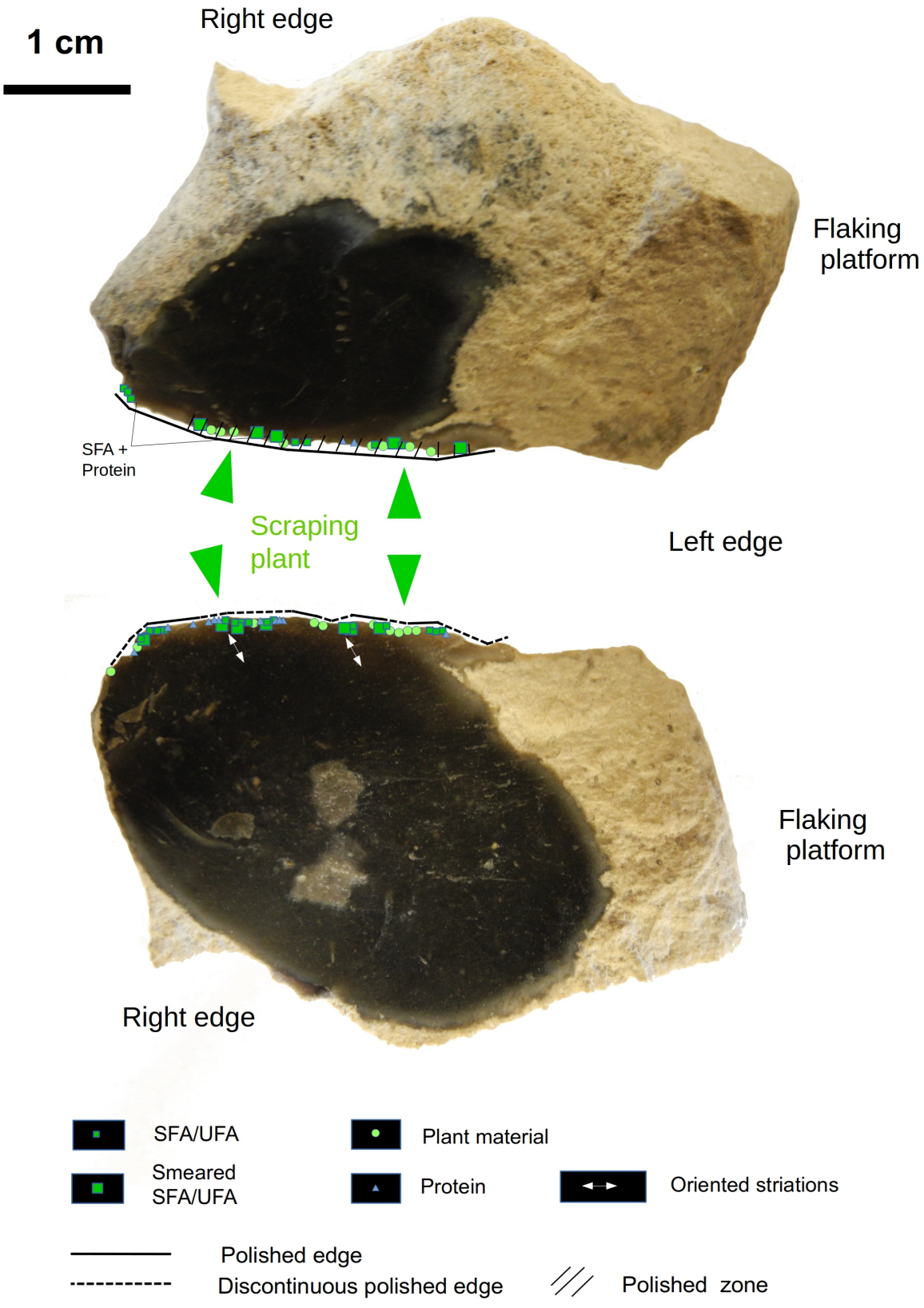

Figure 5 : Micro-residues distribution on artefact Blindtest5.

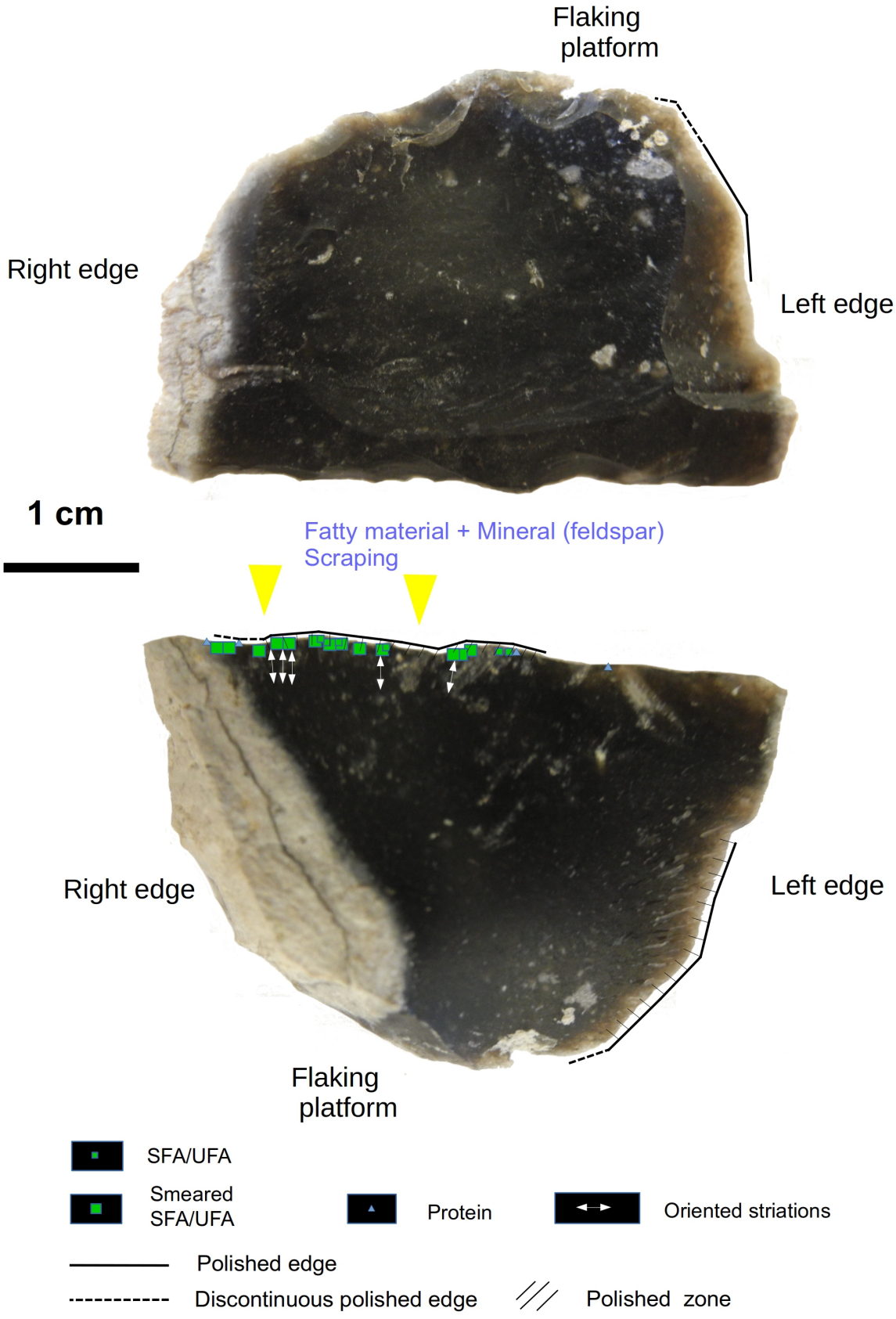

Figure 6 : Micro-residues distribution on artefact Blindtest6.

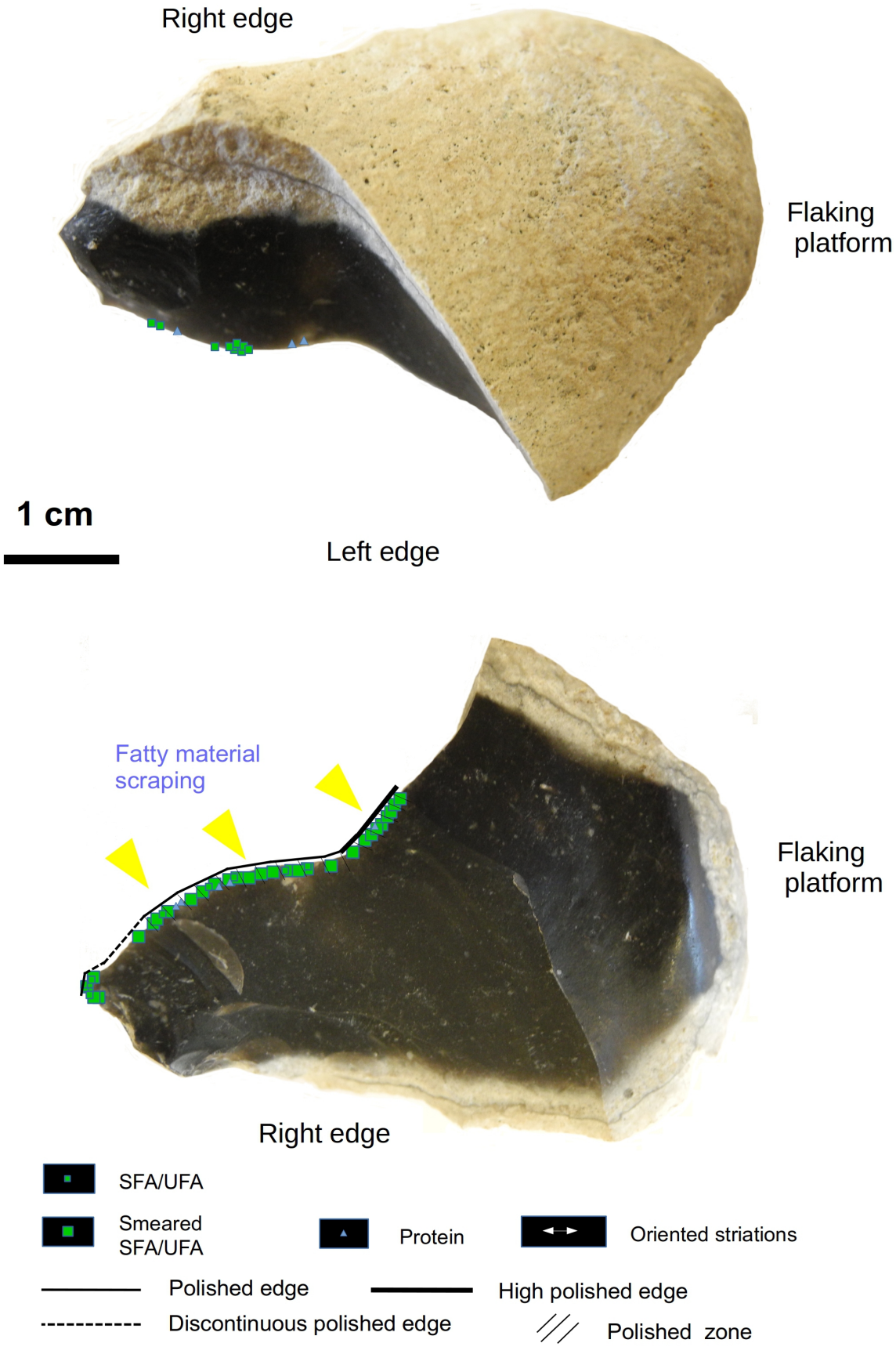

Figure 7: Micro-residues distribution on artefact Blindtest7.